Schweizerische Eidgenossenschaft
Confédération suisse
Confederazione Svizzera
Confederaziun svizra

Eidgenössisches Departement für Umwelt, Verkehr, Energie und Kommunikation UVEK
Département fédéral de l'environnement, des transports, de l'énergie et de la communication DETEC
Dipartimento federale dell'ambiente, dei trasporti, dell'energia e delle comunicazioni DATEC

Bundesamt für Strassen
Office fédéral des routes
Ufficio federale delle Strade

Interaktion Strasse Hangstabilität: Monitoring und Rückwärtsrechnung

Interaction route – stabilité des versants: Monitoring et calcul à rebours

Road – Landslide Interaction: Monitoring and Inverse Stability Analysis

ETH Zürich
Institut für Geotechnik

Alexander Puzrin, Prof.
Andreas Schmid, dipl. Bauing.
Michael Iten, dipl. Bauing.
Markus Schwager, MSc.
Dominik Hauswirth, MSc.

Forschungsauftrag VSS 2005/502 auf Antrag der des Schweizerischen Verbandes der Strassen- und Verkehrsfachleute (VSS)

1270

I. Impressum

Forschungsstelle und Projektteam

Projektleitung

Alexander Puzrin, Prof.

Mitglieder

Markus Caprez, Dr.
Andreas Schmid, dipl. Bauing.
Michael Iten, dipl. Bauing.
Markus Schwager, MSc.
Dominik Hauswirth, MSc.

Federführende Fachkommission

Fachkommission 5: Bautechnik

Begleitkommission

Präsident

Jean-Louis Amiguet

Mitglieder

Walter Steiner, Dr.
Hansjürg Gysi

Antragsteller

Schweizerischer Verband der Strassen- und Verkehrsfachleute (VSS)

Bezugsquelle

Das Dokument kann kostenlos von http://partnershop.vss.ch herunter geladen werden.

II. Inhaltsverzeichnis

III. Zusammenfassung

Dieses Pilotprojekt hatte zum Ziel, an ausgewählten Kriechhängen der Schweiz die Methoden für die Langzeitstabilität zu identifizieren, die dafür nötigen Daten zu sammeln sowie den Einfluss auf die Infrastruktur Strasse zu untersuchen. Nachfolgend sind die im Rahmen dieses Projektes erzielten Resultate aufgelistet.

- Eine neuartige Methode zur Rückrechnung der Langzeitstabilität von natürlich oder künstlich am Fuss gestützten Rutschungen wurde entwickelt und erfolgreich an den Kriechhängen von St. Moritz und Combe Chopin angewandt.
- Im Sommer 2006 wurde in St. Moritz eine gross angelegte geodätische Messkampagne durchgeführt zur Identifizierung der wirklichen Länge und des Verschiebungsfeldes des Brattas Kriechhanges, um diese Daten in der anschliessenden Rückrechnung der Stabilität zu verwenden.
- Zum ersten Mal wurden der Cambridge Insitu und der Marchetti Flat Dilatometer in solch schwierigen Bodenverhältnissen erfolgreich benutzt, um die Bodensteifigkeit in der sich bewegenden Schicht der Brattas Rutschung in St. Moritz zu bestimmen.
- Ein neuartiges Ringschergerät mit bedeutend reduzierter Reibung und fortschrittlicher Kraftmessung wurde entwickelt und zur Bestimmung der Restscherfestigkeit in der Scherfläche des Kriechhanges in Braunwald eingesetzt.
- Ein neuartiges Gerät mit dem Namen Inclinodeformometer (IDM) wurde entwickelt und im Labor kalibriert. Der Inclinodeformometer dient der Rückrechnung der Erddruckänderungen in der sich bewegenden Schicht durch Messung der Änderungen des Durchmessers und der Form eines Inklinometerrohres. Die ersten Anwendungen im Feld sind an den Kriechhängen Brattas und Berisal-Ganter vorgesehen.
- In der Rutschung von St. Moritz wurde durch die Verwendung von Dehnungsmessungen in Glasfaserkabeln (distributed fiber optic strain measurements, BOTDA) eine neuartige Technik zur Bestimmung der Grenzen der Rutschung angewendet. Zum ersten Mal wurden erfolgreich Glasfaserkabel in den Strassenasphalt integriert. Dies ermöglichte, die Strasse als eine Art riesigen Dehnmessstreifen zur Messung der Deformationen zu benutzen und gleichzeitig Informationen zur Gebrauchstauglichkeit der Strasse zu erhalten.
- Dieselbe Technik (BOTDA) wurde bei einem bereits abgescherten Inklinometerrohr in St. Moritz angewendet, um die Verschiebungen auf der Scherfläche zu messen. Hierfür wurden Glasfaserkabel in ein altes Inklinometerrohr eingelegt und das Rohr anschliessend ausinjiziert.
- Abschliessend wurden erste Empfehlungen formuliert betreffend Analyse, Überwachung und Stabilisierung von Kriechhängen, die am Fuss gestützt werden.

Es zeigte sich im Verlauf, dass der Fokus dieses Pilotprojektes auf die Entwicklung von neuartigen Geräten und Methoden zur Analyse und Überwachung sowie auf Techniken zu Labor- und Feldversuchen gerichtet werden musste, um die fehlenden Informationen zur Rückrechnung der Langzeitstabilität und Verschiebungen von Kriechhängen zu sammeln. Diese Entwicklungen wurden in zahlreichen wissenschaftlichen Publikationen präsentiert und von der internationalen geotechnischen Gemeinschaft gut aufgenommen.
Als Folgearbeit zu diesem Pilotprojekt schlagen wir ein vollständiges Projekt vor, bei dem die neuen Geräte zur Datensammlung angewendet und diese Informationen zur Berechnung der Langzeitstabilität und Verschiebungen sowie zur Untersuchung von möglichen Stabilisierungsmassnahmen in den betrachteten Kriechhänge verwendet werden.

IV. Résumé

Le but poursuivi par ce projet pilote est d'établir une méthode de calcul de la stabilité à long terme des versants en reptation. Les données nécessaires ont été récoltées sur un choix de versants en mouvement situés sur le territoire suisse. L'influence de ces phénomènes sur l'infrastructure des routes a aussi été analysée. Les résultats obtenus dans le cadre de cette étude sont listés ci-dessous:

- Une nouvelle méthode de calcul à rebours de la stabilité à long terme des versants en reptation butés en pied de versant,de façon artificielle ou naturelle, a été développée. Cette méthode a été appliquée avec succès aux versants en reptation de St Moritz et de Combe Chopin.
- En été 2006, une campagne géodésique à grande échelle a été effectuée à St Moritz. Le but de celle-ci était d'identifier la longueur réelle du terrain en mouvement du versant en reptation de Brattas. Ces données ont servi aux calculs rétroactifs de la stabilité.
- Pour la première fois, le dilatomètre "in situ" de Cambridge et le flat-dilatomètre Marchetti ont été utilisés avec succès dans ces sols au comportement complexe. Les mesures ont permis de déterminer la rigidité du terrain dans la couche en mouvement du versant en reptation de Brattas à St Moritz.
- Un nouveau dispositif de cisaillement annulaire, présentant un frottement fortement réduit et sur lequel ont été intégrés des capteurs de forces de dernière génération, a été développé. Cet appareil a été utilisé pour mesurer la résistance au cisaillement résiduelle dans les plans de cisaillement du versant en reptation du Braunwald.
- Un nouvel appareil portant le nom d'inclino-déformomètre (IDM) a été développé puis calibré en laboratoire. Cet inclino-déformomètre sert au calcul rétroactif des modifications de contraintes dans la couche de sol en mouvement. Les modifications de pression sont estimées par les mesures de variations du diamètre et de la forme du tube de l'inclinomètre. Les premières applications dans des versants instables sont prévues dans ceux du Brattas et du Bérisal près du pont du Ganter.
- L'utilisation innovatrice de capteurs de dilatation par fibres optiques (distributed fiber optic strain measurements, BOTDA) a permis de déterminer l'extension du glissement de St Moritz. Pour la première fois, des dilatomètres à fibres optiques ont été intégrés dans le revêtement routier en asphalte. Ceci a permis d'utiliser la route, d'une part pour mesurer à grande échelle les déformations et d'autre part pour récolter des informations sur l'aptitude au service de celle-ci.
- La même technique (BOTDA) a été mise en place, à St Moritz, dans un tube d'inclinomètre déjà cisaillé afin de mesurer les déplacements sur le plan de cisaillement. Pour ce faire, des fibres optiques ont été mises en place dans un ancien tube d'inclinomètre. Après la mise en place des fibres optiques, le tube a été injecté.
- Finalement, les premières recommandations ont été formulées pour l'analyse, le contrôle et la stabilisation des versants en reptation appuyés en pied de versant.

Au cours des études, une réorientation de la focalisation de ce projet pilote sur le développement de nouveaux appareils et méthodes pour analyser et surveiller ainsi que sur des techniques d'essai in situ et en laboratoire a été nécessaire. Cette réorientation a permis de récolter les informations manquantes, mais nécessaires au calcul à rebours de la stabilité à long terme des versants en reptation.
Ces développements ont été présentés dans un grand nombre de publications scientifiques. Ils ont été très bien accueillis par la communauté géotechnique internationale.
En corollaire à ce projet pilote, nous pensons que le développement devrait se poursuivre par un projet complet où, d'une part les nouveaux appareils ainsi que les informations pour le calcul de la stabilité à long terme et des déplacements seraient utilisés, et où, d'autre part, l'analyse prenne en compte les moyens mis en place pour la stabilisation des versants en reptation.

V. Abstract

This pilot project had an objective to identify the methods and to collect the necessary data for investigation of the long term stability of a number of Swiss creeping landslides and their effects on road infrastructure. The main achievements of the project are listed below.

- A novel inverse analysis approach to the long term stability of artificially or naturally constrained landslides has been developed and successfully applied to the St Moritz and Combe Chopin landslides.
- An extensive geodetical measurements program allowed for identifying the true length and velocity field for the St Moritz landslide to be used in the inverse analysis of its stability.
- For the first time, both the Cambridge and Marcchetti Dilatometers have been successfully applied in such difficult soil conditions to determine the stiffness of the sliding layer in the St Moritz landslide.
- A novel ring shear apparatus, with significantly reduced friction and advanced measurement of forces has been developed and applied to determine the residual shear strength on the sliding surface in the Braunwald landslide.
- A novel inclinodeformometer (IDM) device for backcalculating the earth pressure changes in the sliding layer (by measuring the change in size and shape of an inclinometer pipe cross-section) has been developed and calibrated. Its first applications are for the St Moritz and Ganter landslides.
- A novel technique for determining the landslide boundaries using distributed fiber optic strain measurements (BOTDA) have been applied in the St Moritz landslide. For the first time the fiber optic cable was successfully integrated into an asphalt road, which allows for the road to be used as a gigantic strain gauge for monitoring the landslide deformation, at the same time providing information on the health of the road pavement.
- The same BOTDA technique used by grouting a fiber optic sensor cable into an old inclinometer pipe in the St Moritz landslide allows for the displacements on the sliding surface to be monitored long after the pipe was sheared.
- Preliminary recommendations for analysis, monitoring and stabilization of the constrained creeping landslides have been formulated.

As is seen, the main focus of this pilot project had to be shifted towards development of the novel tools for analysis, monitoring and laboratory and field testing techniques, in order to be able to collect the missing information for the inverse analysis of the long term stability and displacements of the creeping landslides. These developments have been presented in numerous scientific publications and have been well received by the international geotechnical community.
The suggested follow up of this pilot research should be a full scale project, where the new tools are used to collect the data, perform the stability and displacement analysis, and propose the mitigation measures.

VI. Frühere Arbeiten zu Kriechhängen in der Schweiz

Schon 1945 hat sich Prof. Haefeli (1945) an der ETH Zürich mit der Erd- und Kriechdrucktheorie und deren direkten Anwendung beschäftigt. Damit legte Prof. Haefeli den Grundstein zur Berechnung und Modellierung von Kriechhangphänomenen, worauf dieser Arbeit eine ganze Reihe von verschiedenen Untersuchungen und Forschungen in diesem Gebiet folgten (z. B. Lang und Schaerer 1970, Schlüchter 1988, Wullimann 1990 und Lang 1994). Diese einzelnen Untersuchungen gingen meist mit einer direkten Anwendung der Untersuchungsresultate einher und werden bis zum jetzigen Zeitpunkt weitergeführt (Puzrin und Sterba 2006).

Parallel dazu wurde im Jahre 1980 an der ETH Lausanne das Projekte DUTI (Detection and Use of Landslide-prone Areas) gestartet und dabei technische Berichte zu verschiedenen Hangrutschungen in der Schweiz verfasst. Es sind dies die Hangrutschungen von La Chenaula (Noverraz, F. 1986a), Cergnat La Frasse (Noverraz, F. 1986b) und Arveyes (Gabus, 1986a und 1986b). Aus diesen einzelnen Untersuchungen gingen eine Vielzahl von weiteren Berichten zur Modellierung solcher Hangbewegungen hervor. Dabei stellten Vulliet und Hutter (1988a und 1988b) ein Modell zur Berechnung von sich langsam bewegenden Rutschungen vor, das auf den Grundlagen der Kontinuumsmechanik basiert. Dieses wurde anschliessend auf die bereits untersuchten Kriechhänge und Rutschungen, so wie auch später auf neue Gebiete angewendet (z. B. Vulliet und Bonnard, 1996, François et al., 2007).

Das vorliegende Forschungsprojekt baut auf den vorangegangenen Forschungen an der ETHZ und EPFL auf und möchte die bisher durchgeführten Arbeiten mit neuen Untersuchungsmethoden erweitern.

VII. Abgegebene Forschungsarbeit

1 Abgegebenes Forschungsgesuch

1.1 Einführung

Viele Strassen und Geleise in der Schweiz liegen im Einflussgebiet von aktiven oder ehemaligen Rutschungen. Dies führt teilweise zu Unsicherheiten in der Planung, Konstruktion und Unterhalt. Aus diesem Grund soll im vorliegenden Forschungsbericht ein Vorgehen zur Rückrechnung der Hangstabilität aus im Feld gemessenen Verschiebungen und der Interaktion zwischen der Rutschung und der darauf erstellten Bauten vorgestellt werden. Dies soll in Zukunft zu einer Optimierung im Bezug der zu sammelnden Daten und Kosten der Bauwerksüberwachung und der Überwachung der Rutschung selber führen.
Um den Einfluss verschiedener Randbedingungen genauer zu untersuchen, wurden vier unterschiedliche Rutschungen, die sich stetig mit einer geringen Geschwindigkeit bewegen, untersucht. Es sind dies: Braunwald (GL), Brattas in St. Moritz (GR), Ganter-Berisal (VS) und Combe Chopin (BE).

Das nun durchgeführte Forschungsprojekt sollte einerseits die noch vorhandenen Lücken zur Rückrechnung der einzelnen untersuchten Gebiete aufzeigen und andererseits bereits Versuchen diese Lücken durch neue Messkampagnen oder Messmethoden zu schliessen. Dabei stellte sich heraus, dass teilweise eine Neuentwicklung von Messgeräten und des Weiteren eine Anpassung von neuen Messverfahren angebracht war. Da das Forschungsprojekt als Pilotprojekt zu verstehen ist, wurde ein Augenmerk auf diese „Lücken“ gerichtet, bevor mit der eigentlichen Berechnung der Stabilität und der Verschiebungen mit Hilfe von analytischen und numerischen Modellen begonnen werden kann.

1.2 Zielsetzungen

Das Hauptziel bestand darin ein Vorgehen zur Analyse von lang- und kurzfristiger Stabilität von Rutschungen und deren Einflussfaktoren zu entwickeln. Um dieses Ziel zu erreichen wurde das Problem in weitere Fragestellungen untereilt und mit Zwischenzielen versehen. Im folgenden Abschnitt wird auf diese Zwischenziele kurz eingegangen und Bilanz gezogen.

1.3 Erreichte Ziele und Schwierigkeiten

Auswahl von geeigneten Gebieten um eine vereinfachte Analyse der langfristigen Stabilität durchzuführen und Anlegung einer Datenbank um die nötigen Überwachungsmassnahmen herauszufiltern:

Es wurden vier sich langsam bewegende Hänge aufgrund ihrer unterschiedlichen Randbedingungen ausgesucht:

- Brattas (Vergleiche Kapitel 2)
- Combe Chopin (Vergleiche Kapitel 5.1)
- Ganter (Vergleiche Kapitel 5.2)
- Braunwald (Vergleiche Kapitel 5.3)

Das Anlegen einer Datenbank über die bis anhin gemachten Beobachtungen hat sich leider teilweise als schwierig herausgestellt. Dies einerseits wegen fehlender oder verschollener Messdaten, andererseits

wegen nicht optimaler oder fehlender Geräte zur Messung. Auf die Neu- und Weiterentwicklungen wird in den folgenden Kapiteln eingegangen.

Entwicklung einer Analyse im Bezug auf Rückrechnungen von Beobachtungen, um das Verhalten des Hanges auf äussere Einflüsse zu quantifizieren.

Entwicklung von theoretischen und analytischen Modellen (Vergleiche Kapitel 2 und 5.1)
Entwicklung von numerischen Modellen (noch nicht durchgeführt)

Anwendung der theoretischen, analytischen und numerischen Modelle auf die gesammelten Daten.

Die Entwicklung von Modellen konnte nur im beschränkten Rahmen durchgeführt werden, da es sinnvoller erschien zuerst ein Augenmerk auf die Datenerfassung und die Geräte zur Datenerfassung zu richten. Im Fall wo bereits eine grössere Datensammlung vorhanden war, wurde ein analytisches Modell erstellt (Vergleiche Kapitel 2 Brattas und Kapitel 5.1 Combe Chopin). Die numerischen Modelle gelangten noch in keinem Gebiet zur Anwendung, da diese den analytischen Modellen gegenüber gestellt werden sollen.

Ausarbeitung von Empfehlungen zur Überwachung von Rutschhängen im Bezug zur Bau- und Betriebsphase von Strassen und Bahntrasses.

Optimierung der Anzahl von Messungen und der Anzahl unterschiedlichen Messsystemen.
Empfehlungen zu den Methoden der Beobachtungen
Empfehlungen zu den nötigen Beobachtungsmethoden während dem Bau und während dem Betrieb von Strassen und Bahntrasses, so wie deren Hilfsbauwerken.

Die restlichen Schritte sollten im Rahmen eines Folgeprojektes weitergeführt und ergänzt werden.

1.4 Weiteres Vorgehen

Die Anwendung der neu entwickelten Geräte soll zusätzliche Informationen über die beobachteten Hänge liefern. Weiter sollen die restlichen analytischen und die numerischen Modelle erstellt werden. Zur gleichen Zeit sind die Überlegungen zur Stabilisierung der Rutschungen und der Einfluss solcher Massnahmen mit Hilfe der entwickelten Modelle zu verifizieren und die Auswirkungen von Extremereignissen (Starkregen, Erdbeben, usw.) auf die untersuchten Gebiete zu quantifizieren.

1.5 Einführung zum weiteren Teil des Berichtes

Der eigentliche Bericht wurde gemäss den vier ausgewählten Hängen gegliedert. Des Weiteren wird im Bericht, im Gegensatz zur geologischen Definition, jeder sich langsam bewegende Hang als Kriechhang bezeichnet, dessen Verschiebungen sich mit Hilfe der Kriechtheorie analytisch beschreiben lässt.

Der folgende schematische Schnitt durch einen Kriechhang, wie er in unserem Fall vorkommt, dient dazu, die Bedingungen für die Ränder zu verstehen.

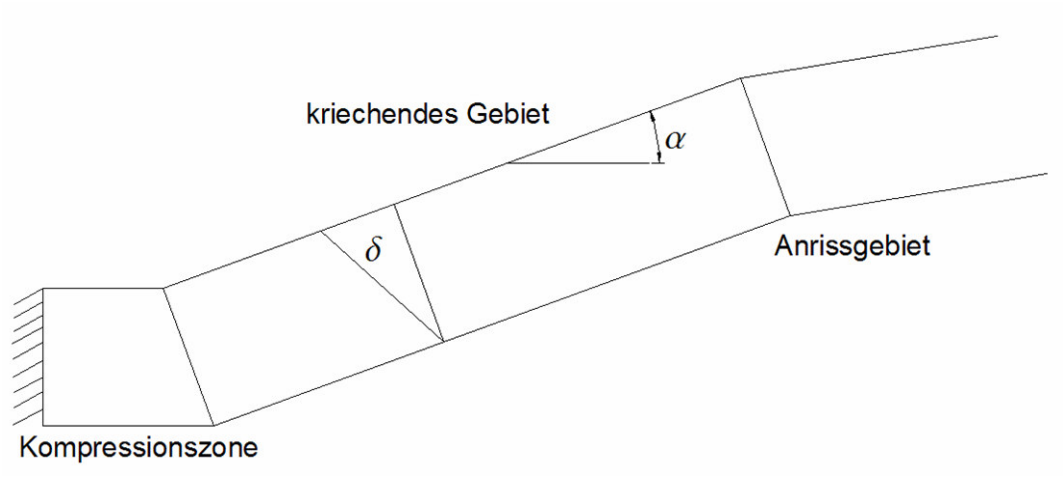

Bild 1: Schematischer Schnitt durch einen Kriechhang

Ein Kriechhang mit seinem Verschiebungsfeld δ und der Hangneigung α besteht aus drei verschiedenen Gebieten (Bild 1). Von unten beginnend mit einer Kompressionszone, die einerseits steif (Brattas Rutschung in St. Moritz), nachgiebig (Ganter im Wallis und Combe Chopin im Kanton Bern) oder gar nicht vorhanden sein kann (Braunwald Glarus). An diese Kompressionszone schliesst das eigentliche kriechende Gebiet an, das in seinem oberen Rand durch das Anrissgebiet begrenzt wird. Im Bericht wird ersichtlich, dass der „Kompressionszone“ eine tragende Rolle zugeteilt wird, da diese das Verhalten des gesamten Kriechhanges im „Kriechzustand“ oder sogar im „Versagenszustand“ massgebend beeinflusst.

2 Brattas Kriechhang

Erdrutsche, so wie Kriechhänge gehören zu den geotechnischen Hauptgefährdungen und beeinflussen das Leben und die Wirtschaft. Etwa 6 Prozent der Fläche der Schweiz befindet sich in Gebieten mit potentiellen Rutschhängen. Meist findet man die Rutsch- und Kriechhänge in ländlichen Gebieten. Hier verursachen sie grosse Schäden an der bestehenden Infrastruktur wie Strassen, Gleisen, etc.. Jedoch von noch grösserer Bedeutung für die Bevölkerung sind aktive Rutschungen oder Kriechhänge in überbauten Gebieten. In diesem Zusammenhang nimmt die aktive Rutschung von St. Moritz (Bild 2a) mit ihrer berühmten Sehenswürdigkeit, dem „Schiefen Turm“ (Bild 2b) aus folgenden Gründen eine Sonderstellung ein. Die aktive Rutschung kommt erst im überbauten Gebiet von St. Moritz Dorf zum Stillstand. Trotzdem ist die Bautätigkeit im sich bewegenden Gebiet enorm. Um die Bautätigkeit in diesem Gebiet zu regeln, wurden von der Gemeinde St. Moritz spezielle Bauvorschriften erlassen. Zusätzlich wird der Hang mit einem umfangreichen Messprogramm überwacht.

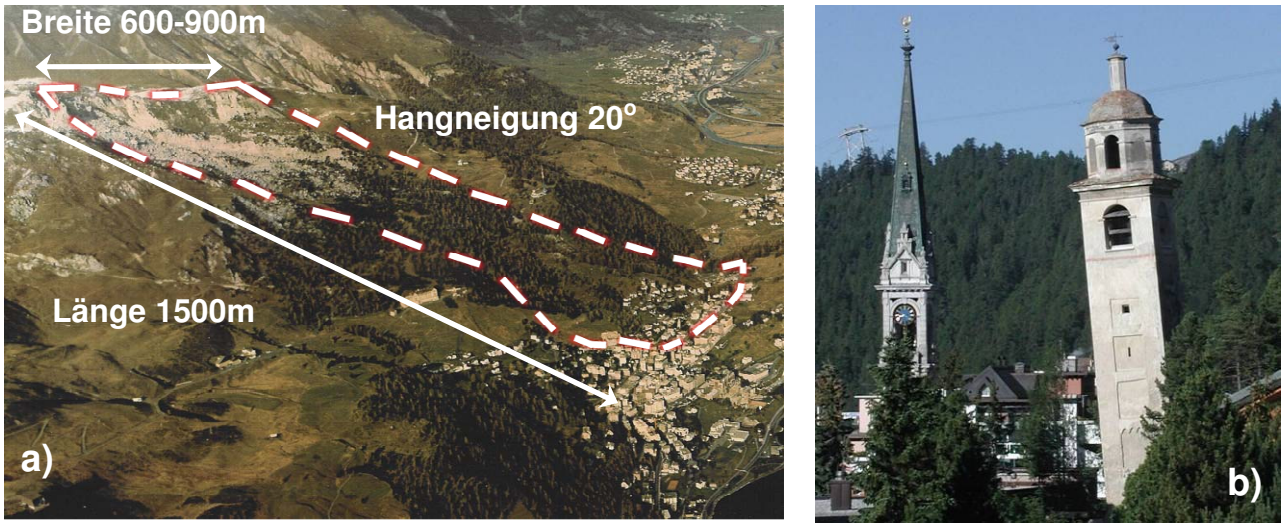

Bild 2: a) Rutschung von St. Moritz (weiss gestrichelte Umrandung), b) Schiefer Turm von St. Moritz (Turm im Vordergrund).

Das Institut für Geotechnik (IGT) der ETH Zürich ist seit über 30 Jahren bei allen geotechnischen Aspekten der Hangrutschung miteinbezogen worden und berät die Gemeinde. Um das Gefahrenpotential des Hanges abzuschätzen, wurde in den letzten drei Jahren ein neues Forschungsprogramm mit folgenden Zielen gestartet:

- ein besseres Verständnis der Mechanismen von aktiven Rutschungen zu erlangen,
- Rutschungen in ihrer Ausdehnung klarer zu definieren,
- Vorhersagen über die langfristige Stabilität und Verschiebungen zu ermöglichen,
- neue Methoden zur Untersuchung und Überwachung zu testen.

2.1 Rückrechnung der Stabilität

2.1.1 Geologie und Verschiebungen

Der unstabile nördliche Hang oberhalb des Dorfes von St. Moritz (Bild 2a) kann in zwei Zonen gegliedert werden (Bild 3a, nach Müller und Messina, 1992). Die obere Zone besteht aus dem Bergsturz von Gianda Laret, welcher von seinem Anrissgebiet auf 2400 m ü. M. bis zu einem lokal anstehenden Fels in 2100 m ü. M. reicht. Die untere Zone wird als Brattas Rutschung bezeichnet. Diese besteht aus mächtigen Lockergesteinsschichten, innerhalb derer Bewegungen stattfinden. An ihrem Fuss wird sie von einem Felsriegel unterhalb der Via Maistra gestoppt (Bild 3b, nach Schlüchter, 1988). Diese untere Zone erstreckt sich von 2100 m ü. M. bis 1800 m ü. M. und weist eine Horizontaldistanz von 800 m auf. Die Rutschung wird von beiden Seiten durch parallele Scherzonen begrenzt und ist 600-900 m breit. Die mittlere Neigung des Hanges beträgt 20°. Bei Bohrungen in diesem Gebiet konnte die Basisgleitfläche in einer Tiefe von rund 20-50 m lokalisiert werden. Das Rutschmaterial besteht aus unterschiedlichen Lockergesteinsschichten, die extrem heterogen sowohl in ihrem Aufbau, als auch in ihren bodenmechanischen Eigenschaften sind.

Die verschiedenen tektonischen Schichten werden als Hauptursache der Rutschung betrachtet. Die mesozoischen Sedimente der Bernina Decke werden über das kristalline Gestein der Err-Decke geschoben. Des Weiteren tragen auch die hydrologischen Verhältnisse zur Instabilität des Hanges bei. Unterschiedlich tief liegende Wasserträger mit unabhängigen Wasserständen wurden beobachtet. Der Scherwiderstand des Bodens wird durch die Porenwasserdrücke, die während des Jahres schwanken, beeinflusst.

Im Bereich, wo sich die Rutschung der Via Maistra nähert, wird die Strasse jedes Jahr ca. 0.5 cm schmäler. Von der Via Maistra nimmt die jährliche Verschiebungsrate hangaufwärts zu (Bild 3b). Die Verschiebungen wurden jedoch nur im überbauten Gebiet gemessen. Aus den bis jetzt vorhandenen Messungen lässt sich nicht schliessen, ob sich die Brattas Rutschung und der Gianda Laret Bergsturz gegenseitig beeinflussen.

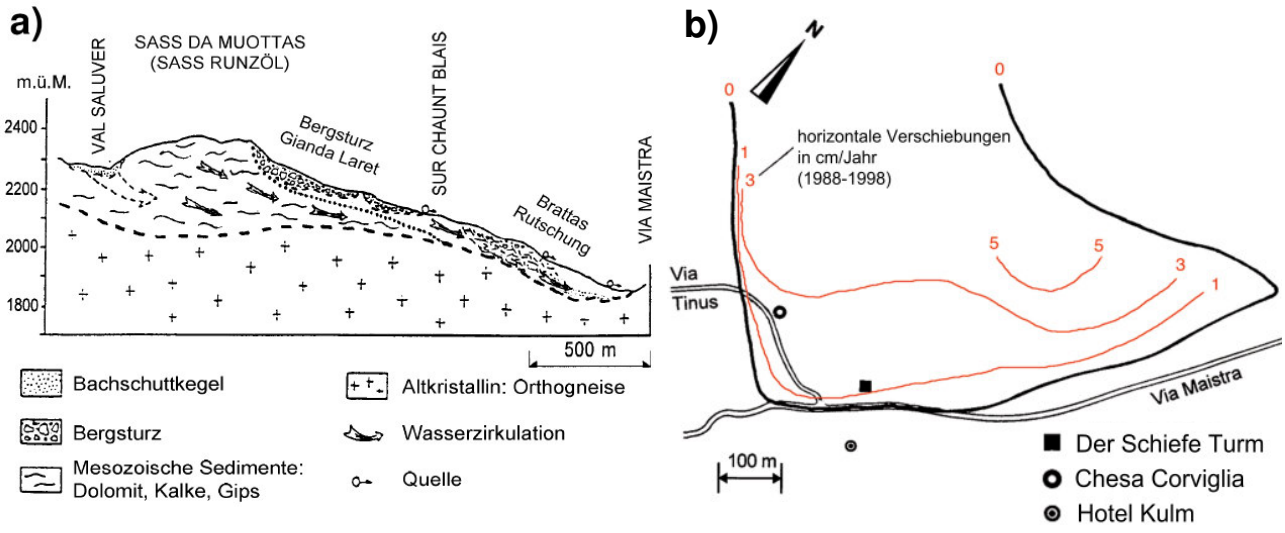

Bild 3: a) geologisches Profil nach Müller und Messina, 1992, b) jährliche Verschiebungen im unteren überbauten Gebiet der Rutschung nach Schlüchter, 1988

2.1.2 Näherungsmethode zur Analyse der Langzeitstabilität

Für die Betrachtung der Verschiebungen und der Langzeitstabilität wurde ein einfaches Modell für einen am Hangfuss begrenzten Rutschhang verwendet (Bild 4a, nach Puzrin und Sterba 2006). Das ungewöhnliche

an dieser Rutschung ist die Tatsache, dass diese am Fuss durch einen Felsriegel gestoppt wird und dadurch die Verschiebungsgeschwindigkeiten mit der Zeit abnehmen. Dies könnte zum voreiligen Schluss verführen, dass der Hang sich nach unbekannter Zeit stabilisieren wird. Tatsächlich jedoch verringert sich der Scherwiderstand an der Gleitfläche durch die Verlangsamung der Rutschung, was zu einer Zunahme des Erddrucks am Hangfuss und schlussendlich zum Versagen führen könnte.

In diesem einfachen Modell wird der Kriechhang als ein „Dehnmessstreifen" betrachtet. Der Sicherheitsfaktor wird als Verhältnis des passiven Erddrucks und des maximal auftretenden Erddrucks am Hangfuss berechnet. In den Formeln im Bild 4b (nach Puzrin und Sterba, 2006) stehen p'_a und p'_p für den aktiven und passiven Erddruck, die sich mit den zugehörigen Bodenparametern nach Chu (1991) berechnen lassen; der Faktor *b/a* kann durch eine Anpassung einer analytischen Kurve an die geodätisch gemessenen Verschiebungen entlang der Rutschung berechnet werden (nach Puzrin und Sterba, 2006). Falls die Sicherheit gegen Versagen am Hangfuss grösser als eins ist, lassen sich die Endverschiebungen bestimmen. Der hierfür nötige Parameter *c* lässt sich durch die Anpassungen einer Kurve als Funktion der Zeit an die gemessenen Verschiebungen bestimmen. Liegt hingegen der Sicherheitsfaktor unter eins, so lässt sich der Versagenszeitpunkt abschätzen. Dafür wären jedoch zusätzlich Erddruckmessungen am Hangfuss nötig.

Damit dieses Modell für die Brattas Rutschung verwendet werden kann, sind weitere Messungen im oberen und mittleren Bereich des Brattas Hanges nötig. Insbesondere soll damit auch abgeklärt werden, in wie weit der Gianda Laret Bergsturz die Brattas Rutschung beeinflusst. Diese zusätzlichen Daten können auch helfen, die Lage der oberen Begrenzung der Rutschung, so wie die dort vorherrschenden Bedingungen zu definieren. Zu diesem Zweck wurde in den Jahren 2006 bis 2008 ein umfangreiches Untersuchungsprogramm erarbeitet und teilweise schon ausgeführt.

a)

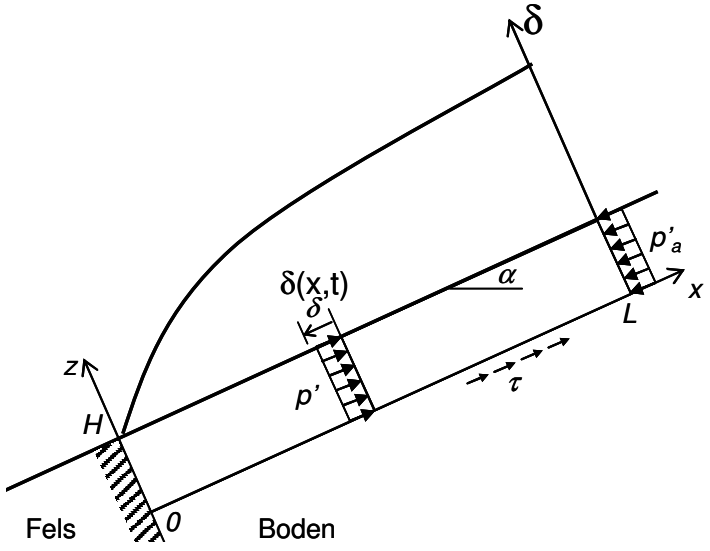

b) Sicherheitsfaktor

$$F_s = \frac{p'_p}{p'(0,\infty)} = \frac{1-2b/a}{p'_a / p'_p}$$

Endverschiebung (falls F_S>1)

$$\delta_\infty(x) = \frac{\delta_M(x)}{1-\exp(-c(t_M - t_1))}$$

Versagenszeitpunkt (falls F_S<1)

$$t_f = t_0 + \frac{1}{c}\ln\frac{\Delta p'/p'_p}{(1-e^{-c\Delta t})(1/F_s - 1)}$$

Bild 4: a) Model des Hanges, b) aus dem Model gewonnene Gleichungen nach Puzrin und Sterba (2006)

2.2 Geodätische Feldmessungen

Während des Untersuchungsprogrammes im Sommer 2006 wurde ein neues Raster von Messpunkten im Gianda Laret Bergsturz und der Brattas Rutschung angelegt. Im Übergangsbereich der beiden Gebiete wurde das Netz verdichtet (Bild 5a). Die Folgemessungen haben in den Jahren 2007 und 2008 stattgefunden, womit eine Bestimmung der verschiedenen Verschiebungsgeschwindigkeiten über den gesamten Hang möglich war (Bild 5b). Die Geschwindigkeiten nehmen mit zunehmender Distanz vom Hangfuss kontinuierlich zu, aber nur in den unteren 700 m, d.h. bis zur wahrscheinlichen Grenze zwischen dem Bergsturz von Gianda Laret und der Brattas Rutschung im Bereich Sur Chaunt Blais (Siehe Bild 3a). Dies legt die Vermutung nahe, dass die beiden Gebiete Bergsturz Gianda Laret und Brattas Rutschung nicht miteinander verbunden sind. Die neu durchgeführte Berechnung der Sicherheit gegen Versagen am Hangfuss bei der Berücksichtigung einer Länge der Rutschung von nur noch 700 m liegt zwischen 1.5 und 2.6, womit das Versagen ausgeschlossen wäre. Weitere Messungen sollen dies noch bestätigen.

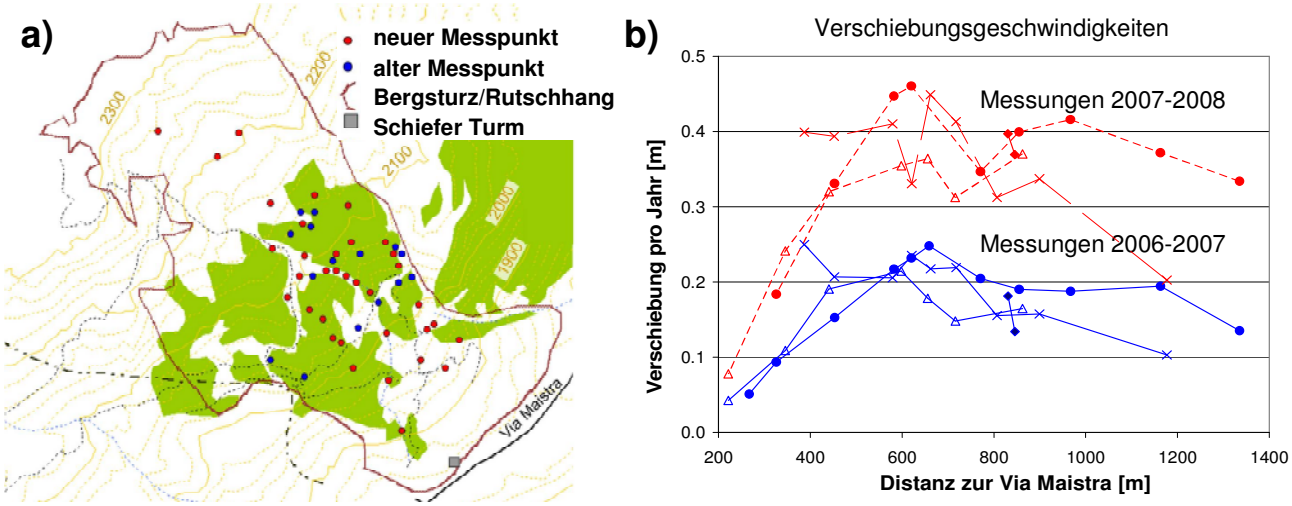

Bild 5: a) Lage der Messpunkte, b) Geschwindigkeitsverlauf entlang des Hanges

2.3 Labor- und Feldversuche

Eine genauere Stabilitätsberechnung erfolgt durch die FEM (Finite-Elemente-Methode), die eine vertiefte Kenntnis der Bodenparameter voraussetzt. Die nötigen Parameter sind die Scherfestigkeit auf der Gleitfläche, die Steifigkeit der kriechenden Schicht und ihre Abhängigkeit vom Druck und der Verschiebungsgeschwindigkeit. Diese sind durch Labor- und Feldversuche zu bestimmen.

2.3.1 Bestimmung der Scherfestigkeit

Zur Ermittlung der Höchst- bzw. Restscherfestigkeit und deren Abhängigkeit der Verschiebungsgeschwindigkeit sollen Ringscherversuche bei verschiedenen Geschwindigkeiten und Spannungen durchgeführt werden. Um die bestehenden Ringschergeräte im Bezug auf den Einbau und die Handhabung zu vereinfachen und eine bessere Reproduzierbarkeit zu erreichen, wurde ein neues Ringschergerät entwickelt (Bild 6a und 6b). Ein weiterer Schritt war die Minimierung des Verlustes durch Reibung in vertikaler Richtung während der Konsolidation und der Reibung zwischen den Ringen während dem Abscheren. Um die restliche noch vorhandene Reibung zu quantifizieren, wird einerseits der Druck

ober- und unterhalb der Probe gemessen und andererseits die Reibung zwischen den Ringen vor und nach jedem Versuch bestimmt.

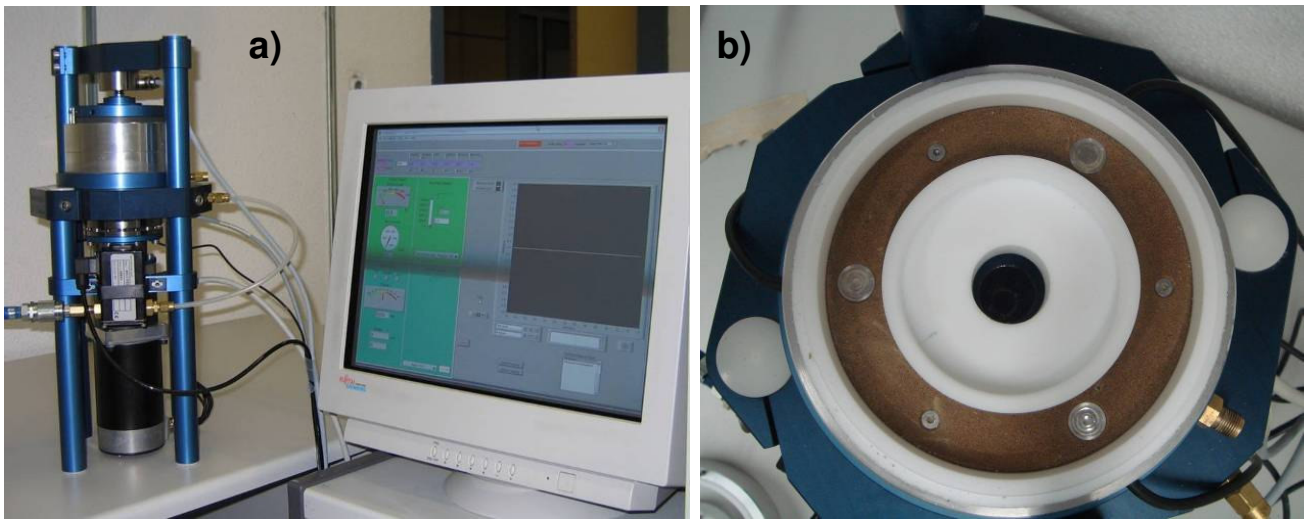

Bild 6: a) Computer gesteuertes Ringschergerät, b) unterer Probenring mit eingebauten Druckmessdosen und Teflonzylindern (Rüttimann, 2008)

Eine ausführliche Beschreibung des Ringschergerätes IGT und seiner Bestandteile ist in Rüttimann (2008) zu finden. In diesem Abschnitt werden das Ringschergerät IGT und die letzten Modifikationen kurz vorgestellt.

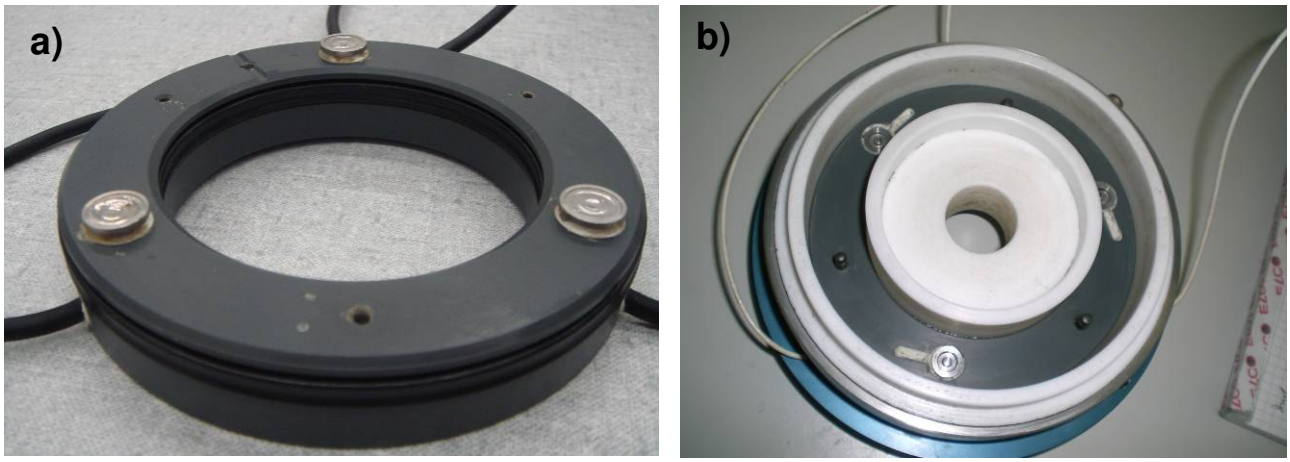

Bild 7: a) PVC Ring mit eingebauten Druckmessdosen (Rüttimann, 2008), b) untere Ringhälfte mit den drei Kraftmessdosen im Boden (Villiger, 2008)

In der Version des von Rüttimann benutzten Ringschergerätes sind in die Filterplatte und das darunter liegende PVC-Zylinderelement am Zellenboden drei Druckaufnehmer integriert (Bild 6b und Bild 7a). Diese Druckaufnehmer besitzen einen Sensor, welcher in ein Ölkissen gebettet ist. Das Öl ist durch eine Aluminiummembran gegen aussen hin abgegrenzt und somit vor dem Auslaufen geschützt. Wird nun Druck auf die Membran ausgeübt, so wird dieser über das Ölkissen auf den Sensor geleitet, welcher den Messwert angibt.

Die eingebauten Druckaufnehmer sind im Vergleich mit den alten Ringschergeräten, welche nicht mit diesen Messinstrumenten ausgestattet sind, eine grosse Neuerung. Mit dieser Massnahme möchte man während dem Versuch genau bestimmen, wie gross der Verlust durch Reibung an den Ringinnenwänden ist. Dazu werden die Messwerte am Probenboden mit der aufgebrachten Normalspannung am Probenkopf verglichen und die tatsächlich wirkende Normalspannung im Material bei der Scherfuge anhand eines Reibungsgesetzes berechnet. Dabei hat sich bei mehreren Versuchen gezeigt, dass der Spannungsverlust, der sich bei den Druckaufnehmer wegen der Bogenwirkung ergibt, grösser und unsteter war als angenommen. Aus diesem Grund wurde das Ringschergerät für die Versuche von Villiger modifiziert.

Anstelle der bei Rüttimann (2008) verwendeten Druckaufnehmer im Boden der Probenzelle sind drei Kraftmessdosen angebracht (Bild 7b). Die Spannungen im Boden werden nun vom Boden auf die Filterplatte und eine darunter liegende Lastverteilungsplatte, die auf den Kraftmessdosen gelagert ist, übertragen. Damit wird das Problem einer Bogentragwirkung in der Bodenprobe rund um die Druckaufnehmer gelöst, woraus verlässlichere Normalspannungen resultieren.
Durch diese Modifikationen wird die Aussagekraft der aufgezeichneten Kräfte und der über die Probenfläche gemittelten effektiven Spannungen grösser. Der Normalspannungsverlust aufgrund der seitlichen Reibung an den Teflonringen über die Probenhöhe kann besser quantifiziert werden und die Korrektur der Scherspannung um den Anteil der Reibung zwischen den Teflonringen wird präziser.

Im Folgenden werden die Resultate von Rüttimann (2008) als Serie 1 und die neuen Resultate von Villiger (2008) als Serie 2 bezeichnet.

Im Bild 8 sind die Mittelwerte der Messresultate von Serie 1 und Serie 2 graphisch dargestellt. Zu jeder Serie ist eine lineare Trendlinie durch den Nullpunkt vorhanden.
Die Resultate beider Serien liegen in derselben Grössenordnung. Dies bedeutet, dass die mit dem Ringschergerät ermittelten Resultate am „Kloten“ Ton gut reproduzierbar sind. Die beiden Serien sind unabhängig voneinander zu betrachten, da die Versuche von unterschiedlichen Personen durchgeführt wurden.

Weiter ist ersichtlich, dass die Streuung der Messwerte der Serie 1 mit dem Bestimmtheitsmass R^2=0.8220 grösser ist als jene aus Serie 2 mit R^2=0.9974. Diese Veränderung kann auf die genauere Bestimmung der effektiven Spannungen mittels Kraftmessdosen anstelle von Druckaufnehmern zurückgeführt werden. Dadurch kann einerseits der Einfluss der Reibung zwischen den Teflonringen und andererseits die effektiv vorhandene Spannung in der Scherfuge genauer bestimmt werden. Zusätzlich wurden dem Bild 8 die Resultate der Triaxialversuche von Küng (2003) an demselben Material als unabhängige Messungen hinzugefügt. Dabei ist zu bemerken, dass bei den Triaxialversuchen nicht die Restscherfestigkeit (Scherwinkel=φ'_r) erreicht werden kann, sondern nur die Scherfestigkeit bei kritischem Volumen (Scherwinkel=φ'_{cv}), die bei Tonen höher liegt als die Restscherfestsigkeit.

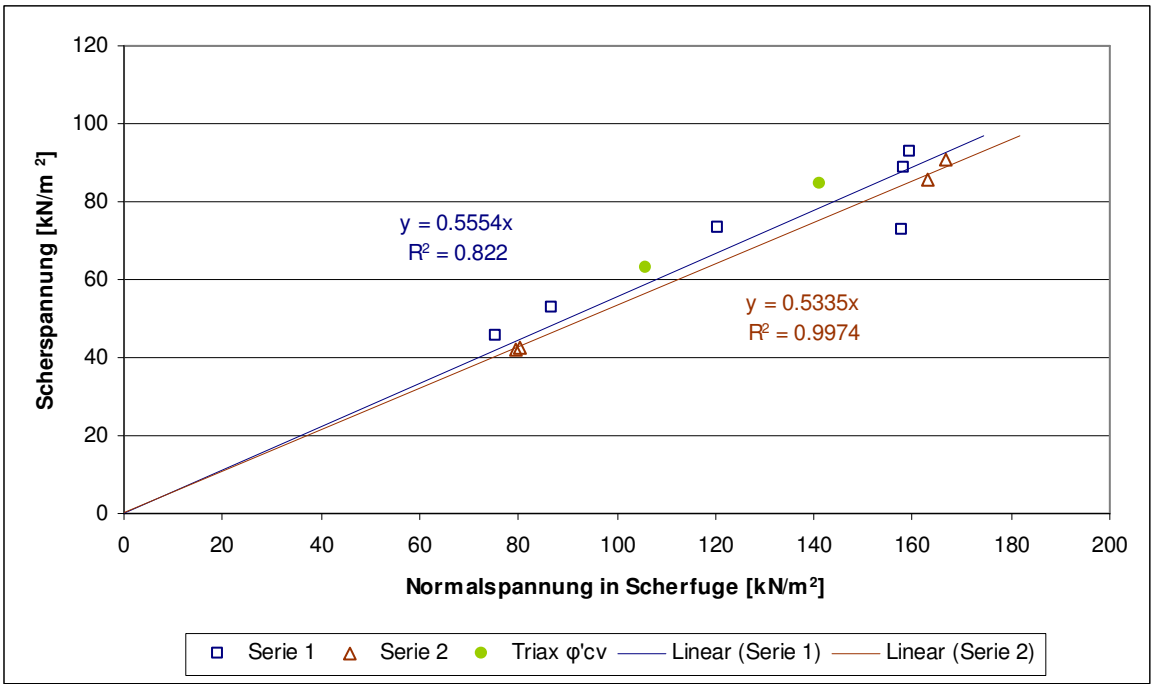

Bild 8: Vergleich der Resultate der Ringscherversuche von Rüttimann (2008) Serie 1 und Villiger (2008) Serie 2 an Kloten Ton mit den Triaxial Versuchen (Triax nur φ'_{cv} möglich) von Küng (2003) am selben Material.

Die Punkte der Serie 1 liegen bis auf einen Messwert stets oberhalb der Trendlinie der Serie 2. Dies kann durch erklärt werden, dass die am Boden vorhandenen Normalspannung durch die Messung mit den drei Kraftmessdosen unterschätzt wurde. Durch eine Bogenbildung im Material aufgrund der weichen Membran und dem steifen Ring der Kraftmessdose ist dies eine plausible Erklärung.

Nach der Validierung der letzten Modifikationen wurden erste Versuche an den Proben aus Braunwald bei unterschiedlichen Normalspannungen und Schergeschwindigkeiten durchgeführt (Beispiel: Bild 9). Diese Arbeiten sind nicht abgeschlossen und werden noch weitergeführt (Vergleiche Kapitel 5.3 Braunwald).
Anschliessend stehen Ringscherversuche der Bodenproben aus St. Moritz bei unterschiedlichen Normalspannungen und Schergeschwindigkeite auf dem Programm.

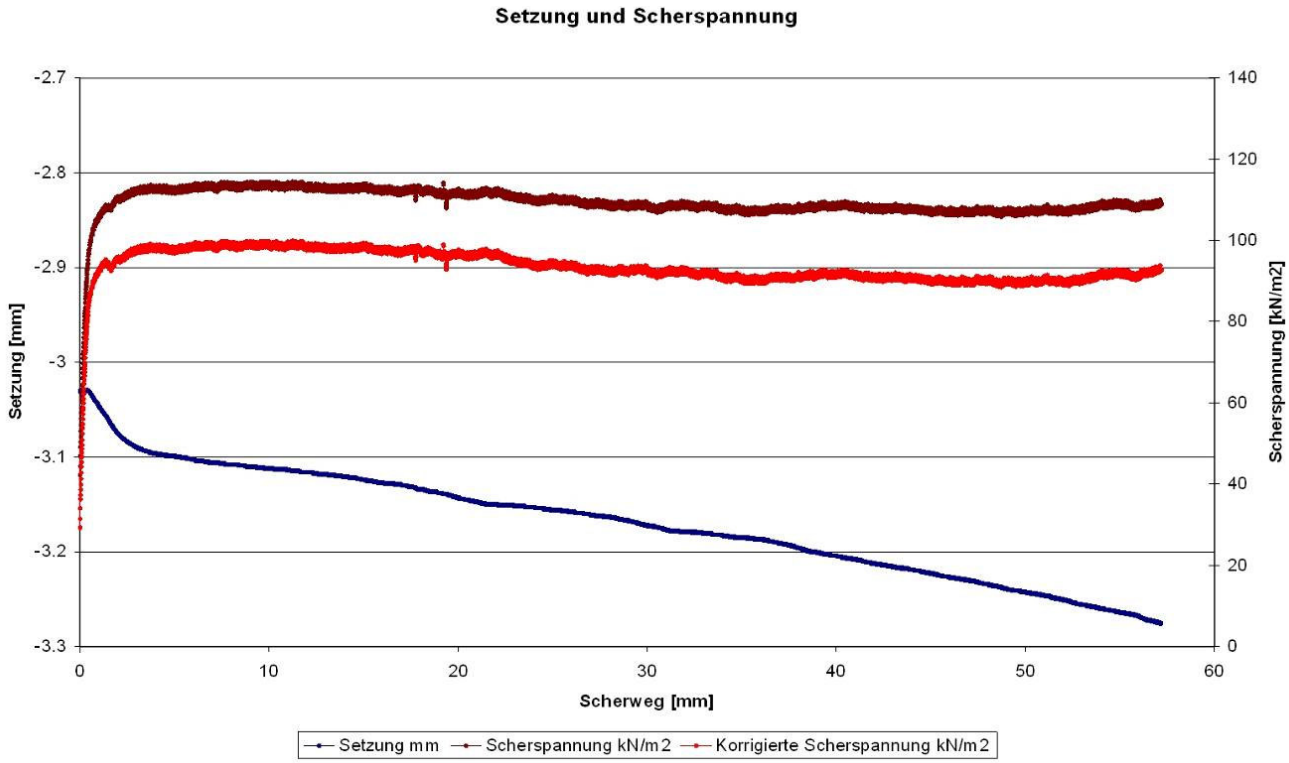

Bild 9: Versuche an der nicht ausgesiebten Bodenprobe 2 aus Braunwald bei einer Normalkraft von ca. 200 kN/m^2 und einer Schergeschwindigkeit von 0.01 mm/min (Villiger, 2008)

2.3.2 Bestimmung der Steifigkeit

Zur Ermittlung der Steifigkeit wurden Oedometerversuche gemacht. Für die Durchführung der Oedometerversuche musste die Kornfraktion grösser als 4 mm ausgesiebt werden (ca. 30 % des Probenmaterials), dadurch zeigen die Oedometerversuche ein eher zu weiches Verhalten des Bodens. Aus diesem Grund wurden zusätzlich zwei Arten von Dilatometer Tests zur Bestimmung der Bodensteifigkeit in unterschiedlichen Tiefen in einem Bohrloch in der Nähe des Schiefen Turms durchgeführt.

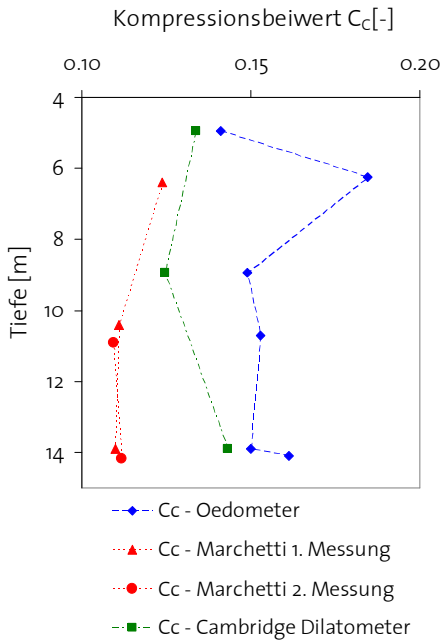

Bild 10: Vergleich der Dilatometerversuche.

Das erste Gerät war der Cambridge Insitu Dilatometer: Ein zylinderförmiges Prüfgerät bestehend aus einer zylinderförmigen, aufblasbaren Gummimembran mit Wegaufnehmern, das in das vorgebohrte Bohrloch eingeführt wird. Das zweite Messgerät war der Marchetti Flat Dilatometer: Dieses Gerät besteht aus einer spatenförmigen Prüfspitze mit einer runden, flachen und aufblasbaren Stahlmembran. Diese Prüfspitze wurde am Bohrlochende bis zu einem Meter tief in den Boden gepresst. Es war das erste Mal, dass diese beiden Methoden in solch schwierigen Bodenverhältnissen (Ton, Silt, Kies und Steine vermischt) erfolgreich eingesetzt werden konnten. Der Vergleich (Bild 10) der Dilatometermessungen untereinander und mit den Oedometerversuchen hat gezeigt, dass die Messungen mit dem Cambridge Insitu Dilatometer wegen dem vorgängigen Bohren generell ein zu weiches Verhalten widerspiegeln. Die Messungen mit dem Marchetti Flat Dilatometer hingegen zeigen ein etwas zu steifes Verhalten des Bodens, da das Einpressen des Spatens zu einer zusätzlichen Verdichtung des Bodens führt. Dagegen zeigen die Oedometer Versuche ein eher zu weiches Verhalten des Bodens. Somit liegt die tatsächliche Steifigkeit zwischen den Marchetti und Cambridge Dilatometer Versuchen. Die Untersuchungen und der Vergleich der Resultate wurden von Puzrin et al. (2008) in einem Bericht festgehalten und werden in den folgenden Kapiteln genauer ausgeführt.

Um die vorherrschenden Verhältnisse des Randewertproblems der Brattas Rutschung zu verdeutlichen, kann das Schema einer dünnen, am Fuss gehaltenen Rutschung, wie im Bild 11a dargestellt, herbeigezogen werden (nach Puzrin und Sterba 2006). Das Kräftegleichgewicht der sich bewegenden Schicht wird gebildet durch den Scherwiderstand τ^* auf der Scherfläche, die Normalspannung p und den effektiven aktiven Erddruck p_a', so wie die Porenwasserspannungen u_a im Anrissgebiet, die auf das obere Ende der Schicht wirken.

$$p(x,t)H + \int_x^L \tau^*(x,t)dx = \gamma_t H(L-x)\sin\alpha + (p_a' + u_a)H \tag{2.1}$$

Wobei γ_t das totale Raumgewicht, α die mittlere Hangneigung, L und H die Länge bzw. die Höhe der sich bewegenden Masse angibt.

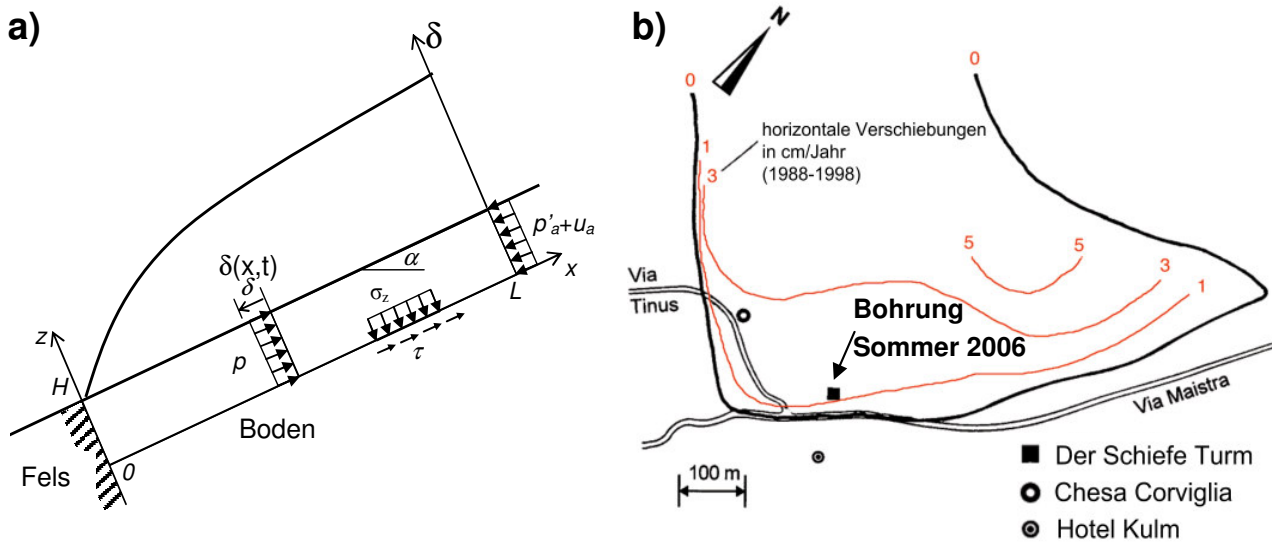

Bild 11: a) Schematische Darstellung der am Fuss gehaltenen Rutschung, b) Standort der neuen Bohrung im Sommer 2006 (Hintergrundbild nach Schlüchter, 1988).

Wie im Bild 11a ersichtlich spielt die Verteilung der Scherspannung entlang der Scherfläche in einer dünnen, rutschenden Schicht eine wichtige Rolle, um die vorherrschenden Spannungen und damit auch die Verschiebungen, so wie die Stabilität des Hanges zu ermitteln. Zusätzlich werden die Scherspannungen stark durch die Porenwasserdrücke $u(x,t)$, die saisonal und örtlich schwanken können, beeinflusst.

$$\tau^*(x,t) = (\sigma_z - u(x,t))\tan\varphi' \qquad \sigma_z = \gamma_t H\cos\alpha \tag{2.2}$$

Leider lassen sich die Porenwasserspannungen in der Scherzone nicht direkt messen. Der einzige Weg um sie dennoch zu ermitteln ist eine Rückrechnung, in der der gesamte Rutschhang als eine Art Dehnmessstreifen betrachtet wird. Dieses Vorgehen wird in den folgenden Abschnitten beschrieben.

Falls die räumliche Verteilung der mittleren Spannungen $p(x,t)$ in der Rutschmasse bekannt ist, können die Porenwasserdrücke $u(x,t)$ mit den Gleichungen 2.1 und 2.2 rückgerechnet werden:

$$u(x,t) = \gamma_t H\left(\cos\alpha - \frac{\sin\alpha}{\tan\varphi'}\right) - \frac{\partial p(x,t)}{\partial x}\frac{H}{\tan\varphi'} \tag{2.3}$$

Jedoch stellt uns auch diese Methode der Bestimmung der Porenwasserdrücke vor einzelne Schwierigkeiten. So ist es bis zum heutigen Zeitpunkt kaum möglich verlässliche Erddruckmessungen in heterogenen Böden durchzuführen. Hingegen sind die Messungen der Verschiebungen entlang der Rutschung $\delta(x,t)$ (Bild 11a) mit Hilfe von geodätischen Messungen und Inklinometermessungen relativ einfach. Nehmen wir nun zum Beispiel ein einfaches linear elasto-plastisches, geschwindigkeits-unabhängiges Model für das Verhalten der sich bewegenden Schicht an, so können die Spannungen wie folgt berechnet werden:

$$p(x,t) = E\varepsilon(x,t) \qquad \varepsilon(x,t) = \partial\delta(x,t)/\partial x \tag{2.4}$$

wobei ε für die über die Tiefe gemittelte, linearen Dehnung steht; *E* ist das elasto-plastische Modul des Bodens. Die Substituierung der Gleichung 2.4 in die Gleichung 2.3 erlaubt die Berechnung der Änderung der Porenwasserspannungen entlang der Scherfläche zu jeder Zeit Δt zwischen den Verschiebungsmessungen:

$$\Delta u(x) = u(x,t_0+\Delta t) - u(x,t_0) = -E\left(\frac{\partial^2\delta(x,t_0+\Delta t)}{\partial x^2} - \frac{\partial^2\delta(x,t_0)}{\partial x^2}\right)\frac{H}{\tan\varphi'} \tag{2.5}$$

Dieser Ausdruck gilt jedoch nur, falls die Änderung des Porenwasserdrucks positiv ist, was zu einer Abnahme der Scherspannungen und somit zu einer Zunahme der Verschiebungen führt. (Hingegen kann eine Zunahme der Scherspannungen nicht dazu führen, dass sich der Hang auf einmal nach oben bewegt, wenn die Änderung der Porenwasserspannung negativ ist!)
Diese Zunahme der Porenwasserspannungen kann mit den saisonalen und jährlichen Schwankungen der Niederschlagsmenge in Verbindung gebracht werden. Die Lokalisierung der unterschiedlichen Porenwasserspannungen führt zu einem effizienteren Design von Drainagesystemen, letztere können mit Hilfe dieser Methode anschliessend auf ihre effektive Wirkung hin überprüft werden.
Bei diesem neuen Rückrechnungsverfahren wird der Rutschhang als eine Art riesiger Dehnmessstreifen betrachtet, der zur Messung des Scherwiderstandes und der Porenwasserspannnungen entlang der

Scherfläche benutzt wird. Wie bei jedem gewöhnlichen Dehnmessstreifen ist die Steifigkeit *E* von grösster Bedeutung. Jedoch stellt die Messung der Bodensteifigkeit parallel zur Hangneigung in solchen heterogenen Böden (kiesige Tone und Silte der Rutschmasse in St. Moritz) eine Herausforderung dar. Verlässliche Daten über die Steifigkeit des Bodens können nur mit Hilfe von Feldversuche erlangt werden, allerdings wird die Anwendung beider Dilatometerversuche (Cambridge Insitu und Marchetti Flat Dilatometer) für solche Böden ausdrücklich nicht empfohlen.
Die Rutschmasse in St. Moritz kann aufgrund ihrer Kornverteilung mit einer Moräne verglichen werden. Nur wenige Untersuchungen der Bodensteifigkeit in Moränen konnten mit Hilfe von Dilatometerversuchen erfolgreich durchgeführt werden (z.B. Akbar and Clarke, 2001; Powell and Butcher, 2003; Long and Menkiti; 2007). Dies liegt an zwei Tatsachen: Einerseits ist die Festigkeit des Bodens nicht genügend gross, dass ein offenes Bohrloch stehen bleibt; andererseits verunmöglichen grössere Steine ein Einpressen oder die Benutzung von selbstbohrenden Dilatometern. Laborversuche zur Bestimmung der Steifigkeit stellen keine Alternative zu den Feldversuchen dar, da die Laborversuche an gestörten und neu angemischten Proben, Partikel grösser als 4 mm werden entfernt, durchgeführt werden (z.B. Gens and Hight, 1979; Clarke et al., 1998).
In den folgenden Abschnitten wird auf die Messung der Bodensteifigkeit der Rutschmasse in St. Moritz eingegangen, wobei beide Arten von Dilatometern eingesetzt wurden. Im Sommer 2006 konnten beide Messungen in der Nähe des Schiefen Turmes erfolgreich durchgeführt werden. Dabei wurden verschiedene Messungen in unterschiedlichen Tiefen durchgeführt und anschliessend die beiden Methoden zur Messung der insitu Steifigkeit des Bodens mit einander verglichen. Zusätzlich wurden Oedometerversuche an Bodenproben aus derselben Bohrung den Resultaten der Dilatometerversuche gegenübergestellt.

2.3.2.1 Die Bohrung in St. Moritz

Im Sommer 2006 wurde ein 25 m tiefes Bohrloch mit einem Innendurchmesser von 101 mm in der Nähe des Schiefen Turms von St. Moritz abgeteuft (Bild 11b, 12a und 12b). Der eigentliche Zweck der Bohrung bestand im Einbau eines neuen Inklinometerrohres zur Überwachung des Schiefen Turmes. Der Fels wurde in einer Tiefe von 19 m angetroffen, überdeckt von einer durchmischten Masse aus Ton und Silt mit Kies und Steinen. Die Scherfläche konnte anhand von früheren Inklinometermessungen in einer Tiefe von 17 m lokalisiert werden. Die Dilatometerversuche wurden in vier verschiedenen Tiefen durchgeführt. In jeder Tiefe konnte mindesten mit einem Dilatometer erfolgreich Versuche durchgeführt werden. Gestörte Bodenproben wurden anschliessend aus denselben Tiefen entnommen wie die Dilatometermessungen gemacht wurden. Im Labor wurde an den gesammelten Bodenproben Oedometerversuche durchgeführt.

Bild 12: a) Ansicht der Bohrstelle und des Bohrgerätes, b) der Schiefe Turm von St. Moritz.

2.3.2.2 Versuche mit dem Cambridge Insitu Dilatometer

Für lockere, weiche Böden sind Cambridge Insitu Dilatometer Versuche grundsätzlich nicht geeignet, da das Bohrloch auch ohne Verrohrung offen bleiben muss. Trotzdem konnten Dilatometerversuche in der Tiefe von 5 m, 9 m und 14 m mit dem Cambridge Insitu Dilatometer durchgeführt werden. Dazu wurde zuerst ein 101 mm Bohrloch ohne Verrohrung vorgebohrt und anschliessend das zylinderförmige Messgerät mit einem Durchmesser von 94 mm (Bild 13a) hinabgelassen. Die Versuche wurden nach einem Standardverfahren von der Firma Stump ForaTec AG (Sambeth, 2006) durchgeführt. Resultate aus den Versuchen sind in Bild 13b für die Erst- (E_{comp}), so wie die Wiederbelastung (E_{ur}) dargestellt.
Grundsätzlich kann festgehalten werden, dass die insitu Bodensteifigkeit, die aus solchen Versuchen erhalten wird, aus folgenden Gründen dem unteren Grenzwert entspricht:

- Zerstörung der Bodenstruktur durch vorgängiges Bohren.
- Relativ grosse Verschiebungen der Messmembrane (3 - 6 mm) schliessen den Effekt von höherer Steifigkeit bei kleinen Dehnungen („small-strain stiffness“) aus.

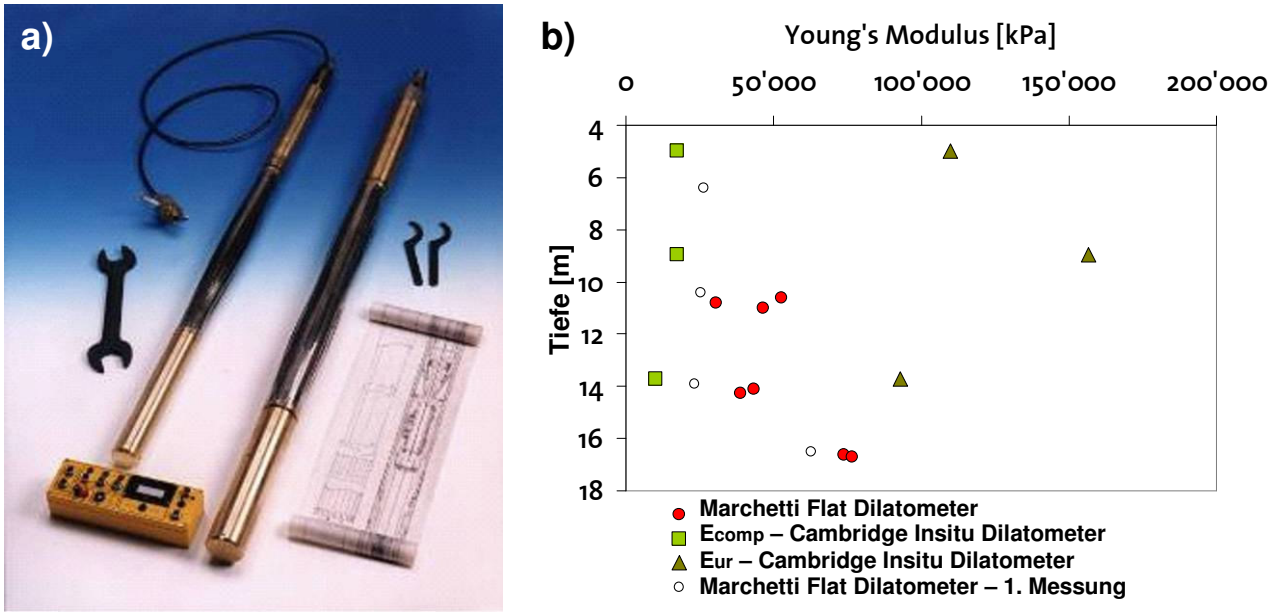

Bild 13: a) Cambridge Insitu Dilatometer (Internet, 2007a), b) Bodensteifigkeit aus Dilatometerversuchen

2.3.2.3 Versuche mit dem Marchetti Flat Dilatometer

Der Marchetti Flat Dilatometer wird prinzipiell nicht für Böden mit Steinen empfohlen, weil diese mit dem Prüfspaten nicht durchdrungen werden können und somit Hindernisse darstellen. Trotzdem konnten in St. Moritz erfolgreich Versuche in der Tiefe von 6.5 m, 11 m, 14 m und 17 m durchgeführt werden. Hierfür wurde eine spatenförmige Prüfspitze (Bild 14) von einem vorgebohrten Bohrloch weiter in den Boden gepresst. Auf der jeweiligen Tiefe wurden Versuche alle 20 cm gemacht. Die Versuche mit dem Marchetti Dilatometer wurden nach einem Standardverfahren von Marchetti et al. (2001) durchgeführt.
Die Resultate der Erstbelastung E_{comp} (nur diese können mit dem Marchetti Dilatometer „gemessen“ werden) sind in Bild 13b dargestellt. Hierbei zeigen die Messungen 20 cm unterhalb des vorgebohrten Bohrlochs geringere Steifigkeiten gegenüber den Werten aus einer Tiefe von 40 und 60 cm unterhalb der Bohrung, weil der Einfluss des Aufbohrens oberhalb der Messung und der damit verbundenen Änderung des Spannungszustandes im Boden ab 40 cm kaum mehr einen Einfluss spielt.
Generell stellt die durch die Marchetti Versuche erhaltenen Steifigkeiten des Bodens aus folgenden Gründen den oberen Grenzwert dar:

- Durch das Einpressen des Prüfspatens wird der Boden um den Spaten verdichtet.
- Relativ kleine Verschiebungen der Messmembrane (1.1 mm) schliesst den Effekt der geringeren Steifigkeit bei grossen Dehnungen (large-strain stiffness) aus.
- Da die Messung nur in einer Richtung erfolgt, führt der 3D-Effekt zu einem steiferen Verhalten (Hingegen wird bei den Versuchen mit dem Cambridge Insitu Dilatometer die Membrane in alle Richtungen der x-y-Ebene aufgeblasen).

Für die oben genannten Effekte gibt es nach Marchetti et al. (2001) verschiedene Korrekturfunktion die auf die einzelnen Messungen in den verschiedenen Böden angewendet werden können. Leider existiert für die Messung in Böden mit einer moräneähnlichen Kornverteilung keine verlässliche Korrekturfunktion, weshalb im Folgenden die unkorrigierten Werte aus den Versuchen mit dem Marchetti Flat Dilatometer verwendet wurden.

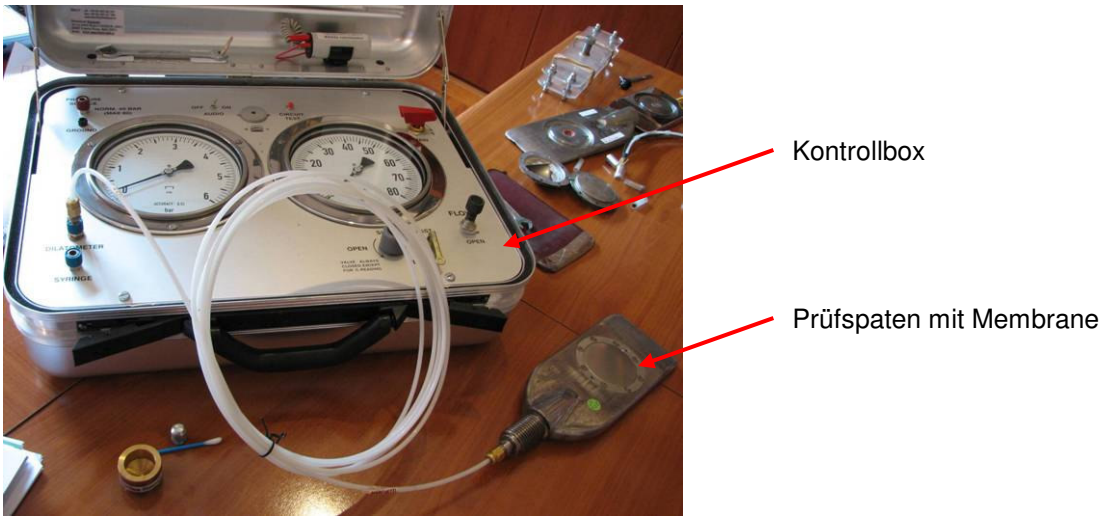

Bild 14: Marchetti Flat Dilatometer

2.3.2.4 Oedometer Versuche

Es wurden 16 gestörte Bodenproben aus denselben Tiefen entnommen, in denen Dilatometerversuche durchgeführt wurden. Dies mit dem Ziel, die Resultate der Bodensteifigkeit aus den Feld- und Laborversuchs einander gegenüber zu stellen.
Grundsätzlich wurden zwei Oedometerversuche an einer Probe aus derselben Tiefe durchgeführt. Wo die Resultate signifikant von einander abwichen wurde ein dritter Test durchgeführt.

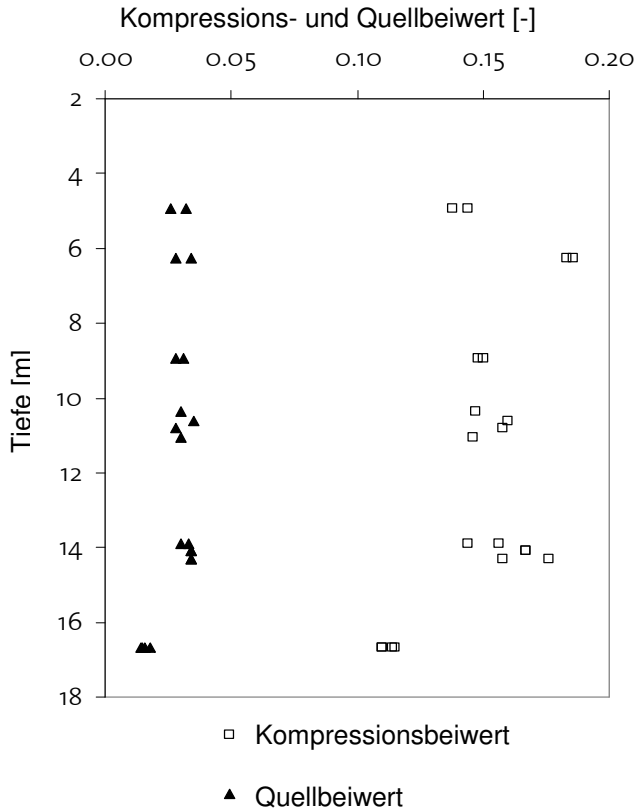

Bild 15: Bodensteifigkeit (Kompressions- CS und Quellbeiwert CC) aus den Oedometerversuchen

Den neu angemischten Proben wurde der Anteil grösser als 4 mm durch Sieben entfernt, womit sich in den Proben keine grösseren Steine, Kies und Holzstücke mehr befanden. Anschliessend wurde den Proben so viel Wasser hinzugegeben bis sie eine pastenartige Konsistenz aufwiesen. Die Proben wurden mit Hilfe von einem Spachtel in die Oedometerringe eingebracht. Jede Probe wurde schrittweise bis 400 kPa belastet, danach bis 50 kPa entlastet und wieder bis 3200 kPa belastet. Aus der Zeit-Setzungskurve ergab sich eine Konsolidationszeit der einzelnen Belastungsschritte zwischen 30 und 45 Minuten. Bild 15 gibt eine Übersicht aller Kompressions- und Quellbeiwerte der Oedometerversuche. Diese Werte zeigen eine gute Übereinstimmung mit den Versuchen die Clark et al. (1998) an Moränen durchgeführt hat.
Generell ist die durch die Oedometerversuche bestimmte Bodensteifigkeit durch folgende Tatsachen geringer als die tatsächlich im Boden vorherrschende:

- Das Material für die Versuche wurde neu angemischt, womit vorherrschende Gefügestrukturen zerstört wurden.
- Für die Durchführung der Oedometerversuche musste die Fraktion grösser als 4 mm ausgesiebt werden.

Gens und Hight (1979) haben gezeigt, falls der Kiesanteil geringer als 12% ist, kann dieser ohne das Endresultat zu verfälschen entfernt werde. Im vorliegenden Fall mit den Bodenproben aus St. Moritz beträgt dieser Anteil jedoch ca. 30%.

2.3.2.5 Vergleich zwischen Labor- und Feldversuchen

Um die einzelnen Resultate der unterschiedlichen Versuchsmethoden miteinander zu vergleichen, eignen sich das Erst- (E_{comp}) und Wiederbelastungsmodul (E_{ur}) nicht, da diese eine grosse Spannungsabhängigkeit aufweisen und die Versuche teilweise bei unterschiedlichen Spannungen durchgeführt wurden. Im Gegensatz dazu sind der Kompressions- und Quellbeiwert spannungsunabhängig und stellen damit „wahre“ Bodenkennwerte dar. Während bei Oedometerversuche C_C und C_S direkt aus den Versuchen hergeleitet werden können, benötigt die Umrechnung von E_{comp} und E_{ur} der Dilatometerversuche Kenntnis über die jeweiligen mittleren Normalspannungen σ'_m die während der Versuche vorherrschten.

Im Allgemeinen sind der Kompressions- und Quellbeiwert wie folgt mit dem Verformungsmodulus M_{Ecomp} bzw. M_{Eur} verknüpft:

$$C_c = \frac{2.3 \cdot (1+e_0)}{M_{Ecomp}} \sigma'_m \qquad C_s = \frac{2.3 \cdot (1+e_0)}{M_{Eur}} \sigma'_m \tag{2.6}$$

Für einen isotrop-elastischen Boden kann das Verformungsmodul durch den Young's Modulus (Erst- bzw. Wiederbelastungsmodul) folgendermassen ersetzt werden:

$$M_{Ecomp} = \frac{(1-\nu)}{(1+\nu)(1-2\nu)} E_{comp} \qquad M_{Eur} = \frac{(1-\nu)}{(1+\nu)(1-2\nu)} E_{ur} \tag{2.7}$$

Mit der Annahmen einer Querdehnzahl von 0.25 können die Formeln aus 2.7 direkt in Verbindung mit den Dilatometerversuchen gebracht werden, und wir erhalten die nachfolgenden Umrechnungsformeln:

$$C_c = \frac{1.92 \cdot (1+e_0)}{E_{comp}} \sigma'_m \qquad C_s = \frac{1.92 \cdot (1+e_0)}{E_{ur}} \sigma'_m \tag{2.8}$$

In diesen Formeln entspricht e_0 der insitu Porenzahl (für St. Moritz zwischen 0.75 und 1.0).

Für die Versuche mit dem Marchetti Dilatometer kann die mittlere Spannung σ'_m aus dem aufgebrachten Druck während des Versuches ermittelt werden. Die Bodensteifigkeit wird mit Hilfe der beiden Drücke p_0 und p_1 berechnet, die nötig sind die Membrane gerade zu öffnen bzw. 1.1 mm zu verschieben (Marchetti et al., 2001). Somit ergibt sich die mittlere Spannung σ'_m, die zur Umrechnung des Erstbelastungsmoduls E_{comp} in einen Kompressionsbeiwert benötigt wird, aus dem arithmetischen Mittel der Drücke p_0 und p_1.

Für die Versuche mit dem Cambridge Insitu Dilatometer wurden für die mittlere Spannung σ'_m ebenfalls der mittlere Druck in der Membrane verwendet. Die Berechnung der Bodensteifigkeit erfolgt durch die Steigung einer Geraden durch zwei Punkte auf dem Spannungsdehnungsdiagramm der Erst- bzw. Wiederbelastung. Durch das arithmetische Mittel der Spannungen an denselben Punkten ergibt sich die zugehörige mittlere Spannung σ'_m für die Umrechnungsformel 2.8.

Im Bild 16 werden die einzelnen Resultate aus den Feld- und Laborversuchen auf der Basis des Kompressionsbeiwerts aus den Oedometerversuchen miteinander verglichen. Hierfür wurde der mittlere Kompressionsbeiwert der Oedometerversuchen aus derselben Tiefe als 100% angenommen und anschliessend für die Feldversuche der Kompressions- bzw. Quellbeiwert nach der Formel 2.8 berechnet. In einem letzten Schritt wurden die Resultate der jeweiligen Tiefen durch den Kompressionsbeiwert aus den Oedometerversuchen geteilt und mit 100% multipliziert.

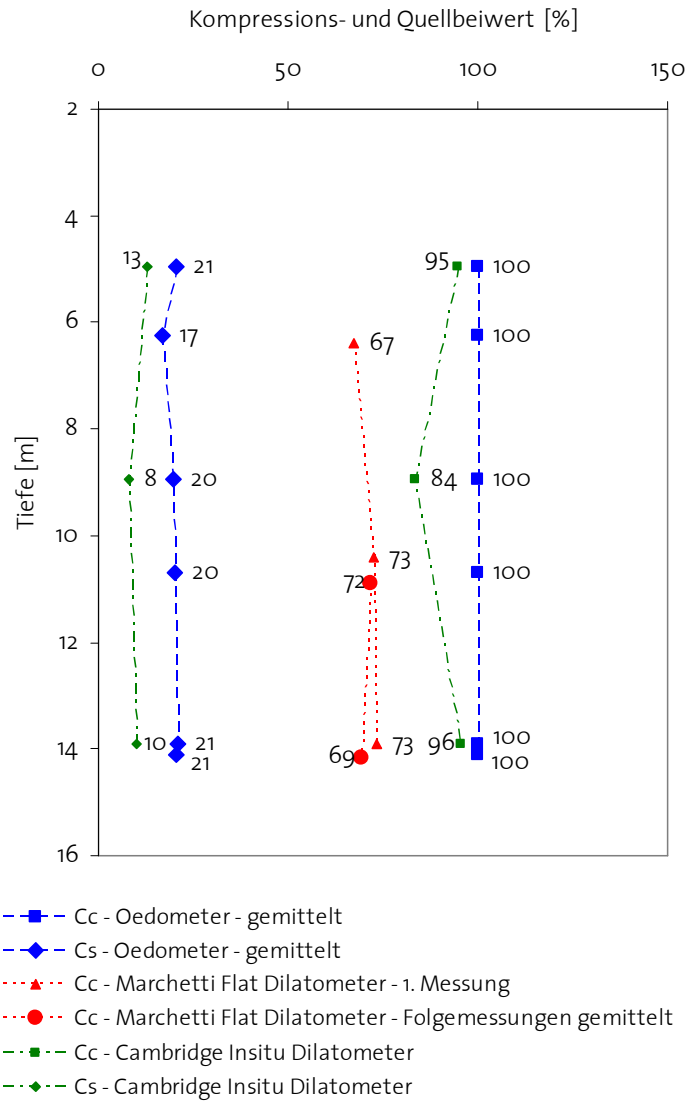

Bild 16: Vergleich der Bodensteifigkeiten aus Feld- und Laborversuchen

2.3.2.6 Diskussion der Resultate

Wie in Bild 16 gezeigt, lassen sich unterschiedliche Labor- und Feldversuchen am besten untereinander vergleichen, wenn die Resultate in die „spannungsunabhängigen“ Kompressions- und Quellbeiwerte umgerechnet werden. Alle drei Untersuchungsmethoden ergeben qualitativ dasselbe Ergebnis über die Tiefe hinweg. Es können folgende Beobachtungen im Bezug auf die Steifigkeit bei der Erstbelastung (Kompressionsbeiwert) gemacht werden:

- Wird davon ausgegangen, dass der Versuch mit dem Cambridge Insitu Dilatometer einen oberen und der Versuch mit dem Marchetti Dilatometer einen unteren Grenzwert für den Kompressionsbeiwert ergeben, so lässt sich eine vernünftige Bandbreite der insitu Bodensteifigkeit abstecken.
- Trotz dem Entfernen der Fraktion grösser als 4 mm (ca. 30%) ergeben die Oedometerversuchen einen vernünftigen oberen Grenzwert für den Kompressionsbeiwert.
- Das elastische Kompressionsmodul E_{comp} der ersten Marchetti Versuche der jeweiligen Bohrlochtiefe (20 cm unterhalb der Bohrung) wird stark durch die Veränderung des Spannungszustandes durch die Bohrung beeinflusst. Hingegen zeigen diese Werte eine gute Übereinstimmung mit den Werten aus den Cambridge Insitu Dilatometerversuche (Vergleiche Bild 15b).
- Die Folgemessungen mit dem Marchetti Dilatometer (40 cm und 60 cm unterhalb der Bohrung) zeigen im Bezug auf den Kompressionsbeiwert ähnliche Resultate, wie die Erstmessung (20 cm unterhalb der Bohrung). Dies lässt darauf schliessen, dass das Bohren keinen störenden Einfluss auf den Kompressionsbeiwert aus den Messresultaten der Marchetti Versuchen hat (Bild 16).

Im Bezug auf die Steifigkeit bei der Wiederbelastung (Quellbeiwert) können folgende Aussagen gemacht werden:

- Geht man davon aus, dass die Versuche mit dem Cambridge Dilatometer einen oberen Grenzwert für den Quellbeiwert angeben, zeigen die Oedometerversuche an den neu angemischten Proben ein zu „weiches“ Verhalten und können nicht zur Findung eines oberen Grenzwertes herbeigezogen werden.
- Dies zeigt, dass das Verhalten bei der Wiederbelastung sensibler auf die Anwesenheit von Kies und Steinen im Feld und auf allfällige Störungen der Probe im Labor reagiert als die Erstbelastung.

2.3.2.7 Zusammenfassung und Schlussfolgerungen

Das erste Mal konnte bei geotechnischen Versuchen beide Arten von Dilatometerversuchen in solch einem schwierigen Boden (siltiger Kies mit Ton und Steinen) erfolgreich eingesetzt werde. Die Feldversuche zeigten eine gute Übereinstimmung untereinander und mit den zusätzlich durchgeführten Laborversuchen. Folgende Schlussfolgerungen können gezogen werden:

- Der Kompressions-(C_C) und Quellbeiwert (C_S) repräsentieren eine gute Grundlage um verschiedene Arten von Feld- und Laborversuchen über einen grossen Spannungsbereich mit einander zu vergleichen.
- Die Versuche mit dem Cambridge Insitu Dilatometer, falls sie überhaupt durchführbar sind, geben einen oberen Grenzwert für den Kompressions- und Quellbeiwert an. (Sie zeigen ein eher zu weiches Verhalten des Bodens, da vorgängig gebohrt werden musste.)
- Der Marchetti Dilatometer gibt die untere Grenze für den Kompressions- und Quellbeiwert an. (Durch das Einpressen des Versuchsspatens wird der Boden teilweise verdichtet, was zu einem eher zu steifen Verhalten des Bodens führt. Hierfür existieren für eine Vielzahl von Böden semi-empirische Korrekturfaktoren.)

- Oedometerversuche an gestörten und neu angemischten Proben, falls der ausgesiebte Teil (> 4 mm) über 12 % beträgt, ergeben einen oberen Grenzwert für den Kompressionswert und einen noch höheren Gernzwert für den Quellbeiwert. (Der Boden zeigt ein zu weiches Verhalten, da ihm die Anteile > 4 mm entzogen wurden, zusätzlich gehen vorher vorhandene Bindungen zwischen den einzelnen Bodenpartikeln verloren.)
- Es hat sich gezeigt, dass um eine vernünftige Bandbreite des wirklichen Bodenverhaltens von moräneähnlichen Böden zu erreichen, eine Kombination von Cambridge Insitu Dilatometer und Marchetti Dilatometer Versuchen von Nöten ist. Eine einzelne Versuchsart von Feldversuchen ist nicht ausreichend.

Die erhaltenen Werte für die Steifigkeit des Bodens können nun in die Rückrechnung der Verschiebungen und somit zur Berechnung der Porenwasserdrücke und der Scherspannungen entlang der Scherfläche miteinfliessen. Womit anschliessend eine Analyse der Stabilität und allfälliger Stabilisierungsmassnahmen (z.B. Drainagesysteme) ermöglicht wird.

3 Neue Sensortechnologien

3.1 Erddruckmessungen

Die meisten Rutschhänge sind mit Inklinometerrohren ausgestattet. Aus diesem Grund war es naheliegend, diese Rohre für zusätzliche Messungen zu benutzen. Da auch auf diese Rohre der Erddruck wirkt, lässt sich durch die Änderung des Durchmessers der Rohre auf den herrschenden Druck schliessen (Bild 17a).

Dafür wurde eine Sonde gebaut (Bild 17b), welche in den Rillen geführt nach unten gleitet und fortlaufend die Inklination, den Wasserdruck und den Durchmesser misst. Eine Vielzahl von zusätzlichen Einflüssen: Rohreigenschaften, Bettung des Rohres, Biegung des Rohres etc. wird im Rahmen einer Doktorarbeit am IGT genauer untersucht (Schwager et al. 2009, Siehe Anhang). Erste Versuche wurden im Herbst 2008 in St. Moritz (Bild 17c) durchgeführt. Die Ergebnisse (Bild 17a) zeigen eine starke Spannungsanisotropie in der Kompressionszone des Rutschhanges.

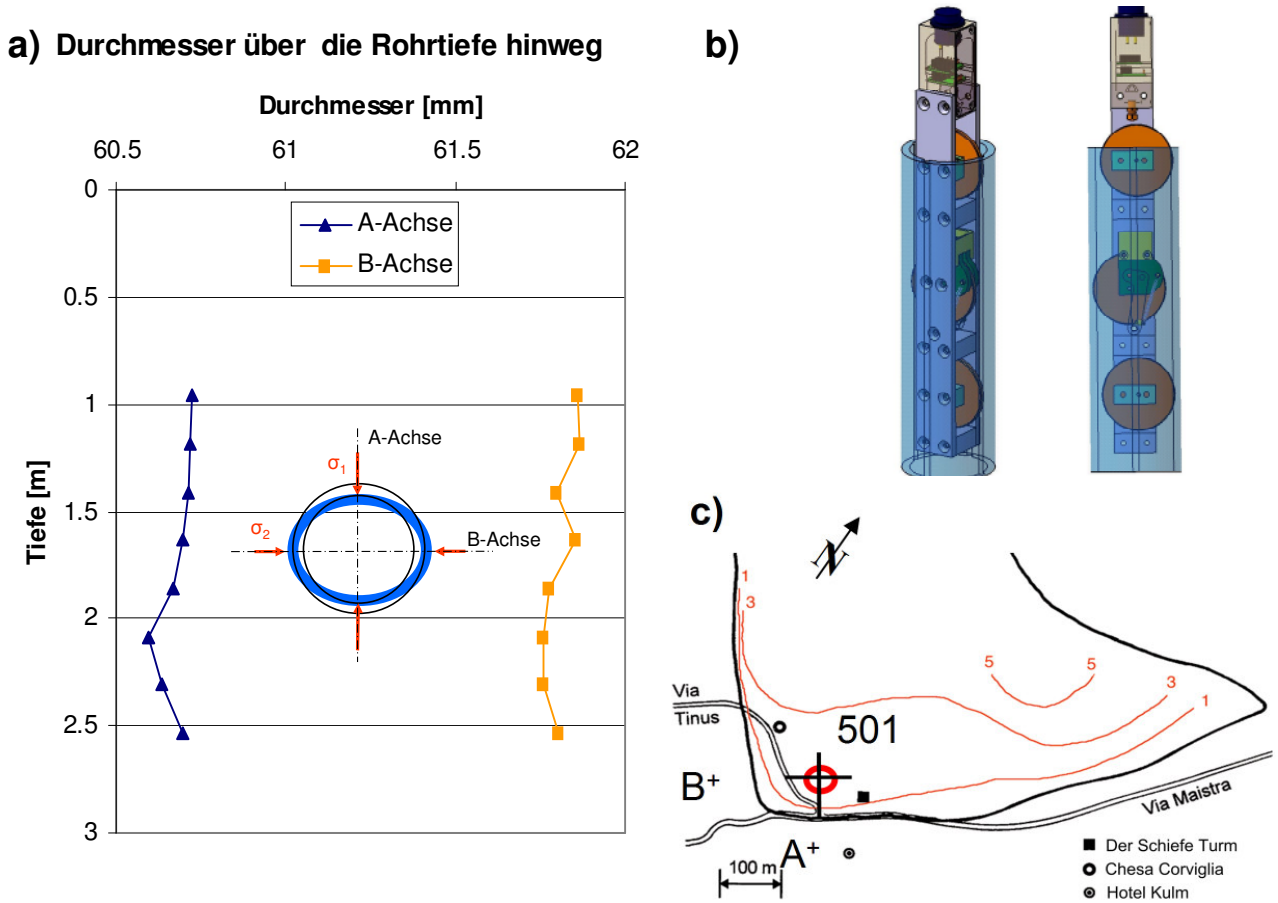

Bild 17: a) Messung eines deformierten Inklinometerrohres mit Spannungsachsen, b) am Institut entwickeltes Messgerät, c) Standort des Inklinometerrohres (Hintergrundbild nach Schlüchter, 1988).

3.2 Bestimmungen der Grenzen

Eine weitere neue Anwendung ist die Glasfasertechnik zur Bestimmung der seitlichen Ausdehnung der Rutschung innerhalb des bebauten Gebietes. Aufgrund der Bauvorschriften der Gemeinde von St. Moritz ist das Bauen innerhalb des Rutschgebietes deutlich teurer und komplexer als ausserhalb. Die westliche Begrenzung der Rutschung durchschneidet das Dorf von St. Moritz und kann durch geodätische Messungen

nicht genau lokalisiert werden. Dies führt zu einer gesetzlichen und technischen Unsicherheit bei Baugesuchen auf den Parzellen, die sich an der Grenze zwischen beweglichem und ruhendem Gebiet befinden. So eine unklare Übergangszone stellt die westliche Begrenzung der Rutschung bei der Via Tinus dar (Bild 17c). Es wurde entschieden die Strasse Via Tinus als einen riesigen Dehnmessstreifen zu verwenden. Zu diesem Zweck wurde ein 88 m langes Glasfaserkabel in einen 7 cm tiefen Schlitz eingelegt (Bild 18a) und mit dem Strassenbelag verklebt. Erste Messungen im darauffolgenden Jahr zeigten eine rund 15 m lange Scherzone (Bild 18b), die etwa in einem 45° Winkel zur Strasse verläuft. Die Verschiebung über die ganze Scherzone beträgt ca. 2 cm, was mit vorgängigen geodätischen Messkampagnen aus den Jahren 1998 und 2006 übereinstimmt.

Des Weiteren wurden Mikro-Anker entwickelt um dieselbe Technik auch unabhängig von Asphaltstrassen anwenden zu können. Die ersten Versuche mit den Mikro-Ankern geschahen im Rahmen einer Masterarbeit am Institut für Geotechnik. Im Sommer 2008 wurde das erste mit Ankern fixierte Kabel in St. Moritz in einem Naturweg eingebaut. Erste Resultate werden voraussichtlich im Sommer 2009 vorliegen.

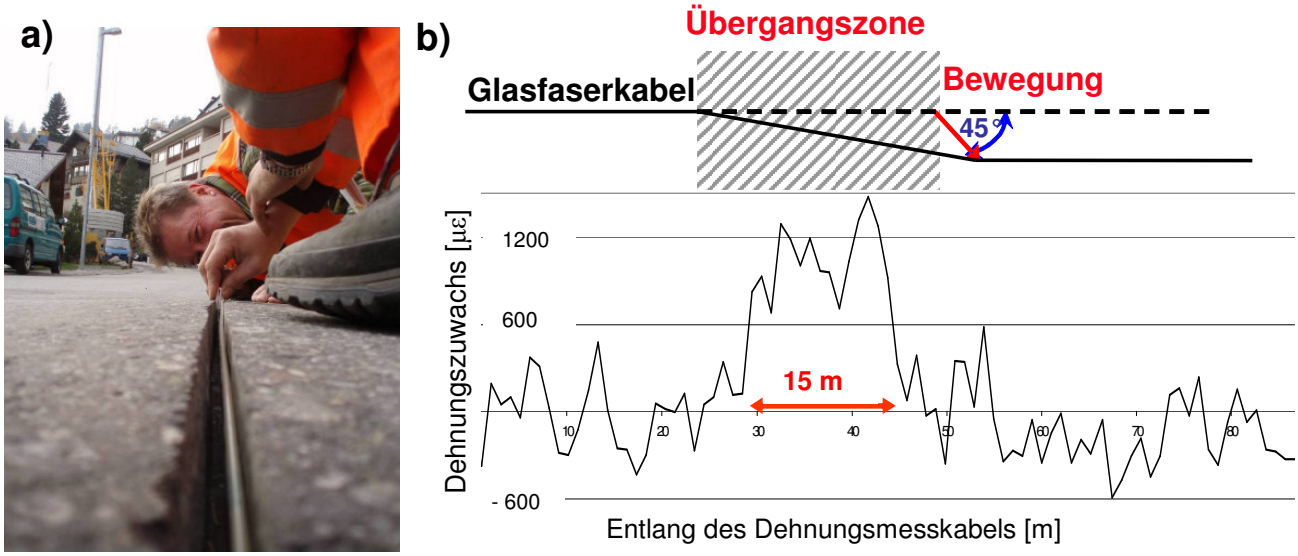

Bild 18: a) Einbau des Glasfaserkabels in der Strasse, b) Interpretation und Dehnungsmessungen im Kabel

Da im gesamten Bereich des überbauten Brattas Hanges Inklinometerrohre eingebaut wurden, die teilweise schon abgeschert sind, besteht eine weitere Idee mit Hilfe von Glasfaserkabeln diese zum heutigen Zeitpunkt abgescherten Inklinometerrohre (für Inklinometersonden nicht mehr durchgängig) wieder funktionstüchtig zu gestalten. Zu diesem Zweck wurde in einem Inklinometerrohr bei der Kreuzung Via Tinus - Via Maistra (Bild 17c) ein Glasfaserkabel eingebaut und das Rohr ausinjiziert. Die ersten Folgemessung des Glasfaserkabels wies auf eine Scherfläche in 6 - 7 m hin, was mit den alten Inklinometermessungen übereinstimmt (Bilder 19a und 19b). Ebenfalls die Grösse der Verschiebung, die aus den Dehnungen im Glasfaserkabel zurückgerechnet wurde, liegt im Bereich der früheren Inklinometermessungen.

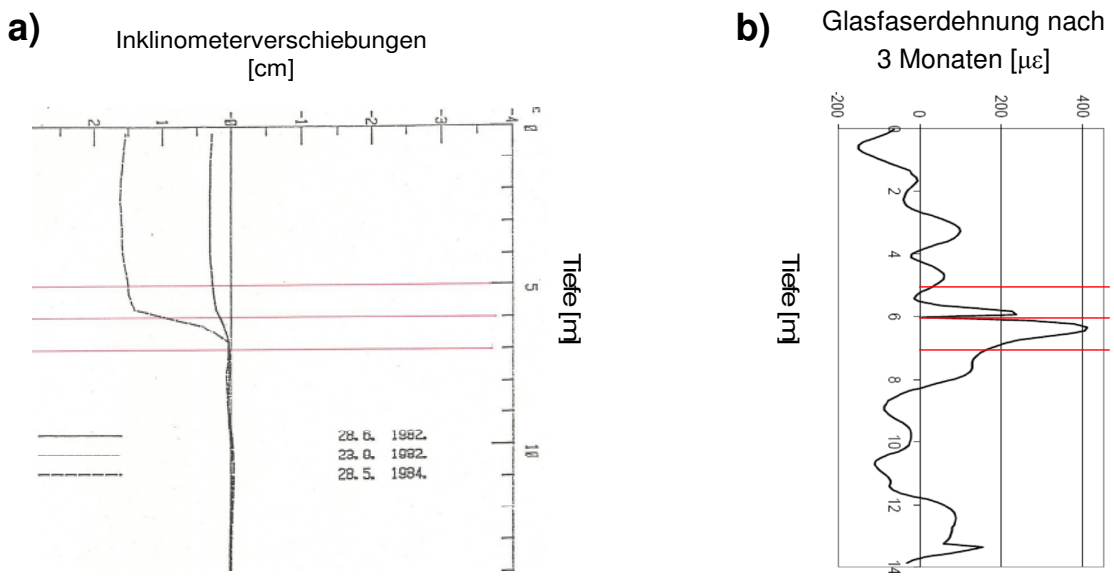

Bild 19: a) Inklinometermessungen aus den Jahren 1982-1984, b) Glasfaserdehnung im selben Inklinometerrohr aus dem Jahr 2008

Das riesige Potential dieser neuen Technologie im Bereich der Überwachung von sich langsam bewegenden Rutschhängen wird von Iten et al. (2009) genauer beschrieben und ist dem Anhang beigelegt.

4 Zusammenfassung Brattas Kriechhang

Die langfristige Stabilität des Brattas Kriechhanges muss noch weiter untersucht werden. Die Abschätzung des Sicherheitsgrades erfolgt durch Rückrechnungen mit Hilfe einer Näherungsmethode, die die jährlichen Verschiebungen des Kriechhanges nutzt. Die Verschiebungen sollen entlang des gesamten Hanges gemessen werden. Eine genauere Abschätzung des Sicherheitsgrades erfolgt durch FE-Stabilitätsberechnungen, die die Kenntnis der Bodenparameter verlangen. Die Bodenparameter werden durch Labor- und Feldversuche bestimmt. Hierbei darf die Versuchsgeschwindigkeit nicht ausser Acht gelassen werden und Versuchsresultate sind durch Rückrechnungen zu überprüfen. Die modernen Sensortechnologien bieten neue Möglichkeit zur Überwachung von Kriechhängen.

5 Weitere Projekte

5.1 Combe Chopin (BE)

Wird ein aktiver Kriechhang an seinem Fuss durch eine natürliche oder künstliche Barriere gestoppt, so verlangsamen sich die Verschiebungen im gesamten Hang. Dies führt meist zur intuitiven Annahme, dass der gesamte Hang dadurch stabilisiert ist. Doch gerade wegen dieser Zwängung am Fuss des Hanges kann es zu einem Versagen kommen. Dies geschieht dadurch, dass durch die Verlangsamung der kriechenden Schicht der viskose Anteil der Scherspannungen in der Übergangszone zwischen Kriechhang und stabilem Untergrund abnimmt. Diese Verminderung der Scherspannung in der Scherzone wird durch eine Zunahme des Erddrucks am Fuss kompensiert, jedoch nur so lange bis der Erddruck am Fuss den passiven Erddruck erreicht. Danach tritt ein Versagen des Hanges ein. Nun gilt es abzuklären, ob die Spannungen am Fuss überhaupt bis zum passiven Erddruck zunehmen können, oder ob der Hang schon vorher zum Stillstand gekommen ist.
Ein solches Beispiel einer künstlichen Barriere stellt die Stützmauer bei Combe Chopin (BE) einem Teilstück der Autobahn A16 dar.

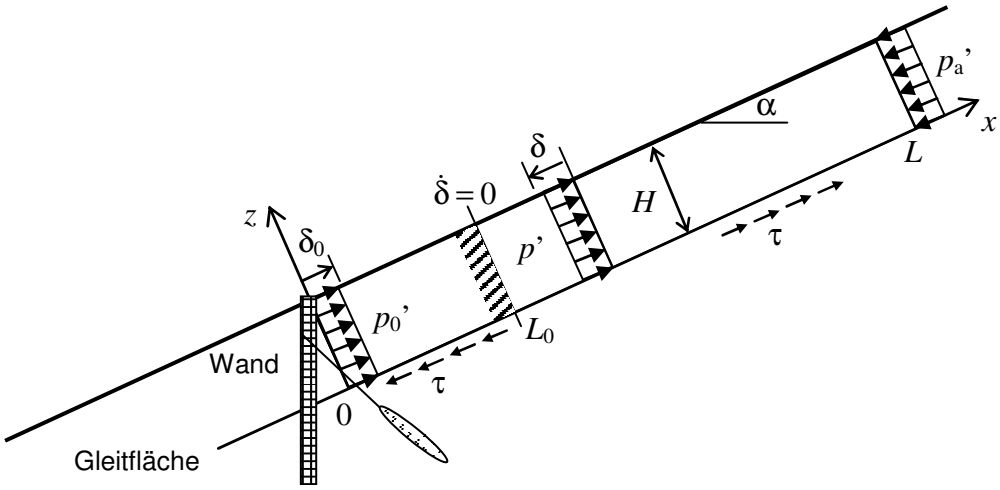

Bild 20: Modell der analytischen Berechnung des Hanges bei Combe Chopin

Ob hier das Versagen durch das Erreichen des passiven Erddrucks im Bereich vor der Mauer auftreten kann oder nicht, wurde mit Hilfe von geodätischen Messungen, TRIVEC und Ankerkraftmessungen abgeklärt (Puzrin und Schmid, 2007). Hierbei stellte sich heraus, dass ein „Überfliessen“ der verankerten Wand nicht ausgeschlossen werden kann.

5.1.1 Einleitung Combe Chopin

In der folgenden Stabililtätsberechnung wurden die Daten aus den Überwachungsmassnahmen bei der Bohrpfahlwand des Autobahnneubaus Combe Chopin verwendet. Hier muss zusätzlich erwähnt werden, dass zum Zeitpunkt der Berechnungen nicht alle aktuellen Daten zur Verfügung standen, somit kann eine definitive Aussage erst nach dem Eintreffen und Miteinfliessen der neusten Daten über die Stabilität der Rutschung bei Combe Chopin gemacht werden. Die in diesem Bericht gemachten Aussagen sollen hauptsächlich als Anleitung zu einer Überprüfung der Stabilität eines am Fusse durch eine flexible Wand gestützten Hanges dienen.

Der Autobahnneubau der A 16 von Bern nach Delémont und Basel stellt eine wichtige Verbindung zwischen Bern als Bundeshauptstadt und Frankreich dar (Bild 21a). Für den Neubau musste der Kriechhang bei Combe Chopin angeschnitten werden. Dieser wird auf beiden Seiten im Norden und Süden von Hügeln umrahmt (Bild 21b). Die Kriechverformungen der Rutschung bei Combe Chopin werden seit 1976 überwacht und gemessen (Bapst, 2002). Die Neigung des Hanges liegt zwischen 25° und 30° und verläuft in Ost West Richtung. Am Fuss der Rutschung befindet sich der Fluss Birs. Die Ausdehnung des sich bewegenden Gebietes entspricht in der Breite 150 - 200 m und in der Länge 140 – 190 m. Das Rutschgebiet kann in einen grösseren südlichen und einen kleineren nördlichen Teil mit einer Länge von ca. 90 m unterschieden werden. Die Dicke der sich bewegenden Schicht beträgt im nördlichen Teil zwischen 5 und 7 m und im südlichen Teil bis zu 14 m. Die Rutschmasse besteht aus einer durchmischten Masse von schlecht abgestuftem Kies bis siltigem Kies teilweise sogar mit Ton vermengt. Darunter befindet sich eine ähnliche Schicht mit einer Dicke von 0.5 bis 1 m, die aber noch zusätzlich mit Lehm aus dem verwitterten Mergel angereichert ist. Unterhalb dieser Schicht befindet sich der Übergang vom gesunden zum verwitterten Mergel mit einer Dicke zwischen 2 und 4 m. Die hydrologischen Verhältnisse werden hauptsächlich durch den weniger durchlässigen Mergel bestimmt, womit Niederschläge durch die sich bewegende Schicht sickern und auf der weniger durchlässigen Mergelschicht dem Rutschhorizont folgen.

Im Rahmen der Baumassnahmen wurde der nördliche Teil des Kriechhanges mit Hilfe von rückverankerten Bohrpfählen stabilisiert. Im Folgenden wird nur der mit Hilfe der Wand „stabilisierte“ nördliche Teil der Rutschung betrachtet.

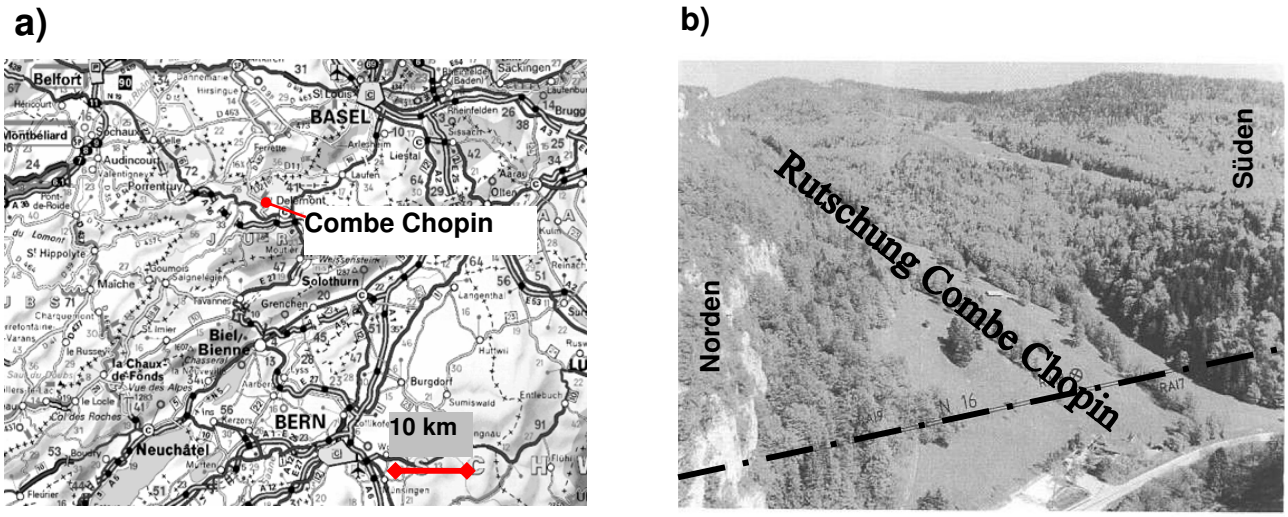

Bild 21: Die Rutschung von Combe Chopin: a) Lage (Internet, 2007b), b) Blick auf die Rutschung (Bapst, 2002).

Zur Überwachung des Langzeitverhaltens der Wand wurden geodätischen Messungen, so wie TRIVEC Messungen in der Bohrpfahlwand durchgeführt. Die TRIVEC Messungen der Wand erlauben eine Verschiebungsmessung in alle drei Achsen und mit Hilfe der Wandverschiebung und Ankerkräfte eine Abschätzung der Wandbelastungen.

5.1.2 TRIVEC Messungen

Bei der TRIVEC Sonde handelt es sich um ein portables Gerät, das die Messung drei zu einander orthogonal stehenden Verschiebungsvektoren mit einer hohen Genauigkeit erlaubt (Bild 22a). Mit dem Gerät

lassen sich direkt die axiale Dehnung, so wie die Neigungswinkel in zwei zu einander orthogonal stehende Ebenen messen (Koeppel et al, 1983).

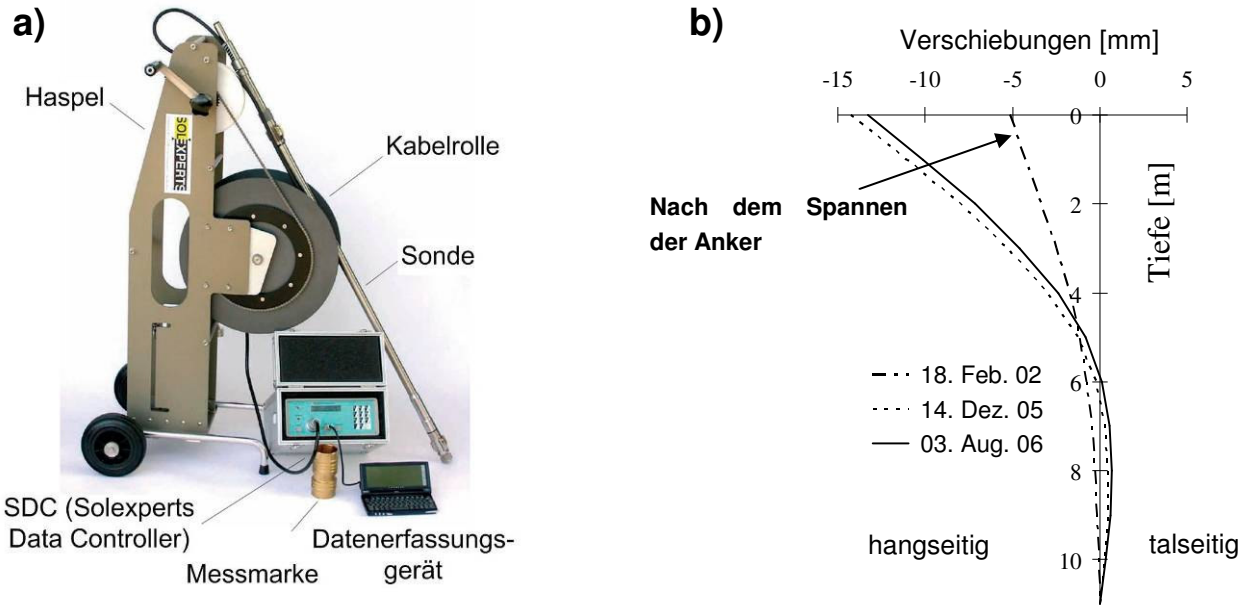

Bild 22: TRIVEC Messungen: a) das Messgerät (SOLEXPERTS, 2007), b) TRIVEC Messungen in der Bohrpfahlwand bei Combe Chopin.

Die ersten Messungen der Bohrpfahlwand nach dem Spannen der Anker hat eine Verschiebung der Wand Hang aufwärts gezeigt (Bild 22b). Die Messungen in den darauffolgenden drei Jahren bis zum Dezember 2005 haben ebenfalls eine Zunahme der Verschiebungen Hang aufwärts ergeben. Wurde nun der Hang oberhalb der Wand stabilisiert? Oder haben Kriecheffekte im Boden hinter der Wand zu einer Zunahme der Verschiebungen Hang aufwärts geführt? Die Messungen im August 2006 zeigten jedoch, dass sich die Verschiebungsrichtung geändert hat und die Verschiebungen nun wieder talwärts gerichtet sind (Bild 22b ausgezogene Linie). Da Messungen der Ankerkräfte in demselben Zeitraum jedoch keine Abnahme der Ankerkräfte gezeigt haben, kann diese Änderung der Verschiebungsrichtung nur durch eine Druckzunahme vor der Wand erklärt werden. Eine erste Betrachtung der Messungen aus dem Herbst 2008 bestätigen, dass sich die Verschiebungsrichtung geändert hat. Weitere Messungen im Jahre 2009 sollen zeigen, ob sich die Tendenz der Verschiebungsgeschwindigkeit fortsetzt.

5.1.3 Model zur Berechnung

Zur Berechnung der Langzeitstabilität des Hanges wurde das Modell aus den Berechnungen des Brattas Hanges in St. Moritz angepasst (Bild 20). Die Rutschung wird nun am Fuss nicht mehr durch eine unverschiebliche Wand gehalten, sondern von einer flexiblen Wand gestützt. Da nach dem Bau der Wand die Anker gespannt werden und der so aufgebrachte Druck grösser sein kann als der Erdruhedruck vor der Wand, kann sich der untere Teil sogar Hang aufwärts bewegen. Trotz alledem bewegt sich der obere Teile der Rutschung noch immer talwärts. Dadurch befindet sich oberhalb der Wand eine Stelle L_0, wo die Verschiebungsgeschwindigkeiten zum Zeitpunkt t Null sind. Womit sich das Problem in zwei einzelnen Teilen betrachten lässt.

Das Kräftegleichgewicht der sich bewegenden Schicht im oberen Teil wird gebildet aus den Scherspannungen τ auf der Gleitschicht, der mittleren effektiven Spannung p' in der gleitenden Schicht und dem effektiven aktiven Erddruck p'_a beim Anrissgebiet:

$$p'(x,t)H + \int_x^L \tau(x,t)dx = \gamma_t H(L-x)\sin\alpha + p'_a H \qquad \text{für } L_0 \le x \le L \tag{5.1a}$$

In der oben stehenden Formel bezeichnet γ_t das totale Raumgewicht des Bodens; α die mittlere Hangneigung; L und H die Länge bzw. Breite der Rutschung.

Das Kräftegleichgewicht des unteren Teiles des Hanges bezieht sich auf die Scherspannungen τ (die immer entgegen der Bewegungsrichtung agiert) auf der Gleitschicht, der mittleren effektiven Spannung p' in der gleitenden Schicht und dem Erddruck p'_0 vor der Wand.

$$p'(x,t)H + \int_0^x \tau(x,t)dx = p'_0 H - \gamma_t H x \sin\alpha \qquad \text{für } 0 \le x \le L_0 \tag{5.1b}$$

In den Fromeln 5.1a und 5.1b wird der effektive Erddruck verwendet mit der Annahme, dass der durchschnittliche Porenwasserdruck entlang des Hanges konstant ist: $u(x,t) = u(t)$, d.h. dass die Grundwasserströmung parallel zur Hangneigung erfolgt, oder keine verbundenen Grundwasserspeicher vorhanden sind.

Die Stelle, wo die Geschwindigkeit Null ist, lässt sich finden, indem in beiden Gleichungen (5.1a und 5.1b) x durch L_0 ersetzt wird und diese anschliessend nach der Spannung $p'(L_0,t)$ auflöst. Dadurch ergibt sich die folgende Gleichung:

$$\int_{L_0}^{L} \tau(x,t)dx - \int_0^{L_0} \tau(x,t)dx = \gamma_t HL\sin\alpha - (p'_0 - p'_a)H \tag{5.2}$$

Um die Gleichungen 5.1a und 5.1b in einer Vorwärtsrechnung des dazugehörigen Randwertproblems zu lösen, müssen die Ausdrücke $\tau(x,t)$ und $p'(x,t)$ der Gleichungen durch die folgenden rheologischen Stoffgesetze ersetzt werden:

$$\tau(x,t) = \tau_r + \eta_\tau \dot{\delta}(x,t) \tag{5.3a}$$

$$p'(x,t) = E\varepsilon(x,t) + \eta_p(\varepsilon,\dot{\varepsilon})\dot{\varepsilon}(x,t) \tag{5.3b}$$

Somit führt uns die Lösung der Gleichungen 5.1a und 5.1b zu den Verschiebungen $\delta(x,t)$, Dehnungen $\varepsilon(x,t)$ und dem Erddruck $p'(x,t)$, womit sich das Verhalten der Rutschung Voraussagen lässt. Dabei stellt E den elasto-plastischen (während der Belastung) Modul des Bodens; τ_r die Restscherfestigkeit der

Gleitfläche dar, η_τ und $\eta_p(\varepsilon,\dot{\varepsilon})$ stehen für die viskosen Koeffizient der Scherspannung bzw. der Normalspannung. Es wird angenommen, dass die Scherfestigkeit mit zunehmender Geschwindigkeit zunimmt, was durch Experimente an natürlichen Böden gezeigt wurde (z.B. Skempton, 1985). Die Steifigkeit des Bodens in der Rutschmasse wird ebenfalls als geschwindigkeitsabhängig angenommen. Weil die Geschwindigkeiten einer am Fuss gestützten Rutschung langsamer sind als einer ungestützten, kann angenommen werden, dass der Porenwasserüberdruck genügend Zeit hat um sich abzubauen, wodurch die Zeitabhängigkeit der Verschiebungen nur vom viskosen Teil des Bodens bestimmt wird.
Der Nachteil in der direkten Vorwärtsrechnung liegt darin, dass beobachtete Verschiebungen nicht in die Berechnung einfliessen. Die Inhomogenität des Bodens, so wie die Versuchsdurchführung zur Bestimmung der Bodenparameter mit Hilfe von Labor- bzw. Feldversuchen, führt zu einer grossen Unsicherheit der so gewonnen Bodenparameter. Dadurch kommt es oft zu erheblichen Unterschieden zwischen dem beobachteten und dem vorausgesagten Verhalten. Hier kann die Rückrechnung von Bodenparameter aus dem beobachteten Verhalten zu Hilfe kommen. Dies zählt insbesonders für die Voraussage des Verhaltens eines Rutschhanges, das nicht allein auf Untersuchungen an einzelnen Bodenproben gemacht werden kann. In einem solchen Fall liefert die Rückrechnung verlässlichere Parameter. Jedoch sollte auch die so gewonnen Parameter kritisch betrachtet und teilweise deren Plausibilität durch Versuche erörtert werden.
Zur Überprüfung der Langzeitstabiliät des Hanges bei Combe Chopin wurde die Methode der Rückrechnung angewendet und in den folgenden Abschnitten dargelegt.

5.1.4 Funktion der Kurvenanpassung

Um die Berechnung etwas zu vereinfachen, wird die folgende analytische Funktion zur Kurvenanpassung der gemessenen und normalisierten Verschiebungen $\bar{\delta}(\bar{x},t)=\delta(x,t)/(L-L_0)$ im oberen Bereich der Rutschung $L_0 \le x \le L$ vorgeschlagen:

$$\bar{\delta}(\bar{x},t)=\bar{\delta}_x(\bar{x})\bar{\delta}_t(t)=\bar{x}(a-b\bar{x})\left(1-e^{-c(t-t_0)}\right), \qquad \text{wobei} \qquad 0\le b/a<0.5\,;\; c>0 \tag{5.4}$$

Hier steht $\bar{x}$ für die normalisierte Stelle der Vermessung $\bar{x}=(x-L_0)/(L-L_0)$. Mit dieser Funktion werden Verschiebungen beschrieben, die an der Stelle L_0 Null sind und monoton (falls $0\le b/a<0.5$) bis zum Anrissgebiet ansteigen (Bild 23a), während die Verschiebungen mit der Zeit abnehmen bis sie asymptotisch auf eine Endverschiebung zulaufen (Bild 23b). Diese Funktion wurde bereits von Puzrin und Sterba (2006) für die Stabilitätsberechnung des Brattas Hanges bei St. Moritz vorgeschlagen.

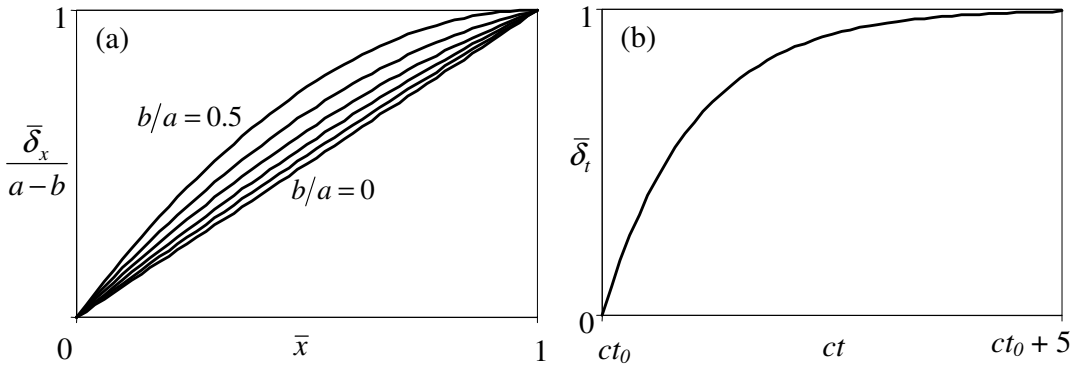

Bild 23: Normalisierte Verschiebungen für die Kurvenanpassung in Raum a) und Zeit b).

Bei der Funktion 5.4 handelt es sich um eine relativ einfache Formel, die aber trotzdem genügend Flexibilität zeigt, um sich an die gemessenen Verschiebungen in Raum (Parameter *a* and *b*) und Zeit (Parameter *c*) anzupassen.
In der Tat stellt diese Funktion die exakte Lösung des Randwertproblems (Formeln 5.1-5.3) für den Fall $\eta_\tau = 0$ und $\eta_p(\varepsilon, \dot{\varepsilon}) = \eta_p = const$ dar. (z.B. falls die Scherfestigkeit geschwindigkeitsunabhängig ist und die Viskosität der sich bewegenden Schicht linear ist.) In diesem Fall können die Koeffizienten aus der Gleichung 5.4 direkt in Bezug zu den Modelparametern gesetzt werden:

$$a = \frac{p'_a + \bar{p}(L - L_0)}{E} \qquad b = \frac{\bar{p}(L - L_0)}{2E} \qquad \bar{p} = \gamma_t \sin\alpha - \tau_r / H \qquad c = \frac{E}{\eta_p} \tag{5.5}$$

wobei L_0 sich mit Hilfe der Gleichung 5.2 herleiten lässt:

$$L_0 = \frac{p'_0 - p'_a - \bar{p}L}{2(\gamma_t \sin\alpha - \bar{p})} \tag{5.6}$$

Hieraus folgt, wenn der Erddruck vor der Wand p_0 konstant über die Zeit bleibt, bewegt sich die Stelle mit der Geschwindigkeit Null L_0 nicht. Womit sich in diesem Fall die exakte Lösung für die normalisierten Verschiebungen $\bar{\delta}(\bar{x}, t) = \delta(x, t)/L_0$ im unteren Bereich der Rutschung ($0 \le x \le L_0$) berechnen lassen:

$$\bar{\delta}(\bar{x}, t) = \bar{\delta}_x(\bar{x})\bar{\delta}_t(t) = \bar{x}(a - b'\bar{x})\left(1 - e^{-c(t - t_0)}\right) \tag{5.7}$$

wobei $\bar{x} = (x - L_0)/L_0$; die Koeffizienten *a* und *c* sind identisch mit jenen aus der Gleichung 5.4; hingegen muss *b* durch *b'* wie folgt ersetzt werden.

$$b' = b\frac{\gamma_t H \sin\alpha + \tau_r}{\gamma_t H \sin\alpha - \tau_r} \tag{5.8}$$

Folglich ist die Verschiebung der Wand (an der Stelle $x = 0$ und $\bar{x} = -1$) Hang aufwärts gerichtet und nimmt mit dem Verlauf der Zeit zu:

$$\delta_0(t) = -L_0(a + b')\left(1 - e^{-c(t - t_0)}\right) \tag{5.9}$$

In Wirklichkeit kann die Hypothese des sich nicht ändernden Drucks p_0 nicht gehalten werden. Die Beziehung zwischen dem Druck und den Verschiebungen bei der Wand wird durch folgende Gleichung beschrieben:

$$\Delta p_0 = K\Delta\delta_0 \tag{5.10}$$

Wobei *K* in der Gleichung für die Wandsteifigkeit steht. Nehmen die Verschiebungen Hang aufwärts zu, muss der Druck, der auf die Wand wirkt, abnehmen. Aus der Gleichung 5.6 ist ersichtlich, dass diese Abnahme des Drucks zu einer Abwärtsbewegung der Nullgeschwindigkeits-Grenze L_0 führt. Daraus folgt, dass die Gleichung 5.7 nicht die exakte Lösung unseres Problems im unteren Teil darstellt. Trotz allem kann

die Gleichung 5.4 für den Fall der Geschwindigkeitsunabhängigkeit der Scherfestigkeit ($\eta_\tau = 0$) als exakte Lösung des Problems im oberen Teil verwendet werden. Vorausgesetzt die Position der Nullgeschwindigkeits-Grenze $L_0(t)$ ist zu jedem Zeitpunkt bekannt. Diese Stelle ($L_0(t)$) kann durchaus auf einen negativen Wert zulaufen (Nullgeschwindigkeits-Grenze unterhalb der Wand).

5.1.5 Rückrechnung

Da die Scherfestigkeit in Wirklichkeit Geschwindigkeitsabhängig ist ($\eta_\tau \neq 0$), besteht die Möglichkeit, dass die Nullgeschwindigkeits-Grenze L_0 die Wand erreicht und danach der Erddruck vor der Wand wieder zunimmt. Der Erddruck vor der Wand könnte mit der Zeit sogar den Wert des passiven Erddrucks erreichen, was dann zu einem „Überfliessen“ der Wand führt. Wir nehmen nun an, sobald die Nullgeschwindigkeits-Grenze die Wand erreicht ($L_0(t_1 - t) = 0$), sich diese Grenze nicht mehr bewegt, womit das Verfahren zur Rückrechnung der Hangstabilität nach Puzrin und Sterba (2006) anwendbar ist.
Die Sicherheit der Langzeitstabilität kann als Verhältnis zwischen dem Widerstand des Bodens (passiver Erddruck) und dem maximalen Erddruck, der sich auf Grund der Abnahme der Scherfestigkeit mit der Zeit vor der Wand aufbauen kann, definiert werden:

$$F_s = \frac{p'_p}{p'(0,\infty)} = \frac{p'_p}{p'_a + \overline{p}L} \tag{5.11}$$

Wobei die Werte des effektiven aktiven und passiven Erddrucks in einem Hang nach Chu (1991) folgendermassen berechnet werden können:

$$\begin{Bmatrix} p'_a \\ p'_p \end{Bmatrix} = \frac{1}{2}\gamma' H \cos\alpha \left[1 + 2\tan^2\varphi'_p \mp 2\sqrt{\left(1+\tan^2\varphi'_p\right)\left(\tan^2\varphi'_p - \tan^2\alpha\right)}\right] \tag{5.12}$$

In der Formel nach Chu (1991) stehe φ'_p und γ' für den effektiven maximalen Reibungswinkel bzw. für das effektive Raumgewicht des Bodens der Rutschmasse. Bevor der Erddruck vor der Wand wieder zugenommen hat, lässt sich der Parameter $\overline{p}$ mit der Gleichung 5.5 und der Kurvenanpassung aus der Gleichung 5.4 an die gemessenen Verschiebungen berechnen.

$$\overline{p} = \frac{p'_a}{(a/2b - 1)(L - L_0)} \tag{5.13}$$

Die Definition des Sicherheitsfaktors der Geleichung 5.11 zeigt ein Versagen auf, so bald $F_s < 1$ ist. Im Fall des Versagens lässt sich nach Puzrin und Sterba (2006) der Versagenszeitpunkt wie folgt abschätzen:

$$t_f = t_0 + \frac{1}{c}\ln\frac{\Delta p'_0 / p'_p}{\left(1 - e^{-c\Delta t}\right)\left(1/F_s - 1\right)} \tag{5.14}$$

Hier steht $\Delta p_0'$ für die Zunahme des Erddrucks vor der Wand während dem Zeitraum Δt. Mit t_0 wird der Zeitpunkt der ersten Erddruckmessung bezeichnet. Diese Änderung des Erddrucks vor der Wand kann mit Hilfe der TRIVEC Messungen berechnet werden.

5.1.6 TRIVEC Messungen

Die Druckänderung $\Delta p_0'$ im Zeitraum t_0 bis $t_0 + \Delta t$ kann aus einer Rückrechnung der Änderungen in der Biegelinie der Wand $\Delta\delta_0(z)$ mit der dazugehörigen Differentialgleichung und unter der Hilfenahme der TRIVEC und der Ankerkraftmessungen erfolgen.
Als Alternative zu diesem doch eher komplexen Problem kann das folgende Vorgehen angesehen werden. Zu einem frühen Zeitpunkt, so lange die Nullgeschwindigkeits-Grenze L_0 noch nicht die Wand erreicht hat (so lange der Druck vor der Wand noch abnimmt.) folgt aus den Gleichungen 5.6 und 5.5:

$$\Delta p_0' = \frac{2\tau_r}{H}\Delta L_0 = 2(\gamma_t \sin\alpha - \bar{p})\Delta L_0 \tag{5.15}$$

ΔL_0 ist die gemessene Änderung der Nullgeschwindigkeits-Grenze zwischen den Zeitpunkten t und $t + \Delta t$. Die mittlere Verschiebung der Wand während demselben Zeitraum wird mit den TRIVEC Messungen wie folgt ermittelt.

$$\Delta\delta_0 = \frac{1}{H}\int_0^H \Delta\delta_0(z)dz \tag{5.16}$$

Mit der Gleichung 5.10 lässt sich nun die Wandsteifigkeit berechnen:

$$K = \Delta p_0' / \Delta\delta_0 \tag{5.17}$$

Nach dem der Erddruck vor der Wand wieder ansteigt, wird die vorher berechnete Wandsteifigkeit zusammen mit der durchschnittlichen Wandverschiebung im Zeitraum t_0 bis $t_0 + \Delta t$ aus der Gleichung 5.16 in die Gleichung 5.10 eingesetzt. Daraus ergibt sich dann der für die Berechnung der Langzeitstabilität (Gleichung 5.14) erforderliche Zuwachs des Erddrucks vor der Wand $\Delta p_0'$ während dem Zeitraum t_0 bis $t_0 + \Delta t$.

5.1.7 Analyse der Stabilität

Angenommen alle folgenden Verschiebungsmessungen wären in Raum und Zeit bekannt: $\delta(x_i, t_j)$, wobei $i = 1,\ldots,N$; $j = 1,\ldots,M$; *N* und *M* stehen für die Anzahl Messungen in Raum und Zeit; entsprechend wäre x_N der oberste auf der Rutschung gemessene Punkt. An jeder Stelle i werden die Anfangsverschiebungen zum Zeitpunkt t_0 Null gesetzt ($\delta(x_i, 0) = 0$ an jeder Stelle $i = 1,\ldots,N$).

1. Bestimmen der Nullgeschwindigkeits-Grenze $L_{0j} = L_0(t_j)$, für jeden Zeitpunkt $j = 1,\ldots,M$.

2. Für jeden Zeitpunkt $j = 1,\ldots,M$ aufzeichnen der normalisierten gemessenen Verschiebung $y_{i,j} = \delta(x_i,t_j)/\delta(x_N,t_j), \quad i = 1,\ldots,N;$ gegenüber der normalisierten Messstelle $x_i' = (x_i - L_0)/(x_N - L_0)$. Bestimmung des Koeffizienten $k_j = b/a$ durch Anpassen der folgenden Funktion an die aufgezeichneten Werte:

$$y = x' \frac{L_j' - k_j x'}{L_j' - k_j} \tag{5.18}$$

wobei $L_j' = (L - L_{0j})/(x_N - L_{0j})$ für die normalisierte Länge der Hangrutschung steht.

3. Berechnung des maximalen Erddruckzuwachses zum Zeitpunkt *j* mit Hilfe der Faktoren k_j und dem effektiven aktiven Erddruck nach Gleichung 5.12:

$$\overline{p}_j = \frac{2k_j p_a'}{(1-2k_j)(L - L_{0j})} \tag{5.19}$$

4. Berechnung des Parameters $\overline{p}$:

$$\overline{p} = \sum_{j=1}^{M} \overline{p}_j / M \qquad \text{, wobei } \overline{p}_j = \frac{2k_j p_a'}{(1-2k_j)(L - L_{0j})} \tag{5.20}$$

5. Berechnung des Sicherheitsfaktors nach Gleichung 5.11: Falls $F_s > 1$ ist die Stabilität gewährleistet, falls $F_s < 1$ ist die Stabilität nicht gewährleistet.

6. Abwarten des Zeitpunktes t_k bei dem die Nullgeschwindigkeits-Grenze die Wand erreicht $L_{0k} = 0$. Aufzeichnen der normalisierten gemessenen Verschiebungen $w_{i,j} = (\delta(x_i,t_j) - \delta(x_i,t_k))/(\delta(x_i,t_M) - \delta(x_i,t_k))$, für $i = 1,\ldots,N;\ j = k,\ldots,M$ gegenüber t_j. Anpassen der folgenden Funktion an die aufgezeichneten Daten durch Variation von *c*:

$$w = \frac{1 - \exp(-c(t - t_k))}{1 - \exp(-c(t_M - t_k))} \tag{5.21}$$

7. Falls $F_s > 1$, Berechnung der Endverschiebung an jeder Stelle $i = 1,\ldots,N$ mit der Formel:

$$\delta_\infty(x_i) = \delta(x_i,t_k) + \frac{\delta(x_i,t_M) - \delta(x_i,t_k)}{1 - \exp(-c(t_M - t_k))} \tag{5.22}$$

8. Falls $F_s < 1$, Verwendung der TRIVEC Messungen nach Kapitel 5.1.6 zur Berechnung der Erddruckzunahme vor der Wand $\Delta p'_0$ während der Zeitspanne Δt. Anschliessend Berechnung des Versagenszeitpunktes mit der Gleichung 5.14.

5.1.8 Anwendung auf die Rutschung von Combe Chopin

Es soll hier noch einmal festgehalten werden, dass zum Zeitpunkt des Erstellens des Berichtes die Messdaten unvollständig waren und eine klare Aussage erst noch der Vervollständigung der Messdaten gemacht werden kann. Nichts desto trotz wird das in den vorangegangenen Abschnitten vorgestellte Verfahren mit einzelnen Annahmen auf die noch aktive Rutschung von Combe Chopin angewendet.

Die folgenden Parameter für die Rutschung bei Combe Chopin wurden nach Bapst (2002) und Bisetti (2002) verwendet: $H = 5\,\mathrm{m}$, $L = 90\,\mathrm{m}$, $\gamma' = 20 kN/m^3$ and $\alpha = 27^\circ$. Der effektive Reibungswinkel der Höchstscherfestigkeit der sich bewegenden Schicht wurde nach Bisetti (2002) mit $\varphi'_p = 30^\circ$ angenommen. Daraus folgt nach der Gleichung 5.12 für den effektiven aktiven Erddruck $p'_a = 46.32 kN/m^2$ bzw. für den effektiven passiven Erddruck $p'_p = 102.18 kN/m^2$.
Für die Berechnung der Langzeitstabilität wurde die Funktion aus der Gleichung 5.4 in die gemessenen Verschiebungen eingepasst. Ein Beispiel einer solchen Anpassung über $k_j = b/a$ für die gemessenen Verschiebungen im März 2003 sind in Bild 24a dargestellt. Die nun daraus resultierenden Werte für $\bar{p}$ aus der Gleichung 5.13 variieren zwischen 0.13 und 0.97 kN/m^3, woraus sich ein Sicherheitsfaktor zwischen 0.8 und 1.8 berechnen lässt. Um diesen weiten Bereich etwas einzuengen wären weitere Messungen notwendig. Unterdessen werden wir die Annahme von einem Sicherheitsfaktor um 0.9 und dem dazugehörigen $\bar{p} = 0.75 kN/m^3$ weiterverfolgen und den hierfür möglichen Versagenszeitpunkt berechnen.
Der Standort der Nullgeschwindigkeits-Grenze wurde 2002 ca. 5m oberhalb der Bohrpfahlwand lokalisiert. Im Dezember 2005 hatte sie bereits die Bohrpfahlwand erreicht($L_0 = 0$) wie die Messungen mit der TRIVEC Sonde gezeigt haben (Bild 24b). Die Messungen zeigen eine deutliche Änderung der Verschiebungsrichtung nach dem Dezember 2005 (Bild 24b).
Mit der Annahme einer linearen Abnahme der Distanz der Nullgeschwindigkeits-Grenze L_0 zur Wand, lässt sich für den Zeitraum Juni 2005 bis Dezember 2005 $\Delta L_0 = 0.697\,\mathrm{m}$ berechnen, womit aus Gleichung 5.15 eine Druckänderung von $\Delta p'_0 = 11.62\,\mathrm{kN/m^2}$ erfolgt. Zur selben Zeit betrug die mittlere Wandverschiebung $\Delta\delta_0 = 0.285\,\mathrm{mm}$. Setzt man diese Angabe in die Gleichung 5.17 ein ergibt sich eine Wandsteifigkeit von $K = 40.85\,\mathrm{MN/m^3}$.

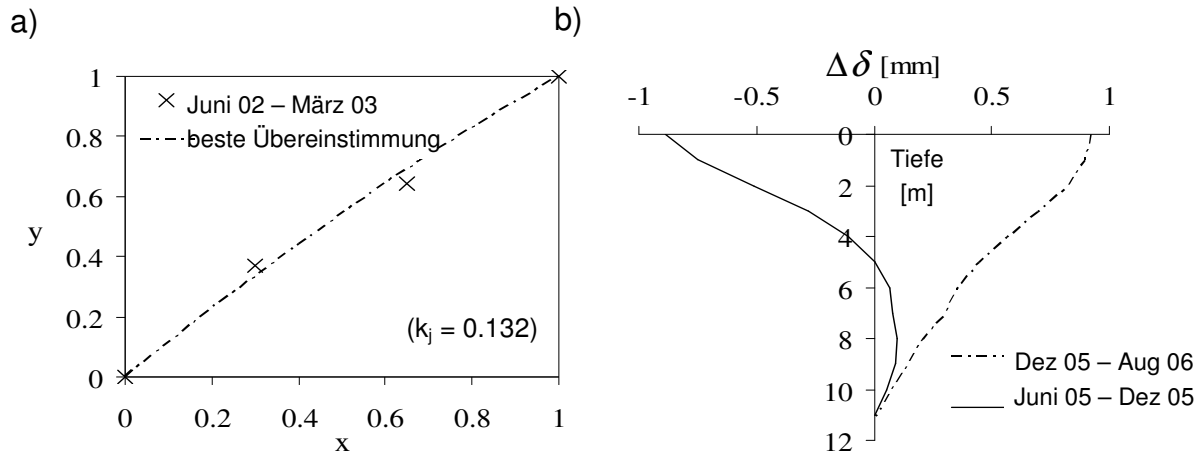

Bild 24: a) Kurvenanpassung im Raum der gemessenen Verschiebungen bei Combe Chopin nach der Gleichung 5.4. b) Änderung der Wandverschiebungen der Bohrpfahlwand bei Combe Chopin mit Hilfe von TRIVEC Messungen durch die Firma Solexperts.

Die mittleren Verschiebungen der Wand betrugen zwischen Dezember 2005 und August 2006 0.674mm zusammen mit der vorgängig berechneten Wandsteifigkeit ergibt sich eine Erddruckzunahme vor der Wand von $\Delta p'_0 = 27.54\,\mathrm{kPa}$ in einem Zeitraum von 230 Tagen. Für den Koeffizient von *c* in der Gleichung 5.14 nehmen wir $c = 1\times10^{-3}\ \mathrm{Tagen}^{-1}$ an, was es durch weitere Messungen noch zu überprüfen gilt. Werden nun all diese Werte zusammen mit einem Sicherheitsfaktor von $F_s = 0.9$ in die Gleichung 5.14 eingesetzt, ergibt sich ein Versagenszeitpunkt um den Herbst 2012. Das Versagen in der Form vom „Überfliessen" der Bohrpfahlwand stellt jedoch kein Problem für das Bauwerk dar, da schon während der Planungsphase an ein mögliches Versagen in dieser Form gedacht wurde.

5.1.9 Zusammenfassung Combe Chopin

Wird versucht eine aktive Hangrutschung mit Hilfe einer verankerten Wand zu stabilisiert und ist der durch die vorgespannten Anker auf den Boden vor der Wand aufgebrachten Erddruck grösser als der vorgängig vorhandene, ist es möglich, dass sich die Wand Hang aufwärts bewegt. Dies könnte nun zum Schluss verleiten, dass mit Hilfe der Wand der gesamte Hang stabilisiert wurde. In Wirklichkeit können die Bewegungen der Wand Hang aufwärts nur von temporärem Charakter sein und sich die Richtung der Bewegung im Verlauf der Zeit ändern, womit auch der Erddruck vor der Wand wieder zunimmt. Dies kann zu einem passiven Versagens des Bodens vor der Wand führen, was sich in einem „Überfliessen" der Wand bemerkbar macht. Das hier vorgestellte Verfahren mit Hilfe von geodätischen und TRIVEC Messungen erlaubt eine Abschätzung eines solchen Versagens schon zu einem früheren Zeitpunkt. Die aktive Rutschung bei Combe Chopin wurde hier vor allem zur Illustration des Problems benutzt, da eine definitive Aussage in diesem Fall noch nicht möglich ist. Zusätzliche Messungen sollen hier Abhilfe schaffen.

5.2 Berisal-Ganter (VS)

Die markante Ganterbrücke, die den Ganterbach überspannt, gehört zu der Simplonnordrampe und verbindet die Schweiz via Simplonpass mit Italien.

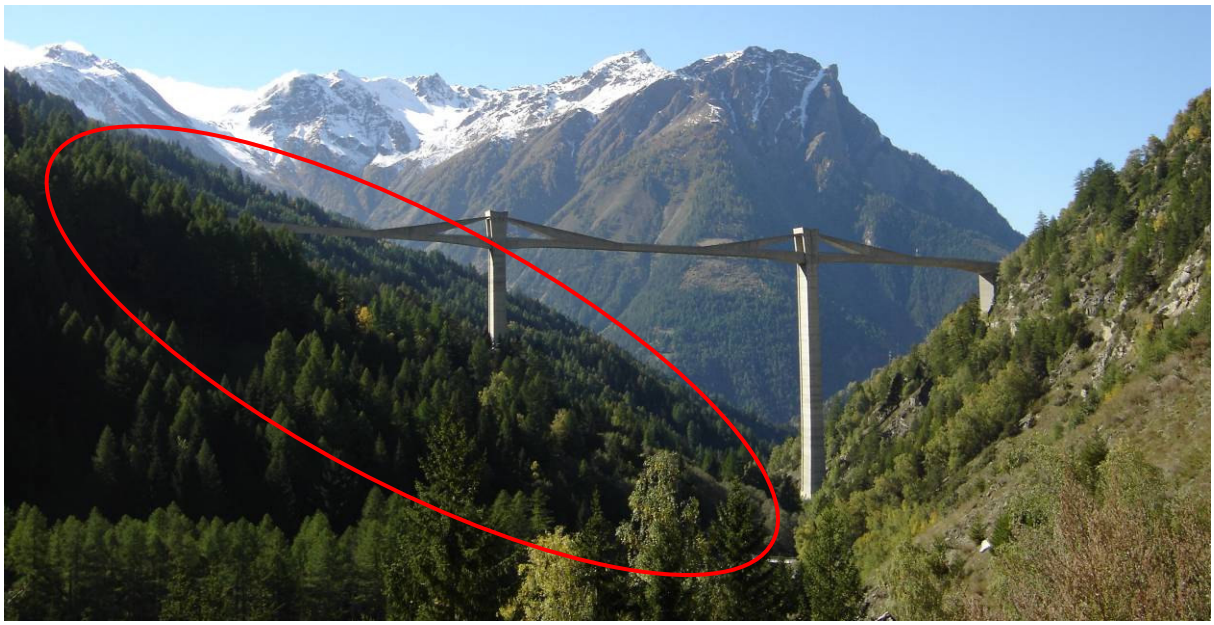

Bild 25: Kriechhang am linken Ufer des Ganterbaches (Blickrichtung Westen)

Schon die ersten geologischen und geotechnischen Abklärungen für das Variantenstudium in den Jahren 1966 bis 1970 durch Lang und Schärer (1970) zeigten, dass sich das Gebiet südlich des Ganterbaches (Bild 25) bewegt. Um diesen Teil des Hanges nicht zusätzlich zu belasten, wurden die Pfeiler in Schächte gestellt. Dies geschah einerseits, um einen Massenausgleich zu schaffen, in dem der Aushub der Schächte genau so viel betragen sollte, wie die Kraft, die später wieder durch die Stützen in den Boden abgeleitet wird. Andererseits sollten die Schächte die Pfeiler vom Kriechhang abschirmen und eine Möglichkeit bieten, die Pfeiler bei zu grossen Verschiebungen wieder nachstellen zu können. Die Schächte sind im Kriechhang nicht speziell verankert, sondern bewegen sich mit dem Hang. Dies war nötig, da sich ansonsten an den Schächten ein so grosser Druck entwickelt hätte, den diese nicht im Stande gewesen wären aufzunehmen.

Da es unausweichlich war das Bauwerk auf dem sich bewegenden Hang zu fundieren, stellt sich hier die Frage des Verschiebungsverlaufs mit der Zeit. Weiter soll ebenfalls die Frage eines möglichen passiven Versagens im Bereich der Kompressionszone (Ganterbach) abgeklärt werden. Um diese Fragen genauer zu errörter wurden im Sommer Sondierbohrungen (Bild 26a und 26b) im Bereich der Kompressionszone abgeteuft. Mit Hilfe von Inklinometerrohren sollen in diesem Bereich die eher gering ausfallenden Verschiebungen gemessen werden. Der eigentliche Grund des Einbaus von Inklinometerrohren stellt die Erddruckmessung und dessen Verlauf mit der Zeit im Bereich der Kompressionszone mit Hilfe des IDM's dar (Siehe Kapitel 3.1).

Bild 26: a) und b) Bohrung an der gegenüberliegenden Seite des Pfeilers 3 der Ganterbrücke

Durch die neuen Messdaten soll ein analytisches und numerisches Modell zur Berechnung der Langzeitstabilität und dem Verlauf der Verschiebungen mit der Zeit erstellt werden.

5.3 Braunwald

Oberhalb der Gemeinden Linthal und Rüti im Kanton Glarus befindet sich die hoch gelegene Sonnenterrasse von Braunwald (Bild 27). Das gesamte Gemeinde Gebiet ist autofrei und eine Standseilbahn verbindet die Terrasse, die sich zwischen 1200 und 1700 m ü. M. befindet, mit dem Tal.

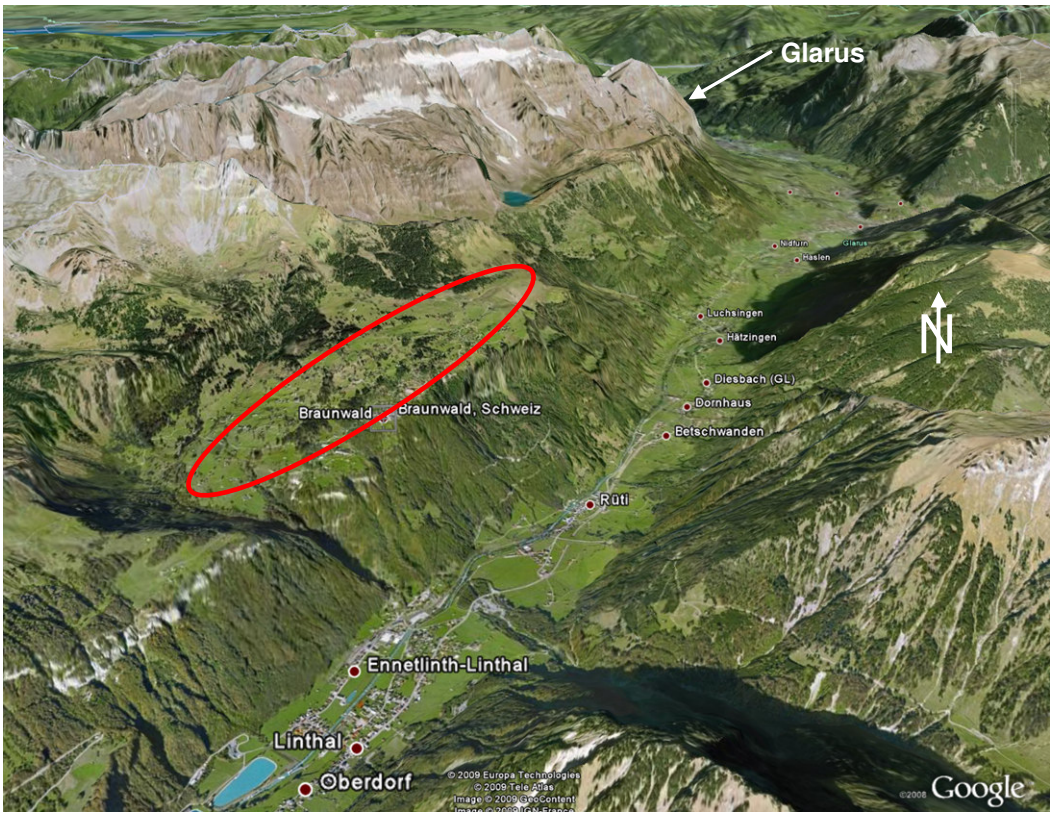

Bild 27: Lage von Braunwald (Internet 2009)

Die sich langsam bewegende Terrasse, abgesehen von einzelnen Abbrüchen an der Kante, stellt noch nicht eine unmittelbare Gefahr für die Gemeinde Braunwald und die unterhalb liegenden Gemeinden dar, da die Situation schon seit längerem bekannt ist und die Verschiebungsgeschwindigkeiten im Grossen und Ganzen über die Jahre konstant waren. Das hauptsächliche Problem stellt jedoch die Gebrauchstauglichkeit und die teilweise Zerstörung sensitiver Infrastruktur und die intensive Überbauung des Gebietes dar. So ergeben sich zum Beispiel Probleme bei der Braunwaldbahn, bei den Wasserleitungen und bei der Kanalisation.
Falls diese Hangbewegungen gestoppt werden könnten, würden kostspielige Instandsetzungsarbeiten der Vergangenheit angehören. Gemäss Dr. von Moos AG (2003) beträgt der jährliche Sachschaden durch die Hangbewegungen rund eine Million CHF.
Um einen kurzen Überblick über die Geschichte und die bereits getätigten Arbeiten im Gebiet Braunwald zu geben wird hier ein Abriss der neueren Geschichte nach Gallusser (1981) wiedergegeben:

Bereits 1932 mussten bei der Bergstation der Braunwaldbahn, wie auch in einzelnen Dorfteilen, grössere Sanierungsmassnahmen getroffen werden. Diese Massnahmen bestanden aus der Erstellung von Entwässerungsstollen. Bei der Neuvermessung 1954 wurde bei den Triangulationspunkten aus dem Jahr 1925 festgestellt, dass sich die ganze Terrasse von Braunwald talwärts bewegt hatte. Darauf wurde im Jahre 1954 aufgrund weiterer Geländebewegungen von politischer Seite der Wunsch geäussert, die Entwässerungskorporation Braunwald zu gründen. Ein Sanierungsprojekt, das eine grossflächig angelegte Oberflächenentwässerung vorsah, wurde 1971 nicht ausgeführt, da die Niederschlagsmengen zu gross und

der Boden in vielen Gebieten zu durchlässig für eine effiziente Oberflächenentwässerung gewesen wäre. Bei einer grossen Rutschung, die sich 1979 ereignete, stürzten einige Tausend Kubikmeter Erdmasse ins Tal. Seit den 80er Jahren sind Untersuchungen betreffend der Hangstabilität und dem Kriechverhalten von Braunwald am Laufen.

Die detaillierte geologische Beschreibung des Gebietes bei Braunwald kann Schindler (1982) entnommen werden. In einer vereinfachten Betrachtungsweise kann die Geologie in eine flach geschliffene Felsoberfläche mit darüber liegender hart gelagerten und unverrutschten Grundmoräne und das ganze überlagert von einer Rutschmasse gegliedert werden. Hierbei liegt der Rutschhorizont nicht im Übergang von Fels zu Lockergesteinsmasse, sondern innerhalb der Schuttmasse selber. Der Rutschhorizont besteht aus einem so genannten „Blue Clay“, einem Ton der aus der Verwitterung der anstehenden Gesteinsmasse entstanden ist.

In den Bilder 27 und 28a ist das steile Felsbord unterhalb Braunwald mit vielen Bachläufen erkennbar. Das Rutschgebiet lässt sich durch folgende Grössen charakterisieren:

- Länge: 500 – 1500m
- Breite: rund 2000m
- Fläche: rund 3km^2
- Mittlere Neigung 12-13° (Hang aufwärts abflachend)
- Lage Rutschhorizont ab OKT 15-40 m (+)
  (Bergseitig zunehmende Rutschmasse)
- Boden im Rutschhorizont Blue Clay

Aufgrund der beobachteten Verschiebungen kann eine Einteilung gemäss Schindler (1982) in drei Bereiche gemacht werden (Bild 28a):

Der unterste Bereich im Steilbord mit einer Länge von rund 200 m zeigt die höchsten Bewegungsgeschwindigkeiten (mit Extremwerten über 10 cm/Jahr). Oberhalb von diesem Bereich liegt ein Gebiet mit mittleren Geschwindigkeiten (2 – 6 cm/Jahr mit wenigen schnelleren Phasen), gefolgt vom obersten Bereich mit den niedrigsten Geschwindigkeiten (bis 2 cm/Jahr).
Diese Abfolge von Bereichen unterschiedlicher Geschwindigkeiten kann mit der nach oben gewölbten Basisgleitfläche erklärt werden. Durch diese Form ist die Neigung am talseitigen Ende mit Abbruchbord der Rutschung grösser als bergseitig.

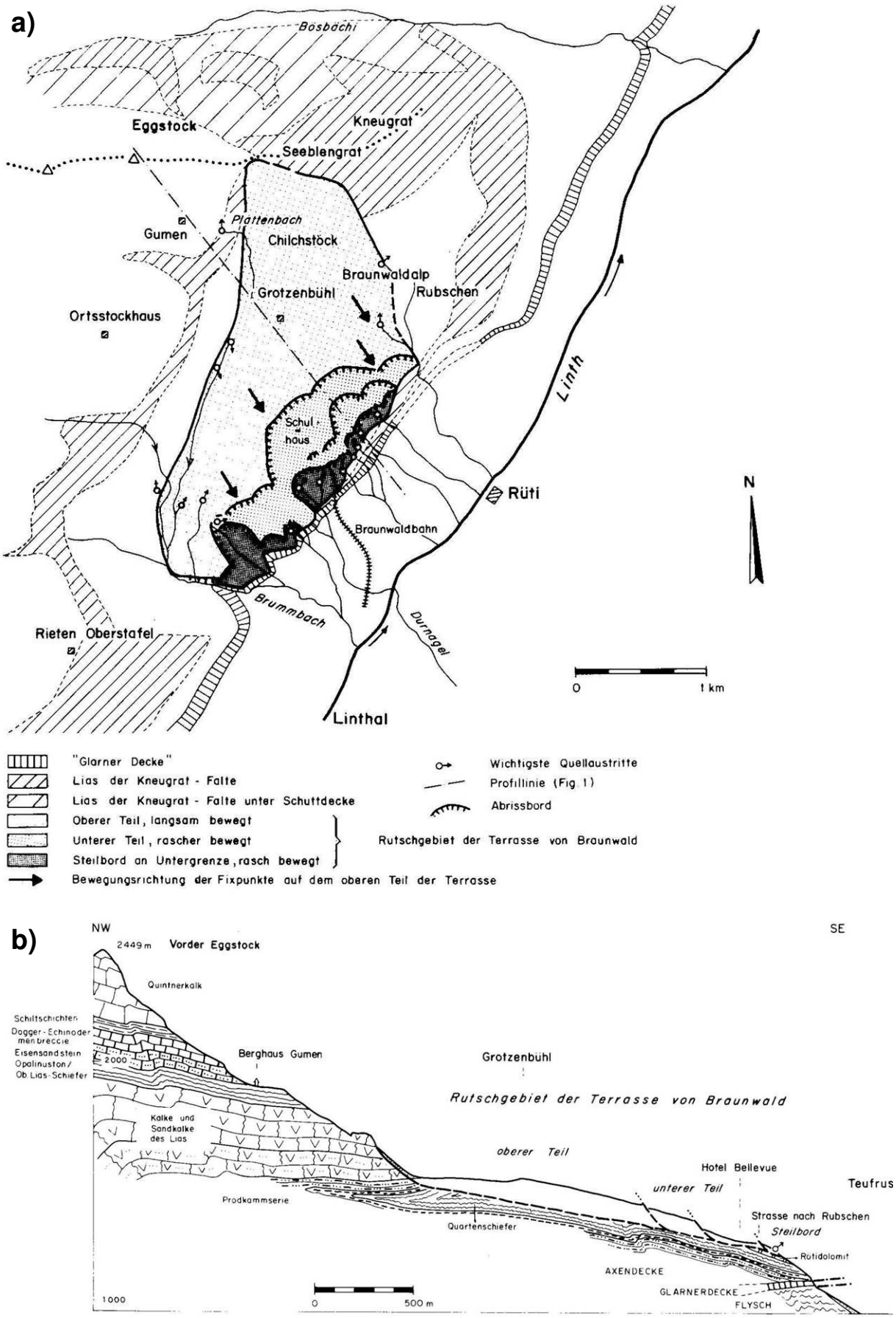

Bild 28: a) und b) Schematische Darstellung des Rutschgebiets und Geologisches Querprofil Braunwald, nicht überhöht (Schindler, 1982)

Zur Erkundung der Geologie und um Bodenproben für Laborversuche zu entnehmen wurden insgesamt 34 Bohrungen im Kerngebiet von Braunwald abgetäuft, zusätzlich wurden Inklinometer und Piezometer eingebaut: 1980 wurden 6 Bohrungen, 1982 in einer grossen Kampagne 10 Bohrungen, 1983 3 Bohrungen, 1985 2 Bohrungen (zusätzlich Installation eines Tiefentwässerungssystems) und 2002 in einer zweiten grossen Kampagne 13 Bohrungen durchgeführt. Bergseitig im oberen Teil der Rutschung ausserhalb des Siedlungsgebiets wurden keine Messinstrumente installiert.

In einem Sanierungsprojekt wurde 1985 im Dorfbereich Grantenboden das bereits erwähnte Tiefentwässerungssystem von rund 200m Länge eingerichtet. Zu diesem Bauwerk gehört auch der Hauptschacht Grantenboden, der den Verschiebungen des Hanges nicht standhalten konnte. Dies äusserte sich im Bruch von Versteifungsringen, so wie einer Kombination von Schub- und Biegerissen in den Pfählen (Dr. Von Moos AG, 2003). Ebenfalls die Pressstollen, die das Wasser zum Hauptschacht leiten, haben in einigen Abschnitten starke Schäden erlitten und wurden im Oktober und Dezember 2002 mit Stahlringen gesichert (Dr. Von Moos AG, 2003). Dieses Beispiel zeigt deutlich, dass Massnahmen mit steifen Konstruktionen, die durch den Rutschhorizont hindurch führen, über kurz oder lang abgeschert und beschädigt werden.

5.3.1 Durchgeführte Versuche

Im Rahmen der Untersuchung des Kriechhanges von Braunwald wurden und werden noch zahlreiche Laborversuche an Bodenproben durchgeführt. Zur Illustration werden im Folgenden Resultate der Probe 2 gezeigt.

Die Probe 2 wurde in einer Tiefe von rund 13 m ab OKT aus dem Hauptschacht entnommen. Aufgrund der Lage der versteifenden Betonringe des Hauptschachts musste für die Entnahme schräg nach oben gebohrt werden.

Bild 29: Ausgestossene Probe 2 (Villiger, 2008)

Die Probe wurde bis zur ihrer Verwendung verschlossen im Klimaschrank des IGT ETH Zürich gelagert. Die ausgestossene Probe ist in Bild 29 zu sehen.
Das Probenmaterial ist grösstenteils sehr dunkel und weist einige, vor allem im hinteren Bereich bräunlich verfärbte Stellen auf. Es kann sein, dass durch die schräge Bohrung aus der „Blue Clay“ Schicht heraus

oder zumindest in eine Übergangsschicht hinein gebohrt wurde. Der verfärbte Teil wurde für die durchgeführten Ringscherversuche nicht verwendet.
Der Wassergehalt der ausgestossenen Probe liegt bei knapp 9%. Die Resultate aus Sieb- und Schlämmanalyse sind in Bild 30 dargestellt. Der grobe Fraktionsanteil ist ziemlich dominant.

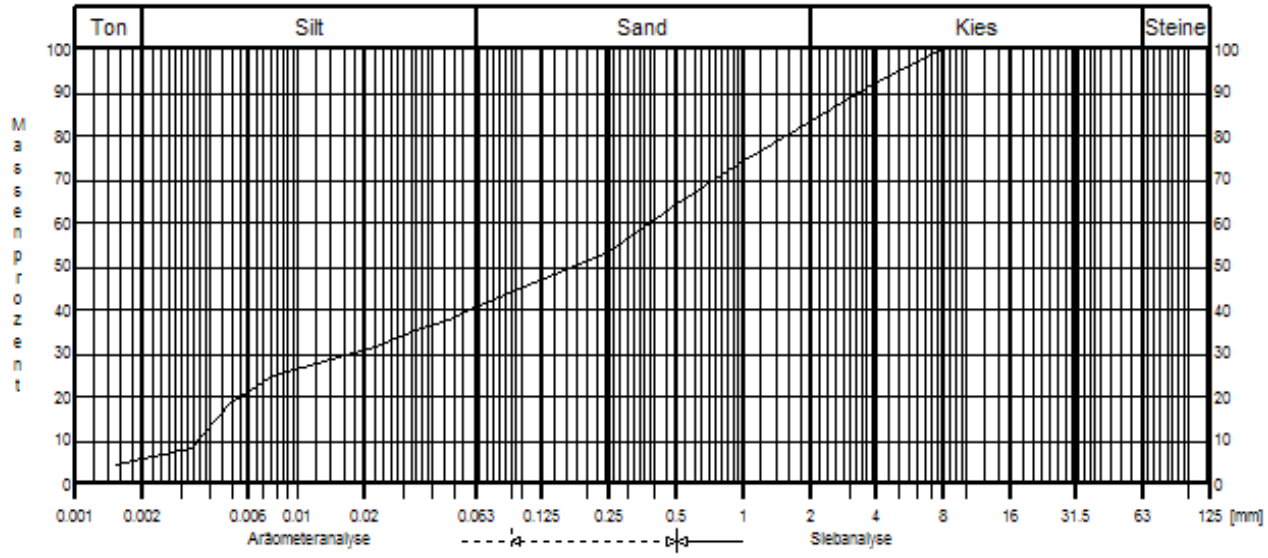

Bild 30: Korngrössenverteilung der Probe 2 als Summationskurve

Die Probe 2 wurde einem totalen Scherweg von 66 mm ausgesetzt, welcher sich auf 32 mm bei 100 kN/m^2 und 34 mm bei 200 kN/m^2 aufteilt.
Wie bei einer normal konsolidierten Probe erwartet sind die Setzungen bei 100 kN/m^2 Belastung zu Versuchsbeginn grösser und flachen ab bis ein konstanter Wert erreicht wird. Bei 200 kN/m^2 zeigen die Setzungen dasselbe Bild wie in den anderen Versuchen. Zu Beginn des Versuches verhalten sie sich wie zu erwarten, werden anschliessend aber nicht konstant sondern nehmen weiter zu. Die gemessenen Kräfte am Boden sind im Gegensatz zu 100 kN/m^2 in der Summe relativ konstant. Die Schwankungen in den einzelnen Kraftmessdosen können auf die Unebenheit der Probe zurückgeführt werden.

Der Einfluss der Geschwindigkeit und der Normalspannung kann durch zwei Graphen mit Gruppen jeweils gleicher Geschwindigkeiten resp. gleicher Normalspannungen aufgezeigt werden. In Bild 31 und Bild 32 sind diese beiden Darstellungen zu sehen.

Aus Bild 31 ist ersichtlich, dass die Geschwindigkeit einen geringen Einfluss auf die Scherspannung hat, da die Neigung der Trendlinien unterschiedlich verlaufen. Es ist zu beachten, dass die Steigung der Trendlinie bei 0.01 mm/min einen grösseren Wert zeigt als bei 0.05 mm/min. Dies kann einerseits darauf zurückgeführt werden, dass die verschiedenen Geschwindigkeiten in denselben Versuchen gefahren werden und dementsprechend die Scherfläche nicht bei jeder Geschwindigkeit gleich ausgebildet ist. Andererseits kann die Geschwindigkeit von 0.05 mm/min bei gering durchlässigen Böden schon ausreichen, um Porenwasserüberdrücke in der Scherfuge auszubilden, was ebenfalls zu einer Abnahme des Scherwiderstandes führen würde.

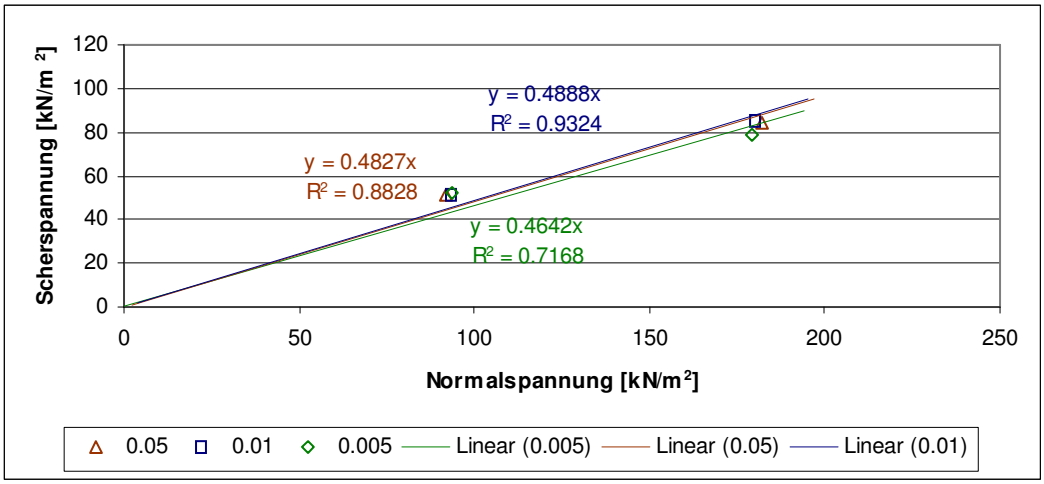

Bild 31: σ – τ Diagramm für Gruppen gleicher Geschwindigkeit [mm/min], Probe 2 (Villiger, 2008)

In Bild 32 hingegen ist kein klar erkennbarer Trend eines Einflusses der Schergeschwindigkeit auf die Scherspannung zu erkennen. Da die beiden Gruppen in unterschiedlichen μ-Werten zu liegen kommen, ist ein Einfluss der Normalspannung nicht auszuschliessen. Die Werte bei 200 kN/m^2 Normalspannung liegen tiefer als diejenigen bei 100 kN/m^2. Dies könnte dadurch erklärt werden, dass die Probe bei 200 kN/m^2 bereits einen grösseren totalen Scherweg zurückgelegt hat als bei 100 kN/m^2 und der Scherwiderstand am Sinken war, jedoch noch nicht den residualen Endwert erreichte. Dies hat nur dann einen Einfluss, wenn durch die langen Scherwege, sowie die mechanische Beanspruchung der Probe durch das Abscheren einzelne grössere Partikel zerbrochen werden. Um dies genauer zu untersuchen wurden Versuche an Proben, bei denen die Fraktionen grösser als 2 mm entfernt wurden, durchgeführt.

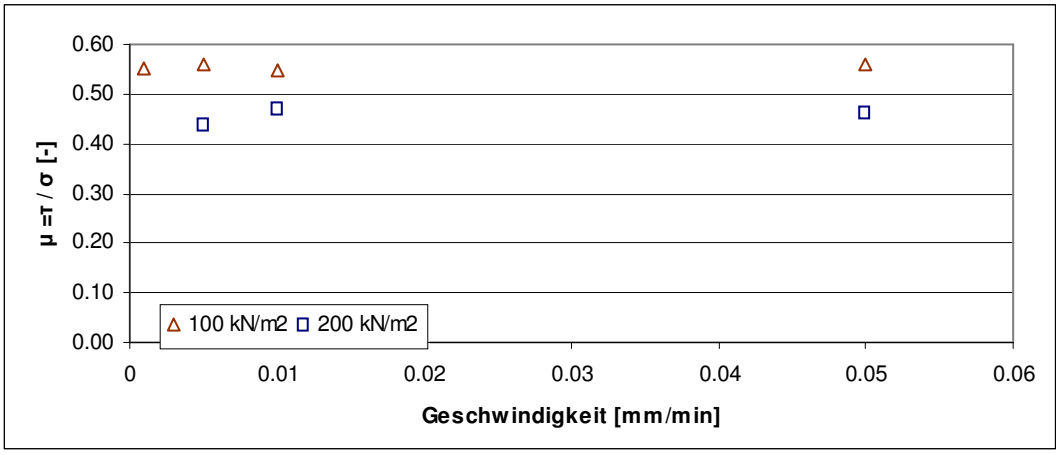

Bild 32: μ –v Diagramm für Gruppen gleicher Normalspannung, Probe 2 (Villiger, 2008)

Aus den Steigungen der Trendlinien in Bild 31 kann ein Reibungswinkel im Bereich von 25° bestimmt werden.
Als Vergleichswert für den residualen Scherwinkel liegt aus Rageth (1987) ein Winkel von 13° - 14° vor. Dieser Wertebereich ist mit Vorsicht zu betrachten, da einerseits die Abschergeschwindigkeit der Versuche unbekannt ist und andererseits der maximale Scherwinkel zu rund 20° bestimmt wurde. Ungewiss ist ebenfalls, wie die Probe aufbereitet wurde.
Der grosse Unterschied der Scherwinkel kann einerseits durch die ziemlich kurzen Scherwege und andererseits durch den Einfluss der groben Fraktion erklärt werden.

Versuche an ausgesiebten Proben

Die Versuche der ausgesiebten Fraktion wurden wie die vorherigen Versuche bei 100 kN/m^2 und 200 kN/m^2 aufgebrachter Normalspannung, jedoch nur noch bei den Geschwindigkeiten 0.01mm/min und 0.05mm/min durchgeführt. Aus Zeitgründen musste die geringste Geschwindigkeit von 0.005mm/min weggelassen werden.

Der total zurückgelegte Scherweg beträgt 264 mm, welcher sich auf 131 mm bei 100kN/m^2 und 133 mm bei 200 kN/m^2 aufteilt. Diese Wege sind einiges länger als bei den Versuchen bei den nicht ausgesiebten Proben. Dementsprechend konnte beim Ausbau der Probe eine eindeutig ausgebildete Scherfläche auf der Höhe des Ringspaltes des Probenbehälters gefunden werden (Bild 33).

Bei 100 kN/m^2 Belastung ist das Verhalten der Probe bis rund 40 mm wie zu erwarten. Die gemessenen Setzungen verhalten sich wie bei einer normal konsolidierten Probe. Bei zunehmendem Scherweg werden diese aber wieder grösser und auch die Normalspannungen wie die Scherspannungen nehmen zu. Bei 200 kN/m^2 können die Setzungen beinahe an den Setzungsverlauf bei 100 kN/m^2 angehängt werden. Nach rund 100 mm Scherweg bei der grösseren Belastung (200kN/m^2) werden die Setzungen konstant. Die Bodenkraft nimmt mit zunehmendem Scherweg etwas zu und wird zum Schluss konstant. Die Scherspannungen sind stetig am Fallen und würden bei der Fortsetzung des Versuches noch weiter sinken.

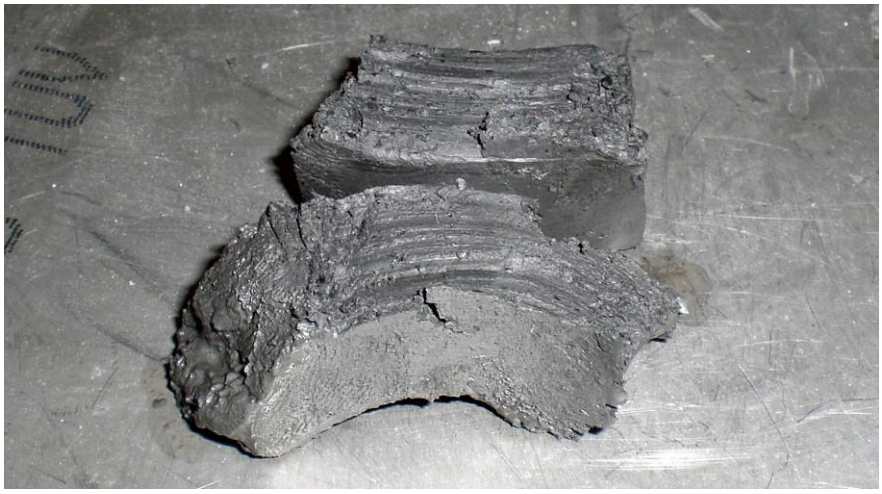

Bild 33: Deutlich ausgebildete Scherfläche, Probe 2 < 2mm (Villiger, 2008)

Die Steigungen der Trendlinien in Bild 34 liegen gegenüber den Versuchen an der nicht ausgesiebten Probe rund 30% tiefer. Dies liegt einerseits am viel längeren Scherweg, der in diesem Versuch zurückgelegt wurde und andererseits am Aussieben der Fraktion > 2 mm. Wie gross der Einfluss der einzelnen Ursachen ist, kann hierbei leider nicht geklärt werden. Aus der Steigung der Trendlinien in Bild 34 kann ein Scherwinkel im Bereich von 20° bestimmt werden. Dieser Wert ist gleich gross wie der maximalen Scherwinkel in den Versuchen von Rageth (1987). Wie bereits erwähnt, zeigen die gemessenen Werte einen deutlichen Trend zu geringeren Scherspannungen. Das bedeutet, dass der residuale Zustand im Versuch noch nicht erreicht wurde. Weitere Versuche an den Proben aus Braunwald und Verbesserungen am Ringschergerät sind geplant und wurden teilweise bereits durchgeführt.

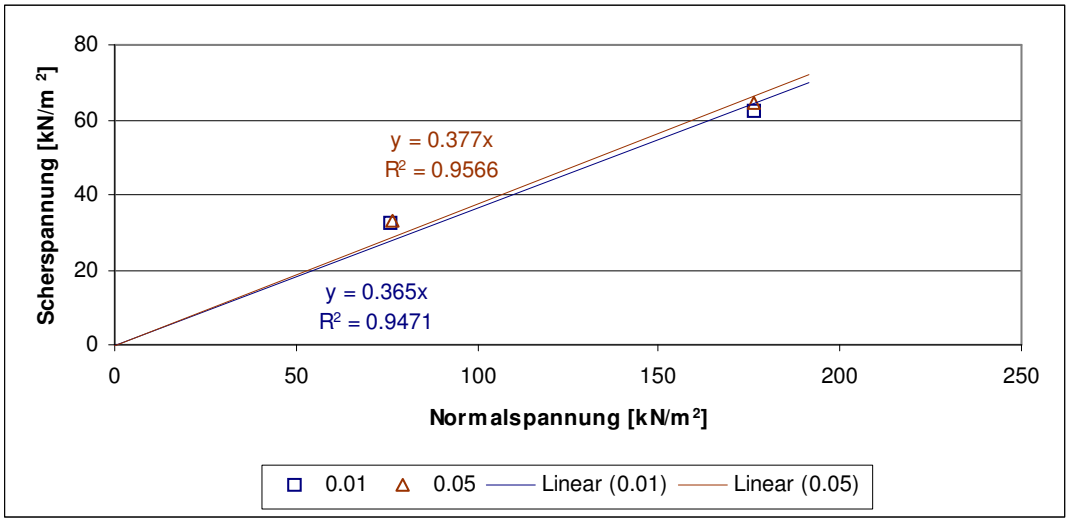

Bild 34: σ – τ Diagramm für Gruppen gleicher Geschwindigkeit, Probe 2 < 2mm (nach Villiger, 2008)

In Bild 34 ist wie bei der unausgesiebter Probe 2 durch die grössere Steigung der Trendlinie bei höherer Geschwindigkeit ein Einfluss der Geschwindigkeit auf die Scherspannung zu erkennen. Dieser Einfluss ist in Bild 35 in den zwei Gruppen kaum erkennbar. Hingegen ist wieder ein Einfluss der Normalspannung ersichtlich, da die beiden Gruppen nicht dieselben μ-Werte zeigen. Folglich ist fraglich, ob nicht auch die Normalspannung einen Einfluss auf den viskosen Teil ausübt. Dies bedeutet, dass der viskose Anteil der Scherspannung ebenfalls spannungsabhängig ist.

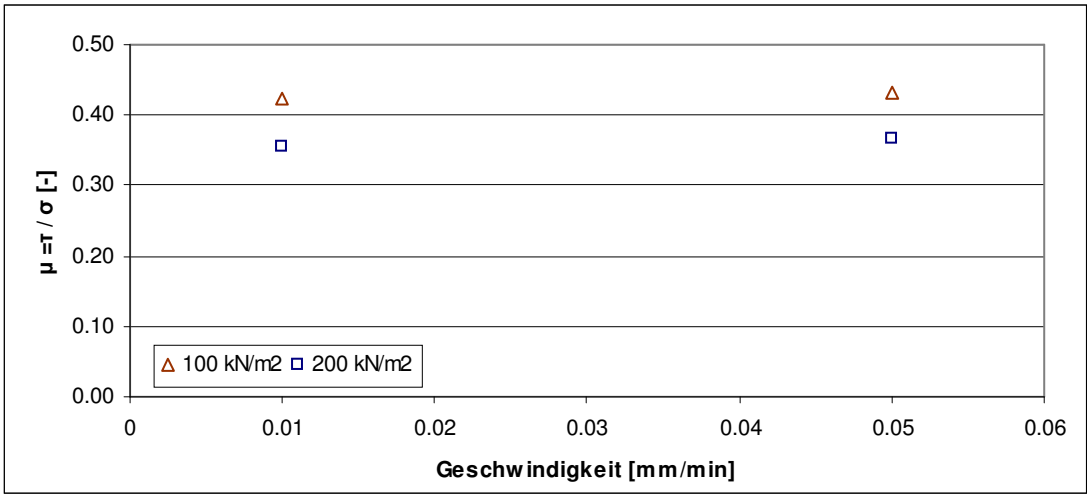

Bild 35: μ – v Diagramm, Probe 2 < 2 mm (Villiger, 2008)

Vergleich der Resultate aus den nicht ausgesiebten und ausgesiebten Versuchen

Werden die Resultate der Versuche an der ausgesiebten Probe und der nicht ausgesiebten Probe verglichen, fallen die deutlich geringeren Scherspannungen der ausgesiebten Probe auf. Zudem ist das Setzungsverhalten der nicht ausgesiebten Probe ungleichmässig, was auf den groben Fraktionsanteil zurückgeführt werden kann.

Weitere Versuchsresultate und Überlegungen zur Auswertung der Versuche können der Projektarbeit von Villiger (2008) „Versuche mit dem neuen Ringschergerät und Anwendung der Versuchsresultate“

entnommen werden. Desweitern sind Versuche an mechanisch aufbereiteten Probe, was einem unendlichen Scherweg entsprechen soll, geplant.

5.3.2 Rückrechnung der Stabilität

Um Sanierungsvorschläge auszuarbeiten und deren Effektivität zu überprüfen sind Bodenparameter eine unerlässliche Grösse. Da die Bodenparameter jedoch nicht zuverlässig nur aus einzelnen Proben gewonnen werden können, wird folgendes Vorgehen mit Hilfe einer Rückrechnung zur Bestimmung der Bodenparameter vorgeschlagen. Die so gewonnen Bodenparameter sollen anschliessend mit den durch Laborversuche bestimmten Werten verglichen werden.

Rückrechnung von Bodenparametern aus Feldmessungen

Bei den FE-Stabilitätsberechnungen werden die in Labor- und Feldversuchen bestimmten Bodenparameter verwendet. Die Schwierigkeit liegt in der unterschiedlichen Deformationsgeschwindigkeit der Versuche und der Wirklichkeit. Die Versuche werden bis 100-mal schneller als die tatsächlichen Kriechgeschwindigkeiten (1 - 10 cm pro Jahr) durchgeführt. Deswegen wäre es vorteilhaft diese Parameter durch eine Rückrechnung von tatsächlichen Kriechbewegungen zu überprüfen. Dazu wird der gesamte Hang als eine Art Dehnmessstreifen betrachtet (Bild 36a), so lassen sich folgende Parameter zurückrechnen (Bild 36b): die Steifigkeit der kriechenden Schicht *E* und der Reibungswinkel der Scherfläche φ'. Hierfür sind nicht nur Inklinometermessungen, Piezometermessungen und geodätische Messungen nötig, sondern auch die Messungen von Erddruckänderungen Δp. Diese Erddruckänderungen zu messen ist jedoch schwierig, neue Sensortechnologien können hier aber hilfreich sein.

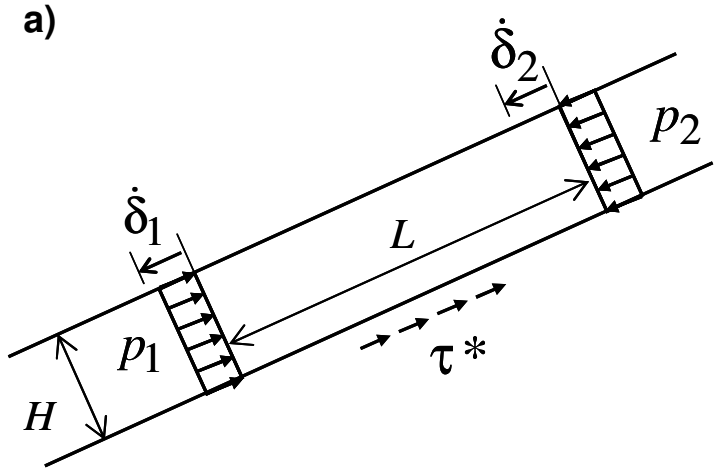

b) Scherfestigkeit:

$$\Delta\tau^* = \frac{H}{L}\left(\Delta p_2 - \Delta p_1\right)$$

$$\tan\varphi'_r = -\frac{\Delta\tau^*}{\Delta u}$$

Steifigkeit:

$$E = \frac{\Delta p}{\Delta\varepsilon} \qquad \Delta\varepsilon = \frac{\dot{\delta}_2\Delta t - \dot{\delta}_1\Delta t}{L}$$

$$\Delta p = \frac{\Delta p_2 + \Delta p_1}{2}$$

Bild 36: a) Model zur Rückrechnung von Bodenparametern, b) Berechnung der Bodenparameter

Dieses System zur Rückrechnung von Bodenparametern soll im Bereich von Braunwald eingesetzt und mit Bodenparametern aus konventionellen Laborversuchen verglichen werden. Anschliessend soll mit Hilfe von Modellen die Wirksamkeit von Drainagen im Gebiet Braunwald abgeklärt und nötigenfalls optimiert werden.

Ein erster Ansatz solch einer kombinierten Betrachtung der Feldversuche und Laborversuchen wurde ebenfalls im Rahmen der Projektarbeit von Villiger (2008) für den Fall Braunwald angewendet. Dabei zeigte

sich jedoch, dass einige Daten, wie die Piezometermessungen der letzten Jahrzehnte, verschwunden sind und durch neue Messungen und Messsysteme zu ersetzten bzw. zu ergänzen sind. Dies ist bereits geschehen, wobei diese Daten für weitere Überlegungen beigezogen werden sollen.

6 Empfehlungen: Strasse-Kriechhang Interaktion

Wird versucht eine aktive Rutschung durch eine künstliche Barriere aufzuhalten, so ist die Möglichkeit des passiven Versagens des Erdkeils vor der Wand zu überprüfen und die Wand auf das „Überfliessen“ zu dimensionieren, wie dies bereits beim Beispiel Combe Chopin geschehen ist. Des Weiteren soll mit Hilfe von Rückrechnungen der Verschiebungen die Bodenparameter berechnet werden, um den möglichen Versagenszeitpunkt voraussagen zu können. Weiter ist der Einfluss von Extremereignissen (Starkregen, Erdbeben, usw.) auf den Hang abzuschätzen. Kann ein Überfliessen der Wand nicht ausgeschlossen werden, so ist ein genügend grosser Abstand zwischen der rückhaltenden Wand und dem zu schützenden Bauwerk vorzusehen. Dabei muss auch an die Möglichkeit der Räumung nach einem Ereignis gedacht werden.

Das Erstellen von Bauwerken in aktiven Rutschungen stellt eine grosse Herausforderung dar. Hierbei steht nicht nur der Bau sonder auch die Überwachung des Bauwerks nach dessen Fertigstellung im Vordergrund. Dabei kann die neue Technologie der Messung von Dehnungen in Glasfaserkabeln, die in Strassen eingebaut werden, helfen. Zum Ersten kann damit die Gebrauchstauglichkeit festgestellt werden, und zum Zweiten liefern die Glasfaserkabel weitere Daten um die Verschiebungen des Hanges und somit die Lebensdauer der Strasse vorauszusagen. Sei dies nun bei gleichbleibenden Einflüssen oder selten auftretenden Ereignissen.

Ein bis anhin eher nachlässig behandeltes Szenario stellt das passive Versagen des Hanges in seiner Kompressionszone dar, womit die Stützung am Fuss des Hanges teilweise wegfällt und die Verschiebungsgeschwindigkeiten rasch ansteigen können. Dies führt zu einer akuten Gefährdung aller Bauten auf und unterhalb des Hanges. Zur Überprüfung des jetzigen Zustandes und für Voraussagen der Druckentwicklung in dieser Zone ist eine Erddruckmessung unerlässlich. In diesem Punkt soll das neue Inclinodeformometer Abhilfe schaffen.

7 Danksagung

Die Autoren möchten an dieser Stelle den zahlreichen Helfern, die an diesem Forschungsprogramm teilgenommen haben, danken: den Studenten Pascal Minder, Damian Senn, und Sebastian Villiger; den Doktoranden Dominik Hauswirth, Michael Iten, Erich Saurer, Markus Schwager und Rolf Zumsteg; den wissenschaftlichen Mitarbeitern Dr. Markus Caprez, Dr. Sophie Messerklinger, Dr. Jacqueline Tront und Dr. Michael Plötze; den Mitarbeitern der Werkstatt und dem Laboranten ohne deren Hilfe eine Umsetzung der noch so „verrücktesten“ Ideen erst gar nicht möglich wäre: Ernst Bleiker, Heinz Buschor, Fredy Ehrbar, René Rohr und Adrian Zweidler.

Des Weiteren geht ein grosser Dank an die Gemeinde von St. Moritz und insbesondere Herrn Pietro Baracchi für die freundliche Unterstützung während der verschiedenen Messprogramme.

Die Forschung wurde hauptsächlich durch den VSS/ASTRA Fond "Strasse-Erdrutsch Interaktion" unterstützt, wobei der Teil der Bestimmung der Grenzen mit Hilfe von Glasfaserkabeln durch ein KTI-Projekt zwischen der ETH Zürich, Omnisens und Brugg Cables getragen wurde.

8 Literatur

Akbar, A. and Clark, B. G. (2001). “A Flat Dilatometer to Operate in Glacial Tills”, *Geotechnical Testing Journal*, Vol. 24, No. 1, 51-60.

Bapst, A. (2002). “N16 – Traversée de la Combe Chopin Conditions géologiques“, *Publication de la Société Suisse de Mécanique des Sols et des Roches*, Réunion d’automne, 8. nov. 2002, Olten, 59-72.

Bisetti, A. (2002). “Confortation et Assainissement de la Combe Chopin Analyse de Stabilité“, *Publication de la Société Suisse de Mécanique des Sols et des Roches*, Réunion d’automne, 8. nov. 2002, Olten, 73-82.

Bollinger, D. (2000), “Ursachenanalyse der Hanginstabilitäten 1999”, *Bull. angew. Geol.*, 5, No 1, 5-38.

Chu, S. (1991). “Rankine analysis of active and passive pressures in dry sands”, *Soils Found*. 31 (4), 115-120.

Clark, B. G., Chen, C.-C. and Aflaki, E. (1998), “Intrinsic compression and swelling properties of a glacial till”, *Quarterly Journal of Engineering Geology*, 31, 235-246.

Dr. Von Moos AG (2003). “Rutschgebiet Braunwald, Sondier- und Messkampagne 2002/03, Stabilitätsbetrachtungen, Bauliche Sanierungsmöglichkeiten”, *Bericht Nr. 7008* für die Entwässerungskorporation Braunwald, 8784 Braunwald.

François, B., Bonnard, L., Laloui, L., Triguero, V. (2007). “Numerical modelling of the hydrological and geomechanical behaviour of a large slope movement: the Triesberg landslide (Liechtenstein)”, *Can. Geotech. J.* 44: 840-857.

Gabus, J. H. (1986a). “Le glissement d'Arveyes, approche pluridisciplinaire“, *Technical Report*, GEOLEP-REPORT-1986-002, Laboratoire de mécanique des sols, EPFL (ETH Lausanne).

Gabus, J. H. (1986a). “Arveyes, un glissement, une correction“, *Technical Report*, GEOLEP-REPORT-1986-001, Laboratoire de mécanique des sols, EPFL (ETH Lausanne).

Galluser, H. (1981). “Braunwald – Entwässerung – Geschichtliches und Gedanken von Hans Gallusser“, Küsnacht, 30. September 1981.

Gens, A. and Hight, D. W. (1979), “The laboratory measurement of design parameters for a glacial till”, Design parameters in geotechnical engineering, *Proceedings of the 7th Eur Conf Soil Mech Found Engng, Brighton*, Vol. 2, 57-65.

GVH Tramelan SA (2003). “Rapport de synthese No. 1: Tunnels du Raimeux et de la Roche St-Jean – Surveillance de la Combe Chopin“.

Haefeli, R. (1945). “Zur Erd- und Kriechdrucktheorie: Mit einer Anwendung auf den Castieler Viadukt der Linie Chur-Arosa der Rhätischen Bahn“, *Mitteilung aus der Versuchsanstalt für Wasserbau an der Eidgen. Techn. Hochschule, Nr. 9*, Zürich und Leipzig Verlag AG. Gebr. Leemann & Co.

Houriet, B. (2002). “N16 – Confortation de la Combe Chopin: Dimensionnement de la paroi de pieux ancrée“, *Publication de la Société Suisse de Mécanique des Sols et des Roches*, Réunion d’automne, 8. nov. 2002, Olten, 83-92.

Internet (2007a), “95mm and 73mm High Pressure Dilatometers side by side”, http://www.cambridge-insitu.com/specs/ Instruments/95_73_Pic.html.

Internet (2007b). http://www.viamichelin.de/viamichelin/deu/dyn/controller/Karten.

Internet (2009). “3-D Ansicht Brauwald, Schweiz“, Ausschnitt wurde mit dem Programm Google Earth erstellt, http://earth.google.com/intl/de/.

Iten, M., Schmid, A., Hauswirth, D., Puzrin, A. M. (2009). “Defining and monitoring of landslide boundaries using fiber optic systems“, submitted paper for the *International Symposium on Prediction and Simulation Methodes for Geohazard Mitigation, IS Kyoto 09*, May 25-27 2009, Kyoto, Japan.

Koeppel, J., Amstad, Ch. and Kovari, K. (1983). “The measurement of displacement vectors with the TRIVEC borehole probe”, *International Symposium on Field Measurements in Geomechanics*, 5-8 Sept. 1983, Zurich, Switzerland, 209-218.

Lang, H. J. und Schaerer, Ch. (1970). “Zwischenbericht über die geotechnischen Untersuchungen bis 1970 im Hinblick auf die Wahl der Fundationsart des Bauwerks zur Überquerung der Ganter“, *Bericht 2774/1*, Versuchsanstalt für Wasserbau und Erdbau an der ETH Zürich.

Lang, H. J. (1994). “Brattas-Hang, St. Moritz: Vorschriften über das Bauen im Brattas-Hang“, *Bericht Nr. 3922/24*, Institut für Geotechnik an der ETH Zürich.

Long, M. and Menkiti, C. O. (2007). “Geotechnical properties of Dublin Boulder Clay”, *Géotechnique 57*, No. 7, 595-611.

Marchetti, S. et al. (2001). “The Flat Dilatometer Test (DMT) in soil investigations”, A Report by the ISSMGE Committee TC 16, Proc. IN SITU 2001, *Intnl. Conf. On In situ Measurement of Soil Properties*, Bali, Indonesia, May 2001.

Müller und Messina (1992). “Geotechnisches Gutachten 1992, Rutschung Sass Runzöl-Brattas, St. Moritz“, *Büchi und Müller AG*, beratende Geologen SIA/ASIC, Chur.

Naterop, D. (2002). “Deformationsmessungen in der Pfahlwand Combe Chopin“, *Mitteilung der Schweizerischen Gesellschaft für Boden- und Felsmechanik,* Herbsttagung, 8. Nov. 2002, Olten: 93-100.

Noverraz, F. (1986a). “Le glissement de la Chenaula“, *Technical Report*, GEOLEP-REPORT-1986-004, Laboratoire de mécanique des sols, EPFL (ETH Lausanne).

Noverraz, F. (1986b). “Le glissement de Cergnat La Frasse“, *Technical Report*, GEOLEP-REPORT-1986-003, Laboratoire de mécanique des sols, EPFL (ETH Lausanne).

Powell, J. J. M. and Butcher, A. P. (2003). “Characterisation of a glacial clay till at Chowden, Humberside”, *Characterisation and Engineering Properties of Natural Soils*, Vol. 2, 983-1020.

Puzrin, A. M. and Sterba, I. (2006). “Inverse long-term stability analysis of a constrained landslide”, *Géotchnique,* 56, No. 7, 483–489.

Puzrin, A. and Schmid, A. (2007). “TRIVEC Measurements in the Inverse Analysis of the Long-Term Stability of a Constrained Landslide.”, *Proceedings of the 7th International Symposium on Field Measurements in Geomechanics Boston, FMGM 07*, Massachusetts, USA, September 24-27.

Puzrin, A. M., Messerklinger, S., Schmid, A. (2008). “The in-situ stiffness of the sliding layer in a creeping landslide”, *Proceedings of the 4th International Symposium on Deformation Characteristics of Geomaterials, IS Atlanta 2008*, September 22-24 2008, Atlanta, Georgia, USA, Vol. 1, pp 407-412.

Rageth, R. (1987). “Analyse und Sanierungsmöglichkeiten grosser Rutschgebiete – Braunwald, Unterlagen zur Bauwerksbesichtigung vom 30. 10. 1987“, *unvollendete Doktorarbeit* am Institut für Ingenieurgeologie der ETH Zürich.

Sambeth, U. (2006). “Brattashang St. Moritz, Dilatometerversuche”, *Stump ForaTec AG*, Stationsstrassse 57, 8606 Nänikon-Uster, Schweiz.

Schindler, C. (1982). “Problemreiche Hinterlassenschaften, Geologie und Wasserverhältnisse in Braunwald”, Seperatdruck aus dem Neujahrsboten 1982 für das Glarnerland.

Schlüchter, Ch. (1988). “Instabilities in the area of St. Moritz, Switzerland – Geology, chronology, geotechnology“, *Proc. of the fifth international symposium on landslides*, Lausanne 10.-15. July 1988, 1375-1380.

Schwager, M. V., Schmid, A. M., Puzrin, A. M. (2009). “Inclinodeformometer: a novel device for measuring earth pressure in creeping landslides“, submitted paper for the *International Symposium on Prediction and Simulation Methodes for Geohazard Mitigation, IS Kyoto 09*, May 25-27 2009, Kyoto, Japan.

Rüttimann, M. (2008). “Neues, innovatives Ringschergerät”. *Masterarbeit in Geotechnik FS 2008*, Institut für Geotechnik der ETH Zürich.

Skempton, A.W. (1985). “Residual strength of clays in landslides, folded strata and the laboratory”, *Geotechnique*, 35(1), 3-18.

SOLEXPERTS (2007). “TRIVEC”, *Solexperts AG*, Mönchaltdorf, Switzerland http://www.solexperts.com/pdfs/en/geo_trivec_en.pdf.

Küng, H. (2003). “Undrainierte Scherfestigkeit an aufbereitetem Seebodenlehm“. *Diplomarbeit in Geotechnik*, Institut für Geotechnik der ETH Zürich.

Villiger, S. (2008). “Versuche mit dem neuen Ringschergerät und Anwendung der Versuchsresultate“ *Projektarbeit in Geotechnik HS 2008,* Institut für Geotechnik der ETH Zürich.

Vulliet, L. and Hutter, K. (1988a). “Set of constitutive models for soils under slow movement”, *Journal of Geotechnical Engineering*, Vol. 114, No. 9, 1022-1041.

Vulliet, L., Hutter K. (1988b). “Continuum model for natural slopes in slow movement”, *Géotechnique*, 38(2), 199-217.

Wullimann, R. (1990). “Geotechnische Überwachung zweier Gebiet am Uetliberghang in Zürich“, *Mitteilungen des Instituts für Grundbau und Bodenmechanik*, Eidgenössische Technische Hochschule Zürich.

9 Anhang

Im Rahmen des Forschungsprojektes 'Interaktion Strasse Hangsatbilität: Monitoring und Rückwärtsrechnung' sind die folgenden Berichte, die im Anhang wiedergegeben werden, entstanden:

Puzrin, A. M. and Sterba, I. (2006). "Inverse long-term stability analysis of a constrained landslide", *Géotchnique,* 56, No. 7, 483–489.

Messerklinger, S., Schmid, A., Rohr, R. Sterba, I. und Puzrin, A.M. (2007)."Interaktion Strasse - Hangstabilität, Monitoring und Rückwärtsrechnung, VSS – Forschungsarbeit Nr. 2005/502 1. Zwischenbericht Field expedition St. Moritz – Juli 2006" Bericht Nr. 4714, Institut für Geotechnik, ETH Zürich

Messerklinger, S., Schmid, A., Rohr, R. Sterba, I. und Puzrin, A.M. (2007)."Interaktion Strasse - Hangstabilität, Monitoring und Rückwärtsrechnung, VSS – Forschungsarbeit Nr. 2005/502 1. Zwischenbericht Field expedition St. Moritz – Juli 2006" Bericht Nr. 4714/1, Institut für Geotechnik, ETH Zürich

Puzrin, A.M. and Schmid, A. (2007). "TRIVEC Measurements in the Inverse Analysis of the Long-Term Stability of a Constrained Landslide." *Proceedings of the 7th International Symposium on Field Measurements in Geomechanics Boston, FMGM 07*, Massachusetts, USA, September 24-27.

Puzrin, A.M., Messerklinger, S., Schmid, A. (2008),"The in-situ stiffness of the sliding layer in a creeping landslide", *Proceedings of the 4th International Symposium on Deformation Characteristics of Geomaterials, IS Atlanta 2008*, 22-24 September 2008, Atlanta, Georgia, USA, Vol. 1, pp 407-412.

Schwager, M. V., Schmid, A. M., Puzrin, A. M. (2009), „Inclinodeformometer: a novel device for measuring earth pressure in creeping landslides", submitted paper for the *International Symposium on Prediction and Simulation Methodes for Geohazard Mitigation, IS Kyoto 09*, May 25-27 2009, Kyoto, Japan.

Iten, M., Schmid, A., Hauswirth, D., Puzrin, A. M. (2009), „Defining and monitoring of landslide boundaries using fiber optic systems", submitted paper for the *International Symposium on Prediction and Simulation Methodes for Geohazard Mitigation, IS Kyoto 09*, May 25-27 2009, Kyoto, Japan.

9.1 Inverse long-term stability analysis of a constrained landslide

Puzrin, A. M. and Sterba, I. (2006). “Inverse long-term stability analysis of a constrained landslide”, *Géotchnique,* 56, No. 7, 483–489.

Puzrin, A. M. & Sterba, I. (2006). *Géotechnique* **56**, No. 7, 483–489

Inverse long-term stability analysis of a constrained landslide

A. M. PUZRIN* and I. STERBA*

This paper deals with long-term stability analysis of a constrained landslide. The landslide has 'nowhere' to go and its downhill movement is slowing in time, which intuitively implies its long-term stability. However, exactly because the landslide is slowing, the shear strength on the sliding surface may decrease, leading to increase in compressive stresses at the landslide foot and, ultimately, to a failure. The proposed long-term stability analysis of such a landslide is based on an inverse analysis, which allows for the safety factor to be determined solely by curve-fitting the observed displacement data. For a safety factor lower than 1, the time of failure can be predicted using additional earth pressure measurements in the sliding layer. The proposed procedure is illustrated using the observation data from the Brattas–St Moritz landslide.

KEYWORDS: creep; failure; landslides; shear strength; slopes

Cette étude se penche sur l'analyse de stabilité à long terme d'un glissement de terrain confiné. Le glissement ne peut s'évacuer nulle part et son mouvement descendant se ralentit au fil du temps, ce qui implique intuitivement sa stabilité à long terme. Cependant, parce que le glissement se ralentit, la résistance au cisaillement sur la surface de glissement peut décroître, ce qui finit par augmenter les contraintes compressives au pied du glissement et, en fin de compte, mener à la rupture. L'analyse de stabilité à long terme que nous proposons est basée sur une analyse inversée qui permet de déterminer le facteur sécurité uniquement en faisant la courbe des données de déplacement observées. Pour un facteur sécurité inférieur à 1, le moment de la rupture peut être prédit en utilisant d'autres mesures de pression terrestre dans la couche glissante. La procédure proposée est illustrée en utilisant les données observées sur le glissement de terrain Brattas–St Moritz.

INTRODUCTION

The long-term stability of slowly moving landslides was a subject of early interest in soil mechanics (e.g. Terzaghi, 1936; Skempton, 1964; Bjerrum, 1967). In these and later studies the analysis focused mainly on progressive failure in overconsolidated clays, where the failure is delayed in time by the development of the negative excess pore water pressure caused by shearing. As soon as this excess pore water pressure dissipated, the landslides, which did not have any kinematic constraints, accelerated and failed. But what would happen if a landslide did have a constraint, such as a natural (rock outcrop) or man-made (landslide protection wall) obstacle, at its bottom end?

This question is not a purely academic one: one such landslide is, in fact, rather famous—the Brattas landslide in St Moritz, Switzerland—and its stability is of the greatest concern for the community. The Leaning Tower of St Moritz (Fig. 1(a)) is probably the most striking evidence of this landslide. It used to be a part of St Mauritius Church, which was built in the 12th century and had to be demolished in 1893 in view of inevitable collapse due to enormous differential settlements. The continuing displacements of the tower have been monitored for almost a century (in 1984 the tower was partially propped up). A detailed geological and geotechnical description of the landslide and the history of the tower are presented elsewhere (Schluechter, 1988; Sterba *et al.*, 2000). What is of particular interest here is that the landslide is constrained by the rock outcrop along the Via Maistra (Fig. 1(b)), where zero displacements are observed. Also, monitoring of the tower displacements before 1984 (Sterba *et al.*, 2000) and more recent measurements of the slide displacements (Tschudi & Angst, 1999; Lang & Sterba, 2002) indicate that the slide is gradually slowing down. Intuitively, it is tempting to conclude that the landslide will eventually stop. But is this really the case?

The purpose of this paper is to suggest the mechanisms of both the safe and failure scenarios of a constrained landslide evolution, and to find, by using the monitored displacement data, a way to distinguish which scenario has a higher probability. In the *safe scenario*, the landslide will eventually stop. In this case, it is important to be able to estimate the final displacements. In the *failure scenario*, the landslide will keep slowing down until the earth pressure at its bottom exceeds the soil resistance and the slope fails catastrophically. In this case, it is necessary to predict the time of the future failure. These objectives are achieved with the help of the inverse analysis procedure developed in this work. It allows for both the safety factor for long-term slope stability and the final displacements to be determined solely from the observed slope displacements. This helps to reduce uncertainties caused by the spatial variability of soil properties. The time of the failure can then be calculated using some additional field measurements. The proposed procedure is illustrated using selected observation data from the St Moritz landslide. The proper long-term stability analysis of this landslide, however, will be performed after additional monitoring and field test data are acquired.

Manuscript received 18 January 2005; revised manuscript accepted 16 May 2006.
Discussion on this paper closes on 1 March 2007, for further details see p. ii.
* Institute for Geotechnical Engineering, Swiss Federal Institute of Technology (ETHZ), Zurich.

2. THE CONSTRAINED LANDSLIDE MODEL

The schematic layout of the boundary value problem of a slowing constrained landslide is given in Fig. 2. Equilibrium of the sliding layer relates the shear stress τ on the sliding surface to the average effective normal stress in the layer, p', and the effective active earth pressure p'_a acting at the top of the layer:

$$p'(x, t)H + \int_x^L \tau(x, t)\mathrm{d}x = \gamma_t H(L - x)\sin\alpha + p'_a H \qquad (1)$$

where γ_t is the total unit weight of soil; α is the slope inclination; and L and H are the landslide length and thickness, respectively. In equation (1) the effective earth

(a)

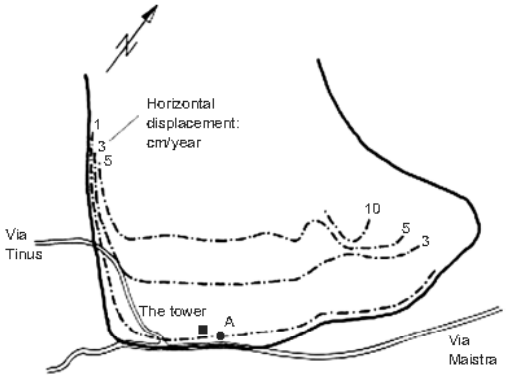

(b)

Fig. 1. The Brattas landslide of St Moritz: (a) the Leaning Tower; (b) the landslide displacements in the lower 200 m, long-term survey until 1982 (after Schluechter, 1988)

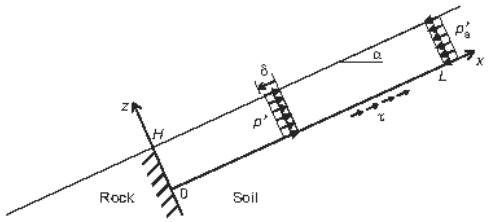

Fig. 2. Schematic layout of constrained landslide model

pressures are used assuming that the average pore water pressure is constant along the slope: $u(x, t) = u(t)$, that is, either there is a flow parallel to the slope surface, or there is no connected water.

In a forward boundary value problem equation (1) would be supplemented with constitutive equations and solved together in order to obtain displacements $\delta(x, t)$ and earth pressures $p'(x, t)$ and to predict the landslide behaviour. Because the processes in a constrained landslide are slower than in one that is free to slide, it is assumed that the excess pore water pressure has enough time to dissipate. Therefore the time dependence of displacements is due solely to the viscous properties of soil. Several possible constitutive models can then be suggested (Fig. 3). As can be seen from equation (1) and Fig. 2, the weight and the active force in the layer are resisted by the earth pressure in the layer and the shear stress on the sliding surface. These are schematically represented in Fig. 3(a) by the elastic spring (with elastic modulus E) and the slip element (with slip stress τ_r) respectively. This simple model is time-independent. In order to introduce time dependence one could, for example, add a viscous dashpot to the system. One possibility would be to assume that all viscous processes (i.e. the secondary compression) take place only within the soil layer, while on the sliding surface the shear strength has reached its residual value τ_r, which is constant in time. In this case, the dashpot should be added in parallel to the spring (Fig. 3(b)). In a more complex model, however, it can be assumed that the shear strength on the sliding surface is also time dependent. In this case, an additional dashpot should be added in parallel to the slip element (Fig. 3(c)).

The disadvantage of the forward approach is that it does not take the observed slope displacements into account. The spatial variability of soil properties results in high levels of indeterminacy in constitutive models and their parameters obtained in laboratory tests. This often causes large discrepancies between the calculated and observed behaviour. In contrast to the forward approach, inverse analysis of the problem would allow for the material properties to be back-calculated directly from the observed displacements. This would account for the global slope behaviour, as opposed to the behaviour of the locally extracted soil samples, and would provide a more reliable basis for future predictions. The purpose of this paper is to develop such an approach.

In order to simplify the analysis, the following analytical function is proposed to fit the observed normalised displacements data $\bar{\delta}(\bar{x}, t) = \delta(x/L, t)/L$.

$$\bar{\delta}(\bar{x}, t) = \bar{\delta}_x(\bar{x})\bar{\delta}_t(t) = \bar{x}(a \quad b\bar{x})(1 \quad e^{\ c\bar{x}+d}) \tag{2}$$

where $0 \leqslant b/a < 0{\cdot}5$; $c > 0$ and $\bar{x} = x/L$. This function describes displacements that are zero at the landslide foot and increase monotonically (when $0 \leqslant b/a < 0{\cdot}5$) along the

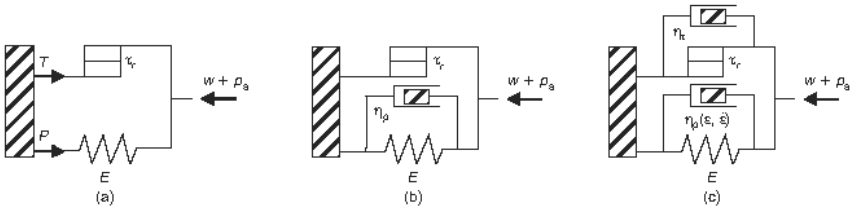

Fig. 3. Schematic layout of the constitutive behaviour: (a) time independent; (b) viscoelastic-purely plastic (VEPP); (c) viscoelastic-viscoplastic (VEVP)

slope towards its crest (Fig. 4(a)), while slowing with time and approaching an asymptotic value (Fig. 4(b)).

Equation (2) is simple, and yet provides sufficient flexibility to fit the observation data in both the space domain (parameters a and b) and the time domain (parameters c and d). In fact, as will be shown below, this function also has a certain theoretical background. In the following two sections we use this function to back-calculate the material parameters of the two constitutive models outlined in Figs 3(b) and 3(c) respectively.

3. THE VISCOELASTIC PURELY PLASTIC (VEPP) MODEL

It is first assumed that all viscous processes take place only within the soil layer, while on the sliding surface the shear strength has reached its residual value τ_r, which is constant in time. In this case, the dashpot is added in parallel to the spring (Fig. 3(b)), resulting in the following viscoelastic and purely plastic constitutive equations.

$$p'(x, t) = E\varepsilon(x, t) + \eta_p\dot{\varepsilon}(x, t) \tag{3a}$$

$$\tau(x, t) = \tau_r \tag{3b}$$

where $\varepsilon(x, t) = \partial\delta(x, t)/\partial x$ is the average linear strain over the layer thickness; η_p is the viscosity coefficient of the soil in the layer; E is the elasto-plastic (loading) modulus of the soil; and τ_r is the residual shear strength of the soil on the sliding surface. Substitution of equation (3b) into equation (1) yields the following expression for the earth pressure p'.

$$p'(x, t) = \left(\gamma_t \sin\alpha - \frac{\tau_r}{H}\right)(L - x) + p'_a \tag{4}$$

As can be seen, the earth pressure is time independent.

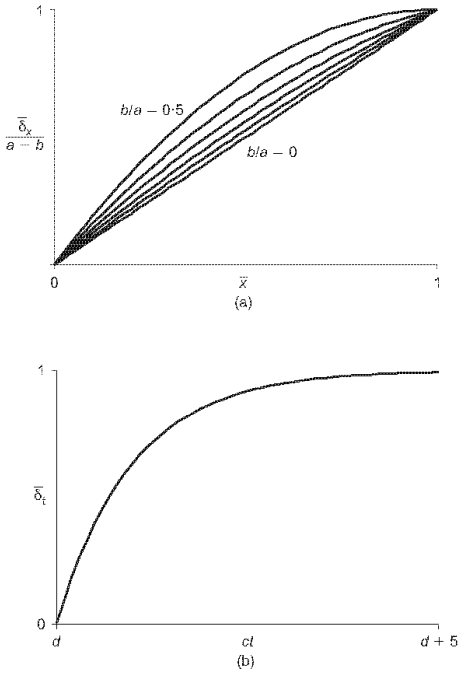

Fig. 4. Normalised functions for curve-fitting of slope displacements: (a) in space; (b) in time

Therefore, according to the adopted model, if the slope is currently stable, its long-term stability is also ensured. But how would this agree with the observed displacements (equation (2)) in terms of the coefficients a, b, c and d?

Substitution of equation (3a) into equation (4) yields

$$E\varepsilon(x, t) + \eta_p\dot{\varepsilon}(x, t) = \left(\gamma_t \sin\alpha - \frac{\tau_r}{H}\right)(L - x) + p'_a \tag{5}$$

By solving this standard viscoelastic equation with the initial condition $\varepsilon(x, t_0) = 0$

$$\varepsilon(x, t) = \frac{1}{E}\left[\left(\gamma_t \sin\alpha - \frac{\tau_r}{H}\right)(L - x) + p'_a\right] \times (1 - e^{-E(t-t_0)/\eta_p}) \tag{6}$$

is obtained. Integrating equation (6) and normalising it by L gives

$$\bar{\delta}(\bar{x}, t) = \frac{1}{L}\int_0^x \varepsilon(x, t)\mathrm{d}x = \frac{\bar{x}}{E}\left[\left(\gamma_t L \sin\alpha - \tau_r\frac{L}{H}\right)\left(1 - \frac{\bar{x}}{2}\right) + p'_a\right] \times (1 - e^{-E(t-t_0)/\eta_p}) \tag{7}$$

Comparing equations (2) and (7) we notice that they become identical when their parameters are related in the following way.

$$\left.\begin{aligned} E &= \frac{p'_a}{a - 2b} \\ \tau_r &= \gamma_t H \sin\alpha - \frac{2bp'_a}{a - 2b}\frac{H}{L} \\ \eta_p &= \frac{p'_a}{ac - 2bc} \\ t_0 &= \frac{d}{c} \end{aligned}\right\} \tag{8}$$

As can be seen, the curve-fitting function (equation (2)) in fact provides the exact solution for the VEPP model and allows for the model parameters to be determined solely from the monitored landslide displacements (via coefficients a, b, c and d). It follows, however, that these parameters should satisfy certain restrictions. First, because the elasto-plastic modulus E can only be positive, it is required that $2b/a < 1$. This condition is in fact identical to the restriction we imposed on equation (2) in order to provide monotonic growth of displacements uphill from the landslide bottom (Fig. 4(a)). It is even more important, however, to ensure that the slope is indeed stable, as implied by the VEPP model. According to equation (4), the largest earth pressure is at the bottom of the landslide, and, for the slope to be stable, it should not exceed the passive earth pressure p'_p.

$$p'(0, t) = \left(\gamma_t \sin\alpha - \frac{\tau_r}{H}\right)L + p'_a < p'_p \tag{9}$$

which, after substitution of τ_r from equation (8), gives

$$2\frac{b}{a} < 1 - \frac{p'_a}{p'_p} \tag{10}$$

which is an even more stringent condition than $2b/a < 1$.

The condition specified in equation (10) is the key criterion for the validity of the proposed inverse analysis. It

gives a mathematical expression for the case that was termed the *safe scenario* in the Introduction. When the coefficients a and b (obtained from curve-fitting of the observed data) satisfy this criterion, the VEPP model can be calibrated using equations (8), and the displacements and earth pressures are predicted at any point in time and space using equations (2) and (4) respectively. Obviously, according to this model, the long-term stability of the slope is satisfied and the displacements will gradually cease to increase. The question then is: what happens if the criterion in equation (10) is *not* satisfied?

4. THE VISCOELASTIC-VISCOPLASTIC (VEVP) MODEL

The case in which coefficients a and b of the curve-fitting function (equation (2)) do not satisfy equation (10) corresponds to the *failure scenario*. In this case, according to the VEPP model, the earth pressure at the bottom of the landslide exceeds the passive earth pressure, causing the development of new slip surfaces and leading to slope failure. However, because the VEPP model implies that the earth pressures in the slope should stay constant over time, this slope should have failed a long time ago, contradicting the observations. This inability of the VEPP model to accommodate a possibility of a future failure is rooted in the assumption that the shear strength has dropped to its final residual value τ_r along the entire sliding surface. It is this assumption that makes the equilibrium equation (1) time independent, whereas, in order to allow for future failure, the earth pressure in the slope must increase over time.

In the viscoelastic-viscoplastic (VEVP) model proposed below, this time dependence of the earth pressure is accommodated by assuming that the shear strength of soil on the sliding surface is rate dependent (Fig. 3(c)).

$$\tau(x,\, t) = \tau_r + \eta_\tau \dot{\delta}(x,\, t) \tag{11}$$

where η_τ is the corresponding viscosity coefficient. In other words, the residual shear strength decreases with decreasing shearing rate, which has been experimentally confirmed for natural soils (e.g. Skempton, 1985). The stiffness of the soil in the sliding layer is also assumed to be rate dependent (Fig. 3(c)),

$$p'(x,\, t) = E\varepsilon(x,\, t) + \eta_p(\varepsilon,\, \dot{\varepsilon})\dot{\varepsilon}(x,\, t) \tag{12}$$

though not necessarily linearly: the functional form of the viscosity coefficient $\eta_p(\varepsilon,\, \dot{\varepsilon})$ will be determined from the inverse analysis.

Substitution of the constitutive equations (11) and (12) into the equilibrium equation (1) yields

$$p'(x,\, t) + \frac{\eta_\tau}{H}\int_x^L \dot{\delta}(x,\, t)\mathrm{d}x = \left(\gamma_t \sin\alpha - \frac{\tau_r}{H}\right)(L - x) + p'_a \tag{13}$$

The parameters of the VEVP model can be determined using the following inverse analysis procedure. First, by substituting the observation data (equation (2)) into equation (13), differentiating and integrating we obtain

$$p'(\bar{x},\, t) = p'_a + \frac{L}{H}(\gamma_t H \sin\alpha - \tau_r)(1 - \bar{x}) - \frac{L^2}{H} c\eta_\tau e^{-ct+d}\left[\frac{a}{2}(1 - \bar{x}^2) - \frac{b}{3}(1 - \bar{x}^3)\right] \tag{14}$$

Next, from equation (2), expressions for the linear strain and its rate are derived.

$$\varepsilon(\bar{x},\, t) = (a - 2b\bar{x})(1 - \mathrm{e}^{-ct+d}) \tag{15a}$$

$$\dot{\varepsilon}(\bar{x},\, t) = (a - 2b\bar{x})c\mathrm{e}^{-ct+d} \tag{15b}$$

which can then be resolved with respect to t and x,

$$\mathrm{e}^{-ct+d} = \frac{\dot{\varepsilon}/c}{\varepsilon + \dot{\varepsilon}/c} \tag{16a}$$

$$\bar{x} = \frac{a - \varepsilon - \dot{\varepsilon}/c}{2b} \tag{16b}$$

and substituted into equation (14)

$$p' = p'_a + \frac{L}{H}(\gamma_t H \sin\alpha - \tau_r)\left(1 - \frac{a - \varepsilon - \dot{\varepsilon}/c}{2b}\right) - \frac{L^2}{H}\eta_\tau \frac{\dot{\varepsilon}}{\varepsilon + \dot{\varepsilon}/c}\left\{\frac{a}{2}\left[1 - \left(\frac{a - \varepsilon - \dot{\varepsilon}/c}{2b}\right)^2\right] - \frac{b}{3}\left[1 - \left(\frac{a - \varepsilon - \dot{\varepsilon}/c}{2b}\right)^3\right]\right\} \tag{17}$$

Comparing equations (12) and (17) we find the relationship between the parameters of the VEVP constitutive model (equations (12) and (13)) and the coefficients of the curve-fitting function (equation (2))

$$E = \frac{p'_a}{a - 2b} \tag{18a}$$

$$\tau_r = \gamma_t H \sin\alpha - \frac{2bp'_a}{a - 2b}\frac{H}{L} \tag{18b}$$

$$\eta_p(\varepsilon,\, \dot{\varepsilon}) = \frac{p'_a}{ac - 2bc} - \frac{L^2}{H}\frac{\eta_\tau}{\varepsilon + \dot{\varepsilon}/c}\left\{\frac{a}{2}\left[1 - \left(\frac{a - \varepsilon - \dot{\varepsilon}/c}{2b}\right)^2\right] - \frac{b}{3}\left[1 - \left(\frac{a - \varepsilon - \dot{\varepsilon}/c}{2b}\right)^3\right]\right\} \tag{19}$$

Note that equations (18) and the constant term in equation (19) are identical to the corresponding expressions (equations (8)) for the VEPP model. As can be seen, derived via inverse analysis, the expression for the non-constant term of the viscosity coefficient in equation (19) is rather complex. The good news, however, is that, unlike the viscosity coefficient η_τ, it does not anywhere enter the expression for the earth pressure evolution (equation (14)). However, it is not sufficient to determine η_τ with the existing observation data (equation (2)), and this has to be supplemented by some other kind of measurement. The time changes in the earth pressure p' at the bottom of the slope ($x = 0$) are of the utmost importance in this analysis. Therefore it would be logical to insert a pressure transducer at the rock/soil interface and measure the increase in the earth pressure, Δp, over the time period Δt.

$$\Delta p = p'(0,\, t_0 + \Delta t) - p'(0,\, t_0) \tag{20}$$

where t_0 is the time of the pressure transducer installation. Substituting $x = 0$ into equation (14) derives the following expression for the earth pressure evolution at the bottom end of the landslide.

$$p'(0, t) = p'_a + \frac{L}{H}(\gamma_t H \sin\alpha - \tau_r) - \frac{L^2}{H} c\eta_\tau e^{-ct+d}\left[\frac{a}{2} - \frac{b}{3}\right] \quad (21)$$

Then substitution of equation (21) into equation (20) gives the desired expression for η_τ

$$\eta_\tau = \frac{\Delta p\, H\, e^{ct_0 - d}}{L^2 c(a/2 - b/3)(1 - e^{-c\Delta t})} \quad (22)$$

Equation (22), after being substituted back into equation (21) together with equation (18b), yields the following expression for the earth pressure at the landslide bottom, defined solely through the observation data coefficients.

$$p'(0, t) = \frac{ap'_a}{a - 2b} - \frac{\Delta p\, e^{-c(t - t_0)}}{(1 - e^{-c\Delta t})} \quad (23)$$

It now becomes possible to predict the time of the future failure. From equation (23) it follows that the earth pressure increases monotonically over time. The failure will take place at time t_f, when the earth pressure at the slope bottom reaches the passive earth pressure value $p'(0, t_f) = p'_p$. Then, from equation (23), we find the following expression for the time of failure.

$$t_f = t_0 + \frac{1}{c}\ln\frac{\Delta p}{(1 - e^{-c\Delta t})\left[p'_a/(1 - 2b/a) - p'_p\right]} \quad (24)$$

which, as can be seen, is mathematically meaningful only when

$$2\frac{b}{a} > 1 - \frac{p'_a}{p'_p} \quad (25)$$

that is, when the safe scenario criterion (equation (10)) is violated.

Note, that according to the VEVP model, the slope fails not 'in spite of', but exactly because of the fact that the landslide slows down in time. In fact, the decrease in displacement rate leads to the decrease in the shear strength (equation (11)), which in turn causes an increase in the earth pressures in the soil layer (equation (13)), which can ultimately exceed the passive pressure resistance.

5. THE SAFETY FACTOR

Expression (25) is nothing else but the definition of the failure scenario, which confirms the validity of the adopted VEVP model. However, this model is still applicable even when failure is not possible. First of all, it can be easily shown that the VEPP model is a degenerate case of the VEVP model with $\eta_\tau = 0$. In fact, the VEVP model is even better for the analysis of the safe scenario, because it can account for a more general case of $\eta_\tau \neq 0$ and $2b/a < 1 - p'_a/p'_p$. In this case, equations (2) and (23) will still correctly predict the displacements and earth pressure evolution respectively. The only difference with the failure scenario analysis will be that the passive earth pressure in equation (23) will never be reached, and equation (24) cannot be used. It follows that the VEVP model is the one that should be applied to the analysis of both scenarios. The safety factor for the slope stability can then be defined as the ratio between the soil resistance (passive earth pressure) and the maximum earth pressure that can develop at the landslide foot in time (equation (23)).

$$F_s = \frac{p'_p}{p'(0, \infty)} = \frac{1 - 2b/a}{p'_a/p'_p} \quad (26)$$

This definition, when compared with equations (10) and (25), identifies the safe scenario with $F_s > 1$, and the failure scenario with $F_s < 1$. In the latter case, equation (24) can be rewritten as

$$t_f = t_0 + \frac{1}{c}\ln\frac{\Delta p'/p'_p}{(1 - e^{-c\Delta t})(1/F_s - 1)} \quad (27)$$

and used to predict the time before the slope failure. Note that the entire stability analysis can be performed using only equations (26) and (27), which utilise solely the observed data and the values of the effective active and passive earth pressures in the slope found from Fig. 5 (Chu, 1991).

$$\begin{Bmatrix} p'_a \\ p'_p \end{Bmatrix} = \frac{1}{2}\gamma' H\cos\alpha \times \left[1 + 2\tan^2\phi'_p \mp 2\sqrt{(1 + \tan^2\phi'_p)(\tan^2\phi'_p - \tan^2\alpha)}\right] \quad (28)$$

where ϕ'_p and γ' are, respectively, the effective peak angle of internal friction and the effective unit weight of the soil in the sliding layer.

6. STABILITY ANALYSIS PROCEDURE

The following procedure is recommended for the stability analysis of a constrained landslide. We assume that the following displacement data are available: $\delta(x_i, t_j)$, where $i = 1, \ldots, N$; $j = 1, \ldots, M$; N and M are the number of measurement points in space and time respectively; and at t_1 $\delta(x_i, t_1) = 0$ for any $i = 1, \ldots, N$.

(*a*) Plot the normalised observation data $y_{i,j} = \delta(x_i, t_j)/\delta(x_N, t_j)$, for $i = 1, \ldots, N$; $j = 1, \ldots, M$ against the normalised coordinate $x'_i = x_i/x_N$. Determine the coefficient $k = b/a$ by fitting to these data the following function.

$$y = x'\frac{L' - kx'}{L' - k} \quad (29)$$

where $L' = L/x_N$ is the normalised length of the landslide.

(*b*) Calculate the effective active and passive earth pressures from equations (28) and their ratio p'_a/p'_p.

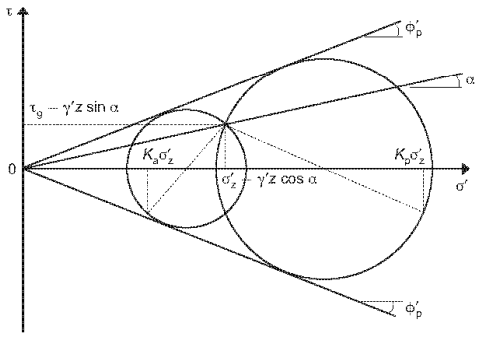

Fig. 5. Mohr circle interpretation of active and passive failure in the slope

$$\frac{p'_a}{p'_p} = \frac{1 + 2\tan^2\phi'_p - 2\sqrt{(1+\tan^2\phi'_p)(\tan^2\phi'_p - \tan^2\alpha)}}{1 + 2\tan^2\phi'_p + 2\sqrt{(1+\tan^2\phi'_p)(\tan^2\phi'_p - \tan^2\alpha)}} \tag{30}$$

(*c*) Substitute $k = b/a$ and p'_a/p'_p into equation (26) to calculate the safety factor. If $F_s > 1$, the slope is stable; if $F_s < 1$, it is not.

Note that the only parameters required for this stability analysis (in addition to the observed displacements) are α, L and ϕ'_p. Not even the thickness of the sliding layer, H, is required at this stage. Also, it has not yet been necessary to define the time-related parameters c and d. These will be defined in the following steps, and used to calculate the final slope displacements δ_∞ for the safe scenario ($F_s > 1$) and the time to failure t_f for the failure scenario ($F_s < 1$).

(*d*) Plot the normalised observation data $w_{i,j} = \delta(x_i, t_j)/\delta(x_i, t_M)$ for i = 1, ..., N; $j = 1, \ldots, M$ against tj. Determine the coefficient c by fitting to these data the following function.

$$w = \frac{1 - \exp[-c(t - t_1)]}{1 - \exp[-c(t_M - t_1)]} \tag{31}$$

(*e*) If $F_s > 1$ the final displacement increments are defined for each $i = 1, \ldots, N$ by

$$\delta_\infty(x_i) = \frac{\delta(x_i, t_M)}{1 - \exp[-c(t_M - t_1)]} \tag{32}$$

(*f*) If $F_s < 1$, install at some time t_0 a pressure transducer at the rock/soil interface and measure the increase in earth pressure Δp over the period of time Δt. Calculate the time of the future failure from equation (27).

7. EXAMPLE

In the following example of a constrained landslide stability analysis we utilise selected observation data from the St Moritz landslide. It is important to emphasise that these data are not sufficient to make definite conclusions about the landslide stability; they are used solely as an illustration of the above procedure.

The following landslide parameters are adopted here (Sterba *et al.*, 2000): $L = 1500$ m and $\alpha = 20°$. The peak effective angle of internal friction is assumed (after Vermeer, 1997) to be within the range $\phi'_p = 28–35°$, so that from equation (30) $p'_a/p'_p = 0{\cdot}28 - 0{\cdot}15$. The best fit of the analytical curve (equation (29)) to the normalised displacement data monitored at different points in the lower 200 m of the landslide (Fig. 1(b)) is achieved at $b/a = 0{\cdot}39$ (Fig. 6(a)). Substituting these parameters into equation (26), we obtain the range for the safety factor: $F_s = 0{\cdot}78–1{\cdot}46$. As can be seen, this analysis does not exclude the possibility of future failure. But let us first focus on the safe scenario. The best fit to the normalised displacement data (Lang & Sterba, 2002) monitored between 1979 and 1999 at point A on the slope located 15 m east from the Tower (Fig. 1(b)) is achieved using the analytical curve (equation (31)) with $c = 0{\cdot}045$ (Fig. 6(b)). The total downhill displacement of point A between 1979 and 1999 was 177 mm: therefore in the safe scenario case, according to equation (32), the final displacement of this point will be 298 mm.

Of greater concern here is the fact that this preliminary stability analysis of the Brattas landslide does not exclude the possibility of the failure scenario. However, it is too early to panic: as mentioned above, the data used in this example are far from being reliable. First of all, the data in Fig. 6(a) are obtained by monitoring only a few points along the slide, all of them within the lower 200 m of the landslide (out of a total of 1500 m). When the curve (equation (29)) is fitted in such a small portion of the range, its ability to represent the entire range is very limited, and the parameter b/a becomes very sensitive to the measurement accuracy. A proper stability analysis of the St Moritz landslide requires additional displacement measurements along the entire landslide length. Also, the data in Fig. 6(b) are obtained by monitoring the displacements of one point on the slope over a relatively short period of time. Proper time-related predictions can be achieved only by monitoring the long-term displacements of the soil along the entire landslide and measuring the earth pressure changes in time in the area of high compression at the landslide bottom. Finally, the effects of climatic changes and groundwater conditions should be also studied and incorporated in the analysis.

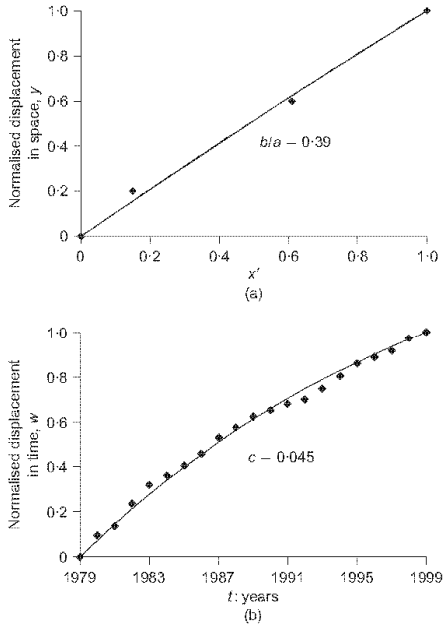

Fig. 6. Curve-fitting of normalised displacement data monitored for St Moritz landslide: (a) in space (before 1983), using equation (29); (b) in time (1979–1999), using equation (31)

8. CONCLUSIONS

This paper deals with the stability analysis of a constrained landslide. The landslide has 'nowhere' to go, and its downhill movement is slowing in time, which intuitively implies landslide stability. However, exactly because the landslide is slowing, the shear strength on the sliding surface may decrease, leading to an increase in the compressive stresses at the landslide foot and, ultimately, to a failure.

The stability analysis of such a landslide proposed here is based on an inverse analysis of the observed displacements. A new curve-fitting function for the observed displacements is suggested, which is rather simple to fit and yet provides sufficient flexibility for the fitting. In addition, this function represents an exact solution for the simple viscoelastic purely plastic model. It is, however, a more complex visco-elastic-viscoplastic model that allows for both the safe and failure scenarios of the landslide evolution to be identified and explored within a unified framework.

The inverse analysis of the viscoelastic-viscoplastic model results in a procedure that allows for the slope safety factor and final slope displacements (when $F_s > 1$) to be determined solely by curve-fitting the observed displacement data, using only one additional soil parameter, ϕ'_p. For the case of $F_s < 1$, the time of failure can be predicted using additional earth pressure measurements in the sliding layer. The proposed procedure is illustrated using observation data from the Brattas–St Moritz landslide. It would be interesting to learn about other cases of landslides that are being slowed down by natural or man-made obstacles.

ACKNOWLEDGEMENTS

The authors would like to thank Professor Hans-Jürgen Lang for his valuable comments. The work has been partially supported by the ASTRA/VSS grant VSS 2005/502 'Landslide-Road-Interaction'.

NOTATION

a, b curve-fitting coefficients for displacement data (in space)
c, d curve-fitting coefficients for displacement data (in time)
E elasto-plastic (loading) modulus of soil
F_s safety factor for long-term stability of slope
H landslide thickness
K_a, K_p active and passive earth pressure coefficients
k ratio between coefficients b and a: $k = b/a$
L landslide length
L' normalised landslide length
p' average effective normal stress (earth pressure) in the layer
p'_a effective active earth pressure
p'_p effective passive earth pressure
t time
t_f time of failure
t_0 time of pressure transducer installation
u average pore water pressure across thickness of layer
w displacement data normalised in time
x space coordinate
$\bar{x}$ normalised space coordinate: $\bar{x} = x/L$
y displacement data normalised in space
z depth below surface
α slope inclination
γ_t total unit weight of soil
γ' effective unit weight of soil
δ downhill displacements of landslide
$\bar{\delta}$ normalised displacements: $\bar{\delta} = \delta/L$
δ_∞ final slope displacements
ε average linear strain over layer thickness
η_p viscosity coefficient of soil in layer
η_s viscosity coefficient of soil on sliding surface
σ'_z normal stress on the z plane
τ shear stress on sliding surface
τ_g gravitational shear stress
τ_r residual shear strength of soil on sliding surface
ϕ'_p effective peak angle of internal friction of soil in sliding layer

REFERENCES

Bjerrum, L. (1967). Progressive failure in slopes of overconsolidated plastic clay and clay shales. *J. Soil Mech. Found. Engng Div. ASCE* **93**, No. 5, 1–49.

Chu, S. (1991). Rankine analysis of active and passive pressures in dry sands. *Soils Found.* **31**, No. 4, 115–120.

Lang, H.-J. & Sterba, I. (2002). *Schiefer Turm, St Moritz: Stellungnahme zu den Messungen*, Bericht 3676/10. Zurich: Institut für Geotechnik, ETH Zürich.

Schluechter, Ch. (1988). Instabilities in the area of St Moritz, Switzerland: geology, chronology, geotechnology. *Proc. 5th Int. Symp. on Landslides, Lausanne* **1**, 1375–1380.

Skempton, A. W. (1964). Long-term stability of clay slopes. *Géotechnique* **14**, No. 2, 77–102.

Skempton, A. W. (1985). Residual strength of clays in landslides, folded strata and the laboratory. *Géotechnique* **35**, No. 1, 3–18.

Sterba, I., Lang, H.-J. & Amann, P. (2000). The Brattas landslide in St Moritz. *Proceedings of the international conference on geotechnical and geological engineering: GeoEng 2000, Melbourne* **2**, 144.

Terzaghi, K. (1936). Stability of slopes of natural clay. *Proc. 1st Int. Conf. Soil Mech. Found. Engng, Cambridge, MA* **1**, 161–165.

Tschudi, D. & Angst, R. (1999). *Diplomvermessungskurs Samedan 1998, Rutschhang Brattas, St Moritz*, Bericht 283. Zurich: Institut für Geodäsie und Photogrammetrie, ETH Zürich.

Vermeer, P. A. (1997). PLAXIS Practice I: The leaning Tower of St Moritz. *PLAXIS Bulletin*, No. 4, 4–7.

9.2 Bericht Nr. 4714

Messerklinger, S., Schmid, A., Rohr, R. Sterba, I. und Puzrin, A.M. (2007).“Interaktion Strasse - Hangstabilität, Monitoring und Rückwärtsrechnung, VSS – Forschungsarbeit Nr. 2005/502 1. Zwischenbericht Field expedition St. Moritz – Juli 2006“ Bericht Nr. 4714, Institut für Geotechnik, ETH Zürich

Bundesamt für Strassen ASTRA
Abteilung Strassennetze
3003 Bern

Interaktion Strasse - Hangstabilität
Monitoring und Rückwärtsrechnung

****

VSS - Forschungsarbeit Nr. 2005/502
1. Zwischenbericht
Field expedition St. Moritz - July 2006

Bericht Nr. 4714

Zürich, 1. November 2007

1

VSS, Vereinigung Schweizerischer Strassenfachleute
Forschungsarbeit Nr. VSS 2005/502

Interaktion Strasse – Hangstabilität: Monitoring und Rückrechnung

1. Zwischenbericht

Field expedition St. Moritz - July 2006

S. Messerklinger, A. Schmid, R. Rohr, I. Sterba and A.M. Puzrin

Institut für Geotechnik

Bericht Nr. 4714
Zürich, 1. November 2007

Field expedition St. Moritz - July 2006

Content:

Tables and Figures:

Figures:

Tables:

Literature:

Lichtenberger, M. (2006). "Bestimmen von Spannungen in der Lithosphäre aus geogener elektromagnetischer Strahlung" Dissertation. Geologisch-Paläontologisches Institut, Ruprecht-Karls-Universität Heidelberg, ISSN 1612-5452.

Appendix:

Appendix I: Staub P. (2006) "Geodätische Geländeüberwachung: Hangrutschungsmessungen im Gebiet Gianda Laret-Brattas, Gemeinde St. Moritz".

Appendix II: Sambeth U. (2006) "Brattashang, St. Moritz: Dilatometerversuche".

Appendix III: Marchetti S., Monaco P., Totani G. and Calabrese M. (2001) "The Flat Dilatometer Test (DMT) in soil investigations" Report by the ISSMGE Committee TC16.

Appendix IV: Company Pergam: Data CD with the infrared pictures.

Appendix V: Sauerbier M. (2006) "Arbeitstitel: Photogrammetrische Auswertung". In preparation.

Appendix VI: Data and analysis of the Electromagnetic Radiation Measurements.

4

Introduction

In July 2006 the Institute for Geotechnical Engineering of ETH Zürich made a field expedition to St. Moritz with the aim:

- to verify and compare various insitu test methods and
- to establish the existence of compression zones at the bottom of the Brattas slide.

The following program points were performed:

1) Installation of new geodetical points on the top and middle part of the Brattas slide for the future geodetical observation of the displacements along the landslide.

2) Investigation and observation of former geodetical points and other significant marks (e.g. the road shown by the surveyor of the community Mr. P. Baracchi) for the investigation of the landslide displacements over the past century.

3) Installation of borehole No. 0601 with a piecometer and an inclinometer and extraction of soil samples.

4) Dilatometer-Pressiometer tests in the borehole for the investigation of soil stiffness over the depth and to compare the stiffness measurements to the measurement data given by the Marchetti dilatometer (point 5) and by Oedometer test (Report No.: 4714/1) performed on samples taken from the borehole.

5) Marchetti dilatometer tests in the borehole for the investigation of soil stiffness over the depth and to compare the stiffness measurements to the measurement data given by the Dilatometer-Pressiometer (point 4) and by Oedometer test (Report No.: 4714/1) performed on samples taken from the borehole.

6) Infrared pictures of the Brattas slide for the investigation of temperature variations along the landslide with the aim to observe the location of compression zones and/or water flows.

7) Photographs of the Brattas slide with the aim to photogrammetrical evaluation the coordinates of the newly installed geodetical points (point 1).

8) Electromagnetic radiation measurements for the observation of compression zones along the landslide.

This report (Report No.: 4714) summarizes the first field expedition to St. Moritz in summer 2006 and presents all measurement results observed in these two weeks of field testing.

Additional investigations on data or samples from St. Moritz are/will be presented in subsequent reports:

- Report No.: 4714/1: Borehole No.: 0601, St. Moritz. Oedometer Tests and Comparison to the Insitu Stiffness Measurements.

1. Installation of new geodetical points on the Brattas slide.

Contributor: S. Annen, M. Iten, E. Saurer, R. Rohr, S. Messerklinger, A.M. Puzrin

New geodetical points were installed on the top and middle part of the Brattas slide. On the bottom side, in the settled regions, there are already geodetical points installed and their movement is observed over the past decades.

The aim of installing new points on the top and middle part of the Brattas slide is to observe the displacements along the entire landslide in the future.

32 points were marked on three longitudinal and nine cross sections. Each point was named with SM for St. Moritz; L, C or R for the left, centre or right longitudinal section and with a number between 01 and 13 corresponding to the cross section. A map of the points marked is shown in Fig. 1.

Attention: cross section 6 was left out; no points were marked on cross section 6. In cross section 7, two points were marked close to the centre section: SMC07_2 on the centre section and SMC07 between the centre and the right section. In cross profiles 01 and 03 respectively, one point at the centre section (SMC01 & SMC03) was marked only. In cross profile 02 one point was marked on the centre and one on the right section (SMC02 & SMR02).

Attention: point SML04 and SMC04 were destroyed and reinstalled.

Each point was marked with:

- a steel nail appropriate for geodetical measurements and
- a white plastic plate or a coloured circle appropriate for photogrammetric evaluation of the pictures taken from the helicopter (paragraph 7).
- additionally, a wooden stick was placed, when possible, in order to find the points again.

Nail:

The steel nails were provided by the group of Prof. Carosio (IGP ETHZ).

- When the point was marked at rock, a hole was drilled which was filled with cement lime before the nail was put inside.
- When the point was marked on soil, a steel tube was driven into the ground with a hammer and the nail was clamped into the topside of the tube.

Photogrammetric markings:

- When the point was marked on a rocky area, an orange circle with a diameter of approx. 50 cm was sprayed around the nail.
- When the point was marked on a grassy area, a square (40 x 40 cm), white plastic plate was placed under the head of the nail.

Stick:

A wooden stick of a length of approx. 50 cm and an orange painted top was placed next to the point at a distance of max. 2 metre. Where it was not possible to fix a stick in the ground (in the rocky areas) a rock-tip next to the point was painted orange.

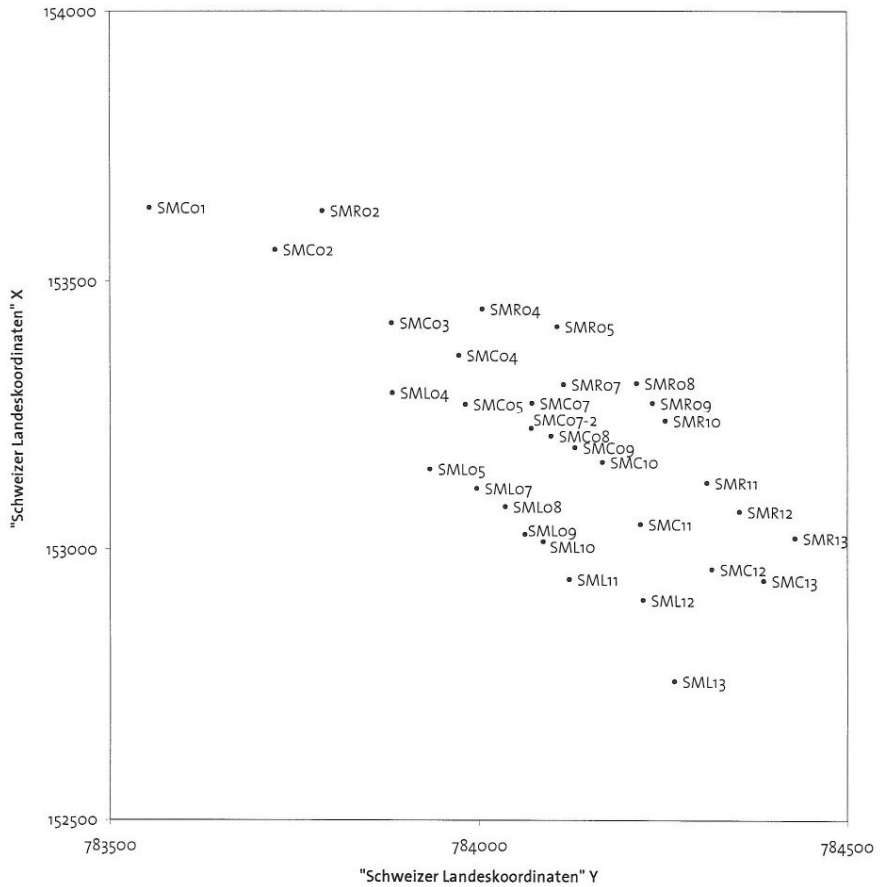

Fig. 1: Newly marked points for the future geodetical observation of the landslide, presented in "Schweizer Landeskoordinaten".

For each newly marked point the geodetical coordinates (in Schweizer Landeskoordinaten) were determined with the IGT-GPS within an accuracy of ± 5 metres. These coordinates are given in Tab. 1 together with the approximate height above see level. Additionally, the coordinates and height of the major spring close to cross section 5 is given at the bottom of Tab. 1.

Tab. 1: Coordinates and height above see level of the newly marked points.

Point No.	Coordinates		Height above see level
SMC01	783554	153636	2261 m
SMC02	783723	153558	2207 m
SMC03	783881	153423	2163 m
SMC04	783973	153362	2128 m
SMC05	783981	153271	2103 m
SMC07	784072	153273	2095 m
SMC07-2	784071	153225	2093 m
SMC08	784098	153211	2079 m
SMC09	784131	153190	2064 m
SMC10	784168	153163	2048 m
SMC11	784220	153047	1994 m
SMC12	784317	152961	1969 m
SMC13	784387	152940	1951 m
SML04	783882	153292	2143 m
SML05	783933	153150	2095 m
SML07	783997	153114	2086 m
SML08	784036	153080	2087 m
SML09	784063	153028	2062 m
SML10	784088	153014	2068 m
SML11	784123	152942	2012 m
SML12	784223	152905	1984 m
SML13	784266	152756	1945 m
SMR02	783787	153630	2205 m
SMR04	784005	153448	2135 m
SMR05	784107	153416	2110 m
SMR07	784115	153308	2096 m
SMR08	784215	153310	2087 m
SMR09	784236	153274	2069 m
SMR10	784254	153239	2056 m
SMR11	784310	153124	2010 m
SMR12	784354	153071	1965 m
SMR13	784429	153021	1933 m
SMquelle01	783963	153211	2103 m

9

In collaboration with Prof. Carosio (Institute of Geodesy and Photogrammetry; Room No.: HIL D46.3; Tel. No.: +41-44-633 3052; email: carosio@geod.aug.ethz.ch) and his assistance Janine Sutter (Room No.: HIL D54.3; Tel. No.: +41-44-633 3062; sutter@geod.baug.ethz.ch) and Peter Staub (Room No.: HIL D46.2; Tel. No.: +41-44-633 3846; email: staub@geod.baug.ethz.ch) a student course was organized.

In this course the students performed geodetical measurements on the:

- 31 of the 74 existing points at the bottom side of the Brattas slide.
- 32 new installed points at the middle and top part of the Brattas slide.
- 4 points

Not all points are measured with the same accuracy. Prior to the measurements the Brattas slide was divided into three zones with different accuracies asked for and after the measurements the actually reached accuracies for each zone were determined (after Staub, 2006; see Appendix I):

Zone 1: all points and cross-section 8, 9, 10	location accuracy: 1.1 cm; height accuracy: 1.5 cm
Zone 2: cross-section 4, 5, 7, 12, 13	location accuracy: 1.4 cm; height accuracy: 1.5 cm
Zone 3: cross-section 1, 2, 3, 11, 3 old points	location accuracy: 1.9 cm; height accuracy: 1.7 cm

The detailed report "Geodätische Geländeüberwachung: Hangrutschungsmessungen im Gebiet Gianda Laret-Brattas, Gemeinde St. Moritz" is attached in **Appendix I**.

2. Investigation and observation of former geodetical points and other significant marks.

Contributor: S. Annen, R. Rohr, I. Sterba, A.M. Puzrin and Mr. P. Baracchi, surveyor of the community of St. Moritz

For the investigation of the displacements along the Brattas slide over the past century it was tried to find former geodetical points and other significant marks for which the coordinates were determined long time ago (e.g. 80 years).

Two groups of marks were identified:

- The road crossing the Brattas slide (close to cross-section 10, Fig. 1). Unfortunately, only one old geodetical point (point no. 2338) could be found.
- Former geodetical points (no. 2320 and 2323) in the Brattas slide (2 points at cross-section 4, Fig. 1 and Appendix I, page 61).

The coordinates of these three points were determined in the measurement campaign (described in the previous chapter) and are presented in **Appendix I**.

3. Installation of borehole No. 0601 with a piecometer and an inclinometer and extraction of soil samples.

Contributor: S. Annen, A. Schmid, R. Rohr, S. Messerklinger, I. Sterba, A.M. Puzrin and A. Mehrstetter (Bohrmeister, Fa. Stump ForaTec AG, Chur)

A boring with the diameter of 131 mm was installed by the company Stump ForaTec AG, Chur. The tests performed in the borehole during its installation and the samples taken from the borehole are listed in Table 2.

Subsequently, a piecometer and an inclinometer (Inkrex tube diameter 71 mm) were installed in the borehole.

4. Dilatometer-Pressiometer tests in the borehole.

Contributor: S. Annen, S. Messerklinger, A.M. Puzrin, U. Sambeth (Fa. Stump ForaTec AG, Zürich)

Dilatometer-Pressiometer tests were performed in the borehole to investigate the soil stiffness over the depth and to compare the stiffness determined with the Dilatometer-Pressiometer to the stiffness measurement data given by the:

- Marchetti dilatometer tests also performed in the borehole (point 5) and
- Oedometer test performed subsequently in the laboratory on samples taken from the borehole (Report No.: 4714/1).

The detailed report of the 4 Dilatometer-Pressiometer tests performed by U. Sambeth in the borehole at depths of 5.0, 8.9, 13.9 and 13.7 m is presented in the report "Brattashang, St. Moritz: Dilatometerversuche" by U. Sambeth (**Appendix II**).

An overview of the location of the tests with respect to the samples taken from the borehole and the Marchetti-Dilatometer tests is given in Table 2 as well as the average Young's Modulus for compression and un-reloading for each test performed.

5. Marchetti Dilatometer tests in the borehole.

Contributor: A. Schmid, R. Rohr, S. Messerklinger, A.M. Puzrin

Marchetti dilatometer tests were performed in the borehole to investigate the soil stiffness over the depth and to compare the stiffness determined with the Marchetti Dilatometer to the stiffness measurement data given by the:

- Dilatometer-Pressiometer tests also performed in the borehole (point 4) and
- Oedometer test performed subsequently in the laboratory on samples taken from the borehole (Report No.: 4714/1).

The Marchetti dilatometer tests were performed with the equipment of IGT ETHZ. The test procedure is as follows:

- The membrane of the Dilatometer is calibrated by measuring the ΔA and ΔB values (The internal pressure at which the membrane separates from the contact at atmospheric pressure).

- The Dilatometer was inserted into the borehole and pressed into the soil.
- Pressure was slowly applied and the pressure at which the membrane separates from the contact (when the peep signal stops) and the pressure at which the membrane 1.1 mm perpendicular to the membrane surface (when the peep signal starts again) is recorded which represents the A and B value respectively.
- The measurement data of the A and B reading for each of the 11 tests performed is presented in Table 2.

The data evaluation is done according to the recommendations in Marchetti et al. (2001) "The Flat Dilatometer Test (DMT) in soil investigations" which is attached in **Appendix III**. The evaluation procedure is highlighted on the results of test 1:

Corrected first reading:

$$p_o = 1.05\ (A + \Delta A) - 0.05(B - \Delta B) = 1.05\ (4.25 + 0.29) - 0.05(12.5 - 0.28) = 4.16 \text{ bar}$$

Corrected second reading:

$$p_1 = B - \Delta B = 12.5 - 0.28 = 12.22 \text{ bar}$$

Material Index: (u_o = pore water pressure; it is assumed that the soil behaves drained, therefore u_o is always zero. The groundwater level is only considered for the calculation of the effective vertical overburden pressure, see footnote.)

$$I_D = (p_1 - p_o) / (p_o - u_o) = (12.22 - 4.16) / (4.16 - 0) = 1.94$$

Horizontal stress index:[a]

$$K_D = (p_o - u_o) / \sigma'_{vo} = (4.16 - 0) / (1.5 * 18\ KN/m^3 + (6.4 - 1.5\ m) * (18 - 10\ KN/m^3) = \\ = 66.2\ kPa = 0.66\ bar) = 6.28$$

Dilatometer Modulus:

$$E_D = 34.7\ (p_1 - p_o) = 34.7\ (12.22 - 4.16) = 280\ bar = 28\ MPa$$

---

[a] Therefore the mean effective vertical stress σ_m' is needed. A unit soil weight of 18 KN/m3 is assumed (such as for the Marchetti Dilatometer data evaluation, Report No.: 4714/1) and the pore water pressure distribution over depth is taken from former piecometer measurements (Report No. 3676/10, Beilage Nr. 7) next to the tower in St. Moritz were also the herein investigated boring No. 0601 is situated. (3 piecometers are installed in boring 11 at depth of 10.3, 14 and 17 m which measured over the past 15 years water pressures of 8.8 m @ 10.3 m depth, 10.0 m @ 14.0 m depth and 15.0 m @ 17.0 m depth). Therefore

Tab. 2: Overview of the tests performed in and the samples taken from the borehole.

Depth [m]	Sample number	Marchetti dilatometer: A, B [bar], Young's Modul E [MPa] & Earth pressure coefficient K_o [-]	Dilatometer-Pressiometer: Young's Modulus E compression and swelling [MPa]
4.85 – 5.05	1		
5.00			E_{comp} = 15.0 E_{ur} = 110.0
6.20 – 6.30	2		
6.40		1/a[b]: A: 4.25 B: 12.5 - E: 48 – K_o: 1.4 No 1/b measurement!	
8.82 – 9.04	3		
8.50 – 8.75	3a		
8.94			E_{comp} = 15.0 E_{ur} = 156.5
9.10 – 9.55	3b		
10.20 – 10.50	4		
10.40		2/a[c]: A: 4.5 B: 12.5 - E: 39 – K_o: 1.1	
10.50 – 10.70	5		
10.60		2/b[c]: A: 6.5 B: 22.5 - E: 96 – K_o: 1.3 (I_D>1.2!)	
10.70 – 10.90	6		
10.80		2/c[c]: A: 7.0 B: 16.5 - E: 56 – K_o: 1.4	
10.90 – 11.20	7		
11.00		2/d[c]: A: 5.8 B: 20.0 - E: 79 – K_o: 1.2 (I_D>1.2!)	
13.80 – 14.00	8		
13.70			E_{comp} = 10.0 E_{ur} = 93.0 After the test at 13.90 m! Only loading &unloading
13.90		3/a[b]: A: 4.1 B: 11.5 - E: 26 – K_o: 0.7	E_{comp} = 8.0 E_{ur} = 178.0 Only loading & unloading!
14.00 – 14.20	9		
14.10		3/b[b]: A: 6.2 B: 19.5 - E: 62 – K_o: 1.0 (I_D>1.2!)	
14.20 – 14.40	10		
14.25		3/c[b]: A: 8.2 B: 20.1 - E: 64 – K_o: 1.2	
15.80 – 16.00	11		
16.30 – 16.47	12		
16.47 – 16.85	13		
16.50		4/a[b]: A: 5.1 B: 24.0 - E: 85 – K_o: 0.8 (I_D>1.2!)	
16.62		4/b[b]: A: 10.8 B: 33.0 - E: 138 – K_o: 1.4 (I_D>1.2!)	
16.70		4/c[b]: A: 14.5 B: 37.5 - E: 162 – K_o: 1.7	
17.00 – 17.25	14		

the groundwater level for test 1 and 2 is 1.5 m below surface, for test 3 the groundwater level is 4 m below surface and for test 4 the groundwater level is 2 m below surface.

[b] Calibration values: ΔA = 0.29 ΔB = 0.28 bar.

[c] Calibration values: ΔA = 0.31 ΔB = 0.30 bar.

Vertical drained constraint Modulus:

$$\text{for } 0.6 < I_D < 3: \quad R_M = R_{M,o} + (2.5 - R_{M,o}) \log K_D = 0.34 + (2.5 - 0.34) \log (6.28) = 2.06$$

$$R_{M,o} = 0.14 + 0.15 (I_D - 0.6) = 0.14 + 0.15 (1.94 - 0.6) = 0.34$$

$$M_{DMT} \text{ (for } 0.6 < ID < 3) = R_M * E_D = 2.06 * 28 = 57.7 \text{ MPa}$$

Young's Modulus: (with $\nu = 0.25$)

$$E = (1 + \nu)(1 - 2\nu) M / (1 - \nu) = 0.83 M_{DMT} = 0.83 * 57.7 = \underline{\mathbf{48 \text{ MPa}}}$$

Earth pressure coefficient (the formulation is valid if $I_D < 1.2$):

$$K_{o,DMT} = (K_D / 1.5)^{0.47} - 0.6 = (6.28 / 1.5)^{0.47} - 0.6 = \underline{\mathbf{1.36}}$$

6. Infrared pictures of the Brattas slide.

Contributor: S. Messerklinger, A.M. Puzrin, T. Walther and W. Trefzer both company Pergam

Infrared pictures were taken from the Brattas slide with the aim to observe the location of compression zones and/or water flows.

The basic idea: Infrared cameras record the temperature distribution on the surface. When one picture is taken in the morning and another in the evening two phenomena's are visible:

- An area where water is flowing stays cold over the day.
- During the day areas with high pressure heat up more than areas with lower pressures (comparison between morning and evening temperature distribution).

Infrared pictures of the Brattas landslide were made from a helicopter by the company Pergam (Pictures taken by Thomas Walther, Helicopter pilot: Werner Trefzer; Company: Pergam-Suisse AG Talacker 42, 8001 Zürich).

The pictures were taken on Tuesday 11th July 2006 between 6 and 6:30 pm and on Wednesday 12th July 2006 between 8 and 8:30 am. On Tuesday it was sunny all day only at about 5:30 pm a thunderstorm occurred between the airport in Samaden and the landslide in St. Moritz.

The files of the infrared pictures taken are on the CD in **Appendix IV**.

7. Photographs and their photogrammetrical evaluation of the geodetical points.

Contributor: M. Sauerbier (Institute of Geodesy and Photogrammetry (IGP), ETH Zurich), S. Messerklinger, A.M. Puzrin, T. Walther and W. Trefzer both company Pergam

Photographs of the Brattas slide were made from the helicopter, next to the infrared pictures, with the aim to photogrammetrical evaluation the pictures and to determine the coordinates of the newly installed geodetical points (point 1) also with this method.

The photogrammetrical evaluation was done by M Sauerbier (Room No.: HIL D52.4; Tel. No.: +41 44 633 32 87 ; email: martin.sauerbier@geod.baug.ethz.ch).

His detailed report **(Appendix V)** is still in preparation and will be attached later.

8. Electromagnetic radiation measurements.

Contributor: A. Schmid, S. Messerklinger, A.M. Puzrin and M. Lichtenberger (Geologisch-Paläontologisches Institut der Ruprechts-Karls-Universität Heidelberg)

Electromagnetic radiation measurements were made with the aim to observe compression zones along the Brattas landslide.

The principle:

When stones are under pressure inside the stone mass micro-cracks develop. These cracks separate the material and consequently the atomic net locally, therefore some of the atoms at the crack have to relocate themselves in the remaining atomic net. This "movement" of atoms produces electromagnetic waves.

The special characteristic of these waves is that they are "pulsed", which means their amplitude reduces with the number of peaks (Fig. 2). These pulsed waves can be measured. The difficulty in this measurement is to filter the electromagnetic emission caused by the civilized environment.

The apparatus:

For the measurement of electromagnetic emission of rocks and stones an apparatus with the corresponding software was developed in the Ukraine. This apparatus is called CERESCOP and is commercially offered e.g. by Dr. Hennes Obermeyer from the "Gesellschaft für Erkundung & Ortung, Yorckstrasse 36, D-76185 Karlsruhe, e-mail: hennes.obermeyer@inka.de. The two apparatuses used for the radiation measurements in St. Moritz were as well provided by him.

The apparatus consists of a box and an antenna, which is connected to the box via a cable and a plug. The box contains a screen, a keypad and three plugs for the antenna, the charging unit and the data transfer, respectively.

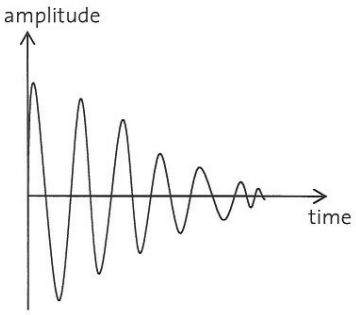

Fig. 2: Principles of electromagnetic radiation: pulsed wave.

The measurements

On Thursday the 13th and Friday the 14th of July 2006, radiation measurements were performed using two apparatuses in parallel. An "old" apparatus which was operated by Marco Lichtenberger and a "new" apparatus operated by S. Messerklinger.

With the old apparatus M. Lichtenberger performed "horizontal radiation measurements". He was held the antenna horizontally, starting towards the north and subsequently turning clockwise in steps of 5°, and logged the received magnitude of electromagnetic radiation at each step for one rotation of 360°. This measurement gave next to the magnitude also the horizontal orientation of the radiation.

With the new apparatus S. Messerklinger performed "vertical radiation measurements". She held the antenna vertically towards the ground and logged the received electromagnetic radiation. At each point the radiation was logged ten times and the average was used. In this measurements the receiving frequency ranges was set to comparable low values of 5 – 15 MHz with the aim to receive radiations from depth of up to approximately 20 metres (M. Lichtenberger, 2006).

- **Initial settings**

At the start of a measurement series the spectrum and the amplification has to be set.

Spectrum: The cerescop measures within a frequency spectrum of 5 to 50 MHz. The received magnitudes for the corresponding frequency can be plotted on the screen of the apparatus. Peaks in this plot indicate interferences at the related frequency and jumping curves indicate general interferences. To avoid influences due to interferences at certain frequencies, the frequency spectrum, considered for the measurement, can be defined by the user. Typically, a range next to the peaks but within the boundaries of 5 and 50 MHz is selected.

Attention: By choosing a frequency range it has to be considered that the frequency is related to the measurement distance. Low frequencies result in a larger observation distance than higher. The observation distance can be calculated after (Lichtenberger, 2006) and is typically in a range of 2 to 20 metres for the given frequency spectrum of 5 to 50 MHz. The spectrum set in the new apparatus was 5,0 to 15,2 MHz.

Amplification: One the one hand the received signals are amplified by a given factor, on the other hand the zero line, above which the signals are considered, is moved towards the peaks so that only the most top peak of the wave is used in the data evaluation. Any combination of amplification and "cut-off" can be defined by the user. However, the best data resolution is given when the Parameter A results in values between 100 and 3000 for the regions with low and high compression, respectively (Lichtenberger, 2006).

These amplification factors are next to the signals also dependent on the type and quality of the antenna. Therefore different values had to be chosen for the new and the old apparatus. For the old apparatus the factors were set to 14 and 44 and in the new apparatus to 2 and 16.

The results:

The parameter A was used for the data analysis of the horizontal as well as the vertical measurements. The data of all measurements are presented in **Appendix VI**.

The analysis:

Electromagnetic radiation is sent in the direction of the micro-crack. Micro-cracks develop in the plane of the maximal and the intermediate stress direction and perpendicular to the minimum stress direction. The antenna can measure only waves which propagate in the direction of the antenna.

This means:

At the top of the landslide, the maximum stress direction is vertical towards the ground due to gravity, the intermediate stress direction is towards the width of the landslide due

to lateral earth pressure and the minimum stress direction is along the sliding direction of the landslide. (This is the case close to a tension crack, when no additional weight acts on the topside of the landslide.)

At the bottom end of the landslide at a compression zone, the maximum stress direction is the sliding direction of the landslide because the entire soil-mass above is pushing. The intermediate stress direction is vertical towards the ground due to gravity. The minimum stress direction is towards the width of the landslide due to lateral earth pressure. The stress magnitude of the gravity and the resulting lateral earth pressure is the same as at the top of the landslide (assuming the landslide has a constant depth/thickness).

In between the principal stress directions will change more or less suddenly from the top to the bottom state.

The orientation of the microcracks developing at the different stress states along a landslide with a compression zone at the bottom side and a tension zone at the top side is shown in Fig. 3.

EMR measurements:

Horizontal antenna:

At the top side the direction of the antenna is perpendicular to the direction of the microcracks. Consequently, the radiation possible to receive by the antenna will be small. Additionally, the magnitude of radiation will be small, close to the tension zone.

At the bottom side, after the change of the principal stress directions, the direction of the antenna is parallel to the direction of the micro-cracks. Consequently, the radiation possible to receive by the antenna will be large. Additionally, the magnitude of radiation will be high, close to the compression zone.

Vertical antenna:

At the top side the direction of the antenna is parallel to the direction of the microcracks. Consequently, the radiation possible to receive by the antenna will be large. But the magnitude of radiation will be small, close to the tension zone.

At the bottom side, after the change of the principal stress directions, the direction of the antenna is again parallel to the direction of the micro-cracks. Consequently, the radiation possible to receive by the antenna will be large such as at the top side. And the magnitude of radiation will be high, close to the compression zone.

19

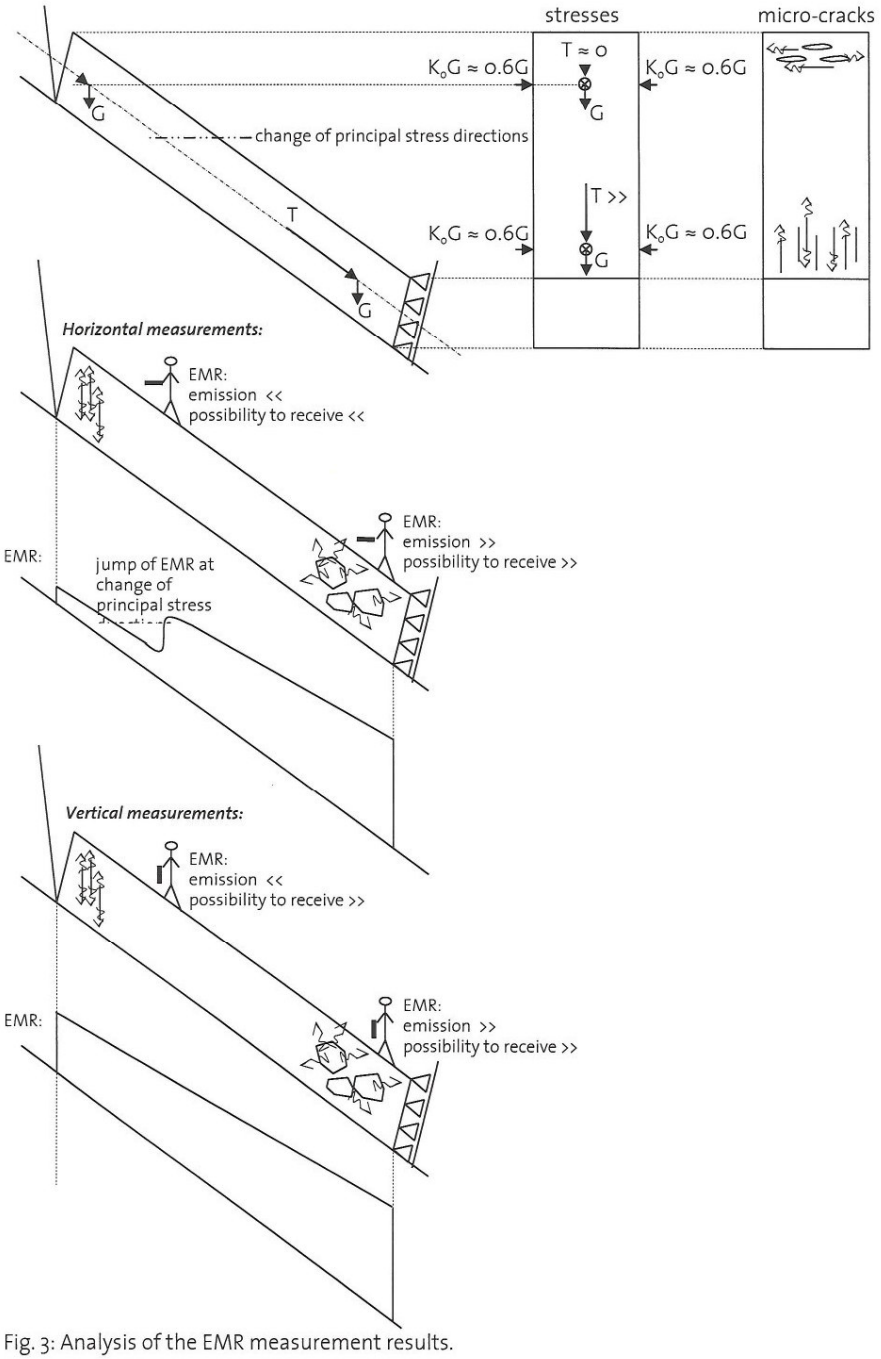

Fig. 3: Analysis of the EMR measurement results.

Conclusions:

It should be possible to detect a compression zone in a landslide with the measurement of electromagnetic radiation along the landslide.

With vertical measured EMR the magnitude of EMR should increase continuously towards the compression zone.

With horizontal measured EMR the magnitude should increase as well continuously, starting from very low magnitudes at the tension zone and with a sudden increase in magnitude at the location of the change of the principal stress direction.

The analysis of the vertical and horizontal measurements performed on the newly installed geodetical points (point 1) on the Brattas slide and the data of every single measurement are presented in **Appendix VI**.

Report No. 4714 Mes/Schm/Rr/IS/AMP

Zurich, 1. November 2007

ETH Zurich
Institute for Geotechnical Engineering

Dr. Sophie Messerklinger
Dipl. Bauing.

Appendix I:

Staub P. (2006)

"Geodätische Geländeüberwachung: Hangrutschungsmessungen im Gebiet Gianda Laret-Brattas, Gemeinde St. Moritz".

Der Bericht:

"Geodätische Geländeüberwachung:
Hangrutschungsmessungen im Gebiet Gianda Laret-Brattas,
Gemeinde St. Moritz"
Staub P. (2006)

befindet sich am Institut für Geotechnik, Wolfgang-Pauli-Str. 15, 8093 Zürich und kann jederzeit eingesehen oder zugestellt werden.

Appendix II:

Sambeth U. (2006)

"Brattashang, St. Moritz: Dilatometerversuche".

V 14/08/06 Ds.

Stump ForaTec AG

Die Spezialisten für:
Sondierbohrungen, Zweckbohrungen, Tiefbohrungen, Pendelbohrungen
Grundwasserarbeiten, Gefrierverfahren, Messtechnik

Zertifiziertes Management System **SGS ISO 9001:2000**

MWST-Nr. 563 955

Messtechnik

Stationsstrasse 57
CH-8606 Nänikon
Telefon: 043 399 29 29
Fax: 043 399 29 39
www. stump.ch

51-1657

Brattashang

St. Moritz

Dilatometerversuche

Bauleitung: ETH Zürich
Institut für Geotechnik
8093 Zürich

Verfasser: Stump ForaTec AG
Stationsstrasse 57, 8606 Nänikon-Uster
Vertreten durch: Hr. Sambeth, Hr. Wolfensberger

Nänikon den 8. August 2006

Inhaltsverzeichnis

Anhang:

1. Einführung

Dilatometermessungen dienen der Ermittlung der Verformungseigenschaften im Bohrloch. Dabei werden Verformungs- und Elastizitäts-Modul im Felsverband und unter dem herrschenden hydrostatischen Druck bestimmt.

Im Auftrag des Instituts für Geotechnik der ETH Zürich, wurden von der Stump ForaTec AG, Abteilung Messtechnik, vier Dilatometerversuche in der Bohrung 0601 durchgeführt. Die Bohrung von 101mm Durchmesser wurde im anstehenden Gehängeschutt abgeteuft. Die Dilatometerversuche erfolgten am 11. bis 13. Juli 2006.

Die Bohrung ist vertikal. Bei sämtlichen Versuchen lag der Wasserspiegel tiefer als die Versuchsstrecke.
Die Versuche eins (Tiefe von 5.0m) und zwei (bei 8.95m) wurden plangemäss ohne spezielle Vorkommnisse beendet.
Der dritte Versuch in 13.9m Tiefe wurde bei etwas über 2 Bar Versuchsdruck vorzeitig abgebrochen, da der Messgeber Nummer 2 eine unverhältnismässig schnelle Deformationszunahme zeigte und deshalb ein Bruch der Membrane befürchtet werden musste.
Nach dem dritten Versuch wurde der Dilatometer 20cm nach oben gezogen und der vierte Versuch begonnen. Dabei bot der sandige Ton/Lehm so wenig Widerstand, dass der Versuch bei etwas über 60 Bar Druck aufgrund der grossen aufgetretenen Deformationen wiederum abgebrochen werden musste.

Um die Verformungs- und Elastizitätsmoduli (Young's modul) in situ zu bestimmen, wurde für die Dilatometerversuche eine Schlauchsonde Typ „Cambridge Insitu", verwendet (siehe Anhang A2).

2. Technische Grundlagen

Die Dilatometersonde, Typ „Cambridge Insitu", besteht aus einem Metallzylinder, wobei dessen mittlerer Teil mit einer speziellen Gummimembrane versehen ist. Mit Hilfe von Gestängen wird diese Sonde an die zu untersuchende Stelle geführt. Um die Verformung des Gesteins zu analysieren, wird die Membrane unter hohem Druck an die Bohrlochwandung gepresst.

Der Druck wird von Druckflaschen (durch Kompressor gespiesen) über einen Hochdruckschlauch zur Sonde geführt. Dieser Schlauch kann in verschiedene Längen unterteilt werden und enthält ebenfalls das Elektrokabel für die Übertragung der Messresultate. Der Druck wird in der Sonde von zwei Druckzellen gemessen. Eine Druckkontroll-Vorrichtung erlaubt, den Druck von der Oberfläche aus zu regulieren. Der Arbeitsdruck reicht bis 20 MPa.

Die Verformung wird von 6 Wegaufnehmern registriert, deren Orientierung mittels eines Kompasses bestimmt wird. Die Messwerte werden mit einer Auflösung von 0,001 mm automatisch und kontinuierlich auf einen angeschlossenen Computer digital übertragen, wo sie alle 10 Sekunden graphisch und tabellarisch dargestellt und gespeichert werden. Mittels der internen Elektronik werden alle Signale schon in der Sonde digitalisiert. Die digitale Übertragung verhindert Verfälschungen der Messresultate auf der Übertragungsstrecke.

Das Instrument misst Wegänderungen (radiale Deformation, in mm) gegenüber Druck (in Pa). Die Analyse beruht darauf, dass das Material homogen, isotropisch und als Kontinuum angenommen werden kann.

Die moderne Messvorrichtung erlaubt einen sehr flexiblen Einsatz dieser Sonde auch bei relativ komplizierten Verhältnissen. Jeder Messgeber (Druck, Kompass, usw.) wird zweimal aufgeführt um redundante Messwerte zu erhalten. Je nach Durchmesser der Bohrung, 76mm, 96mm oder 101 mm, stehen Sonden mit einem Durchmesser von 73mm, 93mm und 95 mm zur Verfügung.

3. Ablauf der Messungen

Die Teststrecke wurde vor Ort festgelegt. Anhand der zur Verfügung stehenden Bohrkerne wurde die genaue Position der Versuchsstrecke bestimmt. Die Messungen wurden von Messtechnikern der Firma Stump ForaTec AG, und mit Hilfe des Bohrpersonals durchgeführt. Die Dilatometersonde wurde vorgängig in unserer Werkstatt kalibriert und geeicht.

Die Versuche wurden wenn möglich in 2 Lastzyklen durchgeführt. Der erste Lastzyklus besteht aus einer Erstbelastung und einer Entlastung. Danach folgt eine Wiederbelastung (bis zum maximalen Belastungswert des ersten Lastzyklus), eine Erstbelastung und Entlastung. Es wurde folgendes Belastungs-Entlastungs-Schema gewählt:

1. Lastzyklus: Belastung bis ca. 80 bar
   Entlastung bis ca. 25 bar
2. Lastzyklus: Belastung bis ca. 100 bar
   Entlastung bis 0 bar

4. Resultate und Auswertung

Die aus dem Dilatometerversuch gewonnenen Messdaten werden in einem Belastungs-Verformungsdiagramm dargestellt, aus dem die Verformungs- und Schermoduli abgeleitet werden können.

Die Verformungsmoduli werden aus den Daten der jeweiligen Erstbelastung berechnet. Die Daten der nachfolgenden Entlastung liefern die Entlastungsmoduli.
Das Schermodul G ist die Änderung der Scherbeanspruchung durch die Änderung der Scherdeformation. Die Scherbeanspruchung ist gegeben durch die Änderung des Druckes während eines Entlastungs- bzw. Belastungszyklus.
Die Deformation ist gegeben durch die Änderung des Radius des Instrumentes. Die radiale Deformation ist gegeben durch die Zunahme des Radius durch den Originalradius der Sonde. Die doppelte radiale Deformation ist gleich der Scherdeformation.

Der E-Modul (Young's Modul) wird schliesslich durch folgende Formel berechnet:

$$E = 2 G (1 + v)$$

G = Schermodul; E = Elastizitätsmodul oder Young's modul
v = Poisson-Zahl (Annahme v = 0,25)

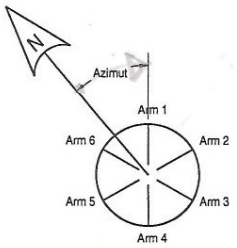

Die gemessene Orientation entspricht dem Azimut des Weggebers 1 = Arm 1
Bei der horizontalen Bohrung 2 wurde Arm 1 nach oben gerichtet.

Die ausführlichen Messresultate befinden sich im Anhang. Dabei bedeuten

- Ave of 6 Arms vs Total Pressure = Durchschnitt aller 6 Arme gegen Druck
- All 6 Arms vs Total Pressure = Alle 6 Arme einzeln gegen Druck
- Arm pairs vs Total Pressure = Armpaare gegen Druck
- True Strain vs Pressure = Verformung (Ln [R/R_0]) gegen Druck

Ebenfalls liegt eine CD-ROM mit den Rohdaten (für das Programm logger.exe, v7.14, Cambridge Insitu) und den kalibrierten Deformationswerten (.csv, ASCII-Dateien) bei. Die kalibrierten Versuchsdaten liegen zumTeil in zwei Versionen vor, mit für den jeweils angegebenen Druckbereich optimierten Eichwerten.
Der Versuch T1T1 ist die Eichung, welche vorgängig im Aluminium-Testrohr Ø 127x108mm durchgeführt wurde.

Stump ForaTec AG

U. Sambeth

i.V. M. Wolfensberger

M. Wolfensberger

BE51-1657.doc, 08.08.06

Anhang A1

Belastungs-/ Verformungsdiagramme aller Versuche

Brattashang, St. Moritz

B6 / Test 1

Dilatometerversuche

Datum: 11. 07. 2006	Azimut: 283°	Sondendurchm. ($D_{Sond.}$): 95.0 mm
Tiefe: 5.00 m	Wasserdruck: 0 kPa	Poissonzahl (v): 0.25

Punkt	Druck	Arm 1	Arm 2	Arm 3	Arm 4	Arm 5	Arm 6
1	236 kPa	4.151 mm	3.731 mm	3.211 mm	3.059 mm	3.503 mm	4.006 mm
2	932 kPa	6.816 mm	6.160 mm	6.323 mm	7.121 mm	6.232 mm	6.430 mm
3	956 kPa	7.410 mm	6.746 mm	7.046 mm	8.077 mm	6.754 mm	6.934 mm
4	234 kPa	6.981 mm	6.325 mm	6.683 mm	7.679 mm	6.379 mm	6.564 mm
5	954 kPa	7.503 mm	6.888 mm	7.241 mm	8.392 mm	6.932 mm	7.098 mm
6	955 kPa	7.451 mm	6.836 mm	7.189 mm	8.341 mm	6.880 mm	7.046 mm
7	1'043 kPa	7.730 mm	7.113 mm	7.505 mm	8.740 mm	7.134 mm	7.298 mm
8	1'022 kPa	8.319 mm	7.699 mm	8.160 mm	9.597 mm	7.638 mm	7.769 mm
9	833 kPa	8.275 mm	7.666 mm	8.135 mm	9.572 mm	7.604 mm	7.740 mm

Stufe			Arme 1/4	Arme 2/5	Arme 3/6	Arme 1-6
1-2	**Erstbelastung**	Durchm. (D_1)	102.210 mm	102.234 mm	102.217 mm	102.220 mm
	Zyklus Start: 236 kPa	Def. (ΔD)	6.727 mm	5.158 mm	5.536 mm	5.807 mm
	Zyklus Ende: 932 kPa	Schermod. (G)	5 MPa	7 MPa	6 MPa	**6 MPa**
	Scherbeanspr. (ΔP): 696 kPa	E-Modul (E)	13 MPa	18 MPa	15 MPa	**15 MPa**
3-4	**Entlastung**	Durchm. (D_3)	110.487 mm	108.500 mm	108.980 mm	109.322 mm
	Zyklus Start: 956 kPa	Def. (ΔD)	-0.827 mm	-0.796 mm	-0.733 mm	-0.785 mm
	Zyklus Ende: 234 kPa	Schermod. (G)	48 MPa	49 MPa	54 MPa	**50 MPa**
	Scherbeanspr. (ΔP): -722 kPa	E-Modul (E)	120 MPa	123 MPa	135 MPa	**125 MPa**
4-5	**Wiederbelastung**	Durchm. (D_4)	109.660 mm	107.704 mm	108.247 mm	108.537 mm
	Zyklus Start: 234 kPa	Def. (ΔD)	1.235 mm	1.116 mm	1.092 mm	1.148 mm
	Zyklus Ende: 954 kPa	Schermod. (G)	32 MPa	35 MPa	36 MPa	**34 MPa**
	Scherbeanspr. (ΔP): 720 kPa	E-Modul (E)	80 MPa	88 MPa	90 MPa	**85 MPa**
6-7	**Erstbelastung**	Durchm. (D_5)	110.792 mm	108.716 mm	109.235 mm	109.581 mm
	Zyklus Start: 955 kPa	Def. (ΔD)	0.678 mm	0.531 mm	0.568 mm	0.592 mm
	Zyklus Ende: 1'043 kPa	Schermod. (G)	7 MPa	9 MPa	8 MPa	**8 MPa**
	Scherbeanspr. (ΔP): 88 kPa	E-Modul (E)	18 MPa	23 MPa	20 MPa	**20 MPa**
8-9	**Entlastung**	Durchm. (D_7)	112.916 mm	110.337 mm	110.929 mm	111.394 mm
	Zyklus Start: 1'022 kPa	Def. (ΔD)	-0.069 mm	-0.067 mm	-0.054 mm	-0.063 mm
	Zyklus Ende: 833 kPa	Schermod. (G)	155 MPa	156 MPa	194 MPa	**167 MPa**
	Scherbeanspr. (ΔP): -189 kPa	E-Modul (E)	388 MPa	390 MPa	485 MPa	**418 MPa**

$$G = \frac{\Delta P}{\Delta r} = \frac{\Delta P}{\frac{\Delta D}{2}}$$

$$E = 2G(1+\nu) \qquad \text{Annahme} \quad \nu = 0{,}25$$

$$M_E = \frac{(1+\nu)(1-2\nu)}{(1-\nu)} \approx \frac{E}{0{,}8}$$

51-1657 Dilato Bohrung 0601.xls, 5m, 04.08.2006, 14:44

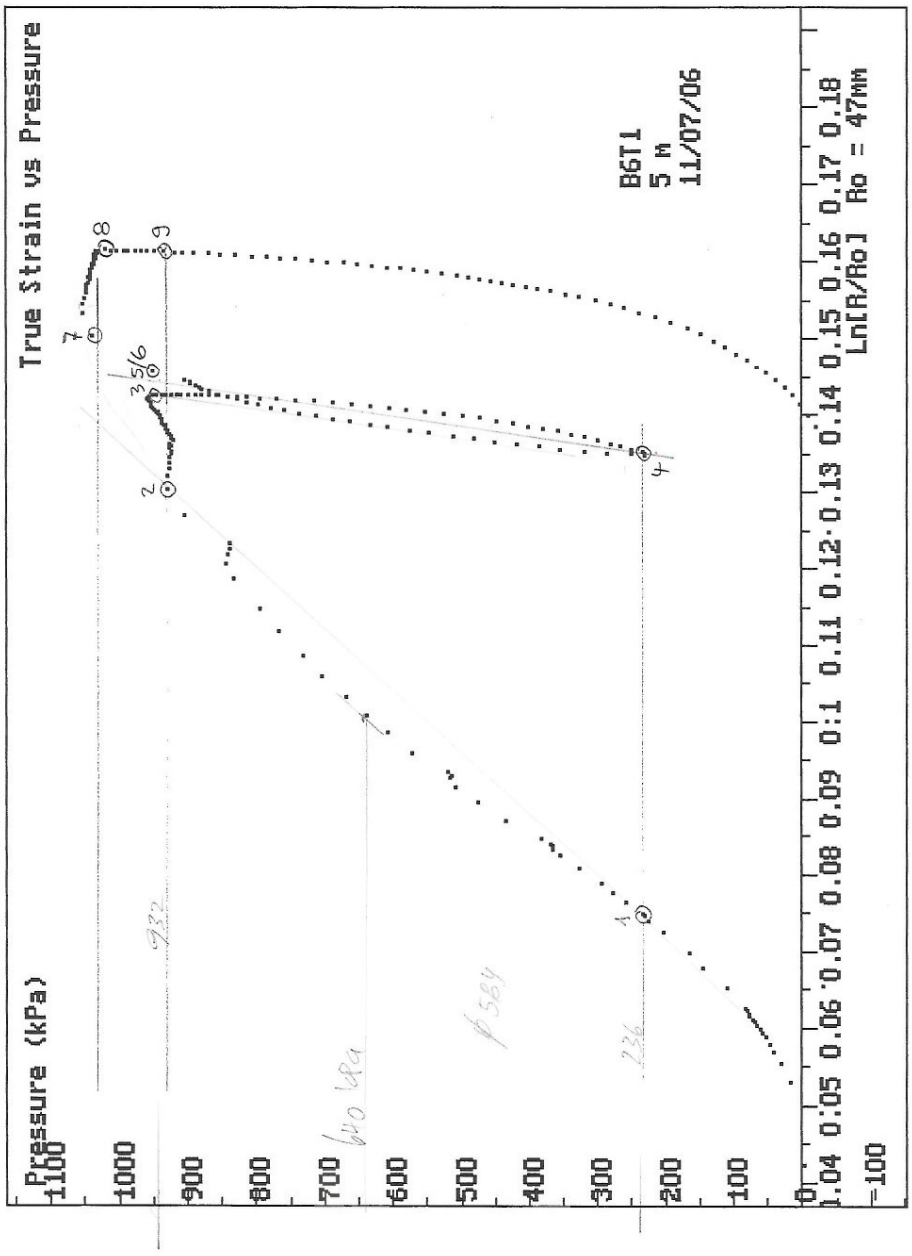

SCREEN DUMP Test: B6T1 Date: 11/07/06 Depth: 5.00m
Dilatometerversuche ausgefuehrt durch die Abt. Messtechnik
der Stump ForaTec AG. www.stump.ch messtechnik@stump.ch

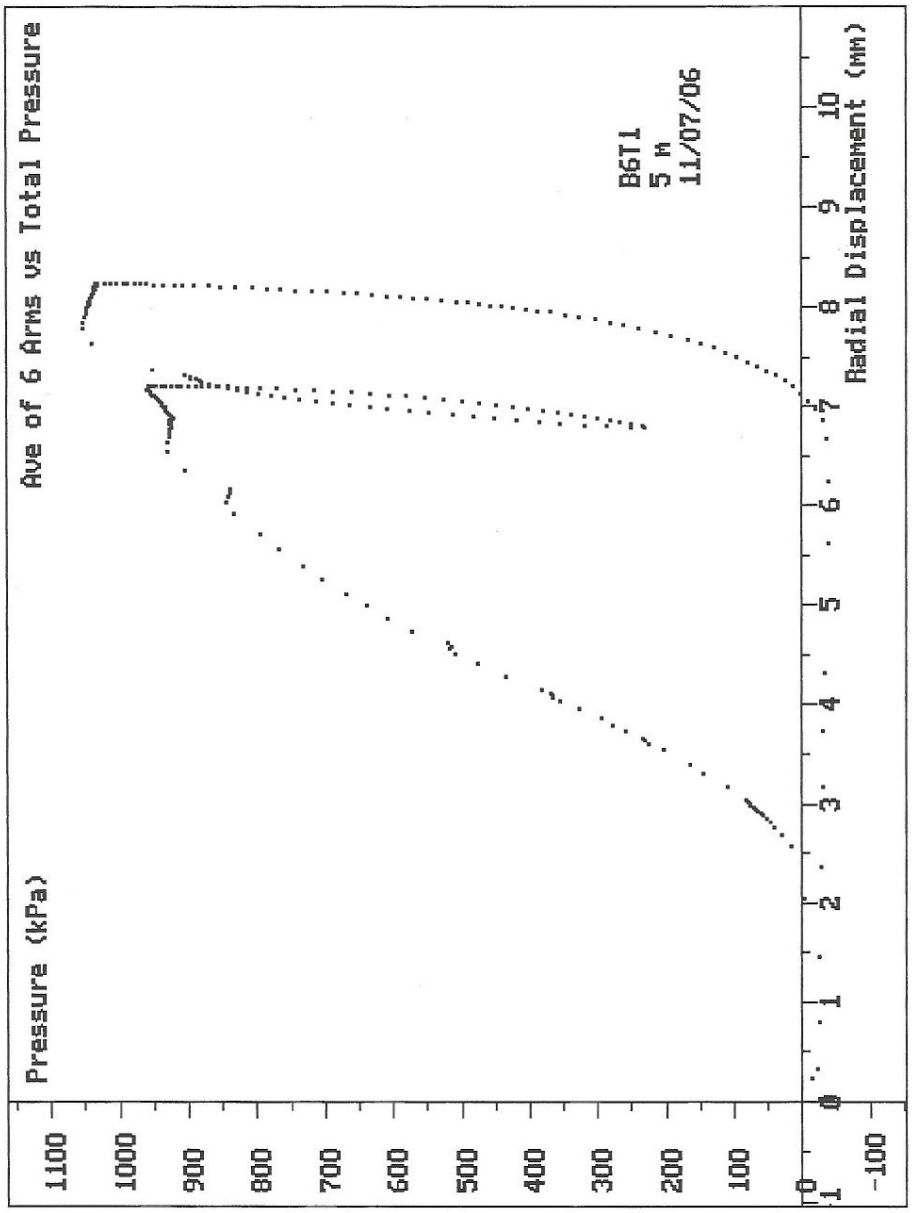

SCREEN DUMP Test: B6T1 Date: 11/07/06 Depth: 5.00m
Dilatometerversuche ausgefuehrt durch die Abt. Messtechnik
der Stump ForaTec AG. www.stump.ch messtechnik@stump.ch

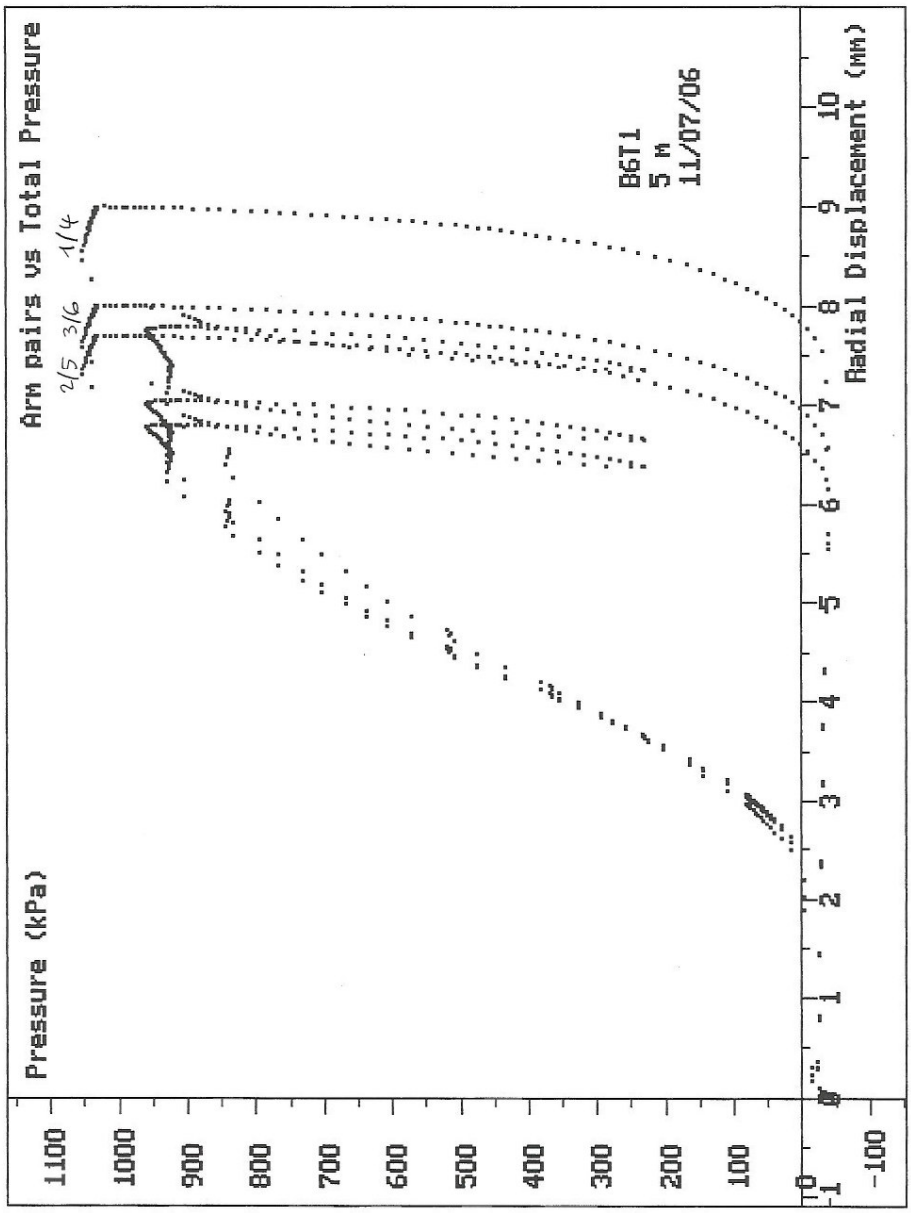

SCREEN DUMP Test: B6T1 Date: 11/07/06 Depth: 5.00m
Dilatometerversuche ausgefuehrt durch die Abt. Messtechnik
der Stump ForaTec AG. www.stump.ch messtechnik@stump.ch

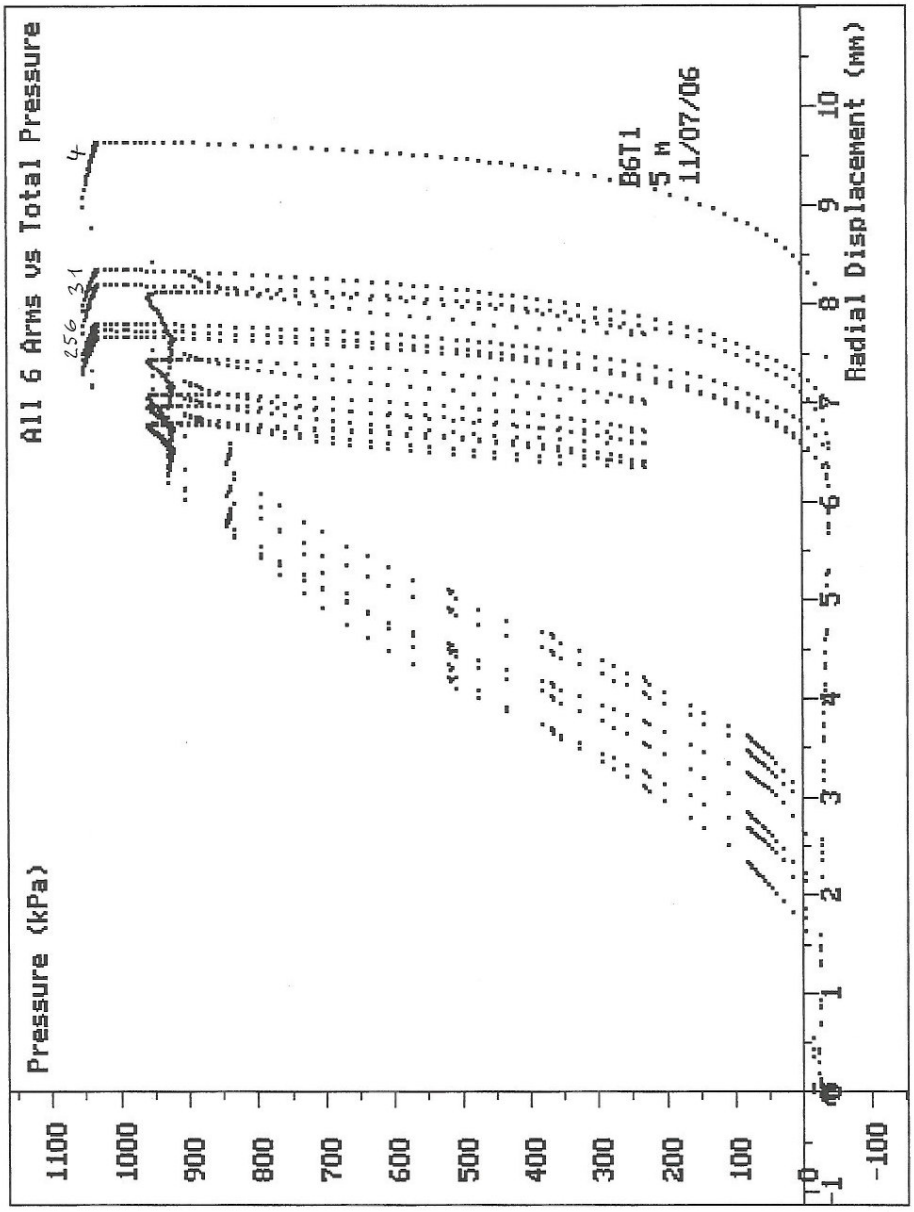

SCREEN DUMP Test: B6T1 Date: 11/07/06 Depth: 5.00m
Dilatometerversuche ausgefuehrt durch die Abt. Messtechnik
der Stump ForaTec AG. www.stump.ch messtechnik@stump.ch

Brattashang, St. Moritz

B6 / Test 2

Dilatometerversuche

Datum: 12. 07. 2006 | Azimut: 165 ° | Sondendurchm. ($D_{Sond.}$): 95.0 mm
Tiefe: 8.94 m | Wasserdruck: 0 kPa | Poissonzahl (v): 0.25

Punkt	Druck	Arm 1	Arm 2	Arm 3	Arm 4	Arm 5	Arm 6
1	259 kPa	6.772 mm	10.082 mm	9.644 mm	9.763 mm	4.925 mm	7.933 mm
2	827 kPa	8.933 mm	13.726 mm	13.234 mm	13.008 mm	6.418 mm	9.164 mm
3	860 kPa	9.630 mm	14.520 mm	14.006 mm	13.754 mm	7.049 mm	9.614 mm
4	252 kPa	9.355 mm	14.132 mm	13.740 mm	13.425 mm	6.938 mm	9.542 mm
5	861 kPa	9.734 mm	14.699 mm	14.146 mm	13.872 mm	7.148 mm	9.664 mm
6	860 kPa	9.785 mm	14.750 mm	14.198 mm	13.923 mm	7.199 mm	9.715 mm
7	1'009 kPa	10.290 mm	15.276 mm	14.628 mm	14.367 mm	7.619 mm	10.020 mm
8	1'012 kPa	11.488 mm	16.428 mm	15.528 mm	15.168 mm	8.410 mm	10.670 mm
9	848 kPa	11.462 mm	16.411 mm	15.517 mm	15.142 mm	8.382 mm	10.648 mm

Stufe			Arme 1/4	Arme 2/5	Arme 3/6	Arme 1-6
1-2	**Erstbelastung**	Durchm. (D_1)	111.535 mm	110.007 mm	112.577 mm	111.373 mm
	Zyklus Start: 259 kPa	Def. (ΔD)	5.406 mm	5.137 mm	4.821 mm	5.121 mm
	Zyklus Ende: 827 kPa	Schermod. (G)	6 MPa	6 MPa	7 MPa	**6 MPa**
	Scherbeanspr. (ΔP): 568 kPa	E-Modul (E)	15 MPa	15 MPa	18 MPa	**15 MPa**
3-4	**Entlastung**	Durchm. (D_3)	118.384 mm	116.569 mm	118.620 mm	117.858 mm
	Zyklus Start: 860 kPa	Def. (ΔD)	-0.604 mm	-0.499 mm	-0.338 mm	-0.480 mm
	Zyklus Ende: 252 kPa	Schermod. (G)	60 MPa	71 MPa	107 MPa	**75 MPa**
	Scherbeanspr. (ΔP): -608 kPa	E-Modul (E)	150 MPa	178 MPa	268 MPa	**188 MPa**
4-5	**Wiederbelastung**	Durchm. (D_4)	117.780 mm	116.070 mm	118.282 mm	117.377 mm
	Zyklus Start: 252 kPa	Def. (ΔD)	0.826 mm	0.777 mm	0.528 mm	0.710 mm
	Zyklus Ende: 861 kPa	Schermod. (G)	43 MPa	45 MPa	68 MPa	**50 MPa**
	Scherbeanspr. (ΔP): 609 kPa	E-Modul (E)	108 MPa	113 MPa	170 MPa	**125 MPa**
6-7	**Erstbelastung**	Durchm. (D5)	118.708 mm	116.949 mm	118.913 mm	118.190 mm
	Zyklus Start: 860 kPa	Def. (DD)	0.949 mm	0.946 mm	0.736 mm	0.877 mm
	Zyklus Ende: 1'009 kPa	Schermod. (G)	9 MPa	9 MPa	12 MPa	**10 MPa**
	Scherbeanspr. (DP): 149 kPa	E-Modul (E)	23 MPa	23 MPa	30 MPa	**25 MPa**
8-9	**Entlastung**	Durchm. (D7)	121.656 mm	119.838 mm	121.198 mm	120.897 mm
	Zyklus Start: 1'012 kPa	Def. (DD)	-0.052 mm	-0.045 mm	-0.033 mm	-0.043 mm
	Zyklus Ende: 848 kPa	Schermod. (G)	192 MPa	218 MPa	301 MPa	**231 MPa**
	Scherbeanspr. (DP): -164 kPa	E-Modul (E)	480 MPa	545 MPa	753 MPa	**578 MPa**

51-1657 Dilato Bohrung 0601.xls, 8.94m, 04.08.2006, 14:44

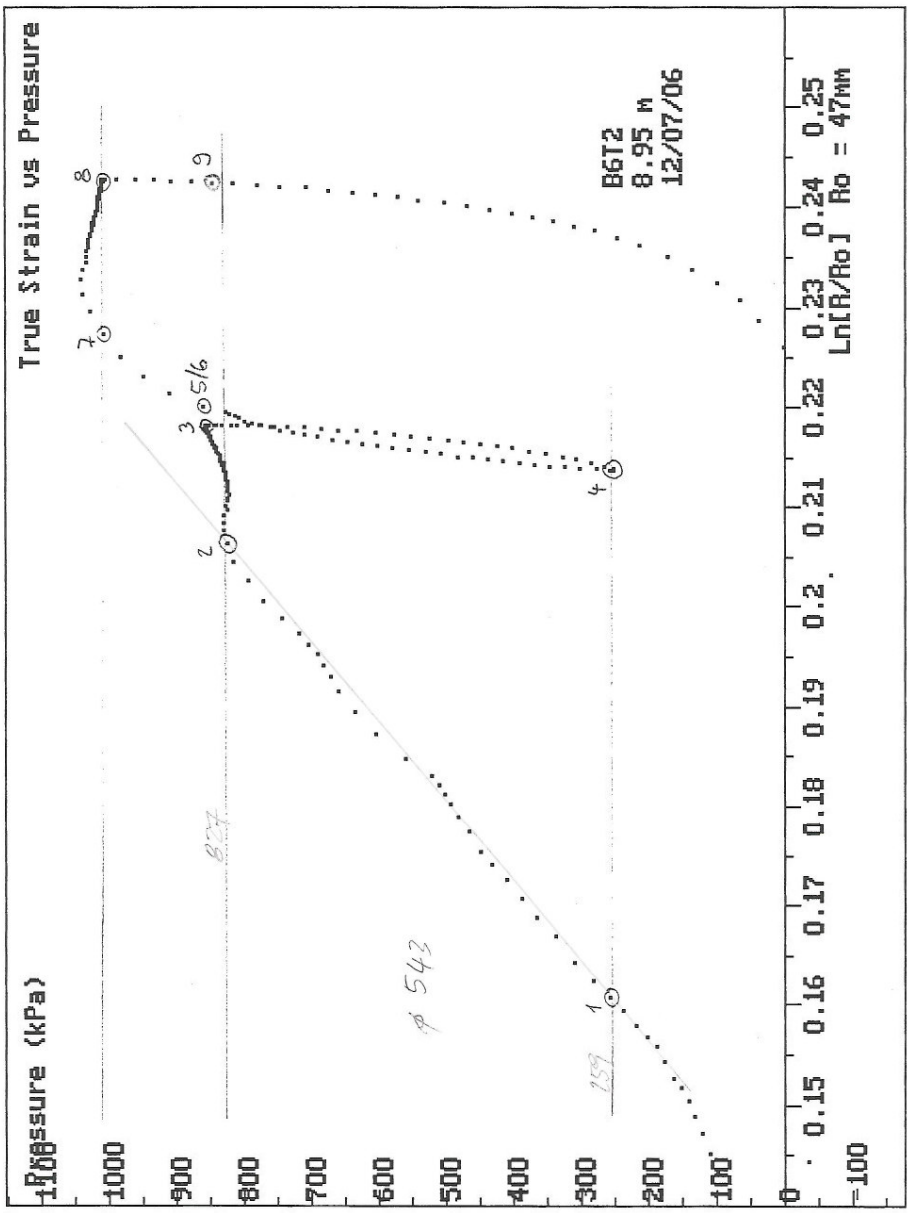

SCREEN DUMP Test: B6T2 Date: 12/07/06 Depth: 8.95m
Dilatometerversuche ausgefuehrt durch die Abt. Messtechnik
der Stump ForaTec AG. www.stump.ch messtechnik@stump.ch

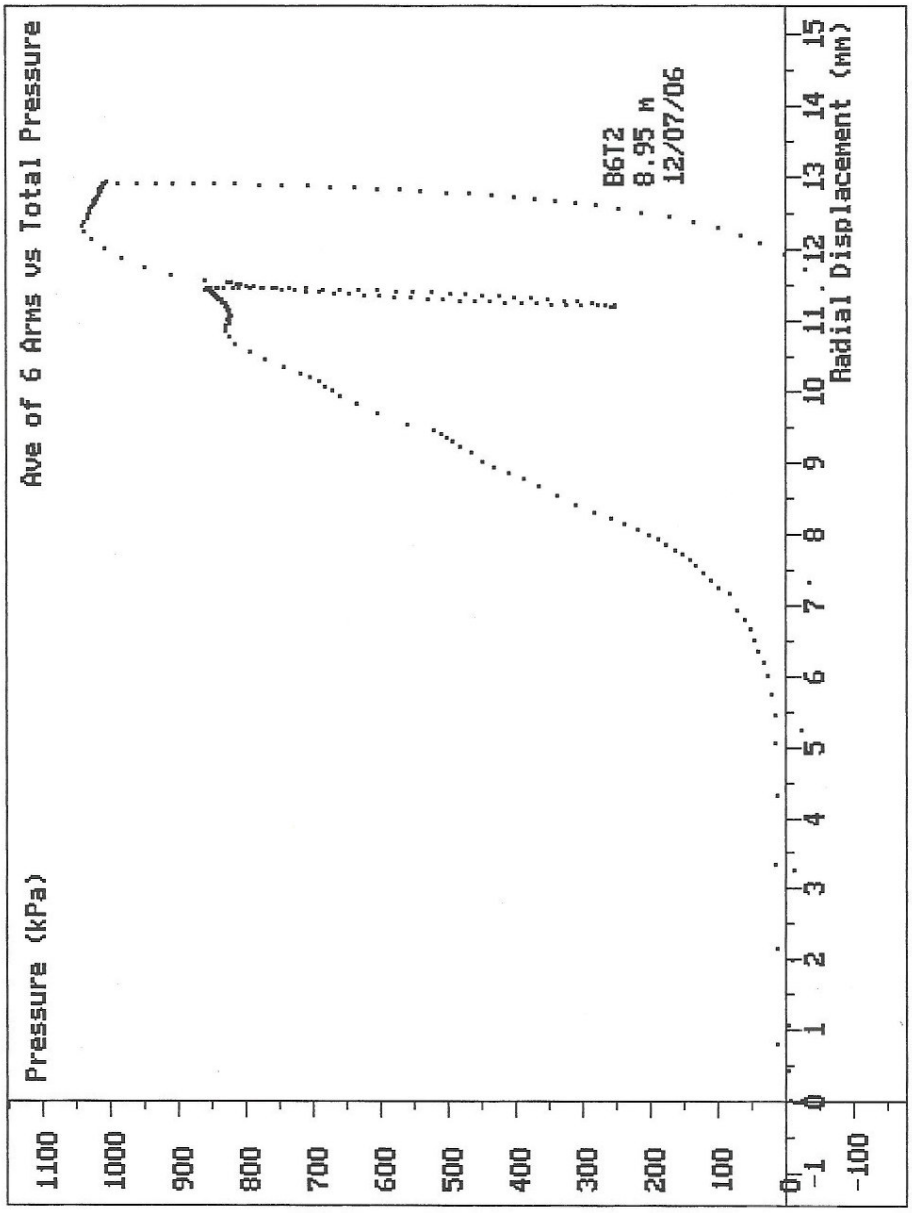

SCREEN DUMP Test: B6T2 Date: 12/07/06 Depth: 8.95m
Dilatometerversuche ausgefuehrt durch die Abt. Messtechnik
der Stump ForaTec AG. www.stump.ch messtechnik@stump.ch

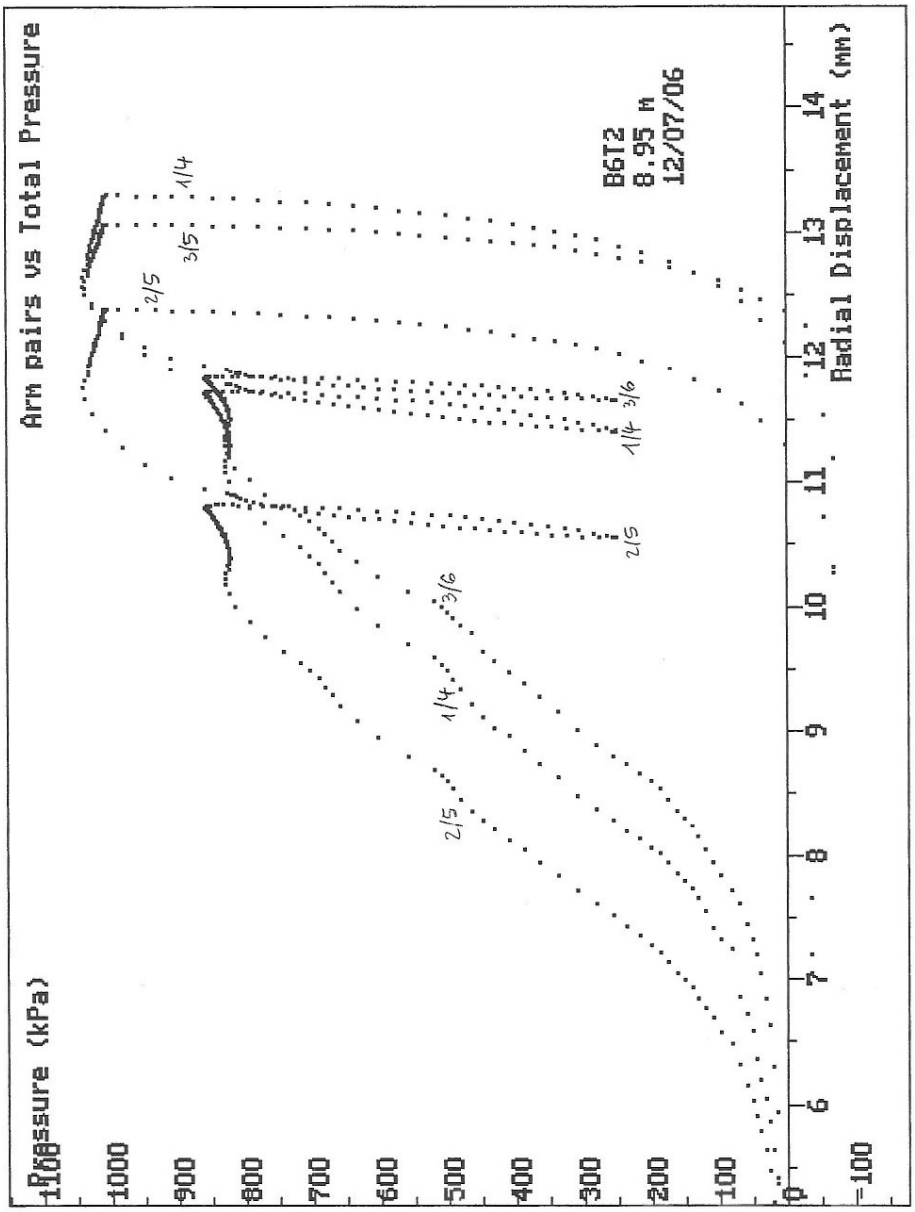

SCREEN DUMP Test: B6T2 Date: 12/07/06 Depth: 8.95m
Dilatometerversuche ausgefuehrt durch die Abt. Messtechnik
der Stump ForaTec AG. www.stump.ch messtechnik@stump.ch

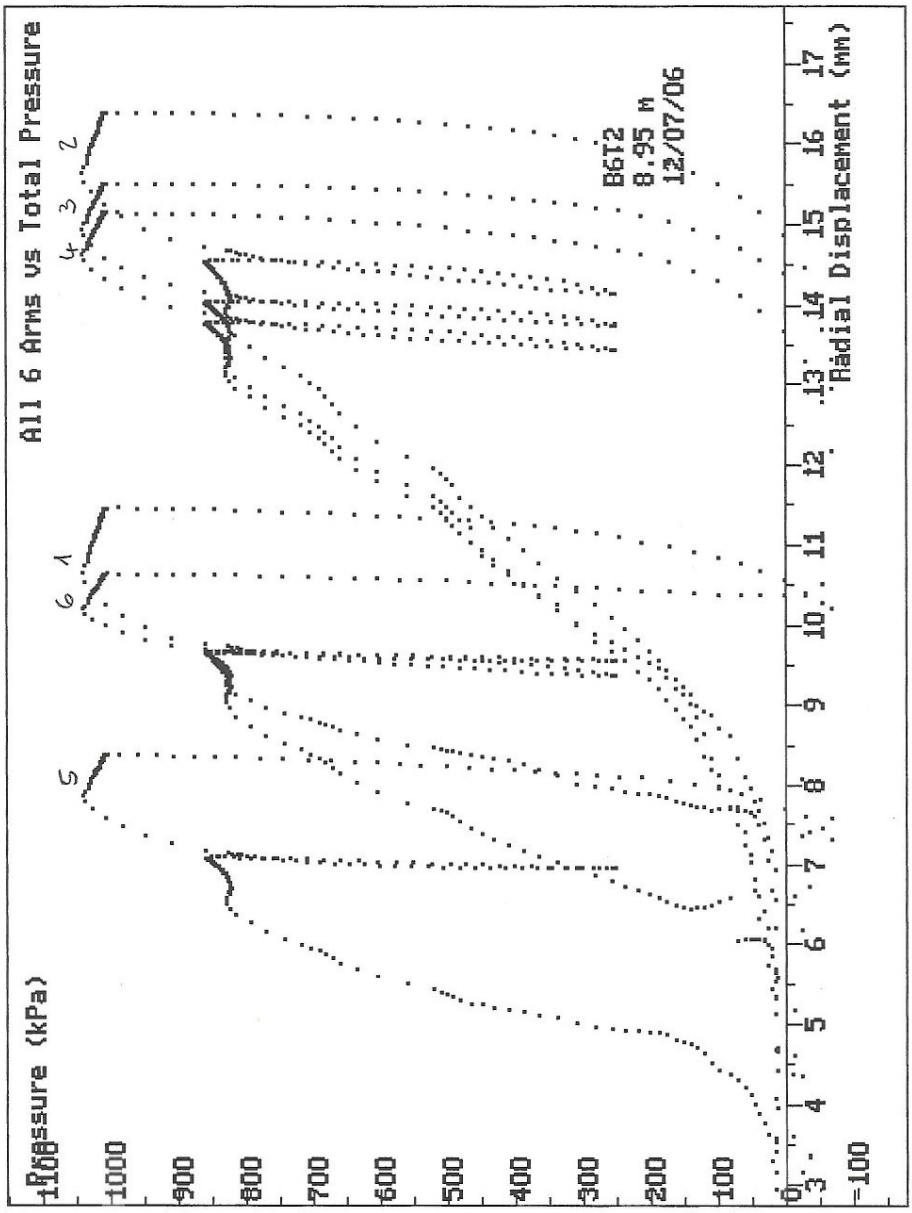

SCREEN DUMP Test: B6T2 Date: 12/07/06 Depth: 8.95m
Dilatometerversuche ausgefuehrt durch die Abt. Messtechnik
der Stump ForaTec AG. www.stump.ch messtechnik@stump.ch

Brattashang, St. Moritz

B6 / Test 3

Dilatometerversuche

Datum: 12. 07. 2006 | Azimut: 239 ° | Sondendurchm. ($D_{Sond.}$): 95.0 mm
Tiefe: 13.90 m | Wasserdruck: 0 kPa | Poissonzahl (v): 0.25

Punkt	Druck	Arm 1	Arm 2	Arm 3	Arm 4	Arm 5	Arm 6
1	108 kPa	0.454 mm	0.943 mm	0.855 mm	0.385 mm	0.146 mm	0.537 mm
2	231 kPa	1.708 mm	2.755 mm	1.772 mm	1.174 mm	0.982 mm	1.679 mm
3	227 kPa	1.749 mm	2.813 mm	1.812 mm	1.225 mm	1.032 mm	1.733 mm
4	105 kPa	1.694 mm	2.792 mm	1.750 mm	1.183 mm	1.008 mm	1.681 mm

Stufe			Arme 1/4	Arme 2/5	Arme 3/6	Arme 1-6
1-2	**Erstbelastung**	Durchm. (D_1)	95.839 mm	96.089 mm	96.392 mm	96.107 mm
	Zyklus Start: 108 kPa	Def. (ΔD)	2.043 mm	2.648 mm	2.059 mm	2.250 mm
	Zyklus Ende: 231 kPa	Schermod. (G)	3 MPa	2 MPa	3 MPa	**3 MPa**
	Scherbeanspr. (ΔP): 123 kPa	E-Modul (E)	8 MPa	5 MPa	8 MPa	**8 MPa**
3-4	**Entlastung**	Durchm. (D_3)	97.974 mm	98.845 mm	98.545 mm	98.455 mm
	Zyklus Start: 227 kPa	Def. (ΔD)	-0.097 mm	-0.045 mm	-0.114 mm	-0.085 mm
	Zyklus Ende: 105 kPa	Schermod. (G)	62 MPa	134 MPa	53 MPa	**71 MPa**
	Scherbeanspr. (ΔP): -122 kPa	E-Modul (E)	155 MPa	335 MPa	133 MPa	**178 MPa**

51-1657 Dilato Bohrung 0601.xls, 13.90m, 04.08.2006, 13:40

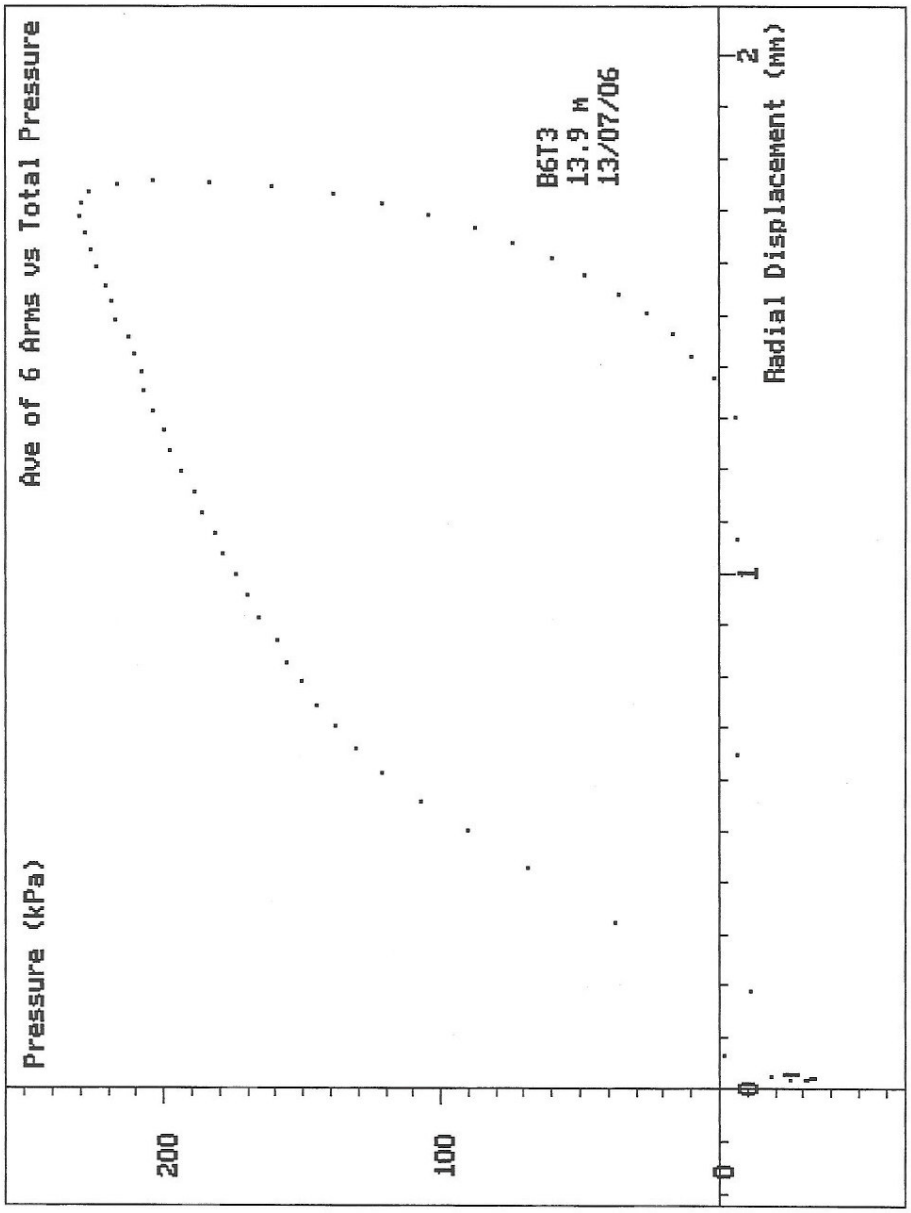

SCREEN DUMP Test: B6T3 Date: 13/07/06 Depth: 13.90m
Dilatometerversuche ausgefuehrt durch die Abt. Messtechnik
der Stump ForaTec AG. www.stump.ch messtechnik@stump.ch

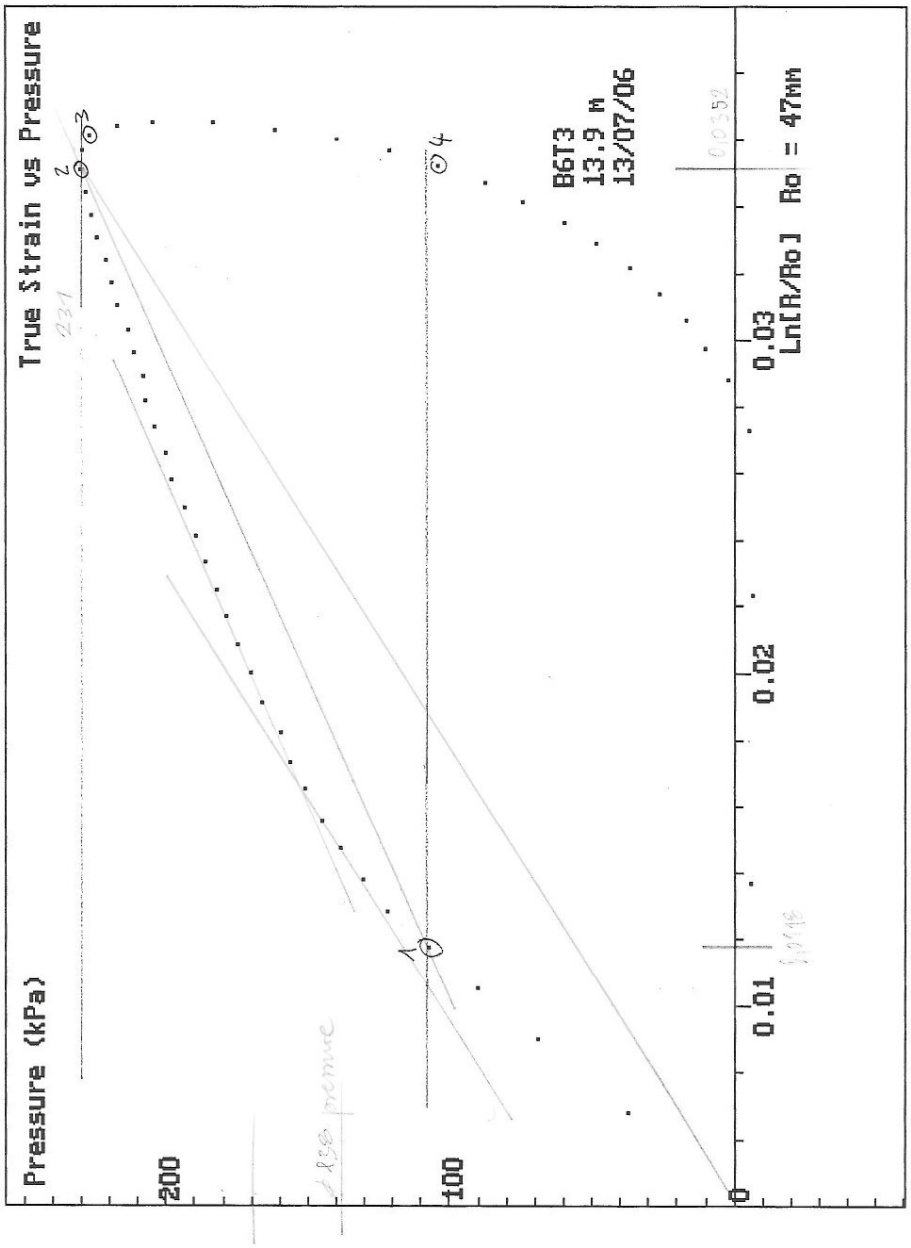

SCREEN DUMP Test: B6T3 Date: 13/07/06 Depth: 13.90m
Dilatometerversuche ausgefuehrt durch die Abt. Messtechnik
der Stump ForaTec AG. www.stump.ch messtechnik@stump.ch

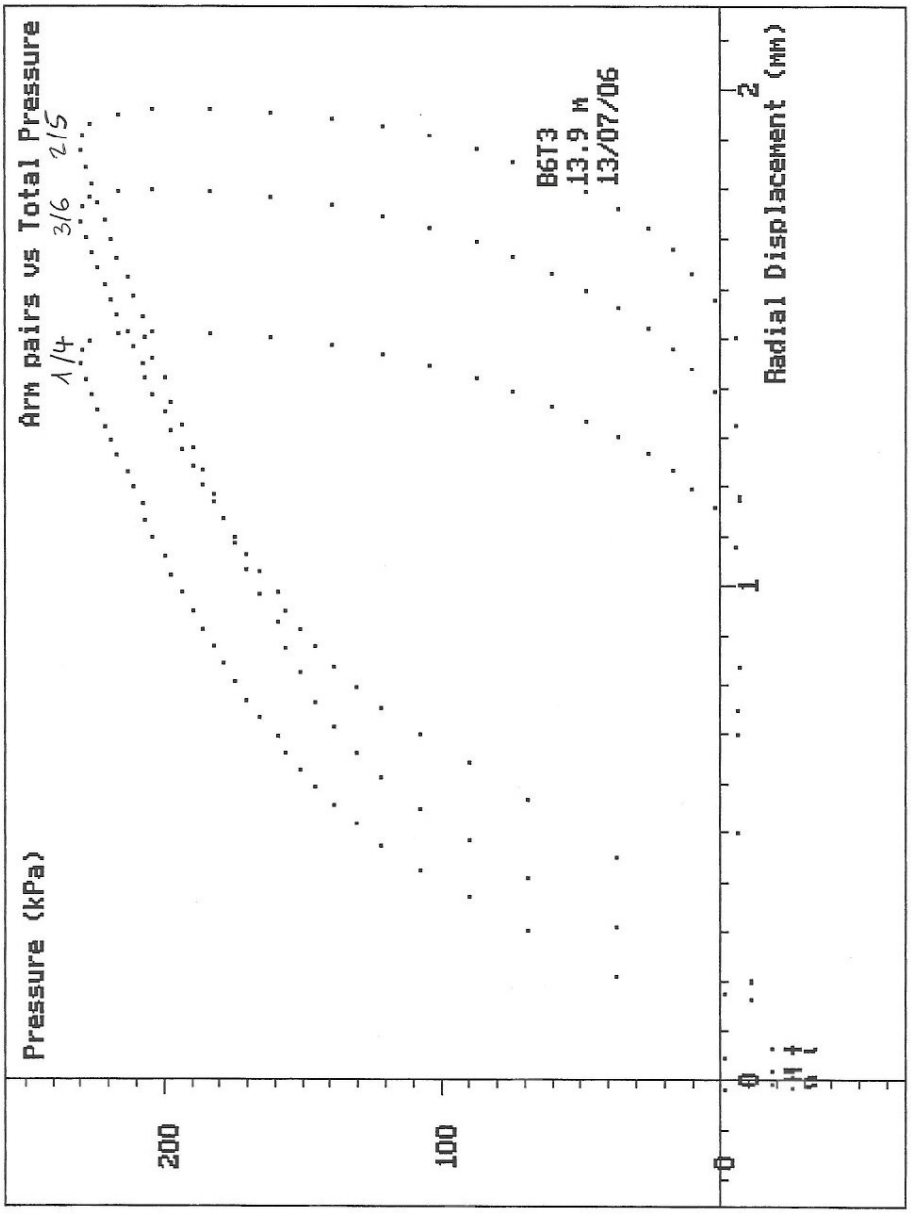

SCREEN DUMP Test: B6T3 Date: 13/07/06 Depth: 13.90m
Dilatometerversuche ausgefuehrt durch die Abt. Messtechnik
der Stump ForaTec AG. www.stump.ch messtechnik@stump.ch

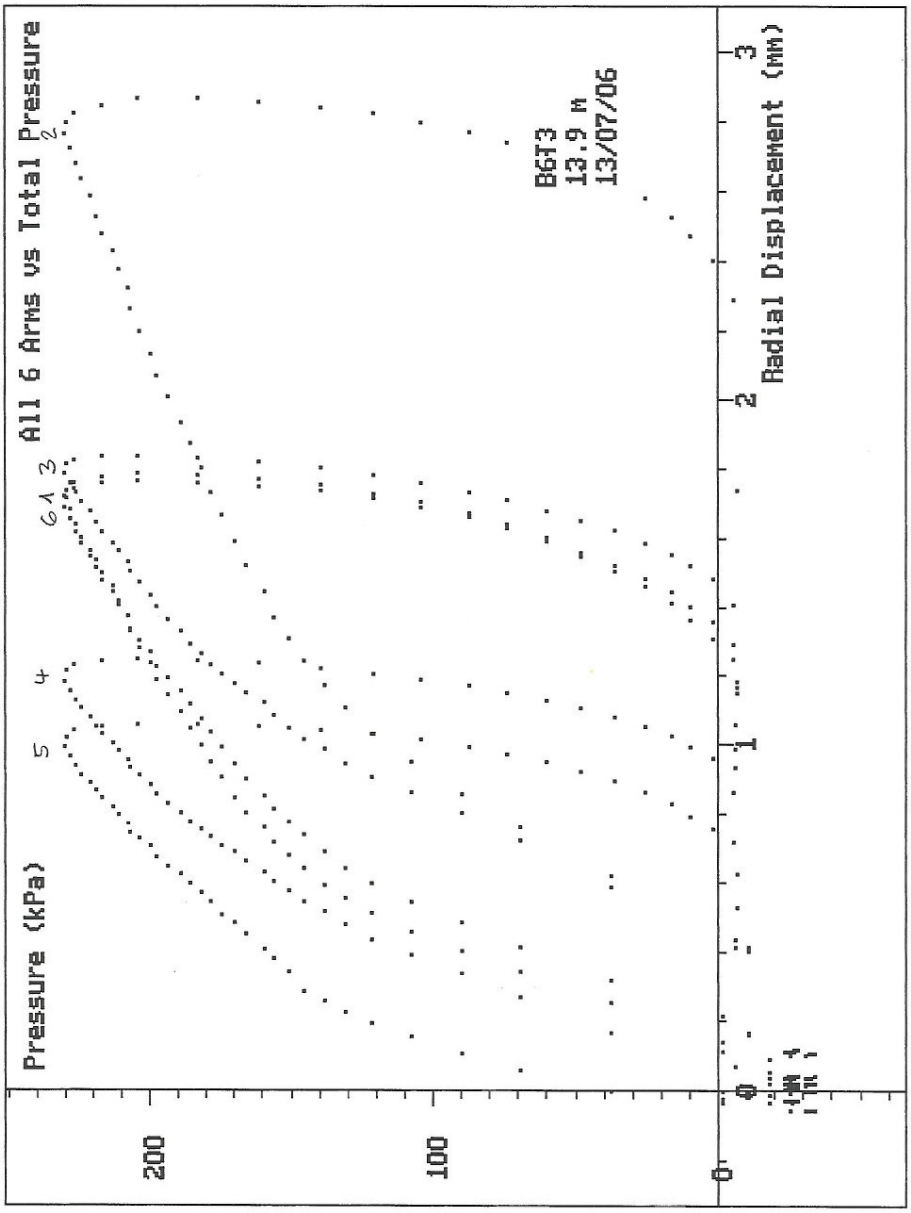

SCREEN DUMP Test: B6T3 Date: 13/07/06 Depth: 13.90m
Dilatometerversuche ausgefuehrt durch die Abt. Messtechnik
der Stump ForaTec AG. www.stump.ch messtechnik@stump.ch

Anhang A2

Beschrieb der Dilatometersonde

Stump ForaTec AG
Abt. Messtechnik
Dép. technique de mesure Dip. tecnica di misurazione

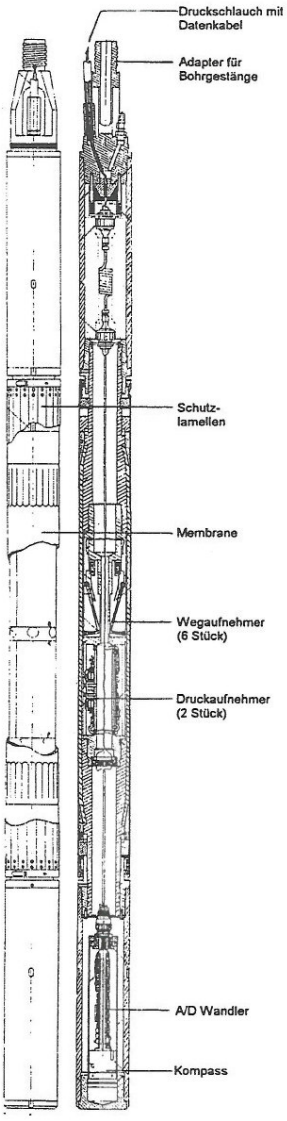

High Pressure Dilatometer

- **Cambridge Insitu**
- **93/95mm**

Beschreibung

Die Dilatometersonde Cambridge Insitu wurde konzipiert , um die Festigkeit von Erdreich (z.B. feste Tone, kompakte Sande) und von Gesteinen zu bestimmen.

Während dem Versuch wird die Vergrösserung des Bohrlochdurchmessers gemessen. Diese wird durch eine mittels Druckluft (oder Hydrauliköl) aufgeweitete Gummi-membrane verursacht.

Sechs gleichmässig auf einer horizontalen Ebene angeordnete Wegaufnehmer messen die Deformation des Untergrundes. Die Digitalisierung der Messwerte erfolgt bereits in der Sonde. Die geografische Orientierung der Geber wird durch einen eingebauten elektrischen Kompass ermittelt. Alle 10 Sekunden werden die Werte der Druck- und Wegaufnehmer automatisch registriert. Da keine Volumenänderung, sondern direkt die Deformation gemessen wird, ist es nicht nötig die Messwerte zu korrigieren, ausser für die Membransteifheit.

Der Druck wird direkt in der Sonde gemessen, um Druckunterschiede auszuschliessen. Der Arbeitsdruck beträgt bis zu 20MPa (200bar).

Der Versuch wird in einem vorgebohrtem Loch mit 96 oder 101mm Durchmesser durchgeführt. In nicht standfähigen Böden muss die Bohrung mit Bentonit-suspension stabilisiert werden oder auszementiert und nachgebohrt werden.

Technische Daten

Bohrdurchmesser:	96mm(HQ), 101mm(CHD)
Ausdehnung, max. Durchmesser:	140mm
Auflösung der Wegaufnehmer:	0.001mm
Arbeitsdruck max.:	20MPa
Auflösung der Druckaufnehmer:	0.001MPa
Durchmesser der Sonde:	93 oder 95mm
Länge der Sonde:	2030mm
Expansionslänge der Membrane:	575mm

Internet: www.stump.ch E-mail: messtechnik@stump.ch

Anhang A3

CD-Rom mit Datenfiles

Die CD-Rom mit Datenfiles:

“51-1657
Brattashang
St. Moritz
Dilatometerversuche”
Sambeth und Wolfensberger (2006)

befindet sich am Institut für Geotechnik, Wolfgang-Pauli-Str. 15, 8093 Zürich und kann jederzeit eingesehen oder zugestellt werden.

Appendix III:

Marchetti S., Monaco P., Totani G. and Calabrese M. (2001)

"The Flat Dilatometer Test (DMT) in soil investigations"

Report by the ISSMGE Committee TC16.

International Society for Soil Mechanics and Geotechnical Engineering (ISSMGE)

The Flat Dilatometer Test (DMT) in Soil Investigations

Report of the ISSMGE
Technica1 Committee 16
on
Ground Property Characterisation from In-situ Testing

2001

IN SITU 2001, Intnl. Conf. On In situ Measurement of Soil Properties, Bali, Indonesia

The Flat Dilatometer Test (DMT) in soil investigations
A Report by the ISSMGE Committee TC16

Marchetti S., Monaco P., Totani G. & Calabrese M.
University of L'Aquila, Italy

TC16 (2001) - Marchetti S., Monaco P., Totani G. & Calabrese M. "The Flat Dilatometer Test (DMT) in Soil Investigations" A Report by the ISSMGE Committee TC16. Proc. IN SITU 2001, Intnl. Conf. On In situ Measurement of Soil Properties, Bali, Indonesia, **May 2001, 41 pp.**

ABSTRACT: This report presents an overview of the DMT equipment, testing procedure, interpretation and design applications. It is a statement on the general practice of dilatometer testing and is not intended to be a standard.

FOREWORD

This report on the flat dilatometer test is issued under the auspices of the ISSMGE Technical Committee TC16 (Ground Property Characterization from In-Situ Testing). It was authored by the Geotechnical Group of L'Aquila University with additional input from other members of the Committee.

The first outline of this report was presented and discussed at the TC16 meeting in Atlanta – ISC '98 (April 1998). The first draft was presented and discussed at the TC16 meeting in Amsterdam – 12th ECSMGE (June 1999).

Members of the Committee and practitioners were invited to review the draft and provide comments. These comments have been edited and taken into account by the original authors and incorporated in this report.

AIMS OF THE REPORT

This report describes the use of the flat dilatometer test (DMT) in soil investigations. The main aims of the report are:

- To give a general overview of the DMT and of its design applications
- To provide "state of good practice" guidelines for the proper execution of the DMT
- To highlight a number of significant recent findings and practical developments.

This report is not intended to be (or to originate in the near future) a Standard or a Reference Test Procedure (RTP) on DMT execution.

Efforts have been made to preserve similarities in format with previous reports of the TC16 and other representative publications concerning in situ testing.

The content of this report is heavily influenced by the experience of the authors, who are responsible for the facts and the accuracy of the data presented herein.

Efforts have been made to keep the content of the report as objective as possible.

Occasionally subjective comments, based on the authors experience, have been included when considered potentially helpful to the readers.

SECTIONS OF THIS REPORT

PART A – PROCEDURE AND OPERATIVE ASPECTS

1. BRIEF DESCRIPTION OF THE FLAT DILATOMETER TEST
2. DMT EQUIPMENT COMPONENTS
3. FIELD EQUIPMENT FOR INSERTING THE DMT BLADE
4. MEMBRANE CALIBRATION
5. DMT TESTING PROCEDURE
6. REPORTING OF TEST RESULTS
7. CHECKS FOR QUALITY CONTROL
8. DISSIPATION TESTS

PART B – INTERPRETATION AND APPLICATIONS

9. DATA REDUCTION AND INTERPRETATION
10. INTERMEDIATE DMT PARAMETERS
11. DERIVATION OF GEOTECHNICAL PARAMETERS
12. PRESENTATION OF DMT RESULTS
13. APPLICATION TO ENGINEERING PROBLEMS
14. SPECIAL CONSIDERATIONS
15. CROSS RELATIONS WITH RESULTS FROM OTHER IN SITU TESTS

BACKGROUND AND REFERENCES

BACKGROUND

The flat dilatometer test (DMT) was developed in Italy by Silvano Marchetti. It was initially introduced in North America and Europe in 1980 and is currently used in over 40 countries.

The DMT equipment, the test method and the original correlations are described by Marchetti (1980) "In Situ Tests by Flat Dilatometer", ASCE Jnl GED, Vol. 106, No. GT3. Subsequently, the DMT has been extensively used and calibrated in soil deposits all over the world.

BASIC DMT REFERENCES / KEY PAPERS

Various international standards and manuals are available for the DMT. An ASTM Suggested Method was published in 1986. A "Standard Test Method for Performing the Flat Plate Dilatometer" is currently being prepared by ASTM (approved Draft 2001). The test procedure is also standardized in the Eurocode 7 (1997). National standards have also been developed in various countries (e.g. Germany, Sweden). A comprehensive manual on the DMT was prepared for the United States Department of Transportation (US DOT) by Briaud & Miran in 1992. Design applications and new developments are covered in detail in a state of the art report by Marchetti (1997). A list of selected comprehensive DMT references is given here below.

STANDARDS

ASTM Subcommittee D 18.02.10 - Schmertmann, J.H., Chairman (1986). "Suggested Method for Performing the Flat Dilatometer Test". ASTM Geotechnical Testing Journal, Vol. 9, No. 2, June.

Eurocode 7 (1997). Geotechnical design - Part 3: Design assisted by field testing, Section 9: Flat dilatometer test (DMT).

MANUALS

Marchetti, S. & Crapps, D.K. (1981). "Flat Dilatometer Manual". Internal Report of G.P.E. Inc.

Schmertmann, J.H. (1988). Rept. No. FHWA-PA-87-022+84-24 to PennDOT, Office of Research and Special Studies, Harrisburg, PA, in 4 volumes.

US DOT - Briaud, J.L. & Miran, J. (1992). "The Flat Dilatometer Test". Departm. of Transportation - Fed. Highway Administr., Washington, D.C., Publ. No. FHWA-SA-91-044, 102 pp.

STATE OF THE ART REPORTS

Lunne, T., Lacasse, S. & Rad, N.S. (1989). "State of the Art Report on In Situ Testing of Soils". Proc. XII ICSMFE, Rio de Janeiro, Vol. 4.

Lutenegger, A.J. (1988). "Current status of the Marchetti dilatometer test". Special Lecture, Proc. ISOPT-1, Orlando, Vol. 1.

Marchetti, S. (1997). "The Flat Dilatometer: Design Applications". Proc. Third International Geotechnical Engineering Conference, Keynote lecture, Cairo University, 28 pp.

CONFERENCES, SEMINARS, COURSES

Several conferences, seminars and courses have been dedicated to the DMT. The most important are mentioned here below.

- First International Conference on the Flat Dilatometer, Edmonton, Alberta (Canada), Feb. 1983.
- One-day Short Course on the DMT held by S. Marchetti in Atlanta (GA), USA, in connection with the First International Conference on Site Characterization (ISC '98), Apr. 1998.
- International Seminar on "The Flat Dilatometer and its Applications to Geotechnical Design" held by S. Marchetti at the Japanese Geotechnical Society, Tokyo, Feb. 1999.

DMT ON THE INTERNET

Key papers on the DMT can be downloaded from the bibliographic site: http://www.marchetti-dmt.it

PART A

PROCEDURE AND OPERATIVE ASPECTS

1. BRIEF DESCRIPTION OF THE FLAT DILATOMETER TEST

The flat dilatometer is a stainless steel blade having a flat, circular steel membrane mounted flush on one side (Fig. 1).

The blade is connected to a control unit on the ground surface by a pneumatic-electrical tube (transmitting gas pressure and electrical continuity) running through the insertion rods. A gas tank, connected to the control unit by a pneumatic cable, supplies the gas pressure required to expand the membrane. The control unit is equipped with a pressure regulator, pressure gage(s), an audio-visual signal and vent valves.

Fig. 1. The flat dilatometer - Front and side view

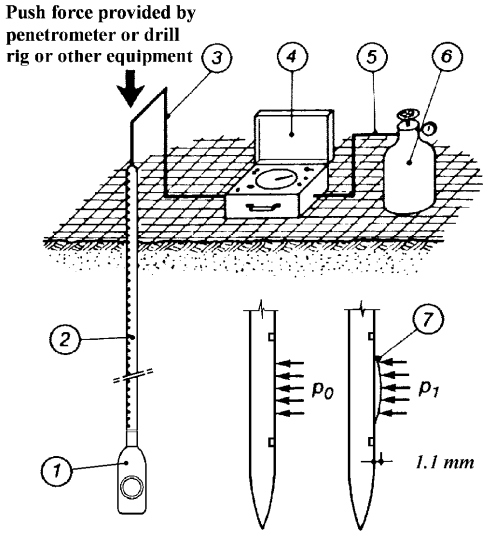

1. Dilatometer blade	4. Control box
2. Push rods (eg.: CPT)	5. Pneumatic cable
3. Pneumatic - electric cable	6. Gas tank
7. Expansion of the membrane	

Fig. 2. General layout of the dilatometer test

The blade is advanced into the ground using common field equipment, i.e. push rigs normally used for the cone penetration test (CPT) or drill rigs. Push rods are used to transfer the thrust from the insertion rig to the blade.

The general layout of the dilatometer test is shown in Fig. 2. The test starts by inserting the dilatometer into the ground. Soon after penetration, by use of the control unit, the operator inflates the membrane and takes, in about 1 minute, two readings:

1) the *A*-pressure, required to just begin to move the membrane against the soil ("lift-off")
2) the *B*-pressure, required to move the center of the membrane 1.1 mm against the soil.

A third reading *C* ("closing pressure") can also optionally be taken by slowly deflating the membrane soon after *B* is reached.

The blade is then advanced into the ground of one depth increment (typically 20 cm) and the procedure for taking *A*, *B* readings repeated at each depth.

The pressure readings *A*, *B* are then corrected by the values ΔA, ΔB determined by calibration to take into account the membrane stiffness and converted into p_0, p_1.

The *field of application* of the DMT is very wide, ranging from extremely soft soils to hard soils/soft rocks. The DMT is suitable for sands, silts and clays, where the grains are small compared to the membrane diameter (60 mm). It is not suitable for gravels, however the blade is robust enough to cross gravel layers of about 0.5 m thickness.

Due to the balance of zero pressure measurement method (null method), the DMT readings are highly accurate even in extremely soft - nearly liquid soils. On the other hand the blade is very robust (can safely withstand up to 250 kN of pushing force) and can penetrate even soft rocks. Clays can be tested from c_u = 2-4 kPa up to 1000 kPa (marls). The range for moduli *M* is from 0.4 MPa up to 400 MPa.

2. DMT EQUIPMENT COMPONENTS

The basic equipment for dilatometer testing consists of the components shown in Fig. 2.

2.1 DILATOMETER BLADE

2.1.1 Blade and membrane characteristics

The nominal dimensions of the blade are 95 mm width and 15 mm thickness. The blade has a cutting edge to penetrate the soil. The apex angle of the edge is 24° to 32°. The lower tapered section of the tip is 50 mm long. The blade can safely withstand up to 250 kN of pushing thrust.

The circular steel membrane is 60 mm in diameter. Its normal thickness is 0.20 mm (0.25 mm thick membranes are sometimes used in soils which may cut the membrane). The membrane is mounted flush on the blade and kept in place by a retaining ring.

2.1.2 Working principle

The working principle of the DMT is illustrated in Fig. 3 (see also the photo in Fig. 4). The blade works as an electric switch *(on/off)*. The insulating seat prevents electrical contact of the sensing disc with the underlying steel body of the dilatometer. The sensing disc is stationary and is kept in place press-fitted inside the insulating seat. The contact is signaled by an audio/visual signal. The sensing disc is grounded (and the control unit emits a sound) under one of the following circumstances:

1) the membrane rests against the sensing disc (as prior to membrane expansion)
2) the center of the membrane has moved 1.1 mm into the soil (the spring-loaded steel cylinder makes contact with the overlying sensing disc).

There is no electrical contact, hence no signal, at intermediate positions of the membrane.

When the operator starts increasing the internal pressure (Fig. 3), for some time the membrane does not move and remains in contact with its metal support (signal *on*). When the internal pressure

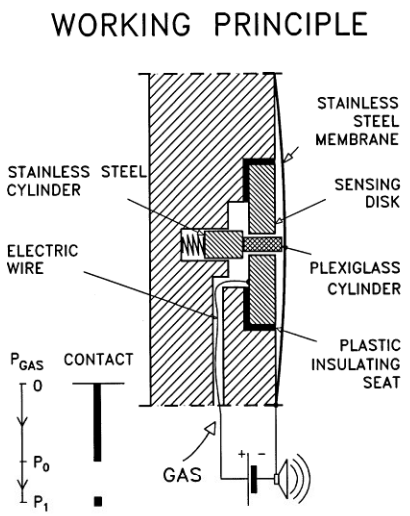

Fig. 3. DMT working principle

Fig. 4. Particular of the DMT blade

counterbalances the external soil pressure, the membrane initiates its movement, losing contact with its support (signal *off*). The interruption of the signal prompts the operator to read the "lift-off" *A*-pressure (later corrected into p_0). The operator, without stopping the flow, continues to inflate the membrane (signal *off*). When the central movement reaches 1.1 mm the spring-loaded steel cylinder touches (and grounds) the bottom of the sensing disc, reactivating the signal. The reactivation of the signal prompts the operator to read the "full expansion" *B*-pressure (later corrected into p_1).

The top of the sensing disc carries a 0.05 mm feeler having the function to improve the definition of the lift-off of the membrane, i.e. the instant at which the electrical circuit is interrupted.

The fixed-displacement system insures that the membrane expansion will be 1.10 mm ± 0.02 mm regardless of the care of the operator, who cannot vary or regulate such distance. Only calibrated quartz (once plexiglas) cylinders (height 3.90 ± 0.01 mm) should be used to insure accuracy of the prefixed movement.

NOTE: Remarks on the DMT working principle

- The membrane expansion is not a load controlled test - apply the load and observe settlement - but a displacement controlled test - fix the displacement and measure the required pressure. Thus in all soils the central displacement (and, at least approximately, the strain pattern imposed to the soil) is the same.
- The membrane is not a measuring organ but a passive separator soil-gas. The measuring organ is the gage at ground surface. The accuracy of the measurements is that of the gage. The zero offset of the gage can be checked at any time, being at surface. A low range pressure gage can be used, e.g. in very soft soils, to increase accuracy to any desired level.
- The method of pressure measurement is the balance of zero (null method), providing high accuracy.
- The blade works as an electric switch *(on/off)*, without electronics or transducers.
- Given the absence of delicate or regulable components, no special skills are required to operate the DMT.

2.2 Control unit

2.2.1 Functions and components

The control unit on ground surface is used to measure the *A, B (C)* pressures at each test depth.

The control unit (Fig. 5) typically includes two pressure gages, a pressure source quick connect, a quick connect for the pneumatic-electrical cable, an electrical ground cable connection, a galvanometer and audio buzzer signal (activated by the electric switch constituted by the blade) which prompt when to read the *A, B (C)* pressures, and valves to control gas flow and vent the system.

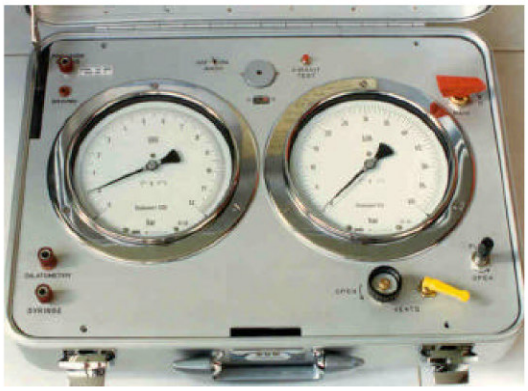

Fig. 5. Control unit

2.2.2 Pressure gages

The two pressure gages, connected in parallel, have different scale ranges: a low-range gage (1 MPa), self-excluding when the end of scale is reached, and a high-range gage (6 MPa). The two-gage system ensures proper accuracy and, at the same time, sufficient range for various soil types (from very soft to very stiff).

According to Eurocode 7 (1997), the pressures should be measured with a resolution of 10 kPa and a reproducibility of 2.5 kPa, at least for pressures lower than 500 kPa. Gages should have an accuracy of at least 0.5 % of span.

In case of discrepancy between the two gages, replace the malfunctioning gage or correct as appropriate. In case of single-gage (old control units), the gage should be periodically calibrated.

Though the control unit is encased in an aluminium carrying case, it should be handled with care to avoid damaging the gages.

2.2.3 Gas flow control valves

The valves on the control unit panel permit to control the gas flow to the blade.

The *main valve* provides a positive shutoff between the gas source and the blade-control unit system. The *micrometer flow valve* is used to control the rate of flow during the test. It also provides a shutoff between the source and the DMT system (anyway it is advisable to close the *main valve* and to open the *toggle vent valve* if the control unit is left unattended for some time). The *toggle vent valve* allows the operator to vent quickly the system pressure to the atmosphere. The *slow vent valve* allows to vent the system slowly for taking the *C*-reading.

2.2.4 Electrical circuit

The electrical circuitry in the control unit has the scope of indicating the *on/off* condition of the blade-switch. It provides both a visual galvanometer and an audio buzzer signal to the operator. The buzzer is *on* when the blade is in the short circuit condition, i.e. collapsed against the blade or fully expanded. The buzzer is *off* when between these two positions. The transitions from buzzer *on* to *off* and then *off* to *on* as the membrane expands are the prompts for the operator to take respectively the *A* and *B* pressure readings.

A 9-Volt battery supplies electrical power to the wire inside the pneumatic-electrical cable quick-connect. The power is returned at the ground cable jack if the blade is in the short circuit condition.

A test button permits to check the vitality of the battery and the operation of the galvanometer and buzzer. Note that it simply shorts across the blade portion of the circuit and hence provides no information about the status of the blade, the pneumatic-electrical cable or the ground cable. If annoyed by the sound during test delays, the operator may disable the buzzer. However, quieting the buzzer involves the risk of missing the prompts to take the readings and overinflating the membrane.

2.3 PNEUMATIC-ELECTRICAL CABLE

The pneumatic-electrical (p-e) cable provides pneumatic and electrical continuity between the control unit and the dilatometer blade. It consists of a stainless steel wire enclosed within nylon tubing with special metal connectors at either end. Two different cable types are normally used (Fig. 6):

- *Non-extendable cable:* this cable has an insulated male metal connector for the DMT blade on one end, and a non-insulated quick-connect for attachment to the control unit on the other end. The cable length (minus a working length at the surface) limits the maximum sounding depth: once the test depth is such that all the cable is inside the soil, the cable cannot be extended and the test must be stopped. This inconvenience is balanced by the simplicity of the cable and its lower cost.
- *Extendable cable:* by using an extendable cable, the operator may connect additional cable(s) as needed during the sounding. The female terminal of such cable (insulated) cannot fit directly into the corresponding quick connector in the control unit. Therefore a *cable leader* (or *short connector cable*) permitting such a connection must be used in conjunction with this cable. This short adaptor is removed when a new cable is added. Though slightly more complex, this type of cable provides the operator with greater flexibility.

The proper type and length of cable should be chosen based on the expected sounding depth. For ease of handling and to minimize pressure lag at the control unit gage, always use the shortest length practical.

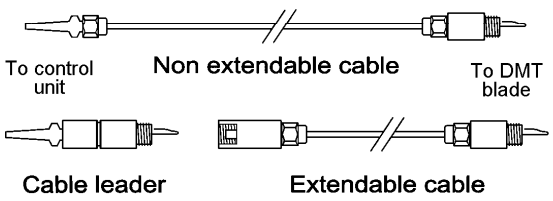

Fig. 6. Types of pneumatic-electrical cables

Short cables are easier to handle, but require junctions. Junctions normally work well and do not represent a problem as long as care is exercised to avoid particles of soils getting into the conduits.

To keep contaminants out, the terminals and connectors must always be protected with caps when disconnected.

The metal connectors are electrically insulated from the inner wire to prevent a short circuit in the ground and sealed by washers to prevent gas leakage.

The cables and terminals are not easily repairable in the field.

2.4 GAS PRESSURE SOURCE

The pressure source is a gas tank equipped with a pressure regulator, valves and pneumatic tubing to connect to the control unit.

The pressure regulator (suitable to gas type) must be able to supply a regulated output pressure of at least 7-8 MPa.

When testing in most soils the output pressure is set at 3-4 MPa. In very hard soils the output pressure is further increased (without exceeding the high-range gage capacity).

Any non flammable, non corrosive, non toxic gas may be used. Compressed nitrogen or compressed air (scuba tanks) are most generally used.

Gas consumption increases with applied pressure (*A*, *B* readings) and test depth (cable length). In "average" soils a scuba size tank (≈ 0.6 m high), initially at 15 MPa, contains gas to perform approximately 70-100 m of "standard" sounding (≈ one day of testing). In general, it is more economical and efficient to have a large tank (≈ 1.5 m high) when more than one day of testing is anticipated.

2.5 ELECTRICAL GROUND CABLE

The ground cable provides electrical continuity between the push rods and the control unit. It returns to the control unit the simple *on/off* electrical power carried to the blade by the pneumatic-electrical cable.

3. FIELD EQUIPMENT FOR INSERTING THE DMT BLADE

3.1 PUSHING EQUIPMENT

The dilatometer blade is advanced into the ground using common field equipment.

The blade can be pushed with a cone penetrometer rig or with a drill rig (Fig. 7).

The penetration rate is usually 2 cm/s as in the CPT (for DMT rates from 1 to 3 cm/s are acceptable, see Eurocode 7 1997).

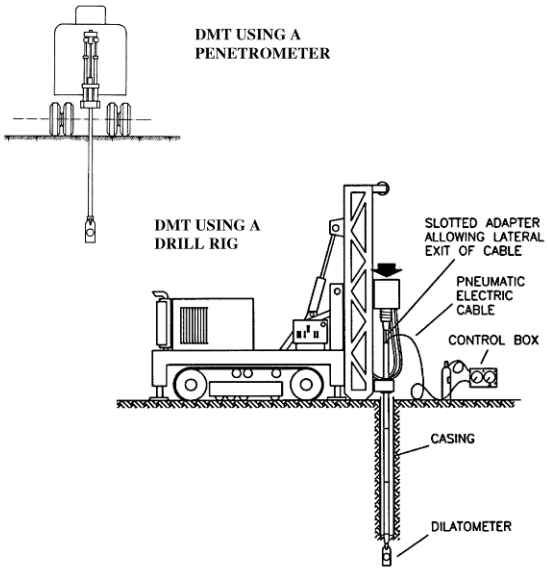

Fig. 7. Equipment for inserting the DMT blade

The DMT can also be driven, e.g. using the SPT hammer and rods, but statical push is by far preferable.

Heavy truck-mounted penetrometers are incomparably more efficient than drill rigs. Moreover the soil provides lateral support to the rods (which is not the case in a borehole). Pushing the blade with a 20 ton penetrometer truck is most effective and yields the highest productivity (up to 80 m of sounding per day).

Drill rigs or light rigs may be used only in soft soils or to very short depths. In all other cases (especially in hard soils) light rigs may be inadequate and source of problems. However drill rigs may be necessary in soils containing occasional boulders or hard layers, where the obstacle-destroying capability will permit to continue the test past the obstacle.

When the DMT sounding is resumed after preboring, the initial test results, obtained in the zone of disturbance at hole bottom (≈ 3 to 5 borehole diameters), should be regarded with caution.

When the DMT is performed inside a borehole, the diameter of the borehole (and casing, if required) should be as small as possible to minimize the risk of buckling (possibly 100-120 mm).

In all cases the penetration must occur in "fresh" (not previously penetrated) soil. The minimum recommended distance from other nearby DMT (or CPT) soundings is 1 m (25 diameters from unbackfilled/uncased borings).

NOTE: Possible problems with light rigs
Possible problems with light rigs (such as many SPT rigs) are:
- Light rigs have typically a pushing capacity of only 2 tons, hence refusal is found very soon (often at 1-2 m depth).
- Often there is no collar near ground surface (i.e. no ground surface side-guidance of the rods).
- There is a hinge-type connection in the rods just below the pushing head, which permits excessive freedom and oscillations of the rods inside the hole.
- The distance between the pushing head of the rig and the bottom of the hole is several meters, hence the free/buckling length of the rods is high. In some cases the loaded rods have been observed to assume a "Z" shape.
- Oscillations of the rods may cause wrong results. In case of short penetration in hard layers it was occasionally observed that the "Z" shape of the rods suddenly reverted to the opposite side. This is one of the few cases in which the DMT readings may be instrumentally incorrect: oscillations of the rods cause tilting of the blade, and the membrane is moved without control close to/far from the soil.

NOTE: Pushing vs driving
Various researchers (US DOT 1992, Schmertmann 1988) have observed that "hammer-driving alters the DMT results and decreases the accuracy of correlations", i.e. the insertion method does affect the test results, and static penetration should be preferred.

According to ASTM (1986), in soils sensitive to impact and vibrations, such as very loose sand or very sensitive clays, dynamic insertion methods can significantly change the test results compared to those obtained using a static push. In general, structurally sensitive soils will appear conservatively more compressible when tested using dynamic insertion methods. In such cases the engineer may need to check such dynamic effects and, possibly, calibrate and adjust test interpretation accordingly. US DOT (1992) recommends that, if the driving technique is used, as a minimum 2 soundings be performed side by side, one by pushing and one by driving. This would give a site/soil specific correlation, which would allow to get back to the parameters obtained from correlations based on the pushing insertion (with added imprecision, however).

According to Eurocode 7 (1997), driving should be avoided except when advancing the blade through stiff or strongly cemented layers which cannot be penetrated by static push.

3.2 PUSH RODS

While in principle any kind of rod can be used, most commonly CPT rods or drill rig rods are employed.

A friction reducer is sometimes used. However the consequent reduction in rod friction is moderate, because of the multi-lobate shape of the cavity produced in the penetrated soil by the blade-rod system.

If used, the friction reducer should be located at least 200 mm above the center of the membrane (Eurocode 7 1997).

NOTE: Use of stronger rods
Many heavy penetrometer trucks performing DMT are today also equipped with rods much stronger than the common 36 mm CPT rods. Such stronger rods are typically 44 to 50 mm in diameter, 1 m length, same steel as CPT rods (yield strength > 1000 MPa). A very suitable and convenient type of rod is the commercially available 44 mm rod used for pushing 15 cm^2 cones.

The stronger rods have been introduced since the rods are "the weakest element in the chain" when working with heavy trucks and the current high strength DMT blades, able to withstand a working load of approximately 250 kN.

The stronger rods have several advantages:
- Capability of penetrating through cemented layers/obstacles.
- Better lateral stability against buckling in the first few meters in soft soils or when the rods are pushed inside an empty borehole.
- Possibility of using completely the push capacity of the truck.
- Reduced risk of deviation from the verticality in deep tests.
- Drastically reduced risk of loosing the rods.

Obvious drawbacks are the initial cost and the heavier weight. Also, their use may not be convenient in OC clay sites because of the increased skin friction.

3.3 ROD ADAPTORS

The DMT blade is connected to the push rods by a *lower adaptor* (Fig. 8).

The most common adaptor has its top connectable to CPT rods, its bottom connectable to the DMT blade (ending cylindrical male M27x3mm).

If rods other than CPT rods are used, specific adaptors need to be prepared (see Fig. 8).

An *upper slotted adaptor* is also needed to allow lateral exit of cable, otherwise pinched by the pushing head.

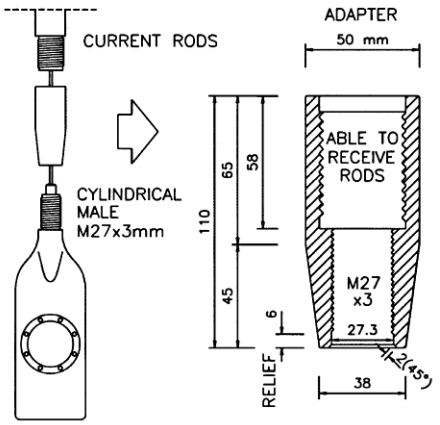

Fig. 8. Lower adaptor connecting the DMT blade to the push rods

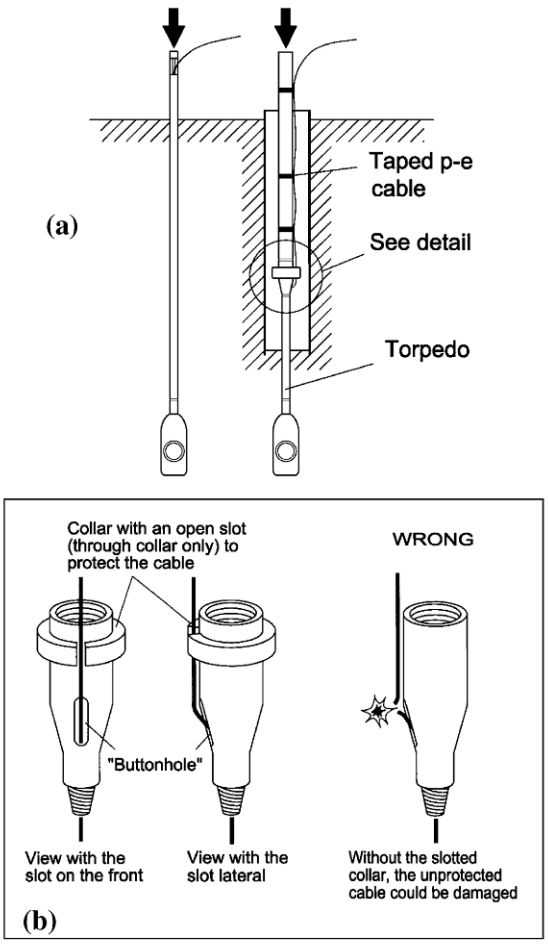

Fig. 9. (a) Possible exits of the cable from the rods (b) Intermediate slotted adaptor joining the upper push rods to the torpedo-like bottom assembly of blade and rods

When using a CPT truck, a DMT sounding normally starts from the ground surface, with the tube running inside the rods (Fig. 9a, left).

When testing starts from the bottom of a borehole, the pneumatic-electrical (p-e) cable can either run all the way up inside the rods, or can exit laterally from the rods at a suitable distance above the blade (Fig. 9a, right). In this case an additional *intermediate slotted adaptor* is needed to permit egress of the cable (Fig. 9a, right). Above this point the cable is taped to the outside of the rods at 1-1.5 m intervals up to the surface.

The torpedo-like bottom assembly in Fig. 9a is composed by the blade, 3 to 5 m (generally) of rods and the *intermediate slotted adaptor*. The "torpedo" is pre-assembled and then mounted at the end of the rods each time. The "torpedo" arrangement speeds production, since it is easier to handle the upper rods free from the cable.

Since the unprotected cable is vulnerable, the *intermediate slotted adaptor* needs a special collar (Fig. 9b). The collar has a vertical channel for the cable and has a diameter larger than the upper rods so as to insure a free space between the upper rods and the casing. The operator should not allow the slotted adaptor and the exposed cable to penetrate the soil, thus limiting the test depth to the length of rods threaded at the bottom.

4. MEMBRANE CALIBRATION

4.1 Definitions of ΔA and ΔB

The calibration procedure consists in obtaining the ΔA and ΔB pressures necessary to overcome membrane stiffness. ΔA and ΔB are then used to correct the A, B readings.

Note that in air, under atmospheric pressure, the free membrane is in an intermediate position between the A and B positions, because the membranes have a slight natural outward curvature (Fig. 10).

ΔA is the external pressure which must be applied to the membrane, in free air, to collapse it against its seating (i.e. A-position). ΔB is the internal pressure which, in free air, lifts the membrane center 1.1 mm from its seating (i.e. B-position).

Various aspects related to the membrane calibration are described in detail by Marchetti (1999) and Marchetti & Crapps (1981).

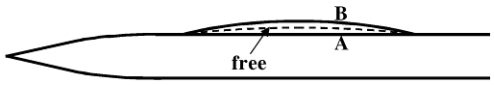

Fig. 10. Positions of the membrane (free, *A* and *B*)

NOTE: Meaning of the term "calibration"
The membrane calibration is not, strictly speaking, a *calibration*, since the term calibration usually refers to the scale of a measuring instrument. The membrane, instead, is a passive separator gas/soil and not a measuring instrument. Actually the membrane is a "tare" and the "calibration" is in reality a "tare determination".

4.2 Determination of ΔA and ΔB

ΔA and ΔB can be measured by a simple procedure using a syringe to generate vacuum or pressure.

During the calibration the high pressure from the bottle should be excluded from the pneumatic circuit by closing the *main valve* on the control unit panel.

To obtain ΔA: quickly pull back (almost fully) the piston of the syringe, in order to apply the maximum vacuum possible (the vacuum causes an inward deflection of the membrane similar to that resulting from the external soil pressure at the start of the test). Hold the piston for sufficient time (at least 5 seconds) for the vacuum to equalize in the system. During this time the buzzer signal should become active. Then slowly release the piston and read ΔA on the low-range gage (gage vacuum reading at which the buzzer stops, i.e. *A*-position). Note this negative pressure as a positive ΔA value (e.g. a vacuum of 15 kPa should be reported as ΔA = 15 kPa). The correction formula for p_0 (Eq. 1 in Section 9.2) is already adjusted to take into account that a positive ΔA is a vacuum.

To obtain ΔB: push slowly the piston into the syringe and read ΔB on the low-range gage when the buzzer reactivates (i.e. *B*-position).

Repeat this procedure several times to have a positive check of the values being read.

Membrane corrections ΔA, ΔB should be measured before a sounding, after a sounding, whenever the blade is removed from the ground.

ΔA, ΔB are usually measured, as a check, in the office before moving to the field. However the initial ΔA, ΔB to be used are those taken just before the sounding (though the difference is generally negligible). The final values of ΔA, ΔB must also be taken at the end of the sounding.

The calibration values of an undamaged membrane remain relatively constant during a DMT sounding. Comparison of before/after values indicates the condition of the membrane and a large difference should prompt a membrane change. Therefore, the calibration procedure is a good indicator of the equipment condition, and consequently of the expected quality of the data.

4.3 Acceptance values of ΔA and ΔB

Acceptance values of ΔA, ΔB are indicated in Eurocode 7 (1997).

- The initial ΔA, ΔB values must be in the following ranges: ΔA = 5 to 30 kPa, ΔB = 5 to 80 kPa. If the values of ΔA, ΔB obtained before inserting the blade into the soil fall outside the above limits, the membrane shall be replaced before testing.
- The change of ΔA or ΔB at the end of the sounding must not exceed 25 kPa, otherwise the test results shall be discarded.

Typical values of ΔA, ΔB are: ΔA = 15 kPa, ΔB = 40 kPa.

ΔA, ΔB values also indicate when it is time to replace a membrane. An old membrane needs not to be replaced as long as ΔA, ΔB are in tolerance.

Indeed an old membrane is preferable, in principle, to a new one, having more stable and lower ΔA, ΔB. However, in case of bad wrinkles, scratches, etc. a membrane should be changed even if ΔA, ΔB are in tolerance (though ΔA, ΔB are not likely to be in tolerance if the membrane is in a really bad shape).

4.4 Configurations during the calibration

The membrane calibration (determining ΔA, ΔB) can be performed in two configurations.

1) The first configuration (*blade accessible*, Fig. 11) is adopted e.g. at the beginning of a sounding, when the blade is still in the hands of the operator.

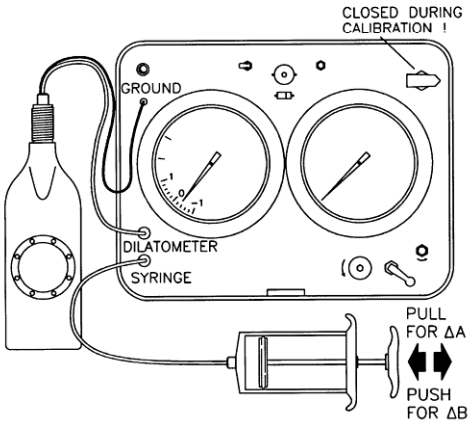

Fig. 11. Layout of the connections during membrane calibration (blade accessible)

The operator will then use the *short calibration cable*, or the *short calibration connector*.

2) The second configuration (*blade not readily accessible*) is used when the blade is under the penetrometer, and is connected to the control unit as during current testing (Fig. 12) with cables of normal length (say 20 to 30 m).

The calibration procedure is the same. The only difference is that, in the second case, due to the length of the DMT tubings, there is some time lag (easily recognizable by the slow response of the pressure gages to the syringe). Therefore, in that configuration, ΔA, ΔB must be taken slowly (say 15 seconds for each determination).

4.5 Exercising the membrane

The exercising operation is to be performed whenever a new membrane is mounted. A new membrane needs to be "exercised" in order to stabilize ΔA, ΔB values (obtain ΔA, ΔB values which will remain constant during the sounding).

The exercising operation simply consists in pressurizing the blade in free air at about 500 kPa for a few seconds two or three times.

If the membrane exercising is performed with the blade submerged in water, it is possible to verify blade airtightness.

After exercising, verify that ΔA, ΔB are in tolerance: ΔA = 5 to 30 kPa (typically 15 kPa), ΔB = 5 to 80 kPa (typically 40 kPa).

4.6 Importance of accurate ΔA and ΔB

The importance of accurate ΔA, ΔB measurements, especially in soft soils, is pointed out by Marchetti (1999). Inaccurate ΔA, ΔB are virtually the only potential source of DMT instrumental error. Since ΔA, ΔB are used to correct all A, B of a sounding, any inaccuracy in ΔA, ΔB would propagate to all the data.

The importance of ΔA, ΔB in soft soils derives from the fact that, in the extreme case of nearly liquid clays, or liquefiable sands, A and B are small numbers, just a bit higher than ΔA, ΔB. Since the correction involves differences between similar numbers, accurate ΔA, ΔB are necessary in such soils.

ΔA, ΔB must be, as a rule, measured before and after each sounding. Their average is subsequently used to correct all A, B readings. Clearly, if the variation is small, the average represents ΔA, ΔB reasonably well at all depths. If the variation is large, the average may be inadequate at some depths. In fact, in soft soils, the operator can be sure that the test results are acceptable only at the end of the sounding, when, checking ΔA, ΔB final, he finds that they are very similar to ΔA, ΔB initial.

In medium to stiff soils ΔA, ΔB are a small part of A and B, so small inaccuracies in ΔA, ΔB have negligible effect.

NOTE: How ΔA, ΔB can go out of tolerance
In practice the only mechanism by which ΔA, ΔB can go out of tolerance is *overinflating the membrane* far beyond the B-position. Once overinflated, a membrane requires excessive suction to close (ΔA generally > 30 kPa), and even ΔB may be a suction.

5. DMT TESTING PROCEDURE

5.1 Preliminary checks and operations before testing

Select for testing only blades respecting the tolerances (have available at least two). Similarly, use only properly checked pieces of equipment.

Pre-thread the pneumatic-electrical (p-e) cable through a suitable number of push rods and the adaptors. During this operation keep the cable terminals protected from dirt with the caps.

Wrench-tighten the cable terminal to the blade. Connect the blade to the bottom push rod (with interposed the *lower adaptor*). Avoid excessive twists in the cable while making the connections.

Insert the electrical ground cable plug into the "ground" jack of the control unit. Clip the other end (electrical alligator clip) to the *upper slotted adaptor* or to one of the push rods (not to the metal frame of the rig, which may be not in firm electrical contact with the rods).

The connections should be as indicated in Fig. 12 (but do not open the valve of the bottle yet!).

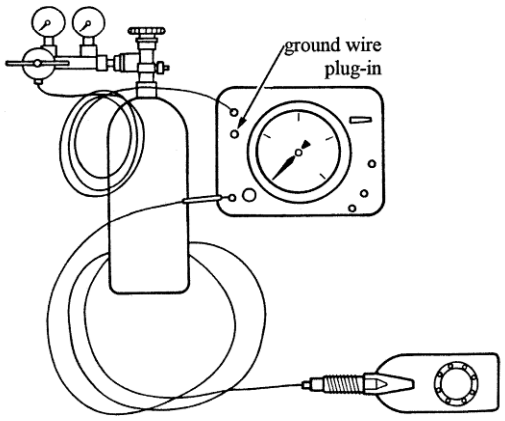

Fig. 12. Layout of the connections during current testing

Check the electrical continuity and the switch mechanism by pressing the center of the membrane. The signal should activate. If not, make the appropriate repair.

Record the zero of the gage Z_M (reading of the gage for zero pressure) by opening the *toggle vent valve* and read the pressure while tapping gently on the glass of the gage.

Perform the calibration as described in detail in Section 4.

With the gas tank valve closed, connect the pressure regulator to the tank and set the regulated pressure to zero (fully unscrew the regulating lever).

Connect the pneumatic cable from the gas tank regulator to the control unit female quick connector marked "pressure source".

Make sure that: the *main valve* is closed, the *toggle vent valve* is open and the *micrometer flow valve* is closed.

Set the regulator so that the pressure supplied to the control unit is about 3 MPa (this pressure can be later increased if necessary). Open the tank valve.

Open the *main valve*. (This valve normally remains always open during current testing. During current testing the operator only uses the *micrometer flow valve* and the *vent* valves).

5.2 STEP-BY-STEP TEST PROCEDURE (*A, B, C* READINGS)

The DMT test basically consists in the following sequence of operations.

1) The DMT operator makes sure that the *micrometer flow valve* is closed and the *toggle vent valve* open, then he gives the go-ahead to the rig operator (the two operators should position themselves in such a way they can exchange control and visual communication easily).
2) The rig operator pushes the blade vertically into the soil down to the selected test depth, either from ground surface or from the bottom of a borehole. During the advancement the signal (galvanometer and buzzer) is normally *on* because the soil pressure closes the membrane. (The signal generally starts at 20 to 40 cm below ground surface).
3) As soon as the test depth is reached, the rig operator releases the thrust on the push rods and gives the go-ahead to the DMT operator.
4) The DMT operator closes the *toggle vent valve* and slowly opens the *micrometer flow valve* to pressurize the membrane. During this time he hears a steady audio signal or buzzer on the control unit. At the instant the signal stops (i.e. when the membrane lifts from its seat and just begins to move laterally), the operator reads the pressure gage and records the first pressure reading *A*.
5) Without stopping the flow, the DMT operator continues to inflate the membrane (signal *off*) until the signal reactivates (i.e. membrane movement = 1.1 mm). At this instant the operator reads at the gage the second pressure reading *B*. After mentally noting or otherwise recording this value, he must do the following four operations:
   1 - Immediately open the *toggle vent valve* to depressurize the membrane.
   2 - Close the *micrometer flow valve* to prevent further supply of pressure to the dilatometer (these first two operations prevent further expansion of the membrane, which may permanently deform it and change its calibrations, and must be performed quickly after the *B*-reading, otherwise the membrane may be damaged).
   3 - Give the rig operator the go-ahead to advance one depth increment - generally 20 cm (the *toggle vent valve* must remain open during penetration to avoid pushing the blade with the membrane expanded).
   4 - Write the second reading *B*.

Repeat the above sequence at each depth until the end of the sounding. At the end of the sounding, when the blade is extracted, perform the final calibration.

If the *C*-reading is to be taken, there is only one difference in the above sequence. In Step 5.1, after *B*, open the *slow vent valve* instead of the fast *toggle vent valve* and wait (approximately 1 minute) until the pressure drops approaching the zero of the gage. At the instant the signal *returns* take the *C*-reading.

Note that, in sands, the value to be expected for *C* is a low number, usually < 100 - 200 kPa, i.e. 10 or 20 m of water.

NOTE: Frequent mistake in C-readings
As remarked in DMT Digest Winter 1996 (edited by GPE Inc., Gainesville, Florida), several users have reported poor *C*-readings, mostly due to improper technique. The frequent mistake is the following. After *B*, i.e. when the slow deflation starts, the signal is *on*. After some time the signal stops (from *on* to *off*). The mistake is to take the pressure at this inversion as *C*, which is incorrect (at this time the membrane is the *B*-position). The correct instant for taking *C* is some time later, when, completed the deflation, after say 1 minute, the membrane returns to the "closed" *A*-position, thereby contacting the supporting pedestal and reactivating the signal.

NOTE: Frequence of C-readings

(a) Sandy sites

In sands ($B \geq 2.5\ A$) *C*-readings may be taken sporadically, say every 1 or 2 m, and are used to evaluate u_0 (equilibrium pore pressure). It is advisable to repeat the *A*-*B*-*C* cycle several times to insure that all cycles provide similar *C*-readings.

(b) Interbedded sands and clays

If the interest is limited to finding the u_0 profile, then *C*-readings are taken in the sandy layers ($B \geq 2.5\ A$), say every 1 or 2 m.

When the interest, besides u_0, is to discern free-draining layers from non free-draining layers, then *C*-readings are taken at each test depth.

NOTE: Electrical connections during testing

The rig operator should never disconnect the ground cable (e.g. to add a rod which requires to remove the electrical alligator) while the DMT operator is taking the readings and anyway not before his go-ahead indication.

NOTE: Expansion rate

Pressures *A* and *B* must be reached slowly.

According to the Eurocode 7 (1997), the rate of gas flow to pressurize the membrane shall be such that the *A*-reading is obtained (typically in 15 seconds) within 20 seconds from reaching the test depth and the *B*-reading (expansion from *A* to *B*) within 20 seconds after the *A*-reading. As a consequence, the rate of pressure increase is very slow in weak soils and faster in stiff soils.

The above time intervals typically apply for cables lengths up to approximately 30 m. For longer cables the flow rate may have to be reduced to allow pressure equalization along the cable.

During the test, the operator may occasionally check the adequacy of the selected flow rate by closing the *micrometer flow valve* and observing how the pressure gage reacts. If the gage pressure drops in excess of 2 % when closing the valve (ASTM 1986), the rate is too fast and must be reduced.

NOTE: Time required for the test

The time delay between end of pushing and start of inflation is generally 1-2 seconds. The complete test sequence (*A*, *B* readings) generally requires about 1 minute. The total time needed for obtaining a "typical" 30 m profile (if no obstructions are found) is about 3 hours. The *C*-reading adds about 45 seconds to 1 minute to the time required for the DMT sequence at each depth.

NOTE: Depth increment

A smaller depth increment (typically 10 cm) can be assumed, even limited to a single portion of the DMT sounding, whenever more detailed soil profiling is required.

NOTE: Test depths

The test depths should be recorded with reference to the center of the membrane.

NOTE: Thrust measurement

Some Authors or existing standards (Schmertmann 1988, ASTM 1986, ASTM Draft 2001) recommend the measurement of the thrust required to advance the blade as a routine part of the DMT testing procedure. The specific aim of this additional measurement is to obtain q_D (penetration resistance of the blade tip). q_D permits to estimate K_0 and Φ in sand according to the method formulated by Schmertmann (1982, 1983).

Measuring q_D directly is highly impractical. One way of obtaining q_D is to derive it from the thrust force, measurable by a properly calibrated load cell.

The preferable location of such load cell would be immediately above the blade to exclude the rod friction (however the lateral friction on the blade has still to be detracted). Even this cell location is impractical and not presently adopted except for research purposes, so that the load cell is generally located above the ground surface.

Practical alternative methods for estimating q_D are indicated in ASTM (1986): (a) Measure the thrust at the ground surface and subtract the estimated parasitic rod friction above the blade. (b) Measure the thrust needed for downward penetration and the pull required for upward withdrawal: the difference gives an estimate of q_D. (c) If values of the cone penetration resistance q_c from adjacent CPT are available, assume $q_D \approx q_c$ (e.g. ASTM 1986, Campanella & Robertson 1991, ASTM Draft 2001).

6. REPORTING OF TEST RESULTS ("FIELD RAW DATA")

A typical DMT field data form is shown in Fig. 13.

Besides the field raw data, the test method should be described, or the reference to a published standard indicated.

7. CHECKS FOR QUALITY CONTROL

7.1 CHECKS ON HARDWARE

7.1.1 Blade

Membrane corrections tolerances

Verify that all blades available at the site are within tolerances (initial ΔA = 5 to 30 kPa, initial ΔB = 5 to 80 kPa).

Typical: 0.15 0.40

FIRM (max characters no.=32)	BLADE No. ↓	ΔA (bar) 0.05-0.20	ΔB (bar) 0.20-0.60	(1) Δmm	Membrane Aspect (2)
CUSTOMER (32)	Start				
JOB (32)	Z_E= (3)				
SITE (32)	Z_E=				
REMARK (32)	Z_E=				

TEST NAME (12) DATE (20)

Absol. elev.(optional) _____ m Z_{water} (necess.) ____ m or ☐ > Z_{final}

Zero of gauge _____ bar γ_{top} _____ t/m³ (default 1.75)

(1) Coaxiality error (L square)
(2) Elastic, overinflated, wrinkled, snapping, scratched, etc.
(3) Depth reached from extracted blade

☐ Rig ☐ Penetrometer

Diameter of rod behind the blade _____

TEST STOPPED BECAUSE → REFUSAL ☐ MEMBRANE † ☐ Z =$Z_{prefixed}$ ☐

OPERATOR _____

0	A	B	C	6				12				18				24			
2				2				2				2				2			
4				4				4				4				4			
6				6				6				6				6			
8				8				8				8				8			
1				7				13				19				25			
2				2				2				2				2			
4				4				4				4				4			
6				6				6				6				6			
8				8				8				8				8			
2				8				14				20				26			
2				2				2				2				2			
4				4				4				4				4			
6				6				6				6				6			
8				8				8				8				8			
3				9				15				21				27			
2				2				2				2				2			
4				4				4				4				4			
6				6				6				6				6			
8				8				8				8				8			
4				10				16				22				28			
2				2				2				2				2			
4				4				4				4				4			
6				6				6				6				6			
8				8				8				8				8			
5				11				17				23				29			
2				2				2				2				2			
4				4				4				4				4			
6				6				6				6				6			
8				8				8				8				8			

Fig. 13. Typical DMT field data form - (1 bar = 100 kPa)

13

Sharpness of electrical signal
Using the syringe (in the calibration configuration) apply 10 or more cycles of vacuum-pressure to verify sharpness of the electrical signal at the *off* and *on* inversions. If the signal inversions are not sharp, the likely reason is dirt between the contacts and the blade must be disassembled and cleaned.

Airtightness
Submerge the blades under water and pressurize them at 0.5 MPa.

Elevations of sensing disc, feeler and quartz (once plexiglas) cylinder
These checks are executed using a special "tripod" dial gage (Fig. 14). The legs of the tripod rest on the surrounding plane and the dial gage permits to measure the elevations above this plane. Their values should fall within the following tolerances:

Sensing disc - Nominal elevation above the surrounding plane: 0.05 mm. Tolerance range: 0.04-0.07 mm.

Feeler - Nominal elevation above the sensing disc: 0.05 mm. Tolerance range: 0.04-0.07 mm.

Quartz cylinder - Only calibrated quartz (once plexiglas) cylinders (height 3.90 ± 0.01 mm) should be used to insure accuracy of the prefixed movement. Therefore checking the elevation of the top of the quartz cylinder is redundant. However such elevation can be checked, and should be in the range 1.13-1.18 mm above the membrane support plane.

Sensing disc extraction force (the sensing disc must be stationary inside the insulating seat)
The disc should fit tightly, thanks to the lateral gripping force, inside the insulating seat. The extraction force should be, as a minimum, equal to the weight of the blade so that, if the sensing disc is lifted, the blade is lifted too without falling.

If the coupling becomes loose (disc free to move) then the gripping force should be increased. One quick fix can be the insertion, while reinstalling the disc, of a small piece of plastic sheet laterally (not on the bottom).

Conditions of the penetration edge
In case of severe denting of blade's edge, straighten the major undulations, then sharpen the edge using a file.

Coaxiality between blade and axis of the rods
With the *lower adaptor* mounted on the blade, place the inside edge of an L-square against the side of the adaptor. Note the distance from the penetration edge of the blade to the side of the L-square. Turn the blade 180° and repeat the measurement. The difference between the two distances should not exceed 3 mm (corresponding to a coaxiality error of 1.5 mm).

Fig. 14. "Tripod" dial gage

Blade planarity
Place a 15 cm ruler against the face of the blade parallel to its long side. The "sag" between the ruler and blade should not exceed 0.5 mm (to be checked with a flat 0.5 mm feeler gage).

Check the blade for electrical continuity
If the calibration has been carried out without irregularities in the expected electrical signal, the calibration itself already proves that the electrical function of the blade is working properly.

Additional electrical checks can be carried out with the membrane removed (but with the quartz cylinder in its place) using a continuity tester. The open blade should respond electrically as follows:

- Continuity between the metal tubelet and the sensing disc
- Continuity between the metal tubelet and blade body if the quartz cylinder is lifted
- No continuity (insulation) between the metal tubelet and blade body if the quartz cylinder is depressed (continuity in this case would mean that the blade is in short circuit).

A recommended check just before mounting the membrane is the following:

- Press 10 times or more on the quartz cylinder to insure that the *on* and *off* signal inversions are sharp and prompt.

Sensing disc, underlying cavity and elements inside cavity must be perfectly clean
The parts of the instrument inside the membrane (disc, spring, metal cylinder, cylinder housing) must be kept perfectly clean (e.g. blowing each piece with compressed air) to insure proper electrical contacts.

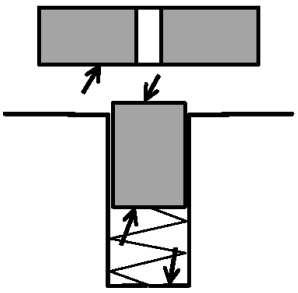

Fig. 15. Electrical contact points to be kept clean to avoid membrane overinflation

A complete guide for disassembling and cleaning the blade can be found in Marchetti & Crapps (1981) and Schmertmann (1988).

In particular, the critical electrical contact points (highlighted in Fig. 15) should be perfectly free from dirt/grains/tissue. If not, the defective electrical contact will cause *severe and costly inconveniences*.

In fact electrical malfunctioning will result in no *B*-signal. In absence of *B*-signal, the operator will keep inflating, eventually overexpanding the membrane beyond ΔA, ΔB tolerances, in which case the test results will be rejected.

The risk of absence of *B*-reading can be reduced by the following check: before starting a sounding, repeat the calibration (ΔA, ΔB) 10 times or more, to make sure that the *B*-signal is regular and sharp.

7.1.2 Control unit

Check the control unit for electrical operation

- Press the test button with the audio switch *on*. The galvanometer and buzzer should activate.
- Connect with a wire the inside of the "ground" jack with the female quick connector marked "dilatometer". The galvanometer and buzzer should activate.

Check the control unit for gas leakage

Close the *vent* valves, open the *main valve* and the *micrometer flow valve*. Pressurize the control unit to the maximum gage range. Close the *main valve* to avoid further pressure supply. Observe the gages for leaks.

7.1.3 Pneumatic-electrical cables

Check the cables for mechanical integrity

Inspect the entire length to determine if the tubing is pinched or broken.

Check the cables for electrical operation

Check by a continuity tester both electrical continuity and electrical insulation between the terminals.

The male quick connectors should be in contact with the inner wire, while the metal terminals should be insulated from the wire.

Check the cables for gas leakage

Plug with the special female closed-ended terminal the blade terminal of the cable and connect the other end of the cable to the control unit. Use the control unit to pressurize the cable to 4-6 MPa. Then close the *micrometer flow valve*. Observe the gage for any loss in pressure. A leak can be localized by immersing the cable and fittings in water.

7.2 CHECKS ON TEST EXECUTION

- Verify that *A* is reached in ≈ 15 seconds (within 20 seconds), *B* in ≈ 15 seconds (within 20 seconds) after *A*.
- The change of ΔA or ΔB before/after the sounding must not exceed 25 kPa, otherwise the test will be rejected.
- The *C*-reading, when taken, should be obtained in 45 to 60 seconds after starting the deflation following *B*.

NOTE: Accuracy of DMT measurements

The prefixed displacement is the difference between the height of the quartz (once plexiglas) cylinder and the thickness of the sensing disc. These components are machined to 0.01 mm tolerance, and their dimensions cannot be altered by the operator. Likely temperature dilatation of such components is less than 0.01 mm. Hence the displacement will be 1.10 mm ± 0.02 mm.

The pressure measurements are balance of zero measurements (null method), providing high accuracy. The accuracy of the pressure measurements is the accuracy of the gages in the control unit.

Since the accuracy of both measured pressure and displacement is high, the instrumental accuracy of the DMT results is also high, and operator independent. Accuracy problems can only arise when the following two circumstances occur simultaneously: (a) The soil is very soft. (b) The operator has badly overinflated the membrane, making ΔA, ΔB uncertain.

NOTE: Reproducibility of DMT results

The high reproducibility of the test results is a characteristic of the DMT unanimously observed by many investigators.

It has been noted that "peaks" or other discontinuities in the profiles repeat systematically if one performs more than one sounding, therefore they are not due to a random instrumental deviation, but reflect soil variability.

Even in sand, which is usually considered inherently variable, the DMT has been found to give repeatable profiles, i.e. the variability can be followed and the instrumental dispersion is negligible.

NOTE: Automatic data acquisition for DMT and "research" dilatometers
While the mechanical DMT is the type most commonly used today, various users have developed automatic data acquisition systems. These systems are outside the scope of this report. Only a few comments are given below.

Automatic data acquisition is not as indispensable as in other in situ tests (e.g. CPT/CPTU), since the DMT generates only a few measurements per minute, that the operator can easily write in the dead time between the operations.

Automatic acquisition does not speed the test or increase productivity or accuracy. Rather, automatic recording is requested nowadays mostly for *quality control checks*, easier when everything is recorded.

"Research" dilatometers, involving blades instrumented with various types of sensors, are outside the scope of this report. The interested reader is referred to Boghrat (1987), Campanella & Robertson (1991), Fretti et al. (1992), Huang et al. (1991), Kaggwa et al. (1995), Lutenegger & Kabir (1988), Mayne & Martin (1998).

One of the interesting findings obtained by testing with different instrumented blades is that the pressure-displacement relationship, between *A* and *B*, is almost linear.

8. DISSIPATION TESTS

In low permeability soils (clays, silts) the excess pore water pressure induced by the blade penetration dissipates over a period of time much longer than required for the DMT test. In these soils it is possible to estimate the in situ consolidation/flow parameters by means of dissipation tests.

A DMT dissipation test consists in stopping the blade at a given depth, then monitoring the decay of the total contact horizontal stress σ_h with time. The flow parameters are then inferred from the rate of decay.

The DMT dissipation method recommended by the authors is the DMT-A method (Marchetti & Totani 1989, ASTM Draft 2001). Other available methods are the DMT-C method (Robertson et al. 1988) and the DMT-A_2 method (ASTM Draft 2001). The interpretation is covered in Section 11.4.1.

Dissipation tests are generally performed during the execution of a standard DMT sounding, stopping the blade at the desired dissipation depth. After the dissipation is completed, the sounding is resumed following the current test procedure. In this case, the time required for the entire DMT sounding includes the time for the dissipation.

Dissipation tests can be time consuming and are generally performed only when information on flow properties is especially valuable. In very low permeability clays, a dissipation can last 24 hours or more. In more permeable silty layers, the dissipation may last hours, if not minutes.

Dissipation tests can also be performed separated from DMT soundings, by means of one or more blades pushed and left in place at the desired depths. This permits to carry out DMT soundings and dissipations simultaneously, with considerable time saving.

The dissipation depths are decided in advance, based on earlier DMT profiles or other available soil information.

It should be noted that DMT dissipations are not feasible in relatively permeable soils (e.g. some sandy silts) whose permeability is such that most of the dissipation occurs in the first minute, because the first reading cannot be taken in less than 10-15 seconds from start. Clearly DMT dissipations are not feasible in sand and gravel.

8.1 DMT-A DISSIPATION METHOD

The DMT-A method (Marchetti & Totani 1989) consists in stopping the blade at a given depth, then taking a timed sequence of *A*-readings. Note that only the *A*-reading is taken, avoiding the expansion to *B*. The operator deflates the membrane by opening the *toggle vent valve* as soon as *A* is reached (this method is also called "*A* & deflate" dissipation).

Procedure:

1) Stop the penetration at the desired dissipation depth and immediately start a stopwatch. The time origin ($t = 0$) is the instant at which pushing is stopped. Then, without delay, *slowly* inflate the membrane to take the *A*-reading. As soon as *A* is reached, immediately vent the blade. Read at the stopwatch the elapsed time at the instant of the *A*-reading and record it together with the *A*-value.
2) Continue to take additional *A*-readings to obtain reasonably spaced points for the time-dissipation curve. A factor of 2 increase in time at each *A*-reading is satisfactory (e.g. 0.5, 1, 2, 4, 8, 15, 30 etc. minutes after stopping the blade). For each *A*-reading record the exact stopwatch time (which has not necessarily to coincide with the above values).

3) Plot in the field a preliminary *A–log t* diagram. Such diagram has usually an S-shape. The dissipation can be stopped when the *A–log t* curve has flattened sufficiently so that the contraflexure point is clearly identified (the time at the contraflexure point t_{flex} is used for the interpretation).

8.2 DMT-A_2 DISSIPATION METHOD

The DMT-A_2 method (described in ASTM Draft 2001) is an evolution of the DMT-C method (Robertson et al. 1988, see also details in Schmertmann 1988 and US DOT 1992).

The DMT-C method consists in performing, at different times, one cycle of readings *A-B-C* and plotting the decay curve of the *C*-readings taken at the end of each cycle.

The DMT-C method relies on the assumption that p_2 (corrected *C*-reading) is approximately equal to the pore pressure u in the soil facing the membrane. Then the method treats the p_2 vs time curve as the decay curve of u (hence p_2 after complete dissipation should be equal to u_o).

The assumption $p_2 = u$ has been found to be generally valid for soft clays, not valid for OC clays. Thus the DMT-C method should be used with caution.

In 1991 (DMT Digest 12) Schmertmann found that a better approximation of the u decay can be obtained in the following way. Perform first one complete cycle *A-B-C* (only one cycle), then take only *A*-readings (called by Schmertmann *"A_2"*) at different times, without performing further *A-B-C* cycles.

The procedure for DMT-A_2 is very similar to the one previously described for the DMT-A dissipation, with the following differences:

1) The readings taken and used to construct the decay curve are the A_2 -readings rather than the *A*-readings.
2) The dissipation is stopped after making at least enough measurements to find t_{50} (time at 50 % of *A*-dissipation). If time permits, the test is continued long enough for the dissipation curve to approach its eventual asymptote at 100 % dissipation A_{100}. Ideally $A_{100} = u_0$ when corrected.

PART B

INTERPRETATION AND APPLICATIONS

9. DATA REDUCTION AND INTERPRETATION

9.1 INTERPRETATION IN TERMS OF SOIL PARAMETERS

The primary way of using DMT results is to interpret them in terms of common soil parameters.

In many cases the parameters estimated by DMT are used by applying the usual design methods. In this way the engineer can compare and check the parameters obtained by other tests, select the design profiles, then apply his usual design methods.

This methodology ("design via parameters") opens the door to a wide variety of engineering applications.

Direct DMT-based methods are limited to some specific applications (e.g. axially loaded piles, *P-y* curves for laterally loaded piles).

9.2 DATA REDUCTION / INTERMEDIATE AND COMMON SOIL PARAMETERS

The basic DMT data reduction formulae and correlations are summarized in Table 1.

Field readings *A*, *B* are corrected for membrane stiffness, gage zero offset and feeler pin elevation in order to determine the pressures p_0, p_1 using the following formulae:

$$p_0 = 1.05\ (A - Z_M + \Delta A) - 0.05\ (B - Z_M - \Delta B) \quad (1)$$

$$p_1 = B - Z_M - \Delta B \quad (2)$$

where

ΔA, ΔB = corrections determined by membrane calibration

Z_M = gage zero offset (gage reading when vented to atmospheric pressure) – For a correct choice of Z_M see Note on next page.

The corrected pressures p_0 and p_1 are subsequently used in place of *A* and *B* in the interpretation.

The original correlations (Marchetti 1980) were obtained by calibrating DMT results versus high quality parameters. Many of these correlations form the basis of today interpretation, having been generally confirmed by subsequent research.

The interpretation evolved by first identifying three "intermediate" DMT parameters (Marchetti 1980):

– the material index I_D
– the horizontal stress index K_D
– the dilatometer modulus E_D

SYMBOL	DESCRIPTION	BASIC DMT REDUCTION FORMULAE	
p_0	Corrected First Reading	$p_0 = 1.05\ (A - Z_M + \Delta A) - 0.05\ (B - Z_M - \Delta B)$	Z_M = Gage reading when vented to atm. If ΔA & ΔB are measured with the same gage used for current readings A & B, set $Z_M = 0$ (Z_M is compensated)
p_1	Corrected Second Reading	$p_1 = B - Z_M - \Delta B$	
I_D	Material Index	$I_D = (p_1 - p_0) / (p_0 - u_0)$	u_0 = pre-insertion pore pressure
K_D	Horizontal Stress Index	$K_D = (p_0 - u_0) / \sigma'_{v0}$	σ'_{v0} = pre-insertion overburden stress
E_D	Dilatometer Modulus	$E_D = 34.7\ (p_1 - p_0)$	E_D is NOT a Young's modulus E. E_D should be used only AFTER combining it with K_D (Stress History). First obtain $M_{DMT} = R_M E_D$, then e.g. $E \approx 0.8\ M_{DMT}$
K_0	Coeff. Earth Pressure in Situ	$K_{0,DMT} = (K_D / 1.5)^{0.47} - 0.6$	for $I_D < 1.2$
OCR	Overconsolidation Ratio	$OCR_{DMT} = (0.5\ K_D)^{1.56}$	for $I_D < 1.2$
c_u	Undrained Shear Strength	$c_{u,DMT} = 0.22\ \sigma'_{v0}\ (0.5\ K_D)^{1.25}$	for $I_D < 1.2$
Φ	Friction Angle	$\Phi_{safe,DMT} = 28° + 14.6°\ \log K_D - 2.1°\ \log^2 K_D$	for $I_D > 1.8$
c_h	Coefficient of Consolidation	$c_{h,DMTA} \approx 7\ cm^2 / t_{flex}$	t_{flex} from A-log t DMT-A decay curve
k_h	Coefficient of Permeability	$k_h = c_h\ \gamma_w / M_h$ ($M_h \approx K_0\ M_{DMT}$)	
γ	Unit Weight and Description	(see chart in Fig. 16)	
M	Vertical Drained Constrained Modulus	$M_{DMT} = R_M E_D$ if $I_D \le 0.6$ $R_M = 0.14 + 2.36 \log K_D$ if $I_D \ge 3$ $R_M = 0.5 + 2 \log K_D$ if $0.6 < I_D < 3$ $R_M = R_{M,0} + (2.5 - R_{M,0}) \log K_D$ with $R_{M,0} = 0.14 + 0.15\ (I_D - 0.6)$ if $K_D > 10$ $R_M = 0.32 + 2.18 \log K_D$ if $R_M < 0.85$ set $R_M = 0.85$	
u_0	Equilibrium Pore Pressure	$u_0 = p_2 = C - Z_M + \Delta A$	In free-draining soils

Table 1. Basic DMT reduction formulae

then relating these intermediate parameters (not directly p_0 and p_1) to common soil parameters.

The intermediate parameters I_D, K_D, E_D are "objective" parameters, calculated from p_0 and p_1 using the formulae shown in Table 1.

The interpreted (final) parameters are common soil parameters, derived from the intermediate parameters I_D, K_D, E_D using the correlations shown in Table 1 (or other established correlations).

The values of the in situ equilibrium pore pressure u_0 and of the vertical effective stress σ'_{v0} prior to blade insertion must also be introduced into the formulae and have to be known, at least approximately.

Parameters for which the DMT provides an interpretation (see Table 1) are:

- vertical drained constrained modulus M (all soils)
- undrained shear strength c_u (in clay)
- in situ coefficient of lateral earth pressure K_0 (in clay)
- overconsolidation ratio OCR (in clay)
- horizontal coefficient of consolidation c_h (in clay)
- coefficient of permeability k_h (in clay)
- friction angle ϕ (in sand)
- unit weight γ and soil type (all soils)
- equilibrium pore pressure u_0 (in sand).

Correlations for clay apply for $I_D < 1.2$. Correlations for sand apply for $I_D > 1.8$.

The constrained modulus M and the undrained shear strength c_u are believed to be the most reliable and useful parameters obtained by DMT.

NOTE: Gage zero offset Z_M

In all the formulae containing Z_M enter $Z_M = 0$ (even if $Z_M \neq 0$) *if* ΔA, ΔB are measured by the *same gage* used for the current A, B readings (this is the normal case today using the dual-gage control unit).

The reason is that the Z_M correction is already accounted for in ΔA, ΔB (this compensation can be verified readily from the algebra of the correction formulae for A, B). Hence entering the real Z_M would result in applying twice the correction to A and B.

To be exact, in general, the value of Z_M to be input in the equations should be the zero offset of the gage used for reading A & B minus the zero offset of the gage used for reading ΔA & ΔB.

NOTE: Correction formula for p_0

Eq. 1 for p_0 (back-extrapolated contact pressure at zero displacement) derives from the assumption of a linear pressure-displacement relationship between 0.05 mm (elevation of the feeler pin above sensing disc) and 1.10 mm (Marchetti & Crapps 1981).

NOTE: Sign of ΔA, ΔB corrections
Although the actual ΔA-pressure is negative (vacuum), it simulates a positive soil pressure. Consequently it is recorded and introduced in the p_0 formula as a positive number when it is a vacuum (which is the normal case). Eq. 1 is already adjusted to take into account that a positive ΔA is a vacuum. ΔB is normally positive.

NOTE: Selecting the "average" ΔA, ΔB to calculate p_0, p_1 (for a detailed treatment of this topic see Marchetti 1999)
Selecting the average ΔA, ΔB from the before/after ΔA, ΔB values must be done by an experienced technician. While performing the average, the entity of ΔA, ΔB and their variations during the sounding will also give him an idea of the care exercised during the execution.

If the test has been regular (e.g. the membrane has not been overinflated, and the Eurocode 7 tolerances for ΔA, ΔB have not been exceeded), the before/after values of ΔA, ΔB are very close, so that their arithmetic average is adequate.

If ΔA or ΔB vary more than 25 kPa during a sounding, the results, according to the Eurocode 7 (1997), should be discarded. However, if the soil is stiff, the results are not substantially influenced by ΔA, ΔB, and using typical ΔA, ΔB values (e.g. 15 and 40 kPa respectively) generally leads to quite acceptable results.

NOTE: Comments on the 3 intermediate parameters
The three intermediate parameters I_D, K_D, E_D are derived from two field readings. Hence, clearly, only two of them are independent (the DMT is just a two-parameter test). I_D, K_D, E_D have been introduced because each one of them has some recognizable physical meaning and some engineering usefulness.

10. INTERMEDIATE DMT PARAMETERS

10.1 MATERIAL INDEX I_D (SOIL TYPE)

The material index I_D is defined as follows:

$$I_D = \frac{p_1 - p_0}{p_0 - u_0} \qquad (3)$$

where u_0 is the pre-insertion in situ pore pressure.

The above definition of I_D was introduced having observed that the p_0 and p_1 profiles are systematically "close" to each other in clay and "distant" in sand.

According to Marchetti (1980), the soil type can be identified as follows:

clay	$0.1 < I_D < 0.6$
silt	$0.6 < I_D < 1.8$
sand	$1.8 < I_D < (10)$

In general, I_D provides an expressive profile of soil type, and, in "normal" soils, a reasonable soil description. Note that I_D sometimes misdescribes silt as clay and vice versa, and of course a mixture clay-sand would generally be described by I_D as silt.

When using I_D, it should be kept in mind that I_D is not, of course, the result of a sieve analysis, but a parameter reflecting mechanical behavior (some kind of "rigidity index"). For example, if a clay for some reasons behaves "more rigidly" than most clays, such clay will be probably interpreted by I_D as silt.

Indeed, if one is interested in mechanical behavior, sometimes it could be more useful for his application a description based on a mechanical response rather than on the real grain size distribution. If, on the other hand, the interest is on permeability, then I_D should be supplemented by the pore pressure index U_D (see Section 11.4.4).

10.2 HORIZONTAL STRESS INDEX K_D

The horizontal stress index K_D is defined as follows:

$$K_D = \frac{p_0 - u_0}{\sigma'_{v0}} \qquad (4)$$

where σ'_{v0} is the pre-insertion in situ overburden stress.

K_D provides the basis for several soil parameter correlations and is a key result of the dilatometer test.

The horizontal stress index K_D can be regarded as K_0 amplified by the penetration. In genuinely NC clays (no aging, structure, cementation) the value of K_D is $K_{D,NC} \approx 2$.

The K_D profile is similar in shape to the *OCR* profile, hence generally helpful for "understanding" the soil deposit and its stress history (Marchetti 1980, Jamiolkowski et al. 1988).

10.3 DILATOMETER MODULUS E_D

The dilatometer modulus E_D is obtained from p_0 and p_1 by the theory of elasticity (Gravesen 1960). For the 60 mm diameter of the membrane and the 1.1 mm displacement it is found:

$$E_D = 34.7\ (p_1 - p_0) \qquad (5)$$

E_D in general should not be used as such, especially because it lacks information on stress history. E_D should be used only in combination with K_D and I_D.

The symbol E_D should not evoke special affinity with the Young's modulus E' (see Section 11.3.2).

11. DERIVATION OF GEOTECHNICAL PARAMETERS

11.1 STRESS HISTORY / STATE PARAMETERS

11.1.1 Unit weight γ and soil type

A chart for determining the soil type and unit weight

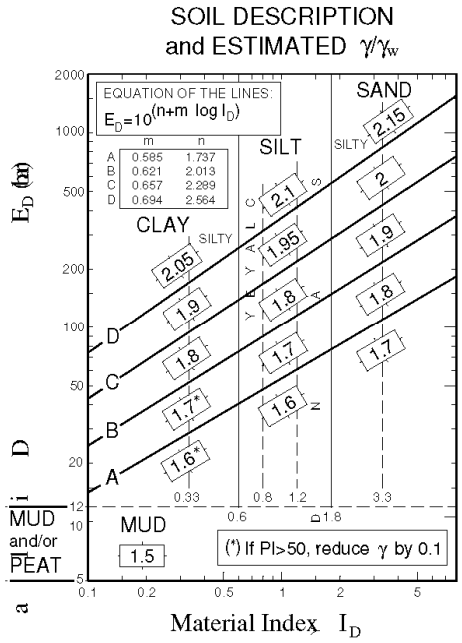

Fig. 16. Chart for estimating soil type and unit weight γ (normalized to γ_w = γ water) - Marchetti & Crapps 1981 - (1 bar = 100 kPa)

γ from I_D and E_D was developed by Marchetti & Crapps 1981 (Fig. 16).

Many Authors (e.g. Lacasse & Lunne 1988) have presented modified forms of such table, more closely matching local conditions. However the original chart is generally a good average for "normal" soils. On the other hand, the main scope of the chart is not the accurate estimation of γ, but the possibility of constructing an approximate profile of σ'_{v0}, needed in the elaboration.

11.1.2 Overconsolidation ratio *OCR*

11.1.2.1 *OCR* in clay

The original correlation for deriving the overconsolidation ratio *OCR* from the horizontal stress index K_D (based on data only for uncemented clays) was proposed by Marchetti (1980) from the observation of the similarity between the K_D profile and the *OCR* profile:

$$OCR_{DMT} = (0.5\ K_D)^{1.56} \qquad (6)$$

Eq. 6 has built-in the correspondence $K_D = 2$ for $OCR = 1$ (i.e. $K_{D,NC} \approx 2$). This correspondence has been confirmed in many genuinely NC (no cementation, aging, structure) clay deposits.

The resemblance of the K_D profile to the *OCR* profile has also been confirmed by many subsequent comparisons (e.g. Jamiolkowski et al. 1988).

Research by Powell & Uglow (1988) on the *OCR*-K_D correlation in several UK deposits showed some deviation from the original correlation. However their research indicated that:

- The original correlation line (Eq. 6) is intermediate between the UK datapoints.
- The datapoints relative to each UK site were in a remarkably *narrow band*, *parallel* to the original correlation line.
- The narrowness of the datapoints band for each site is a confirmation of the remarkable resemblance of the *OCR* and K_D profiles, and the *parallelism* of the datapoints for each site to the original line is a confirmation of its slope.

The original *OCR*-K_D correlation for clay was also confirmed by a comprehensive collection of data by Kamei & Iwasaki 1995 (Fig. 17), and, theoretically, by Finno 1993 (Fig. 18).

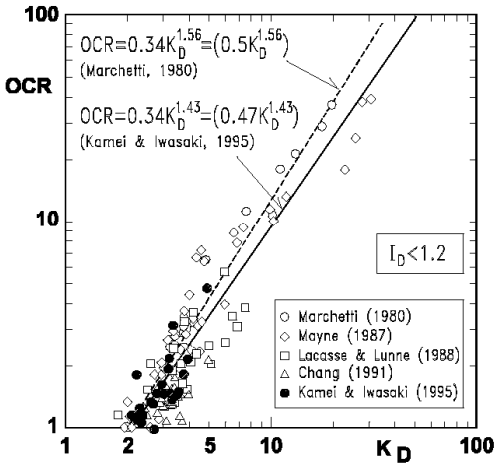

Fig. 17. Correlation K_D-*OCR* for cohesive soils from various geographical areas (Kamei & Iwasaki 1995)

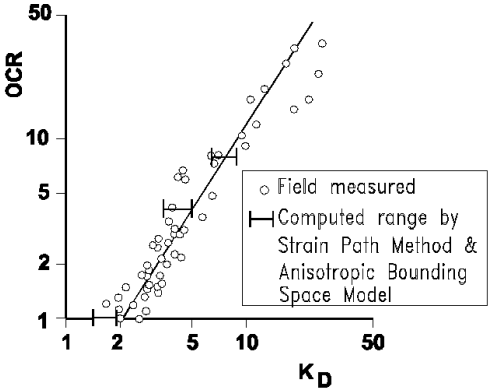

Fig. 18. Theoretical K_D vs *OCR* (Finno 1993)

A confirmation of $K_D \approx 2$ in genuine NC clays comes from recent slip surface research (Totani et al. 1997). In fact: (a) In all the layers where sliding was confirmed by inclinometers, it was found $K_D \approx 2$. (b) The clay in the remolded sliding band has certainly lost any trace of aging, structure, cementation, i.e. such clay is a good example of genuine NC clay.

Thus $K_D \approx 2$ appears the lower bound value for $K_{D,NC}$. If a geologically NC clay has $K_D > 2$, any excess of K_D above 2 indicates the likely existence of aging, structure or cementation.

Cemented-aged-structured clays (for brevity called below "cemented clays")

The original OCR-K_D correlation for clays established by Marchetti (1980) was presented as non applicable to cemented clays. However various researchers have attempted to develop correlations also in cemented clays.

It cannot be expected the existence of a unique OCR-K_D correlation valid for all cemented clays, because the deviation from the uncemented correlation depends on the variable entity of the cementation and the consequent variable increase in K_D. Therefore, in general, datapoints for cemented clays should be kept separated, without attempting to establish a unique average correlation for both cemented and uncemented clays.

Practical indications for estimating OCR in various clays

- The original OCR-K_D correlation (Eq. 6) is a good base for getting a first interpretation of the OCR profile (or, at least, generally accurate information on its shape).
- In general the K_D profile is helpful for "understanding" the stress history. The K_D profile permits to discern NC from OC clays, and clearly identifies shallow or buried desiccation crusts. The K_D profile is often the first diagram that the engineer inspects, because from it he can get at a glance a general grasp on the stress history.
- In NC clays, the inspection of the K_D profile permits to distinguish genuine NC clays ($K_D \approx 2$, constant with depth) from cemented NC clays ($K_D \approx 3$ to 4, constant with depth, e.g. Fucino, Onsøy). In these clays any excess of K_D compared with the "floor" value $K_D \approx 2$ provides an indication of the intensity of cementation/structure/aging. However the NC condition can be easily recognized (despite $K_D > 2$), because K_D does not decrease with depth as in OC deposits.
- In cemented OC clays the inspection of the K_D profile does not reveal cementation as clearly as in NC clays (though the cementation shows up in the form of a less marked decrease of K_D with depth). In cemented clays the geological OCR will be overpredicted by Eq. 6.
- Highly accurate and detailed profiles of the in situ OCR can be obtained by calibrating OCR_{DMT} versus a few (in theory even one or two - see Powell & Uglow 1988) high quality oedometers. Since OCR is a parameter difficult and costly to obtain, for which there are not many measuring options, the possibility of projecting via K_D a large number of high quality data appears useful.
- Stiff fissured OC clays. It is found that in non fissured OC clays the K_D profiles are rather smooth, while in fissured OC clays the K_D profiles are markedly seesaw-shaped. Such difference indicates that fissures are, to some extent, identified by the low points in the K_D profiles. The sensitivity of K_D to fissures may be useful in some studies. Note that the K_Ds in the fissures of an OC clay are still considerably > 2, therefore fissures cannot be confused with slip surfaces - characterized by $K_D = 2$ (see Section 13.4).

11.1.2.2 OCR in sand

The determination (even the definition) of OCR in sand is more difficult than in clay. OCR in sand is often the result of a complex history of preloading or desiccation or other effects. Moreover, while OCR in clay can be determined by oedometers, sample disturbance does not permit the same in sand. Therefore some approximation must be accepted.

A way of getting some information on OCR in sand is to use the ratio M_{DMT}/q_c. The basis is the following:

- Jendeby (1992) performed DMTs and CPTs before and after compaction of a loose sand fill. He found that before compaction (i.e. in nearly NC sand) the ratio M_{DMT}/q_c was 7-10, after compaction (i.e. in OC sand) 12-24.
- Calibration chamber (CC) research (Baldi et al. 1988) comparing q_c with M, both measured on the CC specimen, found ratios M_{cc}/q_c: in NC sands 4-7, in OC sands 12-16.
- Additional data in sands from instrumented embankments and screw plate tests (Jamiolkowski 1995) indicated a ratio (in this case E'/q_c): in NC sands 3-8, in OC sands 10-20.
- The well documented finding that compaction effects are felt more sensitively by M_{DMT} than by q_c (see Section 13.5) also implies that M_{DMT}/q_c is increased by compaction/precompression (see Fig. 42 ahead).

Hence *OCR* in sands can be approximately evaluated from the ratio M_{DMT}/q_c, using the following indicative values as a reference: M_{DMT}/q_c = 5-10 in NC sands, M_{DMT}/q_c = 12-24 in OC sands.

An independent indication of some ability of K_D to reflect *OCR* in sand comes from the crust-like K_D profiles often found at the top of sand deposits, very similar to the typical K_D profiles found in OC desiccation crusts in clay.

11.1.3 In situ coefficient of lateral earth pressure K_0

11.1.3.1 K_0 in clay

The original correlation for K_0, relative to uncemented clays (Marchetti 1980), is:

$$K_0 = (K_D / 1.5)^{0.47} - 0.6 \qquad (7)$$

Various Authors (e.g. Lacasse & Lunne 1988, Powell & Uglow 1988, Kulhawy & Mayne 1990) have presented slightly modified forms of the above equation. However the original correlation produces estimates of K_0 generally satisfactory, especially considering the inherent difficulty of precisely measuring K_0 and that, in many applications, even an approximate estimate of K_0 may be sufficient.

In highly cemented clays, however, the Eq. 7 may significantly overestimate K_0, since part of K_D is due to the cementation.

Example comparisons of K_0 determined by DMT and by other methods at two research sites are shown in Fig. 19 (Aversa 1997).

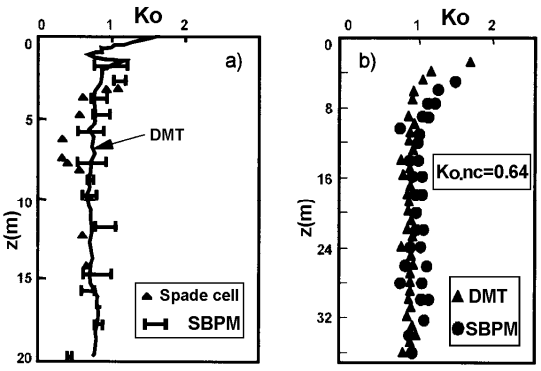

Fig. 19. K_0 from DMT vs K_0 by other methods at two clay research sites (Aversa 1997) (a) Bothkennar, UK (Nash et al. 1992) (b) Fucino, Italy (Burghignoli et al. 1991)

11.1.3.2 K_0 in sand

The original K_0-K_D correlation was obtained by interpolating datapoints relative mostly to clay. The very few (in 1980) datapoints relative to sand seemed to plot on the same curve. However, subsequent sand datapoints showed that a unique correlation cannot be established, since such correlation in sand also depends on ϕ or D_r.

Schmertmann (1982, 1983), based on CC results, interpolated through the CC datapoints a K_0-K_D-ϕ correlation equation (the lengthy fractionlike equation reported as Eq. 1 in Schmertmann 1983 or Eq. 6.5 in US DOT 1992). Such equation is the analytical equivalent of Fig. 10 in Schmertmann (1983), containing, in place of a unique K_0-K_D equation, a family of K_0-K_D curves, one curve for each ϕ. Since ϕ is in general unknown, Schmertmann (1982, 1983) suggested to use also the Durgunoglu & Mitchell (1975) theory, providing an additional condition q_c-K_0-ϕ, if q_c (or q_D) is also measured. He suggested an iterative computer procedure (relatively complicated) permitting the determination of both K_0 and ϕ. A detailed description of the method can be found in US DOT (1992).

To facilitate calculations, Marchetti (1985) prepared a K_0-q_c-K_D chart in which ϕ was eliminated, by combining the Schmertmann (1982, 1983) K_0-K_D-ϕ relation with the Durgunoglu & Mitchell (1975) q_c-K_0-ϕ relation. Such chart (reported as Fig. 6.4 in US DOT 1992) provides K_0, once q_c and K_D are given.

Baldi et al. (1986) updated such K_0-q_c-K_D chart by incorporating all subsequent CC work. Moreover the chart was converted into simple algebraic equations:

$$K_0 = 0.376 + 0.095\ K_D - 0.0017\ q_c/\sigma'_{v0} \qquad (8)$$

$$K_0 = 0.376 + 0.095\ K_D - 0.0046\ q_c/\sigma'_{v0} \qquad (9)$$

Eq. 8 was determined as the best fit of CC data, obtained on artificial sand, while Eq. 9 was obtained by modifying the last coefficient to predict "correctly" K_0 for the natural Po river sand.

In practice the today recommendation for K_0 in sand is to use the above Eqns. 8 and 9 with the following values of the last coefficient: -0.005 in "seasoned" sand, -0.002 in "freshly deposited" sand (though such choice involves some subjectivity).

While this is one of the few methods available for estimating K_0 in sand (or at least the shape of the K_0 profile), its reliability is difficult to establish, due to scarcity of reference values.

Cases have been reported of satisfactory agreement (Fig. 20, Jamiolkowski 1995). In other cases the K_0 predictions have been found to be incorrect as absolute values, though the shape of the profile appears to reflect the likely K_0 profile. The uncertainty is especially pronounced in cemented sand (expectable, due to the additional unknown

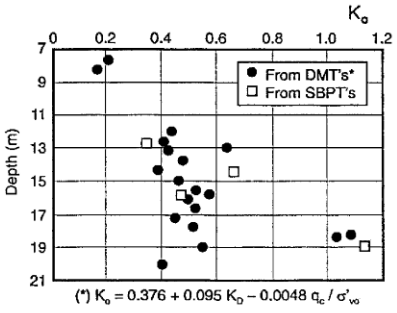

Fig. 20. K_0 from DMTs and SBPTs in natural Ticino sand at Pavia (Jamiolkowski 1995)

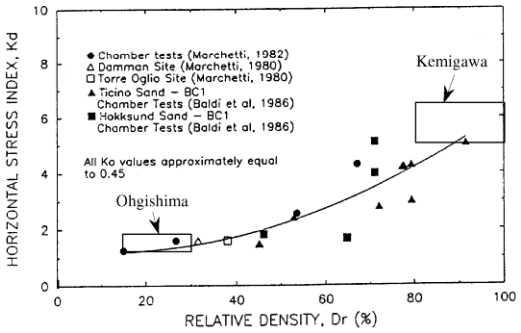

Fig. 21. Correlation K_D-D_r for NC uncemented sands (after Reyna & Chameau 1991, also including Ohgishima and Kemigawa datapoints obtained by Tanaka & Tanaka 1998)

"cementation"). An inconvenience of the method is that it requires both DMT and CPT and proper matching of correspondent K_D and q_c.

11.1.4 Relative density D_r (sand)

In NC uncemented sands, the recommended relative density correlation is the one shown in Fig. 21 (Reyna & Chameau 1991), where D_r is derived from K_D. This correlation is supported by the additional K_D-D_r datapoints (also included in Fig. 21) obtained by Tanaka & Tanaka (1998) at the Ohgishima and Kemigawa sites, where D_r was determined on high quality samples taken by the freezing method.

In OC sands or possibly in cemented sands, Fig. 21 will overpredict D_r, since part of K_D is due to the overconsolidation or cementation, rather than to D_r. The amount of the overprediction is difficult to evaluate at the moment.

11.2 Strength parameters

11.2.1 Undrained shear strength c_u

The original correlation for determining c_u from DMT (Marchetti 1980) is the following:

$$c_u = 0.22\ \sigma'_{v0}\ (0.5\ K_D)^{1.25} \qquad (10)$$

Eq. 10 has generally been found to be in an intermediate position between subsequent datapoints presented by various researchers (e.g. Lacasse & Lunne 1988, Powell & Uglow 1988). Example comparisons between $c_{u\,DMT}$ and c_u by other tests at two research sites are shown in Figs. 22 and 23.

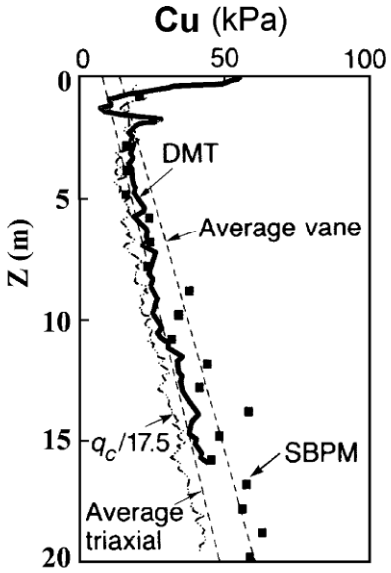

Fig. 22. Comparison between c_u determined by DMT and by other tests at the National Research Site of Bothkennar, UK (Nash et al. 1992)

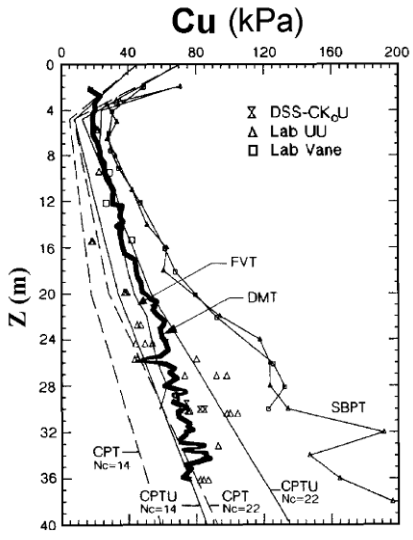

Fig. 23. Comparison between c_u determined by DMT and by other tests at the National Research Site of Fucino, Italy (Burghignoli et al. 1991)

Experience has shown that, in general, $c_{u\,DMT}$ is quite accurate and dependable for design, at least for everyday practice.

11.2.2 Friction angle Φ (sand)

Two methods are currently used today for estimating ϕ from DMT (see also Marchetti 1997).

The first method (Method 1) provides simultaneous estimates of ϕ and K_0 derived from the pair K_D and q_D (Method 1a) or from the pair K_D and q_c (Method 1b). The second method (Method 2) provides a *lower bound* estimate of ϕ based only on K_D.

Method 1a (ϕ from K_D, q_D)
This iterative method, developed by Schmertmann (1982, 1983), described in Section 11.1.3.2 relative to K_0 in sand, permits the determination of both K_0 and ϕ.

Method 1b (ϕ from K_D, q_c)
This method (Marchetti 1985) first derives K_0 from q_c and K_D by Eqns. 8 and 9, as indicated in Section 11.1.3.2 (K_0). Then uses the theory of Durgunoglu & Mitchell (1975), or its handy graphical equivalent chart in Fig. 24, to estimate ϕ from K_0 and q_c.

Method 2 (ϕ from K_D)
Details on the derivation of the method can be found in Marchetti (1997). ϕ is obtained from K_D by the following equation:

$$\phi_{safe,DMT} = 28° + 14.6° \; log\, K_D - 2.1° \; log^2 K_D \quad (11)$$

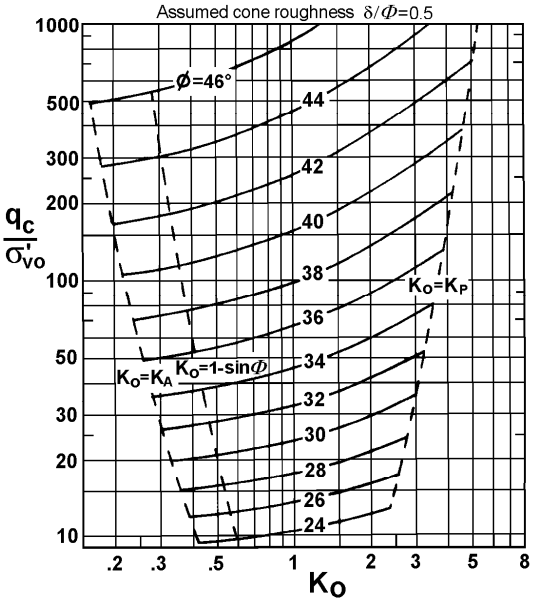

Fig. 24. Chart q_c-K_0-ϕ – graphical equivalent of the Durgunoglu & Mitchell theory (worked out by Marchetti 1985)

As already noted, ϕ from Eq. 11 is intended to be not the "most likely" estimate of ϕ, but a *lower bound* value (typical entity of the underestimation believed to be 2° to 4°). Obviously, if more accurate reliable higher values of ϕ are available, then such values should be used.

It should be noted that in cemented *c*-ϕ sands it is difficult to separate the two strength parameters, because there is an additional unknown.

11.3 Deformation parameters

11.3.1 Constrained modulus *M*

The modulus *M* determined from DMT (often designated as M_{DMT}) is the vertical drained confined (one-dimensional) tangent modulus at σ'_{v0} and is the same modulus which, when obtained by oedometer, is called $E_{oed} = 1/m_v$.

M_{DMT} is obtained by applying to E_D the correction factor R_M according to the following expression:

$$M_{DMT} = R_M \, E_D \quad (12)$$

The equations defining $R_M = f(I_D, K_D)$ (Marchetti 1980) are given in Table 1. The value of R_M increases with K_D (major influence).

It is to be noted that R_M, being dependent on I_D,K_D, is *not* a unique proportionality constant relating *M* to E_D. R_M varies mostly in the range 1 to 3.

Since E_D is an "uncorrected" modulus, while M_{DMT} is a "corrected" modulus, deformation properties should in general be derived from M_{DMT} and not from E_D.

Experience has shown that M_{DMT} is highly reproducible and in most sites variable in the range 0.4 to 400 MPa.

Comparisons both in terms of M_{DMT}–$M_{reference}$ and in terms of predicted vs measured settlements have shown that, in general, M_{DMT} is reasonably accurate and dependable for everyday design practice.

M_{DMT} is to be used in the same way as if it was obtained by other methods (say a good quality oedometer) and introduced in one of the available procedures for evaluating settlements.

Example comparisons between M_{DMT} and *M* from high quality oedometers at two research sites are shown in Figs. 25 and 26.

NOTE: Necessity of applying the correction R_M to E_D
- E_D is derived from soil distorted by the penetration.
- The direction of loading is horizontal, while *M* is vertical.
- E_D lacks information on stress history and lateral stress, reflected to some extent by K_D. The necessity of stress history for the realistic assessment of settlements has been emphasized by

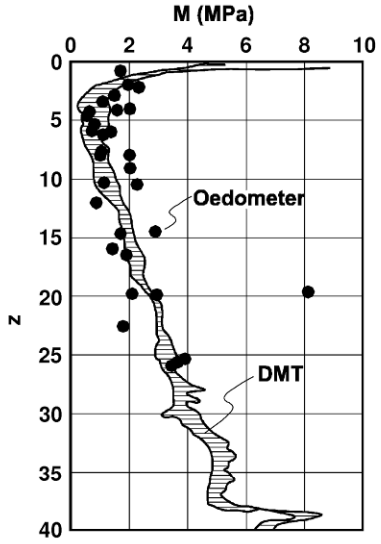

Fig. 25. Comparison between *M* determined by DMT and by high quality oedometers, Onsøy clay, Norway (Lacasse 1986)

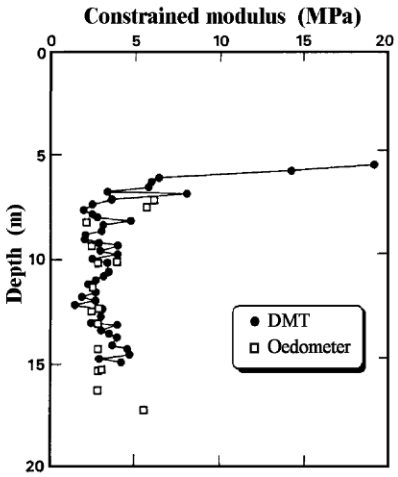

Fig. 26. Comparison between *M* determined by DMT and by high quality oedometers, Komatsugawa site, Japan (Iwasaki et al. 1991)

many researchers (e.g. Leonards & Frost 1988, Massarsch 1994).

– In clays, E_D is derived from an undrained expansion, while M is a drained modulus. (For more details on this specific point see Marchetti 1997).

11.3.2 Young's modulus E'

The Young's modulus E' of the soil skeleton can be derived from M_{DMT} using the theory of elasticity equation:

$$E' = \frac{(1+\nu)(1-2\nu)}{(1-\nu)} M \qquad (13)$$

(e.g. for a Poisson's ratio ν = 0.25-0.30 one obtains $E' \approx 0.8\ M_{DMT}$).

The Young's modulus E' should not be derived from (or confused with) the dilatometer modulus E_D.

11.3.3 Maximum shear modulus G_0

No correlation for the maximum shear modulus G_0 was provided by the original Marchetti (1980) paper.

Subsequently, many researchers have proposed correlations relating DMT results to G_0.

A well documented method was proposed by Hryciw (1990). Other methods are summarized by Lunne et al. (1989) and in US DOT (1992).

Recently Tanaka & Tanaka (1998) found in four NC clay sites (where $K_D \approx 2$) $G_0/E_D \approx 7.5$. They also investigated three sand sites, where they observed that G_0/E_D decreases as K_D increases. In particular they found G_0/E_D decreasing from ≈ 7.5 at small K_D (1.5-2) to ≈ 2 for $K_D > 5$.

Similar trends in sands had been observed e.g. by Sully & Campanella (1989) and Baldi et al. (1989).

11.4 Flow characteristics and pore pressures

11.4.1 Coefficient of consolidation c_h

The method recommended by the authors for deriving c_h from DMT dissipations is the DMT-A method (Marchetti & Totani 1989, ASTM Draft 2001). Another accepted method (ASTM Draft 2001) is the DMT-A_2 method.

The test procedures - and some information on their origin - are described in Section 8.

In all cases the dissipation test consists in stopping the blade at a given depth, then monitoring the decay of the contact pressure σ_h with time. The horizontal coefficient of consolidation c_h is then inferred from the rate of decay.

Note that, as shown by piezocone research, the dissipation is governed in most cases predominantly by c_h rather than by c_v, which is the reason why c_h is the target of these procedures.

c_h from DMT-A dissipation

The interpretation of the DMT-A dissipations for evaluating c_h is very straightforward (Marchetti & Totani 1989):

– Plot the *A–log t* curve
– Identify the contraflexure point in the curve and the associated time (t_{flex})
– Obtain c_h as

$$c_{h,\,OC} \approx 7\ \mathrm{cm}^2 / t_{flex} \qquad (14)$$

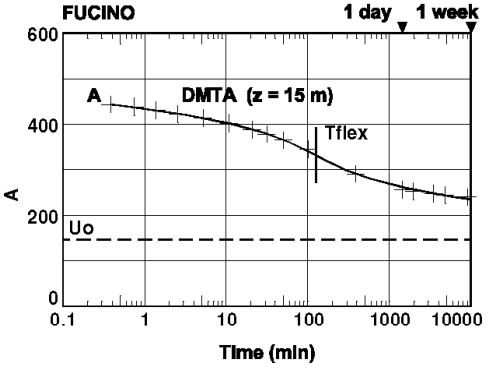

Fig. 27. Example of DMT-A decay curve

It should be noted that c_h from Eq. 14 refers to the soil behavior in the OC range. A c_h value several times lower should be adopted for estimating the settlement rate in a problem involving loading mainly in the NC range.

Comments on the origin of Eq. 14 are given in one of the Notes below.

An example of DMT-A decay curve (Fucino clay) is shown in Fig. 27.

c_h from DMT-A_2 dissipation

Basically the DMT-A_2 method (that can be considered an evolution of the DMT-C method) infers c_h from t_{50} determined from the A_2-decay dissipation curve. c_h is calculated from t_{50} by using an equivalent radius for the DMT blade and a time factor T_{50} obtained from the theoretical solutions for CPTU.

A detailed description of the method for interpreting the DMT-C dissipations can be found in Robertson et al. (1988), Schmertmann (1988) and US DOT (1992). The DMT-A_2 dissipation can be interpreted in the same way as the DMT-C, with the only difference that the readings A_2 are used in place of the readings C.

A detailed description of the method for interpreting DMT-A_2 dissipations can be found in ASTM Draft 2001.

NOTES

- The DMT-A method does not require the knowledge of the equilibrium pore pressure u_o, since it uses as a marker point the contraflexure and not the 50 % consolidation point.
- The use of t_{flex} in the DMT-A method is in line with the recent suggestions by Mesri et al. (1999), advocating the preferability of the "inflection point method" for deriving c_v from the oedometer over the usual Casagrande or Taylor methods.
- The DMT-A dissipation test is very similar to the well-established "holding test" by pressuremeter. For such test the theory is available. It was developed by Carter et al. (1979), who established theoretically the S-shaped decay curve of the total contact pressure σ_h vs time (hence the theoretical time factor T_{flex} for the contraflexure point). A similar theory is not available yet for the decay σ_h vs time in the DMT blade, whose shape is more difficult to model. However, since the phenomenon is the same, the theory must have a similar format, and the link $7\ cm^2$ between c_h and t_{flex} in Eq. 14 was determined by experimental calibration. (Determining $7\ cm^2$ by calibration is similar to determining $T_{50} = 0.197$, in the Terzaghi theory of 1-D consolidation, by field calibration rather than by mathematics). As to *fixity*, in the case of the DMT blade the *fixity* during the holding test is inherently insured, being the blade a solid object.
- Case histories presented by Totani et al. (1998) indicated that the c_h from DMT-A are in good agreement (or "slower" by a factor 1 to 3) with c_h backfigured from field observed behavior.
- The DMT-A_2 method (and the DMT-C method) rely on the assumption that the contact pressure A_2 (or C), after the correction, is approximately equal to the pore pressure u in the soil facing the membrane. Such assumption is generally valid for soft clays, but dubious in more consistent clays. (Note that the DMT-A method does not rely on such assumption).
- The problem of filter smearing or clogging does not exist with the DMT membrane, because the membrane is anyway a non draining boundary, and what is monitored is a *total* contact stress.

11.4.2 Coefficient of permeability k_h

Schmertmann (1988) proposes the following procedure for deriving k_h from c_h:

- Estimate M_h using $M_h = K_0 M_{DMT}$, i.e. assuming M proportional to the effective stress in the desired direction
- Obtain $k_h = c_h \gamma_w / M_h$ (15)

11.4.3 In situ equilibrium pore pressure by *C*-readings in sands

The DMT, though non provided with a pore pressure sensor, permits, in free-draining granular soils ($B \geq 2.5\ A$), the determination of the pre-insertion ambient equilibrium pore pressure u_0. Since analysis of the DMT data depends on the in situ effective stress, water pressure is an important and useful information.

The reason why the DMT closing pressure (*C*-reading) closely approximates u_0 in sand (e.g. Campanella et al. 1985) is the following. During inflation, the membrane displaces the sand away from the blade. During deflation the sand has little tendency to rebound, rather tends to remain away from the membrane, without applying effective pressure to it ($\sigma'_h = 0$, hence $\sigma_h = u_0$). Therefore, at closure, the only pressure on the membrane will be u_0 (see sandy layers in Fig. 28).

This mechanism was well known to pressuremeter investigators, who discovered long ago that the contact pressure, in a disturbed pressuremeter test in sand, is essentially u_0.

In clay the method does not work because, during deflation, the clay tends to rebound and apply to the membrane some effective stresses. Moreover, in general, $u > u_0$ due to blade penetration. Hence $C > u_0$.

u_0 in sand is estimated as p_2, where:

$$p_2 = C - Z_M + \Delta A \qquad (16)$$

(the gage zero offset Z_M is generally taken = 0, more details in Section 9.2).

Before interpreting the *C*-reading the engineer should insure that the operator has followed the right procedure (Section 5.2), in particular has not incurred in the frequent mistake highlighted in Section 5.2. Note that, in sands, the values expected for *C* are low numbers, usually < 100 or 200 kPa, i.e. 10 or 20 m of water.

C-readings typically contain some experimental scatter and the engineer will usually rely on a p_2 profile vs depth, to provide a pore water pressure trend, rather than on individual measurements.

If the interest is limited to finding the u_0 profile, then *C*-readings are taken in the sandy layers ($B \geq 2.5$ *A*), say every 1 or 2 m. When the interest, besides u_0, is to discern free-draining layers from non free-draining layers, then it is recommended to take *C*-readings routinely at each test depth (see next Section).

More details about the *C*-reading can be found in Marchetti (1997) and Schmertmann (1988).

11.4.4 Discerning free-draining from non free-draining layers - Index U_D

In problems involving excavations, dewatering, piping/blowup control, flow nets etc. the identification of free-draining/non free-draining layers is important. For such identification, methods based on the DMT *C*-reading (corrected into p_2 by Eq. 16) have been developed (see Lutenegger & Kabir's 1988 Eq. 2, or Schmertmann's 1988 Eq. 3.7).

The basis of the methods is the following. As discussed in the previous Section, in free-draining layers $p_2 \approx u_0$. In layers not free-draining enough to reach $\Delta u = 0$ in the 1-1.5 min elapsed since insertion, some excess pore pressure will still exist at the time of the *C*-reading, hence $p_2 > u_0$.

Therefore: $p_2 = u_0$ indicates a *free-draining* soil ($\Delta u = 0$ in 1-1.5 min) while $p_2 > u_0$ indicates a *non free-draining* soil (Fig. 28).

Index U_D

Based on the above, the pore pressure index U_D was defined by Lutenegger & Kabir (1988) as:

$$U_D = (p_2 - u_0) / (p_0 - u_0) \qquad (17)$$

In free-draining soils, where $p_2 \approx u_0$, $U_D \approx 0$. In non free-draining soils, p_2 will be higher than u_0 and U_D too.

The example in Fig. 29 (Benoit 1989) illustrates how U_D can discern "permeable" layers ($U_D = 0$), "impermeable" layers ($U_D = 0.7$) and "intermediate permeability" layers (U_D between 0 and 0.7), in agreement with B_q from CPTU.

Note that U_D, while useful for the above scope, cannot be expected to offer a scale over the full range of permeabilities. In fact beyond a certain *k* the test will be drained anyway, below a certain *k* the test will be undrained anyway (see Note on next page).

In layers recognized by U_D as non free-draining, quantitative evaluation of c_h can be obtained e.g. using the DMT dissipations described earlier.

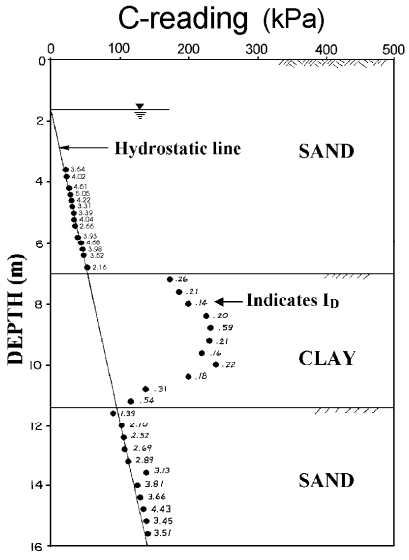

Fig. 28. Use of *C*-readings for distinguishing free-draining from non free-draining layers (Schmertmann 1988)

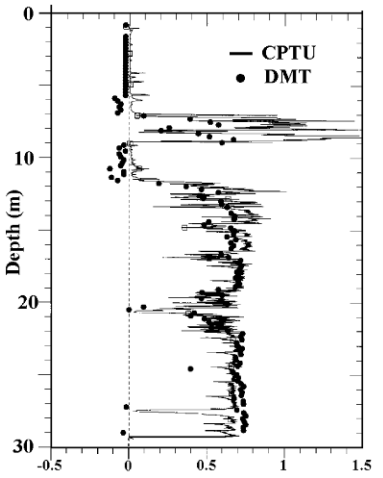

Fig. 29. Use of U_D for discerning free-draining layers (U_D = 0) from non free-draining layers (Benoit 1989)

In layers recognized by U_D as free-draining, the DMT dissipations will not be performed (the DMT dissipations are not feasible if most of the dissipation occurs in the first minute, because readings cannot be taken in the first ≈ 15 sec).

NOTE: Drainage conditions during the test
In a clean sand the DMT is a perfectly drained test. Δu is virtually zero throughout the test, whose duration (say 1 minute) is sufficient for any excess to dissipate. In a low permeability clay the opposite is true, i.e. the test is undrained and the excesses do not undergo any appreciable dissipation during the normal test.

It should be noted that, for opposite reasons, the u values in the soil surrounding the blade are constant with time during the test in both cases. In permeable soils everywhere $u = u_0$. In impermeable soils the pore pressures do not dissipate.

There is however a *niche* of soils (in the silts region) for which 1 minute is insufficient for full drainage, but sufficient to permit some dissipation. In these *partial drainage* soils the data obtained can be misleading to an unaware user. In fact the reading *B*, which follows *A* by say 15 seconds, is not the "proper match" of *A*, because in the 15 seconds from *A* to *B* excess has been dissipating and *B* is too low, with the consequence that the difference *B-A* is also too low and so are the derived values I_D, E_D, M. In such soils I_D will possibly end up in the extreme left hand of its scale (I_D = 0.1 or less) and M will also possibly be far too low. Note that the sites where this occurrence has been encountered are very few (e.g. Drammen, Norway).

To be sure, in case of very low I_D and M there is some ambiguity, because the low values of *B-A* could just be the normal response of a low permeability very soft clay. The ambiguity can be solved with the help of *C*-readings (or U_D). If the U_D values in the "low *B-A*" layers are intermediate between those found in the free-draining layers and those found in the non free-draining layers, than the above interpretation of *partial drainage* is presumably correct.

Of course the *partial drainage* explanation can also be verified by means of laboratory sieve analysis or permeability tests. In practice, if the *partial drainage* explanation of the low *B-A* is confirmed, all results dependent from *B-A* (recognizable by very depressed I_D troughs) have to be ignored.

12. PRESENTATION OF DMT RESULTS

Fig. 30 shows the recommended graphical format of the DMT output. Such output displays four profiles, namely I_D, M, c_u and K_D. Experience has shown that these four parameters are generally the most significant group to plot (for reliability, expressivity, usefulness). Note that K_D, though not a common soil parameter, has been selected as one to be displayed as generally helpful in "understanding" the site history, being similar in shape to the *OCR* profile. It is also recommended that the diagrams be presented side by side, and not separated. It is beneficial for the user to see the diagrams together.

The graphical output contains only the main profiles. The numerical values of these and other parameters are listed in the tabular output normally accompanying the graphical output (see example in Fig. 31).

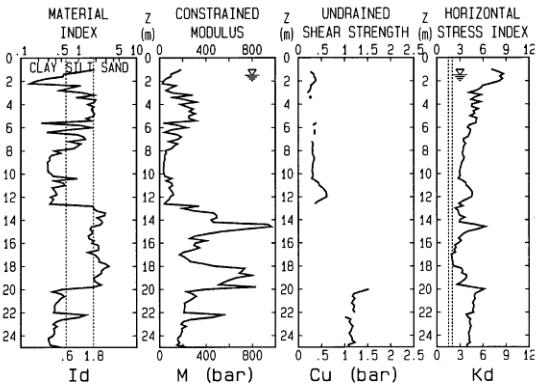

Fig. 30. Recommended graphical presentation of DMT results - (1 bar = 100 kPa)

SOIL TEST — D M T : D3 - 4 OCT 1989 — Reg 1003
LIVORNO HARBOUR — NEW QUAY — WATERTABLE m 1.5

Reduction formulae according to ASCE Geot.Jnl.,Mar. 1980, Vol.109, 299-321
NOTE : OCR = ''relative OCR''. OCR below often reasonable. Accuracy can be improved if precise OCR values are available. Then factorize all OCR below by the ratio OCRreference/OCR

Po = Corrected A reading (bar)
P1 = Corrected B reading (bar)
Gamma = Bulk unit weight/GammaH2O (-)
Sigma'= Effective overb. stress (bar)
U = Pore pressure (bar)
Id = Material Index (-)
Kd = Horizontal stress index (-)
Ed = Dilatometer modulus (bar)

INTERPRETED GEOTECHNICAL PARAMETERS
Ko = In situ earth press. coeff. (-)
Ocr= Overconsolidation ratio (-)
Phi= Safe floor value of friction angle (-)
M = Constrained modulus (at Sigma') (bar)
Cu = Undrained shear strength (bar)

Z (m)	Po	P1	Gamma	Sigma'	U	Id	Kd	Ed	Ko	Ocr	Phi	M	Cu	DESCRIPTION
1.00	1.2	3.5	1.80	0.17	0.00	1.89	7.1	85			39	186		SILTY SAND
1.20	1.6	3.4	1.70	0.21	0.00	1.09	7.9	66	1.6	8.6		150	0.26	SILT
1.40	2.1	3.2	1.70	0.24	0.00	0.56	8.6	43	1.7	9.8		100	0.33	SILTY CLAY
1.60	2.2	3.3	1.70	0.26	0.01	0.53	8.2	43	1.6	9.0		98	0.34	SILTY CLAY
1.80	2.4	3.0	1.60	0.28	0.03	0.27	8.5	23	1.7	9.6		55	0.37	CLAY
2.00	2.4	2.8	1.60	0.29	0.05	0.18	8.2	16	1.6	9.0		36	0.37	CLAY
2.20	2.2	2.5	1.50	0.30	0.07	0.15	7.1	12	1.5	7.3		25	0.32	MUD
2.40	1.9	3.8	1.70	0.31	0.09	1.02	6.0	70	1.3	5.5		139	0.27	SILT
2.60	2.0	3.2	1.70	0.32	0.11	0.68	5.7	47	1.3	5.2		90	0.27	CLAYEY SILT
2.80	1.9	2.7	1.60	0.34	0.13	0.48	5.2	31	1.2	4.4		57	0.25	SILTY CLAY
3.00	1.6	3.4	1.70	0.35	0.15	1.19	4.3	66	1.0	3.3		110	0.20	SILT
3.20	2.2	6.0	1.80	0.36	0.17	1.81	5.7	140			38	276		SILTY SAND
3.40	2.0	3.8	1.70	0.38	0.19	0.96	4.9	66	1.1	4.0		118	0.26	SILT
3.60	2.0	5.4	1.80	0.39	0.21	1.97	4.5	128			37	224		SILTY SAND
3.80	2.5	6.8	1.90	0.41	0.23	1.87	5.6	159			38	312		SILTY SAND
4.00	2.2	5.0	1.70	0.43	0.25	1.45	4.6	105			37	183		SANDY SILT
4.20	2.3	5.9	1.80	0.44	0.26	1.85	4.5	136			37	238		SILTY SAND
4.40	2.7	6.8	1.80	0.46	0.28	1.67	5.4	152			38	289		SANDY SILT
4.60	2.5	6.4	1.70	0.47	0.30	1.73	4.7	144			37	258		SANDY SILT
4.80	2.7	7.2	1.90	0.49	0.32	1.89	4.9	167			37	306		SILTY SAND
5.00	2.5	6.5	1.80	0.50	0.34	1.82	4.4	148			36	253		SILTY SAND
5.20	3.1	6.7	1.80	0.52	0.36	1.37	5.2	136			37	253		SANDY SILT
5.40	3.1	7.6	1.80	0.53	0.38	1.65	5.1	167			37	310		SANDY SILT
5.60	3.2	3.8	1.70	0.55	0.40	0.23	5.1	23	1.2	4.3		42	0.39	CLAY
5.80	2.8	5.4	1.70	0.56	0.42	1.10	4.2	97	1.0	3.2		160	0.32	SILT
6.00	2.7	6.6	1.80	0.58	0.44	1.69	4.0	144			36	233		SANDY SILT
6.20	3.1	4.6	1.70	0.59	0.46	0.61	4.4	58	1.1	3.4		96	0.35	CLAYEY SILT
6.40	3.1	3.8	1.70	0.61	0.48	0.28	4.3	27	1.0	3.3		44	0.35	CLAY
6.60	3.1	5.6	1.70	0.62	0.50	0.97	4.2	93	1.0	3.2		152	0.35	SILT
6.80	3.1	6.2	1.70	0.63	0.52	1.23	4.0	117			36	187		SANDY SILT
7.00	2.8	5.7	1.70	0.65	0.54	1.31	3.5	109			35	159		SANDY SILT
7.20	2.9	4.4	1.70	0.66	0.56	0.69	3.5	58	0.88	2.4		83	0.29	CLAYEY SILT
7.40	3.1	5.8	1.70	0.68	0.58	1.08	3.7	101	0.93	2.6		154	0.32	SILT
7.60	3.0	5.3	1.70	0.69	0.60	0.95	3.5	85	0.89	2.4		124	0.31	SILT
7.80	3.0	5.0	1.70	0.70	0.62	0.83	3.4	74	0.88	2.3		105	0.30	SILT
8.00	3.1	4.0	1.70	0.72	0.64	0.39	3.4	35	0.87	2.3		49	0.31	SILTY CLAY
8.20	3.1	4.2	1.70	0.73	0.66	0.48	3.3	43	0.85	2.2		58	0.30	SILTY CLAY
8.40	3.2	4.0	1.70	0.74	0.68	0.33	3.4	31	0.86	2.3		43	0.32	SILTY CLAY
8.60	3.4	4.2	1.70	0.76	0.70	0.31	3.6	31	0.90	2.4		45	0.34	CLAY
8.80	3.4	4.2	1.70	0.77	0.72	0.31	3.5	31	0.88	2.4		44	0.34	CLAY
9.00	3.3	4.0	1.70	0.79	0.74	0.29	3.3	27	0.84	2.1		37	0.32	CLAY
9.20	3.3	4.0	1.70	0.80	0.76	0.29	3.2	27	0.82	2.1		36	0.31	CLAY
9.40	3.3	4.0	1.70	0.81	0.77	0.29	3.1	27	0.81	2.0		35	0.31	CLAY
9.60	3.3	4.0	1.70	0.83	0.79	0.29	3.0	27	0.79	1.9		35	0.30	CLAY
9.80	3.3	4.0	1.70	0.84	0.81	0.30	3.0	27	0.77	1.8		34	0.30	CLAY
10.00	3.4	4.2	1.70	0.85	0.83	0.33	3.0	31	0.78	1.9		39	0.31	CLAY
10.20	3.5	4.4	1.70	0.87	0.85	0.36	3.0	35	0.79	1.9		45	0.32	SILTY CLAY
10.40	3.3	5.6	1.70	0.88	0.87	0.94	2.8	85	0.74	1.7		104	0.29	SILT
10.60	3.9	5.0	1.70	0.90	0.89	0.39	3.3	43	0.85	2.2		59	0.37	SILTY CLAY

Fig. 31. Example of numerical output of DMT results - (1 bar = 100 kPa)

All input data, in particular the uncorrected field readings *A* and *B* and the calibration values ΔA and ΔB, must always be reported, either in a separate document or as added columns in the above tabular output.

Figs. 32 and 33 show examples of DMT results in predominantly NC and OC sites. The condition NC or OC is clearly identified by K_D (K_D in the vertical band between the two dashed lines (K_D = 1.5-2) in NC sites, higher K_D in OC sites).

13. APPLICATION TO ENGINEERING PROBLEMS

As mentioned earlier, the primary way of using DMT results is "design via parameters".

This Section provides some details on the use of DMT in some specific applications.

13.1 SETTLEMENTS OF SHALLOW FOUNDATIONS

Predicting settlements of shallow foundations is probably the No. 1 application of the DMT, especially in sands, where undisturbed sampling and estimating compressibility are particularly difficult.

Settlements are generally calculated by means of the one-dimensional formula (Fig. 34):

$$S_{1-DMT} = \sum \frac{\Delta\sigma_v}{M_{DMT}} \Delta z \qquad (18)$$

with $\Delta\sigma_v$ generally calculated according to Boussinesq and M_{DMT} constrained modulus estimated by DMT.

It should be noted that the above formula, being based on linear elasticity, provides a settlement *proportional* to the load, and is unable to provide a non linear prediction. The predicted settlement is meant to be the *settlement in "working conditions"* (i.e. for a safety factor Fs = 2.5 to 3.5).

13.1.1 Settlements in sand

Settlements analyses in sand are generally carried out using the 1-D elasticity formula (in 1-D problems, say *large* rafts) or the 3-D elasticity formula (in 3-D problems, say *small* isolated footings).

However, based on considerations by many Authors (e.g. Burland et al. 1977), it is recommended to use the 1-D formula (Eq. 18) in *all* cases. The reasons are illustrated in detail by Marchetti (1997).

In case it is opted for the use of the 3-D formulae, E' can be derived from M using the theory of elasticity, that, for ν = 0.25, provides $E' = 0.83\ M$ (a factor not very far from unity). Indeed M and E' are often used interchangeably in view of the involved approximation.

13.1.2 Settlements in clay

Eq. 18 is also recommended for predicting settlements in clay. The calculated settlement is the *primary* settlement (i.e. net of immediate and secondary), because M_{DMT} is to be treated as the average E_{oed} derived from the oedometer curve

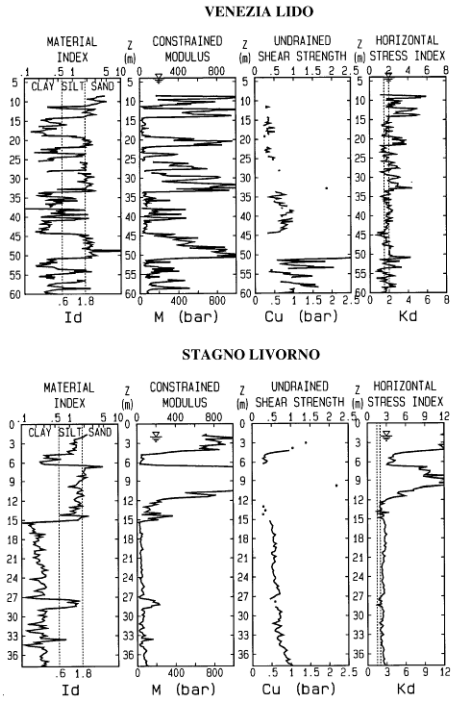

Fig. 32. Examples of DMT results in NC sites ($K_D \approx 2$) - (1 bar = 100 kPa)

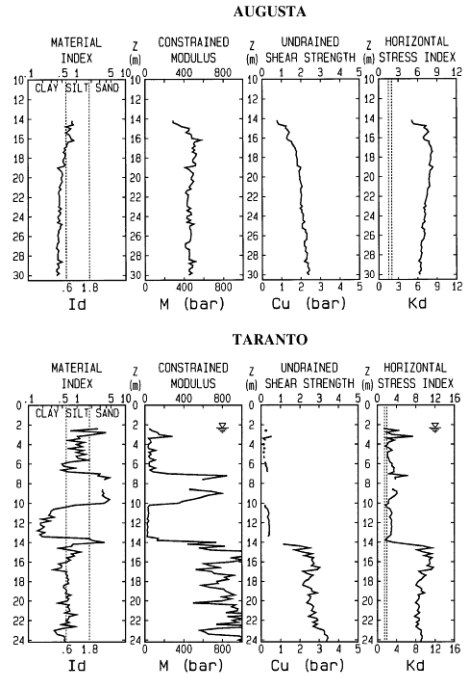

Fig. 33. Examples of DMT results in OC sites ($K_D >> 2$) - (1 bar = 100 kPa)

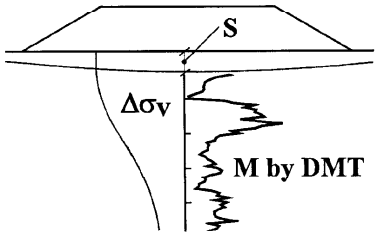

$$S = \sum \frac{\Delta\sigma_v}{M} \cdot \Delta Z$$

Fig. 34. Recommended settlement calculation

in the expected stress range.

It should be noted that in some highly structured clays, whose oedometer curves exhibit a sharp break and a dramatic reduction in slope across the preconsolidation pressure p'_c, M_{DMT} could be an inadequate average if the loading straddles p'_c. However in many common clays, and probably in most sands, the M fluctuation across p'_c is mild, and M_{DMT} can be considered an adequate average modulus.

In 3-D problems in OC clays, "according to the book", the Skempton-Bjerrum correction should be applied. Such correction in OC clays is often in the range 0.2 to 0.5 (<<1). However considering that:

- The application of the Skempton-Bjerrum correction is equivalent to reducing $S_{1\text{-}DMT}$ by a factor 2 to 5
- Terzaghi & Peck's book states that in OC clays "the modulus from even good oedometers may be 2 to 5 times smaller than the in situ modulus"

these two factors approximately cancel out.

Therefore, pending a specific study on this subject, it is suggested to adopt as *primary* settlement (even in 3-D problems in OC clays) directly $S_{1\text{-}DMT}$ from Eq. 18, without the Skempton-Bjerrum correction (while adopting, if applicable, the rigidity and the depth corrections).

13.1.3 Comparison of DMT-calculated vs observed settlements

Many investigators have presented comparisons of observed vs DMT-predicted settlements, reporting generally satisfactory agreement.

Schmertmann (1986) reports 16 case histories at various locations and for various soil types. He found an average ratio calculated/observed settlement ≈ 1.18, with the value of that ratio mostly in the range 0.75 to 1.3.

Fig. 35 (Hayes 1990) confirms the good agreement for a wide settlement range. In such figure the band amplitude of the datapoints (ratio between maximum and minimum) is approximately 2. Or the observed settlement is within ± 50 % from the DMT-predicted settlement.

Similar agreement has been reported by others (Lacasse & Lunne 1986, Skiles & Townsend 1994, Steiner et al. 1992, Steiner 1994, Woodward & McIntosh 1993, Failmezger et al. 1999, Didaskalou 1999, Pelnik et al. 1999).

13.2 AXIALLY LOADED PILES

13.2.1 Driven piles

13.2.1.1 The DMT-σ_{hc} method for piles driven in clay

The DMT-σ_{hc} method (Marchetti et al. 1986) was developed for the case of piles driven in clays. The method is based on the determination of σ'_{hc} (effective horizontal stress against the DMT blade at the end of the reconsolidation). Then a ρ factor is applied to σ'_{hc}, and the product is used as an estimate of the pile skin friction ($f_s = \rho\ \sigma'_{hc}$).

The DMT-σ_{hc} method has conceptual roots in the theories developed by Baligh (1985). However, in practice, the method has two drawbacks:

(a) In clays, the determination of σ'_{hc} can take considerable time (the reconsolidation around the blade of low permeability clays can take many hours, if not one or two days), which makes the σ'_{hc} determination expensive (especially in offshore investigations).

(b) The ρ factor has been found to be not a constant, but a rather variable factor (mostly in the range 0.10 to 0.20). Therefore, until methods for

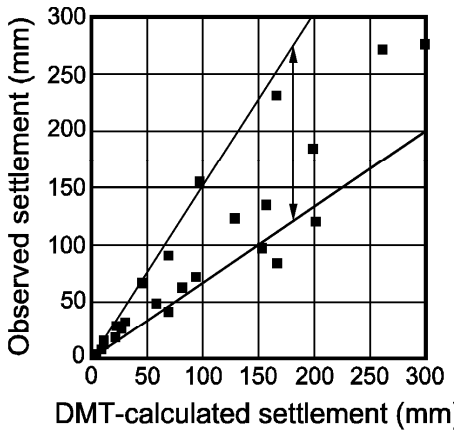

Fig. 35. Observed vs DMT-calculated settlements (Hayes 1990)

guiding the selection of ρ are developed, the uncertainty in f_s is too wide. Nevertheless, in important jobs, the method could helpfully be used to supplement other methods, e.g. for getting information on the shape of the f_s profile, or for estimating a lower bound value of f_s using ρ = 0.10.

13.2.1.2 Method by Powell et al. (2001 b) for piles driven in clay

Powell et al. (2001 b) developed a new method for the design of axially loaded piles driven in clay by DMT. The method was developed based on load tests on about 60 driven or jacked piles at 10 clay sites in UK, Norway, France and Denmark, as part of an EC Brite EuRam Project.

This method predicts the pile skin friction q_s from the material index I_D and $(p_1 - p_0)$. The recommended design formulae for skin friction in clay (both tension and compression piles) are:

$I_D < 0.1$ $\quad q_s/(p_1 - p_0) = 0.5$ (19)

$0.1 < I_D < 0.65$ $\quad q_s/(p_1 - p_0) = -0.73077\, I_D + 0.575$ (20)

$I_D > 0.65$ $\quad q_s/(p_1 - p_0) = 0.1$ (21)

A slightly modified form of the above equations was proposed for predicting q_s of compression piles only:

$I_D < 0.6$ $\quad q_s/(p_1 - p_0) = -1.1111\, I_D + 0.775$ (22)

$I_D > 0.6$ $\quad q_s/(p_1 - p_0) = 0.11$ (23)

For the upper parts of the pile where $h/R > 50$ (h = distance along the pile upwards from the tip, and R = pile radius), in both cases the above values should be multiplied by 0.85.

The pile unit end resistance q_p is evaluated as:

$$q_p = k_{di}\, p_{1e} \quad (24)$$

where p_{1e} is the *equivalent* p_1 (a suitable average beneath the base of the pile) and k_{di} is the "DMT bearing capacity factor". For closed ended driven piles the recommended values for k_{di} are:

for $E_D > 2$ MPa $\quad k_{di} = 1.3$ (25)

for $E_D < 2$ MPa $\quad k_{di} = 0.7$ (26)

For open ended piles multiply these values by 0.5.

The criteria for the variation of k_{di} with soil type need to be established from a larger database of pile and DMT results to establish the transition at $E_D = 2$ MPa.

Based on comparisons with the measured capacity of a large number of piles, Powell et al. (2001 a & b) conclude that the general shaft resistance method for all piles *(both tension and compression)* shows good potential for use in design, and performs at least as well as other methods currently available.

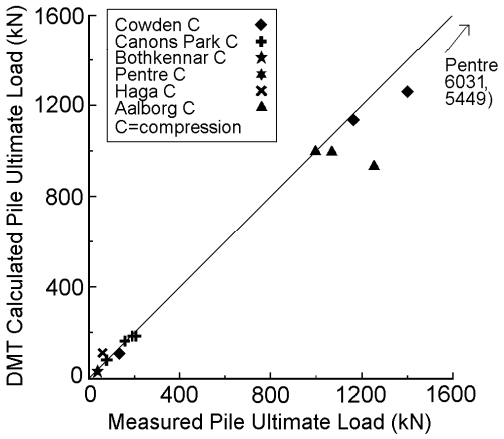

Fig. 36. Predicted vs measured ultimate pile capacity using the DMT compression pile method (Powell et al. 2001 a)

The modified method for estimating q_s for *compression piles only* based on DMT (Eqns. 22 - 23) was found to predict more accurately the observed shaft capacity of compression piles, q_p being derived as above (Fig. 36). This modified method based on DMT was found to outperform other methods investigated for compression piles (Powell et al. 2001 a).

13.2.1.3 Horizontal pressure against piles driven in clay during installation

Totani et al. (1994) report a finding of practical interest to engineers having to decide the thickness of the shell of mandrel-driven piles in clay. The paper describes measurements of σ_h (total) on a pile 57 m long, 508/457 mm in diameter, driven in a slightly OC clay. The pile was instrumented with 8 total pressure cells. Cells readings (σ_h against the pile) were taken during pauses in driving. The σ_h values were found at each depth virtually equal to p_0 determined by a normal DMT.

This finding is in accordance to theoretical findings by Baligh (1985), predicting σ_h independent from the dimensions of the penetrating object (these results suggest independence of σ_h even from the shape).

13.2.1.4 Low skin friction in calcareous sand

Some calcareous sands are known to develop unusually low skin friction, hence very low lateral pile capacity.

DMTs performed in calcareous sand (Fig. 37) have indicated unusually low K_D values in such sands. This suggests: (a) The low f_s in these sands is largely due to low σ'_h. (b) The low K_D measured by DMT in

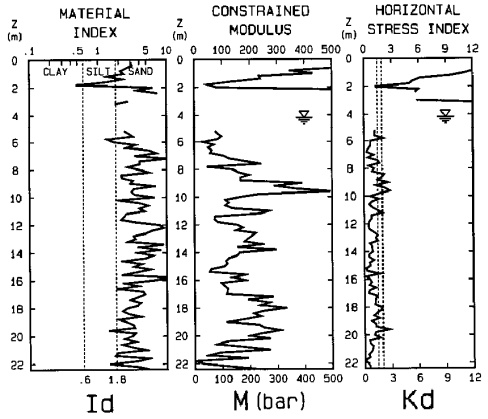

Fig. 37. DMT results in the Plouasne (Brittany) calcareous sand (K_D << 2) - (1 bar = 100 kPa)

calcareous sands is possibly usable as a warning of low skin friction.

13.2.2 Screw piles

Peiffer (1997) developed a method for estimating the skin friction of Atlas screw piles based on p_0 from DMT. The DMT is run in the usual way, but is performed next to the pile (one diameter away from the shaft) after its execution.

This method is intermediate between a real design method and a pile load test. It is not a pre-execution design method because the skin friction is estimated after the pile has been executed. Nor is it a load test, because the skin friction is estimated not by loading the pile, but from DMT-determined properties of the after-pile-installation soil, in accord with the widely recognized notion that pile capacity largely depends on execution, besides soil type.

13.2.3 Bored piles

No special DMT-based methods have been developed for the design of bored piles, which is generally carried out via soil parameters.

However the method developed by Peiffer (1997) for skin friction on screw piles (perform DMT in the soil surrounding the pile, see above Section) is in principle applicable also to bored piles.

13.2.4 Monitoring pile installation effects

The DMT has also been used extensively by Ghent investigators (Peiffer & Van Impe 1993, Peiffer et al. 1993, Peiffer et al. 1994, De Cock et al. 1993) for *comparing soil changes caused by various pile installation methods*. For instance De Cock et al. (1993) describe the use of before/after DMTs to verify, in terms of K_D, the installation effects of the Atlas pile (Fig. 38).

13.3 LATERALLY LOADED PILES

Methods have been developed for deriving *P-y* curves from DMT results. For a single pile the authors recommend the methods developed by Robertson et al. (1987) and by Marchetti et al. (1991). Note that all methods address the case of first time monotonic loading.

13.3.1 Robertson et al. (1987) method (clays and sands)

The Robertson method is an adaptation of the early methods estimating the *P-y* curves from soil properties obtained in the laboratory (Skempton ε_{50} - Matlock 1970 cubic parabola approach). In the Robertson method such "laboratory soil properties" are inferred from DMT results. Then the method continues in the same way as the Matlock method.

A detailed step-by-step procedure to derive the *P-y* curves from DMT, both for sands and clays, can be found in Robertson et al. (1987), or in US DOT (1992).

Validations of the Robertson method by Marchetti et al. (1991) indicated remarkably good agreement between predicted and observed behavior.

13.3.2 Marchetti et al. (1991) method (clays)

Marchetti et al. (1991) developed further the Robertson method for clay, eliminating from the correlation chain the tortuous step of estimating by DMT the "laboratory soil properties", and evolved a straightforward procedure deriving the *P-y* curves directly from DMT data (in clays).

The *P-y* curve at each depth is completely defined by a hyperbolic tangent equation having the

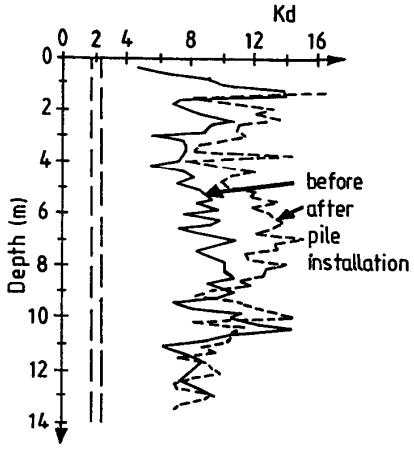

Fig. 38. Before/after DMTs for comparing installation effects of various piles (here an Atlas pile) - DeCock et al. (1993)

non-dimensional form:

$$\frac{P}{P_u} = \tanh\left(\frac{E_{si} \cdot y}{P_u}\right) \quad (27)$$

with

$$P_u = \alpha \cdot K_1 \cdot (p_0 - u_0) \cdot D \quad (28)$$

$$E_{si} = \alpha \cdot K_2 \cdot E_D \quad (29)$$

$$\alpha = \frac{1}{3} + \frac{2}{3} \cdot \frac{z}{7 \cdot D} \leq 1 \quad (30)$$

where

P_u = ultimate lateral soil resistance [F/L]
E_{si} = initial tangent "soil modulus" [F/L^2]
α = non-dimensional reduction factor for depths less than $z = 7\ D$ (α becomes 1 for $z = 7\ D$)
p_0 = corrected first DMT reading
u_0 = in situ pore pressure
D = pile diameter
z = depth
K_1 = empirical soil resistance coefficient: $K_1 = 1.24$
K_2 = empirical soil stiffness coefficient:
$K_2 = 10 \cdot (D / 0.5\ \text{m})^{0.5}$

The authors had several occasions to compare the behaviour of laterally loaded test piles with the behaviour predicted by the Marchetti et al. (1991) method. They found an amazingly good agreement between observed and predicted pile deflections.

A number of independent validations (NGI, Georgia Tech and tests in Virginia sediments) have indicated that the two methods provide similar predictions, in good agreement with the observed behavior.

It may be noted that DMT provides data even at shallow depths, i.e. in the layers dominating pile response.

13.3.3 Laterally loaded pile groups

A method was developed by Ruesta & Townsend in 1997. The method, based on the results of a large-scale load test on a 16 piles group, derives the *P-y* curves from DMT/PMT.

13.4 DETECTING SLIP SURFACES IN OC CLAY SLOPES

Totani et al. (1997) developed a quick method for detecting active or old slip surfaces in OC clay slopes, based on the inspection of the K_D profiles. The method is based on the following two elements:

(a) The sequence of sliding, remolding and reconsolidation (illustrated in Fig. 39) generally creates a remolded zone of nearly normally consolidated clay, with loss of structure, aging or cementation.

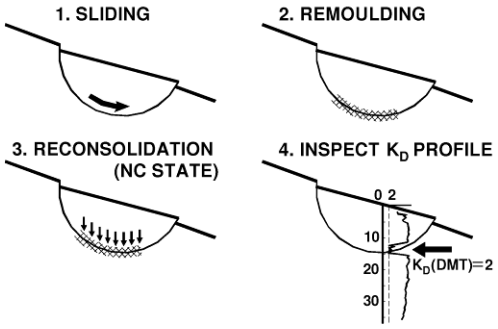

Fig. 39. DMT-K_D method for detecting slip surfaces in OC clay slopes

(b) Since in NC clays $K_D \approx 2$, if an OC clay slope contains layers where $K_D \approx 2$, these layers are likely to be part of a slip surface (active or quiescent).

In essence, the method consists in identifying zones of NC clay in a slope which, otherwise, exhibits an OC profile, using $K_D \approx 2$ as the identifier of the NC zones. Note that the method involves searching for a specific numerical value ($K_D = 2$) rather than for simply "weak zones", which could be detected just as easily also by other in situ tests.

The method was validated by inclinometers or otherwise documented slip surfaces (see Fig. 40).

The "K_D method" provides a faster response than inclinometers in detecting slip surfaces (no need to

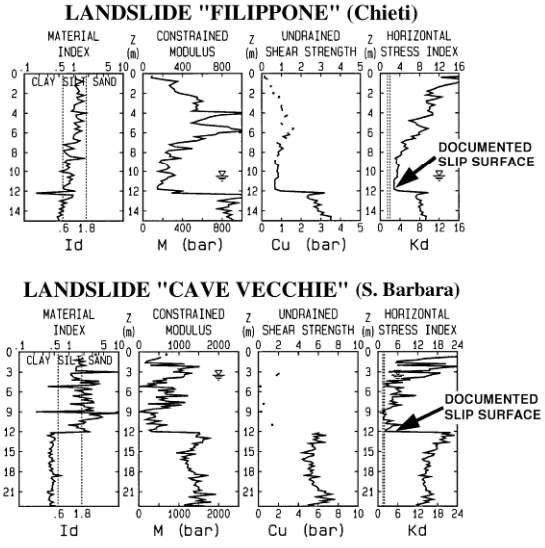

Fig. 40. Examples of $K_D \approx 2$ in documented slip surfaces in two OC clay slopes - (1 bar = 100 kPa)

wait for movements to occur). Moreover, the method enables to detect even possible quiescent surfaces (not revealed by inclinometers), which could reactivate e.g. after an excavation.

On the other hand, the method itself, unlike inclinometers, does not permit to establish if the slope is moving at present and what the movements are. In many cases, DMT and inclinometers can be used in combination (e.g. use K_D profiles to optimize location/depth of inclinometers).

13.5 MONITORING DENSIFICATION / STRESS INCREASE

The DMT has been frequently used for *monitoring soil improvement*, by comparing DMT results before and after the treatment (see e.g. Fig. 41). Compaction is generally reflected by a brisk increase of *both* K_D and M.

Schmertmann et al. (1986) report a large number of before/after CPTs and DMTs carried out for monitoring dynamic compaction at a power plant site (mostly sand). The treatment increased substantially both q_c and M_{DMT}. The increase in M_{DMT} was found to be approximately *twice* the increase in q_c.

Jendeby (1992) reports before/after CPTs and DMTs carried out for monitoring the deep compaction produced in a loose sand fill with the "vibrowing". He found a substantial increase of both q_c and M_{DMT}, but M_{DMT} increased at a faster rate (nearly *twice*, see Fig. 42), a result similar to the previous case.

Pasqualini & Rosi (1993), in monitoring a vibro-

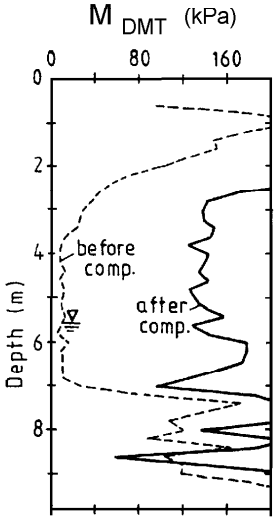

Fig. 41. Before/after DMTs for compaction control (resonant vibrocompaction technique, Van Impe et al. 1994)

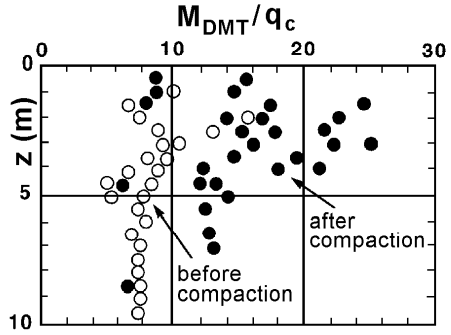

Fig. 42. Ratio M_{DMT}/q_c before/after compaction of a loose sand fill (Jendeby 1992)

flotation treatment, noted that the DMT clearly detected the improvement even in layers marginally influenced by the treatment, where the benefits were undetected by CPT.

All the above results concurrently suggest that the DMT is sensitive to changes of stresses/density in the soil and therefore is well suited to detect the benefits (in particular increased σ_h and increased D_r) of the soil improvement.

An interesting consideration by Schmertmann et al. (1986) is that, since treatments are often aimed at reducing settlements, it would be more rational to base the control and set the specifications in terms of minimum M rather than of minimum D_r.

Stationary DMT as pressure sensing elements

DMT blades have also been used to sense variations in stress state/density using them not as penetration tools, but as stationary spade cells. In this application DMT blades are inserted at the levels where changes are expected, then readings (only A) are taken with time. Various applications of this type have been reported. Peiffer et al. (1994) show (Fig. 43)

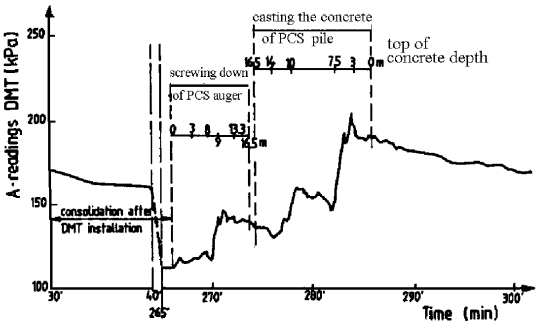

Fig. 43. Stationary DMT blades left in place to feel stress variations caused by the nearby installation of a screw pile (Peiffer et al. 1994)

representative results of such application, where a DMT blade was left in the soil waiting for the installation of a PCS auger pile. The clear distance between the blade and pile face was 1 pile diameter. Sufficient time was allowed for stabilization of the DMT *A*-reading before starting pile insertion.

Fig. 43 shows that the *A*-readings reflected clearly the reconsolidation, the screwing of the piles and the casting of the concrete.

It may be noted that DMT blades used as stationary pressure cells, while able to detect stress *variations*, do not provide *absolute* estimates of the stresses before and after construction, in contrast with before/after continuous DMTs. Note also that each stationary blade can provide information only at one location.

13.6 Monitoring soil decompression

The DMT has been used not only to feel the increase, but also the possible *reduction of density or horizontal stress*.

Peiffer and his colleagues, as mentioned in Section 13.2.4, used the DMT to monitor the decompression caused by various types of piles.

Some investigators (e.g. Hamza & Richards 1995 for Cairo Metro works) have used before/after DMTs to get information on the *decompressed* volume of soil behind diaphragm walls.

13.7 Subgrade compaction control

Some experience exists on the use of DMT for evaluating the suitability of the compacted ground surface (i.e. the subgrade soil) to support the road superstructure (subbase, base, pavements).

Borden (1986), based on laboratory work on A-2-4 to A-7-5 soils, tentatively suggested to estimate CBR % (corrected, unsoaked) as:

$$\text{CBR } \% = 0.058\ E_D\ (\text{bar})^{-0.475} \qquad (31)$$

(1 bar = 100 kPa)

Marchetti (1994) describes the use of DMT as a fast acceptance tool for the subgrade compaction in a road in Bangladesh. The procedure was the following:

- Perform a few preliminary DMTs in the *accepted* subgrade (i.e. satisfying the contract specifications)
- Draw an average profile through the above M_{DMT} profiles and use it as an acceptance profile (Fig. 44).

The acceptance M_{DMT} profile could then be used as an economical production method for quality control of the compaction, with only occasional verifications by the originally specified methods (Proctor, laboratory/in situ CBR and plate load tests).

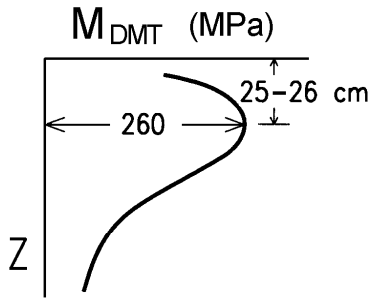

Fig. 44. Example of M_{DMT} acceptance profile for verifying subgrade compaction (Marchetti 1994)

Interestingly, all the after-compaction M_{DMT} profiles had the typical *shape* of the profile shown in Fig. 44, with the maximum M_{DMT} found almost invariably at 25-26 cm depth.

Cases have been reported of after-construction checks with the blade penetrating directly through asphalt.

It can be noted that many today's methods of pavement design make use of moduli rather than other parameters. Hence the availability of the M_{DMT} profiles may be of some usefulness.

13.8 Liquefaction

Fig. 45 summarizes the available knowledge for evaluating sand liquefiability by DMT. The curve currently recommended to estimate the cyclic resistance ratio (*CRR*) from the parameter K_D is the curve by Reyna & Chameau (1991). Such curve is based for a significant part on their curve K_D-D_r (relative to NC sands) shown in Fig. 21.

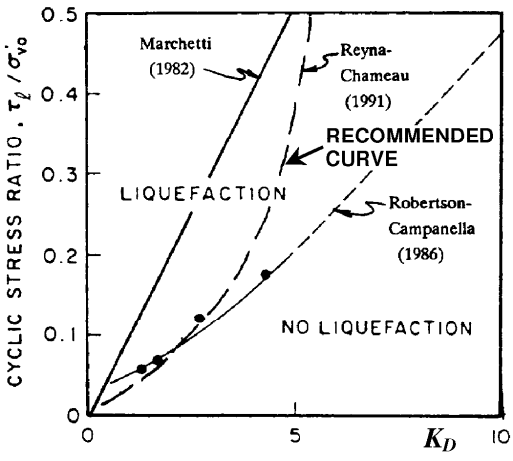

Fig. 45. Recommended curve for estimating *CRR* from K_D (Reyna & Chameau 1991)

This K_D-D_r correlation has been confirmed by additional datapoints obtained by Tanaka & Tanaka (1998) at the sites of Ohgishima and Kemigawa, where D_r was determined on high quality frozen samples.

Once *CRR* has been evaluated from Fig. 45, it is used in liquefaction analysis with the methods developed by Seed (a detailed step-by-step procedure can be found in US DOT 1992).

The demonstrated high sensitivity of the DMT in monitoring densification suggests that the DMT may be a sensitive tool also for sensing sand liquefiability. In fact a liquefiable sand may be regarded as a sort of "negatively compacted" sand, and it appears plausible that the DMT sensitivity holds in the positive and negative range.

Fig. 45, in combination with the available experience (see Marchetti 1997), suggests that a clean sand (natural or sandfill) is adequately safe against liquefaction (M = 7.5 earthquakes) for the following K_D values:

- Non seismic areas: $K_D > 1.7$
- Low seismicity areas ($a_{max}/g = 0.15$): $K_D > 4.2$
- Medium seismicity areas ($a_{max}/g = 0.25$): $K_D > 5.0$
- High seismicity areas ($a_{max}/g = 0.35$): $K_D > 5.5$

13.9 USE OF DMT FOR FEM INPUT PARAMETERS

Various approaches have been attempted so far.

(a) Use the simplest possible model (linear elastic) assigning to the Young's modulus $E' \approx 0.8\ M_{DMT}$. An example of such application is illustrated by Hamza & Richards (1995).

(b) Model the dilatometer test by a finite elements (FEM) computer program by adjusting the input parameters until the DMT results are correctly "predicted". This approach has the shortcoming of requiring many additional (unknown) parameters.

(c) Another more feasible approach, in problems where linear elasticity is known to give inadequate answers (e.g. settlements outside diaphragm walls), is to check the set of intended FEM parameters as follows. Predict for a simple case of simple loading the settlement by DMT (generally predicting well such settlements - see Section 13.1). Then repeat for the same loading case the settlement prediction by FEM. The comparison of the two predicted settlements may help in the final choice of the FEM parameters. Alternatively, simulate by FEM a simple laboratory test (e.g. oedometer), adjusting the FEM input parameters to improve the matching of M_{FEM} vs M_{DMT}.

(d) Other approaches try to identify an "equivalent representative average" DMT strain, with the intent of producing a point in the G-γ degradation curve.

14. SPECIAL CONSIDERATIONS

14.1 DISTORTIONS CAUSED BY THE PENETRATION

Fig. 46 compares the distortions caused in clay by conical tips and by wedges (Baligh & Scott 1975). The deformed grids show that distortions are considerably lower for wedges.

Davidson & Boghrat (1983) observed, using a stereo photograph technique, the strains produced in sand by CPT tips and by DMT blades. The strains in the sand surrounding the cone were found to be considerably higher.

14.2 PARAMETER DETERMINATION BY "TRIANGULATION"

In situ tests represent an "inverse boundary conditions" problem, since they measure *mixed* soil responses rather than *pure* soil properties. In order to isolate *pure* soil properties, it is necessary a "triangulation" (a sort of matrix inversion).

The "triangulation" is possible if more than one response has been measured.

The availability of two independent responses by DMT permits some elementary form of response combination. E.g. M_{DMT} is obtained using both p_0 and p_1.

It may be remarked that one of the two responses, p_0 (hence K_D), reflects stress history, a factor often dominating soil behavior (e.g. compressibility, liquefiability).

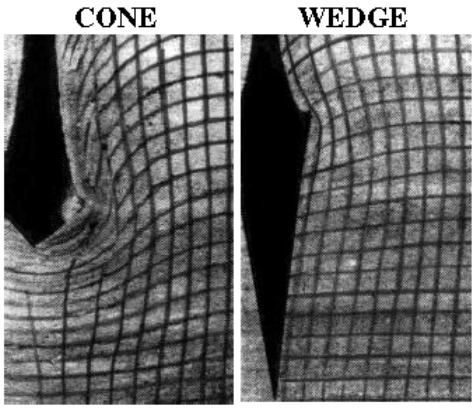

Fig. 46. Deformed grids by Baligh & Scott (1975)

14.3 ARCHING AND SENSITIVITY TO σ_h

Hughes & Robertson (1985) analyzed the horizontal stresses against the CPT sleeve in sands. They showed that at the level of the conical tip σ_h reaches very high values, while, behind the tip, σ_h undergoes an enormous stress reduction.

The penetration of the cone creates of zone of high residual stresses, at some distance from the sleeve. The resulting stiff annulus of precompressed sand is a *screen limiting* σ_h *at interface*, while the enormous unloading *makes undetermined* σ_h. This mechanism may be viewed as a form of an arching phenomenon.

A "plane" tip (DMT width/thickness ratio ≈ 6) should largely reduce arching and improve the possibility of sensing σ_h. Also the stress reduction after the wedge is likewise considerably smaller due to the streamlined shape in the transition zone.

14.4 COMPLEXITY OF THE THEORETICAL MODELS

The DMT is more difficult to model than axisymmetric tips for at least two reasons:

1) The penetration of the DMT blade is a truly three-dimensional problem, in contrast with the two-dimensional nature of cone penetration
2) The DMT is made of two stages:
   - Stage 1. Insertion.
   - Stage 2. Expansion. (Moreover expansion is not the continuation of Stage 1)

A consequence of 1) and 2) is that theoretical solutions have been developed so far only for the first stage (insertion). Solutions have been worked out by Huang (1989), Whittle & Aubeny (1992), Yu et al. (1992), Finno (1993).

15. CROSS RELATIONS WITH RESULTS FROM OTHER IN SITU TESTS

15.1 RELATIONS DMT/PMT

Some information exists about relations between DMT and pressuremeter (PMT) results. Cross relations could help DMT users to apply the design methods developed for PMT.

Preliminary indications, in clays, suggest:

$$p_0 / p_L \approx 0.8,\ p_1 / p_L \approx 1.2 \quad (32)$$

(Schmertmann 1987)

$$p_1 / p_L \approx 1.25,\ E_{PMT} \approx 0.4\ E_D \quad (33)$$

(Kalteziotis et al. 1991)

where p_L = limit pressure from PMT.

Ortigao et al. (1996) investigated the Brasilia porous clay by Menard PMT, Plate Loading Tests (PLT) and DMT. As Kalteziotis, they found that E_{PMT} was less than half E_D and also E_{PLT}. They explained such low PMT moduli with soil disturbance. After careful correction of the PMT field curve, E_{PMT} were similar to E_D and E_{PLT}.

Similar ratios (about 1/2) between PMT moduli and DMT moduli are quoted by Brown & Vinson (1998).

Dumas (1992) reports good agreement between settlements calculated with PMT and with DMT.

Contributions on DMT/PMT have also been presented by Lutenegger (1988), Sawada & Sugawara (1995), Schnaid et al. (2000).

15.2 RELATIONS DMT/CPT

As previously mentioned (Section 11.1.2.2), existing data suggest, in sand, the following broad cross relations:

$$M_{DMT}/q_c = 5\text{-}10 \quad \text{in NC sands} \quad (34)$$

$$M_{DMT}/q_c = 12\text{-}24 \quad \text{in OC sands} \quad (35)$$

15.3 RELATIONS DMT/SPT

According to Schmertmann (1988), the estimation of N_{SPT} from DMT would be "a gross misuse of the DMT data ... any such correlation depends on soil type and is probably site specific and perhaps also rig specific".

As a broad indication, Schmertmann (1988) cites the following relation, based on data from a number of US sites:

$$N_{SPT} = M_{DMT}\ (\text{MPa}) / 3 \quad (36)$$

Tanaka & Tanaka (1998) based on data from three sandy sites (Tokyo and Niigata areas) indicate:

$$N_{SPT} = E_D\ (\text{MPa}) / 2.5 \quad (37)$$

Blowcount SPT vs DMT

A limited number of parallel data, obtained in cases where the DMT was driven with the SPT equipment in gravels and silts, indicated very similar values of N_{SPT} and N_{DMT} (number of blows per 30 cm blade penetration).

SUMMARY

The Flat Dilatometer Test (DMT) is a push-in type in situ test quick, simple, economical, highly reproducible.

It is executable with a variety of field equipment.

It provides estimates of various design parameters/information (M, c_u, soil stratigraphy, deposit history).

One of the most fitting application is investigating the in situ soil compressibility for settlements prediction.

Interpretations and applications described by various Authors include:

- Compaction control
- Sensing the effects of pile installations (increase/ decrease of D_r and σ_h)
- Liquefiability of sands
- Verify if a slope contains slip surfaces
- Axially loaded piles in cohesive soils
- Laterally loaded piles
- Pavement subgrade compaction control
- Coefficient of consolidation and permeability of clays
- Phreatic level in sands
- Help in selecting FEM input parameters.

REFERENCES

ASTM Subcommittee D 18.02.10 - Schmertmann, J.H., Chairman (1986). "Suggested Method for Performing the Flat Dilatometer Test". ASTM Geotechnical Testing Journal, Vol. 9, No. 2, June, 93-101.

ASTM. "Standard Test Method for Performing the Flat Plate Dilatometer ". Approved Draft, 2001.

Aversa, S. (1997). "Experimental aspects and modeling in design of retaining walls and excavations" (in Italian). Proc. IV Nat. Conf. of the Geotechn. National Research Council Group, Perugia, Oct., Vol. II, 121-207.

Baldi, G., Bellotti, R., Ghionna, V. & Jamiolkowski, M. (1988). "Stiffness of sands from CPT, SPT and DMT – A critical review". ICE Proc. Conf. Penetration Testing in the UK, Univ. of Birmingham, July, Paper No. 42, 299-305.

Baldi, G., Bellotti, R., Ghionna, V., Jamiolkowski, M. & Lo Presti, D.C.F. (1989). "Modulus of Sands from CPT's and DMT's". Proc. XII ICSMFE, Rio de Janeiro, Vol. 1, 165-170.

Baldi, G., Bellotti, R., Ghionna, V., Jamiolkowski, M., Marchetti, S. & Pasqualini, E. (1986). "Flat Dilatometer Tests in Calibration Chambers". Proc. In Situ '86, ASCE Spec. Conf. on "Use of In Situ Tests in Geotechn. Engineering", Virginia Tech, Blacksburg, VA, June, ASCE Geotechn. Special Publ. No. 6, 431-446.

Baligh, M.M. (1985). "Strain path method". ASCE Jnl GE, Vol. 111, No. GT9, 1108-1136.

Baligh, M.M. & Scott, R.F. (1975). "Quasi Static Deep Penetration in Clays". ASCE Jnl GE, Vol. 101, No. GT11, 1119-1133.

Benoit, J. (1989). Personal communication to S. Marchetti.

Boghrat, A. (1987). "Dilatometer Testing in Highly Overconsolidated Soils". Technical Note, ASCE Journal of Geotechn. Engineering, Vol. 113, No. 5, May, 516.

Borden, R.H., Aziz, C.N., Lowder, W.M. & Khosla, N.P. (1986). "Evaluation of Pavement Subgrade Support Characteristics by Dilatometer Test". Proc. 64th Annual Meeting of the Transportation Res. Board, June, TR Record 1022.

Brown, D.A. & Vinson, J. (1998). "Comparison of strength and stiffness parameters for a Piedmont residual soil". Proc. First Int. Conf. on Site Characterization ISC '98, Atlanta, GA, Apr., Vol. 2, 1229-1234.

Burghignoli, A., Cavalera, L., Chieppa, V., Jamiolkowski, M., Mancuso, C., Marchetti, S., Pane, V., Paoliani, P., Silvestri, F., Vinale, F. & Vittori, E. (1991). "Geotechnical characterization of Fucino clay". Proc. X ECSMFE, Florence, Vol. 1, 27-40.

Burland, J.B., Broms, B.B. & De Mello, V.F.B. (1977). "Behavior of foundations and structures". Proc. IX ICSMFE, Tokyo, Vol. 2, 495-546.

Campanella, R.G. & Robertson, P.K. (1991). "Use and Interpretation of a Research Dilatometer". Canad. Geotechn. Journal, Vol. 28, 113-126.

Campanella, R.G., Robertson, P.K., Gillespie, D.G. & Grieg, J. (1985). "Recent Developments in In-Situ Testing of Soils". Proc. XI ICSMFE, S. Francisco, Vol. 2, 849-854.

Carter, J.P., Randolph, M.F. & Wroth, C.P. (1979). "Stress and pore pressure changes in clay during and after the expansion of a cylindrical cavity". Int. Jnl Numer. Anal. Methods Geomech., Vol. 3, 305-322.

Davidson, J. & Boghrat, A. (1983). "Displacements and Strains around Probes in Sand". Proc. ASCE Spec. Conf. on "Geotechnical Practice in Offshore Engineering", Austin, TX, Apr., 181-203.

De Cock, F., Van Impe, W.F. & Peiffer, H. (1993). "Atlas screw piles and tube screw piles in stiff tertiary clays". Proc. BAP II, Ghent, 359-367.

Didaskalou, G. (1999). "Comparison between observed and DMT predicted settlements of the Hyatt Regency Hotel shallow foundation on a compressible silt in Thessaloniki". Personal communication to S. Marchetti.

Dumas, J.C. (1992). "Comparisons of settlements predicted by PMT and DMT in a silty-sandy soil in Quebec". Personal communication to S. Marchetti.

Durgunoglu, H.T. & Mitchell, J.K. (1975). "Static Penetration Resistance of Soils, I - Analysis, II - Evaluation of the Theory and Implications for Practice". ASCE Spec. Conf. on "In Situ Measurement of Soil Properties", Raleigh, NC, Vol. 1.

Eurocode 7 (1997). Geotechnical design - Part 3: Design assisted by field testing, Section 9: Flat dilatometer test (DMT). Final Draft, ENV 1997-3, Apr., 66-73. CEN - European Committee For Standardization.

Failmezger, R.A., Rom, D. & Ziegler, S.B. (1999). "Behavioral Characteristics of Residual Soils. SPT? - A Better Approach to Site Characterization of Residual Soils using other In-Situ Tests". ASCE Geot. Special Pub. No. 92, Edelen, Bill, ed., ASCE, Reston, VA, 158-175.

Finno, R.J. (1993). "Analytical Interpretation of Dilatometer Penetration Through Saturated Cohesive Soils". Geotéchnique, 43, No. 2, 241-254.

Fretti, C., Lo Presti, D. & Salgado, R. (1992). "The Research Dilatometer: In Situ and Calibration Chamber Test Results". Riv. Italiana di Geotecnica, 26, No. 4, 237-243.

Gravesen, S. (1960). "Elastic Semi-Infinite Medium Bounded by a Rigid Wall with a Circular Hole". Laboratoriet for Bygninsteknik, Danmarks Tekniske Højskole, Meddelelse No. 10, Copenhagen.

Hamza, M. & Richards, D.P. (1995). "Correlations of DMT, CPT and SPT in Nile Basin Sediment". Proc. XI Afr. Conf. SMFE, Cairo, 437-446.

Hayes, J.A. (1990). "The Marchetti Dilatometer and Compressibility". Seminar on "In Situ Testing and Monitoring", Southern Ont. Section of Canad. Geot. Society, Sept., 21 pp.

Hryciw, R.D. (1990). "Small-Strain-Shear Modulus of Soil by

Dilatometer". ASCE Jnl GE, Vol. 116, No. 11, Nov., 1700-1716.
Huang, A.B. (1989). "Strain-Path Analyses for Arbitrary Three Dimensional Penetrometers". Int. Jnl for Num. and Analyt. Methods in Geomechanics, Vol. 13, 561-564.
Huang, A.B., Bunting, R.D. & Carney, T.C. (1991). "Piezoblade Tests in a Clay Calibration Chamber". Proc. ISOCCT-1, Clarkson Univ., Potsdam, NY, June.
Hughes, J.M.O. & Robertson, P.K. (1985). "Full displacement pressuremeter testing in sand". Canad. Geot. Jnl, Vol. 22, No. 3, Aug., 298-307.
Iwasaki, K., Tsuchiya, H., Sakai, Y. & Yamamoto, Y. (1991). "Applicability of the Marchetti Dilatometer Test to Soft Ground in Japan". Proc. GEOCOAST '91, Yokohama, Sept., 1/6.
Jamiolkowski, M. (1995). "Opening address". Proc. Int. Symp. on Cone Penetration Testing CPT '95, Swedish Geot. Soc., Linköping, Vol. 3, 7-15.
Jamiolkowski, M., Ghionna, V., Lancellotta, R. & Pasqualini, E. (1988). "New Correlations of Penetration Tests for Design Practice". Proc. ISOPT-1, Orlando, FL, Vol. 1, 263-296.
Jendeby, L. (1992). "Deep Compaction by Vibrowing". Proc. Nordic Geotechnical Meeting NGM-92, Vol. 1, 19-24.
Kaggwa, W.S., Jaksa, M.B. & Jha, R.K. (1995). "Development of automated dilatometer and comparison with cone penetration test at the Univ. of Adelaide, Australia". Proc. Int. Conf. on Advances in Site Investig. Practice, ICE, London, Mar.
Kalteziotis, N.A., Pachakis, M.D. & Zervogiannis, H.S. (1991). "Applications of the Flat Dilatometer Test (DMT) in Cohesive Soils". Proc. X ECSMFE, Florence, Vol. 1, 125-128.
Kamey, T. & Iwasaki, K. (1995). "Evaluation of undrained shear strength of cohesive soils using a Flat Dilatometer". Soils and Foundations, Vol. 35, No. 2, June, 111-116.
Kulhawy, F. & Mayne, P. (1990). "Manual on Estimating Soil Properties for Foundation Design". Electric Power Research Institute, Cornell Univ., Ithaca, NY, Report No. EL-6800, 250 pp.
Lacasse, S. (1986). "In Situ Site Investigation Techniques and Interpretation for Offshore Practice". Norwegian Geotechnical Inst., Report 40019-28, Sept.
Lacasse, S. & Lunne, T. (1986). "Dilatometer Tests in Sand". Proc. In Situ '86, ASCE Spec. Conf. on "Use of In Situ Tests in Geotechn. Engineering", Virginia Tech, Blacksburg, VA, June, ASCE Geotechn. Special Publ. No. 6, 686-699.
Lacasse, S. & Lunne, T. (1988). "Calibration of Dilatometer Correlations". Proc. ISOPT-1, Orlando, FL, Vol. 1, 539-548.
Leonards, G.A. & Frost, J.D. (1988). "Settlements of Shallow Foundations on Granular Soils". ASCE Jnl GE, Vol. 114, No. 7, July, 791-809.
Lunne, T., Lacasse, S. & Rad, N.S. (1989). "State of the Art Report on In Situ Testing of Soils". Proc. XII ICSMFE, Rio de Janeiro, Vol. 4, 2339-2403.
Lutenegger, A.J. (1988). "Current status of the Marchetti dilatometer test". Special Lecture, Proc. ISOPT-1, Orlando, FL, Vol. 1, 137-155.
Lutenegger, A.J. & Kabir, M.G. (1988). "Dilatometer C-reading to help determine stratigraphy". Proc. ISOPT-1, Orlando, FL, Vol. 1, 549-554.
Marchetti, S. (1980). "In Situ Tests by Flat Dilatometer". ASCE Jnl GED, Vol. 106, No. GT3, Mar., 299-321.
Marchetti, S. (1982). "Detection of liquefiable sand layers by means of quasi static penetration tests". Proc. 2nd European Symp. on Penetration Testing, Amsterdam, May, Vol. 2, 689-695.
Marchetti, S. (1985). "On the Field Determination of K_0 in Sand". Discussion Session No. 2A, Proc. XI ICSMFE, S. Francisco, Vol. 5, 2667-2673.
Marchetti, S. (1994). "An example of use of DMT as a help for evaluating compaction of subgrade and underlying embankment". Internal Techn. Note, Draft.
Marchetti, S. (1997). "The Flat Dilatometer: Design Applications". Proc. Third International Geotechnical Engineering Conference, Keynote lecture, Cairo University, Jan., 421-448.
Marchetti, S. (1999). "On the calibration of the DMT membrane". L'Aquila Univ., Unpublished report, Mar.
Marchetti, S. & Crapps, D.K. (1981). "Flat Dilatometer Manual". Internal Report of G.P.E. Inc.
Marchetti, S. & Totani, G. (1989). "C_h Evaluations from DMTA Dissipation Curves". Proc. XII ICSMFE, Rio de Janeiro, Vol. 1, 281-286.
Marchetti, S., Totani, G., Calabrese, M. & Monaco, P. (1991). "P-y curves from DMT data for piles driven in clay". Proc. 4th Int. Conf. on Piling and Deep Foundations, DFI, Stresa, Vol. 1, 263-272.
Marchetti, S., Totani, G., Campanella, R.G., Robertson, P.K. & Taddei, B. (1986). "The DMT-σ_{hc} Method for Piles Driven in Clay". Proc. In Situ '86, ASCE Spec. Conf. on "Use of In Situ Tests in Geotechn. Engineering", Virginia Tech, Blacksburg, VA, June, ASCE Geotechn. Special Publ. No. 6, 765-779.
Massarsch, K.R. (1994). "Settlement Analysis of Compacted Granular Fill". Proc. XIII ICSMFE, New Delhi, Vol. 1, 325-328.
Matlock, H. (1970). "Correlation for Design of Laterally Loaded Piles in Soft Clay". Proc. II Offshore Technical Conf., Houston, TX, Vol. 1, 577-594.
Mayne, P.W. & Martin, G.K. (1998). "Seismic flat dilatometer test in Piedmont residual soils". Proc. First Int. Conf. on Site Characterization ISC '98, Atlanta, GA, Apr., Vol. 2, 837-843.
Mesri, G., Feng, T.W. & Shahien, M. (1999). "Coefficient of Consolidation by Inflection Point Method". ASCE Jnl GGE, Vol. 125, No. 8, Aug., 716-718.
Nash, D.F.Y., Powell, J.J.M. & Lloyd, I.M. (1992). "Initial investigations of the soft clay test site at Bothkennar". Geotéchnique, 42, No. 2, 163-181.
Ortigao, J.A.R., Cunha, R.P. & Alves, L.S. (1996). "In situ tests in Brasilia porous clay". Canad. Geot. Jnl, Vol. 33, No. 1, Feb., 189-198.
Pasqualini, E. & Rosi, C. (1993). "Experiences from a vibroflotation treatment" (in Italian). Proc. Annual Meeting of the Geotechn. National Research Council Group, Rome, Nov., 237-240.
Peiffer, H. (1997). "Evaluation and automatisation of the dilatometer test and interpretation towards the shaft bearing capacity of piles". Doctoral Thesis, Ghent University.
Peiffer, H. & Van Impe, W.F. (1993). "Evaluation of pile performance based on soil stress measurements - Field test program". Proc. BAP II, Ghent, 385-389.
Peiffer, H., Van Impe, W.F., Cortvrindt, G. & Bottiau, M. (1993). "Evaluation of the influence of pile execution parameters on the soil condition around the pile shaft of a

PCS-pile". Proc. BAP II, Ghent, 217-220.
Peiffer, H., Van Impe, W.F., Cortvrindt, G. & Bottiau, M. (1994). "DMT Measurements around PCS-Piles in Belgium". Proc. XIII ICSMFE, New Delhi, Vol. 2, 469-472.
Pelnik, T.W., Fromme, C.L., Gibbons, Y.R. & Failmezger, R.A. (1999). "Foundation Design Applications of CPTU and DMT Tests in Atlantic Coastal Plain Virginia". Transp. Res. Board, 78th Annual Meeting, Jan., Washington, D.C.
Powell, J.J.M., Lunne, T. & Frank, R. (2001 a). "Semi-Empirical Design Procedures for axial pile capacity in clays". Proc. XV ICSMGE, Istanbul, Aug., Balkema.
Powell, J.J.M., Shields, C.H., Dupla, J.C. & Mokkelbost, K.H. (2001 b). "A new DMT method for the design of axially loaded driven piles in clay soils". Submitted for publication.
Powell, J.J.M. & Uglow, I.M. (1988). "The Interpretation of the Marchetti Dilatometer Test in UK Clays". ICE Proc. Conf. Penetration Testing in the UK, Univ. of Birmingham, July, Paper No. 34, 269-273.
Reyna, F. & Chameau, J.L. (1991). "Dilatometer Based Liquefaction Potential of Sites in the Imperial Valley". Proc. 2nd Int. Conf. on Recent Advances in Geot. Earthquake Engrg. and Soil Dyn., St. Louis, May.
Robertson, P.K. & Campanella, R.G. (1986). "Estimating Liquefaction Potential of Sands Using the Flat Plate Dilatometer". ASTM Geotechn. Testing Journal, Mar., 38-40.
Robertson, P.K., Campanella, R.G., Gillespie, D. & By, T. (1988). "Excess Pore Pressures and the Flat Dilatometer Test". Proc. ISOPT-1, Orlando, FL, Vol. 1, 567-576.
Robertson, P.K., Davies, M.P. & Campanella, R.G. (1987). "Design of Laterally Loaded Driven Piles Using the Flat Dilatometer". Geot. Testing Jnl, Vol. 12, No. 1, Mar., 30-38.
Ruesta, F. & Townsend, F.C. (1997). "Evaluation of Laterally Loaded Pile Group at Roosvelt Bridge". Jnl ASCE GGE, 123, 12, Dec., 1153-1161.
Sawada, S. & Sugawara, N. (1995). "Evaluation of densification of loose sand by SBP and DMT". Proc. 4th Int. Symp. on Pressuremeter, May, 101-107.
Schmertmann, J.H. (1982). "A method for determining the friction angle in sands from the Marchetti dilatometer test (DMT)". Proc. 2nd European Symp. on Penetration Testing, ESOPT-II, Amsterdam, Vol. 2, 853-861.
Schmertmann, J.H. (1983). "Revised Procedure for Calculating K_o and OCR from DMT's with $I_D > 1.2$ and which Incorporates the Penetration Measurement to Permit Calculating the Plane Strain Friction Angle". DMT Digest No. 1. GPE Inc., Gainesville, FL.
Schmertmann, J.H. (1986). "Dilatometer to compute Foundation Settlement". Proc. In Situ '86, ASCE Spec. Conf. on "Use of In Situ Tests in Geotechn. Engineering", Virginia Tech, Blacksburg, VA, June, ASCE Geotechn. Special Publ. No. 6, 303-321.
Schmertmann, J.H., Baker, W., Gupta, R. & Kessler, K. (1986). "CPT/DMT Quality Control of Ground Modification at a Power Plant". Proc. In Situ '86, ASCE Spec. Conf. on "Use of In Situ Tests in Geotechn. Engineering", Virginia Tech, Blacksburg, VA, June, ASCE Geotechn. Special Publ. No. 6, 985-1001.
Schmertmann, J.H. (1987). "Some interrelationship with p_0 in clays". DMT Digest No. 9, Item 9A, Schmertmann Ed., May.
Schmertmann, J.H. (1988). "Guidelines for Using the CPT, CPTU and Marchetti DMT for Geotechnical Design". Rept. No. FHWA-PA-87-022+84-24 to PennDOT, Office of Research and Special Studies, Harrisburg, PA, in 4 volumes with the 3 below concerning primarily the DMT: Vol. I - Summary (78 pp.); Vol. III - DMT Test Methods and Data Reduction (183 pp.); Vol. IV - DMT Design Method and Examples (135 pp.).
Schmertmann, J.H. (1991). "Pressure Dissipation Tests. A-B-C vs A_2 vs A". DMT Digest No. 12, Section 12C, Schmertmann Ed., Dec.
Schnaid, F., Ortigao, J.A.R., Mantaras, F.M, Cunha, R.P. & MacGregor, I. (2000). "Analysis of self-boring pressuremeter (SBPM) and Marchetti dilatometer (DMT) tests in granite saprolites". Canad. Geot. Jnl, Vol. 37, 4, Aug., 796-810.
Skiles, D.L. & Townsend, F.C. (1994). "Predicting Shallow Foundation Settlement in Sands from DMT". Proc. Settlement '94 ASCE Spec. Conf., Texas A&M Univ., Geot. Spec. Publ. No. 40, Vol. 1, 132-142.
Steiner, W. (1994). "Settlement Behavior of an Avalanche Protection Gallery Founded on Loose Sandy Silt". Proc. Settlement '94 ASCE Spec. Conf., Texas A&M Univ., Geot. Spec. Publ. No. 40, Vol. 1, 207-221.
Steiner, W., Metzger, R. & Marr, W.A. (1992). "An Embankment on Soft Clay with an Adjacent Cut". Proc. ASCE Conf. on Stability and Performance of Slopes and Embankments II, Berkeley, CA, 705-720.
Sully, J.P. & Campanella, R.G. (1989). "Correlation of Maximum Shear Modulus with DMT Test Results in Sand". Proc. Proc. XII ICSMFE, Rio de Janeiro, Vol. 1, 339-343.
Tanaka, H. & Tanaka, M. (1998). "Characterization of Sandy Soils using CPT and DMT". Soils and Foundations, Japanese Geot. Soc., Vol. 38, No. 3, 55-65.
Terzaghi, K. & Peck, R.B. (1967). "Soil Mechanics in Engineering Practice". John Wiley & Sons, NY.
Totani, G., Calabrese, M., Marchetti, S. & Monaco, P. (1997). "Use of in situ flat dilatometer (DMT) for ground characterization in the stability analysis of slopes". Proc. XIV ICSMFE, Hamburg, Vol. 1, 607-610.
Totani, G., Calabrese, M. & Monaco, P. (1998). "In situ determination of c_h by flat dilatometer (DMT)". Proc. First Int. Conf. on Site Characterization ISC '98, Atlanta, GA, Apr., Vol. 2, 883-888.
Totani, G., Marchetti, S., Calabrese, M. & Monaco, P. (1994). "Field studies of an instrumented full-scale pile driven in clay". Proc. XIII ICSMFE, New Delhi, Vol. 2, 695-698.
US DOT - Briaud, J.L. & Miran, J. (1992). "The Flat Dilatometer Test". Departm. of Transportation - Fed. Highway Administr., Washington, D.C., Publ. No. FHWA-SA-91-044, Feb., 102 pp.
Van Impe, W.F., De Cock, F., Massarsch, R. & Menge', P. (1994). "Recent Experiences and Developments of the Resonant Vibrocompaction Technique". Proc. XIII ICSMFE, New Delhi, Vol. 3, 1151-1156.
Whittle, A.J. & Aubeny, C.P. (1992). "The effects of installation disturbance on interpretation of in situ tests in clay". Proc. Wroth Memorial Symp. Predictive Soil Mechanics, Oxford, July, 742-767.
Woodward, M.B. & McIntosh, K.A. (1993). "Case history: Shallow Foundation Settlement Prediction Using the Marchetti Dilatometer". ASCE Annual Florida Sec. Meeting - Abstract & Conclusions.
Yu, H.S., Carter, J.P. & Booker, J.R. (1992). "Analysis of the Dilatometer Test in Undrained Clay". Proc. Wroth Memorial Symp. Predictive Soil Mechanics, Oxford, July, 783-795.

Appendix IV:

Company Pergam

Data CD with the infrared pictures.

Die CD-Rom mit den Infrarotaufnahmen:

Company Pergam (2006)

befindet sich am Institut für Geotechnik, Wolfgang-Pauli-Str. 15, 8093 Zürich und kann jederzeit eingesehen oder zugestellt werden.

Appendix V:

Sauerbier M. (2006)

"Arbeitstitel: Photogrammetrische Auswertung".

In preparation.

Die CD-Rom mit den Luftaufnahmen:

“Arbeitstitel:
Photogrammetrische Auswertung“
Sauerbier M. (2006)

befindet sich am Institut für Geotechnik, Wolfgang-Pauli-Str. 15, 8093 Zürich und kann jederzeit eingesehen oder zugestellt werden.

Appendix VI:

Data and analysis

of the Electromagnetic Radiation Measurements.

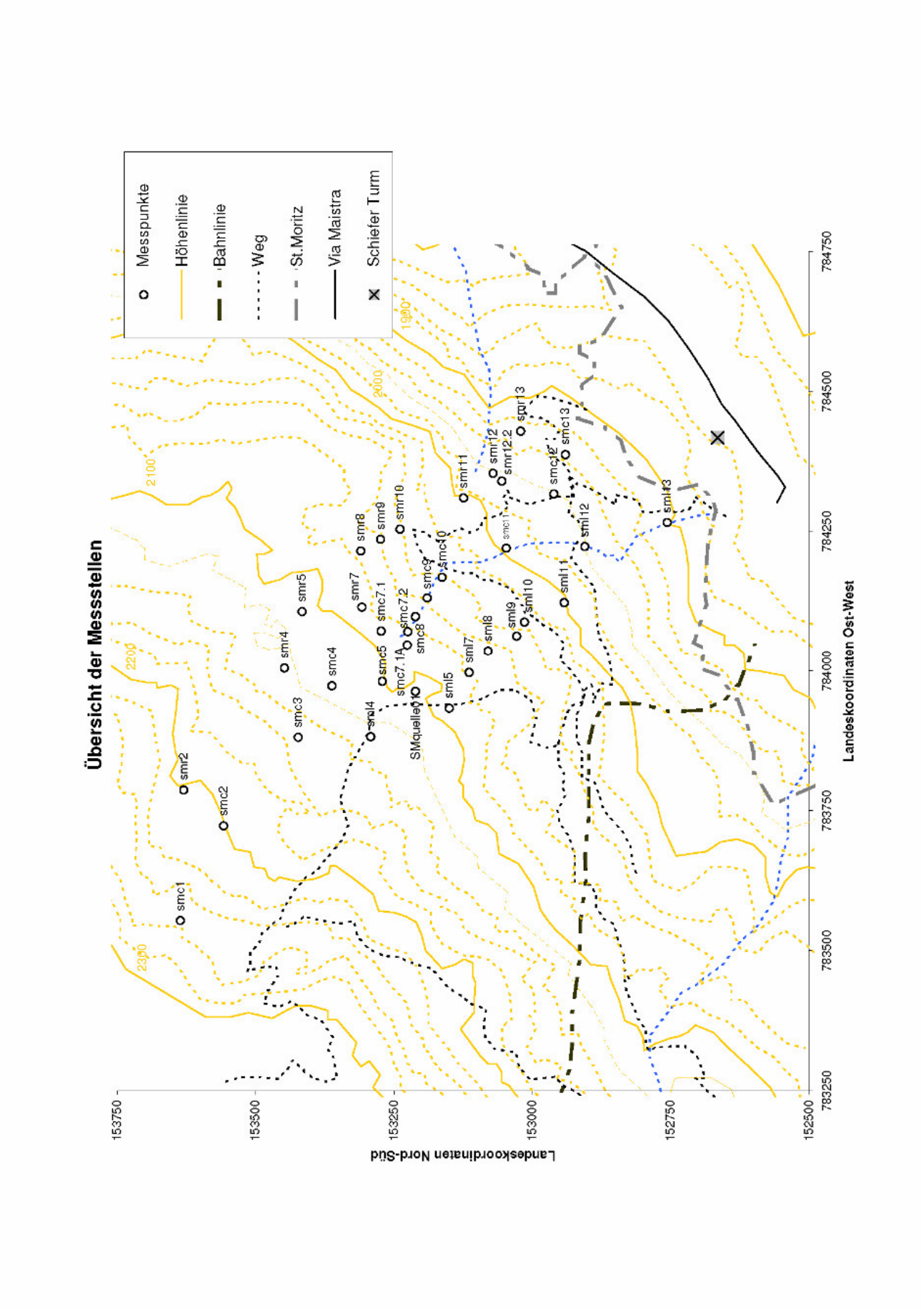
Übersicht der Messstellen
Messpunkte
Höhenlinie
Bahnlinie
Weg
St.Moritz
Via Maistra
Schiefer Turm
2100
2200
2300
2000
1900
smc1
smr2
smc2
smr3
smc3
smr4
smc4
smr5
smc5
smr7
smc7.1
smc7.2
smc8
smc7.1A
SMquelle1
smr4
sml5
sml7
sml8
smr8
smr9
smr10
smc9
smc10
sml9
sml10
smr11
smr12
smr12.2
spr13
smc12
smc13
sml11
sml12
sml13
153750
153500
153250
153000
152750
152500
Landeskoordinaten Nord-Süd
783250
783500
783750
784000
784250
784500
784750
Landeskoordinaten Ost-West

EMR measurements: data analysis

Profile Donnerstag neues Gerät: Vertikalmessungen

C1	232	1
C2	266	2
C3	40	3
C4	220	4
2321	419	4
C5	1578	5
C7	251	6
C8	402	7
C9	519	8
C10	621	9

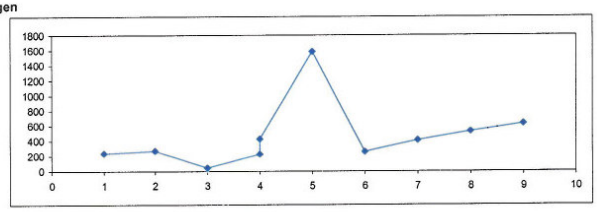

R2	273	2
R4	182	4
R5	788	5
R7	22	6
R8	334	7
R8.5	337	7.5
R9	1029	8
R9.5	1295	8.5
R10	345	9
R10.5	262	9.5

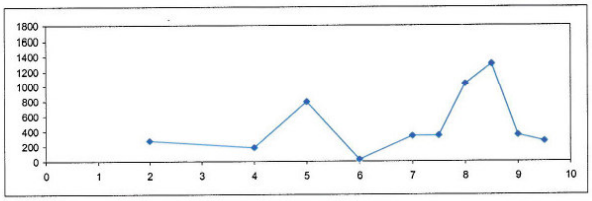

L4	106	4
L5	209	5
L7	414	6
L8	868	7
L9	1178	8
L10	587	9

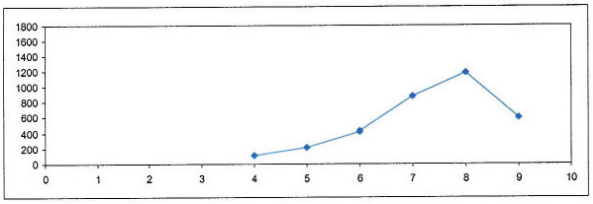

C_Profil_Freitag mit altem Gerät, Vertikalmessungen

SMC04	304	4
SMC04/1	283	4.2
SMC04/2	273	4.4
SMC04/3	253	4.6
SMC04/4	138	4.8
SMC04/5	162	4.9
SMC05	200	5
SMC05/1	240	5.2
SMC05/1	362	5.4
SMC05/1	434	5.7
SMC07	354	6
SMC07	425	6
SMC07	361	6
SMC07	273	6
SMC07	270	6
SMC08	943	7
SMC08	334	7
SMC08	700	7
SMC08	817	7
SMC08	534	7
SMC08/1	376	7.5
SMC09	1063	8
SMC10	1127	9
SMC11	323	10
SMC12	1000	11
SMC13	313	12

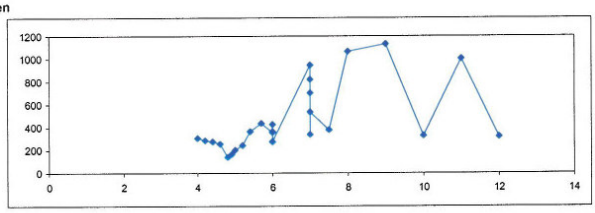

Haupt und Nebenspannungen: altes Gerät, gemessen Do. & Fr., ausgewertet von den Horizontalmessungen

	Hauptsp.	Nebensp.	Querprofil	Verhältnis: Nebensp./Hauptsp.
C1	1200	550	1	0.458333
C2	1350	1100	2	0.814815
C3	1400	100	3	0.071429
C4	1500	400	4	0.266667
C4R	1500	400	4	0.266667
C5	1500	600	5	0.4
C5R	1500	800	5	0.533333
C7_1	1500	1700	6	1.133333
C7_1R	2000	1700	6	0.85
C7_2	2500	3200	6	1.28
C8	2500	3000	7	1.2
C8R	2000	2000	7	1
C9	2500	3000	8	1.2
C9R	2300	2500	8	1.086957
C10	2000	2500	9	1.25
C10R	2000	2200	9	1.1

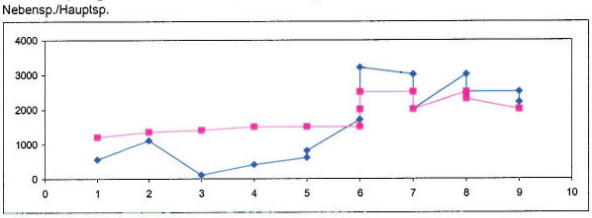

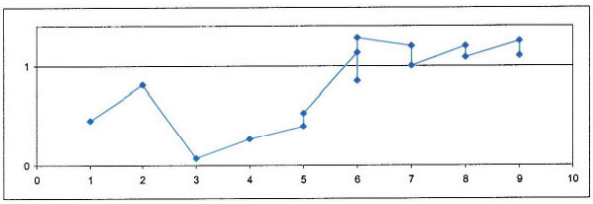

R2	1500	700	2
R4	1500	700	4
R5	1600	1500	5
R7	1500	800	6
R8	1500	2000	7
R9	2000	2000	8
R10	1600	1600	9
R10_5	3200	2800	9.5

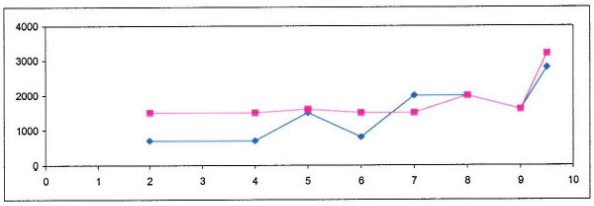

L4	1500	1	4
L5	1400	1100	5
L7	1600	1200	6
L7R	1000	500	6
L8	1800	2500	7
L8R	1800	2200	7
L9	2500	3000	8
L9R	3500	3500	8
L10	1800	1800	9
L11R	1500	2200	10
L12R	1400	1	11
L13R	1200	1	12

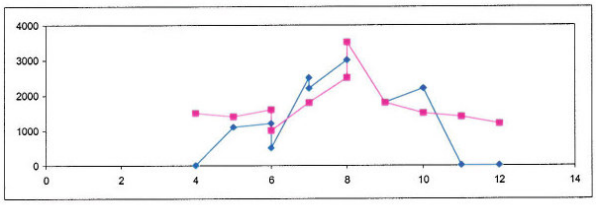

EMR measurement data at single points

SMC01:

Object - sm_____, Profile - c_____,13.07.2006 16:45:48 14/44

Picket	ParametrA	ParametrB	ParametrC	ParametrD	ParametrE	Azimuth	Time
0	1206	57	32	247	86	0	13.07.2004 09:02
5	1215	53	31	251	86	0	13.07.2004 09:02
10	1149	57	31	245	86	0	13.07.2004 09:02
15	1147	61	31	230	86	0	13.07.2004 09:02
20	1138	62	31	236	86	0	13.07.2004 09:02
25	1101						
30	1054						
35	1039						
40	1001						
45	905						
50	783						
55	614						
60	532						
65	480						
70	455						
75	374						
80	300						
85	240						
90	175						
95	162						
100	163						
105	150						
110	164						
115	145						
120	224						
125	251						
130	310						
135	435						
140	550						
145	778						
150	905						
155	977						
160	1099						
165	1145						
170	1157						
175	1191						
180	1227						
185	1198						
190	1184						
195	1130						
200	1159						
205	1076	68	30	212	86	0	13.07.2004 09:03
210	938	96	30	174	86	0	13.07.2004 09:03
215	761	115	27	119	86	0	13.07.2004 09:04
220	744	111	27	118	86	0	13.07.2004 09:04
225	726	120	27	112	86	0	13.07.2004 09:04
230	538	90	26	60	86	0	13.07.2004 09:04
235	326	38	25	16	86	0	13.07.2004 09:04
240	254	24	23	11	105	0	13.07.2004 09:04
245	215	15	23	7	105	0	13.07.2004 09:04
250	182	12	23	4	97	0	13.07.2004 09:04
255	216	21	24	8	105	0	13.07.2004 09:04
260	175	10	23	5	105	0	13.07.2004 09:04
265	197	18	21	6	82	0	13.07.2004 09:04
270	171	12	27	17	71	0	13.07.2004 09:04
275	150	7	33	9	78	0	13.07.2004 09:04
280	166	6	23	2	105	0	13.07.2004 09:04
285	232	21	24	8	82	0	13.07.2004 09:04
290	379	46	23	25	82	0	13.07.2004 09:04
295	554	84	24	60	82	0	13.07.2004 09:04
300	518	75	24	55	86	0	13.07.2004 09:04
305	453	57	25	32	82	0	13.07.2004 09:04
310	422	61	24	35	82	0	13.07.2004 09:04
315	714	95	26	98	86	0	13.07.2004 09:04
320	770	104	27	118	86	0	13.07.2004 09:04
325	1020	82	29	183	86	0	13.07.2004 09:04
330	1102	62	30	213	86	0	13.07.2004 09:04
335	1147	60	30	218	86	0	13.07.2004 09:04
340	1118	56	30	225	86	0	13.07.2004 09:05
345	1142	49	31	237	86	0	13.07.2004 09:05
350	1142	47	30	227	86	0	13.07.2004 09:05
355	1197	45	32	256	86	0	13.07.2004 09:05
360	1220	48	32	249	86	0	13.07.2004 09:05

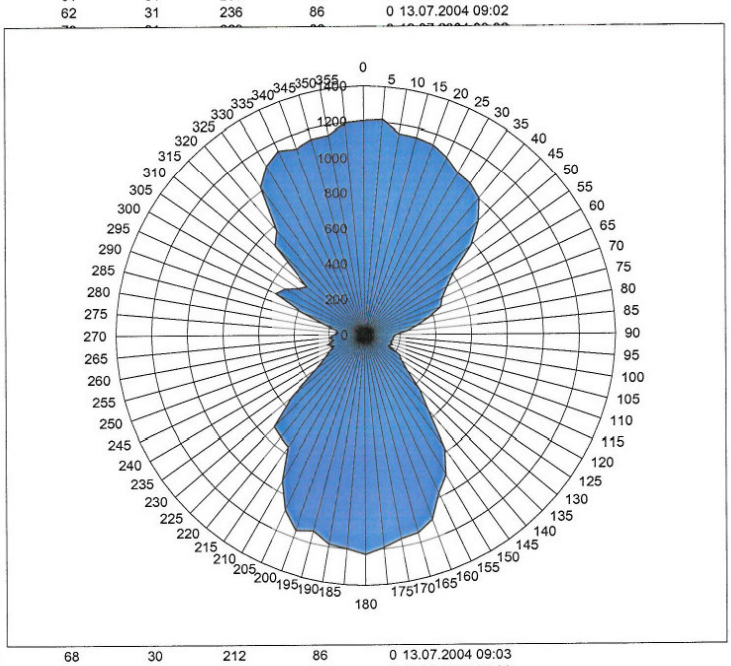

SMCo2:

Object - sm_____, Profile - c2_____,13.07.2006 16:46:53

Picket	ParametrA	ParametrB	ParametrC	ParametrD	ParametrE	Azimuth	Time
0	1342	26	33	287	86	0	13.07.2004 09:48
5	1359	26	34	299	86	0	13.07.2004 09:48
10	1332	29	33	293	86	0	13.07.2004 09:48
15	1308	27	33	293	86	0	13.07.2004 09:48
20	1232	48	33	274	86	0	13.07.2004 09:48
25	1278						
30	1221						
35	1225						
40	1220						
45	1066						
50	907						
55	872						
60	796						
65	729						
70	658						
75	456						
80	403						
85	371						
90	330						
95	247						
100	181						
105	119						
110	131						
115	121						
120	168						
125	211						
130	229						
135	283						
140	398						
145	618						
150	1044						
155	1171						
160	1101						
165	1157						
170	1294						
175	1293						
180	1331						
185	1305						
190	1306						
195	1316						
200	1298						
205	1248	44	33	279	86	0	13.07.2004 09:50
210	1168	50	32	249	86	0	13.07.2004 09:50
215	1090	70	30	215	86	0	13.07.2004 09:50
220	984	84	30	196	86	0	13.07.2004 09:50
225	866	101	28	151	86	0	13.07.2004 09:50
230	748	108	28	114	86	0	13.07.2004 09:50
235	636	97	27	77	82	0	13.07.2004 09:50
240	505	71	25	46	86	0	13.07.2004 09:50
245	444	66	24	38	86	0	13.07.2004 09:50
250	422	55	25	31	86	0	13.07.2004 09:50
255	314	37	24	16	101	0	13.07.2004 09:50
260	233	22	22	9	105	0	13.07.2004 09:50
265	214	14	22	5	82	0	13.07.2004 09:50
270	135	7	20	2	108	0	13.07.2004 09:50
275	130	5	18	1	86	0	13.07.2004 09:50
280	159	12	26	6	97	0	13.07.2004 09:50
285	155	8	21	3	82	0	13.07.2004 09:50
290	224	21	23	8	82	0	13.07.2004 09:50
295	233	15	26	13	82	0	13.07.2004 09:50
300	354	49	24	24	82	0	13.07.2004 09:50
305	420	51	24	36	82	0	13.07.2004 09:50
310	493	65	24	47	82	0	13.07.2004 09:51
315	631	71	25	83	86	0	13.07.2004 09:51
320	760	90	26	119	86	0	13.07.2004 09:51
325	1066	65	28	197	86	0	13.07.2004 09:51
330	998	73	29	181	86	0	13.07.2004 09:51
335	1050	71	30	190	86	0	13.07.2004 09:51
340	1138	54	30	224	86	0	13.07.2004 09:51
345	1240	35	31	262	86	0	13.07.2004 09:51
350	1317	30	32	279	86	0	13.07.2004 09:51
355	1322	29	32	281	86	0	13.07.2004 09:51
360	1343	31	33	293	86	0	13.07.2004 09:51

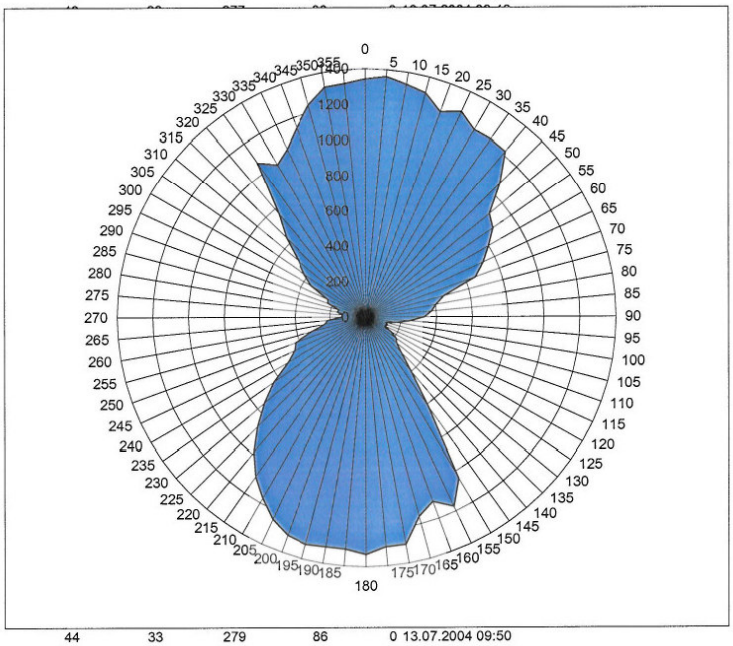

SMR02:

Object - sm_____, Profile - r2_____,13.07.2006 16:46:33

Picket	ParametrA	ParametrB	ParametrC	ParametrD	ParametrE	Azimuth	Time
0	1506	12	36	362	86	0	13.07.2004 09:34
5	1540	10	36	376	86	0	13.07.2004 09:34
10	1524	6	35	366	86	0	13.07.2004 09:34
15	1557	5	36	369	86	0	13.07.2004 09:34
20	1529						
25	1482						
30	1452						
35	1460						
40	1453						
45	1378						
50	1255						
55	1189						
60	1163						
65	938						
70	800						
75	776						
80	694						
85	630						
90	673						
95	560						
100	449						
105	281						
110	404						
115	388						
120	390						
125	411						
130	500						
135	548						
140	740						
145	1007						
150	1225						
155	1320						
160	1380						
165	1415						
170	1450						
175	1508						
180	1524						
185	1537						
190	1547						
195	1498						
200	1494	7	35	361	86	0	13.07.2004 09:35
205	1496	13	37	366	86	0	13.07.2004 09:35
210	1439	19	34	343	86	0	13.07.2004 09:35
215	1367	25	33	314	86	0	13.07.2004 09:35
220	1385	17	33	327	86	0	13.07.2004 09:35
225	1170	63	31	241	86	0	13.07.2004 09:35
230	973	107	29	167	86	0	13.07.2004 09:35
235	891	104	28	142	86	0	13.07.2004 09:35
240	810	113	27	121	86	0	13.07.2004 09:35
245	811	110	27	116	86	0	13.07.2004 09:35
250	648	95	27	80	105	0	13.07.2004 09:35
255	616	87	25	63	108	0	13.07.2004 09:35
260	548	87	25	53	105	0	13.07.2004 09:35
265	512	77	25	46	105	0	13.07.2004 09:36
270	445	68	25	33	105	0	13.07.2004 09:36
275	407	53	25	29	105	0	13.07.2004 09:36
280	405	56	24	32	105	0	13.07.2004 09:36
285	426	64	23	33	82	0	13.07.2004 09:36
290	594	91	23	66	86	0	13.07.2004 09:36
295	596	87	23	66	86	0	13.07.2004 09:36
300	792	96	25	115	86	0	13.07.2004 09:36
305	806	87	25	119	86	0	13.07.2004 09:36
310	924	86	26	144	86	0	13.07.2004 09:36
315	898	91	26	136	86	0	13.07.2004 09:36
320	1023	68	28	180	86	0	13.07.2004 09:36
325	1237	40	31	255	86	0	13.07.2004 09:36
330	1435	14	32	294	86	0	13.07.2004 09:36
335	1442	20	33	300	86	0	13.07.2004 09:36
340	1503	13	34	319	86	0	13.07.2004 09:36
345	1479	16	33	311	86	0	13.07.2004 09:36
350	1538	9	34	339	86	0	13.07.2004 09:36
355	1560	9	35	352	86	0	13.07.2004 09:36
360	1544	9	35	358	86	0	13.07.2004 09:36

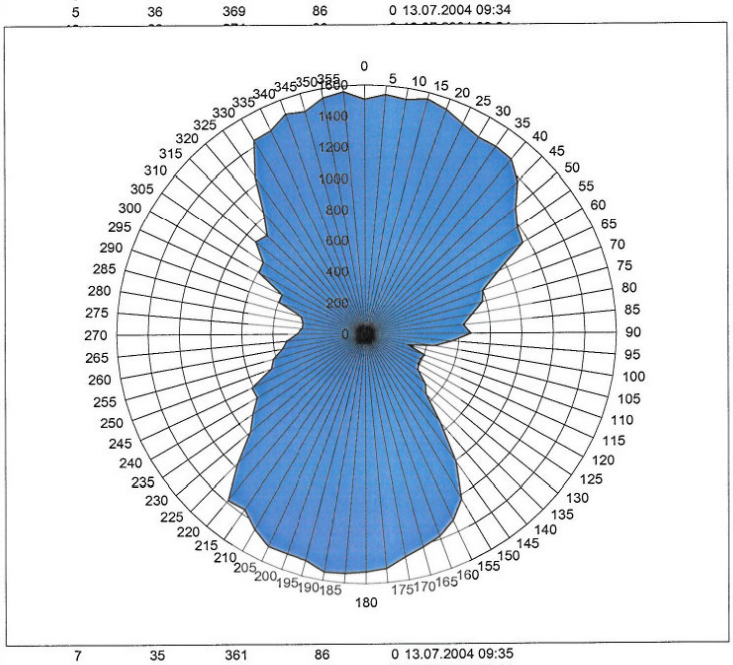

SMC03:

Object - sm_____, Profile - c3_____,13.07.2006 16:47:19

Picket	ParametrA	ParametrB	ParametrC	ParametrD	ParametrE	Azimuth	Time
0	1379	19	35	328	86	0	13.07.2004 10:10
5	1431	12	35	352	86	0	13.07.2004 10:10
10	1435	15	35	353	86	0	13.07.2004 10:10
15	1434	12	36	360	86	0	13.07.2004 10:10
20	1438						
25	1470						
30	1411						
35	1382						
40	1320						
45	1266						
50	1298						
55	1148						
60	1175						
65	1084						
70	839						
75	639						
80	642						
85	580						
90	477						
95	479						
100	440						
105	239						
110	165						
115	194						
120	206						
125	167						
130	196						
135	232						
140	217						
145	429						
150	619						
155	1084						
160	1172						
165	1175						
170	1285						
175	1362						
180	1362						
185	1428						
190	1426						
195	1418						
200	1379	17	35	347	86	0	13.07.2004 10:12
205	1364	18	34	341	86	0	13.07.2004 10:12
210	1355	18	34	334	86	0	13.07.2004 10:12
215	1248	46	33	295	86	0	13.07.2004 10:12
220	1206	49	33	278	86	0	13.07.2004 10:12
225	1113	66	32	246	86	0	13.07.2004 10:12
230	1139	64	32	248	86	0	13.07.2004 10:12
235	850	113	30	158	86	0	13.07.2004 10:12
240	692	112	28	101	105	0	13.07.2004 10:12
245	671	102	27	93	86	0	13.07.2004 10:12
250	565	89	26	64	86	0	13.07.2004 10:12
255	445	68	25	42	105	0	13.07.2004 10:12
260	335	50	24	24	86	0	13.07.2004 10:12
265	298	28	25	17	105	0	13.07.2004 10:12
270	217	17	25	7	105	0	13.07.2004 10:12
275	243	21	23	9	108	0	13.07.2004 10:12
280	207	15	24	6	105	0	13.07.2004 10:12
285	193	19	23	7	105	0	13.07.2004 10:12
290	202	18	22	6	86	0	13.07.2004 10:12
295	300	29	23	11	82	0	13.07.2004 10:12
300	255	21	22	10	82	0	13.07.2004 10:12
305	256	25	22	10	82	0	13.07.2004 10:12
310	317	34	23	17	82	0	13.07.2004 10:12
315	461	71	25	46	86	0	13.07.2004 10:12
320	751	91	26	121	86	0	13.07.2004 10:12
325	891	86	27	151	86	0	13.07.2004 10:13
330	937	74	29	183	86	0	13.07.2004 10:13
335	1130	52	31	229	86	0	13.07.2004 10:13
340	1152	49	30	225	86	0	13.07.2004 10:13
345	1331	29	33	302	86	0	13.07.2004 10:13
350	1377	28	34	314	86	0	13.07.2004 10:13
355	1387	23	34	316	86	0	13.07.2004 10:13
360	1404	14	34	329	86	0	13.07.2004 10:13

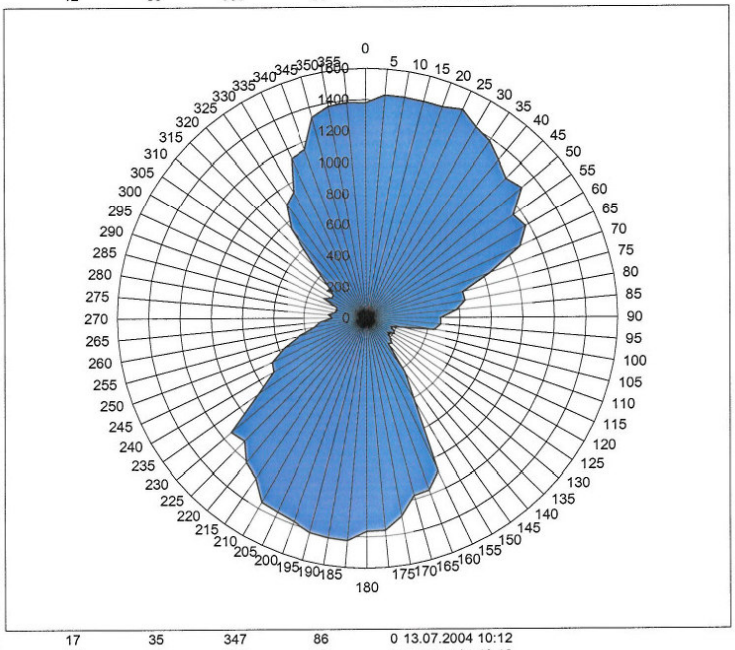

SML04:

Object - sm_____, Profile - l4_____,13.07.2006 16:47:30

Picket	ParametrA	ParametrB	ParametrC	ParametrD	ParametrE	Azimuth	Time
0	1498	8	37	386	86	0	13.07.2004 10:27
5	1511	11	37	392	86	0	13.07.2004 10:27
10	1489	12	37	385	86	0	13.07.2004 10:27
15	1519	11	38	412	86	0	13.07.2004 10:27
20	1523						
25	1521						
30	1523						
35	1504						
40	1559						
45	1449						
50	1446						
55	1369						
60	1136						
65	1157						
70	898						
75	821						
80	755						
85	700						
90	475						
95	441						
100	380						
105	256						
110	160						
115	148						
120	147						
125	241						
130	249						
135	317						
140	576						
145	645						
150	923						
155	970						
160	1165						
165	1291						
170	1360						
175	1437						
180	1479						
185	1517						
190	1525						
195	1539						
200	1521	10	38	413	86	0	13.07.2004 10:28
205	1515	6	38	413	86	0	13.07.2004 10:28
210	1460	17	37	393	86	0	13.07.2004 10:28
215	1483	10	37	407	86	0	13.07.2004 10:28
220	1431	23	37	380	86	0	13.07.2004 10:28
225	1286	35	34	316	86	0	13.07.2004 10:28
230	1052	75	32	231	86	0	13.07.2004 10:28
235	900	103	30	165	86	0	13.07.2004 10:28
240	831	111	28	148	86	0	13.07.2004 10:28
245	770	108	28	121	86	0	13.07.2004 10:28
250	784	109	28	131	86	0	13.07.2004 10:28
255	754	116	29	121	86	0	13.07.2004 10:28
260	564	83	26	74	86	0	13.07.2004 10:28
265	413	57	26	31	105	0	13.07.2004 10:28
270	257	23	25	10	105	0	13.07.2004 10:28
275	207	16	24	7	105	0	13.07.2004 10:29
280	190	13	24	4	82	0	13.07.2004 10:29
285	196	12	24	15	116	0	13.07.2004 10:29
290	172	8	25	5	82	0	13.07.2004 10:29
295	205	14	24	5	86	0	13.07.2004 10:29
300	221	13	22	6	86	0	13.07.2004 10:29
305	403	48	24	32	82	0	13.07.2004 10:29
310	631	80	26	81	86	0	13.07.2004 10:29
315	759	82	28	133	86	0	13.07.2004 10:29
320	784	85	28	139	86	0	13.07.2004 10:29
325	880	87	28	153	86	0	13.07.2004 10:29
330	1276	41	32	265	86	0	13.07.2004 10:29
335	1326	30	34	294	86	0	13.07.2004 10:29
340	1417	20	35	326	86	0	13.07.2004 10:29
345	1468	15	36	366	86	0	13.07.2004 10:29
350	1532	5	37	381	86	0	13.07.2004 10:29
355	1521	5	37	386	86	0	13.07.2004 10:29
360	1522	8	37	402	86	0	13.07.2004 10:29

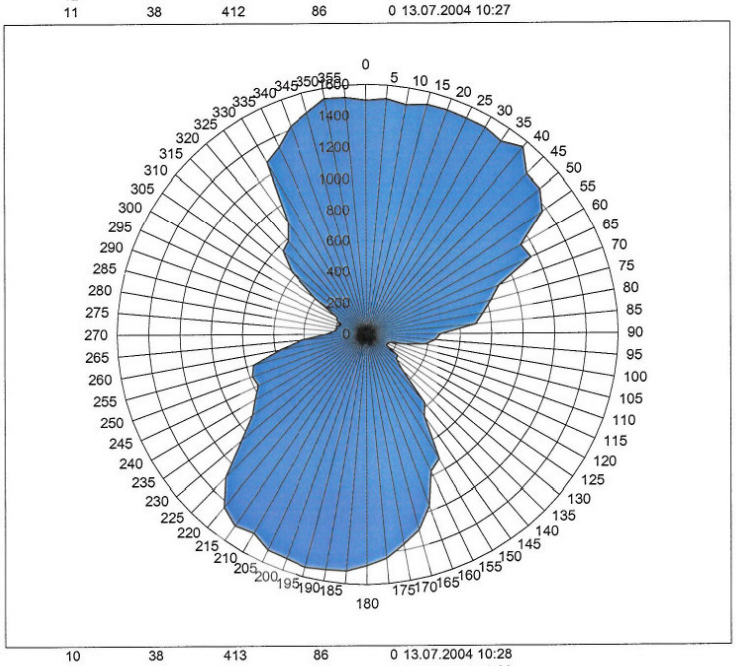

SMC04:

Object - sm , Profile - c4 ,13.07.2006 16:47:44

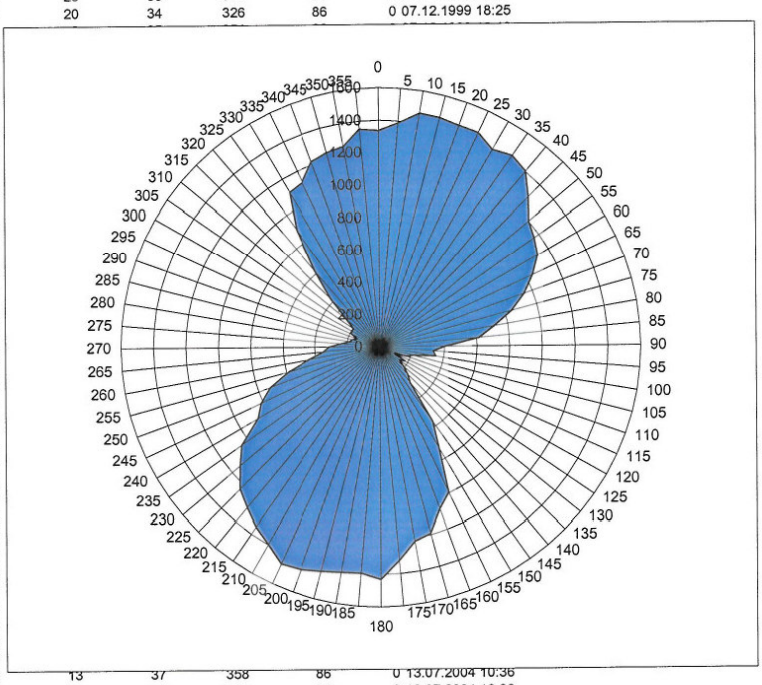

Picket	ParametrA	ParametrB	ParametrC	ParametrD	ParametrE	Azimuth	Time
0	1334	25	33	303	86	0	02.12.1999 02:27
5	1388	20	34	326	86	0	07.12.1999 18:25
10	1461						
15	1462						
20	1451						
25	1453						
30	1399						
35	1431						
40	1404						
45	1300						
50	1201						
55	1165						
60	1125						
65	1039						
70	947						
75	841						
80	717						
85	615						
90	405						
95	332						
100	350						
105	214						
110	180						
115	103						
120	180						
125	148						
130	194						
135	245						
140	294						
145	567						
150	726						
155	996						
160	1069						
165	1192						
170	1217						
175	1320						
180	1430						
185	1396						
190	1406						
195	1426	13	37	358	86	0	13.07.2004 10:36
200	1452	7	39	380	86	0	13.07.2004 10:36
205	1467	11	36	383	86	0	13.07.2004 10:36
210	1398	25	37	366	86	0	13.07.2004 10:36
215	1349	27	34	337	86	0	13.07.2004 10:36
220	1289	42	34	311	86	0	13.07.2004 10:36
225	1232	51	34	291	86	0	13.07.2004 10:36
230	1135	59	33	247	86	0	13.07.2004 10:36
235	1050	73	31	223	86	0	13.07.2004 10:36
240	875	97	30	158	86	0	13.07.2004 10:36
245	814	104	29	143	86	0	13.07.2004 10:36
250	726	112	28	109	86	0	13.07.2004 10:36
255	586	83	27	65	105	0	13.07.2004 10:37
260	442	59	26	36	86	0	13.07.2004 10:37
265	348	46	25	23	105	0	13.07.2004 10:37
270	311	37	26	26	105	0	13.07.2004 10:37
275	234	20	24	7	105	0	13.07.2004 10:37
280	185	11	22	3	105	0	13.07.2004 10:37
285	174	12	22	4	105	0	13.07.2004 10:37
290	145	9	21	3	105	0	13.07.2004 10:37
295	190	11	24	10	82	0	13.07.2004 10:37
300	196	18	22	6	82	0	13.07.2004 10:37
305	195	12	21	4	82	0	13.07.2004 10:37
310	263	20	28	18	86	0	13.07.2004 10:37
315	423	48	23	27	82	0	13.07.2004 10:37
320	621	96	26	76	82	0	13.07.2004 10:37
325	892	82	27	147	86	0	13.07.2004 10:37
330	1106	69	30	215	86	0	13.07.2004 10:37
335	1124	59	31	225	86	0	13.07.2004 10:37
340	1219	51	31	245	86	0	13.07.2004 10:37
345	1242	24	31	266	86	0	13.07.2004 10:37
350	1256	34	32	272	86	0	13.07.2004 10:37
355	1349	18	33	304	86	0	13.07.2004 10:37
360	1427	21	35	334	86	0	13.07.2004 10:37

SMC04:

Object - c4_____, Profile - 2_____,14.07.2006 15:45:34

Picket	ParametrA	ParametrB	ParametrC	ParametrD	ParametrE	Azimuth	Time
0	1458	16	36	365	86	0	14.07.2004 11:23
5	1460	13	37	380	86	0	14.07.2004 11:23
10	1498	11	38	406	86	0	14.07.2004 11:23
15	1477						
20	1515						
25	1487						
30	1438						
35	1443						
40	1446						
45	1373						
50	1402						
55	1355						
60	1202						
65	953						
70	1038						
75	865						
80	858						
85	774						
90	544						
95	457						
100	339						
105	252						
110	244						
115	205						
120	268						
125	244						
130	316						
135	330						
140	734						
145	869						
150	712						
155	945						
160	1118						
165	1409						
170	1432						
175	1463						
180	1480						
185	1502						
190	1482						
195	1506						
200	1513	9	38	415	86	0	14.07.2004 11:24
205	1470	21	38	431	86	0	14.07.2004 11:24
210	1347	32	36	349	86	0	14.07.2004 11:25
215	1408	20	36	369	86	0	14.07.2004 11:25
220	1361	27	36	356	86	0	14.07.2004 11:25
225	1365	29	36	349	86	0	14.07.2004 11:25
230	1260	53	34	286	86	0	14.07.2004 11:25
235	1246	51	34	303	86	0	14.07.2004 11:25
240	1169	60	33	271	86	0	14.07.2004 11:25
245	1114	75	32	244	86	0	14.07.2004 11:25
250	734	111	27	110	112	0	14.07.2004 11:25
255	561	86	27	67	90	0	14.07.2004 11:25
260	352	40	26	24	105	0	14.07.2004 11:25
265	200	19	26	9	108	0	14.07.2004 11:25
270	200	17	32	16	108	0	14.07.2004 11:25
275	196	20	29	9	97	0	14.07.2004 11:25
280	194	13	26	9	82	0	14.07.2004 11:25
285	188	12	24	9	101	0	14.07.2004 11:25
290	276	25	28	19	82	0	14.07.2004 11:25
295	332	32	25	25	82	0	14.07.2004 11:25
300	599	85	25	74	86	0	14.07.2004 11:25
305	553	76	25	56	86	0	14.07.2004 11:25
310	648	96	26	90	86	0	14.07.2004 11:25
315	794	97	26	125	86	0	14.07.2004 11:25
320	665	89	26	94	86	0	14.07.2004 11:25
325	1078	59	30	232	86	0	14.07.2004 11:25
330	1103	65	31	233	86	0	14.07.2004 11:25
335	1009	85	30	188	86	0	14.07.2004 11:26
340	1340	33	33	296	86	0	14.07.2004 11:26
345	1339	20	34	318	86	0	14.07.2004 11:26
350	1393	17	35	330	86	0	14.07.2004 11:26
355	1392	20	34	336	86	0	14.07.2004 11:26
360	1455	16	36	365	86	0	14.07.2004 11:26

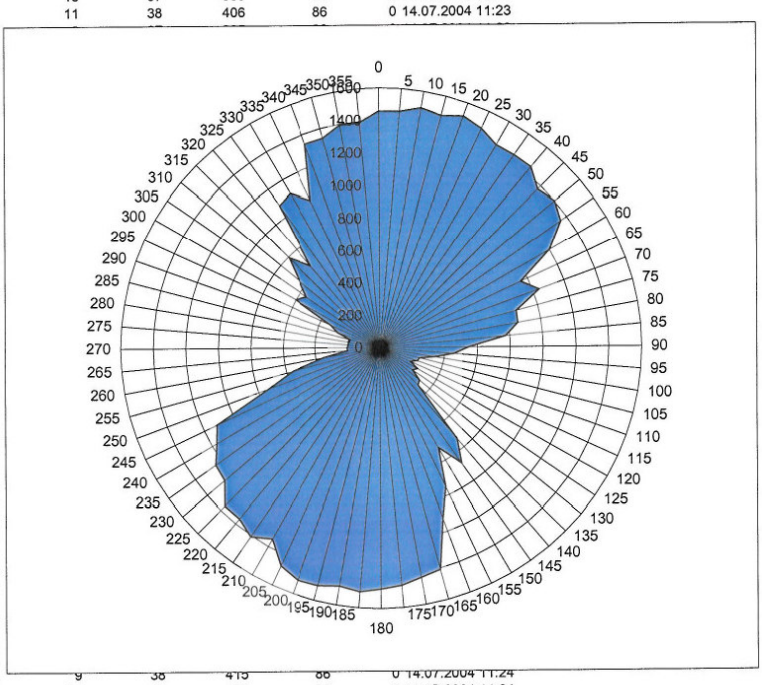

SMR04:

Object - sm_____, Profile - r4_____,13.07.2006 16:48:08

Picket	ParametrA	ParametrB	ParametrC	ParametrD	ParametrE	Azimuth	Time
0	1482	11	36	369	86	0	13.07.2004 10:44
5	1508	7	37	390	86	0	13.07.2004 10:44
10	1511	8	39	422	86	0	13.07.2004 10:44
15	1527						
20	1472						
25	1484						
30	1474						
35	1500						
40	1461						
45	1377						
50	1255						
55	1163						
60	1119						
65	1085						
70	971						
75	661						
80	589						
85	673						
90	535						
95	512						
100	350						
105	295						
110	144						
115	131						
120	152						
125	197						
130	227						
135	389						
140	344						
145	683						
150	929						
155	1168						
160	1327						
165	1381						
170	1488						
175	1464						
180	1488						
185	1493						
190	1529						
195	1487						
200	1513	5	38	429	86	0	13.07.2004 10:46
205	1459	10	38	406	86	0	13.07.2004 10:46
210	1414	16	37	380	86	0	13.07.2004 10:46
215	1343	32	36	356	86	0	13.07.2004 10:46
220	1354	24	36	339	86	0	13.07.2004 10:46
225	1276	38	34	316	86	0	13.07.2004 10:46
230	1172	61	33	267	86	0	13.07.2004 10:46
235	1036	86	32	221	86	0	13.07.2004 10:46
240	765	111	29	118	86	0	13.07.2004 10:46
245	530	90	26	59	86	0	13.07.2004 10:46
250	374	52	25	24	101	0	13.07.2004 10:46
255	337	42	24	20	108	0	13.07.2004 10:46
260	330	40	25	20	105	0	13.07.2004 10:46
265	276	25	26	14	105	0	13.07.2004 10:46
270	134	5	23	1	93	0	13.07.2004 10:46
275	134	11	23	3	105	0	13.07.2004 10:46
280	109	2	20	0	112	0	13.07.2004 10:46
285	133	2	23	0	86	0	13.07.2004 10:46
290	191	10	27	7	82	0	13.07.2004 10:46
295	228	18	22	6	82	0	13.07.2004 10:46
300	295	24	26	17	82	0	13.07.2004 10:46
305	310	29	22	14	82	0	13.07.2004 10:46
310	428	45	24	28	82	0	13.07.2004 10:46
315	672	102	27	85	82	0	13.07.2004 10:46
320	1025	83	30	184	86	0	13.07.2004 10:46
325	1159	52	31	239	86	0	13.07.2004 10:46
330	1306	32	33	283	86	0	13.07.2004 10:46
335	1352	23	34	302	86	0	13.07.2004 10:46
340	1364	22	34	306	86	0	13.07.2004 10:46
345	1458	14	36	353	86	0	13.07.2004 10:46
350	1441	22	37	355	86	0	13.07.2004 10:46
355	1553	7	38	424	86	0	13.07.2004 10:47
360	1507	11	39	416	86	0	13.07.2004 10:47

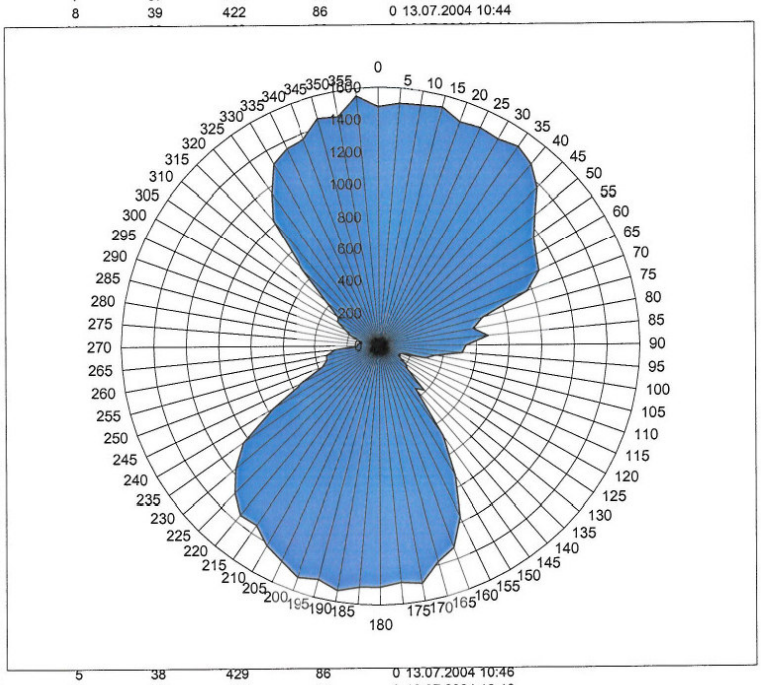

SML05:

Object - sm_____, Profile - l5_____,13.07.2006 16:48:40

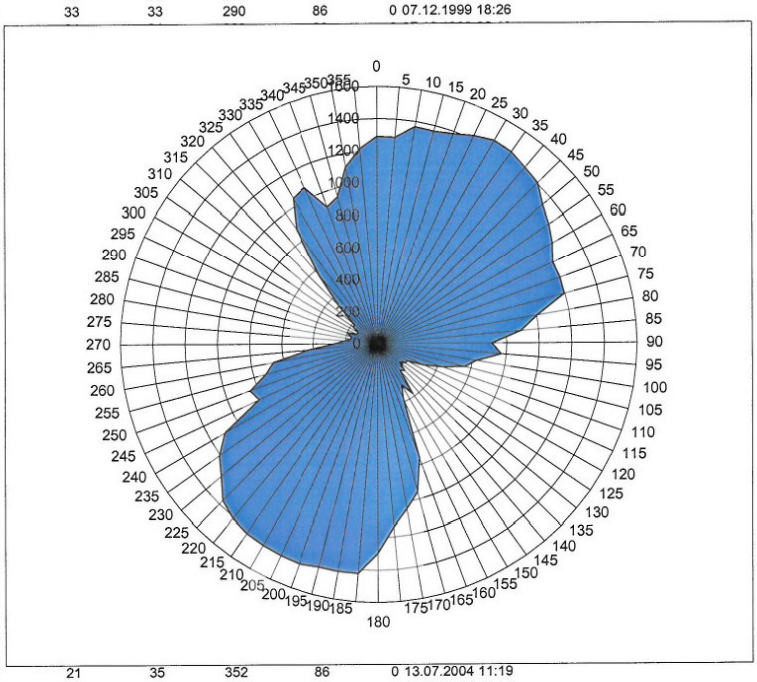

Picket	ParametrA	ParametrB	ParametrC	ParametrD	ParametrE	Azimuth	Time
0	1287	36	32	277	86	0	02.12.1999 02:26
5	1286	33	33	290	86	0	07.12.1999 18:26
10	1366						
15	1363						
20	1384						
25	1421						
30	1452						
35	1449						
40	1423						
45	1404						
50	1335						
55	1295						
60	1249						
65	1194						
70	1200						
75	1194						
80	1003						
85	890						
90	707						
95	767						
100	622						
105	560						
110	425						
115	315						
120	216						
125	207						
130	179						
135	236						
140	217						
145	380						
150	298						
155	377						
160	756						
165	954						
170	1041						
175	1138						
180	1296						
185	1423						
190	1426						
195	1425	21	35	352	86	0	13.07.2004 11:19
200	1444	8	36	369	86	0	13.07.2004 11:19
205	1440	13	36	368	86	0	13.07.2004 11:19
210	1435	13	37	376	86	0	13.07.2004 11:19
215	1428	17	37	390	86	0	13.07.2004 11:19
220	1408	28	37	365	86	0	13.07.2004 11:19
225	1369	20	36	358	86	0	13.07.2004 11:19
230	1274	39	34	313	86	0	13.07.2004 11:19
235	1205	53	33	293	86	0	13.07.2004 11:19
240	1100	70	32	241	86	0	13.07.2004 11:19
245	816	115	30	136	90	0	13.07.2004 11:19
250	848	103	28	149	86	0	13.07.2004 11:19
255	722	107	28	118	86	0	13.07.2004 11:19
260	662	107	27	97	86	0	13.07.2004 11:19
265	431	63	26	37	86	0	13.07.2004 11:19
270	262	26	24	10	105	0	13.07.2004 11:19
275	202	12	25	4	101	0	13.07.2004 11:19
280	167	9	25	3	97	0	13.07.2004 11:19
285	168	5	21	2	108	0	13.07.2004 11:19
290	200	16	24	5	101	0	13.07.2004 11:19
295	143	6	22	2	105	0	13.07.2004 11:19
300	138	9	27	3	101	0	13.07.2004 11:19
305	182	11	27	8	82	0	13.07.2004 11:19
310	186	12	22	7	82	0	13.07.2004 11:19
315	336	30	28	35	82	0	13.07.2004 11:19
320	561	78	27	83	86	0	13.07.2004 11:19
325	877	102	28	145	86	0	13.07.2004 11:20
330	1047	65	29	197	86	0	13.07.2004 11:20
335	1072	69	30	207	86	0	13.07.2004 11:20
340	906	92	28	153	86	0	13.07.2004 11:20
345	945	83	29	162	86	0	13.07.2004 11:20
350	1115	51	30	225	86	0	13.07.2004 11:20
355	1218	43	32	258	86	0	13.07.2004 11:20
360	1391	22	35	319	86	0	13.07.2004 11:20

SMC05:

Object - c5_____, Profile - 1_____,13.07.2006 16:51:15

Picket	ParametrA	ParametrB	ParametrC	ParametrD	ParametrE	Azimuth	Time
0	1526	5	39	440	86	0	13.07.2004 12:53
5	1512	9	40	435	86	0	13.07.2004 12:53
10	1542	4	40	457	86	0	13.07.2004 12:53
15	1544	5	39	438	86	0	13.07.2004 12:53
20	1518	9	39	464	86	0	13.07.2004 12:53
25	1525						
30	1552						
35	1528						
40	1464						
45	1396						
50	1348						
55	1249						
60	1192						
65	963						
70	799						
75	830						
80	806						
85	699						
90	609						
95	319						
100	341						
105	187						
110	188						
115	230						
120	211						
125	203						
130	218						
135	477						
140	815						
145	1065						
150	1234						
155	1308						
160	1360						
165	1397						
170	1500						
175	1497						
180	1512						
185	1554						
190	1556						
195	1543						
200	1551						
205	1486						
210	1486	12	37	414	86	0	13.07.2004 12:55
215	1433	15	37	403	86	0	13.07.2004 12:55
220	1417	21	38	399	86	0	13.07.2004 12:55
225	1297	46	35	340	86	0	13.07.2004 12:55
230	1054	94	33	228	86	0	13.07.2004 12:55
235	943	102	30	179	86	0	13.07.2004 12:55
240	555	92	27	61	82	0	13.07.2004 12:55
245	532	80	27	60	86	0	13.07.2004 12:55
250	519	82	27	68	86	0	13.07.2004 12:55
255	490	60	27	79	75	0	13.07.2004 12:55
260	352	46	24	22	82	0	13.07.2004 12:55
265	359	26	33	93	105	0	13.07.2004 12:55
270	241	19	25	20	116	0	13.07.2004 12:55
275	232	23	28	19	105	0	13.07.2004 12:55
280	182	13	27	13	75	0	13.07.2004 12:55
285	188	13	31	13	82	0	13.07.2004 12:55
290	241	19	27	18	82	0	13.07.2004 12:55
295	259	24	25	14	82	0	13.07.2004 12:55
300	510	67	27	64	86	0	13.07.2004 12:55
305	603	77	28	79	86	0	13.07.2004 12:55
310	759	97	29	114	86	0	13.07.2004 12:55
315	766	82	27	113	86	0	13.07.2004 12:55
320	938	80	29	167	86	0	13.07.2004 12:55
325	1040	80	30	205	86	0	13.07.2004 12:55
330	1263	41	33	309	86	0	13.07.2004 12:55
335	1320	37	34	299	86	0	13.07.2004 12:56
340	1337	42	35	321	86	0	13.07.2004 12:56
345	1409	17	34	351	86	0	13.07.2004 12:56
350	1485	16	39	431	86	0	13.07.2004 12:56
355	1532	12	39	420	86	0	13.07.2004 12:56
360	1538	9	40	449	86	0	13.07.2004 12:56

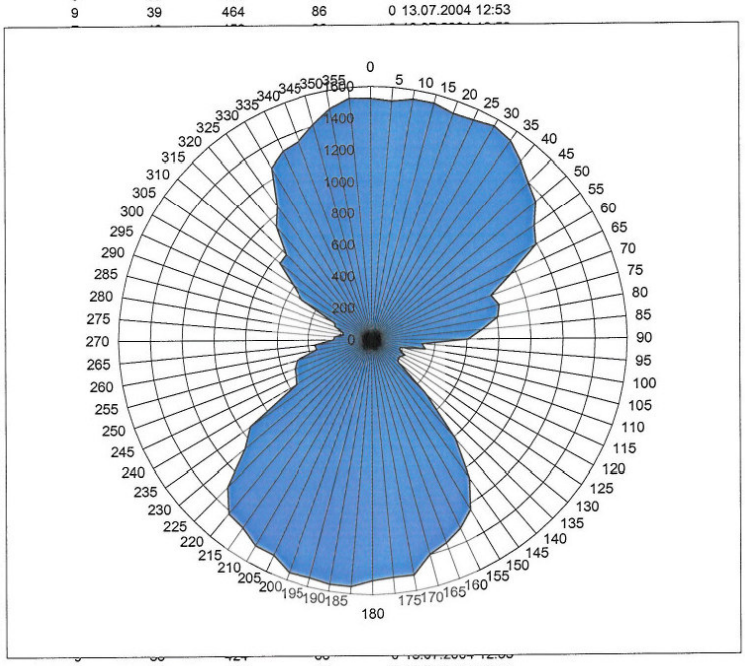

SMC05: with the same frequency range as in the new apparatus for vertical measurements:

Object - c5_tief_, Profile - 1 ,13.07.2006 16:51:29

Picket	ParametrA	ParametrB	ParametrC	ParametrD	ParametrE	Azimuth	Time
0	1662	1	82	1722	86	0	13.07.2004 12:58
5	1667	1	83	1724	86	0	13.07.2004 12:58
10	1692	1	82	1725	86	0	13.07.2004 12:58
15	1691	1	82	1718	86	0	13.07.2004 12:58
20	1676						
25	1665						
30	1647						
35	1686						
40	1654						
45	1642						
50	1596						
55	1577						
60	1567						
65	1523						
70	1471						
75	1397						
80	1316						
85	1320						
90	1219						
95	1218						
100	1211						
105	1137						
110	1110						
115	1126						
120	1162						
125	1309						
130	1349						
135	1408						
140	1497						
145	1552						
150	1617						
155	1598						
160	1621						
165	1618						
170	1668						
175	1656						
180	1641						
185	1673						
190	1653						
195	1679						
200	1657						
205	1664	1	81	1661	86	0	13.07.2004 12:59
210	1657	1	80	1652	86	0	13.07.2004 12:59
215	1620	1	75	1491	86	0	13.07.2004 12:59
220	1607	1	74	1449	86	0	13.07.2004 12:59
225	1562	2	72	1414	86	0	13.07.2004 12:59
230	1574	2	71	1367	86	0	13.07.2004 12:59
235	1512	2	61	1072	86	0	13.07.2004 12:59
240	1391	8	56	888	86	0	13.07.2004 12:59
245	1405	10	54	842	86	0	13.07.2004 12:59
250	1233	18	45	620	45	0	13.07.2004 12:59
255	1214	17	46	630	45	0	13.07.2004 13:00
260	1138	22	43	611	45	0	13.07.2004 13:00
265	1133	18	50	711	45	0	13.07.2004 13:00
270	1100	24	42	546	45	0	13.07.2004 13:00
275	1115	21	45	680	45	0	13.07.2004 13:00
280	1116	27	44	606	45	0	13.07.2004 13:00
285	1140	21	42	552	45	0	13.07.2004 13:00
290	1303	5	50	785	86	0	13.07.2004 13:00
295	1357	4	56	886	86	0	13.07.2004 13:00
300	1380	1	55	903	86	0	13.07.2004 13:00
305	1419	1	57	935	86	0	13.07.2004 13:00
310	1495	2	61	1088	86	0	13.07.2004 13:00
315	1533	1	67	1225	86	0	13.07.2004 13:00
320	1591	1	71	1345	86	0	13.07.2004 13:00
325	1608	1	73	1414	86	0	13.07.2004 13:00
330	1636	1	74	1426	86	0	13.07.2004 13:00
335	1630	1	76	1504	86	0	13.07.2004 13:00
340	1630	1	79	1610	86	0	13.07.2004 13:00
345	1663	1	81	1665	86	0	13.07.2004 13:00
350	1658	1	80	1644	86	0	13.07.2004 13:00
355	1633	1	82	1716	86	0	13.07.2004 13:00
360	1666	1	82	1723	86	0	13.07.2004 13:00

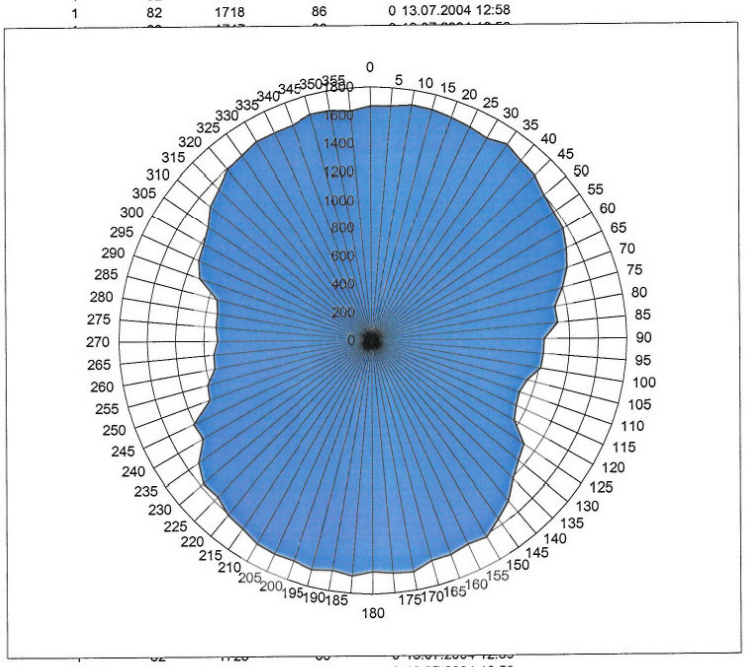

SMC05:

Object - c6_____, Profile - 2_____,14.07.2006 15:44:12

Picket	ParametrA	ParametrB	ParametrC	ParametrD	ParametrE	Azimuth	Time
0	1363	23	33	313	86	0	14.07.2004 11:05
5	1524	5	39	405	86	0	14.07.2004 11:05
10	1483	8	37	405	86	0	14.07.2004 11:05
15	1534	3	38	418	86	0	14.07.2004 11:05
20	1546						
25	1483						
30	1468						
35	1436						
40	1422						
45	1396						
50	1250						
55	1206						
60	1056						
65	1109						
70	1016						
75	1022						
80	748						
85	673						
90	468						
95	510						
100	524						
105	190						
110	200						
115	189						
120	205						
125	258						
130	306						
135	302						
140	621						
145	928						
150	1153						
155	1236						
160	1337						
165	1373						
170	1351						
175	1434						
180	1486						
185	1534						
190	1524						
195	1550						
200	1528						
205	1492	10	38	413	86	0	14.07.2004 11:07
210	1472	11	38	409	86	0	14.07.2004 11:07
215	1486	15	38	414	86	0	14.07.2004 11:07
220	1420	17	36	380	86	0	14.07.2004 11:07
225	1345	31	34	322	86	0	14.07.2004 11:07
230	1253	40	34	307	86	0	14.07.2004 11:07
235	1062	78	32	231	86	0	14.07.2004 11:07
240	1067	86	32	221	86	0	14.07.2004 11:07
245	944	93	30	185	86	0	14.07.2004 11:07
250	626	99	28	84	82	0	14.07.2004 11:07
255	576	96	26	68	86	0	14.07.2004 11:07
260	306	37	25	19	101	0	14.07.2004 11:07
265	211	18	25	11	97	0	14.07.2004 11:07
270	226	13	31	15	105	0	14.07.2004 11:07
275	183	13	21	4	105	0	14.07.2004 11:07
280	260	19	31	38	105	0	14.07.2004 11:07
285	187	16	21	6	105	0	14.07.2004 11:07
290	246	16	27	21	82	0	14.07.2004 11:07
295	304	34	23	14	78	0	14.07.2004 11:07
300	284	24	23	17	86	0	14.07.2004 11:07
305	363	42	27	33	82	0	14.07.2004 11:07
310	386	43	24	33	82	0	14.07.2004 11:07
315	399	56	24	36	82	0	14.07.2004 11:08
320	895	91	27	146	86	0	14.07.2004 11:08
325	1081	64	30	223	86	0	14.07.2004 11:08
330	1205	44	31	246	86	0	14.07.2004 11:08
335	1342	28	33	290	86	0	14.07.2004 11:08
340	1394	20	34	309	86	0	14.07.2004 11:08
345	1464	13	35	353	86	0	14.07.2004 11:08
350	1492	10	39	381	86	0	14.07.2004 11:08
355	1508	6	36	379	86	0	14.07.2004 11:08
360	1510	5	36	398	86	0	14.07.2004 11:08

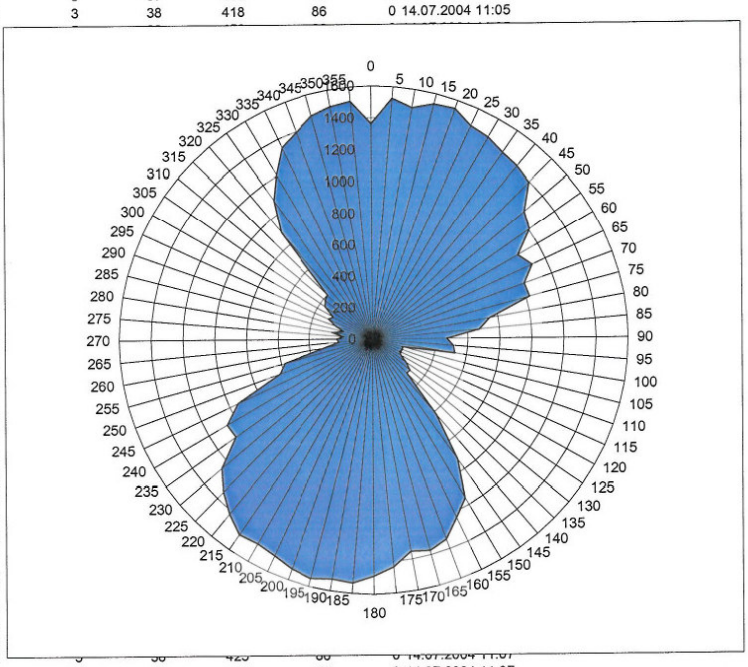

SMR05:

Object - sm_____, Profile - r5_____,13.07.2006 16:48:22

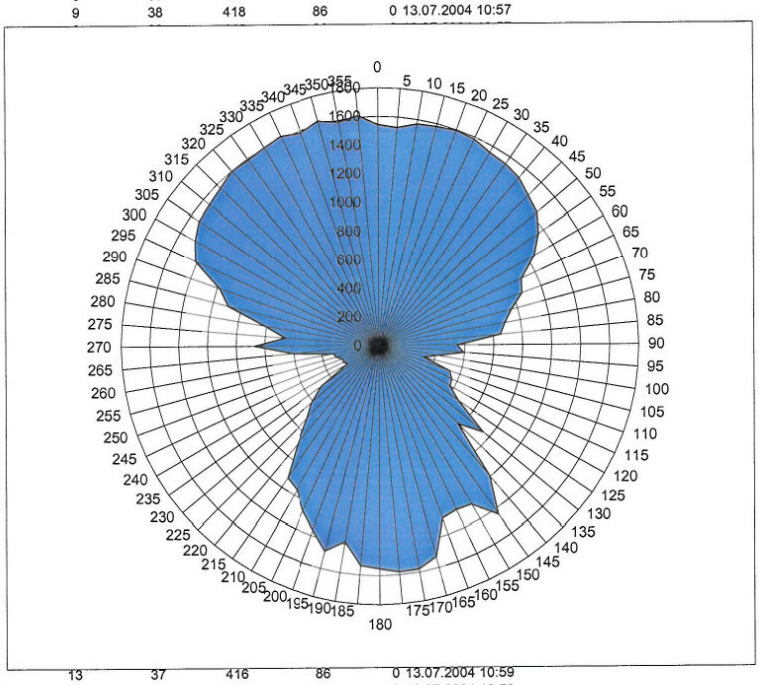

Picket	ParametrA	ParametrB	ParametrC	ParametrD	ParametrE	Azimuth	Time
0	1543	6	38	406	86	0	13.07.2004 10:57
5	1527	9	38	418	86	0	13.07.2004 10:57
10	1568						
15	1580						
20	1595						
25	1585						
30	1552						
35	1542						
40	1521						
45	1473						
50	1438						
55	1355						
60	1248						
65	1095						
70	1058						
75	953						
80	889						
85	849						
90	546						
95	590						
100	409						
105	323						
110	523						
115	560						
120	571						
125	671						
130	945						
135	774						
140	1194						
145	1442						
150	1282						
155	1266						
160	1283						
165	1521						
170	1578						
175	1579						
180	1553						
185	1534						
190	1381						
195	1477	13	37	416	86	0	13.07.2004 10:59
200	1362	27	36	363	86	0	13.07.2004 10:59
205	1266	42	35	310	86	0	13.07.2004 10:59
210	1157	68	32	254	86	0	13.07.2004 10:59
215	1120	71	32	255	86	0	13.07.2004 10:59
220	888	96	29	166	86	0	13.07.2004 10:59
225	711	106	27	110	86	0	13.07.2004 10:59
230	614	102	26	75	90	0	13.07.2004 10:59
235	491	75	26	56	82	0	13.07.2004 10:59
240	248	20	26	10	101	0	13.07.2004 10:59
245	270	27	27	25	105	0	13.07.2004 10:59
250	267	23	22	9	78	0	13.07.2004 10:59
255	305	38	26	29	86	0	13.07.2004 10:59
260	317	38	23	20	82	0	13.07.2004 10:59
265	599	80	26	78	86	0	13.07.2004 10:59
270	868	90	28	146	86	0	13.07.2004 10:59
275	658	81	26	87	86	0	13.07.2004 10:59
280	801	81	27	130	86	0	13.07.2004 10:59
285	1090	61	30	209	86	0	13.07.2004 10:59
290	1184	44	30	244	86	0	13.07.2004 10:59
295	1412	24	35	342	86	0	13.07.2004 10:59
300	1480	14	37	387	86	0	13.07.2004 10:59
305	1533	12	39	416	86	0	13.07.2004 10:59
310	1543	6	39	433	86	0	13.07.2004 10:59
315	1565	6	39	443	86	0	13.07.2004 10:59
320	1597	2	40	471	86	0	13.07.2004 10:59
325	1590	7	40	459	86	0	13.07.2004 10:59
330	1601	8	40	471	86	0	13.07.2004 10:59
335	1616	3	41	482	86	0	13.07.2004 10:59
340	1583	4	41	493	86	0	13.07.2004 11:00
345	1623	6	41	489	86	0	13.07.2004 11:00
350	1586	7	41	488	86	0	13.07.2004 11:00
355	1610	1	41	494	86	0	13.07.2004 11:00

SML07:

Object - sm_____, Profile - I7_____,13.07.2006 16:48:54

Picket	ParametrA	ParametrB	ParametrC	ParametrD	ParametrE	Azimuth	Time
0	1560	5	39	441	86	0	13.07.2004 11:24
5	1513	10	39	402	86	0	13.07.2004 11:24
10	1507						
15	1573						
20	1581						
25	1549						
30	1538						
35	1530						
40	1486						
45	1446						
50	1388						
55	1279						
60	1154						
65	1188						
70	1140						
75	808						
80	792						
85	641						
90	697						
95	590						
100	557						
105	252						
110	177						
115	212						
120	179						
125	135						
130	293						
135	465						
140	634						
145	797						
150	898						
155	978						
160	1319						
165	1383						
170	1462						
175	1490						
180	1567						
185	1584						
190	1570						
195	1570	5	40	453	86	0	13.07.2004 11:25
200	1549	6	39	466	86	0	13.07.2004 11:25
205	1568	8	40	457	86	0	13.07.2004 11:25
210	1537	12	40	450	86	0	13.07.2004 11:25
215	1461	14	39	438	86	0	13.07.2004 11:25
220	1473	11	38	420	86	0	13.07.2004 11:25
225	1402	24	37	371	86	0	13.07.2004 11:25
230	1410	13	36	378	86	0	13.07.2004 11:25
235	1202	51	33	277	86	0	13.07.2004 11:26
240	971	94	30	187	86	0	13.07.2004 11:26
245	946	105	31	182	86	0	13.07.2004 11:26
250	859	119	30	157	86	0	13.07.2004 11:26
255	856	104	30	149	86	0	13.07.2004 11:26
260	693	104	29	128	86	0	13.07.2004 11:26
265	426	60	24	32	86	0	13.07.2004 11:26
270	376	49	25	26	86	0	13.07.2004 11:26
275	341	44	24	23	86	0	13.07.2004 11:26
280	323	42	24	20	105	0	13.07.2004 11:26
285	160	5	24	5	97	0	13.07.2004 11:26
290	206	13	29	11	78	0	13.07.2004 11:26
295	156	6	19	2	82	0	13.07.2004 11:26
300	157	6	22	2	82	0	13.07.2004 11:26
305	168	15	27	13	78	0	13.07.2004 11:26
310	166	10	24	5	78	0	13.07.2004 11:26
315	402	43	24	30	82	0	13.07.2004 11:26
320	961	78	28	177	86	0	13.07.2004 11:26
325	1134	57	31	245	86	0	13.07.2004 11:26
330	1156	53	31	232	86	0	13.07.2004 11:26
335	1204	48	31	249	86	0	13.07.2004 11:26
340	1208	47	31	245	86	0	13.07.2004 11:26
345	1387	18	34	317	86	0	13.07.2004 11:26
350	1392	19	34	323	86	0	13.07.2004 11:26
355	1493	13	37	371	86	0	13.07.2004 11:26
360	1531	9	37	396	86	0	13.07.2004 11:26

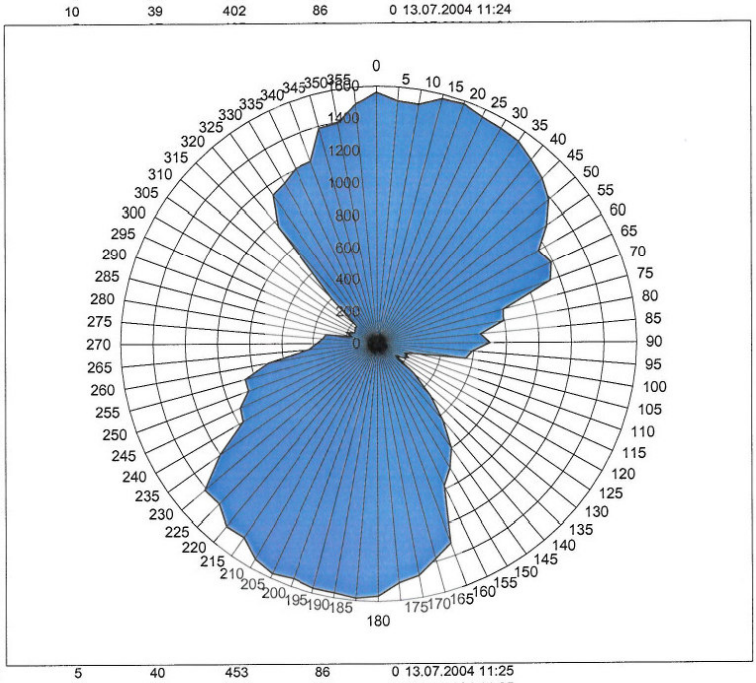

SML07:

Object - I7_____, Profile - 2_____,14.07.2006 15:19:17

Picket	ParametrA	ParametrB	ParametrC	ParametrD	ParametrE	Azimuth	Time
0	897	86	28	154	86	0	14.07.2004 08:02
5	925	101	29	162	86	0	14.07.2004 08:02
10	992						
15	1034						
20	1022						
25	1058						
30	1014						
35	1049						
40	978						
45	983						
50	946						
55	902						
60	751						
65	669						
70	595						
75	558						
80	529						
85	454						
90	376						
95	278						
100	159						
105	115						
110	103						
115	111						
120	79						
125	66						
130	80						
135	95						
140	127						
145	158						
150	345						
155	299						
160	525						
165	646						
170	812						
175	884						
180	958						
185	1003						
190	1019						
195	1004	90	31	193	86	0	14.07.2004 08:04
200	1000	90	31	192	86	0	14.07.2004 08:04
205	1023	83	30	196	86	0	14.07.2004 08:04
210	1007	86	30	189	86	0	14.07.2004 08:04
215	945	107	30	167	86	0	14.07.2004 08:04
220	899	101	28	152	86	0	14.07.2004 08:04
225	852	108	28	137	86	0	14.07.2004 08:04
230	860	103	29	138	86	0	14.07.2004 08:04
235	748	107	27	103	86	0	14.07.2004 08:04
240	550	86	25	56	86	0	14.07.2004 08:04
245	439	64	24	30	86	0	14.07.2004 08:04
250	448	68	24	35	86	0	14.07.2004 08:04
255	457	69	24	35	86	0	14.07.2004 08:04
260	392	43	24	22	90	0	14.07.2004 08:04
265	363	53	24	24	90	0	14.07.2004 08:04
270	195	16	24	5	105	0	14.07.2004 08:04
275	175	10	29	16	71	0	14.07.2004 08:04
280	174	15	20	5	105	0	14.07.2004 08:05
285	159	8	21	2	86	0	14.07.2004 08:05
290	175	13	19	4	75	0	14.07.2004 08:05
295	207	9	22	3	71	0	14.07.2004 08:05
300	220	11	21	4	75	0	14.07.2004 08:05
305	191	8	22	2	78	0	14.07.2004 08:05
310	238	17	21	6	82	0	14.07.2004 08:05
315	497	68	24	35	86	0	14.07.2004 08:05
320	541	75	24	50	86	0	14.07.2004 08:05
325	569	88	25	57	86	0	14.07.2004 08:05
330	550	82	25	56	86	0	14.07.2004 08:05
335	612	90	25	70	86	0	14.07.2004 08:05
340	627	95	26	73	86	0	14.07.2004 08:05
345	629	95	25	71	86	0	14.07.2004 08:05
350	878	102	29	144	86	0	14.07.2004 08:05
355	931	100	29	163	86	0	14.07.2004 08:05

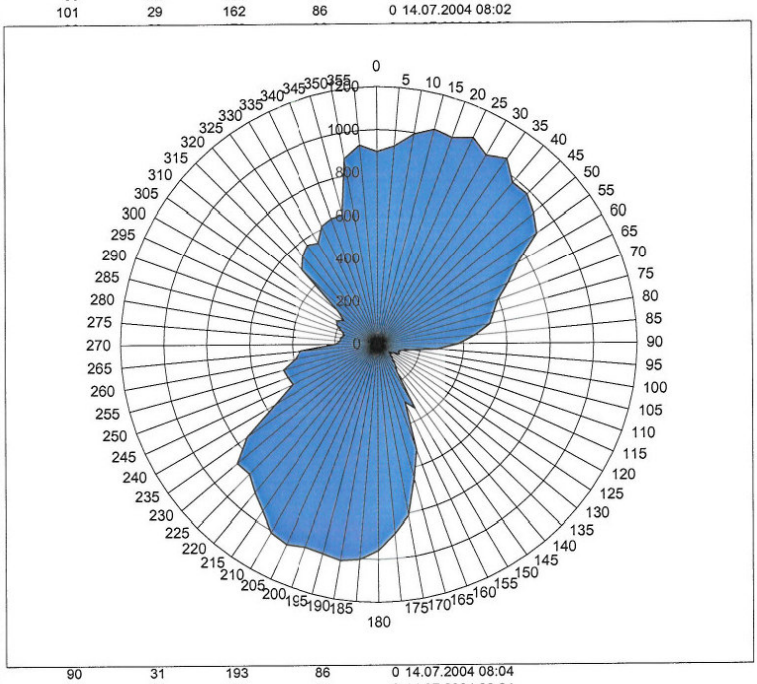

SMC07_2:

Object - c7_2 , Profile - 1 ,13.07.2006 16:51:04

Picket	ParametrA	ParametrB	ParametrC	ParametrD	ParametrE	Azimuth	Time
0	2890	1	83	1753	150	0	13.07.2004 12:47
5	2854	1	79	1643	150	0	13.07.2004 12:47
10	2804	1	77	1569	150	0	13.07.2004 12:47
15	2580	1	73	1452	150	0	13.07.2004 12:47
20	2602	1	73	1435	75	0	13.07.2004 12:47
25	2514						
30	2328						
35	2325						
40	2165						
45	2149						
50	2001						
55	1964						
60	1719						
65	1783						
70	1479						
75	1300						
80	1443						
85	1232						
90	1328						
95	780						
100	518						
105	579						
110	653						
115	480						
120	348						
125	419						
130	495						
135	767						
140	867						
145	996						
150	1053						
155	1395						
160	1407						
165	1953						
170	2152						
175	2517						
180	2681						
185	2716						
190	2697						
195	2801						
200	2791						
205	2673						
210	2688	1	75	1502	150	0	13.07.2004 12:48
215	2628	1	72	1415	150	0	13.07.2004 12:48
220	2444	1	63	1164	150	0	13.07.2004 12:48
225	2268	1	55	919	150	0	13.07.2004 12:49
230	2122	1	51	810	150	0	13.07.2004 12:49
235	2079	4	50	757	150	0	13.07.2004 12:49
240	2223	1	52	842	150	0	13.07.2004 12:49
245	2361	1	58	1030	150	0	13.07.2004 12:49
250	2561	1	58	999	225	0	13.07.2004 12:49
255	2749	1	65	1207	150	0	13.07.2004 12:49
260	2818	1	69	1343	150	0	13.07.2004 12:49
265	2795	1	79	1596	150	0	13.07.2004 12:49
270	2748	1	83	1746	150	0	13.07.2004 12:49
275	2776	1	79	1657	150	0	13.07.2004 12:49
280	2830	1	83	1767	150	0	13.07.2004 12:49
285	2865	1	84	1794	150	0	13.07.2004 12:49
290	2604	1	91	1993	150	0	13.07.2004 12:49
295	2775	1	84	1812	150	0	13.07.2004 12:49
300	2717	1	84	1811	150	0	13.07.2004 12:49
305	2750	1	84	1823	150	0	13.07.2004 12:49
310	3234	1	85	1816	225	0	13.07.2004 12:49
315	3041	1	90	1988	225	0	13.07.2004 12:49
320	2779	1	84	1803	75	0	13.07.2004 12:49
325	2767	1	84	1795	75	0	13.07.2004 12:49
330	2550	1	92	2050	150	0	13.07.2004 12:49
335	2960	1	85	1826	150	0	13.07.2004 12:49
340	2874	1	84	1787	150	0	13.07.2004 12:49
345	2767	1	82	1739	150	0	13.07.2004 12:49
350	2790	1	82	1719	150	0	13.07.2004 12:49
355	2873	1	83	1767	150	0	13.07.2004 12:49

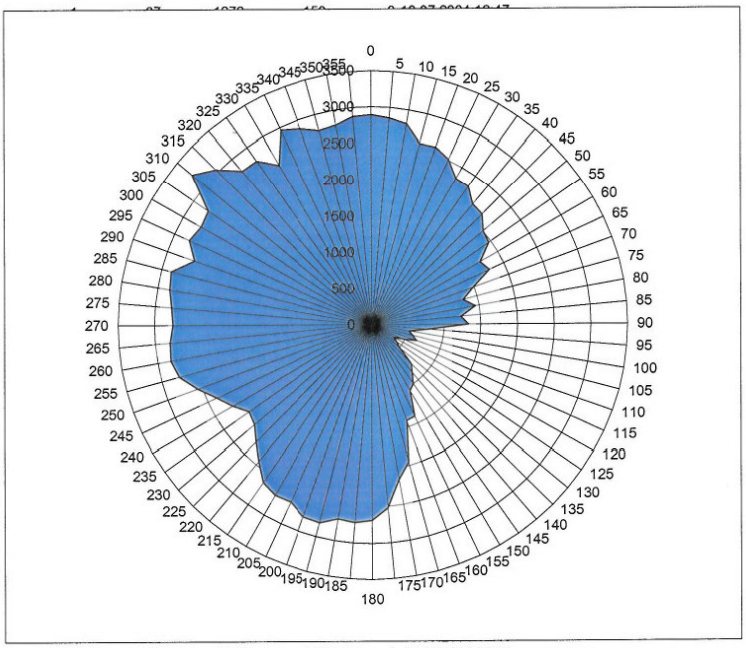

SMC07_2:

Object - c7_____, Profile - 1_____,14.07.2006 15:41:51

Picket	ParametrA	ParametrB	ParametrC	ParametrD	ParametrE	Azimuth	Time
0	1813	3	44	599	86	0	14.07.2004 10:55
5	1835	4	43	625	86	0	14.07.2004 10:55
10	1852						
15	1842						
20	1836						
25	1941						
30	1838						
35	1876						
40	1746						
45	1633						
50	1509						
55	1394						
60	1281						
65	1121						
70	1171						
75	1143						
80	997						
85	880						
90	876						
95	602						
100	581						
105	516						
110	467						
115	382						
120	345						
125	341						
130	720						
135	891						
140	879						
145	1135						
150	1164						
155	1225						
160	1046						
165	1704						
170	1707						
175	1837						
180	1912						
185	1887						
190	2028						
195	2170	1	57	955	150	0	14.07.2004 10:57
200	2028	2	55	889	150	0	14.07.2004 10:57
205	1974	1	53	829	150	0	14.07.2004 10:57
210	1940	1	50	770	150	0	14.07.2004 10:57
215	1683	10	41	540	86	0	14.07.2004 10:57
220	1726	8	43	573	86	0	14.07.2004 10:57
225	1432	26	37	399	86	0	14.07.2004 10:57
230	1143	63	32	254	86	0	14.07.2004 10:57
235	979	88	31	220	86	0	14.07.2004 10:57
240	869	105	30	158	86	0	14.07.2004 10:57
245	808	117	30	144	86	0	14.07.2004 10:57
250	771	114	29	134	86	0	14.07.2004 10:57
255	719	103	28	117	86	0	14.07.2004 10:57
260	426	55	24	32	82	0	14.07.2004 10:57
265	421	61	26	38	86	0	14.07.2004 10:57
270	252	26	26	15	105	0	14.07.2004 10:57
275	285	27	29	19	90	0	14.07.2004 10:57
280	267	27	24	18	82	0	14.07.2004 10:57
285	316	37	23	16	97	0	14.07.2004 10:57
290	322	35	23	15	82	0	14.07.2004 10:57
295	462	67	25	45	86	0	14.07.2004 10:57
300	401	55	25	38	86	0	14.07.2004 10:57
305	682	94	25	93	86	0	14.07.2004 10:57
310	902	90	28	157	86	0	14.07.2004 10:57
315	1095	72	30	220	86	0	14.07.2004 10:58
320	1147	53	30	244	86	0	14.07.2004 10:58
325	1328	40	33	327	86	0	14.07.2004 10:58
330	1536	27	36	401	86	0	14.07.2004 10:58
335	1643	10	38	445	86	0	14.07.2004 10:58
340	1687	12	41	517	86	0	14.07.2004 10:58
345	1881	8	46	651	86	0	14.07.2004 10:58
350	2039	2	48	687	86	0	14.07.2004 10:58
355	1859	4	46	634	86	0	14.07.2004 10:58

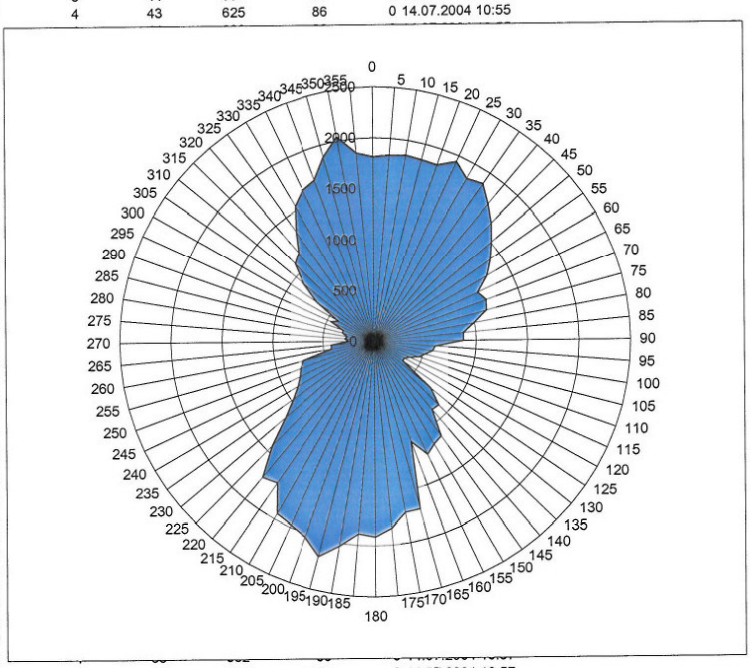

SMC07:

Object - c7_1____, Profile - 1_____,13.07.2006 16:51:42

Picket	ParametrA	ParametrB	ParametrC	ParametrD	ParametrE	Azimuth	Time
0	1511	5	37	414	86	0	13.07.2004 13:05
5	1551	7	40	437	86	0	13.07.2004 13:05
10	1518	7	39	445	86	0	13.07.2004 13:05
15	1524	4	38	413	86	0	13.07.2004 13:05
20	1521						
25	1516						
30	1498						
35	1474						
40	1412						
45	1378						
50	1336						
55	1381						
60	1263						
65	1150						
70	992						
75	705						
80	860						
85	776						
90	505						
95	287						
100	284						
105	362						
110	294						
115	195						
120	203						
125	241						
130	198						
135	537						
140	424						
145	724						
150	1217						
155	1294						
160	1070						
165	1276						
170	1478						
175	1437						
180	1468						
185	1491						
190	1507						
195	1505						
200	1471						
205	1438	13	37	384	86	0	13.07.2004 13:07
210	1448	16	38	439	86	0	13.07.2004 13:07
215	1371	28	37	368	86	0	13.07.2004 13:07
220	1346	33	36	398	86	0	13.07.2004 13:07
225	1000	90	31	229	86	0	13.07.2004 13:07
230	917	105	30	176	86	0	13.07.2004 13:08
235	928	99	30	201	86	0	13.07.2004 13:08
240	1005	93	31	214	86	0	13.07.2004 13:08
245	942	92	30	203	86	0	13.07.2004 13:08
250	565	91	26	72	86	0	13.07.2004 13:08
255	381	54	25	34	86	0	13.07.2004 13:08
260	383	51	25	32	86	0	13.07.2004 13:08
265	390	50	25	31	108	0	13.07.2004 13:08
270	404	48	29	69	105	0	13.07.2004 13:08
275	360	53	25	32	150	0	13.07.2004 13:08
280	472	55	28	86	105	0	13.07.2004 13:08
285	537	67	29	104	86	0	13.07.2004 13:08
290	810	76	28	152	86	0	13.07.2004 13:08
295	792	71	28	155	150	0	13.07.2004 13:08
300	1171	53	30	281	150	0	13.07.2004 13:08
305	1172	50	27	261	150	0	13.07.2004 13:08
310	1324	37	31	322	150	0	13.07.2004 13:08
315	1300	40	30	301	150	0	13.07.2004 13:08
320	1558	17	33	415	150	0	13.07.2004 13:08
325	1654	8	39	497	86	0	13.07.2004 13:08
330	1689	7	39	525	150	0	13.07.2004 13:08
335	1691	2	40	510	150	0	13.07.2004 13:08
340	1609	5	40	479	86	0	13.07.2004 13:08
345	1644	4	41	514	86	0	13.07.2004 13:08
350	1567	5	38	456	86	0	13.07.2004 13:08
355	1614	3	41	495	86	0	13.07.2004 13:09
360	1547	6	38	437	86	0	13.07.2004 13:09

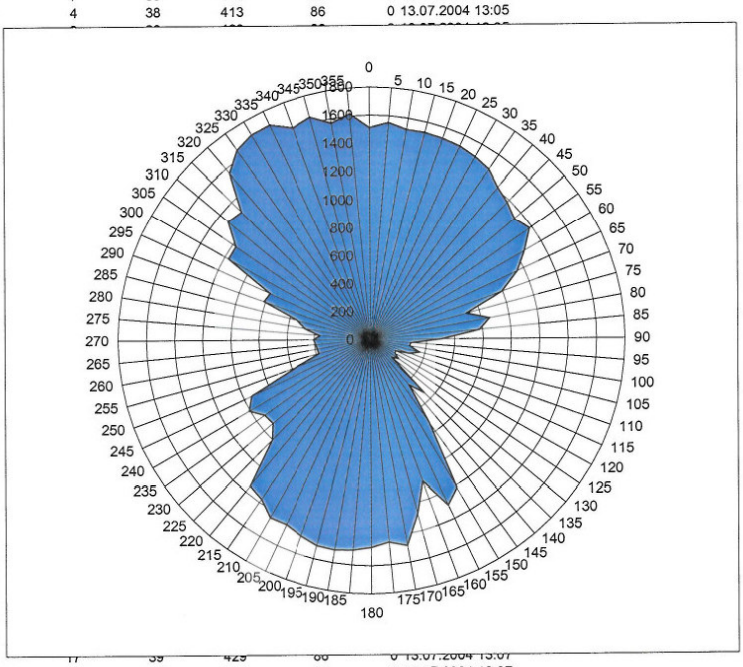

SMR07:

Object - r7_____, Profile - 1_____,13.07.2006 16:51:52

Picket	ParametrA	ParametrB	ParametrC	ParametrD	ParametrE	Azimuth	Time
0	1426	21	36	351	86	0	13.07.2004 13:14
5	1485	10	37	368	86	0	13.07.2004 13:14
10	1476	13	36	373	86	0	13.07.2004 13:14
15	1477	13	38	398	86	0	13.07.2004 13:14
20	1506	7	37	396	86	0	13.07.2004 13:14
25	1524						
30	1470						
35	1455						
40	1448						
45	1384						
50	1330						
55	1316						
60	1232						
65	1135						
70	1008						
75	1000						
80	1015						
85	873						
90	743						
95	578						
100	511						
105	334						
110	322						
115	283						
120	301						
125	319						
130	354						
135	404						
140	555						
145	801						
150	1226						
155	1149						
160	1247						
165	1380						
170	1317						
175	1419						
180	1426						
185	1474						
190	1519						
195	1526						
200	1516						
205	1484						
210	1480	18	40	431	86	0	13.07.2004 13:15
215	1499	13	39	474	86	0	13.07.2004 13:15
220	1353	33	35	369	86	0	13.07.2004 13:15
225	1290	36	35	328	86	0	13.07.2004 13:15
230	1262	47	34	317	86	0	13.07.2004 13:16
235	1193	57	33	278	86	0	13.07.2004 13:16
240	1081	76	33	237	86	0	13.07.2004 13:16
245	877	94	29	161	86	0	13.07.2004 13:16
250	618	97	27	83	105	0	13.07.2004 13:16
255	523	82	27	69	86	0	13.07.2004 13:16
260	448	69	25	41	108	0	13.07.2004 13:16
265	509	71	27	60	105	0	13.07.2004 13:16
270	410	57	25	34	101	0	13.07.2004 13:16
275	306	31	28	27	97	0	13.07.2004 13:16
280	294	32	27	19	90	0	13.07.2004 13:16
285	197	14	22	5	86	0	13.07.2004 13:16
290	236	20	22	9	86	0	13.07.2004 13:16
295	280	31	26	22	82	0	13.07.2004 13:16
300	409	53	28	62	86	0	13.07.2004 13:16
305	456	54	27	66	86	0	13.07.2004 13:16
310	555	62	29	95	82	0	13.07.2004 13:16
315	649	80	31	135	82	0	13.07.2004 13:16
320	929	60	30	182	86	0	13.07.2004 13:16
325	1135	40	32	256	86	0	13.07.2004 13:16
330	1204	46	33	288	86	0	13.07.2004 13:16
335	1232	40	33	274	86	0	13.07.2004 13:16
340	1263	45	33	292	86	0	13.07.2004 13:16
345	1326	46	35	356	86	0	13.07.2004 13:16
350	1355	45	35	331	86	0	13.07.2004 13:16
355	1349	40	35	361	86	0	13.07.2004 13:16
360	1441	33	38	398	86	0	13.07.2004 13:16

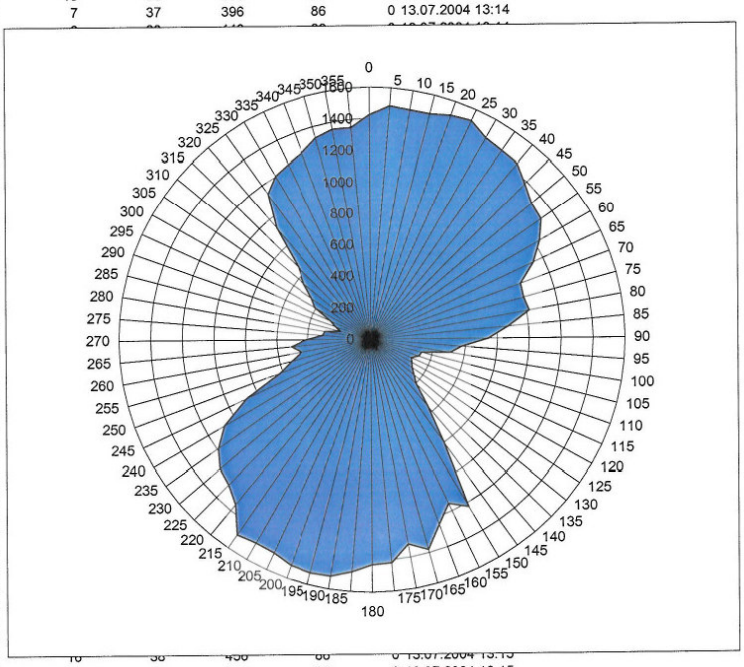

SMLo8:

Object - sm_____, Profile - l8_____,13.07.2006 16:49:05

Picket	ParametrA	ParametrB	ParametrC	ParametrD	ParametrE	Azimuth	Time
0	1755	3	49	741	90	0	13.07.2004 11:29
5	1753	9	46	667	86	0	13.07.2004 11:29
10	1661						
15	1790						
20	1772						
25	1813						
30	1796						
35	1752						
40	1766						
45	1752						
50	1737						
55	1707						
60	1738						
65	1600						
70	1451						
75	1530						
80	1423						
85	1354						
90	1536						
95	1703						
100	1979						
105	2075						
110	2035						
115	2378						
120	2542						
125	2275						
130	1818						
135	2019						
140	1767						
145	1521						
150	1129						
155	1287						
160	1213						
165	1300						
170	1301						
175	1503						
180	1887						
185	2037						
190	1871						
195	1740	4	47	667	90	0	13.07.2004 11:31
200	1824	3	53	828	86	0	13.07.2004 11:31
205	1702	5	48	687	90	0	13.07.2004 11:31
210	1584	29	48	635	90	0	13.07.2004 11:31
215	1612	20	48	654	86	0	13.07.2004 11:31
220	1581	22	47	628	90	0	13.07.2004 11:31
225	1617	24	49	639	90	0	13.07.2004 11:31
230	1547	14	41	517	90	0	13.07.2004 11:31
235	1634	12	42	579	86	0	13.07.2004 11:31
240	1619	19	40	498	86	0	13.07.2004 11:31
245	973	87	29	185	86	0	13.07.2004 11:31
250	890	107	29	163	86	0	13.07.2004 11:31
255	957	100	29	180	90	0	13.07.2004 11:31
260	730	95	26	107	90	0	13.07.2004 11:31
265	701	83	27	125	105	0	13.07.2004 11:31
270	643	99	26	80	86	0	13.07.2004 11:31
275	664	102	27	91	90	0	13.07.2004 11:31
280	856	99	28	148	90	0	13.07.2004 11:31
285	721	89	26	117	90	0	13.07.2004 11:31
290	698	94	26	109	153	0	13.07.2004 11:31
295	874	82	29	164	86	0	13.07.2004 11:31
300	904	81	28	175	150	0	13.07.2004 11:31
305	1082	60	30	261	150	0	13.07.2004 11:31
310	900	86	29	182	150	0	13.07.2004 11:31
315	1110	58	31	255	86	0	13.07.2004 11:32
320	964	72	29	188	86	0	13.07.2004 11:32
325	1063	77	31	211	86	0	13.07.2004 11:32
330	1363	35	36	359	90	0	13.07.2004 11:32
335	1743	6	44	578	150	0	13.07.2004 11:32
340	1618	11	40	489	86	0	13.07.2004 11:32
345	1656	4	41	523	86	0	13.07.2004 11:32
350	1670	11	42	530	86	0	13.07.2004 11:32
355	1796	5	46	662	86	0	13.07.2004 11:32
360	1797	3	47	678	90	0	13.07.2004 11:32

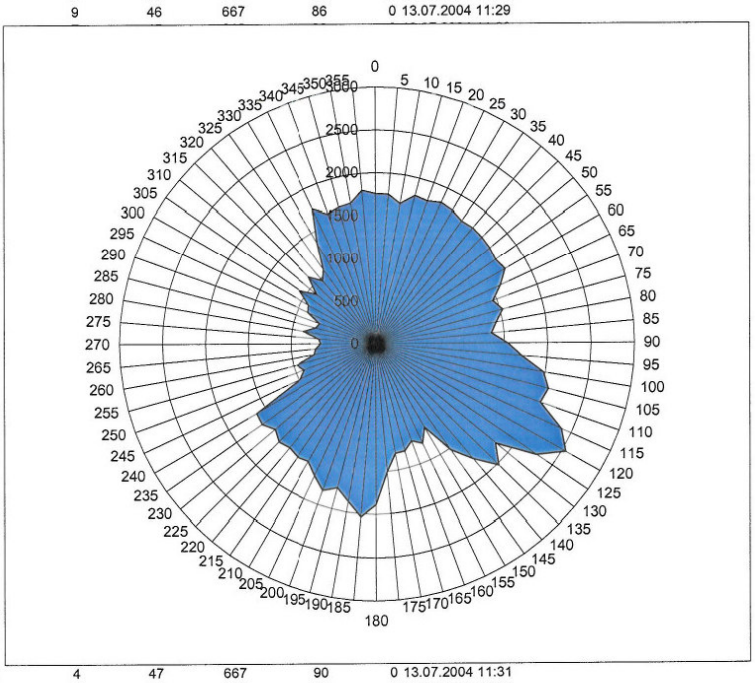

SML08:

Object - I8_____, Profile - 2_____,14.07.2006 15:22:38

Picket	ParametrA	ParametrB	ParametrC	ParametrD	ParametrE	Azimuth	Time
0	1353	40	34	327	86	0	14.07.2004 08:33
5	1586	15	37	430	86	0	14.07.2004 08:34
10	1675	10	40	479	86	0	14.07.2004 08:34
15	1755						
20	1733						
25	1692						
30	1817						
35	1788						
40	1926						
45	2035						
50	2071						
55	2197						
60	2310						
65	2372						
70	2414						
75	2356						
80	2355						
85	2351						
90	2292						
95	2219						
100	2245						
105	2219						
110	2170						
115	2075						
120	2112						
125	1992						
130	2007						
135	1840						
140	1318						
145	1386						
150	1024						
155	1129						
160	1097						
165	1120						
170	1158						
175	1254						
180	1361						
185	1393						
190	1367						
195	1543						
200	1608	18	40	476	86	0	14.07.2004 08:35
205	1843	4	43	591	86	0	14.07.2004 08:35
210	1713	11	39	470	86	0	14.07.2004 08:35
215	1669	22	39	444	86	0	14.07.2004 08:35
220	1635	17	37	412	86	0	14.07.2004 08:35
225	1642	19	37	411	86	0	14.07.2004 08:35
230	1544	24	35	371	86	0	14.07.2004 08:35
235	1579	19	35	386	90	0	14.07.2004 08:35
240	1593	28	36	393	90	0	14.07.2004 08:35
245	1276	42	31	284	150	0	14.07.2004 08:35
250	1205	64	30	235	93	0	14.07.2004 08:35
255	1101	69	30	206	90	0	14.07.2004 08:35
260	1506	32	33	316	90	0	14.07.2004 08:35
265	1018	73	29	181	90	0	14.07.2004 08:35
270	1013	77	29	183	93	0	14.07.2004 08:35
275	824	89	27	117	108	0	14.07.2004 08:35
280	633	92	26	77	90	0	14.07.2004 08:35
285	438	57	24	34	90	0	14.07.2004 08:36
290	821	98	28	133	150	0	14.07.2004 08:36
295	1121	66	31	235	150	0	14.07.2004 08:36
300	1181	57	30	247	150	0	14.07.2004 08:36
305	932	88	28	175	150	0	14.07.2004 08:36
310	694	89	27	107	86	0	14.07.2004 08:36
315	653	81	26	89	86	0	14.07.2004 08:36
320	672	85	27	98	86	0	14.07.2004 08:36
325	846	84	29	146	90	0	14.07.2004 08:36
330	1150	72	31	243	86	0	14.07.2004 08:36
335	1246	50	31	271	90	0	14.07.2004 08:36
340	1311	43	33	310	86	0	14.07.2004 08:36
345	1681	21	39	431	86	0	14.07.2004 08:36
350	1520	33	38	427	90	0	14.07.2004 08:36
355	1512	25	38	432	86	0	14.07.2004 08:36

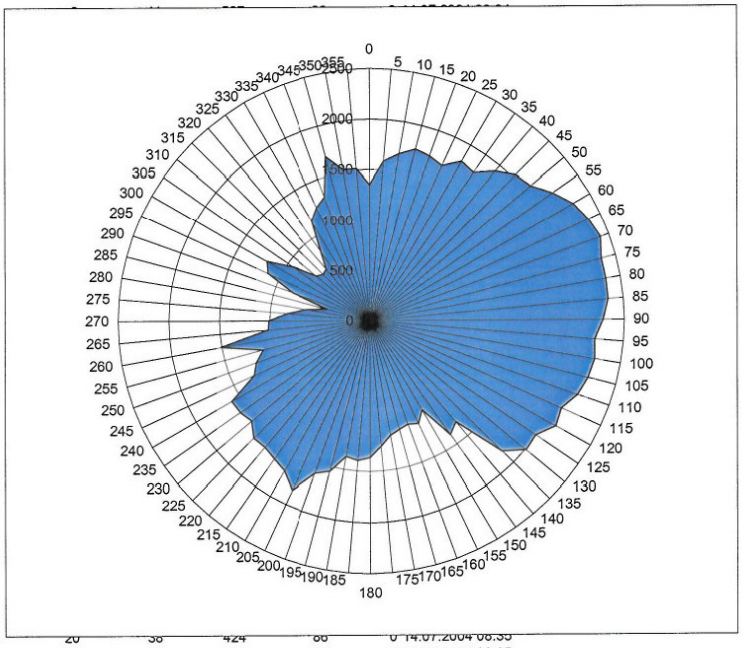

SMCo8:

Object - c8_____, Profile - 1_____,13.07.2006 16:50:51

Picket	ParametrA	ParametrB	ParametrC	ParametrD	ParametrE	Azimuth	Time
0	3012	1	81	1691	225	0	13.07.2004 12:40
5	2638	1	67	1280	225	0	13.07.2004 12:40
10	2380	1	63	1137	150	0	13.07.2004 12:40
15	2810						
20	2476						
25	2070						
30	1833						
35	1900						
40	1793						
45	1770						
50	1696						
55	1611						
60	1733						
65	1609						
70	1625						
75	1501						
80	1517						
85	1591						
90	1415						
95	1185						
100	910						
105	607						
110	490						
115	473						
120	456						
125	395						
130	481						
135	570						
140	752						
145	1111						
150	1585						
155	1672						
160	1731						
165	1991						
170	1984						
175	2453						
180	2447						
185	2492						
190	2780						
195	2659						
200	2516	1	91	2030	150	0	13.07.2004 12:41
205	2567	1	89	1938	150	0	13.07.2004 12:41
210	2435	1	67	1260	150	0	13.07.2004 12:41
215	2376	1	69	1314	150	0	13.07.2004 12:41
220	2366	1	72	1407	150	0	13.07.2004 12:41
225	2092	1	61	1059	150	0	13.07.2004 12:42
230	1956	4	48	721	150	0	13.07.2004 12:42
235	1876	3	43	593	150	0	13.07.2004 12:42
240	2245	1	52	840	150	0	13.07.2004 12:42
245	2230	1	50	799	150	0	13.07.2004 12:42
250	2152	1	47	702	150	0	13.07.2004 12:42
255	2319	1	52	833	150	0	13.07.2004 12:42
260	2207	3	49	755	150	0	13.07.2004 12:42
265	2399	1	54	903	150	0	13.07.2004 12:42
270	2677	1	64	1202	150	0	13.07.2004 12:42
275	2926	1	70	1337	150	0	13.07.2004 12:42
280	3032	1	76	1542	150	0	13.07.2004 12:42
285	3048	1	82	1723	150	0	13.07.2004 12:42
290	3003	1	76	1557	150	0	13.07.2004 12:42
295	3050	1	77	1604	150	0	13.07.2004 12:42
300	2993	1	81	1717	150	0	13.07.2004 12:42
305	2987	1	83	1761	150	0	13.07.2004 12:42
310	2649	1	84	1784	150	0	13.07.2004 12:42
315	2750	1	96	2184	150	0	13.07.2004 12:42
320	2605	1	84	1796	75	0	13.07.2004 12:42
325	2655	1	83	1773	150	0	13.07.2004 12:42
330	2701	1	80	1689	150	0	13.07.2004 12:42
335	2655	1	80	1671	150	0	13.07.2004 12:42
340	2633	1	80	1668	150	0	13.07.2004 12:42
345	2605	1	80	1678	150	0	13.07.2004 12:42
350	2555	1	77	1595	150	0	13.07.2004 12:42
355	2629	1	72	1414	150	0	13.07.2004 12:42
360	2413	1	67	1268	150	0	13.07.2004 12:43

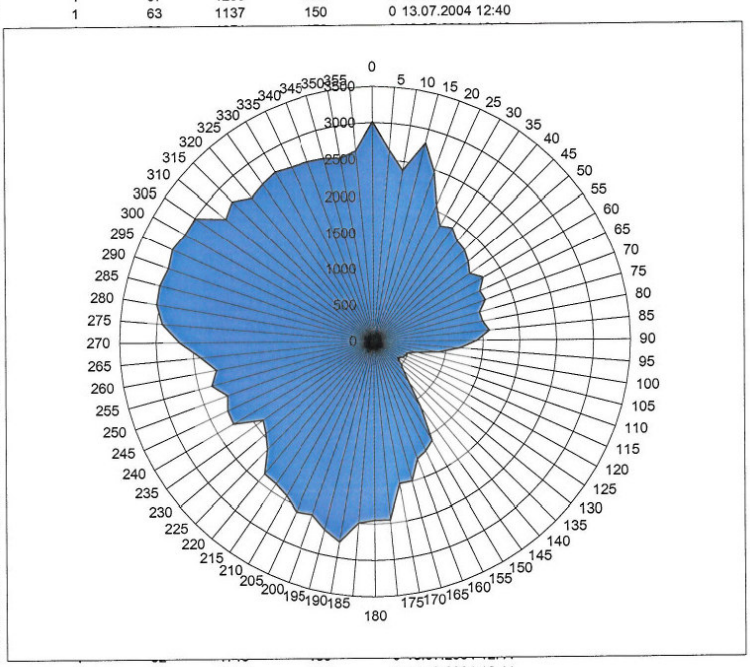

SMCo8:

Object - c8_____, Profile - 2_____,14.07.2006 15:40:12

Picket	ParametrA	ParametrB	ParametrC	ParametrD	ParametrE	Azimuth	Time
0	2006	2	55	920	150	0	14.07.2004 10:49
5	2113	2	55	889	150	0	14.07.2004 10:49
10	2121	1	56	933	150	0	14.07.2004 10:49
15	2371	2	61	1097	150	0	14.07.2004 10:49
20	1895						
25	1603						
30	1665						
35	1619						
40	1553						
45	1532						
50	1319						
55	1216						
60	1163						
65	1087						
70	1013						
75	892						
80	760						
85	716						
90	886						
95	705						
100	515						
105	320						
110	250						
115	265						
120	407						
125	481						
130	632						
135	1092						
140	1136						
145	1478						
150	1738						
155	1882						
160	1969						
165	2137						
170	2160						
175	2198						
180	2062						
185	1920						
190	1949						
195	1947						
200	2079						
205	2265	1	60	1043	150	0	14.07.2004 10:51
210	2355	1	64	1182	150	0	14.07.2004 10:51
215	1899	3	50	792	75	0	14.07.2004 10:51
220	1564	12	38	447	86	0	14.07.2004 10:51
225	1471	28	39	411	86	0	14.07.2004 10:51
230	1211	52	32	266	86	0	14.07.2004 10:51
235	1066	73	30	201	86	0	14.07.2004 10:51
240	1071	87	31	214	86	0	14.07.2004 10:51
245	959	99	29	176	86	0	14.07.2004 10:51
250	785	109	27	119	86	0	14.07.2004 10:51
255	575	83	26	61	90	0	14.07.2004 10:51
260	528	88	26	53	86	0	14.07.2004 10:51
265	450	66	25	36	105	0	14.07.2004 10:51
270	500	78	25	45	108	0	14.07.2004 10:51
275	1049	51	25	185	150	0	14.07.2004 10:51
280	1603	7	35	507	150	0	14.07.2004 10:51
285	1826	1	45	655	150	0	14.07.2004 10:51
290	1902	2	51	798	150	0	14.07.2004 10:51
295	1970	1	53	857	150	0	14.07.2004 10:51
300	1913	1	57	980	150	0	14.07.2004 10:51
305	2089	1	61	1100	150	0	14.07.2004 10:51
310	2263	1	63	1151	150	0	14.07.2004 10:52
315	2065	1	63	1149	150	0	14.07.2004 10:52
320	2208	1	64	1180	150	0	14.07.2004 10:52
325	2295	1	64	1181	150	0	14.07.2004 10:52
330	2266	1	62	1125	150	0	14.07.2004 10:52
335	2302	1	66	1217	150	0	14.07.2004 10:52
340	2140	1	63	1151	150	0	14.07.2004 10:52
345	2205	2	62	1069	150	0	14.07.2004 10:52
350	2041	3	56	1005	150	0	14.07.2004 10:52
355	2347	1	61	1071	150	0	14.07.2004 10:52
360	2222	3	57	965	150	0	14.07.2004 10:52

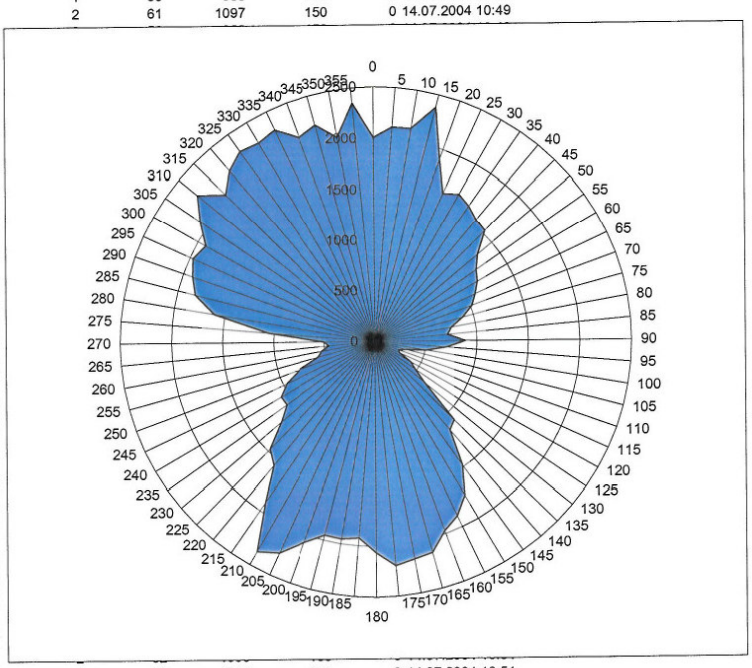

SMR08:

Object - r8_____, Profile - 1_____,13.07.2006 16:52:05

Picket	ParametrA	ParametrB	ParametrC	ParametrD	ParametrE	Azimuth	Time
0	1712	3	43	565	86	0	13.07.2004 13:25
5	1785	3	44	570	150	0	13.07.2004 13:25
10	1977	3	50	727	86	0	13.07.2004 13:25
15	2336	1	56	928	86	0	13.07.2004 13:25
20	2225	1	55	913	86	0	13.07.2004 13:25
25	2202						
30	2317						
35	2207						
40	2377						
45	2481						
50	2365						
55	2012						
60	2052						
65	2013						
70	2248						
75	1892						
80	1866						
85	2052						
90	2060						
95	1732						
100	1730						
105	1386						
110	901						
115	952						
120	588						
125	393						
130	377						
135	470						
140	503						
145	823						
150	1045						
155	1141						
160	1144						
165	1186						
170	1352						
175	1494						
180	1468						
185	1507						
190	1542						
195	1573						
200	1564						
205	1586						
210	1597	6	40	467	86	0	13.07.2004 13:27
215	1616	4	40	469	86	0	13.07.2004 13:27
220	1574	8	40	461	86	0	13.07.2004 13:27
225	1553	13	38	432	86	0	13.07.2004 13:27
230	1452	29	37	371	86	0	13.07.2004 13:27
235	1449	33	35	368	86	0	13.07.2004 13:27
240	1243	57	31	267	86	0	13.07.2004 13:27
245	1166	67	31	240	86	0	13.07.2004 13:27
250	1152	62	30	236	86	0	13.07.2004 13:27
255	1029	82	29	188	86	0	13.07.2004 13:27
260	1010	80	30	265	150	0	13.07.2004 13:27
265	1027	80	29	197	150	0	13.07.2004 13:27
270	710	89	26	107	75	0	13.07.2004 13:27
275	792	88	27	135	150	0	13.07.2004 13:27
280	647	80	28	125	90	0	13.07.2004 13:27
285	563	84	25	67	150	0	13.07.2004 13:27
290	765	86	28	137	150	0	13.07.2004 13:27
295	605	85	26	78	150	0	13.07.2004 13:27
300	932	84	28	179	150	0	13.07.2004 13:27
305	934	83	30	190	150	0	13.07.2004 13:27
310	984	76	28	198	86	0	13.07.2004 13:27
315	1044	81	30	219	86	0	13.07.2004 13:27
320	1510	31	33	407	150	0	13.07.2004 13:27
325	1258	31	32	286	86	0	13.07.2004 13:27
330	1645	4	39	501	86	0	13.07.2004 13:27
335	1561	12	37	424	86	0	13.07.2004 13:27
340	1700	2	41	520	86	0	13.07.2004 13:27
345	1670	2	41	510	150	0	13.07.2004 13:27
350	1882	1	47	680	150	0	13.07.2004 13:27
355	1850	1	46	646	150	0	13.07.2004 13:27

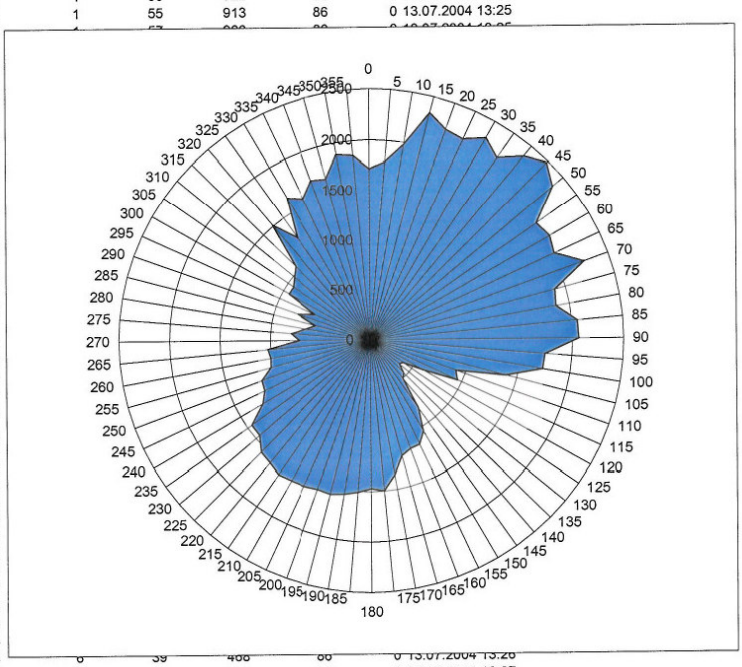

SMLog:

Object - sm_____, Profile - l9_____,13.07.2006 16:49:18

Picket	ParametrA	ParametrB	ParametrC	ParametrD	ParametrE	Azimuth	Time
0	2645	1	101	2367	168	0	13.07.2004 11:36
5	2489	3	97	2365	135	0	13.07.2004 11:36
10	2574	1	98	2282	161	0	13.07.2004 11:36
15	2538						
20	2646						
25	2700						
30	2587						
35	2639						
40	2577						
45	2597						
50	2600						
55	2618						
60	2563						
65	2334						
70	2229						
75	2239						
80	2090						
85	1919						
90	1622						
95	1340						
100	1129						
105	1344						
110	1043						
115	1270						
120	1881						
125	2504						
130	2446						
135	2550						
140	2534						
145	2590						
150	2609						
155	2640						
160	2732						
165	2633						
170	2695						
175	2724						
180	2701						
185	2683						
190	2717						
195	2701						
200	2615	1	93	2101	112	0	13.07.2004 11:38
205	2453	1	96	2207	90	0	13.07.2004 11:38
210	2579	1	85	1829	93	0	13.07.2004 11:38
215	2044	1	62	1092	90	0	13.07.2004 11:38
220	1987	2	53	858	90	0	13.07.2004 11:39
225	1866	5	50	798	86	0	13.07.2004 11:39
230	1778	3	49	728	86	0	13.07.2004 11:39
235	2196	1	61	1070	75	0	13.07.2004 11:39
240	1835	1	52	822	90	0	13.07.2004 11:39
245	2578	1	75	1495	75	0	13.07.2004 11:39
250	2499	1	81	1683	75	0	13.07.2004 11:39
255	2558	1	84	1764	75	0	13.07.2004 11:39
260	2584	1	90	1957	75	0	13.07.2004 11:39
265	2646	1	87	1865	150	0	13.07.2004 11:39
270	2581	1	93	2104	150	0	13.07.2004 11:39
275	2465	1	92	2047	150	0	13.07.2004 11:39
280	2850	1	82	1745	150	0	13.07.2004 11:39
285	2936	1	80	1684	150	0	13.07.2004 11:39
290	2862	1	79	1644	150	0	13.07.2004 11:39
295	2839	1	78	1604	150	0	13.07.2004 11:39
300	2829	1	84	1807	150	0	13.07.2004 11:39
305	2590	1	84	1805	75	0	13.07.2004 11:39
310	2593	1	83	1768	150	0	13.07.2004 11:39
315	2562	1	86	1861	75	0	13.07.2004 11:39
320	2716	1	94	2114	150	0	13.07.2004 11:39
325	2765	1	98	2261	142	0	13.07.2004 11:40
330	2603	1	95	2154	150	0	13.07.2004 11:40
335	2555	1	100	2333	90	0	13.07.2004 11:40
340	2690	1	97	2232	157	0	13.07.2004 11:40
345	2519	2	99	2281	90	0	13.07.2004 11:40
350	2612	1	97	2247	191	0	13.07.2004 11:40
355	2536	1	102	2401	150	0	13.07.2004 11:40
360	2658	1	99	2296	90	0	13.07.2004 11:40

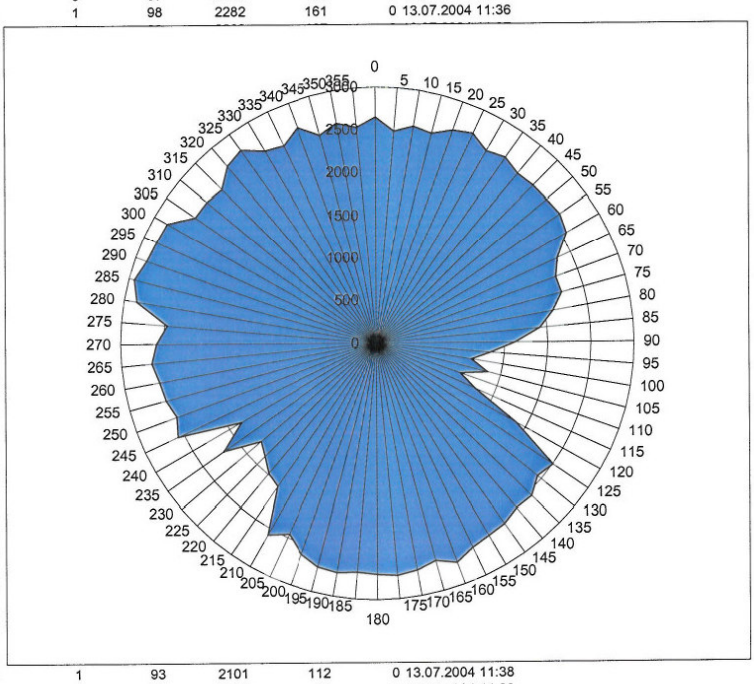

SMLog:

Object - I9_____, Profile - 2_____,14.07.2006 15:25:19

Picket	ParametrA	ParametrB	ParametrC	ParametrD	ParametrE	Azimuth	Time
0	3422	1	88	1937	210	0	14.07.2004 08:42
5	3391	3	88	1958	210	0	14.07.2004 08:42
10	3473	1	87	1894	210	0	14.07.2004 08:42
15	3451						
20	3458						
25	3381						
30	3366						
35	3435						
40	3318						
45	3330						
50	3473						
55	3350						
60	3510						
65	3548						
70	3440						
75	3527						
80	3517						
85	3524						
90	3488						
95	3449						
100	3412						
105	3283						
110	2742						
115	3446						
120	1950						
125	1377						
130	2790						
135	1947						
140	1732						
145	2052						
150	2008						
155	2202						
160	2517						
165	2499						
170	2842						
175	3262						
180	3376						
185	3427						
190	3546						
195	3534						
200	3549	1	89	1938	213	0	14.07.2004 08:44
205	3498	1	89	1944	213	0	14.07.2004 08:44
210	3475	1	89	1951	210	0	14.07.2004 08:44
215	3494	1	89	1948	213	0	14.07.2004 08:44
220	3457	1	89	1946	213	0	14.07.2004 08:44
225	3444	1	90	1994	213	0	14.07.2004 08:45
230	3182	1	79	1619	225	0	14.07.2004 08:45
235	3307	1	89	1970	225	0	14.07.2004 08:45
240	3323	1	87	1900	225	0	14.07.2004 08:45
245	3110	1	87	1882	225	0	14.07.2004 08:45
250	2755	1	87	1898	225	0	14.07.2004 08:45
255	2550	1	87	1921	150	0	14.07.2004 08:45
260	2616	1	90	2014	150	0	14.07.2004 08:45
265	2714	1	90	1999	225	0	14.07.2004 08:45
270	2727	1	92	2069	225	0	14.07.2004 08:45
275	2731	1	92	2080	150	0	14.07.2004 08:45
280	2738	1	92	2086	150	0	14.07.2004 08:45
285	2752	1	92	2079	225	0	14.07.2004 08:45
290	2719	1	93	2119	225	0	14.07.2004 08:45
295	2724	1	91	2054	150	0	14.07.2004 08:45
300	2367	1	87	1928	150	0	14.07.2004 08:45
305	2391	1	86	1887	150	0	14.07.2004 08:45
310	2082	1	79	1663	150	0	14.07.2004 08:46
315	1917	1	78	1629	150	0	14.07.2004 08:46
320	2154	1	77	1597	225	0	14.07.2004 08:46
325	2588	1	74	1495	225	0	14.07.2004 08:46
330	2496	1	77	1571	225	0	14.07.2004 08:46
335	2531	1	77	1563	225	0	14.07.2004 08:46
340	2300	1	75	1517	150	0	14.07.2004 08:46
345	2728	1	74	1489	225	0	14.07.2004 08:46
350	3221	1	75	1524	225	0	14.07.2004 08:46
355	3421	1	84	1797	217	0	14.07.2004 08:46
360	3419	1	85	1818	210	0	14.07.2004 08:46
365	3427	3	86	1846	213	0	14.07.2004 08:46
370	3380	2	86	1875	213	0	14.07.2004 08:46

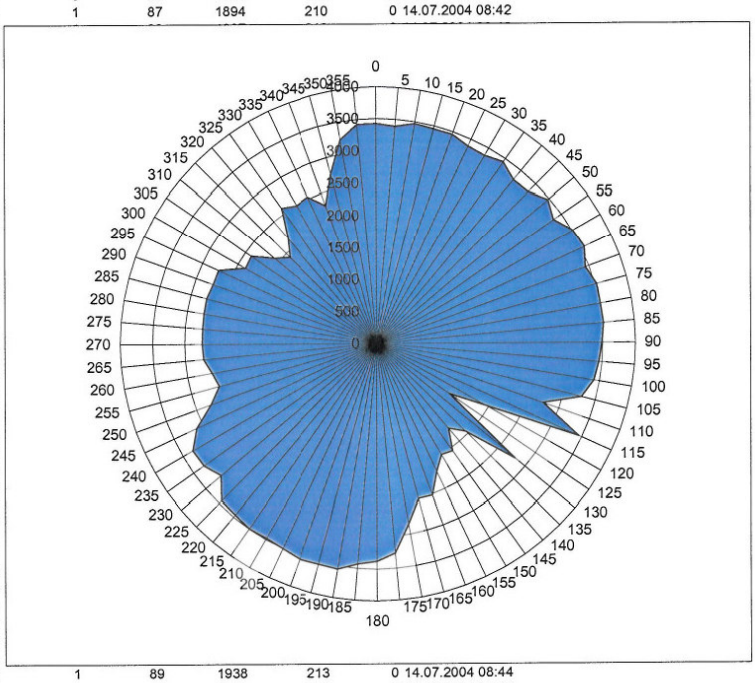

SMCo9:

Object - c9_____, Profile - 1_____,13.07.2006 16:50:37

Picket	ParametrA	ParametrB	ParametrC	ParametrD	ParametrE	Azimuth	Time
0	2940	1	83	1761	150	0	13.07.2004 12:34
5	2824	1	77	1566	150	0	13.07.2004 12:34
10	2519	1	69	1316	150	0	13.07.2004 12:34
15	2544	1	70	1346	86	0	13.07.2004 12:34
20	2412						
25	2371						
30	2444						
35	2407						
40	2348						
45	2248						
50	2004						
55	1897						
60	1848						
65	1696						
70	1604						
75	1533						
80	1499						
85	1180						
90	973						
95	824						
100	833						
105	642						
110	415						
115	239						
120	243						
125	252						
130	290						
135	509						
140	1395						
145	1897						
150	2541						
155	2644						
160	2774						
165	2717						
170	2922						
175	2840						
180	2752						
185	2766						
190	2809						
195	2690						
200	2720						
205	2790	1	82	1737	150	0	13.07.2004 12:36
210	2714	1	77	1568	150	0	13.07.2004 12:36
215	2558	1	72	1429	150	0	13.07.2004 12:36
220	2694	1	76	1526	150	0	13.07.2004 12:36
225	2735	1	81	1711	150	0	13.07.2004 12:36
230	2453	1	68	1273	150	0	13.07.2004 12:36
235	2415	1	64	1193	150	0	13.07.2004 12:36
240	2362	1	62	1134	150	0	13.07.2004 12:36
245	2467	1	61	1097	150	0	13.07.2004 12:36
250	2774	1	68	1287	150	0	13.07.2004 12:36
255	2558	2	59	1021	150	0	13.07.2004 12:36
260	2595	1	65	1168	150	0	13.07.2004 12:36
265	2721	1	65	1211	150	0	13.07.2004 12:36
270	2930	1	75	1503	150	0	13.07.2004 12:36
275	2951	1	88	1933	150	0	13.07.2004 12:36
280	3061	1	83	1755	150	0	13.07.2004 12:36
285	2638	1	88	1917	150	0	13.07.2004 12:37
290	2640	1	89	1935	150	0	13.07.2004 12:37
295	2576	1	91	2006	75	0	13.07.2004 12:37
300	2543	1	93	2067	75	0	13.07.2004 12:37
305	2555	1	92	2044	75	0	13.07.2004 12:37
310	2512	1	94	2112	75	0	13.07.2004 12:37
315	2992	1	94	2139	150	0	13.07.2004 12:37
320	2493	1	97	2225	75	0	13.07.2004 12:37
325	2692	1	91	2042	150	0	13.07.2004 12:37
330	2691	1	90	1973	75	0	13.07.2004 12:37
335	2636	1	88	1921	75	0	13.07.2004 12:37
340	2812	1	85	1817	150	0	13.07.2004 12:37
345	2845	1	85	1836	150	0	13.07.2004 12:37
350	2755	1	81	1702	150	0	13.07.2004 12:37
355	2818	1	78	1596	150	0	13.07.2004 12:37
360	2724	1	76	1527	150	0	13.07.2004 12:37

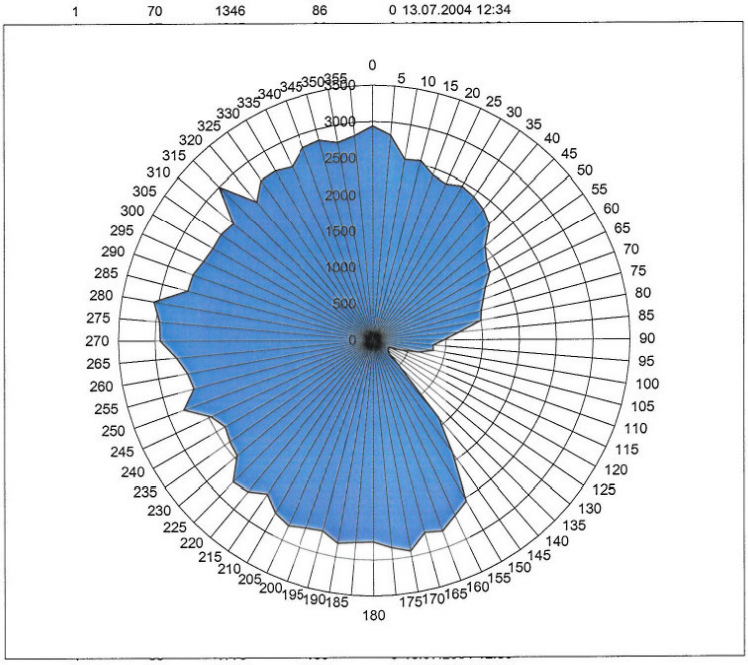

SMCog:

Object - c9 , Profile - 1 ,14.07.2006 15:38:25

Picket	ParametrA	ParametrB	ParametrC	ParametrD	ParametrE	Azimuth	Time
0	2254	2	52	822	86	0	14.07.2004 10:45
5	2272	2	53	865	86	0	14.07.2004 10:45
10	2310	3	55	920	90	0	14.07.2004 10:45
15	2222	2	55	911	90	0	14.07.2004 10:45
20	2287						
25	2347						
30	2230						
35	2144						
40	2261						
45	2097						
50	1859						
55	1698						
60	1618						
65	1376						
70	1191						
75	1138						
80	973						
85	864						
90	893						
95	928						
100	694						
105	911						
110	916						
115	910						
120	1109						
125	1509						
130	1459						
135	1752						
140	1885						
145	1972						
150	2046						
155	2117						
160	2255						
165	2234						
170	2309						
175	2163						
180	2181						
185	2160						
190	2201						
195	2156						
200	2128						
205	2068	3	51	773	86	0	14.07.2004 10:46
210	1776	6	43	575	86	0	14.07.2004 10:46
215	1798	5	45	600	86	0	14.07.2004 10:46
220	1742	3	44	558	86	0	14.07.2004 10:46
225	1400	26	36	366	86	0	14.07.2004 10:46
230	1287	42	34	299	86	0	14.07.2004 10:46
235	1131	69	32	250	86	0	14.07.2004 10:47
240	1082	78	32	237	86	0	14.07.2004 10:47
245	937	89	29	171	86	0	14.07.2004 10:47
250	884	101	29	156	86	0	14.07.2004 10:47
255	776	104	28	117	90	0	14.07.2004 10:47
260	846	103	28	137	86	0	14.07.2004 10:47
265	859	96	28	139	86	0	14.07.2004 10:47
270	1347	28	31	305	150	0	14.07.2004 10:47
275	1470	26	31	357	150	0	14.07.2004 10:47
280	1785	7	38	520	150	0	14.07.2004 10:47
285	1861	7	41	604	150	0	14.07.2004 10:47
290	2093	7	46	728	150	0	14.07.2004 10:47
295	2030	7	41	670	150	0	14.07.2004 10:47
300	2158	3	48	717	150	0	14.07.2004 10:47
305	2220	5	46	708	150	0	14.07.2004 10:47
310	2172	5	45	676	150	0	14.07.2004 10:47
315	2347	2	51	805	225	0	14.07.2004 10:47
320	2440	2	57	944	150	0	14.07.2004 10:47
325	2392	2	52	890	86	0	14.07.2004 10:47
330	2739	1	63	1121	90	0	14.07.2004 10:47
335	2441	2	58	1012	90	0	14.07.2004 10:47
340	2571	1	61	1077	86	0	14.07.2004 10:47
345	2625	1	62	1098	86	0	14.07.2004 10:47
350	2448	1	57	956	86	0	14.07.2004 10:47
355	2411	1	57	974	86	0	14.07.2004 10:47

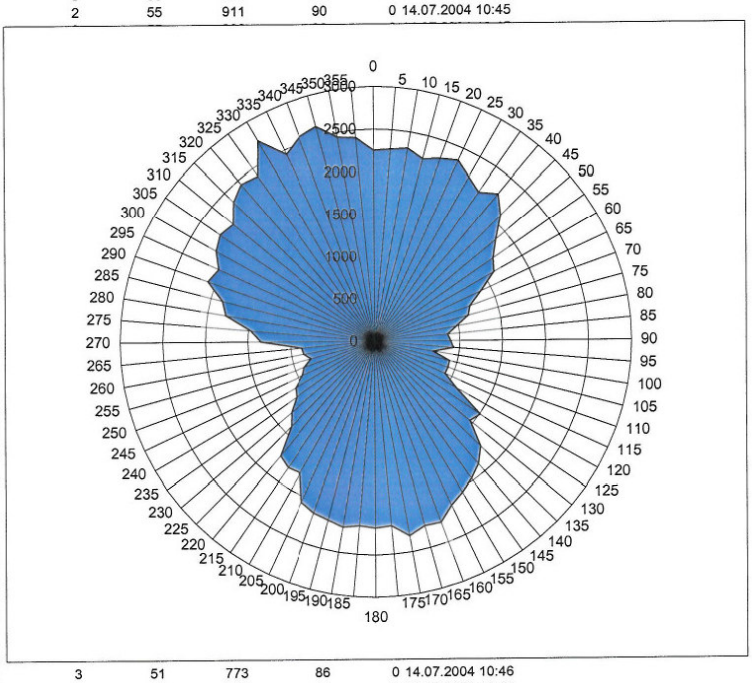

SMR09:

Object - r9_____, Profile - 1_____,13.07.2006 16:52:42

Picket	ParametrA	ParametrB	ParametrC	ParametrD	ParametrE	Azimuth	Time
0	1826	1	47	685	150	0	13.07.2004 13:37
5	1886	1	49	732	150	0	13.07.2004 13:37
10	1868	2	48	707	86	0	13.07.2004 13:37
15	1854	2	48	697	86	0	13.07.2004 13:37
20	1831						
25	1916						
30	1897						
35	1878						
40	1834						
45	1821						
50	1831						
55	1723						
60	1758						
65	1668						
70	1664						
75	1644						
80	1527						
85	1421						
90	1502						
95	1284						
100	1224						
105	689						
110	571						
115	655						
120	839						
125	349						
130	314						
135	959						
140	1029						
145	700						
150	783						
155	1002						
160	1350						
165	1738						
170	1773						
175	1663						
180	1687						
185	1702						
190	1721						
195	1888						
200	2234	2	54	836	86	0	13.07.2004 13:38
205	2041	3	50	793	86	0	13.07.2004 13:38
210	1981	4	45	703	86	0	13.07.2004 13:39
215	1938	7	47	726	86	0	13.07.2004 13:39
220	1998	5	46	671	86	0	13.07.2004 13:39
225	2031	10	48	717	86	0	13.07.2004 13:39
230	2199	5	49	790	86	0	13.07.2004 13:39
235	1992	7	42	668	86	0	13.07.2004 13:39
240	1808	17	40	578	86	0	13.07.2004 13:39
245	1820	20	38	553	86	0	13.07.2004 13:39
250	1585	21	36	427	86	0	13.07.2004 13:39
255	1207	61	32	273	86	0	13.07.2004 13:39
260	971	85	29	181	86	0	13.07.2004 13:39
265	823	112	27	143	112	0	13.07.2004 13:39
270	1177	65	29	336	93	0	13.07.2004 13:39
275	1343	31	32	309	225	0	13.07.2004 13:39
280	1043	58	27	197	75	0	13.07.2004 13:39
285	1464	18	31	418	150	0	13.07.2004 13:39
290	1354	26	31	322	150	0	13.07.2004 13:39
295	1718	18	36	505	150	0	13.07.2004 13:39
300	1754	12	38	573	150	0	13.07.2004 13:39
305	1829	4	47	702	150	0	13.07.2004 13:39
310	1813	2	49	771	150	0	13.07.2004 13:39
315	2066	2	55	889	150	0	13.07.2004 13:39
320	2054	2	60	1080	150	0	13.07.2004 13:39
325	1968	1	57	979	150	0	13.07.2004 13:39
330	1975	1	60	1062	150	0	13.07.2004 13:39
335	1950	1	55	927	150	0	13.07.2004 13:40
340	2040	1	61	1071	150	0	13.07.2004 13:40
345	2028	1	56	945	150	0	13.07.2004 13:40
350	2022	1	56	933	150	0	13.07.2004 13:40
355	1981	1	54	870	75	0	13.07.2004 13:40

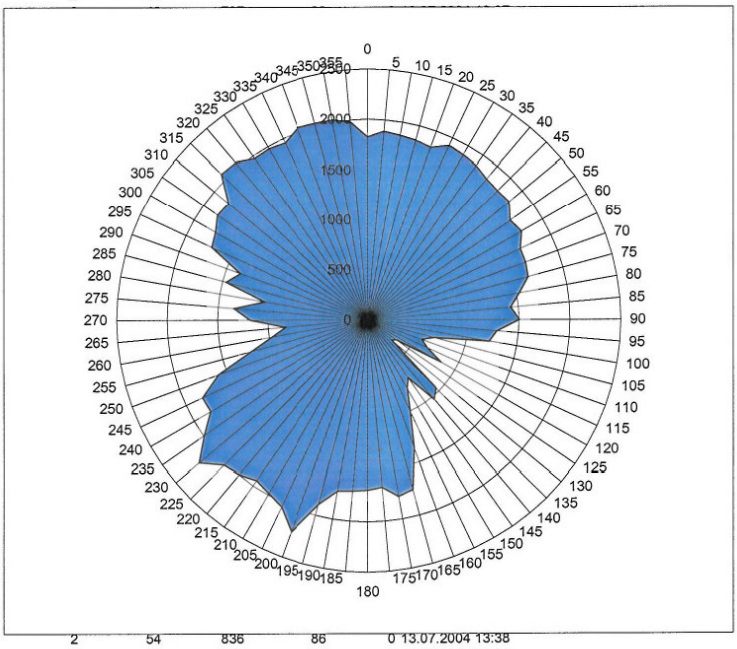

SML10:

Object - I10 , Profile - 1 ,13.07.2006 16:50:02

Picket	ParametrA	ParametrB	ParametrC	ParametrD	ParametrE	Azimuth	Time
0	1660	6	48	688	86	0	13.07.2004 11:43
5	1676	14	49	692	86	0	13.07.2004 11:43
10	1698						
15	1728						
20	1730						
25	1814						
30	1745						
35	1766						
40	1813						
45	1769						
50	1819						
55	1716						
60	1656						
65	1619						
70	1700						
75	1751						
80	1878						
85	1771						
90	1724						
95	1072						
100	1111						
105	1281						
110	1038						
115	1063						
120	823						
125	1264						
130	565						
135	536						
140	856						
145	1196						
150	1307						
155	1757						
160	1541						
165	1559						
170	1663						
175	1750						
180	1805						
185	1833						
190	1708						
195	1626	18	52	708	90	0	13.07.2004 11:44
200	1678	3	47	651	86	0	13.07.2004 11:44
205	1684	10	49	684	90	0	13.07.2004 11:44
210	1680	6	53	754	86	0	13.07.2004 11:45
215	1680	10	50	728	86	0	13.07.2004 11:45
220	1588	12	44	609	86	0	13.07.2004 11:45
225	1542	24	47	606	86	0	13.07.2004 11:45
230	1562	21	43	536	90	0	13.07.2004 11:45
235	1480	33	41	483	86	0	13.07.2004 11:45
240	1351	42	37	383	86	0	13.07.2004 11:45
245	1345	47	37	381	86	0	13.07.2004 11:45
250	1328	44	37	361	86	0	13.07.2004 11:45
255	1106	81	32	247	86	0	13.07.2004 11:45
260	1174	78	34	314	90	0	13.07.2004 11:45
265	710	91	27	106	150	0	13.07.2004 11:45
270	681	94	27	90	90	0	13.07.2004 11:45
275	571	86	26	70	93	0	13.07.2004 11:45
280	518	69	27	66	150	0	13.07.2004 11:45
285	491	68	26	51	150	0	13.07.2004 11:45
290	929	75	28	182	150	0	13.07.2004 11:45
295	601	81	26	83	90	0	13.07.2004 11:45
300	449	58	26	45	86	0	13.07.2004 11:45
305	581	71	27	80	86	0	13.07.2004 11:45
310	1005	63	31	218	86	0	13.07.2004 11:45
315	1102	68	33	252	86	0	13.07.2004 11:45
320	1247	68	38	345	90	0	13.07.2004 11:45
325	1353	48	38	374	86	0	13.07.2004 11:45
330	1491	9	37	437	86	0	13.07.2004 11:45
335	1496	29	42	487	86	0	13.07.2004 11:46
340	1561	14	43	524	90	0	13.07.2004 11:46
345	1504	27	41	468	86	0	13.07.2004 11:46
350	1480	23	43	508	86	0	13.07.2004 11:46
355	1614	12	47	615	86	0	13.07.2004 11:46
360	1653	7	48	658	90	0	13.07.2004 11:46
365	1609	12	45	592	86	0	13.07.2004 11:46

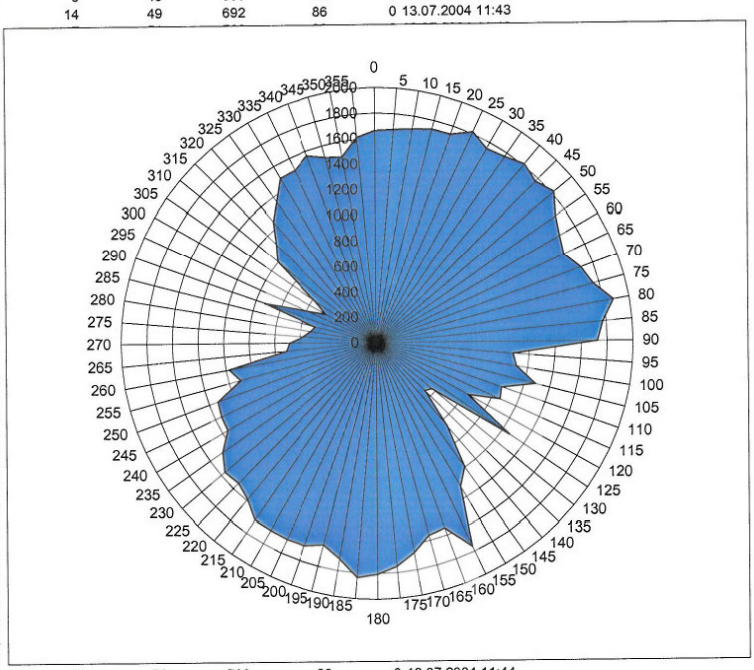

SMC10:

Object - c10 , Profile - 1 ,13.07.2006 16:50:26

Picket	ParametrA	ParametrB	ParametrC	ParametrD	ParametrE	Azimuth	Time
0	2004	1	48	697	86	0	07.12.1999 16:00
5	1810	9	45	638	86	0	12:00:00 AM
10	1908	4	47	668	86	0	12:00:00 AM
15	1869						
20	1958						
25	1829						
30	1788						
35	1756						
40	1712						
45	1637						
50	1540						
55	1576						
60	1588						
65	1487						
70	1354						
75	1107						
80	1079						
85	857						
90	826						
95	755						
100	566						
105	485						
110	287						
115	288						
120	377						
125	506						
130	1049						
135	1479						
140	1961						
145	2348						
150	2171						
155	2469						
160	2499						
165	2427						
170	2412						
175	2280						
180	2278						
185	2177						
190	1972						
195	1923						
200	1844	2	47	663	86	0	13.07.2004 12:30
205	1811	3	47	681	86	0	13.07.2004 12:30
210	1773	3	45	637	86	0	13.07.2004 12:30
215	1729	8	42	575	86	0	13.07.2004 12:30
220	1618	5	40	505	86	0	13.07.2004 12:30
225	1512	15	40	461	86	0	13.07.2004 12:30
230	1530	10	39	442	86	0	13.07.2004 12:30
235	1481	22	37	427	86	0	13.07.2004 12:30
240	1469	32	38	397	86	0	13.07.2004 12:30
245	1599	17	38	469	150	0	13.07.2004 12:30
250	1451	21	36	393	150	0	13.07.2004 12:30
255	1644	11	39	482	150	0	13.07.2004 12:30
260	1605	24	37	431	150	0	13.07.2004 12:30
265	1709	8	40	586	150	0	13.07.2004 12:30
270	1872	3	45	685	150	0	13.07.2004 12:30
275	1876	5	44	660	150	0	13.07.2004 12:31
280	1722	11	39	535	150	0	13.07.2004 12:31
285	1235	58	34	316	75	0	13.07.2004 12:31
290	2411	5	48	753	150	0	13.07.2004 12:31
295	1615	14	37	469	150	0	13.07.2004 12:31
300	2438	1	52	851	150	0	13.07.2004 12:31
305	1708	11	39	518	75	0	13.07.2004 12:31
310	1636	15	39	487	75	0	13.07.2004 12:31
315	2303	6	47	789	150	0	13.07.2004 12:31
320	1904	4	43	602	150	0	13.07.2004 12:31
325	1595	15	38	458	150	0	13.07.2004 12:31
330	1916	4	43	579	150	0	13.07.2004 12:31
335	1779	8	40	512	86	0	13.07.2004 12:31
340	1876	7	44	594	86	0	13.07.2004 12:31
345	1906	6	44	603	86	0	13.07.2004 12:31
350	1990	9	44	665	86	0	13.07.2004 12:31
355	1921	5	47	647	86	0	13.07.2004 12:31
360	1864	8	46	639	86	0	13.07.2004 12:31

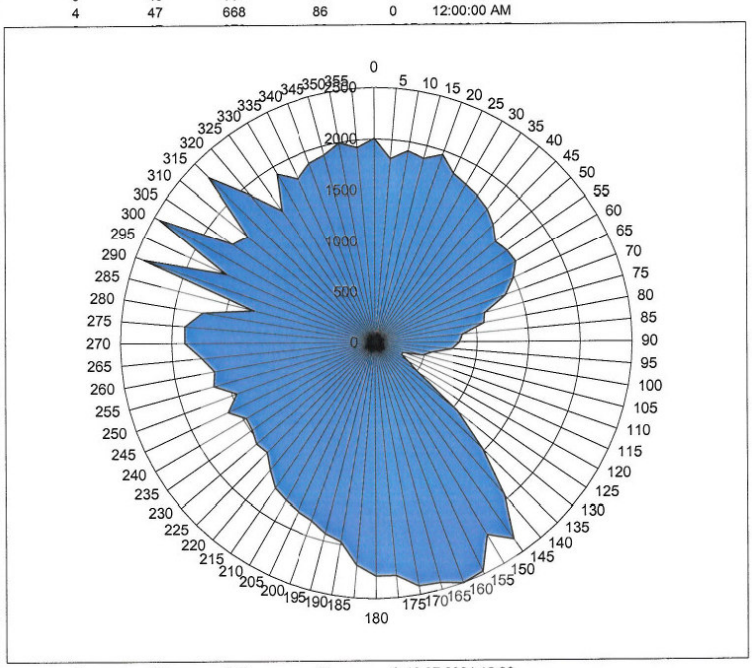

SMC10:

Object - c10_____, Profile - 2_____,14.07.2006 15:36:37

Picket	ParametrA	ParametrB	ParametrC	ParametrD	ParametrE	Azimuth	Time
0	1547	15	41	490	86	0	14.07.2004 10:38
5	1616	5	45	608	86	0	14.07.2004 10:38
10	1651	6	47	640	86	0	14.07.2004 10:38
15	1766	5	50	719	86	0	14.07.2004 10:38
20	1756						
25	1869						
30	1920						
35	1864						
40	1914						
45	2359						
50	2464						
55	2251						
60	2285						
65	2308						
70	2165						
75	2385						
80	2242						
85	2280						
90	1995						
95	1711						
100	1548						
105	1114						
110	1140						
115	1005						
120	938						
125	979						
130	1189						
135	1107						
140	1192						
145	1254						
150	1603						
155	1601						
160	1698						
165	1808						
170	2070						
175	2077						
180	1982						
185	1956						
190	1750						
195	1703						
200	1732						
205	1754	5	47	673	86	0	14.07.2004 10:40
210	1735	6	44	600	86	0	14.07.2004 10:40
215	1634	4	42	526	86	0	14.07.2004 10:40
220	1601	9	41	482	86	0	14.07.2004 10:40
225	1411	20	38	406	86	0	14.07.2004 10:40
230	1298	40	34	315	86	0	14.07.2004 10:40
235	1123	71	32	241	86	0	14.07.2004 10:40
240	995	94	31	202	86	0	14.07.2004 10:40
245	952	93	29	168	86	0	14.07.2004 10:40
250	774	102	28	121	86	0	14.07.2004 10:40
255	769	107	28	119	86	0	14.07.2004 10:40
260	649	95	27	87	86	0	14.07.2004 10:40
265	798	103	27	124	112	0	14.07.2004 10:40
270	1021	65	28	192	150	0	14.07.2004 10:40
275	1017	54	27	192	150	0	14.07.2004 10:40
280	1196	41	27	263	150	0	14.07.2004 10:40
285	1416	29	31	420	150	0	14.07.2004 10:40
290	1247	42	28	303	150	0	14.07.2004 10:40
295	1272	33	30	298	150	0	14.07.2004 10:40
300	1176	56	29	262	75	0	14.07.2004 10:40
305	1154	73	31	284	75	0	14.07.2004 10:40
310	1383	33	32	360	150	0	14.07.2004 10:40
315	1793	8	44	745	150	0	14.07.2004 10:40
320	1480	18	35	438	150	0	14.07.2004 10:40
325	1284	51	35	328	86	0	14.07.2004 10:40
330	1552	15	37	457	86	0	14.07.2004 10:40
335	1438	28	38	403	86	0	14.07.2004 10:41
340	1550	14	40	476	86	0	14.07.2004 10:41
345	1587	11	43	556	90	0	14.07.2004 10:41
350	1563	19	44	543	86	0	14.07.2004 10:41
355	1585	12	43	542	86	0	14.07.2004 10:41

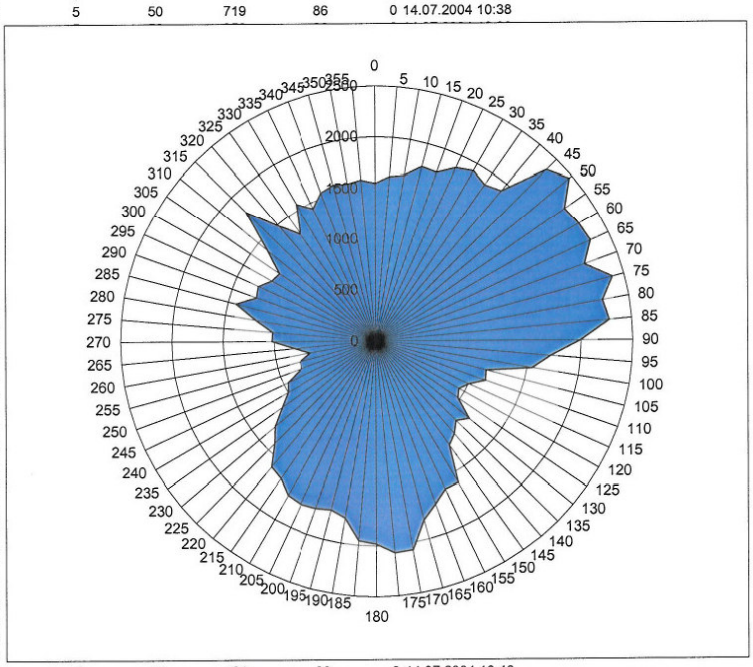

SMR10:

Object - r10_____, Profile - 1_____,13.07.2006 16:52:55

Picket	ParametrA	ParametrB	ParametrC	ParametrD	ParametrE	Azimuth	Time
0	1727	14	47	687	90	0	13.07.2004 13:48
5	1670	12	45	606	90	0	13.07.2004 13:48
10	1566	19	43	537	86	0	13.07.2004 13:48
15	1649	11	44	574	90	0	13.07.2004 13:48
20	1591	14	43	544	86	0	13.07.2004 13:48
25	1636						
30	1737						
35	1665						
40	1570						
45	1723						
50	1714						
55	1649						
60	1384						
65	1277						
70	983						
75	1625						
80	1592						
85	1541						
90	644						
95	717						
100	557						
105	582						
110	807						
115	662						
120	1252						
125	1286						
130	1450						
135	1279						
140	1592						
145	1930						
150	1868						
155	1641						
160	1780						
165	2064						
170	2212						
175	1910						
180	1949						
185	1892						
190	1772						
195	1696						
200	1589						
205	1535	16	40	460	86	0	13.07.2004 13:49
210	1545	12	41	474	86	0	13.07.2004 13:49
215	1541	13	41	474	86	0	13.07.2004 13:49
220	1564	9	39	493	86	0	13.07.2004 13:49
225	1467	27	38	421	86	0	13.07.2004 13:49
230	1418	22	38	415	86	0	13.07.2004 13:49
235	1371	37	35	341	86	0	13.07.2004 13:49
240	1378	27	36	357	86	0	13.07.2004 13:50
245	1254	50	35	317	86	0	13.07.2004 13:50
250	826	107	29	137	86	0	13.07.2004 13:50
255	675	96	26	85	86	0	13.07.2004 13:50
260	590	86	26	86	105	0	13.07.2004 13:50
265	423	64	25	38	112	0	13.07.2004 13:50
270	705	93	27	110	90	0	13.07.2004 13:50
275	720	91	27	107	86	0	13.07.2004 13:50
280	571	79	25	88	105	0	13.07.2004 13:50
285	631	81	23	88	150	0	13.07.2004 13:50
290	815	70	27	187	150	0	13.07.2004 13:50
295	506	63	24	52	75	0	13.07.2004 13:50
300	601	79	25	72	150	0	13.07.2004 13:50
305	786	76	27	133	150	0	13.07.2004 13:50
310	691	79	25	115	75	0	13.07.2004 13:50
315	787	79	26	116	150	0	13.07.2004 13:50
320	797	98	28	153	75	0	13.07.2004 13:50
325	969	109	31	192	86	0	13.07.2004 13:50
330	987	97	30	198	86	0	13.07.2004 13:50
335	1343	44	35	341	86	0	13.07.2004 13:50
340	1437	32	37	383	86	0	13.07.2004 13:50
345	1421	32	37	380	86	0	13.07.2004 13:50
350	1516	24	41	462	86	0	13.07.2004 13:50
355	1542	26	43	526	86	0	13.07.2004 13:50

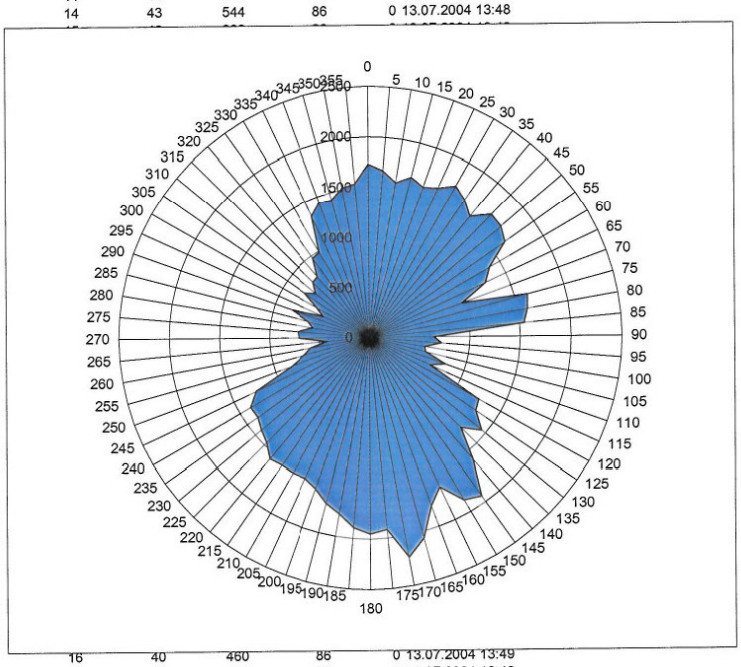

SMR10_5: Measurement in the profile between SMR10 and SMR11 at the intersection with the road:

Object - r10_5___, Profile - 1_____,13.07.2006 16:53:21

Picket	ParametrA	ParametrB	ParametrC	ParametrD	ParametrE	Azimuth	Time
0	1875	4	43	600	86	0	13.07.2004 13:54
5	1944	2	48	739	86	0	13.07.2004 13:54
10	1853	5	45	627	86	0	13.07.2004 13:54
15	2029	2	50	755	86	0	13.07.2004 13:54
20	2082						
25	2059						
30	2062						
35	2161						
40	2208						
45	2304						
50	2257						
55	2309						
60	2316						
65	2383						
70	2332						
75	2280						
80	2232						
85	2312						
90	2264						
95	1780						
100	1213						
105	1562						
110	1659						
115	1634						
120	1688						
125	851						
130	591						
135	602						
140	694						
145	822						
150	998						
155	1223						
160	1480						
165	1583						
170	1690						
175	1846						
180	1825						
185	1807						
190	2115						
195	2806						
200	2695	1	61	1077	90	0	13.07.2004 13:55
205	2968	1	67	1250	213	0	13.07.2004 13:55
210	3079	1	69	1301	180	0	13.07.2004 13:55
215	3227	1	73	1450	206	0	13.07.2004 13:55
220	2983	1	69	1329	183	0	13.07.2004 13:55
225	2900	1	66	1215	206	0	13.07.2004 13:55
230	2729	1	58	980	90	0	13.07.2004 13:55
235	2095	11	44	602	90	0	13.07.2004 13:55
240	2065	8	42	549	90	0	13.07.2004 13:56
245	1484	36	34	328	86	0	13.07.2004 13:56
250	2475	5	52	808	221	0	13.07.2004 13:56
255	2329	8	48	698	210	0	13.07.2004 13:56
260	2035	18	42	533	221	0	13.07.2004 13:56
265	432	60	25	33	105	0	13.07.2004 13:56
270	754	93	26	106	221	0	13.07.2004 13:56
275	722	92	27	113	112	0	13.07.2004 13:56
280	286	26	25	28	108	0	13.07.2004 13:56
285	290	29	26	21	105	0	13.07.2004 13:56
290	225	21	22	12	86	0	13.07.2004 13:56
295	214	20	24	12	82	0	13.07.2004 13:56
300	282	30	29	27	78	0	13.07.2004 13:56
305	500	65	27	68	86	0	13.07.2004 13:56
310	631	91	25	84	86	0	13.07.2004 13:56
315	1089	69	28	211	86	0	13.07.2004 13:56
320	1494	25	32	318	86	0	13.07.2004 13:56
325	1372	39	33	303	86	0	13.07.2004 13:56
330	1687	29	37	411	86	0	13.07.2004 13:56
335	2022	16	39	492	86	0	13.07.2004 13:56
340	2571	3	51	785	86	0	13.07.2004 13:56
345	2164	6	42	599	86	0	13.07.2004 13:56
350	2572	2	54	849	86	0	13.07.2004 13:56
355	2767	2	60	1060	225	0	13.07.2004 13:56

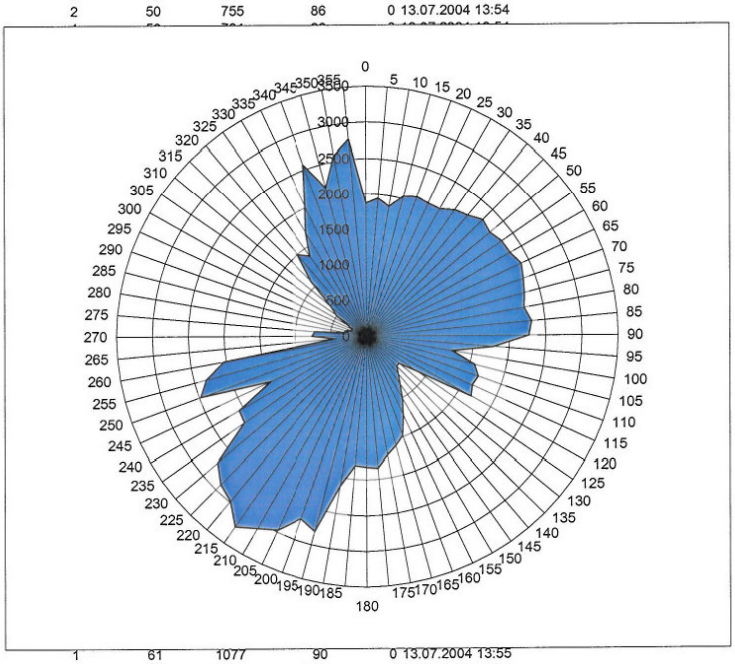

SM 2321: at the geodetical poinz close to SMC04:

Object - 23 , Profile - 21 ,13.07.2006 16:49:50

Picket	ParametrA	ParametrB	ParametrC	ParametrD	ParametrE	Azimuth	Time
0	1433	14	35	341	86	0	13.07.2004 11:07
5	1481	15	37	374	86	0	13.07.2004 11:07
10	1490	11	37	397	86	0	13.07.2004 11:07
15	1490						
20	1473						
25	1503						
30	1454						
35	1450						
40	1385						
45	1356						
50	1322						
55	1243						
60	1124						
65	964						
70	826						
75	752						
80	740						
85	643						
90	464						
95	329						
100	220						
105	236						
110	250						
115	198						
120	171						
125	216						
130	288						
135	364						
140	591						
145	643						
150	881						
155	1061						
160	1179						
165	1306						
170	1457						
175	1397						
180	1409						
185	1468						
190	1492						
195	1489						
200	1487	9	36	385	86	0	13.07.2004 11:08
205	1437	18	37	377	86	0	13.07.2004 11:08
210	1448	11	37	393	86	0	13.07.2004 11:08
215	1418	15	36	374	86	0	13.07.2004 11:08
220	1310	36	35	327	86	0	13.07.2004 11:08
225	1175	60	33	263	86	0	13.07.2004 11:08
230	1041	84	32	224	86	0	13.07.2004 11:08
235	1012	88	31	213	86	0	13.07.2004 11:08
240	901	102	29	165	86	0	13.07.2004 11:08
245	984	88	31	198	86	0	13.07.2004 11:08
250	721	101	29	112	86	0	13.07.2004 11:08
255	706	94	27	101	86	0	13.07.2004 11:08
260	697	106	28	100	86	0	13.07.2004 11:08
265	407	59	27	38	105	0	13.07.2004 11:08
270	421	63	25	34	86	0	13.07.2004 11:08
275	362	43	30	39	108	0	13.07.2004 11:08
280	296	32	24	14	105	0	13.07.2004 11:09
285	166	8	36	23	63	0	13.07.2004 11:09
290	163	11	30	8	75	0	13.07.2004 11:09
295	177	10	20	4	82	0	13.07.2004 11:09
300	227	18	35	21	86	0	13.07.2004 11:09
305	246	23	22	8	82	0	13.07.2004 11:09
310	239	17	21	7	82	0	13.07.2004 11:09
315	312	35	24	19	82	0	13.07.2004 11:09
320	503	72	25	50	86	0	13.07.2004 11:09
325	590	85	26	75	86	0	13.07.2004 11:09
330	1004	82	29	178	86	0	13.07.2004 11:09
335	1054	72	30	194	86	0	13.07.2004 11:09
340	1157	54	31	229	86	0	13.07.2004 11:09
345	1326	25	33	300	86	0	13.07.2004 11:09
350	1371	26	33	300	86	0	13.07.2004 11:09
355	1443	16	34	331	86	0	13.07.2004 11:09

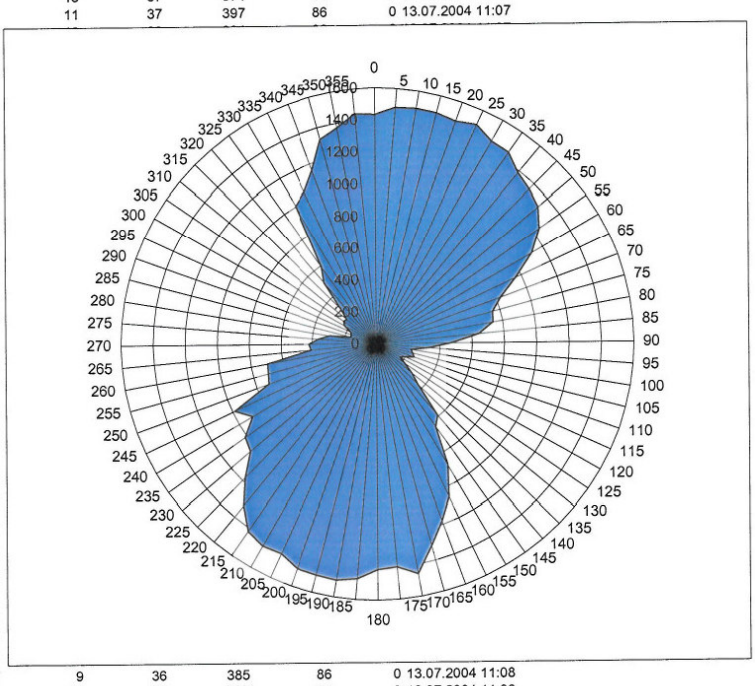

SML11:

Object - I11_____, Profile - 1_____,14.07.2006 15:29:47

Picket	ParametrA	ParametrB	ParametrC	ParametrD	ParametrE	Azimuth	Time
0	1255	45	33	276	86	0	14.07.2004 09:26
5	1338	41	35	316	86	0	14.07.2004 09:26
10	1370	24	34	340	86	0	14.07.2004 09:26
15	1406	20	35	360	86	0	14.07.2004 09:26
20	1403	20	36	363	86	0	14.07.2004 09:26
25	1386	25	36	358	86	0	14.07.2004 09:26
30	1397						
35	1380						
40	1349						
45	1344						
50	1265						
55	1291						
60	1281						
65	1328						
70	1039						
75	531						
80	618						
85	538						
90	644						
95	638						
100	498						
105	505						
110	1228						
115	1248						
120	1502						
125	1215						
130	1806						
135	1913						
140	2159						
145	1975						
150	1787						
155	1703						
160	1888						
165	1718						
170	1491						
175	1886						
180	1732						
185	1609						
190	1634						
195	1638						
200	1438						
205	1440						
210	1371	32	37	372	86	0	14.07.2004 09:28
215	1381	21	36	362	86	0	14.07.2004 09:28
220	1320	31	35	335	86	0	14.07.2004 09:28
225	1164	62	33	270	86	0	14.07.2004 09:28
230	1159	66	33	264	86	0	14.07.2004 09:28
235	1051	85	32	228	86	0	14.07.2004 09:28
240	1017	95	31	200	86	0	14.07.2004 09:28
245	954	94	30	201	86	0	14.07.2004 09:28
250	836	98	30	158	86	0	14.07.2004 09:28
255	812	95	28	135	78	0	14.07.2004 09:28
260	567	85	25	72	86	0	14.07.2004 09:28
265	437	65	25	36	105	0	14.07.2004 09:28
270	415	62	25	38	108	0	14.07.2004 09:28
275	312	40	24	19	105	0	14.07.2004 09:28
280	284	29	23	15	90	0	14.07.2004 09:28
285	157	13	21	4	108	0	14.07.2004 09:28
290	194	16	24	7	78	0	14.07.2004 09:28
295	145	5	24	2	82	0	14.07.2004 09:28
300	137	8	29	6	82	0	14.07.2004 09:28
305	192	10	22	4	82	0	14.07.2004 09:28
310	217	22	22	9	82	0	14.07.2004 09:29
315	316	34	23	18	82	0	14.07.2004 09:29
320	482	74	26	47	82	0	14.07.2004 09:29
325	678	92	26	93	86	0	14.07.2004 09:29
330	745	90	28	111	86	0	14.07.2004 09:29
335	906	91	28	153	86	0	14.07.2004 09:29
340	1099	79	31	217	86	0	14.07.2004 09:29
345	1110	62	31	223	86	0	14.07.2004 09:29
350	1211	56	32	258	86	0	14.07.2004 09:29
355	1257	40	33	281	86	0	14.07.2004 09:29
360	1286	38	34	300	86	0	14.07.2004 09:29

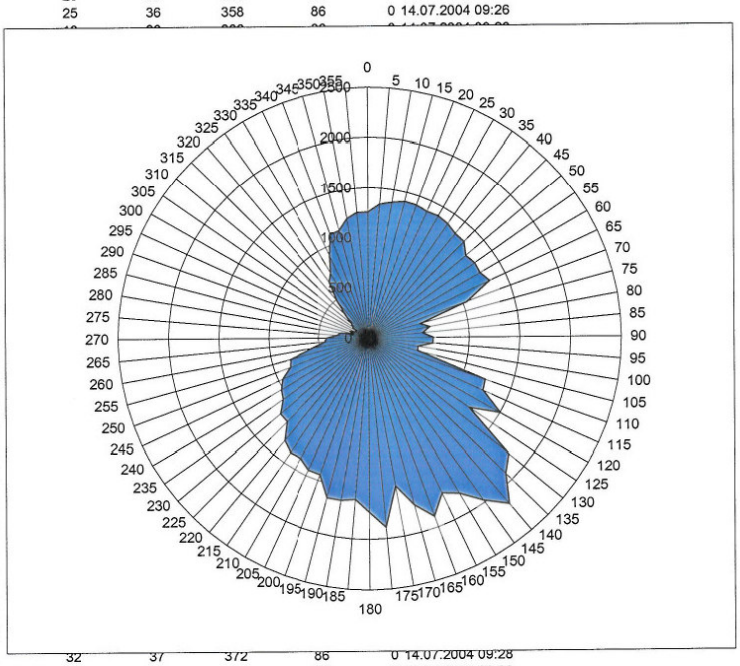

SML12:

Object - I12_____, Profile - 1_____,14.07.2006 15:31:32

Picket	ParametrA	ParametrB	ParametrC	ParametrD	ParametrE	Azimuth	Time
0	1131	69	31	240	86	0	14.07.2004 09:37
5	1220	49	32	266	86	0	14.07.2004 09:37
10	1301	39	34	315	86	0	14.07.2004 09:37
15	1322	26	35	326	86	0	14.07.2004 09:38
20	1394	22	36	354	86	0	14.07.2004 09:38
25	1404	28	37	381	86	0	14.07.2004 09:38
30	1367						
35	1415						
40	1469						
45	1373						
50	1359						
55	1334						
60	1286						
65	1187						
70	1087						
75	977						
80	957						
85	1073						
90	659						
95	444						
100	341						
105	285						
110	209						
115	331						
120	269						
125	252						
130	170						
135	244						
140	249						
145	618						
150	470						
155	607						
160	929						
165	940						
170	1208						
175	1180						
180	1268						
185	1322						
190	1361						
195	1366						
200	1350						
205	1391						
210	1372						
215	1330	29	35	340	86	0	14.07.2004 09:40
220	1336	37	36	346	86	0	14.07.2004 09:40
225	1374	25	37	381	86	0	14.07.2004 09:40
230	1338	34	34	335	86	0	14.07.2004 09:40
235	1260	52	33	303	86	0	14.07.2004 09:40
240	1459	16	36	399	150	0	14.07.2004 09:40
245	1344	41	34	324	150	0	14.07.2004 09:40
250	1261	64	34	297	150	0	14.07.2004 09:40
255	1310	37	32	296	150	0	14.07.2004 09:40
260	1197	47	30	255	150	0	14.07.2004 09:40
265	1093	58	28	215	150	0	14.07.2004 09:40
270	900	88	27	160	75	0	14.07.2004 09:40
275	750	96	25	112	112	0	14.07.2004 09:40
280	602	87	25	71	105	0	14.07.2004 09:40
285	350	47	22	21	71	0	14.07.2004 09:40
290	245	21	22	8	75	0	14.07.2004 09:40
295	239	22	21	9	108	0	14.07.2004 09:40
300	217	13	22	6	105	0	14.07.2004 09:40
305	247	25	22	14	90	0	14.07.2004 09:41
310	328	34	22	15	82	0	14.07.2004 09:41
315	375	53	24	26	82	0	14.07.2004 09:41
320	485	61	24	53	82	0	14.07.2004 09:41
325	736	99	26	106	86	0	14.07.2004 09:41
330	688	108	27	95	82	0	14.07.2004 09:41
335	855	103	27	137	86	0	14.07.2004 09:41
340	925	92	28	174	86	0	14.07.2004 09:41
345	984	90	29	177	86	0	14.07.2004 09:41
350	1202	61	33	260	86	0	14.07.2004 09:41
355	1296	40	33	296	86	0	14.07.2004 09:41
360	1346	31	34	316	86	0	14.07.2004 09:41

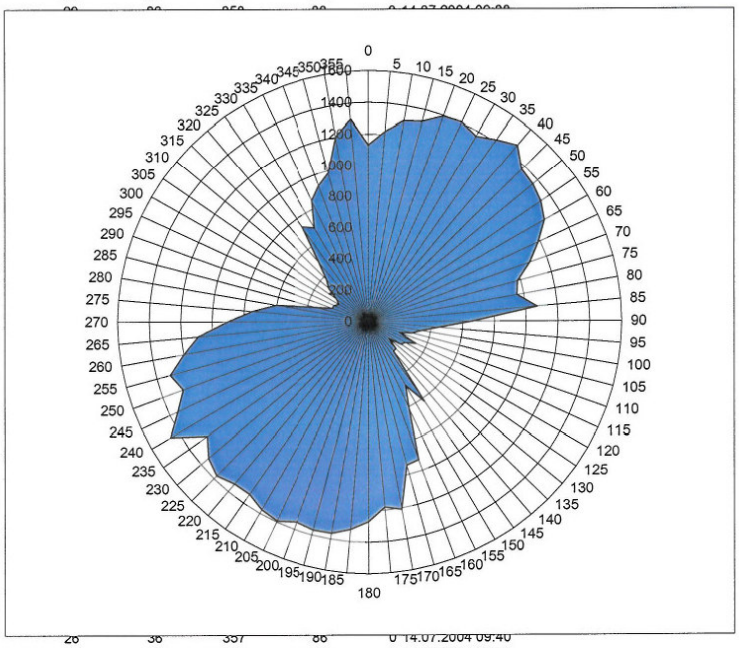

SML13:

Object - I13_____, Profile - 1_____,14.07.2006 15:32:22

Picket	ParametrA	ParametrB	ParametrC	ParametrD	ParametrE	Azimuth	Time
0	914	86	29	177	86	0	03.12.1999 02:27
5	987	84	30	197	86	0	03.12.1999 18:24
10	927	88	30	184	86	0	12:00:00 AM
15	952						
20	1081						
25	1124						
30	1115						
35	1150						
40	1180						
45	1137						
50	1127						
55	1111						
60	1026						
65	948						
70	885						
75	921						
80	891						
85	819						
90	804						
95	654						
100	585						
105	589						
110	482						
115	401						
120	380						
125	408						
130	476						
135	338						
140	516						
145	371						
150	410						
155	623						
160	742						
165	731						
170	760						
175	855						
180	921						
185	992						
190	1016						
195	1076	66	31	232	86	0	14.07.2004 09:53
200	1058	74	32	227	86	0	14.07.2004 09:53
205	1092	69	32	242	86	0	14.07.2004 09:53
210	1130	61	32	249	86	0	14.07.2004 09:53
215	1140	61	32	259	86	0	14.07.2004 09:53
220	1140	65	33	260	86	0	14.07.2004 09:53
225	1119	70	32	253	86	0	14.07.2004 09:53
230	1085	75	32	239	86	0	14.07.2004 09:53
235	977	90	31	190	86	0	14.07.2004 09:53
240	924	95	30	178	86	0	14.07.2004 09:53
245	816	112	29	147	86	0	14.07.2004 09:53
250	845	102	29	149	86	0	14.07.2004 09:53
255	755	112	28	125	86	0	14.07.2004 09:53
260	609	98	28	80	86	0	14.07.2004 09:53
265	595	84	26	69	86	0	14.07.2004 09:53
270	546	93	27	63	86	0	14.07.2004 09:53
275	447	73	25	44	82	0	14.07.2004 09:53
280	407	52	25	31	86	0	14.07.2004 09:53
285	359	40	23	28	90	0	14.07.2004 09:53
290	377	46	24	30	86	0	14.07.2004 09:53
295	309	30	23	17	86	0	14.07.2004 09:53
300	348	40	25	29	108	0	14.07.2004 09:53
305	257	27	23	13	86	0	14.07.2004 09:53
310	274	29	22	14	30	0	14.07.2004 09:53
315	281	32	23	18	82	0	14.07.2004 09:53
320	340	45	23	29	86	0	14.07.2004 09:53
325	432	59	23	44	86	0	14.07.2004 09:54
330	457	64	23	50	82	0	14.07.2004 09:54
335	564	74	26	71	86	0	14.07.2004 09:54
340	655	85	26	97	86	0	14.07.2004 09:54
345	640	85	27	96	86	0	14.07.2004 09:54
350	760	82	27	127	86	0	14.07.2004 09:54
355	819	92	28	145	86	0	14.07.2004 09:54
360	958	86	30	193	86	0	14.07.2004 09:54

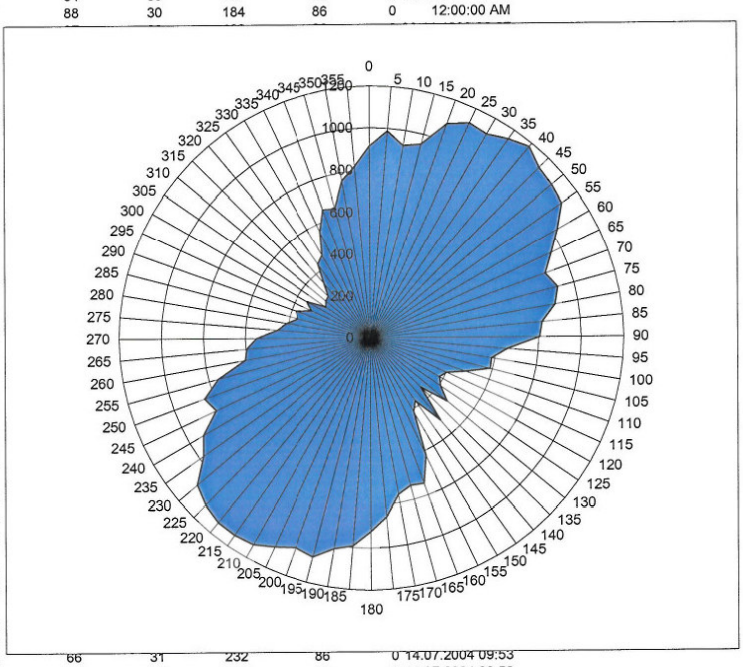

SML14_St.Moritz: next to the stairs at Chesa Corvilia

Object - 43_____, Profile - 1_____,14.07.2006 15:35:09

Picket	ParametrA	ParametrB	ParametrC	ParametrD	ParametrE	Azimuth	Time
0	1270	49	33	291	86	0	14.07.2004 10:05
5	1347	37	34	309	86	0	14.07.2004 10:05
10	1494	19	38	420	86	0	14.07.2004 10:05
15	1585						
20	1599						
25	1641						
30	1616						
35	1615						
40	1607						
45	1590						
50	1600						
55	1555						
60	1570						
65	1589						
70	1593						
75	1517						
80	1447						
85	1408						
90	1420						
95	1283						
100	1164						
105	995						
110	791						
115	981						
120	821						
125	643						
130	496						
135	477						
140	437						
145	996						
150	848						
155	956						
160	937						
165	973						
170	1106						
175	1237						
180	1375						
185	1444						
190	1416						
195	1404	29	37	378	86	0	14.07.2004 10:06
200	1423	31	37	372	86	0	14.07.2004 10:06
205	1425	20	37	387	86	0	14.07.2004 10:06
210	1549	10	43	529	86	0	14.07.2004 10:06
215	1433	20	39	423	86	0	14.07.2004 10:06
220	1371	33	38	390	86	0	14.07.2004 10:06
225	1367	22	36	369	86	0	14.07.2004 10:06
230	1294	45	36	341	86	0	14.07.2004 10:06
235	1229	48	35	311	86	0	14.07.2004 10:06
240	1181	65	33	280	86	0	14.07.2004 10:06
245	1117	70	33	261	86	0	14.07.2004 10:06
250	1065	80	32	229	86	0	14.07.2004 10:06
255	861	105	30	160	86	0	14.07.2004 10:06
260	963	100	30	197	86	0	14.07.2004 10:06
265	833	102	28	143	86	0	14.07.2004 10:07
270	1158	63	34	323	108	0	14.07.2004 10:07
275	924	81	29	180	105	0	14.07.2004 10:07
280	522	69	27	61	108	0	14.07.2004 10:07
285	410	42	26	40	202	0	14.07.2004 10:07
290	367	31	26	37	202	0	14.07.2004 10:07
295	349	31	27	36	202	0	14.07.2004 10:07
300	321	25	26	30	202	0	14.07.2004 10:07
305	399	32	28	49	202	0	14.07.2004 10:07
310	385	36	25	45	202	0	14.07.2004 10:07
315	538	50	26	60	86	0	14.07.2004 10:07
320	634	61	27	86	82	0	14.07.2004 10:07
325	634	59	26	79	86	0	14.07.2004 10:07
330	804	88	27	132	86	0	14.07.2004 10:07
335	966	84	29	176	86	0	14.07.2004 10:07
340	1160	72	31	242	86	0	14.07.2004 10:07
345	1277	60	33	288	86	0	14.07.2004 10:07
350	1331	38	35	333	86	0	14.07.2004 10:07
355	1409	30	37	389	86	0	14.07.2004 10:07

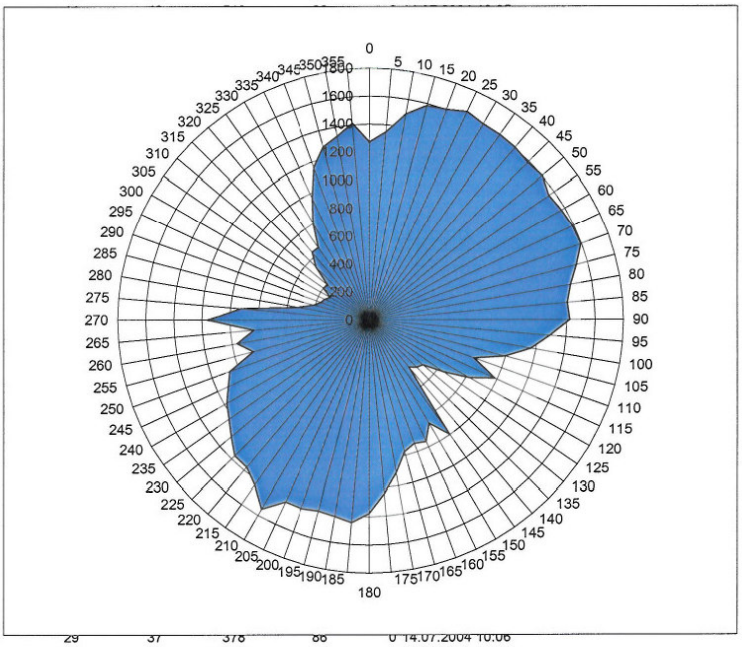

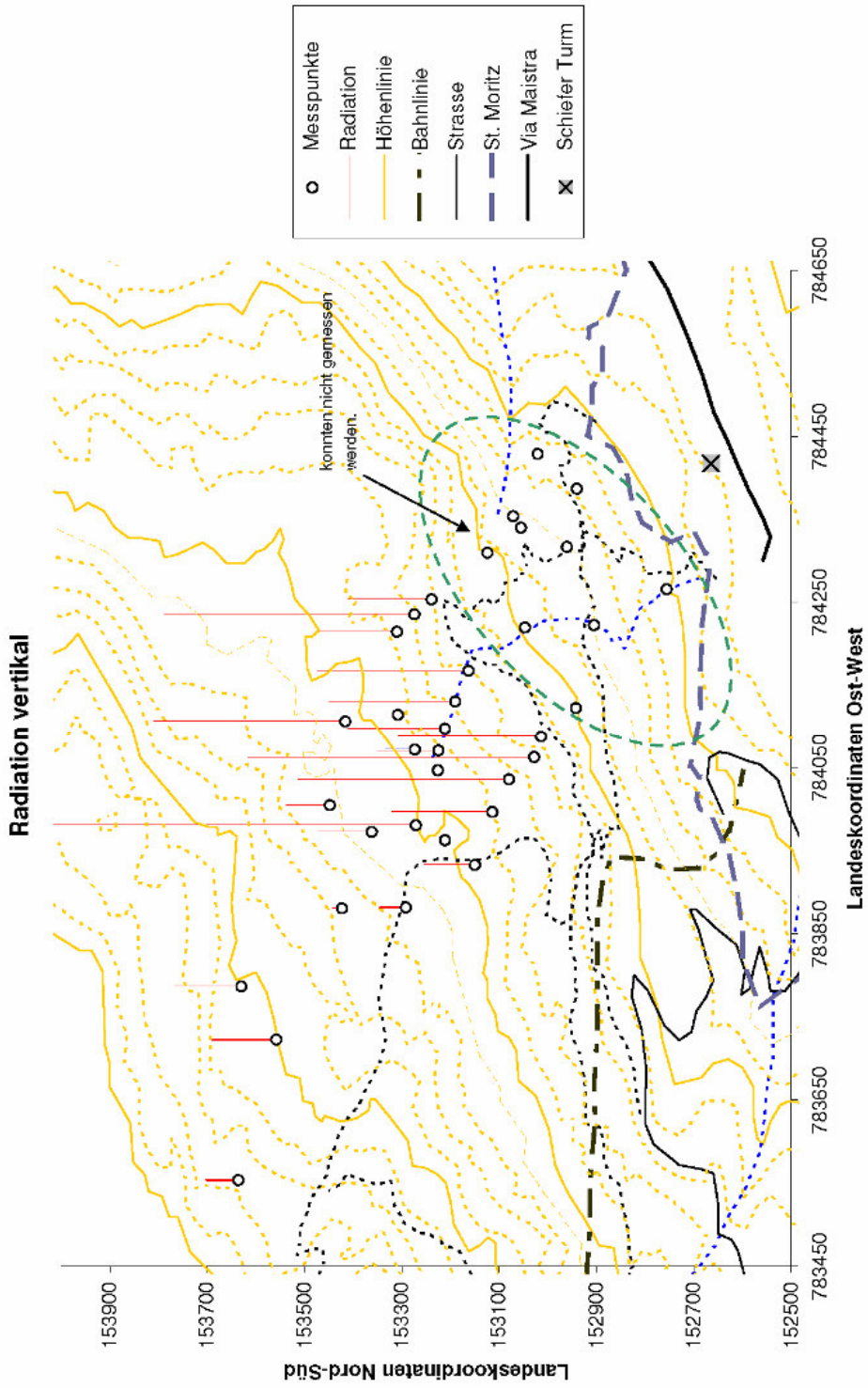
Messpunkte
Radiation
Höhenlinie
Bahnlinie
Strasse
St. Moritz
Via Maistra
Schiefer Turm
konnten nicht gemessen werden.
Radiation vertikal
Landeskoordinaten Ost-West
Landeskoordinaten Nord-Süd
784650
784450
784250
784050
783850
783650
783450
153900
153700
153500
153300
153100
152900
152700
152500

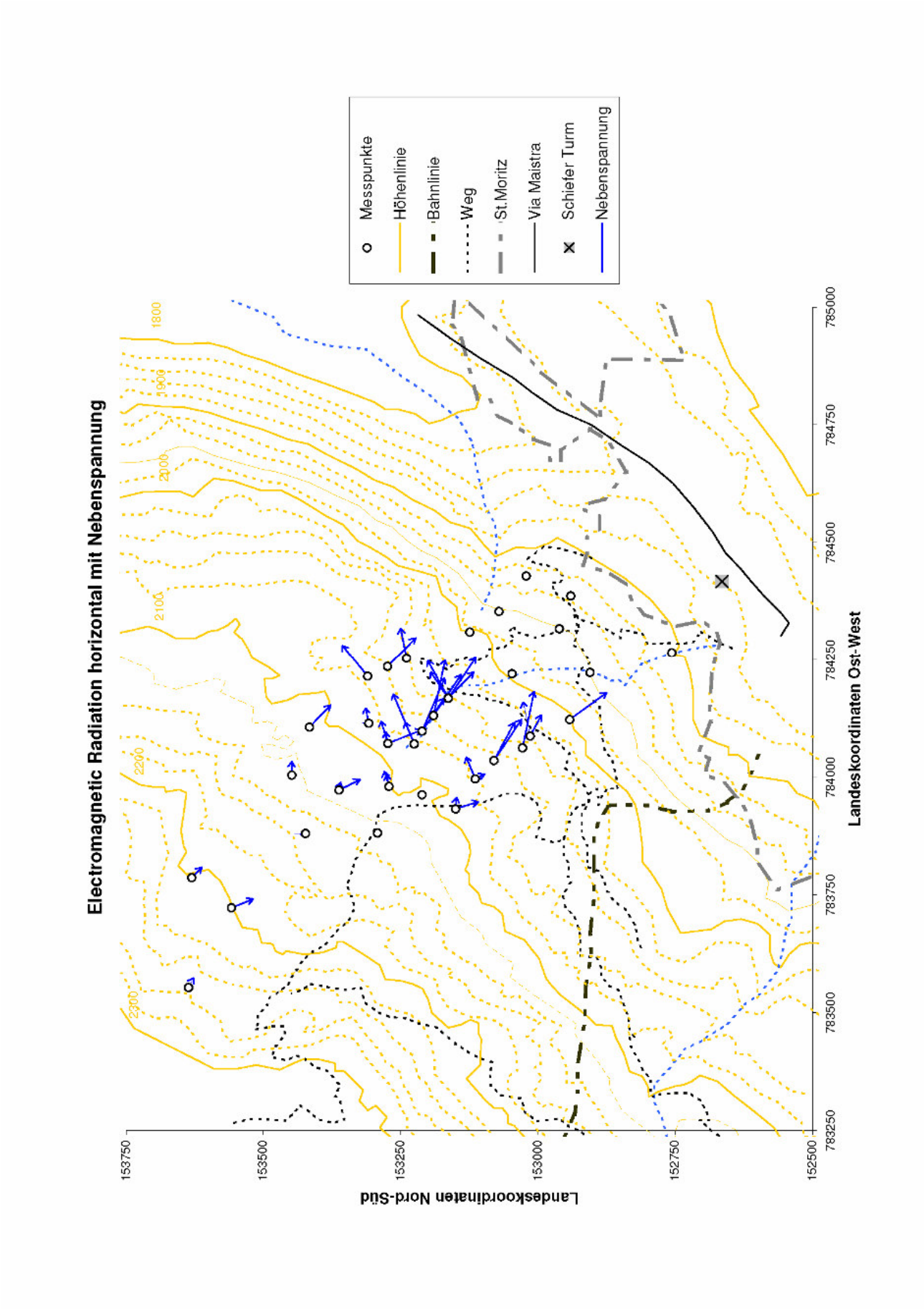
Electromagnetic Radiation horizontal mit Nebenspannung
Messpunkte
Höhenlinie
Bahnlinie
Weg
St.Moritz
Via Maistra
Schiefer Turm
Nebenspannung
1800
1900
2000
2100
2200
2300
Landeskoordinaten Nord-Süd
153750
153500
153250
153000
152750
152500
Landeskoordinaten Ost-West
782250
783500
783750
784000
784250
784500
784750
785000

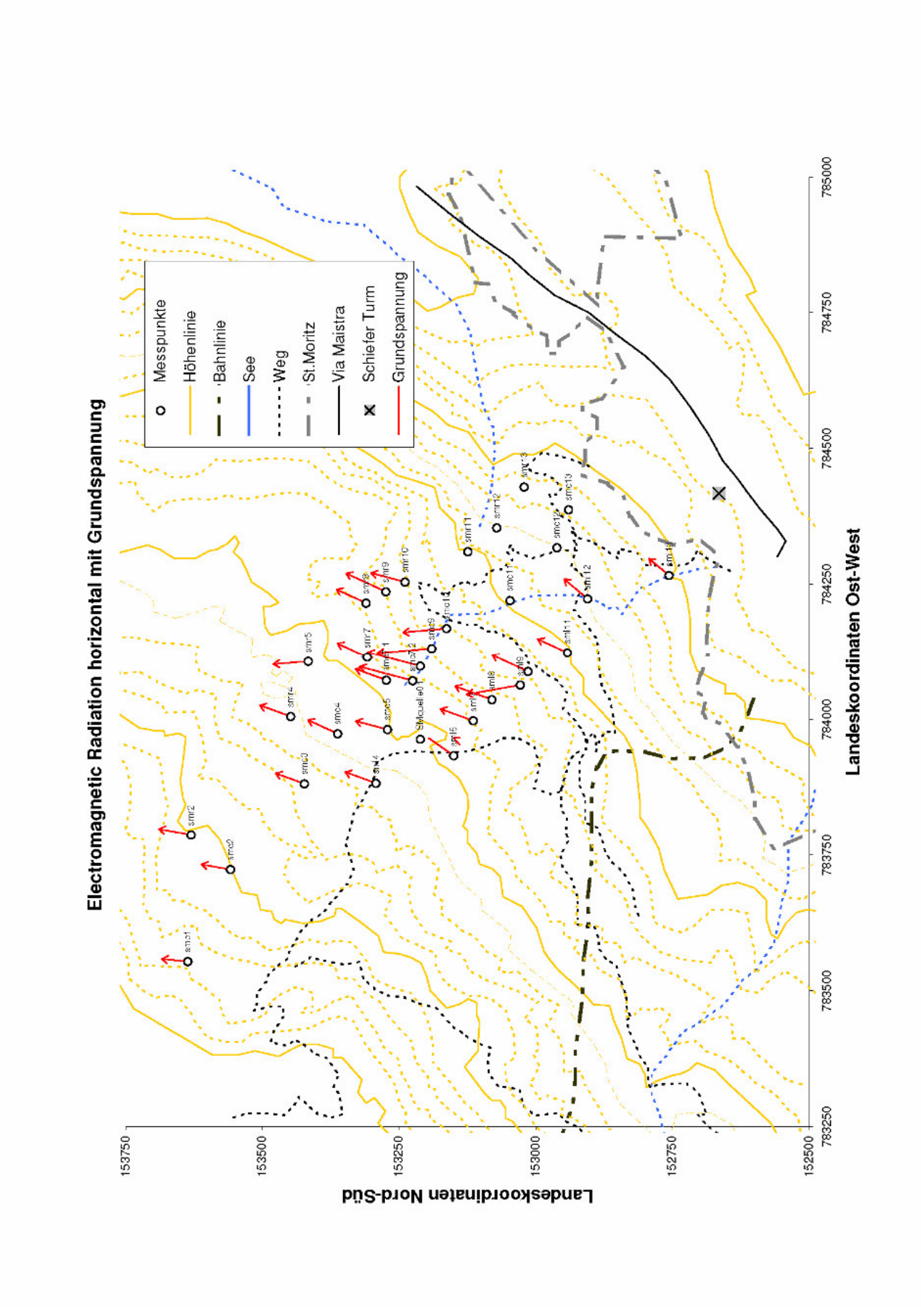
Electromagnetic Radiation horizontal mit Grundspannung
Messpunkte
Höhenlinie
Bahnlinie
See
Weg
St.Moritz
Via Maistra
Schiefer Turm
Grundspannung
Landeskoordinaten Nord-Süd
153750
153500
153250
153000
152750
152500
Landeskoordinaten Ost-West
783250
783500
783750
784000
784250
784500
784750
785000

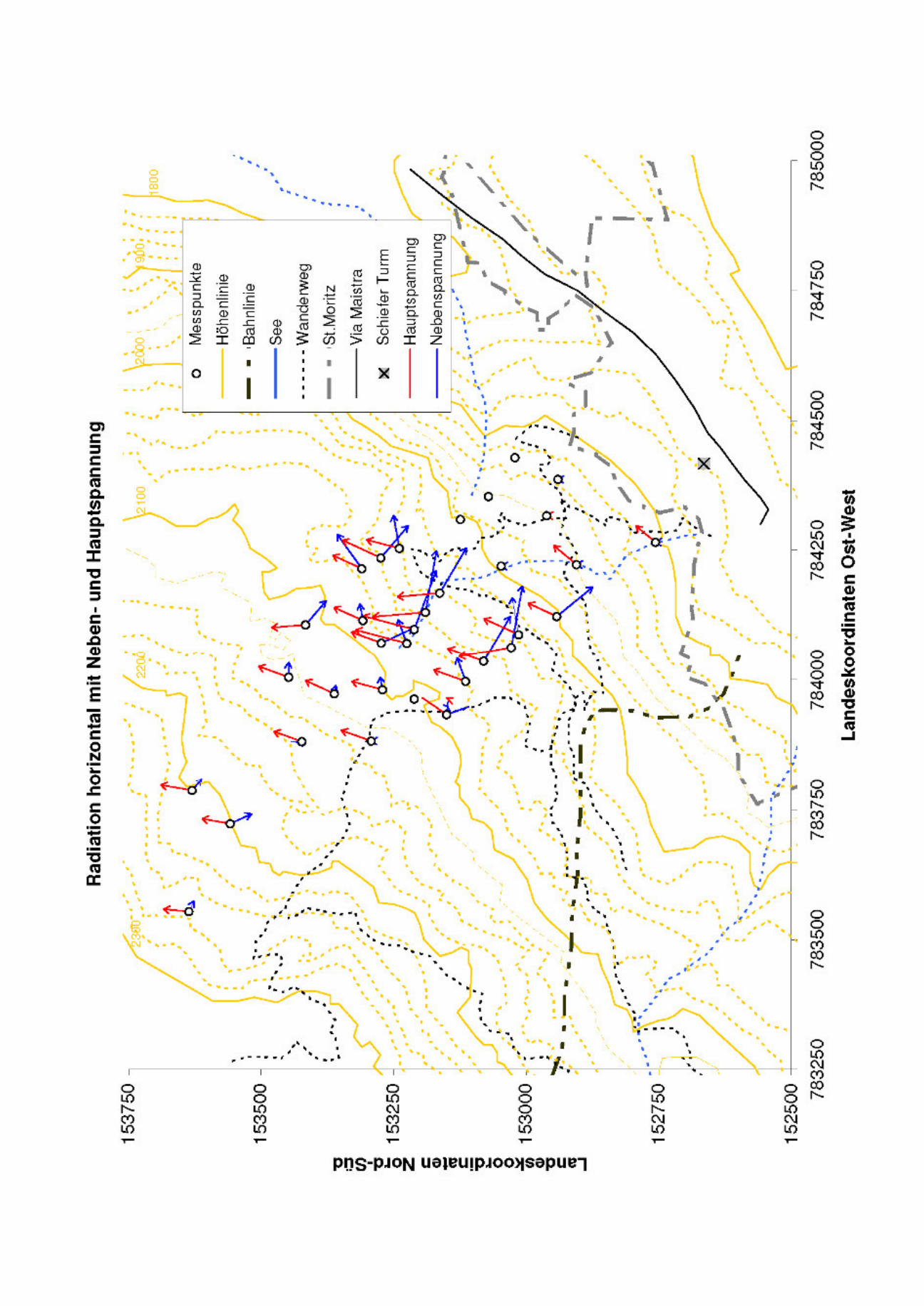
Radiation horizontal mit Neben- und Hauptspannung
Messpunkte
Höhenlinie
Bahnlinie
See
Wanderweg
St.Moritz
Via Maistra
Schiefer Turm
Hauptspannung
Nebenspannung
1800
1900
2000
2100
2200
2360
Landeskoordinaten Nord-Süd
153750
153500
153250
153000
152750
152500
Landeskoordinaten Ost-West
783250
783500
783750
784000
784250
784500
784750
785000

9.3 Bericht Nr. 4714/1

Messerklinger, S., Schmid, A., Rohr, R. Sterba, I. und Puzrin, A.M. (2007).“Interaktion Strasse - Hangstabilität, Monitoring und Rückwärtsrechnung, VSS – Forschungsarbeit Nr. 2005/502 1. Zwischenbericht Field expedition St. Moritz – Juli 2006“ Bericht Nr. 4714/1, Institut für Geotechnik, ETH Zürich

Bundesamt für Strassen ASTRA
Abteilung Strassennetze
3003 Bern

Interaktion Strasse - Hangstabilität
Monitoring und Rückwärtsrechnung

****

VSS - Forschungsarbeit Nr. 2005/502
2. Zwischenbericht
Borehole No 0601, St. Moritz, Oedometer tests and comparison to the insitu stiffness measurements

---

Bericht Nr. 4714/1

Zürich, 15. November 2007

1

VSS, Vereinigung Schweizerischer Strassenfachleute
Forschungsarbeit Nr. VSS 2005/502

Interaktion Strasse – Hangstabilität: Monitoring und Rückrechnung

2. Zwischenbericht

Borehole No.: 0601, St. Moritz. Oedometer Tests and Comparison to the Insitu Stiffness Measurements.

S. Messerklinger, R. Rohr, I. Sterba and A.M. Puzrin

Institut für Geotechnik

Bericht Nr. 4714/1
Zürich, 15. November 2007

Borehole No.: 0601, St. Moritz. Oedometer Tests and Comparison to the Insitu Stiffness Measurements.

Content:

Tables and Figures:

References:

Marchetti S., Monaco P., Totani G. and Calabrese M. (2001). "The Flat Dilatometer Test (DMT) in soil investigations" Report by the ISSMGE Committee TC16.

Atkinson, J.H. & Sällfors, G. (1991). „Experimental determination of stress-strain-time characteristics in laboratory and in situ tests." Proc. 10th European Conference on Soil Mechanics and Foundation Engineering, Florence. 3: 915-956.

Appendix:

Data sheets of the 22 oedometer tests.

1. Introduction

In July 2006 the Institute for Geotechnical Engineering of ETH Zürich made a field expedition to St. Moritz (Report No. 4714) with the aim to:

- verify and compare various insitu test methods and
- establish the existence of compression zones at the Brattas slide.

The following program points were performed:

1) Installation of new geodetical points on the Brattas slide.
2) Investigation and observation of former geodetical points and other significant marks.
3) Installation of borehole No. 0601 with a piecometer and an inclinometer and extraction of soil samples.
4) Dilatometer-Pressiometer tests in the borehole.
5) Marchetti dilatometer tests in the borehole.
6) Infrared pictures of the Brattas slide.
7) Photographs and their photogrammetrical evaluation of the geodetical points.
8) Electromagnetic radiation measurements.

In point 4 and 5 insitu methods for the stiffness determination were applied. The insitu test methods are the Dilatometer-Pressiometer (point 4) and Marchetti dilatometer test (point 5) which were performed in the borehole. The soil stiffness over the depth was investigated and the stiffness measurements of these two field methods were compared to each other (Report No. 4714).

In a second step these insitu stiffness data are compared to the stiffness determined in the laboratory with Oedometer test performed on samples taken from the borehole (point 3). This report is about these Oedometer test on the samples taken from the borehole.

2. Oedometer tests

16 disturbed samples were extracted from borehole No. 0601 form depths at which insitu tests were performed with the aim to determine and compare the oedometer stiffness to the stiffness measurements insitu. An overview of the samples extracted and the insitu tests performed is shown in table 1 together with the oedometer tests performed.

Tab. 1: Overview of the Oedometer and insitu tests performed.

Depth [m]	Labor number	Sample number	Oedometer test number	Marchetti dilatometer test number	Dilatometer-Pressiometer test number
4.85 – 5.05	47134	1	1_1 1_2		1 @ 5.00 m
6.20 – 6.30	47135	2	2_1 2_2 2_3	1/a @ 6.40 m	
8.82 – 9.04	47136	3	3_1 3_2		2 @ 8.94 m
8.50 – 8.75	47137	3a			
9.10 – 9.55	47138	3b			
10.20 – 10.50	47139	4	4_1	2/a @ 10.40 m	
10.50 – 10.70	47140	5	5_1	2/b @ 10.60 m	
10.70 – 10.90	47141	6	6_1	2/c @ 10.80 m	
10.90 – 11.20	47142	7	7_1	2/d @ 11.00 m	
13.80 – 14.00	47143	8	8_1 8_2	3/a @ 13.90 m	3 @ 13.70 m 4 @ 13.90 m
14.00 – 14.20	47144	9	9_1 9_2	3/b @ 14.10 m	
14.20 – 14.40	47145	10	10_1 10_2	3/c @ 14.25 m	
15.80 – 16.00	47146	11			
16.30 – 16.47	47147	12			
16.47 – 16.85	47148	13	13_1 13_2 13_3 13_4 13_5	4/a @ 16.50 m 4/b @ 16.62 m 4/c @ 16.70 m	
17.00 – 17.25	47149	14			

The general idea was to perform 2 tests per sample. When the results of these two tests varied significantly, a third test was performed. Then the two results which were similar were used further and the third test was ignored. For the samples 4 to 7, which are all within one meter, only one test was performed per sample and the results were compared to each other.

a. Sample preparation

The disturbed samples from the borehole were stored in plastic bags and transported in the IGT laboratory. The plastic bags were opened and a representative sample was taken. This sample was sieved through a 4 mm sieve to remove large stones and wood. The remaining soil was wetted until it had a pasty consistence. This is needed to install a rather saturated test specimen in the oedometer ring. Then the pasty soil was filled into the oedometer ring with a spatula and placed in the oedometer apparatus.

b. Test performance

The specimen was loaded stepwise with 4, 12.5, 25, 50, 100, 200 and 400 kPa. Then an un- and reloading cycle was applied with 200, 100, 50, 100, 200 and 400 kPa. Subsequently, the compression path was continued with 800, 1600 and 3200 kPa.

The consolidation time per load step was determined from the load – displacement curve as 30 to 45 minutes.

c. Test data analysis

For each test are the test data and their analysis shown in the appendix. Measured are the vertical displacements and calculated are the compression C_c and swelling index C_s for each load step.

The compression and swelling index are soil constants and should be the same for every load step. Due to influences of the test apparatus on load steps at low stress level and due to the varying initial water content, the results of the first few steps are not always consistent with the results at steps with higher stress levels. Therefore, not the average value for C_c and C_s was used for further comparisons but an "optimized" compression and swelling index was calculated together with the theoretical initial void ratio e_o. These calculations are shown for each test on the data sheet in the appendix and the resulting

stiffness response is highlighted in the diagram. In the e – log σ_v' diagram the green line represents the optimized compression index, the orange line represents the average compression index and the red dot gives the initial void ratio e_o for the optimized compression index. The swelling index was also optimized but remained in general the same or changed only minor.

3. Results

Table 2 presents a summary of the optimized compression and swelling index and the initial void ratio determined from the oedometer test.

Tab. 2: Oedometer test results.

Depth [m]	Sample number	Oedometer test number	Compression index C_c	Swelling index C_s	Initial void ratio e_o	Average initial void ratio
4.85 – 5.05	1	1_1 1_2	0.144 0.138	0.032 0.026	0.797 0.788	0.793
6.20 – 6.30	2	2_1 2_2 2_3	0.21 0.183 0.186	0.022 0.028 0.034	1.146 1.070 0.997	1.071
8.82 – 9.04	3	3_1 3_2	0.15 0.148	0.031 0.028	0.800 0.789	1.195
10.20 – 10.50	4	4_1	0.147	0.030	0.759	0.763
10.50 – 10.70	5	5_1	0.16	0.035	0.796	
10.70 – 10.90	6	6_1	0.158	0.028	0.785	
10.90 – 11.20	7	7_1	0.146	0.030	0.713	
13.80 – 14.00	8	8_1 8_2	0.156 0.144	0.030 0.033	0.759 0.742	0.751
14.00 – 14.20	9	9_1 9_2	0.167 0.167	0.034 0.034	0.826 0.826	0.826
14.20 – 14.40	10	10_1 10_2	0.158 0.176	0.034 0.034	0.715 0.851	0.783
16.47 – 16.85	13	13_1* 13_2 13_3 13_4 13_5	0.155 0.110 0.110 0.115 0.114	0.017 0.014 0.018 0.015 0.016	0.893 0.686 0.676 0.743 0.719	0.706

* The only sample which was not sieved.

Test 2_1 behaves significantly different from tests 2_2 and 2_3, therefore this test was ignored for further analysis. As well as test 13_1, which was the first test and for this test the material was not sieved.

In Fig. 1 an overview of all compression and swelling indices determined from the oedometer tests is presented.

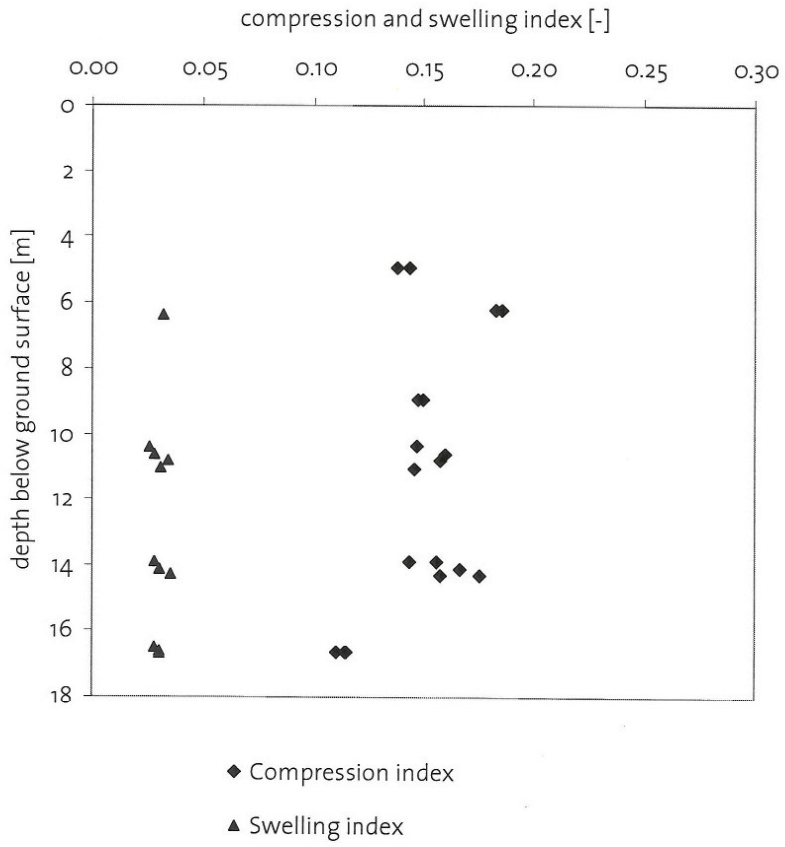

Fig. 1: Comparison of the compression and swelling index determined from the oedometer tests.

4. Comparison to insitu tests

To compare the Young's moduli determined from the Marchetti Dilatometer and the Dilatometer-Pressiometer tests (Report No. 4714) to the soil parameters C_c and C_s determined from the oedometer tests, the Young's moduli are transformed into compression (swelling) indices, using the pressure levels applied by the Marchetti Dilatometer and the Dilatometer-Pressiometer tests, respectively.

Firstly, the Young's moduli (E and E') are transformed to the constraint moduli using isotropic elasticity and a Poisson's ratio of 0.25:

$$E = (1 + \nu)(1 - 2\nu)\, M_E / (1 - \nu) \qquad \text{Eq. 1}$$

(The same formulation is used in the evaluation of the Marchetti data to transform M_{DMT} into E (Report No. 4714). With the Poisson's ratio of 0.25 Eq. 1 transforms into:

$$E = 0.83\, M_E$$

Secondly, the constraint modulus M_E is transformed into the compression and swelling index, respectively.

$$M_E = 2.3^*(1 + e_o)\, \sigma_m' / C_c \qquad \text{Eq. 2}$$

$$M_E' = 2.3^*(1 + e_o)\, \sigma_m' / C_s \qquad \text{Eq. 3}$$

The constraint moduli as well as the Young's moduli are stress dependent parameters while the compression and swelling indices are soil parameters.

Therefore, the stress magnitude σ_m' at which the test was performed, is needed.

For the Marchetti Dilatometer test this stress magnitude is given by the average pressure in the membrane during stiffness measurement. The stiffness is measured by applying 1.1 mm displacement (Marchetti et al., 2001) between the A and the B reading. Therefore, the average pressure between A and B was used for the transformation of the constraint modulus to the compression and swelling indices.

For the Dilatometer Pressiometer test this stress magnitude is as well given by the average pressure in the membrane during stiffness measurement. The evaluation of the stiffness parameter was performed on the stress-strain plot by defining two points on the curve for the compression and the swelling path, respectively and calculating the stress strain ratio in between. From the same two points the average stress was calculated and this is the stress magnitude used for the transformation of the constraint modulus to the compression and swelling indices.

Marchetti Dilatometer:

For the Marchetti Dilatometer tests the average pressure between A and B was used because between these two values the displacement of 1.1 mm is applied and the soil stiffness calculated.
Comparing these average pressure values for all tests performed (Tab. 3 and Fig. 2) it can be seen that for the first test of each series (2/a, 3/a and 4/a) the average pressure is significantly lower than for the following tests of the same series. This might be due to disturbance at the bottom of the borehole.
The values of the subsequent measurements (2/b, 2/c, 2/d & 3/b, 3/c & 4/b, 4/c) are relatively consistent for the series 3 and 4, therefore their average was taken. In series 2 the pressure level of the second measurement is significantly higher than the pressure level of the following measurements as well as the Young's modulus determined from this test. It is assumed that a stone or something else influenced the measurement of test 2/b, therefore the data were not considered further.

The ratio between the first measurements (2/a, 3/a and 4/a) and the average of the following measurements was determined to see the influence of the borehole disturbance. The results are presented in Tab. 3. It can be seen that the first value is always around 60 to 65 % of the following measurements.

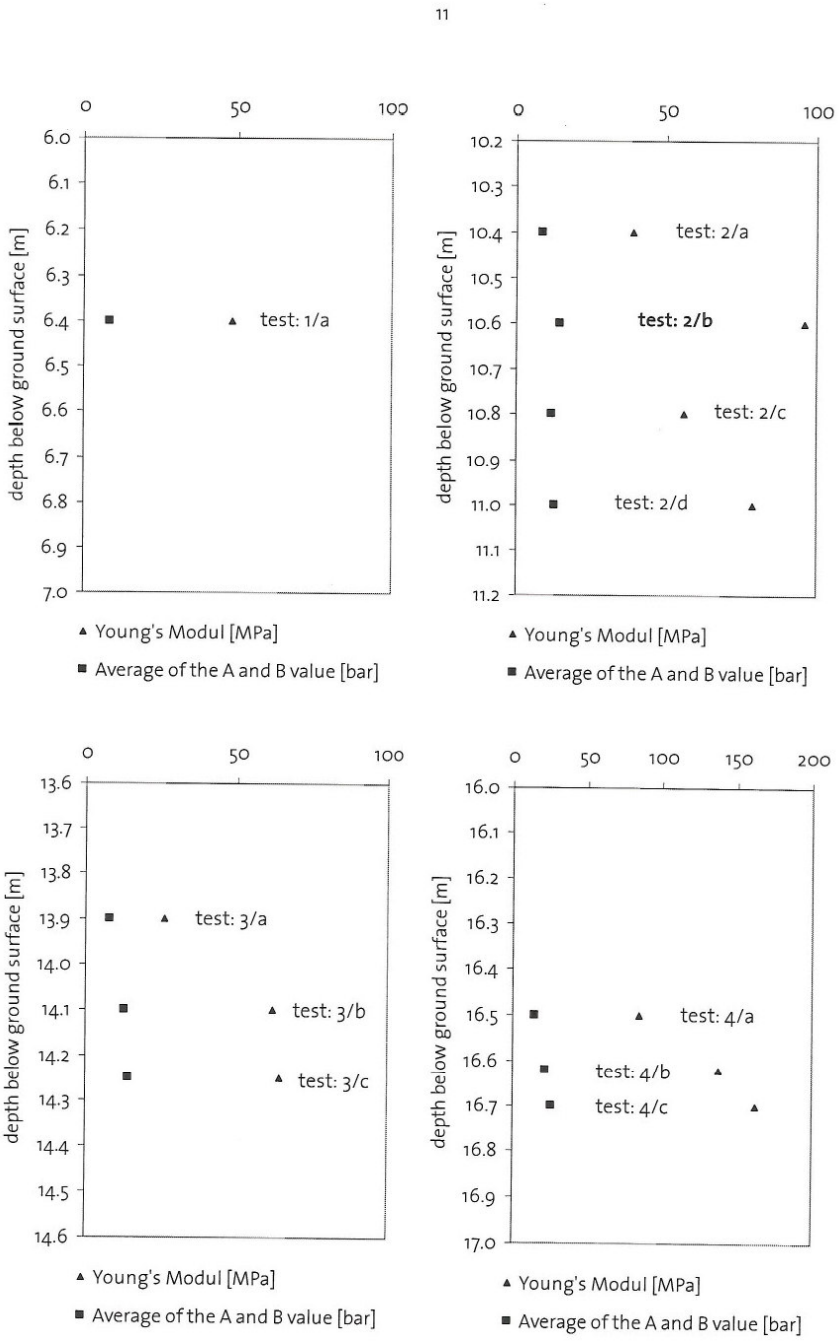

Fig. 2: Comparison of the Young's moduli and the average pressure between A and B determined with the Marchetti Dilatometer tests.

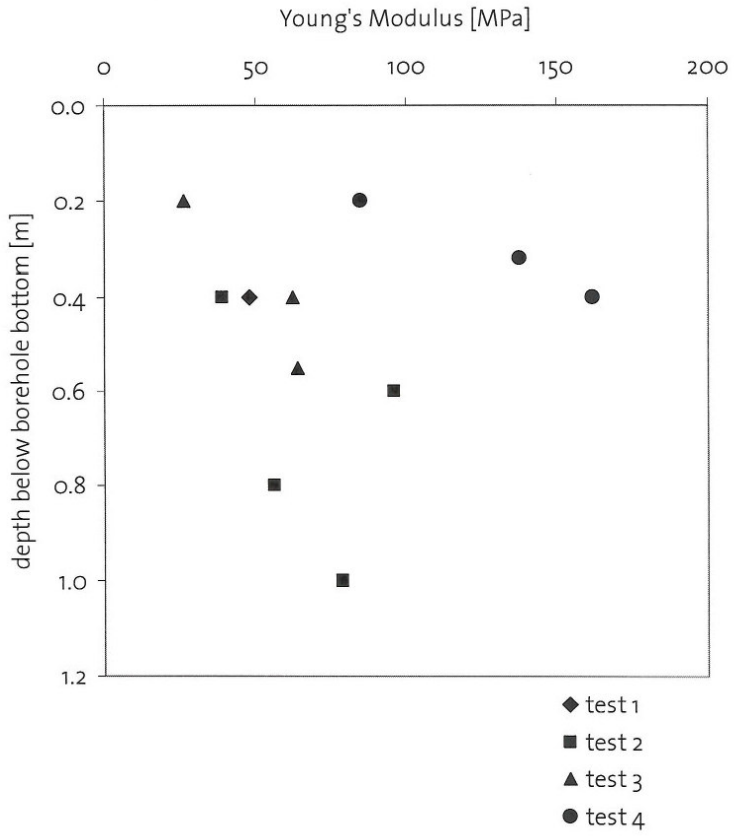

Fig. 3: Comparison of the Young's moduli determined with the Marchetti Dilatometer tests over the depth below the borehole bottom.

Finally, the constraint modulus M_E was calculated using Eq. 1 and subsequently the compression index C_c was determined from M_E using Eq. 2 (Tab. 3).

The initial void ratio is taken from the oedometer tests performed at the corresponding depth (Tab. 2). The stress magnitude σ_m' is the average pressure of A & B (Tab. 3).

Tab. 3: Transformation of Marchetti Dilatometer test data.

Depth [m]	Marchetti dilatometer measurements	Young's Modul E [MPa]	Constraint Modul M_E [MPa]	Ø of A & B [bar]	Ø of A & B [bar]	Average initial void ratio e_o [-]	C_c [-]
6.40	1/a: A: 4.25 B: 12.5 bar No 1/b measurement!	48	57.6	8.4		1.071	0.0695
10.40	2/a: A: 4.5 B: 12.5 bar	39	46.8	8.5	69 %	0.759	0.0735
10.60	2/b: A: 6.5 B: 22.5 bar	(96)		(14.5)			
10.80	2/c: A: 7.0 B: 16.5 bar	56	67.2	11.75	12.3	0.785	0.0718
11.00	2/d: A: 5.8 B: 20.0 bar	79	94.8	12.9		0.713	0.0536
13.90	3/a: A: 4.1 B: 11.5 bar	26	31.2	7.8	57 %	0.751	0.1007
14.10	3/b: A: 6.2 B: 19.5 bar	62	74.4	12.9	13.6	0.826	0.0728
14.25	3/c: A: 8.2 B: 20.1 bar	64	76.8	14.2		0.783	0.0758
16.50	4/a: A: 5.1 B: 24.0 bar	85	102.0	14.6	61 %	0.706	0.0562
16.62	4/b: A: 10.8 B: 33.0 bar	138	165.6	21.9	24.0		0.0519
16.70	4/c: A: 14.5 B: 37.5 bar	162	194.4	26.0			0.0525

An overview of the test results is given in Fig. 4 to Fig. 7. The compression and swelling indices determined from the oedometer tests as well as the compression indices determined from the Marchetti Dilatometer tests, using the pressures applied by the Dilatometer (Tab. 3), are plotted over the depth.

In Fig. 4 the data of all tests are presented and the data of the first measurement of the Marchetti Dilatometer within one series are marked.

The comparison of all indices shows that from 4 to 12 m the indices are slightly increasing with depth. At 14 m the indices increase overproportional while at 16.7 m there is a consistent drop of the values.

The comparison of the compression and swelling indices determined by the oedometer tests to each other show qualitatively the same behaviour. Only at a depth of 6.25 m the compression index is significantly higher than the indices determined above and below (for the depth of 4.95 and 8.93 m, respectively).

The comparison of the Marchetti Dilatometer measurements show that the first measurements give a compression index whose value is on the top side of the average of the following measurements but within the range. In comparison to the Young's moduli determined which are around 60 to 65 % of the Young's moduli determined from the following measurements. This highlights the advantage of the data analysis on real soil parameters which are not stress level dependent and underlines the consistency of the Marchetti Dilatometer tests.

In Fig. 5 and Fig. 6 the average values of the results per depth are plotted. The comparison shows that the Marchetti measurements give an index which is between the swelling and the compression index. This indicates that the strain magnitude applied (1.1 mm) is not large enough to reach the fully plastic state. But it is too large to represent the strain magnitude at the average swelling index.
Due to the non-linearity of the elastic behaviour of real soils the stiffness parameter is strain level dependent and the strain level applied by Marchetti Dilatometer is in this case at a magnitude where the stiffness is twice the plastic stiffness. (In comparison to the small strain "elastic" stiffness which is about 10 times the plastic stiffness, e.g. Atkinson & Sällfors, 1991).

In Fig. 7 is the Oedometer swelling index and the Marchetti Dilatometer compression index given in percentage of the Oedometer compression index. The results show that the swelling index is a fifth of the compression index and the Marchetti Dilatometer index is 40 to 50 % of the Oedometer compression index.

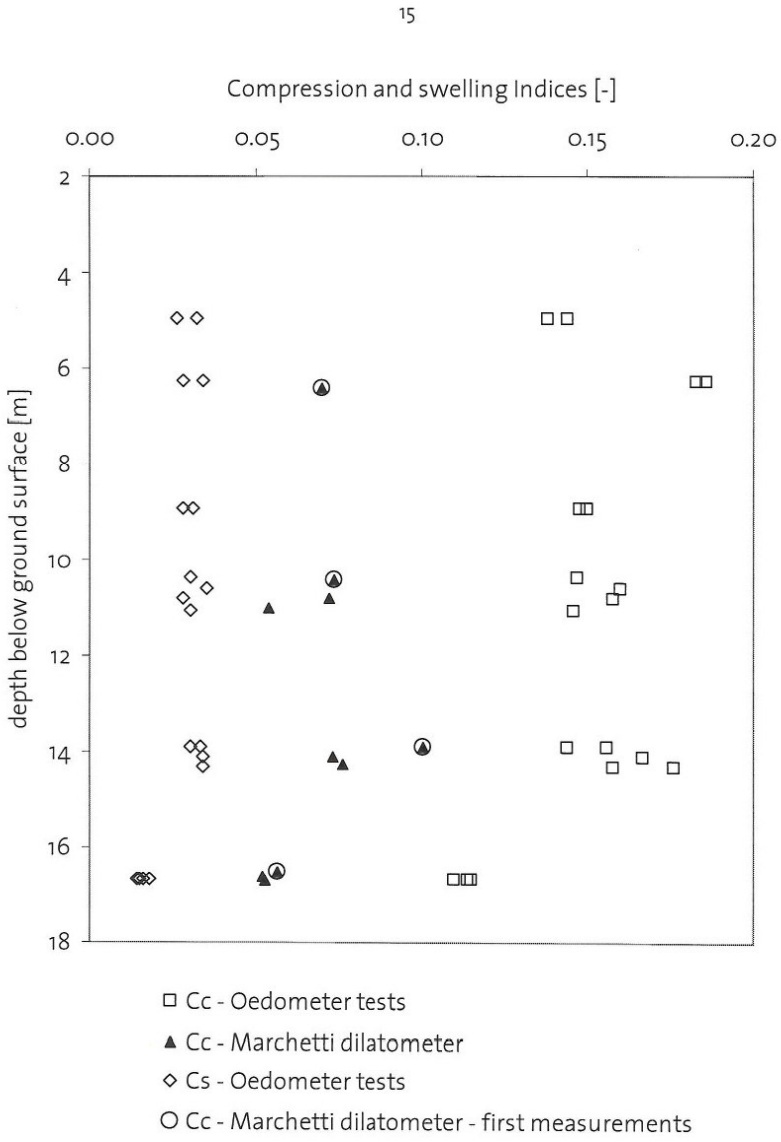

Fig. 4: Comparison of the compression and swelling indices determined from the oedometer and Marchetti Dilatometer tests.

16

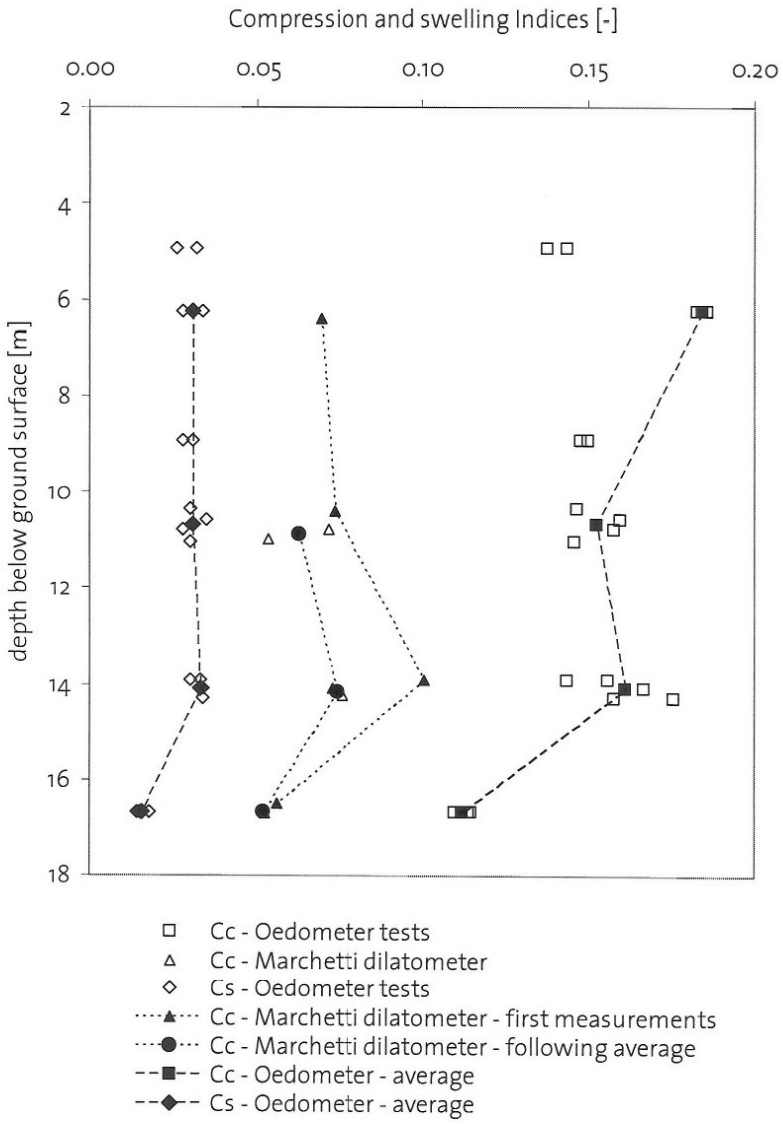

Fig. 5: Comparison of the average compression and swelling indices determined from the oedometer and Marchetti Dilatometer tests.

17

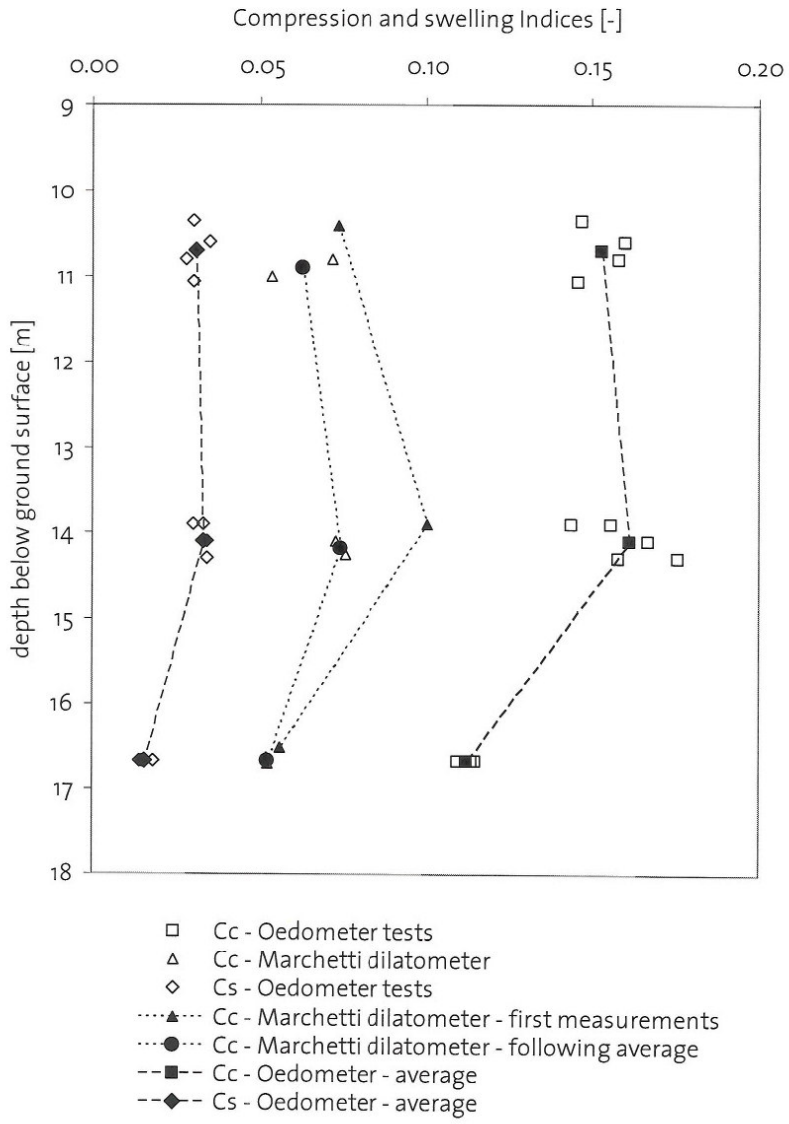

Fig. 6: Comparison of the average compression and swelling indices determined from the oedometer and Marchetti Dilatometer tests.

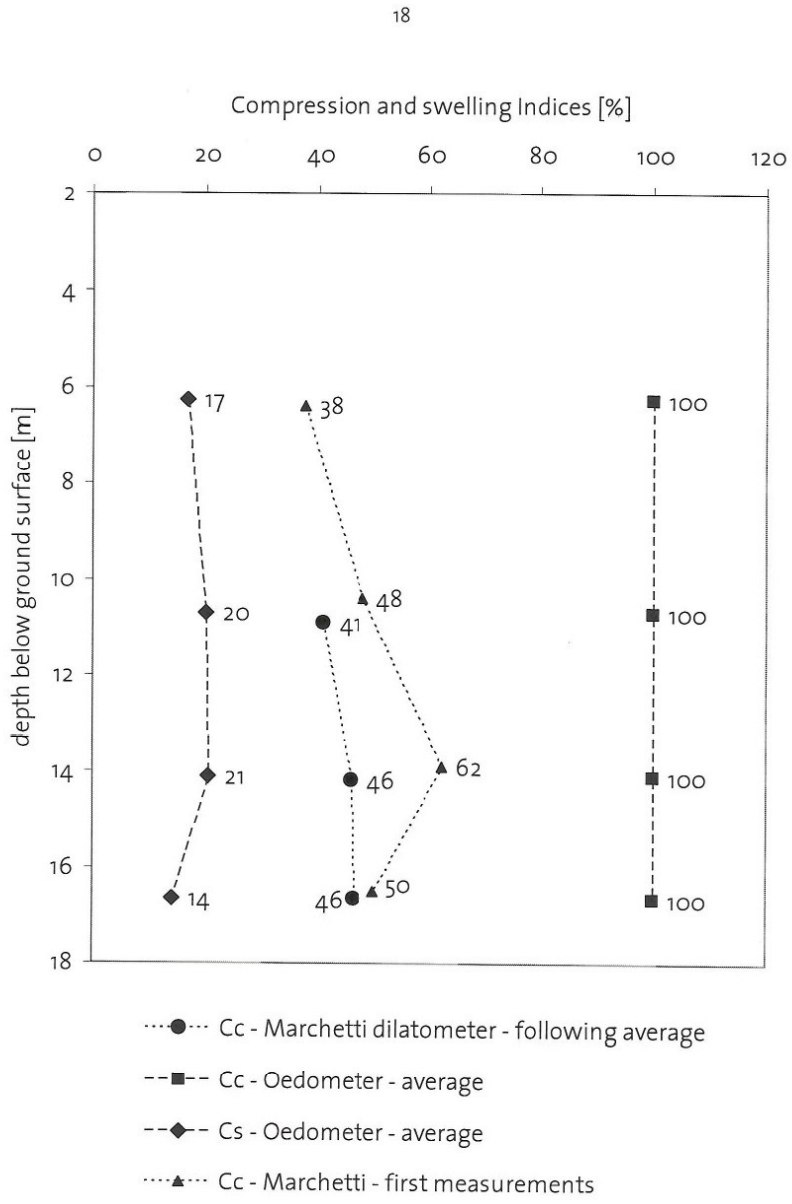

Fig. 7: Comparison of the index ratios of the oedometer and Marchetti Dilatometer tests.

19

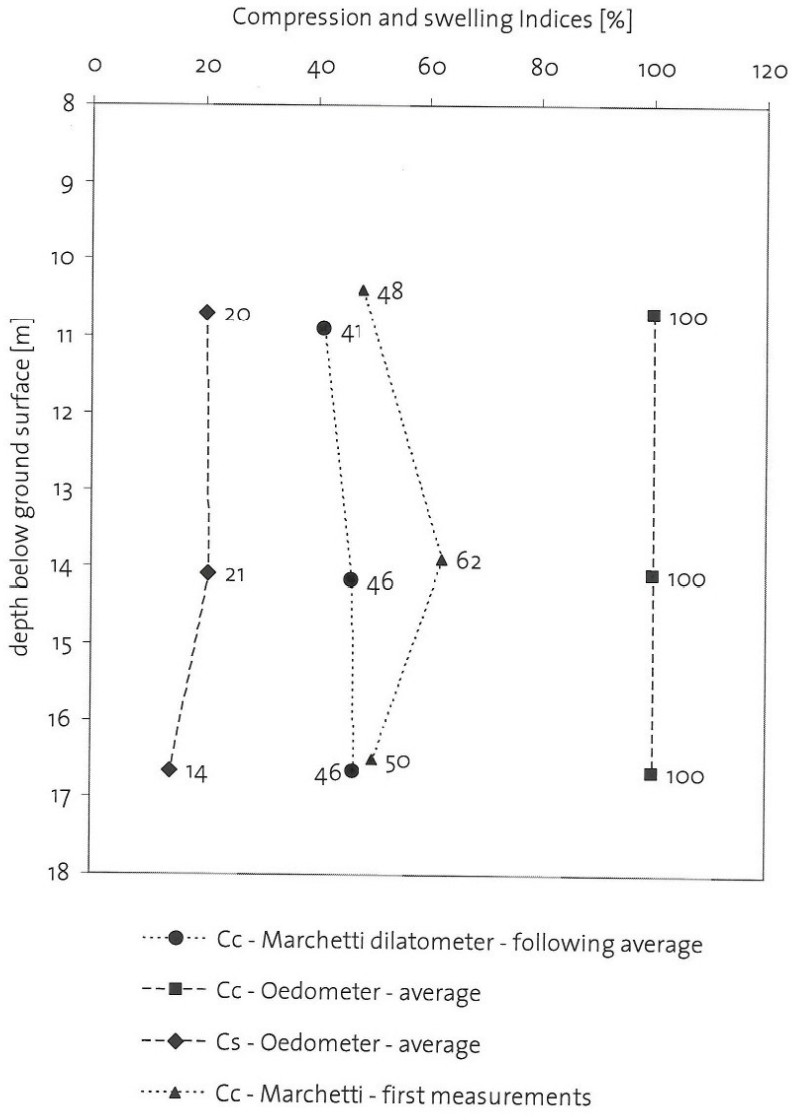

Fig. 8: Comparison of the index ratios of the oedometer and Marchetti Dilatometer tests.

Dilatometer-Pressiometer:

For the Dilatometer-Pressiometer tests the average pressure between the start and end point used for the stiffness data analysis for compression and swelling, respectively, was used.

During the third test the first measurement was performed at a depth of 13.90 m. Problems occurred therefore the test was stopped and the pressiometer was lifted and another test was performed at a depth of 13.7 m. This second test was successful and its results are used further.

Tab. 4: Transformation of Dilatometer-Pressiometer test data.

Depth [m]	Test no	Dilatometer-Pressiometer: Young's Moduli [MPa]	Constraint Moduli [MPa]	Average pressure [kPa]	Average initial void ratio e_o [-]	C_c [-]	C_s [-]
5.00	1	E_{comp} = 15.0 E_{ur} = 110.0	M_E = 18.0 M_E' = 132.0	584	0.793	0.134	0.0182
8.94	2	E_{comp} = 15.0 E_{ur} = 156.5	M_E = 18.0 M_E' = 187.8	543	0.795	0.125	0.0119
13.70	3b	E_{comp} = 10.0 E_{ur} = 93.0	M_E = 12.0 M_E' = 112.0	427	0.751	0.143	0.0154
13.90	3a	E_{comp} = 8.0 E_{ur} = 178.0	M_E = 9.6 M_E' = 213.6	(170)			

An overview of the test results is given in Fig. 9 to Fig. 11. The compression and swelling indices determined from the oedometer tests as well as the compression indices determined from the Dilatometer Pressiometer tests, using the pressures applied by the membrane (Tab. 4), are plotted over the depth.

In Fig. 9 the data of all tests are presented. The comparison shows that the qualitative behaviour observed by both tests has the same trend (Fig. 10)

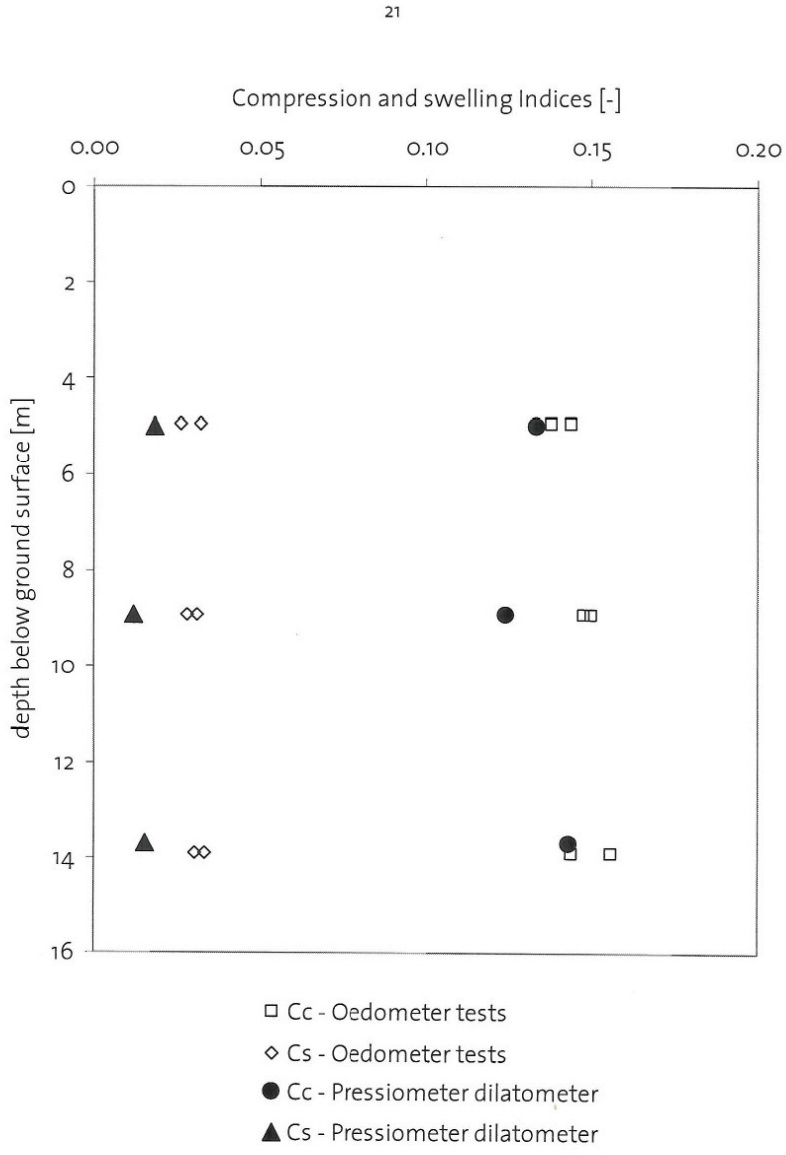

Fig. 9: Comparison of the compression and swelling indices determined from the oedometer and Dilatometer-Pressiometer tests.

The comparison of the compression and swelling index values determined by the oedometer tests to the indices determined by the Pressiometer Dilatometer show that latter values are always below the oedometer indices. While for the compression indices the values of the Pressiometer Dilatometer are only

marginally smaller for the swelling indices the values of the Pressiometer Dilatometer are about a half compared to the Oedometer results (Fig. 11).

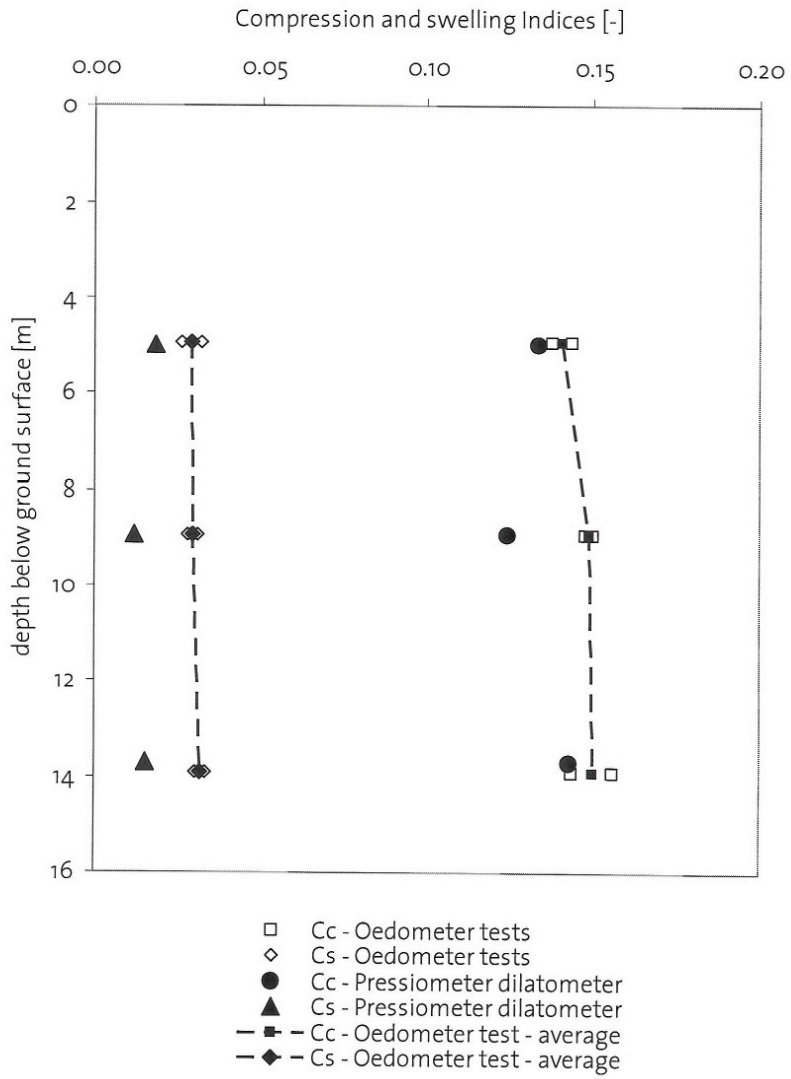

Fig. 10: Comparison of the average compression and swelling indices determined from the oedometer and Dilatometer-Pressiometer tests.

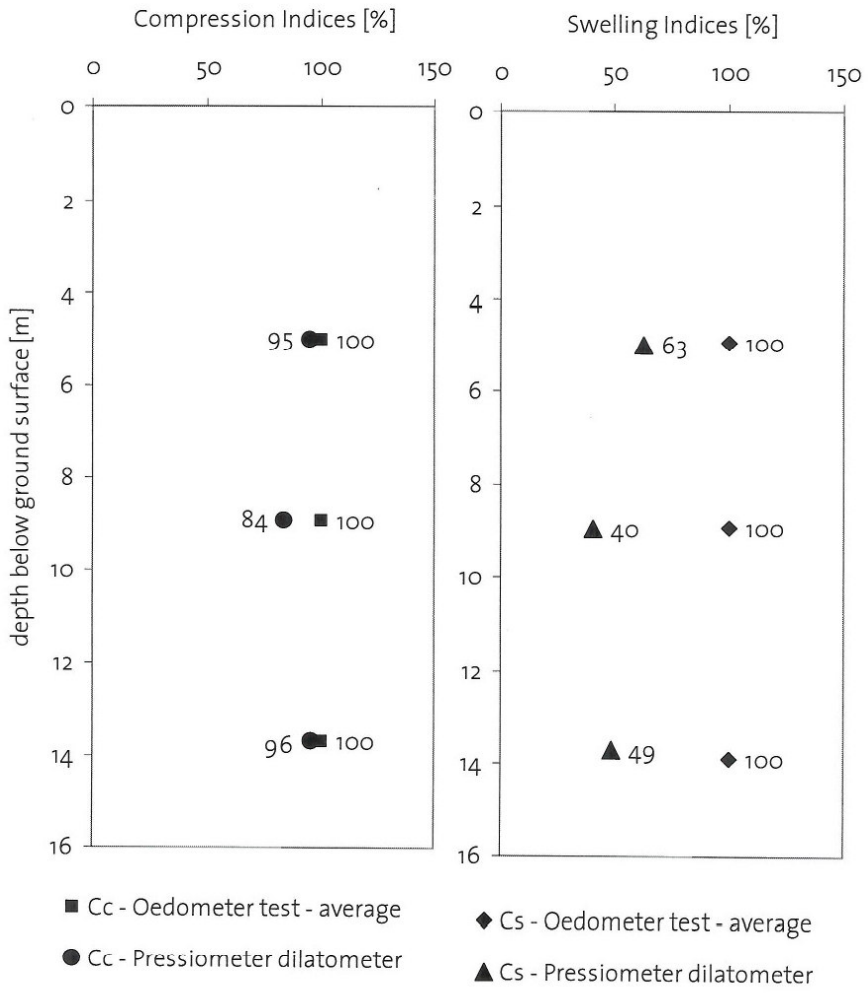

Fig. 11: Comparison of the index ratios of the oedometer and Dilatometer Pressiometer tests.

Finally, the results of all three methods are compared to each other (Fig. 12).

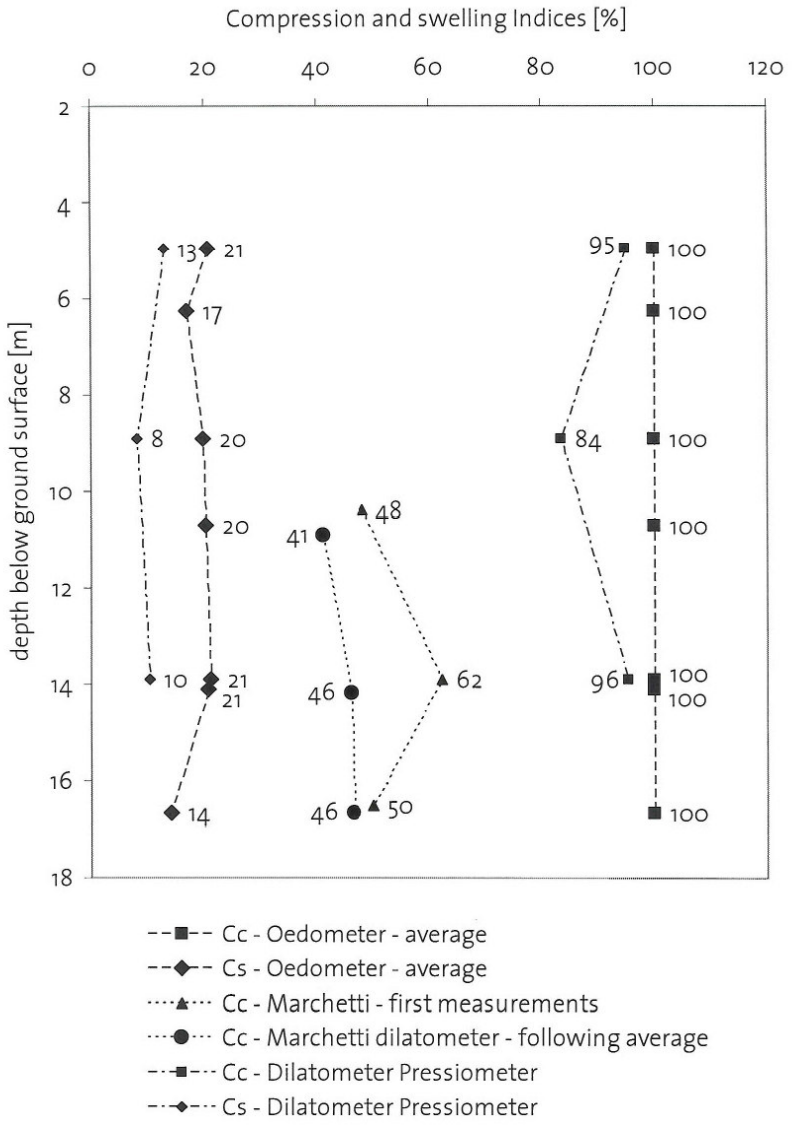

Fig. 12: Comparison of the index ratios of the oedometer, the Marchetti Dilatometer and the Dilatometer Pressiometer tests.

5. Summary and conclusions

- All three methods give qualitatively the same stiffness response over depth.
- Oedometer tests:
  The swelling indices are a fifth of the compression indices.
- Marchetti Dilatometer:
  The compression index is between the swelling and compression index of the oedometer tests and is about a half of the compression index. This might be due to the comparable small displacements applied (1.1 mm).
- Pressiometer Dilatometer:
  The compression index corresponds quantitatively to the compression index determined with Oedometer. This might be due to the comparable large displacements applied (3 to 6 mm).
  The swelling index is about a half of the Oedometer swelling index. This might be due to the unstable unloading behaviour.

This report is part of the field investigations performed 2006 in St. Moritz, which are summarized in detail in Report No. 4714.

Report No. 4714/1 Mes/Rr/IS/AMP
Zurich, 15. November 2007

ETH Zurich
Institute for Geotechnical Engineering

Dr. Sophie Messerklinger
Dipl. Bauing.

Appendix:

Data sheets of the 22 oedometer tests.

Oedometer Test

1_2 St.Moritz

Testaim: Comparison of soil stiffness with measurements of Marchetti and Cambridge Dilatometer tests
Materialnumber: Probe 1
Test apparatus: HIF B 26.1: Oedometer 02 / Zelle 9
File name: Probe_1_2.dat **Testdate:** 14.02.2007
Comments: 4 mm sieved & remoulded - eingestrichen

Measured sample Data:

initial sample height:	H_0	20.00 [mm]
sample diameter:	D	56.40 [mm]
sample area:	A	24.98 [cm²]
initial sample volume:	V_0	49.97 [cm³]
dry sample weight:	m_d	**81.15** [g]
sample volume:	V_s	29.30 [cm³]

Determined sample data:

density	ρ_s	2.77 [g/cm³]

Test Data:

Loadstep σ´ from..to [kPa]	laod σ´ [kPa]	Δσ´ [kPa]	H_{act} [mm]	Δh [mm]	ΔΔh [-]	$\Delta\varepsilon_n$ [-]	$\Delta\varepsilon_e$ [-]	$M(')_{E(n)}$ [kN/m²]	$M(')_{E(e)}$ [kN/m²]	$V_{tot,akt}$ [cm³]	e [-]	C_c [-]	C_s [-]	w act [%]	sample weight [g]
	0		20.00	0.000						49.97	0.71			25.47	101.82
0...4	4	4	19.28	0.720	0.720	0.0373	0.0360	107	111	48.17	0.64			23.26	100.02
4...12.5	13	8.5	18.89	1.108	0.388	0.0205	0.0194	414	438	47.20	0.61	0.0669		22.06	99.05
12.5...25	25	12.5	18.46	1.542	0.434	0.0235	0.0217	532	576	46.11	0.57	0.1229		20.72	97.97
25...50	50	25	18.07	1.929	0.387	0.0214	0.0194	1167	1292	45.15	0.54	0.1096		19.53	97.00
50...100	100	50	17.66	2.344	0.415	0.0235	0.0208	2127	2410	44.11	0.51	0.1176		18.26	95.96
100...200	200	100	17.29	2.706	0.362	0.0209	0.0181	4777	5525	43.21	0.47	0.1026		17.14	95.06
200...400	400	200	16.79	3.210	0.504	0.0300	0.0252	6663	7937	41.95	0.43	0.1428		15.59	93.80
400...200	200	-200	16.83	3.175	-0.035	-0.0021	-0.0018	96143	114286	42.03	0.43		0.0099	15.70	93.89
200...100	100	-100	16.91	3.095	-0.080	-0.0047	-0.0040	21131	25000	42.23	0.44		0.0227	15.94	94.09
100...50	50	-50	17.03	2.971	-0.124	-0.0073	-0.0062	6867	8065	42.54	0.45		0.0351	16.33	94.40
50...100	100	50	16.98	3.025	0.054	0.0032	0.0027	15718	18519	42.41	0.45		0.0153	16.16	94.26
100...200	200	100	16.88	3.122	0.097	0.0057	0.0049	17400	20619	42.17	0.44		0.0275	15.86	94.02
200...400	400	200	16.71	3.288	0.166	0.0099	0.0083	20135	24096	41.75	0.43		0.0470	15.35	93.61
400...800	800	400	16.31	3.691	0.403	0.0247	0.0202	16188	19851	40.75	0.39	0.1142			
800...1600	1600	800	15.82	4.178	0.487	0.0308	0.0244	25991	32854	39.53	0.35	0.1380		12.61	91.38
1600...3200	3200	1600	15.32	4.679	0.501	0.0327	0.0251	48929	63872	38.28	0.31	0.1419		11.07	90.13
										average value		0.117	0.026		

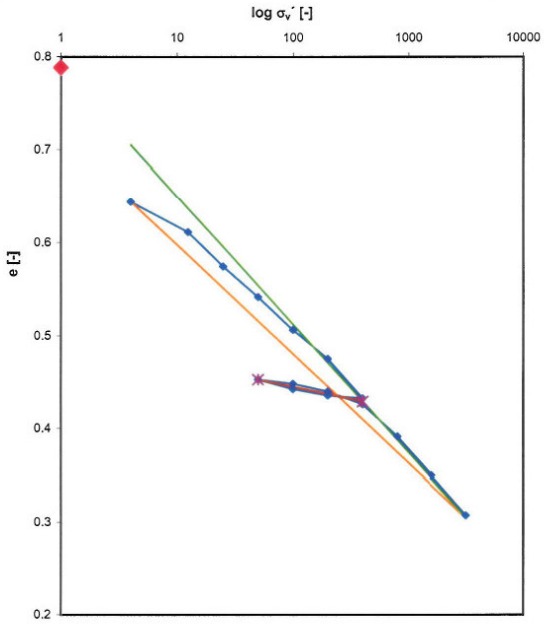

average		optimized	0.138	
sig	e	sig	e	
4	0.64	4	0.705	
3200	0.3034	3200	0.30	
			e0:	0.788

average		optimized	0.026	
sig	e	sig	e	
50	0.45	50	0.45	
400	0.4285	400	0.43	
			e0:	0.496

Oedometer Test

2_1 St.Moritz

Testaim: Comparison of soil stiffness with measurements of Marchetti and Cambridge Dilatometer tests
Materialnumber: Probe 2
Test apparatus: HIF B 26.1: Oedometer 02 / Zelle 09
File name: Probe_2_1.dat **Testdate:** 18.01.2007
Comments: 4 mm sieved & remoulded - eingestrichen

Measured sample Data:

initial sample height:	H_0	20.00 [mm]
sample diameter:	D	56.40 [mm]
sample area:	A	24.98 [cm²]
initial sample volume:	V_0	49.97 [cm³]
dry sample weight:	m_d	63.8 [g]
sample volume:	V_s	23.03 [cm³]

Determined sample data:

density	ρ_s	2.77 [g/cm³]

Test Data:

Loadstep σ´ from..to [kPa]	laod σ´ [kPa]	Δσ´ [kPa]	H_{act} [mm]	Δh [mm]	ΔΔh [-]	$\Delta\varepsilon_n$ [-]	$\Delta\varepsilon_e$ [-]	$M(')_{E(n)}$ [kN/m²]	$M(')_{E(e)}$ [kN/m²]	$V_{tot,akt}$ [cm³]	e [-]	C_c [-]	C_s [-]	w act [%]	sample weight [g]
	0		20.00	0.000						49.97	1.17			42.22	90.73
0...4	4	4	17.96	2.042	2.042	0.1137	0.1021	35	39	44.86	0.95			34.22	85.63
4...12.5	13	8.5	17.38	2.623	0.581	0.0334	0.0291	254	293	43.41	0.88	0.1274		31.94	84.18
12.5...25	25	12.5	16.95	3.055	0.432	0.0255	0.0216	490	579	42.33	0.84	0.1557		30.25	83.10
25...50	50	25	16.46	3.545	0.490	0.0298	0.0245	840	1020	41.11	0.78	0.1766		28.33	81.88
50...100	100	50	15.93	4.072	0.527	0.0331	0.0264	1511	1898	39.79	0.73	0.1899		26.27	80.56
100...200	200	100	15.37	4.630	0.558	0.0363	0.0279	2754	3584	38.40	0.67	0.2011		24.09	79.17
200...400	400	200	14.81	5.194	0.564	0.0381	0.0282	5250	7092	36.99	0.61	0.2032		21.88	77.76
400...200	200	-200	14.82	5.179	-0.015	-0.0010	-0.0007	197613	266667	37.03	0.61		0.0054	21.94	77.80
200...100	100	-100	14.88	5.122	-0.057	-0.0038	-0.0029	26102	35088	37.17	0.61		0.0205	22.16	77.94
100...50	50	-50	14.96	5.037	-0.085	-0.0057	-0.0043	8802	11765	37.38	0.62		0.0306	22.49	78.15
50...100	100	50	14.93	5.067	0.030	0.0020	0.0015	24888	33333	37.31	0.62		0.0108	22.37	78.07
100...200	200	100	14.87	5.129	0.062	0.0042	0.0031	23985	32258	37.15	0.61		0.0223	22.13	77.92
200...400	400	200	14.76	5.242	0.113	0.0077	0.0057	26120	35398	36.87	0.60		0.0407	21.69	77.64
400...800	800	400	14.21	5.788	0.546	0.0384	0.0273	10412	14652	35.51	0.54	0.1967			
800...1600	1600	800	13.61	6.395	0.607	0.0446	0.0304	17931	26359	33.99	0.48	0.2187		17.17	74.76
1600...3200	3200	1600	12.99	7.012	0.617	0.0475	0.0309	33680	51864	32.45	0.41	0.2223		14.76	73.22
										average value		0.188	0.022		

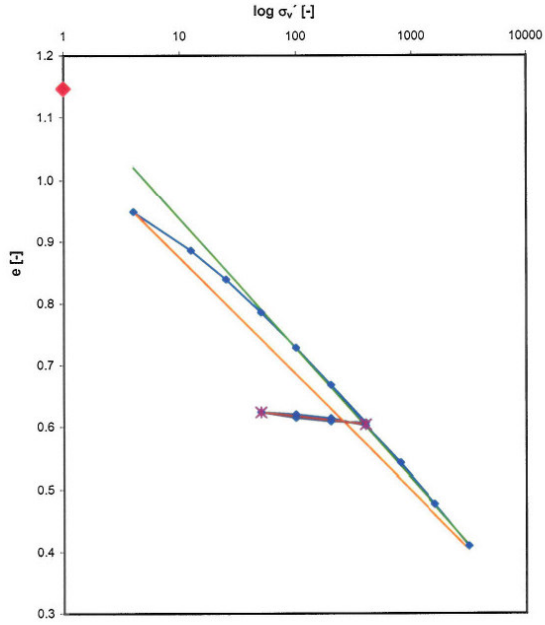

average		optimized	0.21
sig	e	sig	e
4	0.95	4	1.02
3200	0.4023	3200	0.41
			e0: 1.146

average		optimized	0.022
sig	e	sig	e
50	0.62	50	0.62
400	0.6034	400	0.60
			e0: 0.660

Oedometer Test

2_2 St.Moritz

Testaim: Comparison of soil stiffness with measurements of Marchetti and Cambridge Dilatometer tests
Materialnumber: Probe 2
Test apparatus: HIF B 26.1: Oedometer 06 / Zelle 14
File name: Probe_2_2.dat **Testdate:** 18.01.2007
Comments: 4 mm sieved & remoulded - eingestrichen

Measured sample Data:

initial sample height:	H_0	20.00 [mm]
sample diameter:	D	56.40 [mm]
sample area:	A	24.98 [cm²]
initial sample volume:	V_0	49.97 [cm³]
dry sample weight:	m_s	71.23 [g]
sample volume:	V_s	25.71 [cm³]

Determined sample data:

density	ρ_s	2.77 [g/cm³]

Test Data:

Loadstep σ´ from..to [kPa]	Iaod σ´ [kPa]	Δσ´ [kPa]	H_{act} [mm]	Δh [mm]	ΔΔh [-]	$\Delta\varepsilon_n$ [-]	$\Delta\varepsilon_e$ [-]	$M(')_{E(n)}$ [kN/m²]	$M(')_{E(e)}$ [kN/m²]	$V_{tot,akt}$ [cm³]	e [-]	C_c [-]	C_s [-]	w act [%]	sample weight [g]
	0		20.00	0.000						49.97	0.94			34.05	95.48
0...4	4	4	19.44	0.557	0.557	0.0286	0.0279	140	144	48.57	0.89			32.09	94.09
4...12.5	13	8.5	18.92	1.081	0.524	0.0277	0.0262	307	324	47.27	0.84	0.1029		30.26	92.78
12.5...25	25	12.5	18.49	1.510	0.429	0.0232	0.0215	539	583	46.19	0.80	0.1385		28.75	91.71
25...50	50	25	18.05	1.954	0.444	0.0246	0.0222	1016	1126	45.08	0.75	0.1433		27.19	90.60
50...100	100	50	17.51	2.487	0.533	0.0304	0.0267	1643	1876	43.75	0.70	0.1720		25.32	89.27
100...200	200	100	16.96	3.040	0.553	0.0326	0.0277	3067	3617	42.37	0.65	0.1785		23.38	87.89
200...400	400	200	16.42	3.577	0.537	0.0327	0.0269	6117	7449	41.03	0.60	0.1733		21.50	86.55
400...200	200	-200	16.45	3.554	-0.023	-0.0014	-0.0012	143009	173913	41.09	0.60		0.0074	21.58	86.60
200...100	100	-100	16.51	3.487	-0.067	-0.0041	-0.0033	24646	29851	41.25	0.60		0.0216	21.82	86.77
100...50	50	-50	16.62	3.378	-0.109	-0.0066	-0.0055	7625	9174	41.53	0.61		0.0352	22.20	87.04
50...100	100	50	16.58	3.422	0.044	0.0027	0.0022	18839	22727	41.42	0.61		0.0142	22.04	86.93
100...200	200	100	16.49	3.510	0.088	0.0053	0.0044	18739	22727	41.20	0.60		0.0284	21.74	86.71
200...400	400	200	16.37	3.629	0.119	0.0073	0.0060	27514	33613	40.90	0.59		0.0384	21.32	86.42
400...800	800	400	15.86	4.143	0.514	0.0324	0.0257	12340	15564	39.62	0.54	0.1659			
800...1600	1600	800	15.24	4.763	0.620	0.0407	0.0310	19661	25806	38.07	0.48	0.2001		17.34	83.58
1600...3200	3200	1600	14.59	5.412	0.649	0.0445	0.0325	35964	49307	36.45	0.42	0.2095		15.06	81.96
										average value		0.165	0.024		

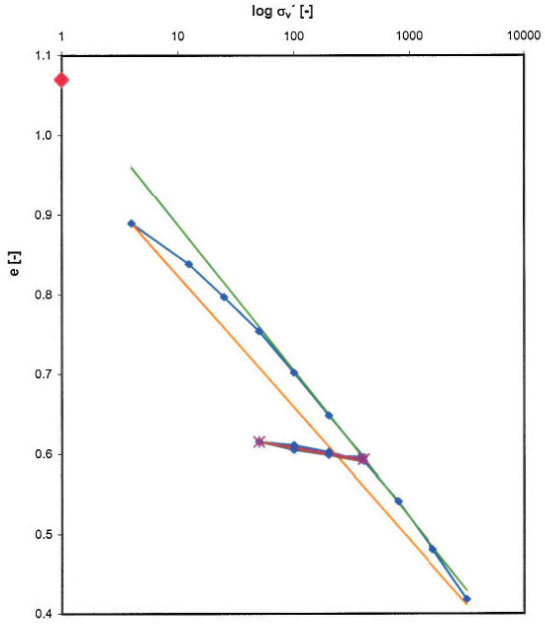

average		optimized	0.183
sig	e	sig	e
4	0.89	4	0.96
3200	0.4103	3200	0.43
			e0: 1.070

average		optimized	0.028
sig	e	sig	e
50	0.61	50	0.61
400	0.593	400	0.59
			e0: 0.662

Oedometer Test

2_3 St.Moritz

Testaim: Comparison of soil stiffness with measurements of Marchetti and Cambridge Dilatometer tests
Materialnumber: Probe 2
Test apparatus: HIF B 26.1: Oedometer 05 / Zelle 12
File name: Probe_2_3.dat **Testdate:** 14.02.2007
Comments: 4 mm sieved & remoulded - eingestrichen

Measured sample Data:

initial sample height:	H_0	20.00 [mm]
sample diameter:	D	56.40 [mm]
sample area:	A	24.98 [cm²]
initial sample volume:	V_0	49.97 [cm³]
dry sample weight:	m_d	74.71 [g]
sample volume:	V_s	26.97 [cm³]

Determined sample data:

density	ρ_s	2.77 [g/cm³]

Test Data:

Loadstep σ´ from..to [kPa]	laod σ´ [kPa]	Δσ´ [kPa]	H_{act} [mm]	Δh [mm]	ΔΔh [-]	$\Delta\varepsilon_n$ [-]	$\Delta\varepsilon_e$ [-]	$M(')_{E(n)}$ [kN/m²]	$M(')_{E(e)}$ [kN/m²]	$V_{tot,akt}$ [cm³]	e [-]	C_c [-]	C_s [-]	w act [%]	sample weight [g]
	0		20.00	0.000						49.97	0.85			30.78	97.71
0...4	4	4	19.89	0.109	0.109	0.0055	0.0055	730	734	49.69	0.84			30.41	97.43
4...12.5	13	8.5	18.95	1.049	0.940	0.0496	0.0470	171	181	47.35	0.76	0.1760		27.27	95.08
12.5...25	25	12.5	18.57	1.431	0.382	0.0206	0.0191	608	654	46.39	0.72	0.1175		25.99	94.13
25...50	50	25	18.10	1.905	0.474	0.0262	0.0237	954	1055	45.21	0.68	0.1459		24.41	92.95
50...100	100	50	17.52	2.482	0.577	0.0329	0.0289	1518	1733	43.77	0.62	0.1775		22.48	91.50
100...200	200	100	16.93	3.075	0.593	0.0350	0.0297	2854	3373	42.28	0.57	0.1825		20.50	90.02
200...400	400	200	16.36	3.638	0.563	0.0344	0.0282	5812	7105	40.88	0.52	0.1732		18.61	88.62
400...200	200	-200	16.39	3.609	-0.029	-0.0018	-0.0015	113041	137931	40.95	0.52		0.0089	18.71	88.69
200...100	100	-100	16.48	3.518	-0.091	-0.0055	-0.0046	18112	21978	41.18	0.53		0.0280	19.02	88.92
100...50	50	-50	16.68	3.325	-0.193	-0.0116	-0.0096	4320	5181	41.66	0.54		0.0594	19.66	89.40
50...100	100	50	16.56	3.445	0.120	0.0072	0.0060	6898	8333	41.36	0.53		0.0369	19.26	89.10
100...200	200	100	16.45	3.551	0.106	0.0064	0.0053	15518	18868	41.09	0.52		0.0326	18.90	88.83
200...400	400	200	16.32	3.678	0.127	0.0078	0.0063	25704	31496	40.78	0.51		0.0391	18.48	88.52
400...800	800	400	15.78	4.222	0.544	0.0345	0.0272	11601	14706	39.42	0.46	0.1674			
800...1600	1600	800	15.16	4.839	0.617	0.0407	0.0309	19658	25932	37.88	0.40	0.1899		14.60	85.62
1600...3200	3200	1600	14.49	5.506	0.667	0.0460	0.0334	34768	47976	36.21	0.34	0.2052		12.37	83.95
										average value		0.171	0.034		

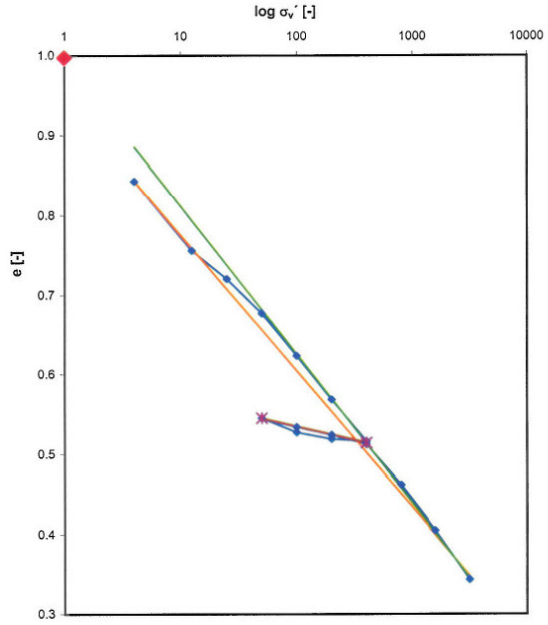

average		optimized	0.186
sig	e	sig	e
4	0.84	4	0.885
3200	0.3473	3200	0.35
			e0: 0.997

average		optimized	0.034
sig	e	sig	e
50	0.54	50	0.54
400	0.5138	400	0.51
			e0: 0.602

Oedometer Test

3_1 St.Moritz

Testaim: Comparison of soil stiffness with measurements of Marchetti and Cambridge Dilatometer tests
Materialnumber: Probe 3
Test apparatus: HIF B 26.1: Oedometer 04 / Zelle 12
File name: Probe_3_1.dat **Testdate:** 18.01.2007
Comments: 4 mm sieved & remoulded - eingestrichen

Measured sample Data:

initial sample height:	H_0	20.00 [mm]
sample diameter:	D	56.40 [mm]
sample area:	A	24.98 [cm²]
initial sample volume:	V_0	49.97 [cm³]
dry sample weight:	m_d	75.3 [g]
sample volume:	V_s	27.18 [cm³]

Determined sample data:

density	ρ_s	2.77 [g/cm³]

Test Data:

Loadstep σ´ from..to [kPa]	∫σ´ [kPa]	Δσ´ [kPa]	H_{act} [mm]	Δh [mm]	ΔΔh [-]	$\Delta\varepsilon_n$ [-]	$\Delta\varepsilon_e$ [-]	$M(')_{E(n)}$ [kN/m²]	$M(')_{E(e)}$ [kN/m²]	$V_{tot,akt}$ [cm³]	e [-]	C_c [-]	C_s [-]	w act [%]	sample weight [g]
	0		20.00	0.000						49.97	0.84			30.26	98.08
0...4	4	4	19.23	0.774	0.774	0.0403	0.0387	99	103	48.03	0.77			27.69	96.15
4...12.5	13	8.5	18.25	1.754	0.980	0.0537	0.0490	158	173	45.58	0.68	0.1820		24.44	93.70
12.5...25	25	12.5	17.22	2.780	1.026	0.0596	0.0513	210	244	43.02	0.58	0.3132		21.03	91.14
25...50	50	25	16.81	3.189	0.409	0.0243	0.0205	1028	1222	42.00	0.54	0.1249		19.67	90.12
50...100	100	50	16.30	3.698	0.509	0.0312	0.0255	1601	1965	40.73	0.50	0.1554		17.99	88.84
100...200	200	100	15.83	4.166	0.468	0.0296	0.0234	3383	4274	39.56	0.46	0.1429		16.43	87.67
200...400	400	200	15.38	4.617	0.451	0.0293	0.0226	6822	8869	38.43	0.41	0.1377		14.94	86.55
400...200	200	-200	15.43	4.575	-0.042	-0.0027	-0.0021	73452	95238	38.54	0.42		0.0128	15.08	86.65
200...100	100	-100	15.52	4.482	-0.093	-0.0060	-0.0047	16686	21505	38.77	0.43		0.0284	15.38	86.88
100...50	50	-50	15.66	4.343	-0.139	-0.0089	-0.0070	5632	7194	39.12	0.44		0.0424	15.85	87.23
50...100	100	50	15.58	4.424	0.081	0.0052	0.0041	9615	12346	38.91	0.43		0.0247	15.58	87.03
100...200	200	100	15.47	4.530	0.106	0.0069	0.0053	14594	18868	38.65	0.42		0.0324	15.23	86.76
200...400	400	200	15.31	4.686	0.156	0.0102	0.0078	19633	25641	38.26	0.41		0.0476	14.71	86.38
400...800	800	400	14.90	5.102	0.416	0.0279	0.0208	14325	19231	37.22	0.37	0.1270			
800...1600	1600	800	14.40	5.598	0.496	0.0344	0.0248	23229	32258	35.98	0.32	0.1514		11.68	84.10
1600...3200	3200	1600	13.87	6.127	0.529	0.0381	0.0265	41960	60491	34.66	0.27	0.1615		9.93	82.78
										average value		0.166	0.031		

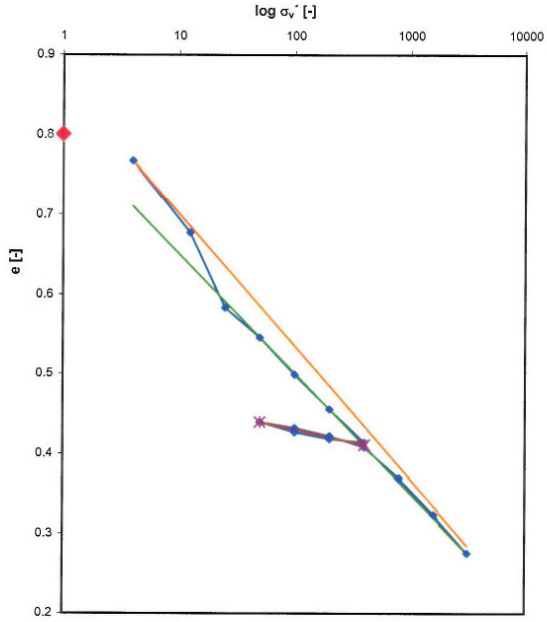

average		optimized	0.15	
sig	e	sig	e	
4	0.77	4	0.71	
3200	0.2844	3200	0.27	
			e0:	0.800

average		optimized	0.031	
sig	e	sig	e	
50	0.44	50	0.44	
400	0.4106	400	0.41	
			e0:	0.492

Oedometer Test

3_2 St.Moritz

Testaim: Comparison of soil stiffness with measurements of Marchetti and Cambridge Dilatometer tests
Materialnumber: Probe 3
Test apparatus: HIF B 26.1: Oedometer 05 / Zelle 10
File name: Probe_3_2.dat **Testdate:** 18.01.2007
Comments: 4 mm sieved & remoulded - eingestrichen

Measured sample Data:

initial sample height:	H_0	20.00 [mm]
sample diameter:	D	56.40 [mm]
sample area:	A	24.98 [cm^2]
initial sample volume:	V_0	49.97 [cm^3]
dry sample weight:	m_d	74.73 [g]
sample volume:	V_s	26.98 [cm^3]

Determined sample data:

density	ρ_s	2.77 [g/cm^3]

Test Data:

Loadstep σ´ from..to [kPa]	laod σ´ [kPa]	Δσ´ [kPa]	H_{act} [mm]	Δh [mm]	ΔΔh [-]	$\Delta\varepsilon_n$ [-]	$\Delta\varepsilon_e$ [-]	$M(')_{E(n)}$ [kN/m^2]	$M(')_{E(e)}$ [kN/m^2]	$V_{tot,akt}$ [cm^3]	e [-]	C_c [-]	C_s [-]	w act [%]	sample weight [g]
	0		20.00	0.000						49.97	0.85			30.76	97.72
0...4	4	4	19.68	0.319	0.319	0.0162	0.0160	247	251	49.17	0.82			29.70	96.92
4...12.5	13	8.5	18.61	1.392	1.073	0.0577	0.0537	147	158	46.49	0.72	0.2008		26.11	94.24
12.5...25	25	12.5	18.53	1.472	0.080	0.0043	0.0040	2895	3125	46.29	0.72	0.0246		25.84	94.04
25...50	50	25	16.56	3.442	1.970	0.1190	0.0985	210	254	41.37	0.53	0.6060		19.25	89.12
50...100	100	50	16.11	3.893	0.451	0.0280	0.0226	1786	2217	40.24	0.49	0.1387		17.75	87.99
100...200	200	100	15.65	4.355	0.462	0.0295	0.0231	3386	4329	39.09	0.45	0.1421		16.20	86.84
200...400	400	200	15.19	4.810	0.455	0.0300	0.0228	6677	8791	37.95	0.41	0.1400		14.68	85.70
400...200	200	-200	15.22	4.778	-0.032	-0.0021	-0.0016	95137	125000	38.03	0.41		0.0098	14.79	85.78
200...100	100	-100	15.31	4.691	-0.087	-0.0057	-0.0043	17597	22989	38.25	0.42		0.0268	15.08	86.00
100...50	50	-50	15.43	4.571	-0.120	-0.0078	-0.0060	6429	8333	38.55	0.43		0.0369	15.48	86.30
50...100	100	50	15.38	4.616	0.045	0.0029	0.0023	17093	22222	38.43	0.42		0.0138	15.33	86.19
100...200	200	100	15.28	4.721	0.105	0.0069	0.0053	14551	19048	38.17	0.41		0.0323	14.98	85.92
200...400	400	200	15.11	4.887	0.166	0.0110	0.0083	18208	24096	37.76	0.40		0.0511	14.42	85.51
400...800	800	400	14.70	5.301	0.414	0.0282	0.0207	14202	19324	36.72	0.36	0.1274			
800...1600	1600	800	14.21	5.795	0.494	0.0348	0.0247	23004	32389	35.49	0.32	0.1520		11.39	83.24
1600...3200	3200	1600	13.68	6.319	0.524	0.0383	0.0262	41774	61069	34.18	0.27	0.1612		9.64	81.93
										average value		0.188	0.028		

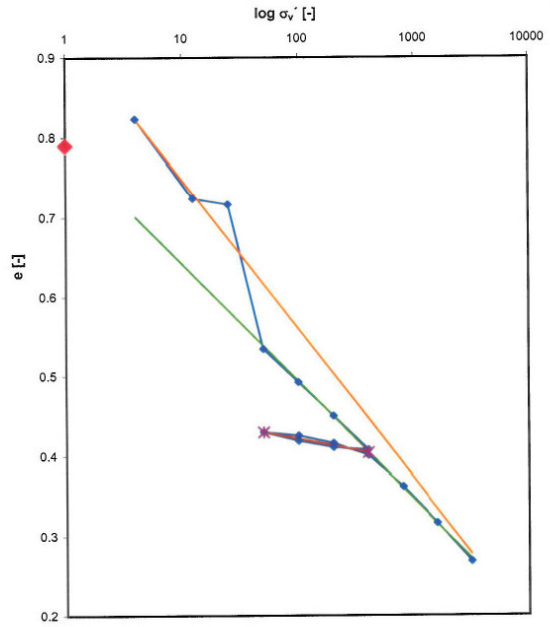

average		optimized	
sig	e	sig	e
4	0.82	4	0.7
3200	0.2765	3200	0.27
			e0: 0.789

average		optimized	0.028
sig	e	sig	e
50	0.43	50	0.43
400	0.4031	400	0.40
			e0: 0.476

Oedometer Test

4_1 St.Moritz

Testaim: Comparison of soil stiffness with measurements of Marchetti and Cambridge Dilatometer tests
Materialnumber: Probe 4
Test apparatus: HIF B 26.1: Oedometer 01 / Zelle 11
File name: Probe_4_1.dat **Testdate:** 18.01.2007
Comments: 4 mm sieved & remoulded - eingestrichen

Measured sample Data:

initial sample height:	H_0	20.00	[mm]
sample diameter:	D	56.40	[mm]
sample area:	A	24.98	[cm²]
initial sample volume:	V_0	49.97	[cm³]
dry sample weight:	m_d	79.24	[g]
sample volume:	V_s	28.61	[cm³]

Determined sample data:

density	ρ_s	2.77	[g/cm³]

Test Data:

Loadstep σ´ from..to [kPa]	laod σ´ [kPa]	Δσ´ [kPa]	H_{act} [mm]	Δh [mm]	ΔΔh [-]	$\Delta\varepsilon_m$ [-]	$\Delta\varepsilon_e$ [-]	$M(')_{E(p)}$ [kN/m²]	$M(')_{E(e)}$ [kN/m²]	$V_{tot,akt}$ [cm³]	e [-]	C_c [-]	C_s [-]	w act [%]	sample weight [g]
	0		20.00	0.000						49.97	0.75			26.96	100.60
0…4	4	4	19.26	0.741	0.741	0.0385	0.0371	104	108	48.12	0.68			24.62	98.75
4…12.5	13	8.5	18.91	1.092	0.351	0.0186	0.0176	458	484	47.24	0.65	0.0619		23.51	97.87
12.5…25	25	12.5	18.41	1.593	0.501	0.0272	0.0251	459	499	45.99	0.61	0.1453		21.93	96.62
25…50	50	25	17.23	2.766	1.173	0.0681	0.0587	367	426	43.06	0.51	0.3403		18.24	93.69
50…100	100	50	16.77	3.235	0.469	0.0280	0.0235	1787	2132	41.88	0.46	0.1361		16.76	92.52
100…200	200	100	16.28	3.721	0.486	0.0299	0.0243	3350	4115	40.67	0.42	0.1410		15.22	91.30
200…400	400	200	15.78	4.217	0.496	0.0314	0.0248	6364	8065	39.43	0.38	0.1439		13.66	90.06
400…200	200	-200	15.83	4.173	-0.044	-0.0028	-0.0022	71941	90909	39.54	0.38		0.0128	13.80	90.17
200…100	100	-100	15.92	4.076	-0.097	-0.0061	-0.0049	16416	20619	39.78	0.39		0.0281	14.10	90.42
100…50	50	-50	16.06	3.941	-0.135	-0.0084	-0.0067	5948	7407	40.12	0.40		0.0392	14.53	90.75
50…100	100	50	16.00	4.002	0.061	0.0038	0.0031	13113	16393	39.97	0.40		0.0177	14.34	90.60
100…200	200	100	15.88	4.116	0.114	0.0072	0.0057	13933	17544	39.68	0.39		0.0331	13.98	90.32
200…400	400	200	15.70	4.299	0.183	0.0117	0.0092	17160	21858	39.23	0.37		0.0531	13.40	89.86
400…800	800	400	15.25	4.753	0.454	0.0298	0.0227	13433	17621	38.09	0.33	0.1317			
800…1600	1600	800	14.72	5.285	0.532	0.0362	0.0266	22128	30075	36.76	0.29	0.1543		10.29	87.40
1600…3200	3200	1600	14.16	5.840	0.555	0.0392	0.0278	40822	57658	35.38	0.24	0.1610		8.54	86.01
										average value		0.157	0.031		

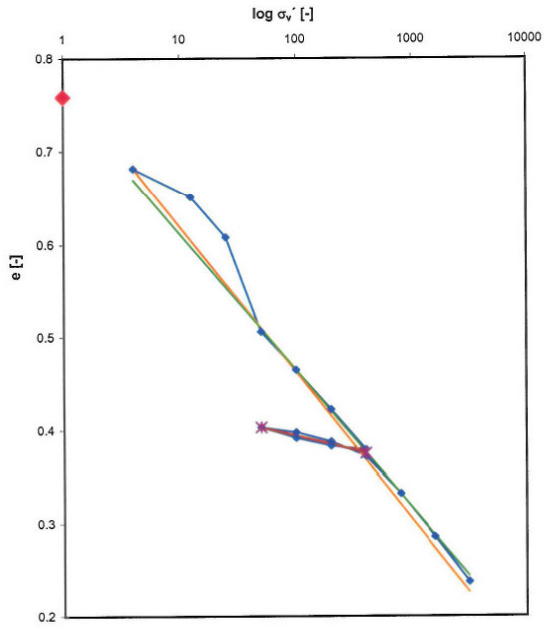

average	
sig	e
4	0.68
3200	0.2253

optimized	
sig	e
4	0.67
3200	0.24
e0:	0.759

average	
sig	e
50	0.40
400	0.3748

optimized	
sig	e
50	0.40
400	0.38
e0:	0.453

Oedometer Test

5_1 St.Moritz

Testaim: Comparison of soil stiffness with measurements of Marchetti and Cambridge Dilatometer tests
Materialnumber: Probe 5
Test apparatus: HIF B 26.1: Oedometer 03 / Zelle 13
File name: Probe_5_1.dat **Testdate:** 18.01.2007
Comments: 4 mm sieved & remoulded - eingestrichen

Measured sample Data:

initial sample height:	H_0	20.00 [mm]
sample diameter:	D	56.40 [mm]
sample area:	A	24.98 [cm^2]
initial sample volume:	V_0	49.97 [cm^3]
dry sample weight:	m_d	**73.96** [g]
sample volume:	V_s	26.70 [cm^3]

Determined sample data:

density	ρ_s	2.77 [g/cm^3]

Test Data:

Loadstep σ´ from..to [kPa]	Iaod σ´ [kPa]	Δσ´ [kPa]	H_{act} [mm]	Δh [mm]	ΔΔh [-]	$\Delta\varepsilon_n$ [-]	$\Delta\varepsilon_e$ [-]	$M(')_{E(n)}$ [kN/m²]	$M(')_{E(e)}$ [kN/m²]	$V_{tot,akt}$ [cm^3]	e [-]	C_c [-]	C_s [-]	w act [%]	sample weight [g]
	0		20.00	0.000						49.97	0.87			31.46	97.23
0…4	4	4	19.76	0.236	0.236	0.0119	0.0118	335	339	49.38	0.85			30.66	96.64
4…12.5	13	8.5	19.60	0.400	0.164	0.0084	0.0082	1016	1037	48.97	0.83	0.0310		30.11	96.23
12.5…25	25	12.5	19.36	0.643	0.243	0.0126	0.0122	996	1029	48.36	0.81	0.0755		29.29	95.62
25…50	50	25	16.27	3.731	3.088	0.1898	0.1544	132	162	40.65	0.52	0.9598		18.85	87.90
50…100	100	50	15.79	4.212	0.481	0.0305	0.0241	1641	2079	39.44	0.48	0.1495		17.23	86.70
100…200	200	100	15.28	4.725	0.513	0.0336	0.0257	2978	3899	38.16	0.43	0.1595		15.50	85.42
200…400	400	200	14.74	5.260	0.535	0.0363	0.0268	5510	7477	36.83	0.38	0.1663		13.69	84.08
400…200	200	-200	14.79	5.210	-0.050	-0.0034	-0.0025	59160	80000	36.95	0.38		0.0155	13.86	84.21
200…100	100	-100	14.91	5.088	-0.122	-0.0082	-0.0061	12223	16393	37.25	0.40		0.0379	14.27	84.51
100…50	50	-50	15.06	4.939	-0.149	-0.0099	-0.0075	5054	6711	37.63	0.41		0.0463	14.77	84.89
50…100	100	50	15.00	4.996	0.057	0.0038	0.0029	13161	17544	37.48	0.40		0.0177	14.58	84.74
100…200	200	100	14.87	5.129	0.133	0.0089	0.0066	11181	15038	37.15	0.39		0.0413	14.13	84.41
200…400	400	200	14.65	5.348	0.219	0.0149	0.0110	13381	18265	36.61	0.37		0.0681	13.39	83.87
400…800	800	400	14.20	5.803	0.455	0.0320	0.0228	12481	17582	35.47	0.33	0.1414			
800…1600	1600	800	13.67	6.327	0.524	0.0383	0.0262	20875	30534	34.16	0.28	0.1629		10.09	81.42
1600…3200	3200	1600	13.14	6.863	0.536	0.0408	0.0268	39215	59701	32.82	0.23	0.1666		8.27	80.08
										average value		0.224	0.038		

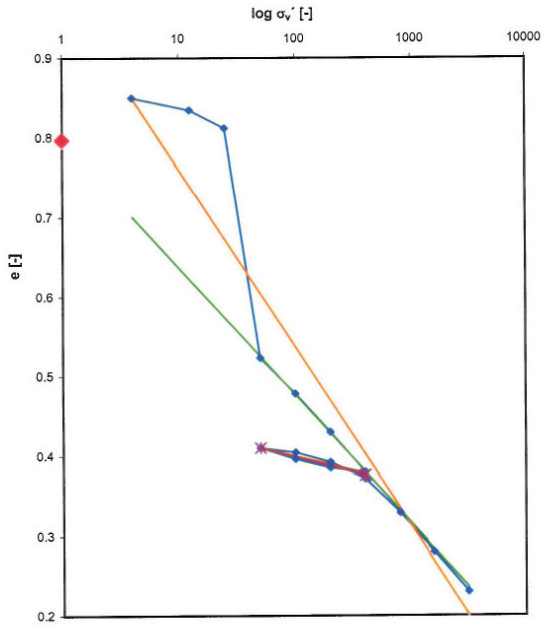

average		optimized		
sig	e	sig	e	0.16
4	0.85	4	0.7	
3200	0.2001	3200	0.24	
			e0:	0.796

average		optimized		
sig	e	sig	e	0.035
50	0.41	50	0.41	
400	0.3751	400	0.38	
			e0:	0.469

Oedometer Test

6_1 St.Moritz

Testaim: Comparison of soil stiffness with measurements of Marchetti and Cambridge Dilatometer tests
Materialnumber: Probe 6
Test apparatus: HIF B 26.1: Oedometer 06 / Zelle 14
File name: Probe_6_1.dat **Testdate:** 16.01.2007
Comments: 4 mm sieved & remoulded - eingestrichen

Measured sample Data:

initial sample height:	H_0	20.00 [mm]
sample diameter:	D	56.40 [mm]
sample area:	A	24.98 [cm²]
initial sample volume:	V_0	49.97 [cm³]
dry sample weight:	m_d	82.33 [g]
sample volume:	V_s	29.72 [cm³]

Determined sample data:

density	ρ_s	2.77 [g/cm³]

Test Data:

Loadstep σ´ from..to [kPa]	laod σ´ [kPa]	Δσ´ [kPa]	H_{act} [mm]	Δh [mm]	ΔΔh [-]	$\Delta\varepsilon_n$ [-]	$\Delta\varepsilon_e$ [-]	$M('')_{E(n)}$ [kN/m²]	$M('')_{E(e)}$ [kN/m²]	$V_{tot,akt}$ [cm³]	e [-]	C_c [-]	C_s [-]	w act [%]	sample weight [g]
	0		20.00	0.000						49.97	0.68			24.59	102.57
0...4	4	4	19.80	0.204	0.204	0.0103	0.0102	388	392	49.46	0.66			23.97	102.06
4...12.5	13	8.5	19.14	0.860	0.656	0.0343	0.0328	248	259	47.82	0.61	0.1114		21.98	100.43
12.5...25	25	12.5	18.70	1.298	0.438	0.0234	0.0219	534	571	46.72	0.57	0.1223		20.65	99.33
25...50	50	25	18.39	1.611	0.313	0.0170	0.0157	1469	1597	45.94	0.55	0.0874		19.70	98.55
50...100	100	50	17.41	2.588	0.977	0.0561	0.0489	891	1024	43.50	0.46	0.2728		16.74	96.11
100...200	200	100	16.91	3.090	0.502	0.0297	0.0251	3369	3984	42.25	0.42	0.1402		15.21	94.85
200...400	400	200	16.38	3.621	0.531	0.0324	0.0266	6169	7533	40.92	0.38	0.1483		13.60	93.53
400...200	200	-200	16.42	3.585	-0.036	-0.0022	-0.0018	91194	111111	41.01	0.38		0.0101	13.71	93.62
200...100	100	-100	16.51	3.486	-0.099	-0.0060	-0.0049	16681	20202	41.26	0.39		0.0276	14.01	93.87
100...50	50	-50	16.66	3.339	-0.147	-0.0088	-0.0074	5667	6803	41.62	0.40		0.0410	14.46	94.23
50...100	100	50	16.61	3.391	0.052	0.0031	0.0026	15970	19231	41.49	0.40		0.0145	14.30	94.10
100...200	200	100	16.48	3.518	0.127	0.0077	0.0063	12978	15748	41.18	0.39		0.0355	13.91	93.79
200...400	400	200	15.81	4.187	0.669	0.0423	0.0335	4727	5979	39.51				0.00	82.33
400...800	800	400													
800...1600	1600	800	15.26	4.741	4.741	0.3107	0.2371	2575	3375	38.12	0.28			10.20	90.73
1600...3200	3200	1600	14.67	5.331	0.590	0.0402	0.0295	39780	54237	36.65	0.23	0.1647		8.41	89.26
										average value		0.150	0.026		

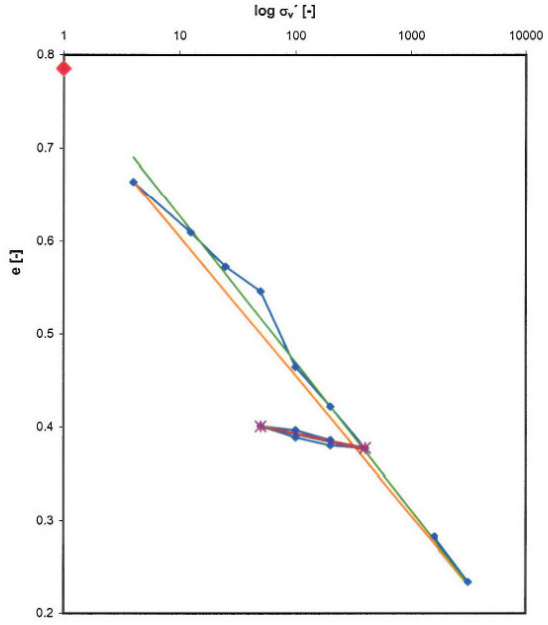

average		optimized	0.158
sig	e	sig	e
4	0.66	4	0.69
3200	0.2297	3200	0.23
			e0: 0.785

average		optimized	0.028
sig	e	sig	e
50	0.40	50	0.40
400	0.3772	400	0.38
			e0: 0.448

Oedometer Test

7_1 St.Moritz

Testaim: Comparison of soil stiffness with measurements of Marchetti and Cambridge Dilatometer tests
Materialnumber: Probe 7
Test apparatus: HIF B 26.1: Oedometer 05 / Zelle 10
File name: Probe_7_1.dat **Testdate:** 16.01.2007
Comments: 4 mm sieved & remoulded - eingestrichen

Measured sample Data:

initial sample height:	H_0	20.00 [mm]
sample diameter:	D	56.40 [mm]
sample area:	A	24.98 [cm²]
initial sample volume:	V_0	49.97 [cm³]
dry sample weight:	m_d	**85.75** [g]
sample volume:	V_s	30.96 [cm³]

Determined sample data:

density	ρ_s	2.77 [g/cm³]

Test Data:

Loadstep σ´ from..to [kPa]	load σ´ [kPa]	Δσ´ [kPa]	H_{act} [mm]	Δh [mm]	ΔΔh [-]	$\Delta\varepsilon_n$ [-]	$\Delta\varepsilon_e$ [-]	$M(')_{E(n)}$ [kN/m²]	$M(')_{E(e)}$ [kN/m²]	V_{totAkt} [cm³]	e [-]	C_c [-]	C_s [-]	w act [%]	sample weight [g]
	0		20.00	0.000						49.97	0.61			22.17	104.76
0...4	4	4	19.99	0.015	0.015	0.0008	0.0008	5329	5333	49.93	0.61			22.13	104.72
4...12.5	13	8.5	19.11	0.890	0.875	0.0458	0.0438	186	194	47.74	0.54	0.1427		19.58	102.54
12.5...25	25	12.5	18.74	1.257	0.367	0.0196	0.0184	638	681	46.83	0.51	0.0984		18.51	101.62
25...50	50	25	18.35	1.647	0.390	0.0212	0.0195	1176	1282	45.85	0.48	0.1046		17.37	100.64
50...100	100	50	17.55	2.450	0.803	0.0458	0.0402	1093	1245	43.85	0.42	0.2153		15.03	98.64
100...200	200	100	17.04	2.961	0.511	0.0300	0.0256	3334	3914	42.57	0.38	0.1370		13.54	97.36
200...400	400	200	16.53	3.475	0.514	0.0311	0.0257	6430	7782	41.28	0.33	0.1378		12.04	96.08
400...200	200	-200	16.57	3.435	-0.040	-0.0024	-0.0020	82825	100000	41.38	0.34		0.0107	12.16	96.18
200...100	100	-100	16.67	3.328	-0.107	-0.0064	-0.0054	15581	18692	41.65	0.35		0.0287	12.47	96.45
100...50	50	-50	16.82	3.178	-0.150	-0.0089	-0.0075	5607	6667	42.03	0.36		0.0402	12.91	96.82
50...100	100	50	16.77	3.235	0.057	0.0034	0.0029	14706	17544	41.88	0.35		0.0153	12.74	96.68
100...200	200	100	16.64	3.362	0.127	0.0076	0.0064	13101	15748	41.57	0.34		0.0340	12.37	96.36
200...400	400	200	16.44	3.564	0.202	0.0123	0.0101	16273	19802	41.06	0.33		0.0542	11.79	95.86
400...800	800	400	15.97	4.034	0.470	0.0294	0.0235	13588	17021	39.89	0.29	0.1260		10.42	94.68
800...1600	1600	800	15.43	4.571	0.537	0.0348	0.0269	22985	29795	38.55	0.25	0.1440		8.85	93.34
1600...3200	3200	1600	14.86	5.136	0.565	0.0380	0.0283	42093	56637	37.14	0.20	0.1515		7.21	91.93
										average value		**0.140**	**0.031**		

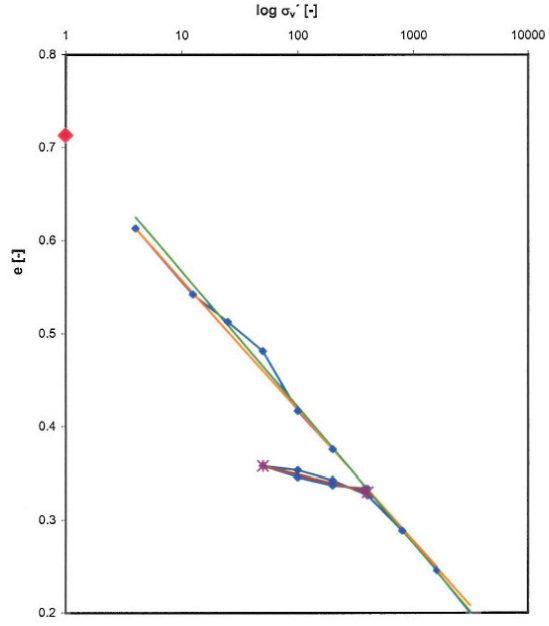

average		optimized	0.146	
sig	e	sig	e	
4	0.61	4	0.625	
3200	0.2073	3200	0.20	
			e0:	0.713

average		optimized	0.03	
sig	e	sig	e	
50	0.36	50	0.36	
400	0.33	400	0.33	
			e0:	0.409

Oedometer Test

8_1 St.Moritz

Testaim: Comparison of soil stiffness with measurements of Marchetti and Cambridge Dilatometer tests
Materialnumber: Probe 8
Test apparatus: HIF B 26.1: Oedometer 03 / Zelle 13
File name: Probe_8_1.dat **Testdate:** 16.01.2007
Comments: 4 mm sieved & remoulded - eingestrichen

Measured sample Data:

initial sample height:	H_0	20.00 [mm]
sample diameter:	D	56.40 [mm]
sample area:	A	24.98 [cm²]
initial sample volume:	V_0	49.97 [cm³]
dry sample weight:	m_s	86.3 [g]
sample volume:	V_s	31.16 [cm³]

Determined sample data:

density	ρ_s	2.77 [g/cm³]

Test Data:

Loadstep σ´ from..to [kPa]	laod σ´ [kPa]	Δσ´ [kPa]	H_{act} [mm]	Δh [mm]	ΔΔh [-]	$\Delta\varepsilon_n$ [-]	$\Delta\varepsilon_e$ [-]	$M(')_{E(n)}$ [kN/m²]	$M(')_{E(e)}$ [kN/m²]	$V_{tot,akt}$ [cm³]	e [-]	C_c [-]	C_s [-]	w act [%]	sample weight [g]
	0		20.00	0.000						49.97	0.60			21.80	105.11
0...4	4	4	19.85	0.152	0.152	0.0077	0.0076	522	526	49.59	0.59			21.36	104.73
4...12.5	13	8.5	19.53	0.474	0.322	0.0165	0.0161	515	528	48.78	0.57	0.0522		20.43	103.93
12.5...25	25	12.5	19.16	0.844	0.370	0.0193	0.0185	647	676	47.86	0.54	0.0986		19.35	103.00
25...50	50	25	18.76	1.244	0.400	0.0213	0.0200	1172	1250	46.86	0.50	0.1066		18.20	102.00
50...100	100	50	18.07	1.935	0.691	0.0383	0.0346	1307	1447	45.13	0.45	0.1841		16.20	100.28
100...200	200	100	17.39	2.606	0.671	0.0386	0.0336	2592	2981	43.46	0.39	0.1787		14.25	98.60
200...400	400	200	16.81	3.190	0.584	0.0347	0.0292	5757	6849	42.00	0.35	0.1556		12.56	97.14
400...200	200	-200	16.86	3.143	-0.047	-0.0028	-0.0024	71732	85106	42.11	0.35		0.0125	12.70	97.26
200...100	100	-100	16.97	3.034	-0.109	-0.0064	-0.0055	15565	18349	42.39	0.36		0.0290	13.01	97.53
100...50	50	-50	17.11	2.888	-0.146	-0.0085	-0.0073	5860	6849	42.75	0.37		0.0389	13.44	97.90
50...100	100	50	17.06	2.943	0.055	0.0032	0.0028	15506	18182	42.61	0.37		0.0147	13.28	97.76
100...200	200	100	16.93	3.071	0.128	0.0076	0.0064	13226	15625	42.29	0.36		0.0341	12.91	97.44
200...400	400	200	16.72	3.281	0.210	0.0126	0.0105	15923	19048	41.77	0.34		0.0559	12.30	96.91
400...800	800	400	16.21	3.786	0.505	0.0311	0.0253	12843	15842	40.51	0.30	0.1345		10.84	95.65
800...1600	1600	800	15.65	4.347	0.561	0.0358	0.0281	22322	28520	39.11	0.26	0.1494		9.21	94.25
1600...3200	3200	1600	15.07	4.930	0.583	0.0387	0.0292	41358	54889	37.65	0.21	0.1553		7.53	92.79
										average value		0.135	0.031		

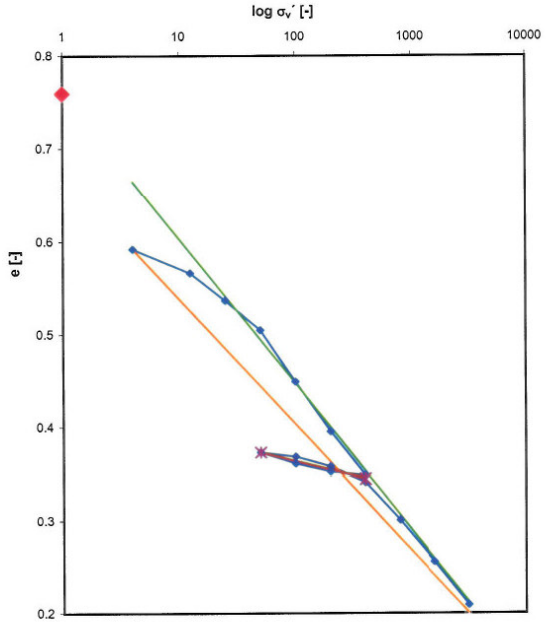

average		optimized	0.156	
sig	e	sig	e	
4	0.59	4	0.665	
3200	0.1997	3200	0.21	
			e0:	0.759

average		optimized	0.03	
sig	e	sig	e	
50	0.37	50	0.37	
400	0.3443	400	0.35	
			e0:	0.423

Oedometer Test

8_2 St.Moritz

Testaim: Comparison of soil stiffness with measurements of Marchetti and Cambridge Dilatometer tests
Materialnumber: Probe 8
Test apparatus: HIF B 26.1: Oedometer 04 / Zelle 12
File name: Probe_8_2.dat **Testdate:** 16.01.2007
Comments: 4 mm sieved & remoulded - eingestrichen

Measured sample Data:

initial sample height:	H_0	20.00 [mm]
sample diameter:	D	56.40 [mm]
sample area:	A	24.98 [cm^2]
initial sample volume:	V_0	49.97 [cm^3]
dry sample weight:	m_d	**86.07** [g]
sample volume:	V_s	31.07 [cm^3]

Determined sample data:

density	ρ_s	2.77 [g/cm^3]

Test Data:

Loadstep σ´ from..to [kPa]	laod σ´ [kPa]	Δσ´ [kPa]	H_{act} [mm]	Δh [mm]	ΔΔh [-]	$\Delta\varepsilon_n$ [-]	$\Delta\varepsilon_s$ [-]	$M(')_{E(n)}$ [kN/m^2]	$M(')_{E(e)}$ [kN/m^2]	V_{solakt} [cm^3]	e [-]	C_c [-]	C_s [-]	w act [%]	sample weight [g]
	0		20.00	0.000						49.97	0.61			21.95	104.96
0...4	4	4	19.92	0.083	0.083	0.0042	0.0042	960	964	49.76	0.60			21.71	104.76
4...12.5	13	8.5	19.53	0.468	0.385	0.0197	0.0193	431	442	48.80	0.57	0.0626		20.59	103.79
12.5...25	25	12.5	19.12	0.885	0.417	0.0218	0.0209	573	600	47.76	0.54	0.1114		19.38	102.75
25...50	50	25	18.80	1.197	0.312	0.0166	0.0156	1507	1603	46.98	0.51	0.0833		18.48	101.97
50...100	100	50	18.07	1.928	0.731	0.0404	0.0366	1236	1368	45.15	0.45	0.1952		16.36	100.15
100...200	200	100	17.53	2.466	0.538	0.0307	0.0269	3259	3717	43.81	0.41	0.1437		14.79	98.80
200...400	400	200	17.02	2.981	0.515	0.0303	0.0258	6609	7767	42.52	0.37	0.1376		13.30	97.52
400...200	200	-200	17.07	2.933	-0.048	-0.0028	-0.0024	71112	83333	42.64	0.37		0.0128	13.44	97.64
200...100	100	-100	17.17	2.828	-0.105	-0.0061	-0.0053	16354	19048	42.90	0.38		0.0280	13.74	97.90
100...50	50	-50	17.34	2.656	-0.172	-0.0099	-0.0086	5042	5814	43.33	0.39		0.0459	14.24	98.33
50...100	100	50	17.26	2.741	0.085	0.0049	0.0043	10152	11765	43.12	0.39		0.0227	14.00	98.12
100...200	200	100	17.13	2.866	0.125	0.0073	0.0063	13707	16000	42.81	0.38		0.0334	13.63	97.80
200...400	400	200	16.94	3.064	0.198	0.0117	0.0099	17107	20202	42.31	0.36		0.0529	13.06	97.31
400...800	800	400	16.47	3.532	0.468	0.0284	0.0234	14075	17094	41.14	0.32	0.1250		11.70	96.14
800...1600	1600	800	15.93	4.071	0.539	0.0338	0.0270	23642	29685	39.80	0.28	0.1440		10.14	94.79
1600...3200	3200	1600	15.35	4.648	0.577	0.0376	0.0289	42571	55459	38.35	0.23	0.1541		8.46	93.35
										average value		0.129	0.033		

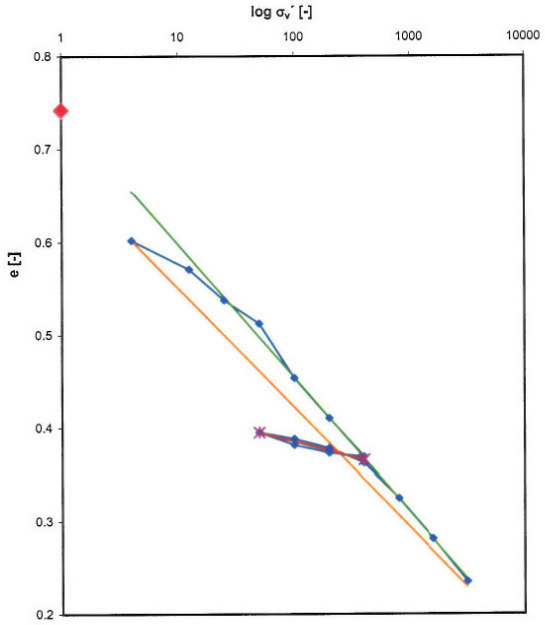

average		optimized		
sig	e	sig	e	
4	0.60	4	0.655	
3200	0.2282	3200	0.24	
			e0:	**0.742**

average		optimized		
sig	e	sig	e	
50	0.39	50	0.39	
400	0.3651	400	0.36	
			e0:	0.451

Oedometer Test

9_1 St.Moritz

Testaim: Comparison of soil stiffness with measurements of Marchetti and Cambridge Dilatometer tests
Materialnumber: Probe 9
Test apparatus: HIF B 26.1: Oedometer 01 / Zelle 11
File name: Probe_9_1.dat **Testdate:** 16.01.2007
Comments: 4 mm sieved & remoulded - eingestrichen

Measured sample Data:

initial sample height:	H_0	20.00 [mm]
sample diameter:	D	56.40 [mm]
sample area:	A	24.98 [cm²]
initial sample volume:	V_0	49.97 [cm³]
dry sample weight:	m_s	79.52 [g]
sample volume:	V_s	28.71 [cm³]

Determined sample data:

density	ρ_s	2.77 [g/cm³]

Test Data:

Loadstep σ´ from..to [kPa]	laod σ´ [kPa]	Δσ´ [kPa]	H_{act} [mm]	Δh [mm]	ΔΔh [-]	$\Delta\varepsilon_n$ [-]	$\Delta\varepsilon_e$ [-]	$M(')_{E(n)}$ [kN/m²]	$M(')_{E(e)}$ [kN/m²]	$V_{tot,akt}$ [cm³]	e [-]	C_c [-]	C_s [-]	w act [%]	sample weight [g]
	0		20.00	0.000						49.97	0.74			26.73	100.78
0...4	4	4	19.50	0.505	0.505	0.0259	0.0253	154	158	48.70	0.70			25.15	99.52
4...12.5	13	8.5	18.90	1.096	0.591	0.0313	0.0296	272	288	47.23	0.65	0.1039		23.29	98.04
12.5...25	25	12.5	18.70	1.302	0.206	0.0110	0.0103	1135	1214	46.71	0.63	0.0596		22.64	97.53
25...50	50	25	18.29	1.706	0.404	0.0221	0.0202	1132	1238	45.70	0.59	0.1168		21.37	96.52
50...100	100	50	18.09	1.906	0.200	0.0111	0.0100	4524	5000	45.20	0.57	0.0578		20.75	96.02
100...200	200	100	16.55	3.448	1.542	0.0932	0.0771	1073	1297	41.35	0.44	0.4458		15.90	92.16
200...400	400	200	15.99	4.013	0.565	0.0353	0.0283	5659	7080	39.94	0.39	0.1633		14.13	90.75
400...800	800	400	15.40	4.605	0.592	0.0385	0.0296	10402	13514	38.46	0.34	0.1711		12.27	89.27
800...400	400	-400	15.44	4.556	-0.049	-0.0032	-0.0025	126073	163265	38.58	0.34		0.0142	12.42	89.40
400...200	200	-200	15.56	4.443	-0.113	-0.0073	-0.0057	27535	35398	38.87	0.35		0.0327	12.78	89.68
200...100	100	-100	15.71	4.288	-0.155	-0.0099	-0.0077	10137	12903	39.25	0.37		0.0448	13.26	90.07
100...200	200	100	15.66	4.345	0.057	0.0036	0.0028	27465	35088	39.11	0.36		0.0165	13.08	89.92
200...400	400	200	15.52	4.480	0.135	0.0087	0.0068	22993	29630	38.77	0.35		0.0390	12.66	89.59
400...800	800	400	15.29	4.711	0.231	0.0151	0.0116	26474	34632	38.20	0.33		0.0668	11.93	89.01
800...1600	1600	800	14.75	5.248	0.537	0.0364	0.0269	21977	29795	36.86	0.28	0.1552		10.25	87.67
1600...3200	3200	1600	14.15	5.849	0.601	0.0425	0.0301	37673	53245	35.35	0.23	0.1737		8.36	86.17
										average value		0.161	0.036		

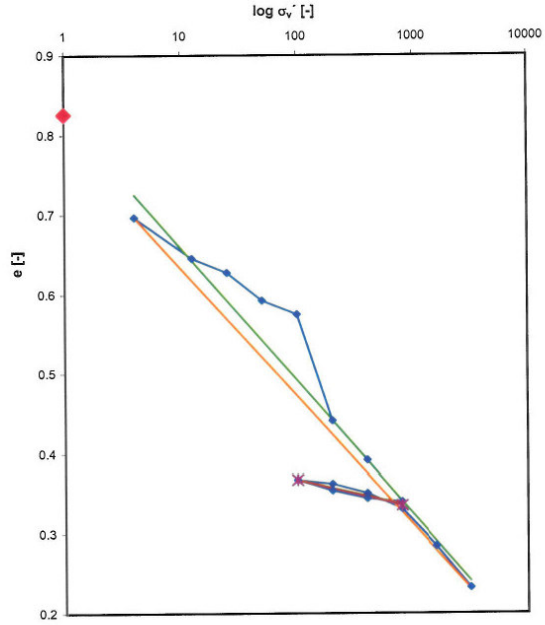

average		optimized	0.167
sig	e	sig	e
4	0.70	4	0.725
3200	0.2297	3200	0.24
			e0: 0.826

average		optimized	0.034
sig	e	sig	e
100	0.37	100	0.37
800	0.3352	800	0.34
			e0: 0.435

Oedometer Test

9_2 St.Moritz

Testaim: Comparison of soil stiffness with measurements of Marchetti and Cambridge Dilatometer tests
Materialnumber: Probe 9
Test apparatus: HIF B 26.1: Oedometer 02 / Zelle 09
File name: Probe_9_2.dat **Testdate:** 16.01.2007
Comments: 4 mm sieved & remoulded - eingestrichen

Measured sample Data:

initial sample height:	H_0	20.00 [mm]
sample diameter:	D	56.40 [mm]
sample area:	A	24.98 [cm²]
initial sample volume:	V_0	49.97 [cm³]
dry sample weight:	m_s	**79.55** [g]
sample volume:	V_s	28.72 [cm³]

Determined sample data:

density	ρ_s	2.77 [g/cm³]

Test Data:

Loadstep σ´ from..to [kPa]	laod σ´ [kPa]	Δσ´ [kPa]	H_{act} [mm]	Δh [mm]	ΔΔh [-]	$\Delta\varepsilon_m$ [-]	$\Delta\varepsilon_e$ [-]	$M(')_{E(n)}$ [kN/m²]	$M(')_{E(e)}$ [kN/m²]	$V_{tot,akt}$ [cm³]	e [-]	C_c [-]	C_s [-]	w act [%]	sample weight [g]
	0		20.00	0.000						49.97	0.74			26.71	100.80
0...4	4	4	19.36	0.645	0.645	0.0333	0.0323	120	124	48.35	0.68			24.68	99.19
4...12.5	13	8.5	18.97	1.032	0.387	0.0204	0.0194	417	439	47.39	0.65	0.0680		23.47	98.22
12.5...25	25	12.5	18.35	1.649	0.617	0.0336	0.0309	372	405	45.85	0.60	0.1783		21.53	96.68
25...50	50	25	17.69	2.310	0.661	0.0374	0.0331	669	756	44.20	0.54	0.1910		19.46	95.03
50...100	100	50	17.15	2.846	0.536	0.0312	0.0268	1600	1866	42.86	0.49	0.1549		17.77	93.69
100...200	200	100	16.61	3.390	0.544	0.0328	0.0272	3053	3676	41.50	0.44	0.1572		16.06	92.33
200...400	400	200	16.04	3.965	0.575	0.0359	0.0288	5577	6957	40.06	0.39	0.1662		14.26	90.89
400...800	800	400	15.45	4.553	0.588	0.0381	0.0294	10508	13605	38.59	0.34	0.1699		12.41	89.42
800...400	400	-400	15.50	4.503	-0.050	-0.0032	-0.0025	123976	160000	38.72	0.35		0.0144	12.57	89.55
400...200	200	-200	15.61	4.391	-0.112	-0.0072	-0.0056	27873	35714	39.00	0.36		0.0324	12.92	89.83
200...100	100	-100	15.77	4.233	-0.158	-0.0100	-0.0079	9979	12658	39.39	0.37		0.0457	13.42	90.22
100...200	200	100	15.72	4.284	0.051	0.0032	0.0026	30816	39216	39.26	0.37		0.0147	13.26	90.10
200...400	400	200	15.57	4.426	0.142	0.0091	0.0071	21935	28169	38.91	0.35		0.0410	12.81	89.74
400...800	800	400	15.34	4.658	0.232	0.0151	0.0116	26452	34483	38.33	0.33		0.0670	12.08	89.16
800...1600	1600	800	14.82	5.177	0.519	0.0350	0.0260	22849	30829	37.03	0.29	0.1500		10.45	87.86
1600...3200	3200	1600	14.24	5.762	0.585	0.0411	0.0293	38942	54701	35.57	0.24	0.1691		8.61	86.40
										average value		0.156	0.036		

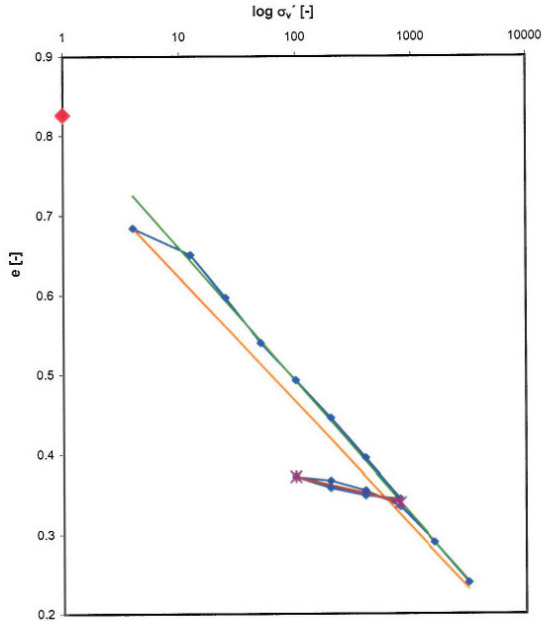

average		optimized	0.167
sig	e	sig	e
4	0.68	4	0.725
3200	0.2307	3200	0.24
			e0: **0.826**

average		optimized	0.034
sig	e	sig	e
100	0.37	100	0.37
800	0.3392	800	0.34
			e0: 0.440

Oedometer Test

10_1 St.Moritz

Testaim: Comparison of soil stiffness with measurements of Marchetti and Cambridge Dilatometer tests
Materialnumber: Probe 10
Test apparatus: HIF B 26.1: Oedometer 04 / Zelle 14
File name: Probe_10_1.dat **Testdate:** 11.01.2007
Comments: 4 mm sieved & remoulded - eingestrichen

Measured sample Data:

initial sample height:	H_0	20.00 [mm]
sample diameter:	D	56.40 [mm]
sample area:	A	24.98 [cm²]
initial sample volume:	V_0	49.97 [cm³]
dry sample weight:	m_d	76.97 [g]
sample volume:	V_s	27.79 [cm³]

Determined sample data:

density	ρ_s	2.77 [g/cm³]

Test Data:

Loadstep σ´ from..to [kPa]	Iaod σ´ [kPa]	Δσ´ [kPa]	H_{act} [mm]	Δh [mm]	ΔΔh [-]	$\Delta\varepsilon_n$ [-]	$\Delta\varepsilon_e$ [-]	$M(')_{E(n)}$ [kN/m²]	$M(')_{E(e)}$ [kN/m²]	$V_{tot,akt}$ [cm³]	e [-]	C_c [-]	C_s [-]	w act [%]	sample weight [g]
	0		20.00	0.000						49.97	0.80			28.82	99.15
0...4	4	4	18.54	1.464	1.464	0.0790	0.0732	51	55	46.31	0.67			24.06	95.49
4...12.5	13	8.5	17.66	2.336	0.872	0.0494	0.0436	172	195	44.13	0.59	0.1584		21.23	93.31
12.5...25	25	12.5	17.30	2.703	0.367	0.0212	0.0184	589	681	43.21	0.56	0.1096		20.04	92.40
25...50	50	25	17.23	2.766	0.063	0.0037	0.0032	6839	7937	43.06	0.55	0.0188		19.84	92.24
50...100	100	50	15.58	4.422	1.656	0.1063	0.0828	470	604	38.92	0.40	0.4946		14.46	88.10
100...200	200	100	15.03	4.971	0.549	0.0365	0.0275	2738	3643	37.55	0.35	0.1640		12.68	86.73
200...400	400	200	14.49	5.508	0.537	0.0371	0.0269	5397	7449	36.21	0.30	0.1604		10.94	85.39
400...200	200	-200	14.54	5.462	-0.046	-0.0032	-0.0023	63209	86957	36.32	0.31		0.0137	11.09	85.50
200...100	100	-100	14.64	5.358	-0.104	-0.0071	-0.0052	14079	19231	36.58	0.32		0.0311	11.42	85.76
100...50	50	-50	14.79	5.208	-0.150	-0.0101	-0.0075	4931	6667	36.96	0.33		0.0448	11.91	86.14
50...100	100	50	14.73	5.274	0.066	0.0045	0.0033	11156	15152	36.79	0.32		0.0197	11.70	85.97
100...200	200	100	14.60	5.403	0.129	0.0088	0.0064	11316	15504	36.47	0.31		0.0385	11.28	85.65
200...400	400	200	14.41	5.591	0.188	0.0130	0.0094	15329	21277	36.00	0.30		0.0562	10.67	85.18
400...800	800	400	13.95	6.049	0.458	0.0328	0.0229	12184	17467	34.85	0.25	0.1368		9.18	84.04
800...1600	1600	800	13.44	6.561	0.512	0.0381	0.0256	20998	31250	33.57	0.21	0.1529		7.52	82.76
1600...3200	3200	1600	12.92	7.076	0.515	0.0398	0.0258	40152	62136	32.29	0.16	0.1538		5.85	81.47
										average value		0.172	0.034		

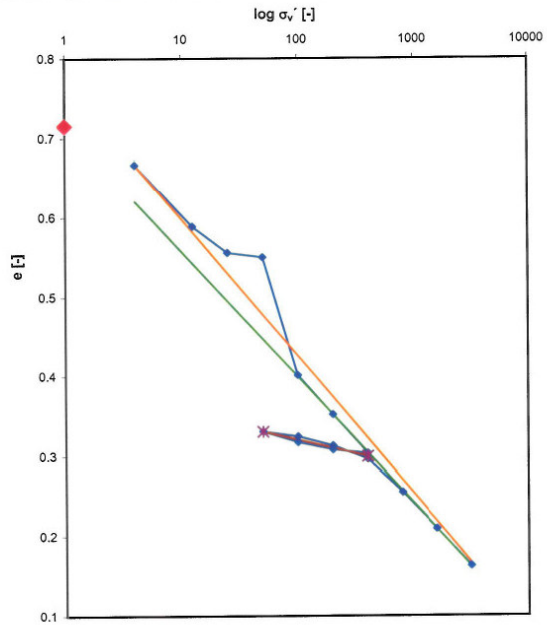

average	
sig	e
4	0.67
3200	0.1668

optimized	
sig	e
4	0.62
3200	0.16
e0:	0.715

average	
sig	e
50	0.33
400	0.2992

optimized	
sig	e
50	0.33
400	0.30
e0:	0.388

Oedometer Test

10_2 St.Moritz

Testaim: Comparison of soil stiffness with measurements of Marchetti and Cambridge Dilatometer tests
Materialnumber: Probe 10
Test apparatus: HIF B 26.1: Oedometer 05 / Zelle 13
File name: Probe_10_2.dat **Testdate:** 11.01.2007
Comments: 4 mm sieved & remoulded - eingestrichen

Measured sample Data:

initial sample height:	H_0	20.00 [mm]
sample diameter:	D	56.40 [mm]
sample area:	A	24.98 [cm²]
initial sample volume:	V_0	49.97 [cm³]
dry sample weight:	m_d	**76.58** [g]
sample volume:	V_s	27.65 [cm³]

Determined sample data:

density	ρ_s	2.77 [g/cm³]

Test Data:

Loadstep σ´ from..to [kPa]	laod σ´ [kPa]	Δσ´ [kPa]	H_{act} [mm]	Δh [mm]	ΔΔh [-]	$\Delta\varepsilon_m$ [-]	$\Delta\varepsilon_e$ [-]	$M(')_{E(p)}$ [kN/m²]	$M(')_{E(e)}$ [kN/m²]	$V_{tot,akt}$ [cm³]	e [-]	C_c [-]	C_s [-]	w act [%]	sample weight [g]
	0		20.00	0.000						49.97	0.81			29.15	98.90
0...4	4	4	19.52	0.485	0.485	0.0249	0.0243	161	165	48.75	0.76			27.56	97.69
4...12.5	13	8.5	19.38	0.624	0.139	0.0072	0.0070	1185	1223	48.41	0.75	0.0254		27.11	97.34
12.5...25	25	12.5	18.94	1.056	0.432	0.0228	0.0216	548	579	47.33	0.71	0.1297		25.70	96.26
25...50	50	25	17.19	2.815	1.759	0.1024	0.0880	244	284	42.93	0.55	0.5280		19.96	91.87
50...100	100	50	16.60	3.404	0.589	0.0355	0.0295	1409	1698	41.46	0.50	0.1768		18.04	90.40
100...200	200	100	16.00	3.997	0.593	0.0371	0.0297	2699	3373	39.98	0.45	0.1780		16.11	88.91
200...400	400	200	15.42	4.581	0.584	0.0379	0.0292	5280	6849	38.52	0.39	0.1753		14.20	87.46
400...200	200	-200	15.46	4.542	-0.039	-0.0025	-0.0020	79272	102564	38.62	0.40		0.0117	14.33	87.55
200...100	100	-100	15.57	4.429	-0.113	-0.0073	-0.0056	13780	17699	38.90	0.41		0.0339	14.70	87.84
100...50	50	-50	15.72	4.277	-0.152	-0.0097	-0.0076	5172	6579	39.28	0.42		0.0456	15.19	88.21
50...100	100	50	15.66	4.336	0.059	0.0038	0.0030	13275	16949	39.13	0.42		0.0177	15.00	88.07
100...200	200	100	15.54	4.465	0.129	0.0083	0.0064	12043	15504	38.81	0.40		0.0387	14.58	87.75
200...400	400	200	15.33	4.666	0.201	0.0131	0.0101	15258	19900	38.31	0.39		0.0603	13.92	87.24
400...800	800	400													
800...1600	1600	800													
1600...3200	3200	1600													
										average value		0.202	0.035		

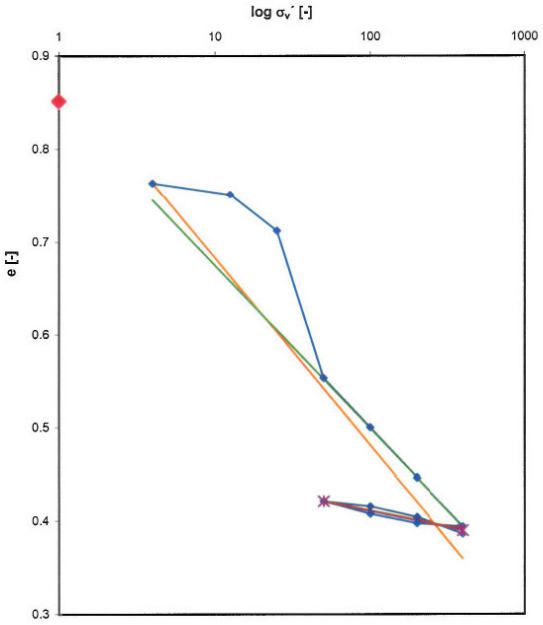

average		optimized	0.176
sig	e	sig	e
4	0.76	4	0.745
400	0.3591	400	0.39
		e0:	0.851

average		optimized	0.034
sig	e	sig	e
50	0.42	50	0.42
400	0.3895	400	0.39
		e0:	0.479

Oedometer Test

13_1 St.Moritz

Testaim: Comparison of soil stiffness with measurements of Marchetti and Cambridge Dilatometer tests
Materialnumber: Probe 13
Test apparatus: HIF B 26.1: Oedometer 01 / Zelle 11
File name: Probe_13_1.dat **Testdate:** 11.01.2007
Comments: remoulded - eingestrichen

Measured sample Data:

initial sample height:	H_0	20.00 [mm]
sample diameter:	D	56.40 [mm]
sample area:	A	24.98 [cm²]
initial sample volume:	V_0	49.97 [cm³]
dry sample weight:	m_d	84.57 [g]
sample volume:	V_s	30.53 [cm³]

Determined sample data:

density	ρ_s	2.77 [g/cm³]

Test Data:

Loadstep σ´ from..to [kPa]	laod σ´ [kPa]	Δσ´ [kPa]	H_{act} [mm]	Δh [mm]	ΔΔh [-]	$\Delta\varepsilon_n$ [-]	$\Delta\varepsilon_e$ [-]	$M(')_{E(n)}$ [kN/m²]	$M(')_{E(e)}$ [kN/m²]	$V_{tot,akt}$ [cm³]	e [-]	C_c [-]	C_s [-]	w act [%]	sample weight [g]
	0		20.00	0.000						49.97	0.64			22.98	104.01
0...4	4	4	20.00	0.000	0.000	0.0000	0.0000	#DIV/0!	#DIV/0!	49.97	0.64			22.98	104.01
4...12.5	13	8.5	19.76	0.245	0.245	0.0124	0.0123	685	694	49.35	0.62	0.0405		22.26	103.39
12.5...25	25	12.5	19.63	0.370	0.125	0.0064	0.0063	1963	2000	49.04	0.61	0.0340		21.89	103.08
25...50	50	25	19.49	0.515	0.145	0.0074	0.0073	3359	3448	48.68	0.59	0.0394		21.46	102.72
50...100	100	50	19.08	0.917	0.402	0.0211	0.0201	2374	2488	47.68	0.56	0.1093		20.27	101.71
100...200	200	100	18.78	1.222	0.305	0.0162	0.0153	6157	6557	46.91	0.54	0.0829		19.37	100.95
200...400	400	200	18.26	1.742	0.520	0.0285	0.0260	7022	7692	45.61	0.49	0.1414		17.84	99.65
400...200	200	-200	18.27	1.729	-0.013	-0.0007	-0.0006	281092	307692	45.65	0.50		0.0035	17.87	99.69
200...100	100	-100	18.31	1.686	-0.043	-0.0023	-0.0022	42591	46512	45.75	0.50		0.0117	18.00	99.79
100...50	50	-50	18.41	1.590	-0.096	-0.0052	-0.0048	9589	10417	45.99	0.51		0.0261	18.28	100.03
50...100	100	50	18.38	1.621	0.031	0.0017	0.0016	29644	32258	45.92	0.50		0.0084	18.19	99.96
100...200	200	100	18.32	1.682	0.061	0.0033	0.0031	30030	32787	45.76	0.50		0.0166	18.01	99.80
200...400	400	200	18.20	1.804	0.122	0.0067	0.0061	29830	32787	45.46	0.49		0.0332	17.65	99.50
400...800	800	400	17.60	2.405	0.601	0.0342	0.0301	11710	13311	43.96	0.44	0.1634		15.88	98.00
800...1600	1600	800	17.01	2.992	0.587	0.0345	0.0294	23180	27257	42.49	0.39	0.1596		14.14	96.53
1600...3200	3200	1600	16.51	3.494	0.502	0.0304	0.0251	52609	63745	41.24	0.35	0.1365		12.66	95.28
										average value		0.101	0.017		

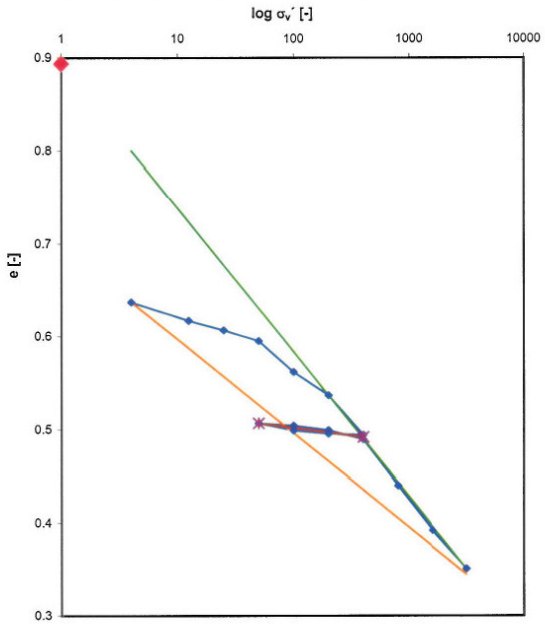

average		optimized	0.155
sig	e	sig	e
4	0.64	4	0.8
3200	0.3441	3200	0.35
			e0: 0.893

average		optimized	0.017
sig	e	sig	e
50	0.51	50	0.51
400	0.4915	400	0.49
			e0: 0.535

Oedometer Test

13_2 St.Moritz

Testaim: Comparison of soil stiffness with measurements of Marchetti and Cambridge Dilatometer tests
Materialnumber: Probe 13
Test apparatus: HIF B 26.1: Oedometer 02 / Zelle 09
File name: Probe_13_2.dat **Testdate:** 11.01.2007
Comments: remoulded - eingestrichen

Measured sample Data:

initial sample height:	H_0	20.00 [mm]
sample diameter:	D	56.40 [mm]
sample area:	A	24.98 [cm²]
initial sample volume:	V_0	49.97 [cm³]
dry sample weight:	m_d	**87.11** [g]
sample volume:	V_s	31.45 [cm³]

Determined sample data:

density	ρ_s	2.77 [g/cm³]

Test Data:

Loadstep σ´ from..to [kPa]	laod σ´ [kPa]	Δσ´ [kPa]	H_{act} [mm]	Δh [mm]	ΔΔh [-]	$\Delta\varepsilon_n$ [-]	$\Delta\varepsilon_v$ [-]	$M(')_{E(n)}$ [kN/m²]	$M(')_{E(e)}$ [kN/m²]	$V_{tot,akt}$ [cm³]	e [-]	C_c [-]	C_s [-]	w act [%]	sample weight [g]
	0		20.00	0.000						49.97	0.59			21.26	105.63
0...4	4	4	19.49	0.514	0.514	0.0264	0.0257	152	156	48.68	0.55			19.78	104.34
4...12.5	13	8.5	19.19	0.812	0.298	0.0155	0.0149	547	570	47.94	0.52	0.0478		18.93	103.60
12.5...25	25	12.5	19.02	0.978	0.166	0.0087	0.0083	1432	1506	47.52	0.51	0.0438		18.45	103.19
25...50	50	25	18.76	1.238	0.260	0.0139	0.0130	1804	1923	46.87	0.49	0.0686		17.71	102.54
50...100	100	50	18.36	1.645	0.407	0.0222	0.0204	2255	2457	45.86	0.46	0.1074		16.54	101.52
100...200	200	100	17.99	2.013	0.368	0.0205	0.0184	4888	5435	44.94	0.43	0.0971		15.49	100.60
200...400	400	200	17.67	2.332	0.319	0.0181	0.0160	11077	12539	44.14	0.40	0.0842		14.57	99.80
400...200	200	-200	17.68	2.321	-0.011	-0.0006	-0.0005	321436	363636	44.17	0.40		0.0029	14.60	99.83
200...100	100	-100	17.73	2.269	-0.052	-0.0029	-0.0026	34098	38462	44.30	0.41		0.0137	14.75	99.96
100...50	50	-50	17.81	2.194	-0.075	-0.0042	-0.0038	11871	13333	44.49	0.41		0.0198	14.97	100.15
50...100	100	50	17.79	2.215	0.021	0.0012	0.0011	42345	47619	44.43	0.41		0.0055	14.91	100.09
100...200	200	100	17.73	2.272	0.057	0.0032	0.0029	31102	35088	44.29	0.41		0.0150	14.74	99.95
200...400	400	200	17.64	2.364	0.092	0.0052	0.0046	38339	43478	44.06	0.40		0.0243	14.48	99.72
400...800	800	400	17.26	2.740	0.376	0.0218	0.0188	18362	21277	43.12	0.37	0.0992		13.40	98.78
800...1600	1600	800	16.85	3.154	0.414	0.0246	0.0207	32553	38647	42.09	0.34	0.1093		12.21	97.75
1600...3200	3200	1600	16.40	3.597	0.443	0.0270	0.0222	59243	72235	40.98	0.30	0.1169		10.94	96.64
										average value		0.086	0.014		

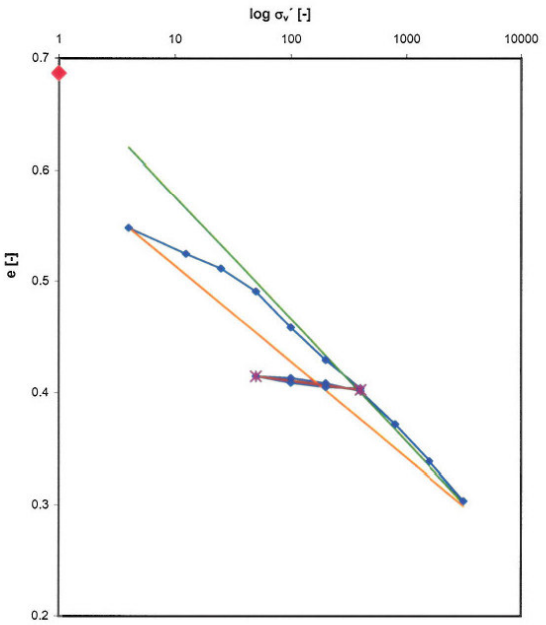

average		optimized	
sig	e	sig	e
4	0.55	4	0.62
3200	0.2983	3200	0.30
			e0: 0.686

average		optimized	0.014
sig	e	sig	e
50	0.41	50	0.41
400	0.4023	400	0.40
			e0: 0.438

Oedometer Test

13_3 St.Moritz

Testaim: Comparison of soil stiffness with measurements of Marchetti and Cambridge Dilatometer tests
Materialnumber: Probe 13
Test apparatus: HIF B 26.1: Oedometer 03 / Zelle 12
File name: Probe_13_3.dat **Testdate:** 11.01.2007
Comments: remoulded - eingestrichen

Measured sample Data:

initial sample height:	H_0	20.00 [mm]
sample diameter:	D	56.40 [mm]
sample area:	A	24.98 [cm²]
initial sample volume:	V_0	49.97 [cm³]
dry sample weight:	m_s	**84.85** [g]
sample volume:	V_s	30.63 [cm³]

Determined sample data:

density	ρ_s	2.77 [g/cm³]

Test Data:

Loadstep σ´ from..to [kPa]	laod σ´ [kPa]	Δσ´ [kPa]	H_{act} [mm]	Δh [mm]	ΔΔh [-]	$\Delta\varepsilon_n$ [-]	$\Delta\varepsilon_e$ [-]	$M(')_{E(n)}$ [kN/m²]	$M(')_{E(e)}$ [kN/m²]	$V_{tot,akt}$ [cm³]	e [-]	C_c [-]	C_s [-]	w act [%]	sample weight [g]
	0		20.00	0.000						49.97	0.63			22.79	104.18
0...4	4	4	19.08	0.925	0.925	0.0485	0.0463	82	86	47.66	0.56			20.06	101.87
4...12.5	13	8.5	18.69	1.308	0.383	0.0205	0.0192	415	444	46.70	0.52	0.0631		18.94	100.92
12.5...25	25	12.5	18.43	1.569	0.261	0.0142	0.0131	883	958	46.05	0.50	0.0707		18.17	100.26
25...50	50	25	18.16	1.840	0.271	0.0149	0.0136	1675	1845	45.37	0.48	0.0734		17.37	99.59
50...100	100	50	17.82	2.181	0.341	0.0191	0.0171	2613	2933	44.52	0.45	0.0924		16.37	98.74
100...200	200	100	17.46	2.543	0.362	0.0207	0.0181	4822	5525	43.61	0.42	0.0981		15.30	97.83
200...400	400	200	17.08	2.920	0.377	0.0221	0.0189	9061	10610	42.67	0.39	0.1021		14.19	96.89
400...200	200	-200	17.10	2.896	-0.024	-0.0014	-0.0012	142533	166667	42.73	0.39		0.0065	14.26	96.95
200...100	100	-100	17.17	2.826	-0.070	-0.0041	-0.0035	24534	28571	42.91	0.40		0.0190	14.47	97.12
100...50	50	-50	17.27	2.733	-0.093	-0.0054	-0.0047	9283	10753	43.14	0.41		0.0252	14.74	97.36
50...100	100	50	17.22	2.779	0.046	0.0027	0.0023	18718	21739	43.02	0.40		0.0125	14.60	97.24
100...200	200	100	17.15	2.851	0.072	0.0042	0.0036	23818	27778	42.84	0.40		0.0195	14.39	97.06
200...400	400	200	17.05	2.947	0.096	0.0056	0.0048	35527	41667	42.60	0.39		0.0260	14.11	96.82
400...800	800	400	16.72	3.285	0.338	0.0202	0.0169	19781	23669	41.76	0.36	0.0916		13.11	95.98
800...1600	1600	800	16.31	3.693	0.408	0.0250	0.0204	31975	39216	40.74	0.33	0.1105		11.91	94.96
1600...3200	3200	1600	15.86	4.137	0.444	0.0280	0.0222	57164	72072	39.63	0.29	0.1203		10.61	93.85
										0	-1.00			-36.10108	54.218231
										0	-1.00			-36.10108	54.218231
										average value		0.091	0.018		

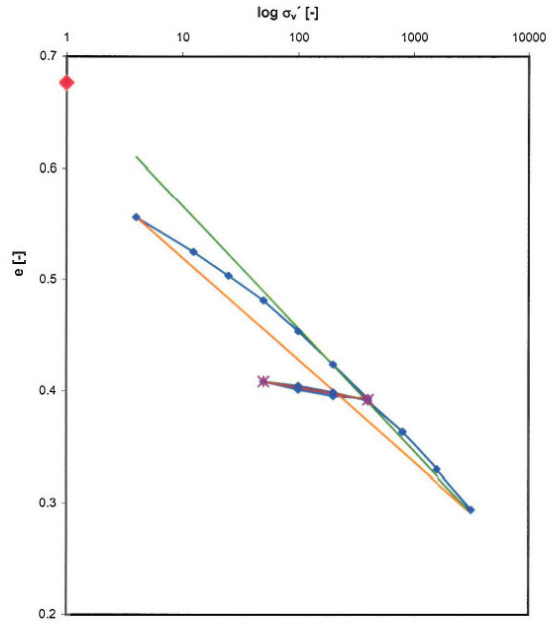

average		optimized	0.11	
sig	e	sig	e	
4	0.56	4	0.61	
3200	0.2905	3200	0.29	
			e0:	0.676

average		optimized	0.018	
sig	e	sig	e	
50	0.41	50	0.41	
400	0.3919	400	0.39	
			e0:	0.439

Oedometer Test

13_4 St.Moritz

Testaim: Comparison of soil stiffness with measurements of Marchetti and Cambridge Dilatometer tests
Materialnumber: Probe 13
Test apparatus: HIF B 26.1: Oedometer 03 / Zelle 14
File name: Probe_13_4.dat **Testdate:** 14.02.2007
Comments: 4 mm sieved & remoulded - eingestrichen

Measured sample Data:

initial sample height:	H_0	20.00 [mm]
sample diameter:	D	56.40 [mm]
sample area:	A	24.98 [cm²]
initial sample volume:	V_0	49.97 [cm³]
dry sample weight:	m_s	**82.29** [g]
sample volume:	V_s	29.71 [cm³]

Determined sample data:

density	ρ_s	2.77 [g/cm³]

Test Data:

Loadstep σ´ from..to [kPa]	laod σ´ [kPa]	Δσ´ [kPa]	H_{act} [mm]	Δh [mm]	ΔΔh [-]	$\Delta\varepsilon_n$ [-]	$\Delta\varepsilon_e$ [-]	$M(')_{E(n)}$ [kN/m²]	$M(')_{E(e)}$ [kN/m²]	$V_{tot,akt}$ [cm³]	e [-]	C_c [-]	C_s [-]	w act [%]	sample weight [g]
	0		20.00	0.000						49.97	0.68			24.62	102.55
0...4	4	4	19.60	0.397	0.397	0.0203	0.0199	198	202	48.97	0.65			23.41	101.56
4...12.5	13	8.5	19.29	0.706	0.309	0.0160	0.0155	531	550	48.20	0.62	0.0525		22.48	100.79
12.5...25	25	12.5	18.90	1.099	0.393	0.0208	0.0197	601	636	47.22	0.59	0.1098		21.28	99.80
25...50	50	25	18.34	1.659	0.560	0.0305	0.0280	819	893	45.82	0.54	0.1564		19.58	98.40
50...100	100	50	17.95	2.054	0.395	0.0220	0.0198	2272	2532	44.83	0.51	0.1103		18.38	97.42
100...200	200	100	17.59	2.410	0.356	0.0202	0.0178	4941	5618	43.95	0.48	0.0995		17.30	96.53
200...400	400	200	17.21	2.793	0.383	0.0223	0.0192	8985	10444	42.99	0.45	0.1070		16.14	95.57
400...200	200	-200	17.23	2.773	-0.020	-0.0012	-0.0010	172270	200000	43.04	0.45		0.0056	16.20	95.62
200...100	100	-100	17.29	2.715	-0.058	-0.0034	-0.0029	29802	34483	43.18	0.45		0.0162	16.38	95.77
100...50	50	-50	17.36	2.643	-0.072	-0.0041	-0.0036	12053	13889	43.36	0.46		0.0201	16.59	95.95
50...100	100	50	17.34	2.661	0.018	0.0010	0.0009	48164	55556	43.32	0.46		0.0050	16.54	95.90
100...200	200	100	17.28	2.725	0.064	0.0037	0.0032	26992	31250	43.16	0.45		0.0179	16.35	95.74
200...400	400	200	17.18	2.825	0.100	0.0058	0.0050	34350	40000	42.91	0.44		0.0279	16.04	95.49
400...800	800	400	16.82	3.184	0.359	0.0213	0.0180	18736	22284	42.01	0.41	0.1003			
800...1600	1600	800	16.38	3.625	0.441	0.0269	0.0221	29705	36281	40.91	0.38	0.1232		13.61	93.49
1600...3200	3200	1600	15.90	4.103	0.478	0.0301	0.0239	53212	66946	39.72	0.34	0.1335		12.16	92.30
										average value		0.110	0.015		

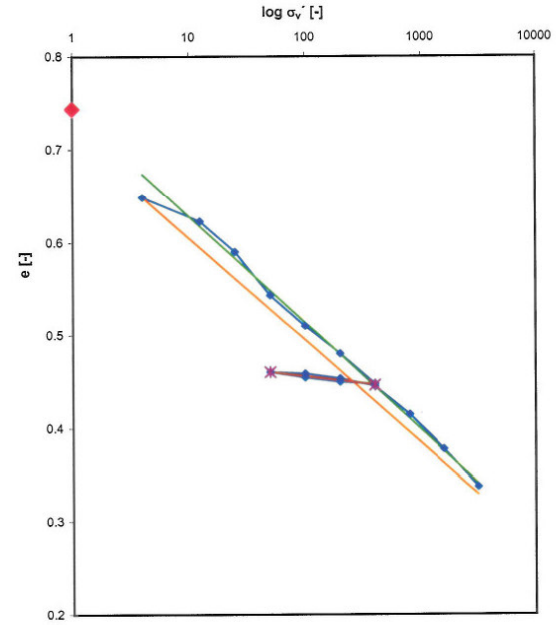

average		optimized	0.115
sig	e	sig	e
4	0.65	4	0.674
3200	0.3284	3200	0.34
			e0: **0.743**

average		optimized	0.015
sig	e	sig	e
50	0.46	50	0.46
400	0.4457	400	0.45
			e0: 0.485

Oedometer Test

13_5 St.Moritz

Testaim: Comparison of soil stiffness with measurements of Marchetti and Cambridge Dilatometer tests
Materialnumber: Probe 13
Test apparatus: HIF B 26.1: Oedometer 04 / Zelle 10
File name: Probe_13_5.dat **Testdate:** 14.02.2007
Comments: 4 mm sieved & remoulded - eingestrichen

Measured sample Data:

initial sample height:	H_0	20.00 [mm]
sample diameter:	D	56.40 [mm]
sample area:	A	24.98 [cm²]
initial sample volume:	V_0	49.97 [cm³]
dry sample weight:	m_d	**82.16** [g]
sample volume:	V_s	29.66 [cm³]

Determined sample data:

density	ρ_s	2.77 [g/cm³]

Test Data:

Loadstep σ' from..to [kPa]	laod σ' [kPa]	Δσ' [kPa]	H_{act} [mm]	Δh [mm]	εΔh [-]	$\Delta\varepsilon_m$ [-]	$\Delta\varepsilon_e$ [-]	$M(')_{E(n)}$ [kN/m²]	$M(')_{E(e)}$ [kN/m²]	$V_{tot,akt}$ [cm³]	e [-]	C_c [-]	C_s [-]	w act [%]	sample weight [g]
	0		20.00	0.000						49.97	0.68			24.71	102.47
0...4	4	4	19.45	0.552	0.552	0.0284	0.0276	141	145	48.59	0.64			23.04	101.09
4...12.5	13	8.5	19.12	0.876	0.324	0.0169	0.0162	502	525	47.78	0.61	0.0551		22.05	100.28
12.5...25	25	12.5	18.95	1.049	0.173	0.0091	0.0087	1369	1445	47.35	0.60	0.0484		21.53	99.85
25...50	50	25	18.06	1.939	0.890	0.0493	0.0445	507	562	45.12	0.52	0.2490		18.82	97.62
50...100	100	50	17.70	2.304	0.365	0.0206	0.0183	2424	2740	44.21	0.49	0.1021		17.71	96.71
100...200	200	100	17.22	2.781	0.477	0.0277	0.0239	3610	4193	43.02	0.45	0.1335		16.26	95.52
200...400	400	200	16.95	3.048	0.267	0.0158	0.0134	12698	14981	42.35	0.43	0.0747		15.45	94.85
400...200	200	-200	16.98	3.022	-0.026	-0.0015	-0.0013	130600	153846	42.42	0.43		0.0073	15.53	94.92
200...100	100	-100	17.03	2.968	-0.054	-0.0032	-0.0027	31541	37037	42.55	0.43		0.0151	15.69	95.05
100...50	50	-50	17.11	2.889	-0.079	-0.0046	-0.0040	10830	12658	42.75	0.44		0.0221	15.93	95.25
50...100	100	50	17.08	2.922	0.033	0.0019	0.0017	25876	30303	42.67	0.44		0.0092	15.83	95.17
100...200	200	100	17.02	2.985	0.063	0.0037	0.0031	27008	31746	42.51	0.43		0.0176	15.64	95.01
200...400	400	200	16.92	3.083	0.098	0.0058	0.0049	34524	40816	42.26	0.42		0.0274	15.34	94.76
400...800	800	400	16.55	3.455	0.372	0.0225	0.0186	17790	21505	41.33	0.39	0.1041			
800...1600	1600	800	16.10	3.905	0.450	0.0280	0.0225	28613	35556	40.21	0.36	0.1259		12.84	92.71
1600...3200	3200	1600	15.62	4.384	0.479	0.0307	0.0240	52162	66806	39.01	0.32	0.1340		11.38	91.51
										average value		0.114	0.016		

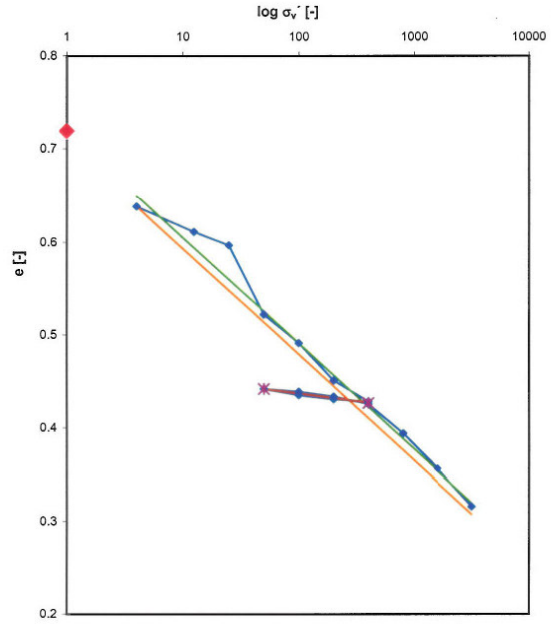

average		optimized	0.114	
sig	e	sig	e	
4	0.64	4	0.65	
3200	0.3069	3200	0.32	
			e0:	0.719

average		optimized	0.016	
sig	e	sig	e	
50	0.44	50	0.44	
400	0.4264	400	0.43	
			e0:	0.468

9.4 TRIVEC Measurements in the Inverse Analysis of the Long-Term Stability of a Constrained Landslide

Puzrin, A.M. and Schmid, A. (2007). “TRIVEC Measurements in the Inverse Analysis of the Long-Term Stability of a Constrained Landslide.” *Proceedings of the 7th International Symposium on Field Measurements in Geomechanics Boston, FMGM 07*, Massachusetts, USA, September 24-27.

FMGM 2007: Seventh International Symposium on Field Measurements in Geomechanics

TRIVEC MEASUREMENTS IN THE INVERSE ANALYSIS OF THE LONG-TERM STABILITY OF A CONSTRAINED LANDSLIDE

by Alexander M. Puzrin[a] and Andreas Schmid[b]

[a] *Professor, Institute for Geotechnical Engineering, ETH Zurich,Wolfgang-Pauli-Str. 15, Zurich CH-8093, Switzerland; Fax: +41-44-633-1429; E-mail: alexander.puzrin@igt.baug.ethz.ch*

[b] *Research Assistant, Institute for Geotechnical Engineering, ETH Zurich, Wolfgang-Pauli-Str. 15, Zurich CH-8093, Switzerland; Fax: +41-44-633-1429; E-mail: andreas.schmid@igt.baug.ethz.ch*

ABSTRACT

When an active creeping landslide is constrained by a retaining structure, it has "nowhere" to go and its downhill movement in the vicinity of the structure may be even reversed (provided the anchor forces are sufficiently large). This intuitively implies that the landslide has been stabilized. However, because the landslide is slowing, the viscous part of the shear strength on the sliding surface may decrease, eventually leading to increase in compressive stresses in soil in front of the structure. If these stresses exceed the passive earth pressure, this can ultimately lead to a failure and the landslide will simply "overflow" the structure. In this paper we propose an inverse analysis procedure for a long-term stability analysis of such a landslide. The procedure is based on the curve fitting of the observed displacement data and back-calculation of earth pressure changes from retaining wall deflections measured using a TRIVEC system. Its application is illustrated on an example of the landslide stabilization project in Combe Chopin, Switzerland.

1. INTRODUCTION

When an active creeping landslide is constrained by a rock outcrop or a retaining structure, it has "nowhere" to go and its downhill movement slows down. This intuitively implies that the landslide has been stabilized. However, exactly because the landslide is slowing, the viscous part of the shear strength on the sliding surface may decrease, leading to increase in compressive stresses in soil in front of the structure.

Puzrin and Sterba (2006a) suggested the mechanism of a *failure scenario* for a constrained landslide evolution. In this scenario, the landslide will keep slowing down till the earth pressure at its bottom exceeds the soil resistance and the slope fails catastrophically. In this case, it is necessary to be able to answer the following three questions:

- Is the residual shear strength on the sliding surface rate dependent?
- If it is, will the earth pressure increase sufficiently to cause a failure?

- If it will, how much time is left before the future failure takes place?

The answered to these questions could be found with the help of the inverse analysis procedure developed by Puzrin and Sterba (2006a). It allows for the safety factor for long-term slope stability and final displacements to be determined solely from the observed slope displacements. This helps to reduce uncertainties caused by spatial variability of soil properties. The time of the failure can then be calculated using the earth pressure measurements at the bottom of the slide.

This procedure has been applied to the St. Moritz landslide in Switzerland (Puzrin and Sterba, 2006b) constrained by a rock outcrop. The advantage of this case is that the constraint is a clear zero velocity boundary and the earth pressure grows on it continuously. The major disadvantage, however, is that direct pressure measurements within the soil mass are not likely to produce reliable results due to high level of heterogeneity of sliding deposits.

In the presented paper we consider a case, where the landslide is constrained by an anchored retaining structure. In this case, changes in earth pressures can be easily back-calculated from retaining wall deflections measured using, e.g., a TRIVEC system, which (together with the changes in anchor forces in time) can be directly incorporated into the inverse stability analysis. The disadvantage of this case, however, is that the retaining structure is not a zero velocity boundary. Furthermore, if the anchor forces are sufficiently large, the lower part of the landslide could initially start moving uphill (!) with the corresponding drop of the earth pressure on the retaining wall, which can be rather misleading for interpretation and long term stability analysis.

The purpose of this paper is to extend the Puzrin and Sterba (2006a) procedure to a case of a flexible anchored retaining structure instrumented by a TRIVEC system and to illustrate its application using the observation data from the landslide stabilization project in Combe Chopin, Switzerland.

2. THE COMBE CHOPIN LANDSLIDE

The highway A16 from Bern to Delemont and Basel is a major north-south link in Switzerland and connects the capital city Bern to France (Fig. 1a). The highway crosses the creeping landslide of Combe Chopin (Fig. 1b), which is bounded by two hills located to the north and south of the landslide, respectively. This landslide is inclined from east to west with an inclination of 25 to 30° (Bapst, 2002) towards the river Birse, which passes on the bottom end of the landslide. The width of the slide is about 150 - 200 m, its length in general is about 140 – 190 m, but in the northern part the length of the active portion is about 90 m. The soil of the landslide is composed of slope debris, a mélange of clay to gravel, a sliding zone with a thickness of 0.5 to 1.0 meters which is as well a mélange of clay to gravel, a zone of weathered rock with a thickness of 2 to 4 meters and then solid rock. The landslide can be divided into a north zone, with a landslide thickness of approximately 5 to 7 meters and a south zone, with a landslide thickness of up to 14 meters. The hydrology is dominated by the less permeable layer of mélange of clay to gravel.

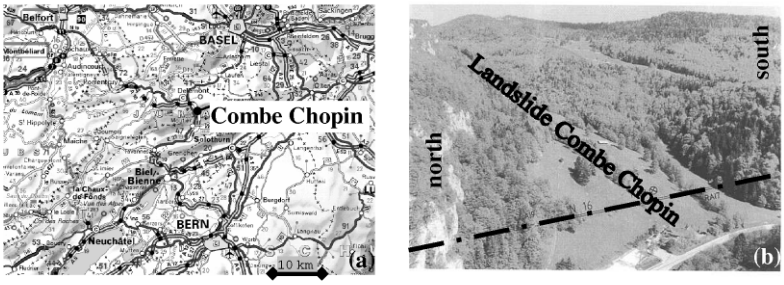

FIG. 1. The Combe Chopin landslide: (a) location (VIAMICHELIN, 2007); (b) view (Bapst, 2002).

Creep deformations in the landslide were observed and monitored since 1976, when the highway project started (Bapst, 2002). The northern zone of the landslide was partially stabilized by an anchored bored piles retaining wall, monitored using a TRIVEC measurement system.

3. TRIVEC MEASUREMENTS

The TRIVEC device is a portable, high precision instrument to measure the distribution of three orthogonal displacement components along a vertical borehole (Fig. 2a). The quantities measured directly are the axial strain and the angles of vertical derivation in two vertical planes normal to each other. (Koeppel et al, 1983).

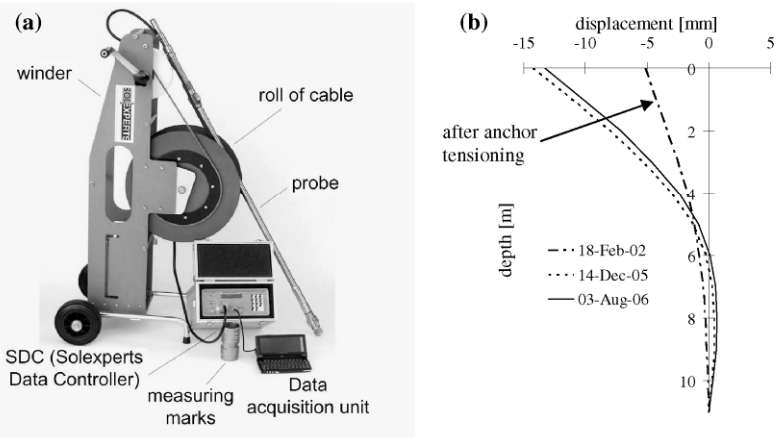

FIG. 2. TRIVEC measurements: (a) the device (SOLEXPERTS, 2007); (b) TRIVEC measurements of the Combe Chopin retaining wall displacements.

The first measurements from the TRIVEC system in the retaining wall after tensioning of the anchors had shown that the wall moved uphill (Fig. 2b). For the first three years, until December 2005, the wall continued moving uphill. Does it mean that the landslide has been stabilized? Or is that just a temporary creep of the soil behind the wall? In the last measurement, which had been taken in August 2006, the movements of the wall had changed their direction (solid line in Fig. 2b). The wall is now moving downhill. What happens with the earth pressure behind the wall? Is it growing, and if it is, will it ever reach the passive pressure? The goal of this paper is to attempt answering these questions.

4. THE CONSTRAINED LANDSLIDE MODEL

The schematic layout of a landslide constrained by an anchored retaining structure is shown in Fig. 3. When the anchor force applied to the structure is sufficiently large, it will push the bottom part of the landslide upwards. The upper part of the landslide will, however, keep moving downwards. The boundary with the zero velocity is located at the distance L_0 from the retaining wall. Equilibrium of the sliding layer in the upper part of the landslide relates the shear stress τ on the sliding surface to the average effective normal stress in the layer p' and the effective active earth pressure p'_a acting at the top of the layer:

$$p'(x,t)H + \int_x^L \tau(x,t)dx = \gamma_t H(L-x)\sin\alpha + p'_a H \quad \text{for} \quad L_0 \le x \le L \tag{1a}$$

Here γ_t is the total unit weight of soil; α is the slope inclination; L and H are the landslide length and thickness, respectively.

Equilibrium in the lower part of the landslide relates the shear stress τ (which always acts against the movement) to the normal stress in the layer p' and the earth pressure p'_0 acting on the wall:

$$p'(x,t)H + \int_0^x \tau(x,t)dx = p'_0 H - \gamma_t H x \sin\alpha \quad \text{for} \quad 0 \le x \le L_0 \tag{1b}$$

We use in (1a, b) the effective earth pressures assuming that the average pore water pressure is constant along the slope: $u(x,t)=u(t)$, i.e. either that there is a flow parallel to the slope surface, or that there is no connected water. The zero velocity boundary is found by substituting $x = L_0$ into both equations (1a) and (1b):

$$\int_{L_0}^{L} \tau(x,t)dx - \int_0^{L_0} \tau(x,t)dx = \gamma_t HL\sin\alpha - (p'_0 - p'_a)H \tag{2}$$

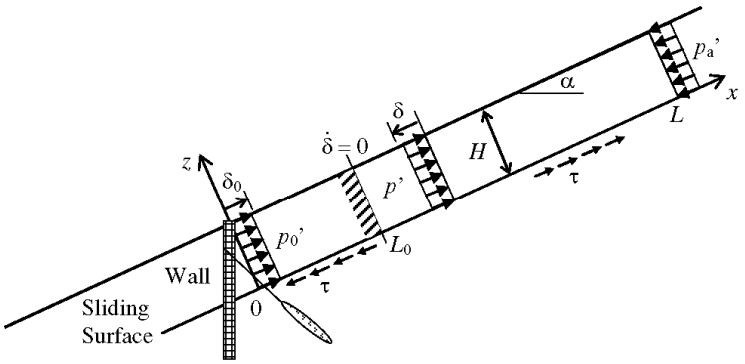

FIG. 3. Schematic layout of the constrained landslide model.

In a forward boundary value problem, we supplement equations (1) with constitutive equations:

$$\tau(x,t) = \tau_r + \eta_\tau \dot{\delta}(x,t) \tag{3a}$$

$$p'(x,t) = E\varepsilon(x,t) + \eta_p(\varepsilon,\dot{\varepsilon})\dot{\varepsilon}(x,t) \tag{3b}$$

and solve them together in order to obtain displacements $\delta(x,t)$, strains $\varepsilon(x,t)$ and earth pressures $p'(x,t)$ and predict the landslide behavior. Here E is the elasto-plastic (loading) modulus of soil; τ_r is the residual shear strength of soil on the sliding surface, η_τ and $\eta_p(\varepsilon,\dot{\varepsilon})$ are the viscosity coefficients for the shear and normal stresses respectively. The residual shear strength is assumed here to decrease with decreasing shearing rate, which has been experimentally confirmed for natural soils (e.g., Skempton, 1985). The stiffness of the soil in the sliding layer is also assumed to be rate dependent. Because the processes in a constrained landslide are slower than in the one which is free to slide, we assume that the excess pore water pressure has enough time to dissipate. Therefore, the time dependency of displacements is solely due to viscous properties of soil.

Disadvantage of the forward approach is that it does not take into account the observed slope displacements. Spatial variability of the soil properties results in high levels of indeterminacy in constitutive models and their parameters obtained in laboratory tests. This often causes large discrepancies between the calculated and observed behavior. In contrast to the forward approach, the inverse analysis of the problem allows for the material properties to be back calculated directly from the observed displacements. This accounts for the global slope behavior, as opposed to the behavior of the locally extracted soil samples, and provides a more reliable basis for the future predictions. The purpose of this paper is to develop such an approach.

5. THE CURVE FITTING FUNCTION

In order to simplify the analysis, the following analytical function is proposed to fit the observed normalized displacements data $\bar{\delta}(\bar{x},t)=\delta(x,t)/(L-L_0)$ in the upper part of the slope ($L_0 \le x \le L$):

$$\bar{\delta}(\bar{x},t)=\bar{\delta}_x(\bar{x})\bar{\delta}_t(t)=\bar{x}(a-b\bar{x})\left(1-e^{-c(t-t_0)}\right), \text{ where } \quad 0 \le b/a < 0.5\,;\; c>0 \qquad (4)$$

where $\bar{x}=(x-L_0)/(L-L_0)$. This function describes displacements that are zero at $x=L_0$ and increase monotonically (when $0 \le b/a < 0.5$) along the slope towards its crest (Fig. 4a), while slowing with time and approaching an asymptotic value (Fig. 4b).

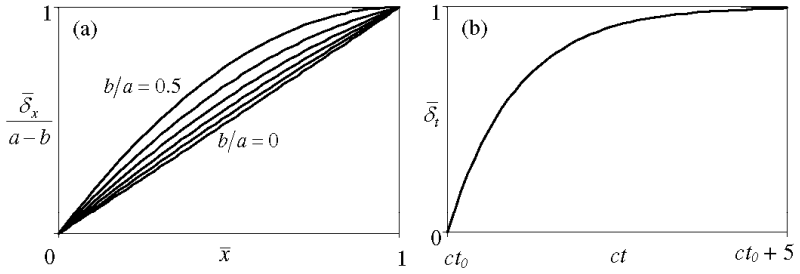

FIG. 4. Normalized functions for curve fitting of slope displacements: (a) in space; (b) in time.

The function (4) is simple and yet provides sufficient flexibility to fit the observation data both in the space (parameters *a* and *b*) and time domain (parameter *c*).

In fact, this function is the exact solution of the boundary value problem (1)-(3), for a particular case of $\eta_\tau=0$ and $\eta_p(\varepsilon,\dot{\varepsilon})=\eta_p=const$, i.e. when the residual shear strength τ_r is rate independent and the viscosity of the sliding layer is linear. In this case, the coefficients of the function (4) can be directly related to the model parameters:

$$a=\frac{p'_a+\bar{p}(L-L_0)}{E} \qquad b=\frac{\bar{p}(L-L_0)}{2E} \qquad \bar{p}=\gamma_t\sin\alpha-\tau_r/H \qquad c=\frac{E}{\eta_p} \qquad (5)$$

where L_0 is determined from equation (2):

$$L_0 = \frac{p_0' - p_a' - \bar{p}L}{2(\gamma_t \sin\alpha - \bar{p})} \tag{6}$$

It follows that if the pressure on the structure p'_0 were constant in time, the zero velocity boundary L_0 would not move. In this case, the exact solution for the normalized displacements $\bar{\delta}(\bar{x},t) = \delta(x,t)/L_0$ in the lower part of the slope ($0 \le x \le L_0$) is given by:

$$\bar{\delta}(\bar{x},t) = \bar{\delta}_x(\bar{x})\bar{\delta}_t(t) = \bar{x}(a - b'\bar{x})\left(1 - e^{-c(t-t_0)}\right) \tag{7}$$

where $\bar{x} = (x - L_0)/L_0$; coefficients a and c are identical to those in the equation (4); and

$$b' = b\frac{\gamma_t H \sin\alpha + \tau_r}{\gamma_t H \sin\alpha - \tau_r} \tag{8}$$

Hence, the displacement of the retaining structure (at $x = 0$ and $\bar{x} = -1$) is directed uphill and increases in time:

$$\delta_0(t) = -L_0(a + b')\left(1 - e^{-c(t-t_0)}\right) \tag{9}$$

In reality, however, the constant p'_0 pressure condition does not hold. The pressure-displacement relationship of the retaining structure is given by:

$$\Delta p'_0 = K\Delta\delta_0 \tag{10}$$

where K is the stiffness of the structure. Therefore, when the uphill displacement increases, the pressure p'_0 on the structure should decrease. Via equation (6) this pressure drop also causes the downhill movement of the zero velocity boundary L_0. As a result, equation (7) does not provide the exact solution for the lower part of the landslide. In spite of this, for the case of rate independent residual strength ($\eta_\tau = 0$), the curve fitting function (4) still gives the exact solution for the upper part of the landslide provided the position of the zero velocity boundary $L_0(t)$ is known at any point in time. This position will eventually converge to some non-zero value.

6. THE INVERSE ANALYSIS

Because the residual strength is in fact rate dependent ($\eta_\tau \neq 0$), the zero velocity boundary L_0 can eventually reach the retaining structure, after which the pressure on the structure will stop decreasing and start increasing. It may eventually reach the passive pressure causing the landslide collapse "overflowing" the retaining structure. Once $L_0 = 0$, we assume that it stays constant and Puzrin and Sterba (2006a) inverse analysis procedure can be applied.

The safety factor for the slope stability can be defined as the ratio between the soil resistance (passive earth pressure) and the maximum earth pressure that can develop at the retaining structure as a result of the residual shear strength decrease:

$$F_s = \frac{p'_p}{p'(0,\infty)} = \frac{p'_p}{p'_a + \bar{p}L} \tag{11}$$

where the values of the effective active and passive earth pressures in the slope are found from Chu (1991):

$$\begin{Bmatrix} p'_a \\ p'_p \end{Bmatrix} = \frac{1}{2}\gamma' H \cos\alpha \left[1 + 2\tan^2\varphi'_p \mp 2\sqrt{\left(1+\tan^2\varphi'_p\right)\left(\tan^2\varphi'_p - \tan^2\alpha\right)}\right] \tag{12}$$

where φ'_p and γ' are the effective peak angle of internal friction and effective unit weight of the soil in the sliding layer, respectively. Parameter $\bar{p}$ can be calculated from equations (5) by curve fitting the observed displacement data using the function (4) long before the pressure on the retaining structure started to increase:

$$\bar{p} = \frac{p'_a}{(a/2b-1)(L-L_0)} \tag{13}$$

Definition of the safety factor in equation (12) identifies the *failure scenario* with $F_s < 1$. In this case the time before the slope failure is given as (Puzrin and Sterba, 2006a):

$$t_f = t_0 + \frac{1}{c}\ln\frac{\Delta p'_0 / p'_p}{\left(1-e^{-c\Delta t}\right)\left(1/F_s - 1\right)} \tag{14}$$

where $\Delta p'_0$ is the increase in the earth pressure at the retaining structure, measured over the period of time Δt, t_0 is the time of the initial pressure measurement. This change in pressure can be determined using the TRIVEC system measurements.

7. PRESSURE CALCULATIONS FROM TRIVEC MEASUREMENTS

The pressure increment $\Delta p'_0$ between the times t_0 and $t_0 + \Delta t$ can be determined by the back analysis of the changes $\Delta\delta_0(z)$ in the deflection line of the retaining wall using the corresponding differential equation, TRIVEC system and anchor load measurements.

An alternative to this rather complex analysis could be the following procedure. At the earlier stages of the landslide evolution, before the zero velocity boundary L_0 moved down to the retaining structure, i.e. when the pressure p'_0 is still decreasing, from equations (6) and (5) it follows:

$$\Delta p'_0 = \frac{2\tau_r}{H}\Delta L_0 = 2(\gamma_t \sin\alpha - \bar{p})\Delta L_0 \tag{15}$$

where ΔL_0 is the measured change in the position of the zero velocity boundary between the times t and $t + \Delta t$. The average displacement of the structure over the same period of time is calculated using TRIVEC measurements:

$$\Delta\delta_0 = \frac{1}{H}\int_0^H \Delta\delta_0(z)dz \tag{16}$$

The structure stiffness is then defined using equation (10):

$$K = \Delta p'_0 / \Delta\delta_0 \tag{17}$$

After the pressure on the retaining structures starts increasing, we substitute this stiffness, together with the average displacement (14) measured between the times t_0 and $t_0 + \Delta t$, into equation (10). This gives the pressure increment $\Delta p'_0$ required for calculation of time to failure using equation (14).

8. THE COMBE CHOPIN LANDSLIDE ANALYSIS

In the following landslide stability analysis we utilize selected observation data from the Combe Chopin landslide in Switzerland. It is important to emphasize that these data are at the moment incomplete and more data will be collected over the following year to definitely conclude about the landslide stability.

The following landslide parameters are adopted here (Bapst, 2002; Bisetti, 2002): $H = 5\,\text{m}$, $L = 90\,\text{m}$, $\gamma' = 20kN/m^3$ and $\alpha = 27°$. The peak effective angle of internal friction is assumed (after Bisetti, 2002) to be $\varphi'_p = 30°$, so that from equation (5): $p'_a = 46.32kN/m^2$ and $p'_p = 102.18kN/m^2$. The safety factor was calculated by

fitting the displacement function (4) to the normalized displacement data. Example of a $k_j = b/a$ derivation for the slope displacements measured in the March 2003 is presented in Fig. 5a. The resulting values for $\bar{p}$ derived from equation (13) vary between 0.13 and 0.97kN/m^3, which results in the safety factors between 0.8 and 1.8. More observation data are required to narrow this safety factor range. Meanwhile let us explore a failure scenario with the safety factor of 0.9 and the corresponding $\bar{p} = 0.75kN/m^3$ and calculate a potential time to failure when the landslide will overflow the retaining structure.

The initial zero velocity boundary was determined in June 2002 to be at the distance 5 m uphill from the wall. By December 2005 it shifted down to the wall ($L_0 = 0$), as confirmed by TRIVEC measurements (Fig. 5b), which show that the incremental displacements of the wall have changed their direction at around this time. In fact, in Fig. 4b the solid line shows incremental displacement measured between June 2005 and December 2005 and it is negative (directed uphill). The broken line gives the incremental displacement between December 2005 and August 2006, and it is positive.

Assuming that the zero velocity boundary L_0 decreases in time linearly we calculate for the period June 2005-Dec 2005 $\Delta L_0 = 0.697$ m and from the formula (15) $\Delta p'_0 = 11.62$ kN/m^2. In the same period of time the average wall displacement was $\Delta\delta_0 = 0.285$ mm. From equation (17) the calculated stiffness of the structure $K = 40.85$ MN/m^3.

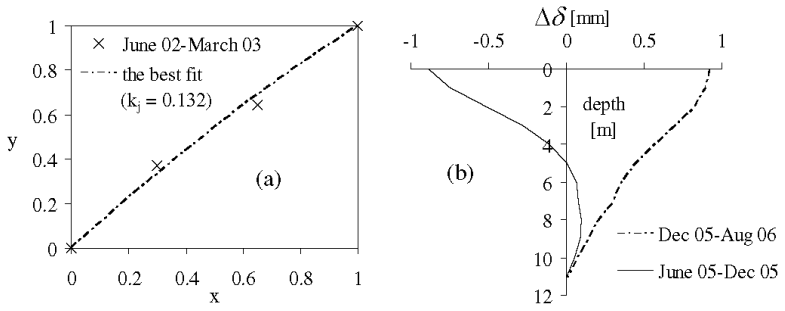

FIG. 5: (a) Curve fitting in space of the normalized displacement data monitored for the Combe Chopin landslide using equation (18). (b) Incremental displacements of the wall from TRIVEC measurements.

The displacement between Dec 2005 and Aug 2006 was 0.674 mm, and using the structure stiffness K calculated above, from equation (10) we obtain the pressure increase on the wall of $\Delta p'_0 = 27.54$ kPa over the period of $\Delta t = 230$ days. For the coefficient c responsible for the creep behavior in time we currently assume a range

$c = 1 \div 2 \times 10^{-3}$ days^{-1}, which will have to be confirmed by future measurements. Substituting all these parameters together with $F_s = 0.9$ into equation (14) we estimate that the failure will potentially take place between summer 2008 and autumn 2012. The retaining structure has been designed with the understanding that it may eventually be overflown and further measures may be required for the subsequent slope stabilization.

9. CONCLUSIONS

After a landslide is stopped by an anchored retaining structure, and the anchor forces are larger than the initial earth pressure, it is possible that the structure displacements are directed uphill and the pressure on the structure decreases in time. This may create an impression that the slope was stabilized. In fact, these negative displacements may be just temporary, and when downhill displacements start to dominate again, the pressure will start increasing. This eventually may lead to the passive failure above the structure and the structure will be overflown. The proposed here procedure based on inverse analysis of geodetic and TRIVEC measurements allows for this failure to be predicted at early stages of the landslide evolution. The Combe Chopin Landslide example has been used here for purely illustrative purposes. Additional data is required to definitely conclude on its long term stability.

10. ACKNOWLEDGEMENTS

The work has been partially supported by the ASTRA/VSS grant VSS 2005/502 "Landslide-Road-Interaction". The Authors are grateful to Mr. A. Bisetti and Mr. B. Houriet (GVH Tramelan SA) for providing the data on the Combe Chopin Landslide and to Mr. D. Naterop (Solexperts AG) for providing the TRIVEC data.

11. REFERENCES

Bapst, A. (2002). "N16 – Traversée de la Combe Chopin Conditions géologiques." *Publication de la Société Suisse de Mécanique des Sols et des Roches*, Réunion d'automne, 8. nov. 2002, Olten, Switzerland, 59-72.

Bisetti, A. (2002). "Confortation et Assainissement de la Combe Chopin Analyse de Stabilite." *Publication de la Société Suisse de Mécanique des Sols et des Roches*, Réunion d'automne, 8. nov. 2002, Olten, Switzerland, 73-82.

Chu, S. (1991). "Rankine analysis of active and passive pressures in dry sands." *Soils and Foundations*, 31 (4), 115-120.

GVH Tramelan SA (2003). "Rapport de synthese No. 1: Tunnels du Raimeux et de la Roche St-Jean – Surveillance de la Combe Chopin."

Houriet, B. (2002). "N16 – Confortation de la Combe Chopin: Dimensionnement de la paroi de pieux ancrée." *Publication de la Société Suisse de Mécanique des Sols et des Roches*, Réunion d'automne, 8. nov. 2002, Olten, Switzerland, 83-92.

Koeppel, J., Amstad, Ch. and Kovari, K. (1983). "The measurement of displacement vectors with the TRIVEC borehole probe." *International Symposium on Field Measurements in Geomechanics*, 5-8 Sept. 1983, Zurich, Switzerland, 209-218.

Naterop, D. (2002). "Deformationsmessungen in der Pfahlwand Combe Chopin." *Mitteilung der Schweizerischen Gesellschaft für Boden- und Felsmechanik,* Herbsttagung, 8. nov. 2002, Olten, Switzerland, 93-100.

Puzrin, A. and Sterba, I. (2006a). "Inverse long-term stability analysis of a constrained landslide." *Geotechnique,* 56, No. 7, 483–489.

Puzrin, A. and Sterba, I. (2006b). "Inverse Stability Analysis of St Moritz Landslide." *Proceedings of the Geotechnical Symposium in Rome*, Italy, March 2006, in press.

Skempton, A.W. (1985). "Residual strength of clays in landslides, folded strata and the laboratory." *Geotechnique*, 35(1), 3-18.

SOLEXPERTS (2007). "TRIVEC" *Solexperts AG*, Mönchaltorf, Switzerland http://www.solexperts.com/pdfs/en/geo_trivec_en.pdf

VIAMICHELIN (2007). http://www.viamichelin.de/viamichelin/deu/dyn/controller /Karten

9.5 The in-situ stiffness of the sliding layer in a creeping landslide

Puzrin, A.M., Messerklinger, S., Schmid, A. (2008),"The in-situ stiffness of the sliding layer in a creeping landslide", *Proceedings of the 4th International Symposium on Deformation Characteristics of Geomaterials, IS Atlanta 2008*, 22-24 September 2008, Atlanta, Georgia, USA, Vol. 1, pp 407-412.

The in-situ stiffness of the sliding layer in a creeping landslide

Puzrin, A. M., Messerklinger, S., & Schmid, A.
Institute for Geotechnical Engineering, ETH Zurich, Switzerland

Keywords: in-situ, soil stiffness, dilatometer test, oedometer test, creeping landslide

ABSTRACT: A long thin creeping landslide can be used as a gigantic strain gage to measure the pore water pressures and shear stiffness on the sliding surface. This requires knowledge of the stiffness of the sliding layer. For the first time in geotechnical practice both the Cambridge High Pressure Dilatometer and the Marchetti Flat Dilatometer tests have been performed in difficult soil conditions of Swiss creeping landslides (gravelly clays and silts with boulders). The field tests produced results consistent with each other and with the corresponding lab oedometer tests. It was shown that in order to produce a reasonably narrow range for the true soil stiffness, a combination of Cambridge and Marchetti tests is necessary – one kind of tests is not sufficient. The obtained stiffness values can now be used in the inverse analysis of the landslide displacements to calculate the excess pore water pressures and shear strength along the sliding surface, leading to the improved stability analysis and better design of mitigation measures (e.g. drainage).

1 INTRODUCTION

Along with the gravity, the ground water is the main driving force of many creeping landslides. It is not, therefore, surprising that changes in the yearly displacements of many landslides in Switzerland (Schindler, 1982, Schlüchter 1988, Bollinger et al, 2000) can be well correlated to the amount of yearly precipitation. Increase in the pore water pressures on the sliding surface leads to a decrease in the shear resistance, which in turn causes acceleration of the landslide displacements and may affect the overall stability.

To illustrate this, a schematic layout of the boundary value problem of a long thin constrained landslide is given in Figure 1 (e.g. St. Moritz Landslide, Puzrin and Sterba 2006). Equilibrium of the sliding layer relates the shear resistance τ^* on the sliding surface to the average normal stress in the layer p and the average effective active earth pressure p'_a and pore water pressure u_a acting at the top of the layer:

$$p(x,t)H + \int_x^L \tau^*(x,t)dx = \gamma_t H(L-x)\sin\alpha + (p'_a + u_a)H \qquad (1)$$

Here γ_t is the total unit weight of soil; α is the slope inclination; L and H are the landslide length and thickness, respectively. As is seen, the distribution of the shear strength along the sliding surface of a long thin landslide plays a major role in defining the stresses in the landing layer, and consequently, its displacements and overall stability. In turn, this shear strength distribution strongly depends on the pore water pressures $u(x,t)$ and their seasonal changes.

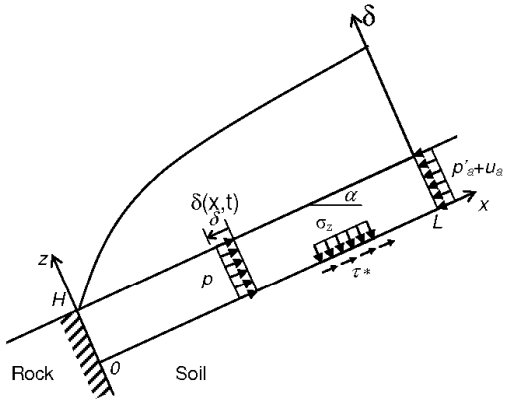

Figure 1. Schematic layout of the constrained landslide model.

$$\tau^*(x,t) = (\sigma_z - u(x,t))\tan\varphi' \qquad \sigma_z = \gamma_t H\cos\alpha \tag{2}$$

Unfortunately, these pore water pressures on the sliding surface are virtually impossible to measure directly. The only way to determine them is via some kind of inverse analysis, using a landslide as a gigantic strain gage, as described below.

If the spatial distribution of the average normal stress in the layer $p(x,t)$ was known, the pore water pressures $u(x,t)$ could be back-calculated from equations (1) and (2):

$$u(x,t) = \gamma_t H\left(\cos\alpha - \frac{\sin\alpha}{\tan\varphi'}\right) - \frac{\partial p(x,t)}{\partial x}\frac{H}{\tan\varphi'} \tag{3}$$

This inverse analysis is, however, also difficult to perform, because the reliable pressure measurements in the heterogeneous soil mass continue to represent a serious challenge.

In contrast, the displacements along the landslide $\delta(x,t)$ (Figure 1) are relatively easy to obtain using geodetic methods and with the help of inclinometers. Assuming, for example, simple linear elasto-plastic rate independent model for soil behaviour in the sliding layer, the stresses can be back calculated:

$$p(x,t) = E\varepsilon(x,t) \qquad \varepsilon(x,t) = \partial\delta(x,t)/\partial x \tag{4}$$

where ε is the average linear strain over the layer thickness; E is the elasto-plastic modulus of soil. Substitution of equations (4) into (3), allows for the changes in the pore water pressure along the sliding surface to be calculated for any period of time Δt between any subsequent displacement measurements:

$$\Delta u(x) = u(x,t_0+\Delta t) - u(x,t_0) = -E\left(\frac{\partial^2\delta(x,t_0+\Delta t)}{\partial x^2} - \frac{\partial^2\delta(x,t_0)}{\partial x^2}\right)\frac{H}{\tan\varphi'} \tag{5}$$

In fact, this expression only works if the pore water pressure increment is positive, in which case it causes further drop in the shear strength and positive landslide displacements (obviously, increase in the shear strength cannot lead to the uphill displacements).

This increase in the pore water pressure can be correlated to the increases in the amount of seasonal and yearly precipitations, and their spatial distribution can then be used for a more efficient design of a drainage system and, later, for the assessment of its effectiveness.

In this new inverse analysis approach, the landslide can be viewed as a gigantic strain gage, used for the measurement of the shear resistance and pore pressures along the sliding surface. Like in any strain gage, the stiffness E is the parameter of the greatest importance. But measuring the stiffness of the soil in the direction parallel to the slope in the heterogeneous soil conditions, such as gravely clays and silts of the St. Moritz landslide, is also a challenge. While reliable stiffness values can be obtained from the field tests only, applications of both Cambridge and Marchetti dilatometer tests are explicitly not recommended for these kinds of soil.

The soils with the grain distribution closest to that of the St. Moritz landslide are glacial tills. Studies of these soils report very limited successful attempts of applying pressuremeter and Marchetti dilatometer tests for in-situ stiffness measurements (e.g. Akbar and Clarke, 2001; Powell and Butcher, 2003; Long and Menkiti, 2007). The reason for that is that these soils are often not strong enough to hold an open borehole, while the stones do not allow for penetration and self-boring. Laboratory stiffness measurements do not provide a proper alternative, because they are normally performed on the reconstituted samples with gravel size particles being removed (e.g. Gens and Hight, 1979; Clarke et al., 1998)

The purpose of this work was to attempt measuring the soil stiffness of the sliding layer of the St. Moritz landslide, using both types of tests. In the summer 2006 these were successfully performed in a borehole close to the Leaning Tower of St Moritz, allowing for the investigation of the distribution of soil stiffness with depth and for comparing the two methods of in-situ stiffness measurements to each other and to oedometer tests performed on samples taken from the same borehole.

2 THE BOREHOLE

In the summer 2006, a 25 m deep 101 mm diameter borehole was drilled in the vicinity of the Leaning Tower of St. Moritz with the purpose of the installation of an inclinometer (Figure 2, Figure 3 and Figure 4). The rock was encountered at the depth of 19 m, with the soil above it being a mixture of clay and silt with gravel and boulders, typical for the creeping landslides in Switzerland. The sliding surface has been encountered at the depth of 17 m, and the series of Cambridge and Marchetti dilatometer tests have been performed at four different locations within the sliding layer. At each of these locations, at least one of the tests was

successful. The disturbed soil samples were collected from the same depths and the consolidation tests were performed.

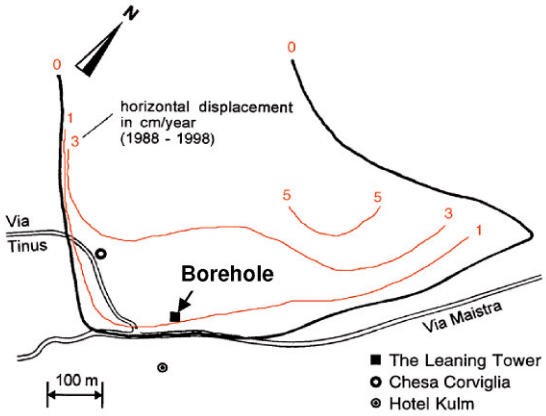

Figure 2. The borehole location on the landslide

Figure 3. Side view of the borehole location

Figure 4. The leaning tower of St. Moritz

3 THE CAMBRIDGE DILATOMETER TESTS

Cambridge High Pressure Dilatometer tests are in general not recommended for soft soils because of the fact that the borehole should be able to stand without support. Nevertheless, in this project the Cambridge dilatometer tests have been successfully performed at the depths of 5 m, 9 m and 14 m, by inserting a 95 mm cylindrical probe (Figure 5) into a predrilled 101 mm hole. The test followed a standard procedure (Sambeth, 2006). The test results are given in Figure 6, both for the compression E_{comp} and unloading-reloading E_{ur} moduli.

In general, the stiffness obtained in these tests is likely to provide a lower bound for the true soil stiffness for the following reasons:

- disturbance of soil by drilling,
- large displacements (3 to 6 mm) exclude effects of the higher small-strain stiffness.

Figure 5. Dilatometer tests: Cambridge (Internet, 2007)

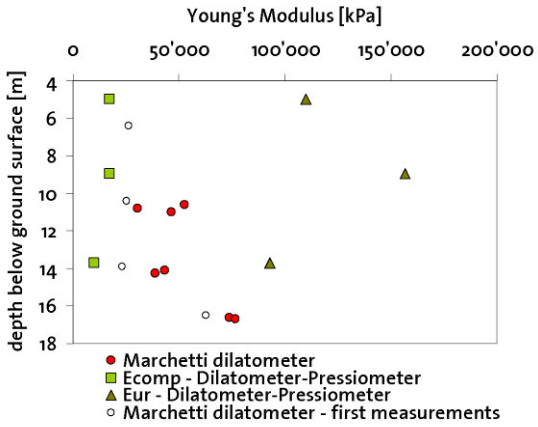

Figure 6. Soil stiffness from the dilatometer tests

4 THE MARCHETTI DILATOMETER TESTS

The Marchetti Flat Dilatometer tests are in general not recommended for soils containing stones, because they represent obstacles for penetration. In spite of that, in this project the Marchetti dilatometer tests have been successfully performed at the depths of 6.5 m, 11 m and 14 m, by penetrating a spade-like probe (Figure 7) from the bottom of a predrilled hole. The tests have been performed at the depth intervals of 20 cm. The test followed a standard procedure (Marchetti et al., 2001). The test results for compression modulus E_{comp} (the only one measured in this kind of test) are given in Figure 6. The smaller value of the measured compression modulus for each depth corresponds to the first measurement (at the depth of 20 cm below the borehole bottom), indicating the pressure relief due to the drilling process. Starting from the 40 cm depth the effect of the pressure relief becomes less significant.

In general, the stiffness obtained in these tests is likely to provide an upper bound for the true soil stiffness for the following reasons:

- compaction of the soil around the probe,
- small displacements (1.1 mm) exclude effects of the lower large-strain stiffness,
- the 3D configuration causes a stiffer soil response.

Figure 7. Dilatometer tests: Marchetti

5 THE OEDOMETER TESTS

Sixteen disturbed samples were extracted from the borehole from depths at which insitu tests were performed with the aim to determine and compare the oedometer stiffness to the stiffness measurements in situ. In general, 2 tests per sample were performed. When the results of these two tests varied significantly, a third test was performed.

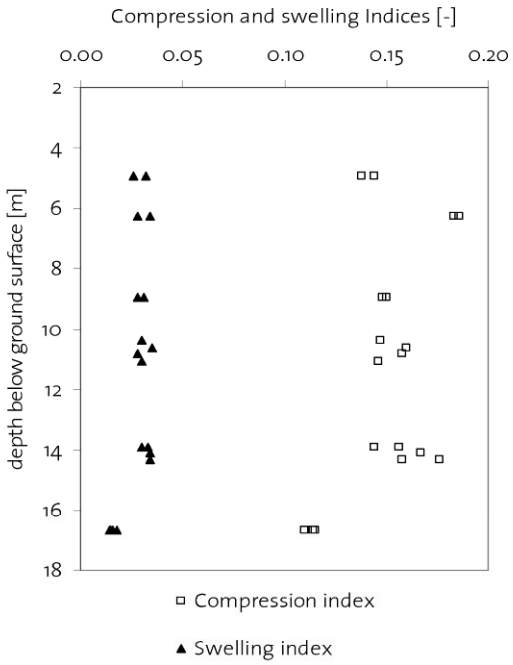

Figure 8. Soil stiffness from the oedometer tests

The reconstituted samples were sieved through a 4 mm sieve to remove large stones and wood. The remaining soil was wetted until it had a pasty consistence, filled into the oedometer ring with a spatula and placed in the oedometer apparatus. Each specimen was loaded stepwise up to 400 kPa, then unloaded to 50 kPa and reloaded to 3200 kPa. The consolidation time per load step was determined from the load – displacement curve as 30 to 45 minutes. Figure 8 gives an overview of all compression and swelling indices determined from the oedometer tests. They are in good agreement with the values obtained for a glacial till by Clarke et al. (1998).

In general, the stiffness obtained in these tests is likely to be lower than the true soil stiffness for the following reasons:

- reconstituted samples,
- removal of stones.

Gens and Hight (1979) have shown that at the gravel content smaller than 12% the gravels can be removed without affecting the soil stiffness. In the soil under study, however, the gravel content is around 30%.

6 COMPARISON BETWEEN IN SITU AND LAB TEST RESULTS

The comparison between the stiffness parameters determined from different tests is not straight-

forward, because of the strong dependency of the compression E_{comp} and unloading-reloading E_{ur} moduli in soils on the current stress state. In contrast, the compression and swelling C_C and C_S indices are stress independent, and are in fact the true soil parameters. While in the oedometer tests, the C_C and C_S are determined directly, for the Marchetti and the Cambridge dilatometer tests the transformation of the E_{comp} and E_{ur} moduli into compression (swelling) indices requires the knowledge of the average normal stresses σ'_m applied in these two dilatometer tests, respectively.

In general, the compression and swelling indices C_C and C_S for clayey soils are related to the constraint modulus M_E as follows:

$$C_C = \frac{2.3 \cdot (1+e_0)}{M_{Ecomp}} \sigma'_m \qquad C_s = \frac{2.3 \cdot (1+e_0)}{M_{Eur}} \sigma'_m \tag{6}$$

which in isotropic elasticity is in turn related to the Young's modulus:

$$M_{Ecomp} = \frac{(1-\nu)}{(1+\nu)(1-2\nu)} E_{comp}$$

$$M_{Eur} = \frac{(1-\nu)}{(1+\nu)(1-2\nu)} E_{ur} \tag{7}$$

Assuming the Poisson's ratio of 0.25, we obtain the transformation formulae for the dilatometer tests:

$$C_c = \frac{1.92 \cdot (1+e_0)}{E_{comp}} \sigma'_m \qquad C_s = \frac{1.92 \cdot (1+e_0)}{E_{ur}} \sigma'_m \tag{8}$$

Here e_0 is the in situ void ratio (for the St. Moritz landslide between 0.75 and 1.0).

For the Marchetti dilatometer test this stress magnitude is given by the average pressure applied by the membrane during the stiffness measurement. The stiffness is measured by applying 1.1 mm displacement (Marchetti et al., 2001) between the p_0 and p_1 pressure readings. Therefore, the average pressure between p_0 and p_1 was used for the transformation of the stiffness moduli into the compression and swelling indices.

For the Cambridge dilatometer test this stress magnitude is as well given by the average pressure applied by the membrane. The evaluation of the stiffness parameter was performed on the stress-strain plot by defining two points on the curve for the compression and the swelling path, respectively, and calculating the stress-strain ratio in between. From the same two points the average stress was calculated and this is the stress magnitude used for the transformation of the stiffness moduli into the compression and swelling indices.

Figure 9 represents a comparison between the compression and swelling indices obtained from the different tests, where for each depth the average value of the corresponding compression index from the oedometer test is taken for 100%.

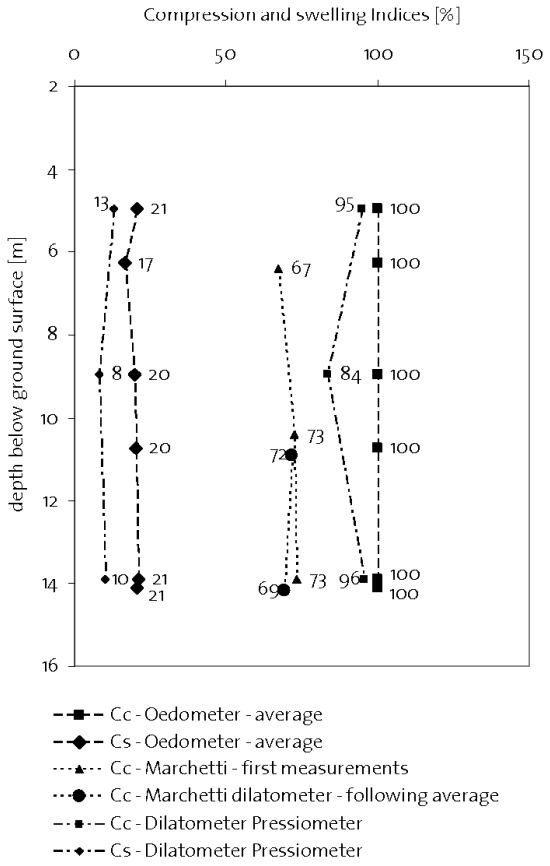

Figure 9. Comparison of the soil stiffness parameters from the field and lab tests

7 DISCUSSION

As is seen in Figure 9, compression and swelling indices appear to be a good comparison basis for different lab and field tests. All three methods gave qualitatively the same stiffness response over depth. The following observations can be made with respect to the stiffness in loading (compression index):

- considering the Cambridge test results as an upper bound and the Marchetti test results as a lower bound, the study produced a reasonably narrow range for the true compression index;
- oedometer tests also produced a reasonably accurate upper bound for the true compression index, in spite of the effect of the stone removal;
- the elastic moduli in compression in the first Marchetti measurements (20 cm below the borehole) are clearly affected by the pressure relief due to drilling, and are very close to the modulus values obtained by the Cambridge dilatometer (Figure 6);
- the soil disturbance due to drilling did not have any effect on the Marchetti measurements of stiffness, because the compression index values appear to be almost identical for the first (20 cm below the borehole) and the following deeper Marchetti measurements (Figure 9).

With respect to the stiffness in unloading (swelling index) it can be observed that:

- considering the Cambridge test results as an upper bound for the true swelling index, oedometer tests produced a much softer response and do not represent a good upper bound;
- this shows that the unloading behavior is more sensitive to the presence of stones in the field and disturbance of the samples in the lab, and is, in general, less stable.

8 SUMMARY AND CONCLUSIONS

For the first time in geotechnical practice, the both types of field dilatometer tests have been performed in difficult soil conditions of Swiss creeping landslides (gravelly silts and clays with boulders). The field tests produced results consistent with each other and with the corresponding lab tests. The following conclusions can be made:

- the compression and swelling indexes represent a good basis of comparison for different in-situ and lab tests over a large range of stresses;
- the Cambridge dilatometer tests, when feasible, produce reliable upper bounds for compression and swelling indexes;
- the Marchetti dilatometer tests produce reliable lower bounds for compression index values, independent of the depth of penetration below the bottom of the borehole;
- oedometer tests on reconstituted samples with the gravel size particles removed produce reasonable upper bound for compression index and too high upper bound for the swelling index;
- in order to produce a reasonably narrow range for the true soil stiffness, a combination of Cambridge and Marchetti tests is necessary – one kind of tests is not sufficient.

The obtained stiffness values can now be used in the inverse analysis of the landslide displacements to calculate the excess pore water pressures and shear strength along the sliding surface, leading to the improved stability analysis and better design of mitigation measures (e.g. drainage).

REFERENCES

Akbar, A. and Clark, B. G. (2001), "A Flat Dilatometer to Operate in Glacial Tills", Geotechnical Testing Journal, Vol. 24, No. 1, 51-60

Bollinger, D. (2000), "Ursachenanalyse der Hanginstabilitäten 1999", Bull. angew. Geol., 5, No 1, 5-38

Clark, B. G., Chen, C.-C. and Aflaki, E. (1998), "Intrinsic compression and swelling properties of a glacial till" Quarterly Journal of Engineering Geology, 31, 235-246

Gens, A. and Hight, D. W. (1979), "The laboratory measurement of design parameters for a glacial till", Design parameters in geotechnical engineering, Proceedings of the 7th Eur Conf Soil Mech Found Engng, Brighton, Vol. 2, 57-65

Internet (2007), "95mm and 73mm High Pressure Dilatometers side by side", http://www.cambridge-insitu.com/specs/Instruments/95_73_Pic.html.

Long, M. and Menkiti, C. O. (2007), "Geotechnical properties of Dublin Boulder Clay", Géotechnique 57, No. 7, 595-611

Marchetti, S. et al. (2001), "The Flat Dilatometer Test (DMT) in soil investigations", A Report by the ISSMGE Committee TC 16, Proc. IN SITU 2001, Intnl. Conf. On In situ Measurement of Soil Properties, Bali, Indonesia, May 2001.

Powell, J. J. M. and Butcher, A. P. (2003), "Characterisation of a glacial clay till at Chowden, Humberside", Characterisation and Engineering Properties of Natural Soils, Vol. 2, 983-1020

Puzrin, A. M. and Sterba, I. (2006). "Inverse long-term stability analysis of a constrained landslide", Geotechnique, 56, No. 7, 483–489.

Sambeth, U. (2006), „Brattashang St. Moritz, Dilatometer-versuche", Stump ForaTec *AG*, Stationsstrasse 57, 8606 Nänikon-Uster, Switzerland.

Schlüchter, Ch. (1988), "Instabilities in the area of St. Moritz, Switzerland", Proceeding 5th Int. Symposium on Landslides, Lausanne.

Schindler, C. (1982), "Problemreiche Hinterlassenschaften, Geologie und Wasserverhältnisse in Braunwald", Seperatdruck aus dem Neujahrsboten 1982 für das Glarnerland.

9.6 Inclinodeformometer: a novel device for measuring earth pressure in creeping landslides

Schwager, M. V., Schmid, A. M., Puzrin, A. M. (2009), „Inclinodeformometer: a novel device for measuring earth pressure in creeping landslides“, submitted paper for the *International Symposium on Prediction and Simulation Methodes for Geohazard Mitigation, IS Kyoto 09*, May 25-27 2009, Kyoto, Japan.

Inclinodeformometer: a novel device for measuring earth pressure in creeping landslides

M. V. Schwager, A. M. Schmid & A. M. Puzrin
Swiss Federal Institute of Technology, Zurich, Switzerland

ABSTRACT: The inclinodeformometer (IDM) is a novel device to measure changes of earth pressure in a sliding layer of a creeping landslide. The device makes use of the existing and widely used technology of the inclinometer measurements. The change of earth pressures in the sliding layer leads to the changes in the inclinometer pipe shape and dimensions. If these changes are carefully measured, the pressure change can be backcalculated, from a solution of a boundary value problem with properly described constitutive behaviors of the pipe and the surrounding soil. An advantage of the inclinodeformometer is that it does not require any additional infrastructure than standard inclinometer pipes, which are being installed anyway for landslide monitoring. Furthermore, these pipes can be used for pressure change measurements in the sliding layer long after they were sheared and became unsuitable for inclinometer measurements. Full scale laboratory tests performed in a 2 m high calibration chamber demonstrated that the pressure measurement accuracy can be as high as 3 kPa. Initial field measurements performed on the St. Moritz landslide confirmed significant stress anisotropy in the compression zone of this constrained creeping landslide.

1 INTRODUCTION

1.1 *Motivation*

Information about the earth pressure changes in a sliding layer of a creeping landslide is a crucial component for understanding, analysis and stabilization of the creeping landslides.

This information is especially important for constrained landslides, where the pressures in the compression zone could reach the passive pressure and lead to a catastrophic failure. Combining the measured increase in pressure with geodetic measurements allows for predicting whether and when the constrained landslide will fail. The procedure for this long-term inverse stability analysis was proposed by Puzrin&Sterba (2006).

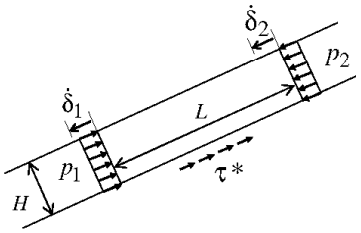

$$\Delta\tau^* = \frac{H}{L}(\Delta p_2 - \Delta p_1) \qquad E = \frac{\Delta p}{\Delta \varepsilon}$$

Figure 1. Backcalculation of the average shear strength on the sliding surface and average lateral stiffness of soil.

In general the combination of the displacements and the changes in pressure observations is very promising for the analysis of landslides. Knowing the pressure changes and displacements in two sections of a long thin sliding layer (Fig. 1) allows for backcalculation of the average shear strength on the sliding surface and average lateral stiffness of the soil in the sliding layer.

Unfortunately, measuring the earth pressures is also one of the most challenging problems in the geotechnical monitoring.

1.2 *The concept*

The inclinodeformometer (IDM) is a new device allowing for backcalculation of the changes of earth pressure using a two step procedure. In the first step, IDM measures the change in dimensions of an inclinometer pipe in the sliding layer. The change in shape is assumed to be caused by the changes in the surrounding stress field. Therefore, in the second step, the measured deformations are used to backcalculate the change in pressure via inverse analysis of the corresponding boundary value problem of a plastic pile surrounded by soil under a changing stress state.

2 MEASURING THE PIPE DEFORMATIONS

2.1 *Principle of measurement*

The inlclindeformometer makes use of the existing and widely used technology of the inclinometer measurements. The IDM probe is being lowered down the depth of the pipe on three wheels guided along the channels of the inclinometer pipe (Fig. 2). Continuous diameter measurements in two perpendicular directions can be taken.

The upper and the lower wheels are rolling in the same channel. These wheels are fixed to the probe. The middle wheel is connected via a lever with two springs, so that it can be pressed against the opposite channel. Change in the diameter of the pipe leads to change of the position of the middle wheel in respect to the probe. There are two tilt sensors (VTI Technologies, 2006) detecting the relative inclination between the probe and the lever of the middle wheel. One sensor is located on the top of the probe, another on the middle wheel (Fig. 2).

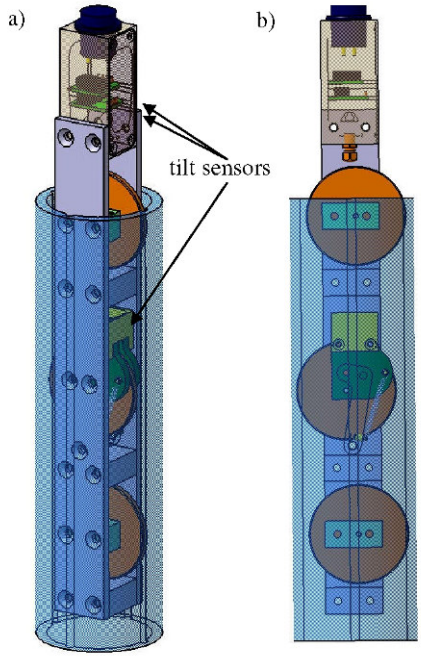

Figure 2. The inclinodeformometer in the inclinometer pipe: a) The complete device, b) The device without the front panel.

In addition to the two tilt sensors in the plane of the measured diameter there is another tilt sensor measuring in a perpendicular direction out of this plane. This sensor is used for correction of the measurements (see Section 2.2). Above the top wheel there is a pressure cell to measure the water pressure in the inclinometer pipe.

At the top of the borehole the cable on which the device is hanging goes around a wheel. An incremental rotation sensor (Wachendorff, 2008) measures the wheel rotation which determines the depth of the device in the inclinometer pipe. As the device is lowered down into the inclinometer pipe, all the sensor measurements get saved on the computer for the corresponding position in the pipe.

The IDM is built for the two most common diameters of inclinometer pipes in Switzerland: 71 and 84 mm. The device can be easily switched between the different inclinometer pipe diameters.

2.2 *Correction for the pipe inclination*

The measured diameter D inside of the pipe is a function of the two angels α_W and α_P measured at the middle wheel and at the probe:

$$D = d + X + \sin(\alpha_W - \alpha_P) \cdot Y \qquad (1)$$

X, Y and d are constants depending on geometry.

The measurements of α_W and α_P are not independent of the inclination β of the device out of the plane. Assuming that the sensors are giving the true (α_W - α_P) value at β=0° there is an error occurring on the tilt measurements, when β is different from 0°. Because the diameter is just a function of the difference (α_W - α_P), it is sufficient to describe the error Δ affecting this difference. This error can be found by calibration measurements on a biaxial inclinable table (Fig. 3).

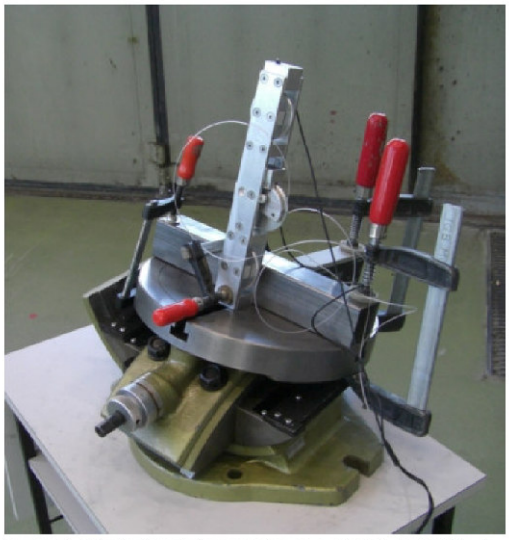

Figure 3. The inclinodeformometer on a biaxial inclinable table for calibration measurements.

The error occurring due to the device inclination out of the plane can be described as a function of α_W, α_T and β as follows:

$$\Delta(\alpha_W - \alpha_P) = (A_1\alpha_W + A_2\alpha_P + A_3)\beta^2 + (C_1\alpha_W + C_2\alpha_P + C_3)\beta \quad (2)$$

A_1, A_2, A_3, C_1, C_2 and C_3 are constants derived by a regression analysis of the calibration measurements. Correcting the difference (α_W - α_P) by the error function leads to the corrected diameter D_{cor}:

$$D_{cor} = d + X + \sin(\alpha_W - \alpha_P - \Delta)\cdot Y \quad (3)$$

By using the error function from Equation 2, the corrected measurements of the diameter D reach the precision of +/- 2 micrometers within β=+/- 4°, compared to the measurement at β=0° (Fig. 4).

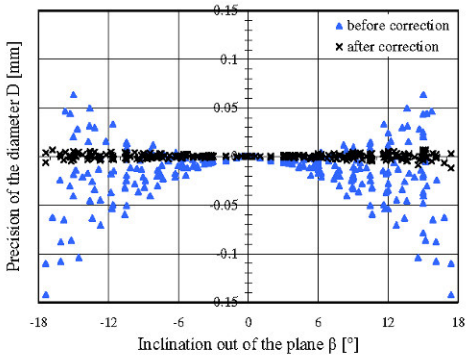

Figure 4. The precision of the diameter D compared to the measurement at β=0°.

2.3 *Calibration of the device*

The aim of IDM is it to have measurements of the diameters of the inclinometer pipes over a period of several years so that the change in shape can be computed. It is therefore important to avoid the influence of a possible shift of the device reference. For this reason the field measurements of different years should be preceded by the calibration in a constant diameter high precision reference gauge. There are two different reference gauges for both types of inclinometer pipes (Fig. 5).

Figure 5. The reference gauges for both types of inclinometer pipes.

3 BACKCALCULATING PRESSURES

3.1 *Boundary value problem*

The pressure change can be backcalculated, from a solution of a boundary value problem. The boundary value problem is given by a horizontal crossection of the pipe and the surrounding soil in plane stress (Fig. 6). The boundary conditions are static: the two principle earth pressures. The major principle stress direction is assumed to coincide with the direction of displacement vector which is known from the conventional inclinometer measurements.

The pressure increments can be backcalculated, from the measured changes in pipe diameters, provided the stiffness of the soil and the stiffness of the

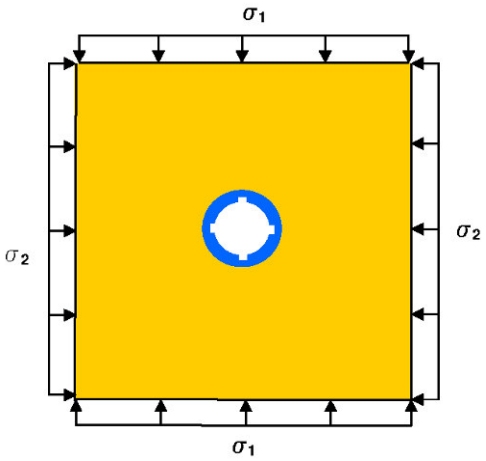

pipe in this range of stresses are known.

Figure 6. Plain strain model in case of principle stresses parallel to the axes of the pipe.

The measured diameters are not only affected by the earth pressure. Also the bending of the inclinometer pipe produced by the movement of the landslide causes changes in diameter. This influence has to be corrected before modeling in the plain stress problem.

3.2 *Effects of stiffness*

The stiffness of the pipe and the soil affect the result of the backcalculation significantly. Therefore, it is very important to describe the constitutive behaviors of the pipe and the surrounding soil in an appropriate way.

3.2.1 *Stiffness of the inclinometer pipe*

In case of the inclinometer pipe the short term Young's modulus for fast loading could be found by compression tests. The pipe was loaded by a linear distributed load in a purpose-built test apparatus (Fig. 7). The deformations had been measured for several angles between the direction of the force and the direction of the channels in the pipe.

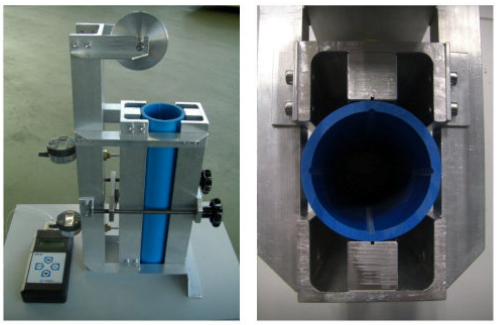

Figure 7. Compression test on the inclinometer pipe.

The tangent stiffness of the pipe k is defined as the ratio between the increment of force f divided by the increment of displacement u (or, more precisely, a half of the displacement due to the symmetry of the setup):

$$k = \frac{\Delta f}{(\Delta u)/2} \qquad (4)$$

The stiffness is strongly dependent on the angel between the direction of force and the direction of the channels in the pipe, because they soften the pipe cross-section. The highest stiffness is achieved at the angle of 45° between the force direction and the channels (Fig. 8). In this configuration there are hardly any bending moments acting in the area of the channels, where the bending stiffness is reduced a lot.

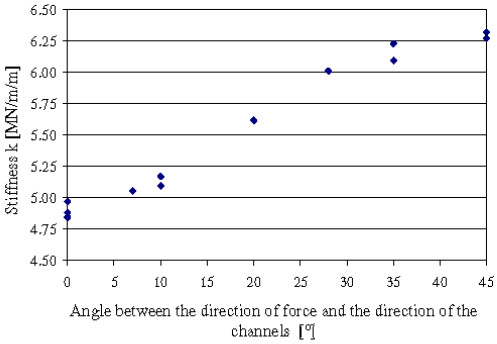

Figure 8. Stiffness k of the pipe as a function of the direction of force.

The Young's modulus E is related to k by an analytical elastic solution for a solid pipe (without channels) loaded by two opposite forces (e.g., Bouma, 1993):

$$E = \frac{2kr}{\pi A} + \frac{2r^3 k}{\pi I}(1/9 + 1/225 + 1/1225 + ..) \qquad (5)$$

where r = middle radius; A = area of the pipe section; and I = moment of inertia of the pipe section

Using Equation 5 with the stiffness k from the 45° constellation (Fig. 7) leads to the immediate Young's modulus of E=2850 MPa for fast loading. In fact this value is a lower bound because the formula is made for pipes without channels. Nevertheless, when used for the modeling of this test with the finite element program ABAQUS, it appeared to reproduce the results for a channeled pipe with high accuracy.

For backcalculations of pressures in creeping landslides, however, the long-term modulus is of much bigger concern then the immediate modulus for fast loading. The viscous behaviour of the pipe has to be considered. The long term creep and relaxation test are currently being carried out.

3.2.2 *Stiffness of the surrounding soil*

The stiffness of the surrounding soil can be measured by dilatometer tests while drilling the borehole for the inclinometer. If no measurements are available the stiffness of the soil can be estimated from results of laboratory tests (e.g., consolidation tests). The major effects on the stiffness of the soil are the loading history and the nonlinearity due to stress dependency of stiffness.

3.2.3 *Linear elastic solution*

In the axisymmetric case of the hydrostatic state of stress, where $\sigma_1 = \sigma_2 = \sigma$, there exists an analytical

elastic solution relating the acting free field stress σ and the radial deformation u:

$$\sigma = u\left(\frac{E_S}{R(1+\upsilon_S)} + \frac{E_P t}{(R-t/2)^2}\right) \quad (6)$$

where E_S = Young's modulus of the surrounding soil; υ_S = Poisson ratio of the soil; E_P = Young's modulus of the inclinometer pipe; R = external radius of the pipe; and t = thickness of the pipe.

Equation 6 clearly shows the effects of the both the pipe and the soil stiffness, but does not consider any channels. This formula can be used as a benchmark for the finite element model.

3.3 *Inverse analysis*

In reality, however, the soil is visco-elasto-plastic and the pipe is visco-elastic with geometric nonlinearity due to the channels. Therefore, the forward boundary value problem has to be solved using numerical analysis. The backcalculation of pressures is performed in two steps: first, a finite element program computes the deformations caused by the trial stresses. An inverse analysis algorithm then solves the optimization problem to minimize the objective function F (the sum of squared errors between the measured and the computed pipe deformations) by changing the trial stresses σ_1 and σ_2.

Figure 8 shows f as a function of σ_1 and σ_2. The Young's moduli of the soil and the pipe were set to 50 MPa and 2850 MPa, respectively. The poisson ratios were assumed to 0.3 and 0.25. The minimum of the objective function is located at σ_1 = 100 kPa and σ_2 = 60 kPa.

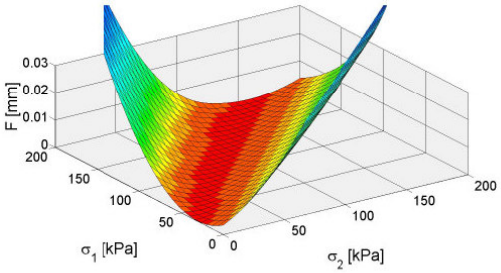

Figure 9. Objective function for inverse analysis.

It can be seen in Fig. 9, that the gradient is quite low along the objection function "valley". This means that a variety of states of stress may lead to similar pipe deformations. This can be explained by the fact, that bending moments cause much bigger deformations of the pipe then normal forces, and different combinations of the stress ratio σ_2/σ_1 and the average stress $(\sigma_1+\sigma_2)/2$ can produce the same bending moments at different levels of compression of the pipe. From Fig. 9 it follows that variation in σ_2/σ_1 at a fixed $(\sigma_1+\sigma_2)/2$ produces larger pipe deformation than other way round. This makes backcalculation of stress increments more challenging.

3.4 *Validation: IDM box*

For validation of the backcalculation full scale laboratory tests were performed in a 2 m high calibration chamber (IDM-box) with a cross-section of 40 by 40 cm. Each of the 4 vertical walls of the chamber is equipped with a pressure membrane allowing for application of 2 independent principle horizontal stresses. The chamber is filled with sand and the inclinometer pipe is fixed in the middle of the chamber. Increase in principle stresses results in the deformations in the pipe which are measured using the inclinodeformometer.

Validation with finite elements showed that the dimensions of 40 by 40 cm, when compared with a free field solution, are sufficient to avoid the effect of the boundaries.

Figure 10. The IDM box.

Preliminary measurements in the calibration chamber demonstrated an accuracy in pressure measurements of about +/- 5 kPa. The comparison between applied and backcalculated pressures is given in Fig. 11.

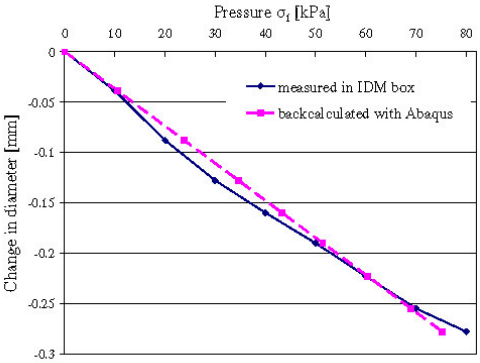

Figure 11. The comparison between the backcalculated and applied pressures in the IDM box experiments; $\sigma_2 = 0.6\ \sigma_1$.

4 INITIAL FIELD MEASUREMENTS

Initial field measurements performed in the compression zone of the St. Moritz landslide confirmed significant stress anisotropy (Fig. 12). The A-axis coincides with the direction of the landslide velocity, B-axis is perpendicular to it. The pipe diameters are averaged every 3 meters – e.g., within each continuous pipe section between the installation joints. The measurements consistently demonstrate an elliptical pipe shape with a smaller diameter parallel to the landslide velocity. The difference between the pipe sections is most likely due to the variation in the initial pipe diameters. In 2009 the measurements of the diameter changes will be taken and the earthpressure changes backcalculated.

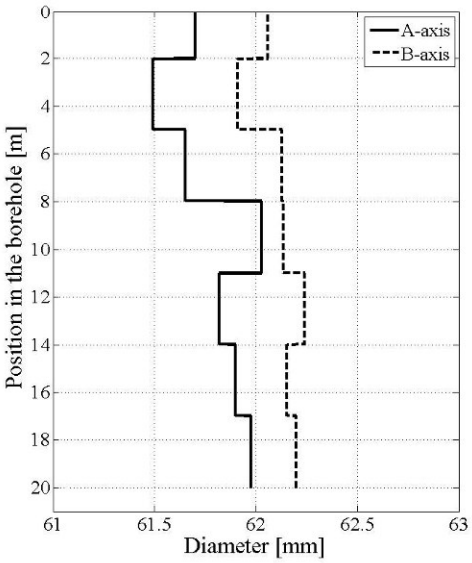

Figure 12. Initial measurements of the sheared inclinometer pipe diameter in the compression zone of the St. Moritz landslide.

5 CONCLUSIONS

The research on the novel inclinodeformometer device is in its preliminary stages. Nevertheless it looks promising, due to simplicity and accuracy of measurements. In addition, it does not require any additional infrastructure than standard inclinometer pipes, which are being installed anyway for landslide monitoring. Furthermore, these pipes can be used for pressure change measurements in the sliding layer long after they were sheared and became unsuitable for inclinometer measurements. Backcalculation of pressures is a challenging task, which requires additional study.

6 ACKNOWLEDGMENTS

The work has been partially supported by the ASTRA/VSS grant VSS 2005/502 "Landslide-Road-Interaction".

7 REFERENCES

Bouma, A.L. 1993. *Mechanik schlanker Tragwerke. Ausgewählte Beispiele in der Praxis*. Berlin: Springerverlag.

Puzrin, A. M., & Sterba, I. 2006. Inverse long-term stability analysis of a constrained landslide. *Géotechnique* 56(7): 483-489.

VTI Technologies Oy. 2006. The SCA103T Differential Inclinometer Series; Data Sheet.

Wachendorff Automation GmbH. 2008. Drehgeber WDG 58E; Datenblatt.

9.7 Defining and monitoring of landslide boundaries using fiber optic systems

Iten, M., Schmid, A., Hauswirth, D., Puzrin, A. M. (2009), „Defining and monitoring of landslide boundaries using fiber optic systems“, submitted paper for the *International Symposium on Prediction and Simulation Methodes for Geohazard Mitigation, IS Kyoto 09*, May 25-27 2009, Kyoto, Japan.

Defining and monitoring of landslide boundaries using fiber optic systems

M. Iten, A. Schmid, D. Hauswirth & A. M. Puzrin
Swiss Federal Institute of Technology, Zurich, Switzerland

ABSTRACT: Defining and monitoring of the landslide boundaries is essential for the landslide understanding, analysis and stabilization. It is, however a rather challenging task in both urban and rural areas. Distributed fiber optic sensors are offering new possibilities in the field of geotechnical monitoring. This paper describes three novel fiber optic landslide boundary monitoring systems, which have been designed, put in place and tested on several locations around St. Moritz, Switzerland.

1 INTRODUCTION

1.1 *Motivation*

Differential soil displacements initiated by creeping landslides can cause immense problems by damaging infrastructure and buildings in the sliding area. Moreover, special construction and reinforcement requirements, or even total halt of construction within a landslide area may be demanded by local construction laws. In some cases it is, therefore, of crucial importance to determine the exact position of the boundary between the landslide and the stable part of the slope. For a comprehensive analysis, this boundary needs to be identified on the surface, as well as in the subsoil.

Traditional monitoring techniques for this problem include geodetic measurements and inclinometers. Geodetic measurements can identify the boundary on the surface, but not necessarily with high precision. Additionally, depending on the amount of required measurement points and survey frequency, this can be a costly campaign. Inclinometers serve for the detection of this boundary underneath the surface, called the sliding surface. Once an inclinometer pipe is sheared, a conventional inclinometer probe can not be inserted anymore and the inclinometer will no longer produce results.

This paper is an attempt to outline new landslide monitoring techniques by means of continuous strain measurements in optical fibers embedded into an asphalt road, an old inclinometer pipe, or even directly into the soil. The necessary technology of measuring continuous longitudinal strain in an optical fiber is based on Brillouin Optical Time Domain Analysis (BOTDA), nowadays commercially available. It offers a great potential for application in the geotechnical field.

1.2 *Projects*

In all the projects presented in this paper, the goal is to determine the boundary between the landslide and the stable part. By performing optical strain measurements along the sensor cable, the transition zone between the sliding and the stable parts can be identified.

The first system, an asphalt road-embedded sensor cable, serves for the evaluation of such a boundary in an urban region. A road, which intersects this boundary, can be seen as a large-scale strain gauge. Commencing in 2006, up to date three such road-embedded sensor systems have been integrated and tested in the field.

For the boundary identification in an area where no road or other infrastructure exists, to which the fiber cable could be attached, a soil-embedded "micro-anchor"-cable system has been developed. The principle of this second system is that a cable fixed to "micro-anchors" buried in soil experiences the same movement than the soil around it. Laboratory testing of system parts started in 2007 and a first field integration of the novel specially developed cables and anchors took place in July 2008.

The third monitoring system takes advantage of old, out of service, inclinometer pipes. In order to continue using such pipes, a fiber cable is placed inside and the pipe is filled with grout. The current sliding surface can then be identified and displacements on this surface backcalculated. Such a fiber optics equipped inclinometer has been installed on site in July 2008.

1.3 *Location*

The two creeping landslides monitored in this work are located in the heart of the renowned mountain resort town of St. Moritz, Switzerland (Fig. 1). The displacements of the Brattas landslide have been monitored by geodetic measurement techniques for over 100 years. The Laret landslide, on the other hand, has not been recognized until recently, and it is still discussed whether it even represents a landslide or just localized displacements.

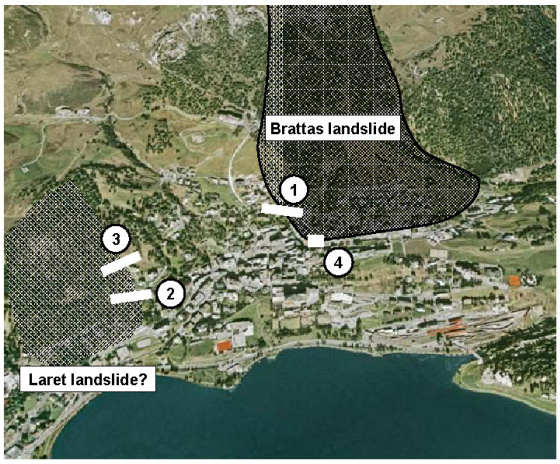

Figure 1. A view of the lake and the town of St. Moritz from the South. The sensors installed are as follows: 1 and 2, road-embedded sensors, 3 soil-embedded sensor system, 4 fiber optics inclinometer.

2 DISTRIBUTED FIBER OPTIC SENSING

2.1 *Brillouin optical time domain analysis*

Distributed temperature and strain sensing along an optical fiber using the effect of Brillouin scattering was proposed by Horiguchi et al. (1990). It has since evolved towards a high performance technology that can achieve 1 meter spatial resolution over long fiber lengths with absolute strain measurements in the range of a few $\mu\varepsilon$ (1 microstrain = 10^{-4}%).

Spontaneous Brillouin scattering occurs when a portion of light guided through a silicia fiber is backscattered by a nonlinear interaction with thermally excited acoustic waves. The scattered light undergoes a frequency shift. This frequency shift depends, among others, on the acoustic wave velocity, which is directly related to the strain and temperature dependent medium density.

In the more refined stimulated Brillouin scattering configuration, two counter-propagating lightwaves, at different frequencies, interact via stimulated acoustic waves. The use of stimulated Brillouin scattering for distributed fiber measurements was demonstrated by Horiguchi et al. (1989) and later named as Brillouin optical time domain analysis (BOTDA).

The Brillouin backscattered light is recorded in the time domain to obtain information of the scattering along the fiber and the frequency shift of the signal is analyzed and converted into strain and temperature data. As the frequency shift is dependent on strain and temperature change in the cable, a temperature reference measurement is needed in order to separate the two components.

Today's commercially available distributed Brillouin scattering measurement units can be operated by an experienced engineer without profound knowledge of the physics behind the phenomenon. For the projects presented in this paper, a BOTDA measurement unit from Omnisens, Switzerland was utilized. It is capable of measuring the strain value with a resolution of 2 $\mu\varepsilon$ continuously along the optical fiber of up to 30km length for any minimally 1m long section of this fiber (Omnisens 2007).

2.2 *Design and selection of fiber optic cables*

Fiber optic cables for integration into different environments have to comply with several requirements, such as being strong enough to withstand harsh installation conditions, transmitting strain applied on the jacket without loss to the fiber core, allowing unproblematic handling and offering flexible adjustment to project modifications.

Specialty fiber optics strain and temperature sensing cables can be found on the market, but they appear to have a series of handicaps varying from high signal loss (attenuation), tricky handling and inflexibility in project alterations to long production and delivery time and high prices. Therefore, it was chosen to custom produce strain sensing cables for the projects in this paper. The first custom sensor has been produced in 2006 at the institute's laboratory, while the later versions where developed in a joint project with a cable manufacturer. The different sensor cables are displayed in Figure 2 and their main characteristics are qualitatively described in Table 1.

2.3 *Laboratory testing of cables*

The strain response of the fiber cables used in this study was separately tested in the laboratory. This has been done using a fiber strain calibration device which allows for fixation and straining of the fiber at known values and reference measurements thereof with Brillouin technology. As a result, the characteristics of all the cables, such as Brillouin shift, fiber slip and temperature influence could be specified and field readings can be, if necessary, adjusted to these values.

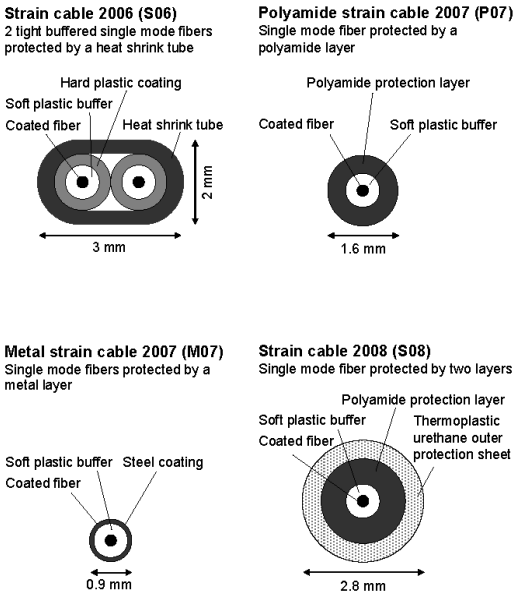

Figure 2. Cross section of strain sensing cables used in this study.

Table 1. Main characteristics of custom produced fiber optic sensors used in the projects described in this paper.

Sensor	Robustness	Handling	Attenuation	Price
S06	- - -	-	- - -	+ + +
P07	+	+ +	+	-
M07	+ +	+	+	-
S08	+ +	+	+	- -

+ advantage
- limitation

3 ASPHALT ROAD-EMBEDDED FIBER OPTIC SENSOR

3.1 *Site description*

The creeping Brattas landslide (Fig. 1) divides the heavily populated hillside into a stable part (outside the landslide boundary) and a moving part (landslide). An asphalt road crosses the landslide boundary in the south-western region of the landslide. The road is surrounded by buildings on both sides. No cracks have been observed in asphalt, indicating that the boundary shear zone is sufficiently wide for the asphalt to absorb deformations without cracking. To locate the boundary shear zone, it was decided to instrument the road with the fiber optic cable (Site 1 in Fig. 1).

3.2 *Installation of sensor*

In October 2006, a 89m long, 10mm wide and 70mm deep trench was cut along the road in the asphalt. The sensor cable S06 was then attached to the bottom of the trench by clips at 2m length intervals. This procedure allowed pre-straining of the cable over the whole length. Subsequently, a two-component epoxy adhesive fixed the cable definitely at 1 meter intervals to the asphalt at the trench bottom. On top of the strain cable, a temperature compensation cable was loosely positioned and the whole trench was filled with an elastic cold sealing compound. The detailed installation procedure is described in Iten et al. (2008).

3.3 *Monitoring process*

Strain and temperature measurements were performed the day following the sensor installation and thereafter every couple of months. There was no need for continuous monitoring, because the landslide is slow moving (creeping) and no large-scale movements have been observed. The monitoring was performed successfully for 7 months until the sensor broke.

3.4 *Monitoring results*

The strain change in the fiber along the road in the 7 months of monitoring is shown in Figure 3. It is clearly recognizable that in a 15m long section (between 30 and 45 meters from the upper shaft), strain increased by about 1000 $\mu\varepsilon$, while in the other parts of the fiber, strain change stays within a 500 $\mu\varepsilon$ band around the zero line.

Temperature measurements could not be successfully performed, as the signal loss was exceeding the required level for measuring with BOTDA. Therefore, temperature compensation is not included in the results of the strain measurements.

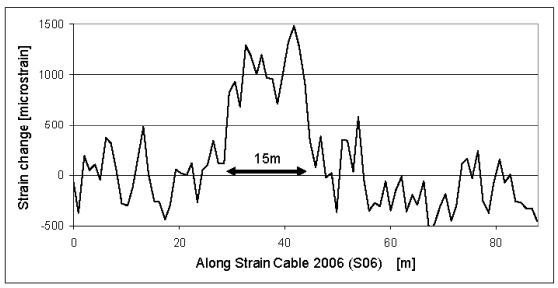

Figure 3. Strain change along road-embedded S06 sensor.

3.5 *Data interpretation*

For the data interpretation of the measured strain in the fiber, a simple model can be considered (Fig. 4). For correct interpretation, the angle between the sensor and the movement needs to be specified. Visual observations of damaged structures, geodetical data, as well as the location of the strained section lead to the assumption, that this angle is around 45°.
In order to achieve a strain of about 1000 $\mu\varepsilon$, over the transition zone of 15m, the landslide movement should be about 20mm. This displacement is of the order of magnitude of the yearly displacement geodetically recorded in this area.

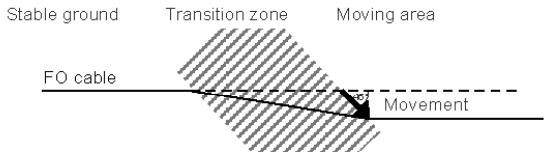

Figure 4. Simple model for movement interpretation from strain data.

3.6 *Application of asphalt road-embedded sensor system in other projects*

Following the cable breaking of the S06, a new set of sensors was installed on the same location in summer 2007. This time, a metal protected strain cable (M07), as well as a polyamide protected strain cable (P07) (Fig. 2), were embedded into the road. In addition, in 2008 an asphalt road crossing the Laret landslide boundary (Site 2 in Fig. 1) was equipped by 47m of the P07 cables. The monitoring of these sensors is still continuing and is beyond the scope of this paper.

4 SOIL-EMBEDDED "MICRO-ANCHOR" – CABLE SYSTEM

4.1 *Site description*

Uphill from the road-embedded sensor on the Laret landslide (Site 2 in Fig. 1), a soil-embedded sensing system was placed beneath a hiking path (Site 3 in Fig. 1). Downhill from that path, and above the road-embedded sensor, a building was severely damaged in 2006 due to differential displacements. At that point, concerns began to rise that a creeping landslide may exist at this location. It is assumed that the landslide is almost not moving under normal conditions, but may be triggered by a nearby excavation, undertaken in 2006 for the construction of a new building.

4.2 *Sensor system*

The soil-embedded sensor system consists of the two parts: "micro-anchors" and optical cable. The purpose of the "micro-anchors" is to connect the cable to the soil at the specified fixation points, so that the cable experiences the same movement than the soil around it, instead of the soil just flowing around the cable. Such a system is sketched in Figure 5.

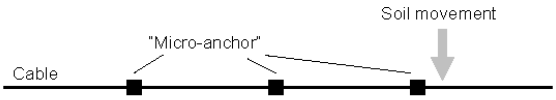

Figure 5. Soil-embedded sensor system.

4.3 *Laboratory testing of sensor system*

In order to dimension the "micro-anchors", a pullout box was used (Fig. 6). The box is 2m long, 0.1m wide and 0.2m deep and has a step motor at the front. For the tests, the box was filled with a poorly graded sand up to the half of its height. The sensor was then placed and the box was entirely filled with sand. On top of this sand, it was possible to add additional weight simulating different sensor depths. Three different tests were carried out: the cable failure test, the anchor failure test and the anchor interaction test (Fig. 7).

The cable failure test allows for the measurement of cable pullout resistance, and therefore, the friction between the cable and the sand. The purpose of the anchor failure test is to determine the anchor bearing capacity (failure load), as well as the design load (before the anchor starts loosing contact with the soil). The anchor interaction test determines the minimal distance d between two identical anchors, at which they do not affect each others performance.

In advance of the field installation, these tests were run in order to design the system components properly. The cable S08 (Fig.2) in connection with a 40x40x40mm anchor was subsequently chosen for field installation.

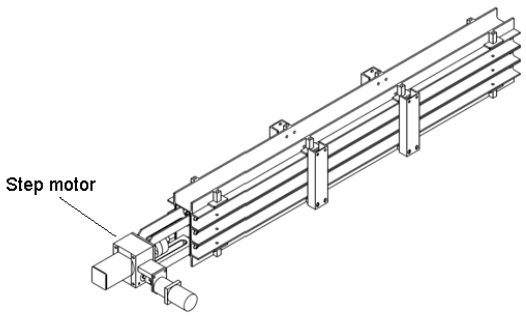

Figure 6. Pullout box.

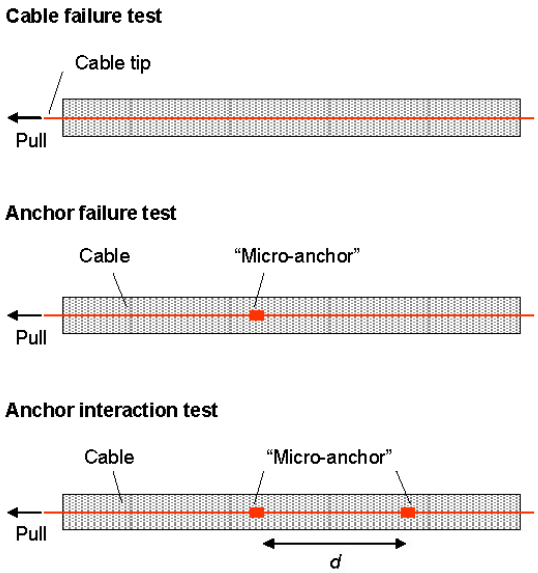

Figure 7. Setup of the laboratory tests with the pullout box.

4.4 *Installation of the sensor system*

For the installation of the sensor system, a 80m long and approximately 0.4m deep trench was cut in the path. The location of the trench was chosen so that part of the trench should be on stable ground while the rest is in the creeping zone. The bottom of the trench was then filled with compacted sand, the sensor was slightly pre-strained, placed and covered with sand again. In addition, a temperature compensation cable as well as a strain cable without anchors was put in the trench. A picture of the installation is shown in Figure 8.

Figure 8. The trench cut in the hiking path with the sensor system already embedded.

4.5 *Monitoring and outlook*

Zero readings of the strain were taken the day following the implementation in July 2008. First results from strain monitoring are expected for summer 2009.

5 REACTIVATION OF OLD INCLINOMETER PIPES

5.1 *Site description*

Close to the compression zone and lower boundary of the Brattas landslide, an inclinometer pipe was installed in 1982 for the localization of the sliding surface and monitoring of displacements (Site 4 in Fig. 1). The inclinometer pipe has a standard 71mm diameter, and goes 14.75m deep into the ground. Since 1987, the inclinometer can not be monitored anymore because the conventional probe does not go all the way through the pipe. For that reason, it was decided to reactivate this inclinometer by installing a fiber optic sensor.

5.2 *Installation of sensor*

The sensor consists of the P07 cable, which was inserted into the inclinometer to 14m depth and slightly prestrained. The whole pipe was then filled with a cement-bentonite grout backfill. This grout is intended for the overall bonding of the fiber along the pipe.

5.3 *Monitoring process*

In July 2008, after hardening of the grout, zero readings of the strain in the fiber were taken. In October, the strain was measured again and monitoring will continue every few months.

5.4 *First monitoring results*

The strain change along the cable between July and October 2009 is displayed in Figure 9. It can be clearly seen, that between 5.5m and 7.5m, the strain in the fiber increased by up to 400 $\mu\varepsilon$, while in the other parts, strain increase stays about +/- 100 $\mu\varepsilon$ around 0. The largest strain increase was measured at 6.2m with 410 $\mu\varepsilon$.

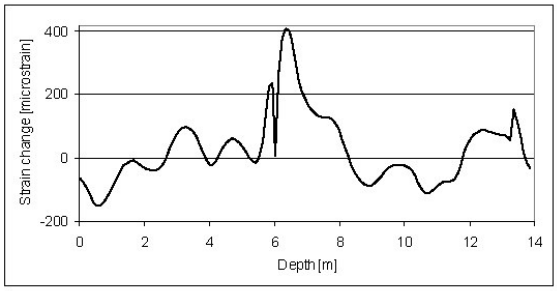

Figure 9. Average strain change in the 3 months period following the sensor installation in the inclinometer.

5.5 *Data interpretation and outlook*

Monitoring data from 1982 to 1984 indicate that the sliding surface lies between 5.8m and 6.7m. By looking at the optically measured strain in the fiber, one can see that principal displacements must occur between 6.2m and 6.8m. The measured strain over the 1 meter thick sliding surface suggests a monthly horizontal displacement of about 1mm, which is in the range measured in 1982-1987. The optical data series at this site consists of just two measurements, one in July and the other one in October. Therefore, it would be too early to give a comprehensive validation of this sensor system. Nevertheless, the agreement between the two methods strongly supports applicability of the fiber optics sensors in old inclinometer pipes.

6 DISCUSSION

6.1 *Cable selection*

In any fiber optic strain sensing project, the selection of the adequate cable is a key issue. The main concern is usually put on the protection and on the strain transfer from the outside sheath of the cable to the optical fiber. Cable manufacturers are increasingly adjusting to the demands of the fiber sensing community and can offer custom made strain sensor cables. Shortly, such cables should be available of the shelf.

6.2 *Attachment of cable to the structure / ground*

For the attachment of a sensor cable to a structure or to the ground, basically two methods exist: continuous bonding and point fixation. It is a difficult task to determine the best fixation method and, especially, to choose a procedure which allows to achieve a durable and trustworthy fixation. The options shown in this paper have demonstrated a good performance.

6.3 *BOTDA technology vs. traditional technologies*

The possibility to measure deformation continuously along a fiber optic cable, presents several advantages over traditional technologies such as geodetic measurements or inclinometers. First, it offers distributed measurements of strain over long distances and therefore, hundreds and thousands of measuring points. This is a clear advantage when soil stability monitoring extends over long distances (e.g. for ground movement detection along roads, train tracks, power lines or pipelines). Second, measurements can be done remotely from the site, as the cable can extend to the instrument placed in an office, and therefore, a large area can be monitored from one source. Other advantages of fiber optic strain sensing include its immunity to electromagnetic hazards (lightning), water resistance and its long lifetime.

In order to deploy BOTDA measurements meaningfully to monitor ground movement, a series of improvements and developments have to be considered, such as commercially available strain sensing cables with known strain behavior parameters, guidelines for structure integration techniques and standards for data processing and evaluation.

7 CONCLUSIONS

The design, implementation and testing of three novel fiber optic landslide boundary monitoring systems using BOTDA technology has been demonstrated. Where the time frame allowed, measurements have been taken and the obtained results were in good agreement with traditional monitoring techniques. This validation leads to the conclusion that distributed BOTDA sensing has the potential to become a widely accepted new tool in landslide monitoring, and, in some cases, might even outperform traditional techniques. At present, until methods and standards in this field are established and reliable, combination with traditional measurements is necessary.

8 ACKNOWLEDGMENTS

The authors would like to thank the cable manufacturer BRUGG CABLES and the measurement unit provider OMNISENS for their collaboration and advice, VSS/ASTRA (the Swiss federal department of transportation) as well as to CTI (the Swiss innovation promotion agency) for funding. In addition, we are grateful to the authorities of the municipality of St. Moritz for the test sites and support during field measurements.

REFERENCES

Horiguchi, T., Kurashima, T. & Tateda, M. 1990. A technique to measure distributed strain in optical fibers. In Photonics Technol. Lett., 2: 352-354.

Horiguchi, T. & Tateda, M. 1989. Optical-fibre-attenuation investigation using stimulated Brillouin scattering between a pulse and a continuous wave. In Optic Letters, 14: 408-410.

Iten, M., Puzrin, A.M. & Schmid, A. 2008. Landslide monitoring using a road-embedded optical fiber sensor. In Smart Sensor Phenomena, Technology, Networks, and Systems 2008; Proceedings of SPIE 6933.

Omnisens SA. 2007. STA100/200 Series, Fiber Optic Distributed Temperature and Strain Analyzer; User Manual.

VIII. Projektabschluss

Schweizerische Eidgenossenschaft
Confédération suisse
Confederazione Svizzera
Confederaziun svizra

Eidgenössisches Departement für
Umwelt, Verkehr, Energie und Kommunikation UVEK
Bundesamt für Strassen ASTRA

FORSCHUNG IM STRASSENWESEN DES UVEK **ARAMIS SBT**

Formular Nr. 3: Projektabschluss

erstellt / geändert am:	27. April 2009

Grunddaten

Projekt-Nr.:	**VSS 2005 / 502**
Projekttitel:	Road-Landslide Interaction: Monitoring and Inverse Stability Analysis; Interaktion Strasse-Hangstabilität: Monitoring und Rückwärtsrechnung
Enddatum:	30. März 2009

Texte:

Zusammenfassung der Projektresultate:

Dieses Pilotprojekt hatte zum Ziel, an ausgewählten Kriechhängen der Schweiz die Methoden für die Langzeitstabilität zu identifizieren, die dafür nötigen Daten zu sammeln sowie den Einfluss auf die Infrastruktur Strasse zu untersuchen. Nachfolgend sind die im Rahmen dieses Projektes erzielten Resultate aufgelistet.

Eine neuartige Methode zur Rückrechnung der Langzeitstabilität von natürlich oder künstlich am Fuss gestützten Rutschungen wurde entwickelt und erfolgreich an den Kriechhängen von St. Moritz und Combe Chopin angewandt.

•Zum ersten Mal wurden der Cambridge Insitu und der Marchetti Flat Dilatometer in solch schwierigen Bodenverhältnissen erfolgreich benutzt, um die Bodensteifigkeit in der sich bewegenden Schicht der Brattas Rutschung in St. Moritz zu bestimmen.

•In der Rutschung von St. Moritz wurde durch die Verwendung von Dehnungsmessungen in Glasfaserkabeln (distributed fiber optic strain measurements, BOTDA) eine neuartige Technik zur Bestimmung der Grenzen der Rutschung angewendet. Zum ersten Mal wurden erfolgreich Glasfaserkabel in den Strassenasphalt integriert. Dies ermöglichte, die Strasse als eine Art riesigen Dehnmessstreifen zur Messung der Deformationen zu benutzen und gleichzeitig Informationen zur Gebrauchstauglichkeit der Strasse zu erhalten.

ARAMIS SBT: VSS-2005-502-projektab.doc Seite 1 / 3

Schweizerische Eidgenossenschaft
Confédération suisse
Confederazione Svizzera
Confederaziun svizra

Eidgenössisches Departement für
Umwelt, Verkehr, Energie und Kommunikation UVEK

Bundesamt für Strassen ASTRA

	Es zeigte sich im Verlauf, dass der Fokus dieses Pilotprojektes auf die Entwicklung von neuartigen Geräten und Methoden zur Analyse und Überwachung sowie auf Techniken zu Labor- und Feldversuchen gerichtet werden musste, um die fehlenden Informationen zur Rückrechnung der Langzeitstabilität und Verschiebungen von Kriechhängen zu sammeln. Diese Entwicklungen wurden in zahlreichen wissenschaftlichen Publikationen präsentiert und von der internationalen geotechnischen Gemeinschaft gut aufgenommen.
Zielerreichung:	Das Ziel wurde erreicht. Die angedachte Methode zur Berechnung der Hangstabilität von Kriechhängen konnte erarbeitet werden.
Folgerungen und Empfehlungen:	Als Folgearbeit zu diesem Pilotprojekt schlagen wir ein vollständiges Projekt vor, bei dem die neuen Geräte zur Datensammlung angewendet und diese Informationen zur Berechnung der Langzeitstabilität und Verschiebungen sowie zur Untersuchung von möglichen Stabilisierungsmassnahmen in den betrachteten Kriechhänge verwendet werden.
Publikationen:	Puzrin, A. M. & Sterba, I. (2006). Geotechnique 56, No. 7, 483–489, Inverse long-term stability analysis of a constrained landslide Messerklinger, S., Schmid, A., Rohr, R. Sterba, I. und Puzrin, A.M. (2007).“Interaktion Strasse - Hangstabilität, Monitoring und Rückwärtsrechnung, VSS – Forschungsarbeit Nr. 2005/502 1. Zwischenbericht Field expedition St. Moritz – Juli 2006“ Bericht Nr. 4714, Institut für Geotechnik, ETH Zürich Messerklinger, S., Schmid, A., Rohr, R. Sterba, I. und Puzrin, A.M. (2007).“Interaktion Strasse - Hangstabilität, Monitoring und Rückwärtsrechnung, VSS – Forschungsarbeit Nr. 2005/502 1. Zwischenbericht Field expedition St. Moritz – Juli 2006“ Bericht Nr. 4714/1, Institut für Geotechnik, ETH Zürich Puzrin, A.M. and Schmid, A. (2007). “TRIVEC Measurements in the Inverse Analysis of the Long-Term Stability of a Constrained Landslide.” Proceedings of the 7th International Symposium on Field Measurements in Geomechanics Boston, FMGM 07, Massachusetts, USA, September 24-27. Puzrin, A.M., Messerklinger, S., Schmid, A. (2008),”The in-situ stiffness of the sliding layer in a creeping landslide”, Proceedings of the 4th International Symposium on Deformation Characteristics of Geomaterials, IS Atlanta 2008, 22-24 September 2008, Atlanta, Georgia, USA, Vol. 1, pp 407-412.M. V. Schwager, M. V., Schmid, A. M., Puzrin, A. M. (2009), „Inclinodeformometer: a novel device for measuring earth pressure in creeping landslides“, submitted paper for the International Symposium on Prediction and Simulation Methodes for Geohazard Mitigation, IS Kyoto 09, May 25-27 2009, Kyoto, Japan. Iten, M., Schmid, A., Hauswirth, D., Puzrin, A. M. (2009), „Defining an monitoring of landslide boundaries using fiber optic systems“, submitted paper for the International Symposium on Prediction and Simulation Methodes for Geohazard Mitigation, IS Kyoto 09, May 25-27 2009, Kyoto, Japan.

Schweizerische Eidgenossenschaft
Confédération suisse
Confederazione Svizzera
Confederaziun svizra

Eidgenössisches Departement für
Umwelt, Verkehr, Energie und Kommunikation UVEK
Bundesamt für Strassen ASTRA

Beurteilung der Begleitkommission:
Diese Beurteilung der Begleitkommission ersetzt die bisherige separate fachliche Auswertung.

Beurteilung:	**Die Begleitkommission schätzt den Wert der erarbeiteten Resultate als hoch ein. Die gewonnenen Erkenntnisse und Methoden lassen sich auf verschiedene Kriechhänge in der Schweiz applizieren.** **Kriechhänge und allgemein instabile Hänge beeinflussen die Linienwahl und die Unterhaltsarbeiten an Verkehrswegen in unserem Land erheblich. Die Theorien zur Berechnung und Bemessung von Kriechhängen und Kriechdrücken beruhen auf relativ alten Annahmen, wobei es zu dieser Zeit noch nicht möglich war moderne Messmittel wie optische Sensoren etc. einzusetzen. Die in diesem Bericht vorgestellten Ansätze sind daher von grossem Wert.** **Allerdings sollten die neuen Messmethoden noch an weiteren praktischen Beispielen verifiziert werden, daher sind noch weitere Arbeiten auf diesem Gebiet wünschenswert.**
Umsetzung:	Die Umsetzung der gewonnenen Resultate in die Praxis geschieht anhand von Publikationen und Vorträgen. Der praktisch tätige Geotechnikingenieur kann die gewonnenen Erkenntnisse anwenden.
weitergehender Forschungsbedarf:	Ja. Bei diesem Projekt handelt es sich um eine sehr breite Machbarkeitsstudie für die realistische Bemessung und Beurteilung der Mechanik von Kriechhängen mit neuen Methoden. In einem weiteren Forschungsprojekt sollten die gewonnenen Erkenntnisse an mehreren Kriechhängen in der Schweiz verifiziert und kalibriert werden.
Einfluss auf Normenwerk:	Noch keinen unmittelbaren, mittelbar wird die Arbeit auf die Normierungstätigkeit wirksam werden.

äsident Begleitkommission:

Name:	Amiguet, Präsident EK 5.08	Vorname:	Jean-Louis
Amt, Firma, Institut:	Geotest SA		
Strasse, Nr.:	EN Budron E7		
PLZ:	CH-1052	Email:	jean-louis.amiguet@geotest.ch
Ort:	Le Mont-sur-Lausanne	Telefon:	+41 21 731 45 65
Kanton, Land:	Vaud, Suisse	Fax:	+41 21 731 43 83

Unterschrift Präsident Begleitkommission:

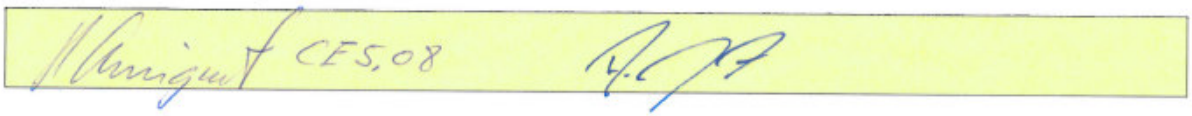

ARAMIS SBT: VSS-2005-502-projektab.doc

Seite 3 / 3

IX. Verzeichnis der Forschungsberichte im Strassenwesen

Verzeichnis der Forschungsberichte

Strassenwesen, Forschungsberichte ab Nr. 1000

Bericht-Nr.	Projekt Nr.	Alte Nr.	Titel	Datum
1000	VSS 1996/035	(20/96)	Evaluation des performances de nouveaux matériaux de revêtement: 1re partie: Enrobés à haut module *Untersuchung des Verhaltens neuer Belagsmaterialien: 1. Teil: Tragschichten hoher Steifigkeit*	2001
1001	VSS 1997/056	(21/97)	Tätigkeitsabläufe und Entscheidungshilfen im Management der Strassenerhaltung *Déroulement des activités et soutien du choix dans le cadre de la gestion de l'entretien des routes*	2001
1002	VSS 1999/119	(11/99)	Analyse des modèles de comportement des chaussées *Analyse der Verhaltensmodelle der Fahrbahnen*	2001
1003	SVI 1999/136	(42/99)	Probleme bei der Einführung und Durchsetzung der im Transportwesen geltenden Umweltschutzbedingungen; unter besonderer Berücksichtigung des Vollzugs beim Strassenverkehrslärm *Problèmes lors de la mise en place et de l'application de la légalisation en vigueur sur la protection de l'environnement dans le domaine des transports; particulièrement en ce qui concerne l'application en cas de bruit engendré par la circulation routière*	2002
1004	VSS 1999/124	(16/99)	Anforderungen an Geokunststoffe mit den Aufgaben Bewehren und Schützen *Exigences relatives aux fonctions de renforcement et de protection pour géosynthétiques*	2002
1005	SVI 1999/138	(44/99)	Nachhaltigkeit und Koexistenz in der Strassenraumplanung *Durabilité et coexistence dans la planification des espaces routiers*	2001
1006	ASTRA 1998/094	(52/98)	Utilisation des matériaux d'excavation de tunnels dans le domaine routier Etat des connaissances actuelles *Verwendung von Tunnelausbruchmaterial im Strassenbau* *Stand der aktuellen Kenntnisse*	2002
1007	VSS 1999/111	(03/99)	Höhengleiche Kreuzungen Schiene/Strasse *Croisements à niveau rail–route*	2001
1008	SVI 1999/141	(47/99)	Nachhaltigkeit im Verkehr; Kriterien für kommunale und kantonale Strassenverkehrsplanungen und -projekte *La durabilité concernant le trafic routier; Critères d'évaluation pour des projets et des planifications routiers*	2002
1009	VSS 1999/218	(17/00)	Voraussetzungen für die dynamische Umwidmung von Standstreifen zu Fahrstreifen *Conditions pour la transformation dynamique des bandes d'arrêts d'urgence en voie de circulation*	2002

Bericht-Nr.	Projekt Nr.	Alte Nr.	Titel	Datum
1010	VSS 1999/289	(19/00)	Modalités de mise en place d'arbres d'alignement Problématique de l'implantation d'allées d'arbres hors des agglomérations *Vorgehen bei der Planung und Realisierung von Alleebaumbepflanzungen ausserorts*	2001
1011	SVI 1999/137	(43/99)	Warum steht Paul Müller lieber im Stau als im Tram? Motive der Verkehrsteilnahme – Teil 2 *Pourquoi dans un bouchon plutôt que dans un tram? Ou les raisons de se déplacer – part 2*	2002
1012	VSS 1999/269	(02/00)	Absturzsicherungen für Personen sowie Passive Sicherheit von Tragkonstruktionen der Strassenausrüstung *Protections des personnes contre les chutes et Securité passive des structures porteuses*	2002
1013	SVI 1998/088	(42/98)	Massnahmen zur Erhöhung der Akzeptanz längerer Fuss- und Velostrecken *Mesures pour une meilleure acceptation des parcours piétonniers et cyclables plus longs*	2002
1014	SVI 1999/321	(37/00)	Carreiseverkehr: Grundlagen und Perspektiven *Transport de voyageurs par car: Caractéristiques et perspectives*	2002
1015	SVI 1998/092	(46/98)	Potentielle Gefahrenstellen *Endroits potentiellement dangereux*	2001
1016	ASTRA 2000/411		Lärmschirme an Strassen; Akustische Quellenhöhe bei der Berechnung der Hinderniswirkung *Parois antibruit; Hauteur de source du trafic routier pour le calcul de l'effet d'écran*	2002
1017	VSS 1996/032	(14/96)	Tägliche äquivalente Verkehrslast TF verschiedener Strassentypen in der Schweiz *Trafic pondéral équivalent journalier TF sur divers types de chaussées en Suisse*	2002
1018	VSS 1996/034	(18/96)	Volumetrische und mechanische Optimierung von Splittmastixasphalt *Optimisation volumétrique et mécanique des splittmastixasphaltes*	2002
1019	SVI 2000/442		Evaluation kurzfristiger Benzinpreiserhöhungen *Evaluation des effects des hausses à court terme du prix de l'essence*	2002
1020	VSS 1999/301		Systeme für die automatische Verkehrskontrolle mit digitaler Bildtechnik *Systèmes pour les contrôles routiers automatiques avec traitement d'images numériques*	2002
1021	ASTRA 1999/151	(62/99)	Exploitation des résultats du congrès de Kuala Lumpur et du concours «Infrastructures et Transports pour le 21e siècle» *Auswertung der Ergebnisse des Weltstrassenkongresses in Kuala Lumpur und des Wettbewerbes «Infrastrukturen und Verkehr für das 21. Jahrhundert»*	2002
1022	ASTRA 2000/447		Erarbeitung der Grundlagen für eine Strassenverkehrssicherheitspolitik des Bundes (VESIPO) *Elaboration des fondements d'une politique nationale de sécurité routière (VESIPO)*	2002

Bericht-Nr.	Projekt Nr.	Alte Nr.	Titel	Datum
1023	ASTRA 2001/060		Erarbeitung der Grundlagen für eine Strassenverkehrssicherheitspolitik des Bundes (VESIPO) Beurteilung betrieblicher und infrastruktureller Massnahmen *Elaboration des fondements d'une politique nationale de sécurité routière (VESIPO)* *Evaluation de mesures d'exploitation et d'infrastructure*	2002
1024	ASTRA 2001/061		Erarbeitung der Grundlagen für eine Strassenverkehrssicherheitspolitik des Bundes (VESIPO) Prognose der Strassenverkehrsunfalle 2010 *Elaboration des fondements d'une politique nationale de sécurité routière (VESIPO)* *Pronostic du nombre des accidents de la circulation routière 2010*	2002
1025	ASTRA 2001/062		Erarbeitung der Grundlagen für eine Strassenverkehrssicherheitspolitik des Bundes (VESIPO) Beitrag der Verkehrstelematik zu einer Verkehrssicherheitsstrategie *Elaboration des fondements d'une politique nationale de sécurité routière (VESIPO)* *Contribution de la télématique des transports à une stratégie de sécurité routière*	2002
1026	ASTRA	2001/063	Erarbeitung der Grundlagen für eine Strassenverkehrssicherheitspolitik des Bundes (VESIPO) Wirtschaftliche Bewertung von Verkehrssicherheitsmassnahmen (WIVSIMA) *Elaboration des fondements d'une politique nationale de sécurité routière (VESIPO)* *Evaluation économique des mesures de sécurité routière (EEMSR)*	2002
1027	SVI 2000/376	(39/00)	Mischverkehr MIV / OEV auf stark befahrenen Strassen *Circulation mixte TMI / TP sur les routes à trafic élevé*	2002
1028	VSS 1995/023	(09/00)	Elektronische Parkgebühreninkassosysteme mit dedizierter Nahbereichskommunikation (DSRC) *Systèmes d'encaissement électronique de taxes de parking (DSRC)*	2002
1029	VSS 1995/023	(09/99)	Datenaustausch mit dem Road Administration Data Exchange Format (RADEF) auf dem Trans European Road Network (TERN) *Echange de données avec le Road Administration Data Exchange Format (RADEF) sur le Trans European Road Network (TERN)*	2002
1030	ASTRA 1999/145	(53/99)	Schädigungsmechanismen der Betonkorrosion in Tunnelbauwerken *Mécanismes d'endommagement du béton par l'eau dans les tunnels*	2002

Bericht-Nr.	Projekt Nr.	Alte Nr.	Titel	Datum
1031	VSS 1995/023	(17/95)	Verfahren zur Bestimmung der Leistungsfähigkeit, der Verkehrsqualität und der Belastbarkeit von Verkehrsanlagen *Méthodes pour les calculs de la capacité, du niveau de service et des charges compatibles*	2002
1032	ASTRA 1999/144	(52/99)	Spritzabdichtungen im Tunnelbau *Etanchéité projetée dans les travaux souterrains*	2002
1033	VSS 1999/126	(18/99)	Annäherung und Parallelführung Schiene – Strasse Abstand und Schutzmassnahmen *Voies de communication du trafic routier et du trafic ferroviaire - Tracés parallèles ou se rejoignant Distances minimales et mesures de protection*	2002
1034	VSS 1999/255	(21/00)	Heutige und künftige Transportketten im Güterverkehr: Analyse und Normierungsbedarf *Les chaînes de transport des marchandises actuelles et futures: analyse et besoin de standardisation*	2002
1035	ASTRA / SRCE		Planches comparatives avec bitumes modifiés et ajouts *Vergleichsstrecken mit polymermodifizierten Bindemitteln und Zusätzen*	2002
1036	VSS 1998/071	(04/98)	Stoffliche Zusammensetzung und Beurteilung der langfristigen Umweltverträglichkeit von Sekundärbaustoffen *Composition des matériaux de récupération et appréciation de leur influence sur l'environnement à long terme*	2002
1037	VSS 1996/031	(11/96)	Entwicklung der Griffigkeit von Strassenbelägen verschiedener Strassentypen in der Schweiz *Développement de l'adhérence de revêtements de chaussées en Suisse*	2003
1038	ASTRA 2000/423		Griffigkeit auf Autobahnen Vergleich der Messergebnisse SRM und SCRIM Unterhalt 2000, Forschungsprojekt 6 *Propriétés antidérapantes aux autoroutes Relation entre SRM et SCRIM Entretien 2000, projet de recherche 6*	2002
1039	SVI 2000/391	(44/00)	Verlässlichkeit als Entscheidungsvariable Vorstudie *La fiabilité comme variable dans la prise de décision Etude préliminaire*	2002
1040	VSS 1999/120	(12/99)	Evaluation des Strassenzustandes *Diagnostic d'état des chaussées*	2000
1041	VSS 1999/297	(13/00)	Grundlagen zur Revision der Norm SN 640 925a inkl. Schadenkatalog *Etudes de base pour la révision de la norme SN 640 925a y compris le catalogue des dégradations*	2002
1042	VSS 1994/015	(19/94)	Schnittstellen zwischen Strassendatenbanken und Geo-Informationssystemen *Interfaces entre des banques de données routière (BDR) et des systèmes d'information géographique*	2003
1043	VSS 1997/051	(13/97)	Assiette des giratoires *Kreiselplatte*	2002

Bericht-Nr.	Projekt Nr.	Alte Nr.	Titel	Datum
1044	VSS 1999/122	(14/99)	Récupération du liant bitumineux provenant d'extraction Mise en application et adaptation de la nouvelle norme européenne vis-à-vis des expériences suisses *Rückgewinnung bituminöser Bindemittel aus Extraktionslösungen* *Ueberprüfung und Anpassung der neuen EN-Norm an die schweizerischen Erfahrungen*	2002
1045	SVI 1999/319	(35/00)	Perspektiven für kurze Autos *Perspectives pour les mini-véhicules*	2003
1046	SVI 1999/135	(41/99)	Strassen mit Gemischtverkehr: Anforderungen aus der Sicht der Zweiradfahrer *Routes à trafic mixte: les exigences du point du vue de cyclistes*	2003
1047	SVI 2000/362		Projet Agram Etude de l'acquisition d'une géométrie de référence des axes de maintenance Base pour la révision des normes VSS SN 640 910, SN 640 911 et SN 640 920, et l'établissement de la norme sur la gestion des géométries d'axe *Projekt Agram* *Beschaffung der Bezugsgeometrie der Unterhaltsachsen Grundlage für die Revision der VSS–Normen SN 640 910, SN 640 911 und SN 640 920 sowie für die Erarbeitung der Norm zur Verwaltung der Achsgeometrien*	2003
1048	SVI 2001/512		Vorstudie zu den Wechselwirkungen Individualverkehr – öffentlicher Verkehr infolge von Verkehrstelematik-Systemen *Etude préliminaire sur les interactions transports individuels – transports en commun suite à la mise en place de systèmes de télématique routière*	2003
1049	VSS 1999/295		Management der Strassenerhaltung (MSE) für Strassennetze in Städten und Gemeinden Erhaltungsplanung bei Infrastrukturanlagen *Système de gestion de l'entretien des réseaux routiers (SGE) dans les villes et les communes* *Planification d'entretien des installations d'infrastructure*	2003
1050	VSS 1999/207	(01/00)	Einfache Kostenkontrolle und -überwachung auf der Baustelle *Suivi et contrôle simple des coûts de construction sur le chantier*	2003
1051	VSS 2000/414	(18/00)	Bewachsene Oberbauten *Superstructures vertes*	2003
1052	VSS 1991/003	(22/91)	Fugenabdichtungen Langzeitverhalten von Fugenvergussmassen aus Polymerbitumen auf einer Versuchsstrecke *Joint d'étanchéité* *Comportement à long terme des joints à base de bitume-polymère sur un tronçon de route témoin*	2003
1053	ASTRA 2000/415	(52/00)	Verifikation von PM10 – Emissionsfaktoren des Strassenverkehrs	2003

Bericht-Nr.	Projekt Nr.	Alte Nr.	Titel	Datum
			Vérification des facteurs d'émission de PM10 du trafic routier	
1054	VSS 1998/079	(20/98)	Geschwindigkeiten in Steigungen und Gefällen *Les vitesses dans les rampes et les pentes*	2003
1055	VSS 2000/436	(31/00)	Standardisierte Verkehrsinformation *Normalisation de l'information d'aide à la mobilité*	2003
1056	VSS 2001/101		Volkswirtschaftliche Nutzen und Kosten einer beschleunigten Realisierung von Autobahnbaustellen mittels Anreizsystemen *Les utilités et coûts économiques d'une réalisation accélérée des chantiers sur les autoroutes moyenant l'application de systèmes d'incitation*	2003
1057	VSS 1996/306	(08/00)	Elektronische Verkehrssignale – Voruntersuchung *Signalisation routière électronique – pré–étude*	2003
1058	VSS 1995/019	(06/95)	Kälteverhalten von bituminösen Bindemitteln *Comportement des liants bitumineux à basse température*	2002
1059	VSS 1999/263		Parkleitsysteme Systemarchitektur und Schnittstellen *Systèmes de guidage pour le stationnement* *Architecture des systèmes et interfaces*	2004
1060	SVI 2000/444		Lange Planungsprozesse im Verkehr Das Gras wächst nicht schneller, wenn man daran zieht *Longs processus de planification dans les transports* *L'herbe ne pousse pas plus vite si on la tire*	2004
1061	ASTRA 2002/009		Site Internet du Comité national suisse de l'AIPCR (www.swissroads.ch) *Website des Schweizer Nationalkomitees des AIPCR (www.swissroads.ch)*	2004
1062	SVI 1999/326		Auswirkungen von Personal Travel Assistance (PTA) auf das Verkehrsverhalten *Influence d'un système d'aide du type „Personal Travel Assistance" sur le comportement des usagers des transports*	2004
1063	SVI 1999/142	(48/99)	Erfolgskontrolle von Umweltschutzmassnahmen bei Verkehrsvorhaben *Suivi des mesures de protection de l'environnement dans la construction de voirie*	2003
1064	VSS 1997/054	(17/97)	Unfallauswertung: Statistik, Auswertung und Analyse von Strassenverkehrsunfällen, Massnahmen *Evaluation des accidents: statistique, traitement et analyse des accidents de la circulation Routière, mesures*	2003
1065	SVI 2001/534		Zeitkostenansätze im Personenverkehr *Valeur du temps concernant le transport des voyageurs*	2004
1066	SVI 2000/379		Methoden zum Erstellen und Aktualisieren von Wunschlinienmatrizen im motorisierten Individualverkehr *Méthodes d'estimation et d'actualisation d'une matrice d'origine – destination dans la Circulation individuelle motorisée*	2004
1067	VSS 1999/256		Telematikanwendungen im kombinierten Güterverkehr	2004

Bericht-Nr.	Projekt Nr.	Alte Nr.	Titel	Datum
			Application de la télématique au transport intermodal de marchandises	
1068	VSS 2000/439	(34/00)	Architecture cadre pour la télématique routière *Rahmenarchitektur für die Verkehrstelematik*	2004
1069	VSS 1997/053	(15/97)	Projektierung der Grünräume im Strassenraum *Projets d'espaces verts le long des axes routières*	2004
1070	VSS 1999/290		Projektierung von Güterstrassen und Parkplätzen *Projets de routes rurales et d'aires de stationnement*	2004
1071	SVI 2000/445	(73/00)	Determinanten des Freizeitverkehrs: Modellierung und empirische Befunde *Facteurs déterminant les déplacements liés aux loisirs*	2004
1072	SVI 2000/443	(71/00)	Verfahren von Technology Assessment im Verkehrswesen *Procédures de TechnologyAssessment dans le domaine du transport*	2003
1073	VSS 1999/110	(02/99)	Erfahrungsbilanz bei der Gestaltung des Strassenraumes in erhaltenswerten Ortskernen *Aménagement de l'espace routier dans les centres de localité dignes d'être sauvegardés*	2003
1074	ASTRA 2001/008		Konfliktanalyse bezüglich Vermeidung eines Versorgungsnotstandes der schweizerischen Bauwirtschaft mit felsgebrochenen Hartgesteinen zur Herstellung hochwertiger Beläge und Bahnschotter *Analyse des conflits pour éviter des problèmes d'approvisionnement de l'industrie suisse de construction en roches dures concassées destinées à la production de revêtements de haute qualité et de ballast*	2004
1075	VSS 1998/084	(25/98)	Einfluss und Wirkung von Dünnschichtbelägen auf die In–Situ–Eigenschaften von Asphaltoberbauten *Influence et effets des revêtements minces sur les caractéristiques in situ des Chaussées bitumineuses*	2004
1076	VSS 2001/301		Stauzeit statt Staulänge *Durée de bouchon au lieu de longueur de bouchon*	2004
1077	SVI 2001/541		Verkehrsumlegungs–Modelle für stark belastete Strassennetze *Modèles d'affectation pour des réseaux fortement chargés*	2004
1078	SVI 2000/386		Wirksamkeit und Nutzen der Verkehrsinformation *Efficacité et bénéfices de l'information routière*	2004
1079	VSS 1998/083	(24/98)	Géométrie tridimensionnelle des voies de circulation *Dreidimensionale Geometrie der Verkehrswege*	2004
1080	VSS 1999/302		Verkehrstelematiksysteme für das Management von Gefahrguttransporten *Systèmes télématiques pour la gestion des transports de marchandises dangereurses*	2004
1081	VSS 1998/074	(12/98)	Elaboration d'une méthode prédictive de l'orniérage des revêtements bitumineux *Erarbeitung einer Methode zur Spurrinnenprognose in bituminösen Belägen*	2004
1082	VSS 1999/283		Beziehung zwischen den Verdichtungswerten AASHTO–Standard und AASHTO–Modified	2005

Bericht-Nr.	Projekt Nr.	Alte Nr.	Titel	Datum
			Corrélation entre les valeurs de compactage AASHTO–Standard et AASHTO–Modified	
1083	VSS 1999/123	(15/99)	Erarbeiten von Grundlagen zur Festlegung von Anforderungskennwerten für den Gyratorversuch *Bases et données pour l'établissement des valeurs caractéristiques requises pour l'essai de presse à cisaillement giratoire*	2004
1084	VSS 1999/244		Lokal verstärkter Schneegriesel bei tiefem Stratus (Industrieschnee) *Amplification locale de la chute de neige granulée par stratus bas (neige industrielle)*	2004
1085	FGU 2003/003		Evaluation der Methodik „Indirekte Vorauserkundung von wasserführenden Zonen mittels Temperaturdaten" in Bezug auf Aussagekraft und Nutzen für den Vortrieb *Evaluation de la méthode «Prédiction indirecte de zones de venue d'eau au moyen de données thermiques» au regard des besoins de l'excavation de tunnel*	2005
1086	ASTRA 2001/013		Beschlagende Scheiben in Strassentunneln – Synthese *Embuage du pare–brise dans les tunnels routiers – synthèse*	2004
1087	VSS 2002/902		Alpentransitbörse Abschätzung der Machbarkeit verschiedener Modelle einer Alpentransitbörse für den Schwerverkehr *La bourse du transit alpin*	2004
1088	SVI 2001/531		Mobilitätsdatenmanagement für lokale Bedürfnisse *Gestion des données de mobilité dans le contexte local*	2004
1089	SVI 2001/515		Auswirkungen neuer Arbeitsformen auf den Verkehr – Vorstudie *Effets de nouvelles formes de travail sur le trafic – Etude préliminaire*	2004
1090	VSS 2000/337		Verkehrsqualität und Leistungsfähigkeit auf Autobahnen *Qualité de service et capacité des autoroutes*	2004
1091	VSS 2001/901		Qualitraffic – Qualität der Verkehrsinformation *Qualitraffic – Qualité de l'information trafic*	2005
1092	VSS 1998/076	(16/98)	Leistungsfähigkeit hochbelasteter Kreisel (Grundlagen) *Capacité des carrefours giratoires encombrés (principes de base)*	2004
1093	VSS 1996/033	(15/96)	Bases, principes et mesures de modération du trafic et de valorisation de l'espace routier *Grundlagen, Grundsätze und Massnahmen zur Verkehrsberuhigung und Aufwertung des Strassenraumes*	2000
1094	VSS 2000/454		Sicherheit und Komfort von Parkierungsanlagen *Sécurité et confort des installations de stationnement*	2004
1095	ASTRA 2002/005		Intervention bei Bränden in Strassentunneln *Interventions lors d'incendies dans les tunnels routiers*	2005
1096	SVI 1999/310		Wirkungsketten Verkehr–Wirtschaft	2005

Bericht-Nr.	Projekt Nr.	Alte Nr.	Titel	Datum
			Interactions entre le transport et l'économie	
1097	SVI 1999/322		Spezialisierung und Vernetzung : Verkehrsangebot und Nachfrageentwicklung zwischen den Metropolitanräumen des Städtesystems Schweiz *Spécialisation et interconnexion: Offre de transport et évolution de la demande entre les espaces métropolitains du réseau urbain Suisse*	2005
1098	SVI 2001/525		Standards für intermodale Schnittstellen im Verkehr *Standards pour les interfaces intermodales en matière de transport*	2004
1099	VSS 1998/078	(17/98)	Evacuation des eaux de chaussées Bases de calcul du débit (2éme partie) *Strassenbewässerung Grundlagen und Abflussberechnung*	2005
1100	SVI 2001/553		Cleaner Drive Hindernisse für die Markeinführung von neuen Fahrzeug-Generationen	2004
1101	VSS 2001/602		Critères d'oppurtunité et de choix des installations automatiques de déverglacages *Zweckmässigkeits- und Auswahlkriterien für automatische Taumittelsprühanlagen*	2005
1102	VSS 2000/340		Standardisierte Erfassung des Gesamtverkehrsaufkommens von einzelnen Verkehrserzeugern *Enregistrement standardisé du volume de trafic global à partir de générateurs individuels de trafic*	2004
1103	VSS 1997/046	(03/97)	Einfluss von Änderungen des Parkierungs-Angebotes auf das Verkehrsverhalten *Influence de changements dans l'offre de stationnement sur le comportement*	2004
1104	VSS 2000/366		Parkplatzbedarf und -angebot für Personenwagen *Besoin et offre en cases de stationnement pour les voitures de tourisme*	2004
1105	SVI 2000/446	(74/00)	Spezifische Anforderungen an Autobahnen in städtischen Agglomerationen *Specificités autoroutières dans les agglomérations urbaines*	2004
1106	SVI 1999/312		Instrumente für die Planung und Evaluation von Verkehrssystem-Management-Massnahmen *Instruments de planification et d'évaluation des mesures de gestion de systèmes de transport*	2004
1107	VSS 1999/270		Vorbereiche vor Tunneln auf Autobahnen *Zones d'approche des tunnels d'autoroutes*	2005
1108	VSS 2002/703		Abschätzung des durchschnittlichen jährlichen Wertverlustes von kommunalen Strassennetzen *Estimation de la dépréciation moyenne annuelle d'un réseau de routes communales*	2005
1109	VSS 1999/293		Optimierungsprozesse im Management der Strassenerhaltung (MSE) *Processus d'optimisation dans le cadre du Système de Gestion de l'Entretien Routier*	2005
1110	VSS 1998/184		Signalisation variable (de danger et de prescription) Panneaux à messages variables *Vorschrifts- und Gefahren-Wechselsignale*	2005

Bericht-Nr.	Projekt Nr.	Alte Nr.	Titel	Datum
			Wechseltextanzeigen	
1111	SVI 1999/143		Trafic de support logistique de grandes manifestations *Betriebsverkehr von Grossanlässen*	2005
1112	VSS 1998/085	(26/98)	Bestimmung des Wassersättigungsgrades von Walzasphalt *Détermination du degré de saturation en eau des enrobés*	2004
1113	VSS 1998/196		Einsatz gelb hinterlegter Signale *Implantation de signaux sur fond jaune*	2005
1114	VSS 1999/246		Wirksamkeit des Winterdienstes *Efficacité du service hivernal*	2005
1117	VSS 2002/201		Unfälle beim Transport wassergefährdender Flüssigkeiten *Accidents routiers avec des liquides polluant l'eau*	2005
1115	SVI 2001/507		Angebote und Erfolgskriterien im nächtlichen Freitzeitverkehr *Trafic de loisirs nocturne*	2005
1118	VSS 1999/307		Systeme für die Fahrzeugführerunterstützung zur Erhöhung der Verkehrssicherheit *Wirksamkeit und Eignung* *Systèmes d'assistance au conducteur destinés à l'amélioration de la sécurité routière*	2005
1119	VSS 2000/365		Geometrie der Parkierungsanlagen *Géométrie des installtions de stationnement*	2005
1120	SVI 2001/514		Untersuchung der Stabilität des Verkehrsverhaltens *Etude de la stabilité des comportements de déplacements*	2005
1121	VSS 2001/202		Bankette bestehender Strassen *Bas-cotés de rotes existantes*	2006
1122	VSS 2000/342		Kosten-Nutzen-Analysen im Strassenverkehr *Analyses coûts/avantages du trafic routier*	2006
1123	VSS 1998/188		Essais croisés interlaboratoires en mécanique des sols et des roches *Ringversuche in Boden- und Felsmechanik*	2006
1124	VSS 1999/127		Baustellen an Hochleistungsstrassen *Chantiers sur routes à grand débit*	2006
1125	VSS 2002/705		Sicherheit von Kabelanlagen *Sécurité dans les installations de câblage*	2006
1126	VSS 2002/407		Complément d'essais Los Angeles en vue de l'introduction de la norme européenne EN 13043 relative aux granulats *Ergänzungsversuch Los Angeles zur Einführung der Europäischen Norm EN 13043 entsprechend den Granulaten*	2006
1127	VSS 1998/189		Ausgestaltung von Terminals für den (unbegleiteten) kombinierten Ladungsverkehr *Aménagement de terminaux pour le transport combiné (non accompagné)*	2006
1128	VSS 1998/193		Verkehrsbeeinflussung an Kreiseln *Influencer le trafic dans les giratoires*	2006
1129	VSS 2000/353		Flächendeckende Verdichtungskontrolle (FDVK) mittels bodenmechanischer Materialkenngrössen	2006

Bericht-Nr.	Projekt Nr.	Alte Nr.	Titel	Datum
			Contrôle continu du compactage (CCC) à l'aide de paramètres géotechniques	
1130	ASTRA 2002/011		Bewertung von Qualitätsmerkmalen im Güterverkehr *Evaluation des attributs de qualité dans le transport de marchandise*	2006
1131	SVI 1999/329		Vor- und Nachlauf im kombinierten Ladungsverkehr *Parcours initiaux et terminaux dans le transport combiné*	2006
1132	SVI 2001/519		Finanzielle Anreize für effiziente Fahrzeuge- Eine Wirkungsanalyse der Projekte VEL2 (Tessin) und NewRide in Basel und Zürich *Incitations Financières pour Véhicules Economes* *Une analyse de l'efficacité des projets VEL2 (Tessin) et NewRide (Bâle et Zürich)*	2006
1133	VSS 1999/285		Remplacement de l'essai oedométrique standard (oedomètre incrémental) par l'essai CRS (Constant Rate of Strain) *Ersetzung von Standard-Oedometerversuchen (Incremental-Oedometer) durch CRS-Oedometer-versuche*	2006
1134	VSS 1993/012		Druckfestigkeit von Gesteinskörnungen am Haufwerk *Résistance à la compression des granulats en vrac*	2006
1135	VSS 1999/259		Développement de modèles suisses pour la prédiction de la demande en transport pour des applications en temps réel *Schätzung Schweizer Verkehrsnachfragemodelle unter Berücksichtigung von Telematiksystemen*	2004
1136	SVI 2001/535		Reduktionsmöglichkeiten externer Kosten des MIV am Beispiel des Förderprogramms VEL2 im Kanton Tessin *Réduction des coûts externes du trafic individuel routier: le cas du programme de promotion VEL2 au Tessin*	2006
1137	VSS 2003/201		Diskontsatz in Kosten-Nutzen-Analysen im Verkehr *Taux d'actualisation pour les analyses coûts/avantages du trafic*	2006
1138	VSS 1998/070		Einfluss schweizerischer Filler auf die Alterung von bituminösen Bindemitteln und die Rissbildung im Belag *Influence des filliers suisses sur le vieillissement des liants bitumineux et la formation des fissures dans le revêtement*	2006
1139	SVI 2001/509		Nachhaltigkeit im Verkehr Indikatoren im Bereich Gesellschaft *Développement durable dans le trafic* *Indicateurs sociaux*	2005
1140	VSS 1999/292		Zerfallzyklen von EM-Anlagen *Durée de vie des installations électromécaniques*	2005
1141	VSS 2000/544		Erhaltungsmanagement: Gesamtbewertung der Fahrbahnen, Substanz- und	2006

Bericht-Nr.	Projekt Nr.	Alte Nr.	Titel	Datum
			Gebrauchswert *Gestion de l'entretien: Evaluation globale des chaussées, valeur intrinsèque et d'usage*	
1142	ASTRA 2000/421-1		Modélisation des charges d'essieu *Modellierung der Axlasten*	2005
1143	ASTRA 2000/421-2		Formulation et optimisation des formules d'enrobés *Mischrezeptur und Optimierung der bituminösen Mischgute*	2005
1144	ASTRA 2001/016		Evolution et impact des systèmes de navigation dynamique multimodale en Suisse *Entwicklung und Auswirkung von multimodalen dynamischen Navigationssystemen in der Schweiz*	2005
1145	SVI 2000/378		Früherkennung von Entwicklungstrends zum Verkehrsangebot *Identification précoce des tendances évolutives en matière d'offre de transport*	2005
1146	SVI 2001/503		Erhebung des Fuss- und Veloverkehrs *Enquête sur le trafic piétonnier et cycliste*	2005
1147	ASTRA 2001/058		Schadstoffe im Strassenabwasser einer stark befahrenen Strasse und deren Retention mit neuartigen Filterpaketen aus Goetextil und Absorbermaterial *Polluants dans les eaux de ruissellement d'un tronçon de route avec trafic intense et leur traitement innovateur avec géotextile et absorbant granulé*	2006
1148	VSS 2000/364		Metaroute Gestion de la qualité des données du repérage spatial et de la géométrie des axes routiers *Management der Datenqualität des Raumbezugs und der Goemetrie der Strassenachse*	2006
1149	VSS 1999/261		Architektur und Zeitaspekte von SVT-Daten *Architecture et aspects temporels des données de la télématique routière*	2005
1150	VSS 1998/187		Dimensionierung der Fussgängerflächen von Haltestellen des strassengebundenen öffentlichen Verkehrs *Dimensionnement des zones destinées aux piétons aux arrêts des transports publics sur voirie*	2006
1151	SVI 2001/545		Publikumsintensive Einrichtungen PE: Planungsgrundlagen und Gesetzmässigkeiten *Installations à forte fréquentation: Bases de planification et normes*	2005
1152	VSS 2000/360		Besoin en adhérence des revêtements de chaussées *Griffigkeitsbedarf von Strassenbelägen*	2006
1153	VSS 2000/412		Schweizerisches Handbuch für die Konzeption des Strassenoberbaus *Manuel Suisse de conception des chaussées*	2005
1154	ASTRA 2001/053		Strassenlärm in grossen Abständen *Bruit routier sur des grandes distances*	2006
1155	VSS 2001/602		Zweckmässigkeits- und Auswahlkriterien	2005

Bericht-Nr.	Projekt Nr.	Alte Nr.	Titel	Datum
			für automatische Taumittelsprühanlagen *Critères d'opportunité et de choix des installations automatiques de déverglaçage*	
1156	VSS 2002/404		Screening moderner chemisch-physikalischer Analysemethoden für bituminöse Baustoffe *Screening des méthodes d'analyse chimico-physiques pour des matériaux bitumineux*	2006
1157	SVI 2004/015		Error Propagation in Macro Transport Models *La propagation d'erreurs dans les macro modèles de transport*	2006
1158	SVI 2003/003		Verkehrstechnische Beurteilung multimodaler Betriebskonzepte auf Strassen innerorts *Evaluation technique de concepts d'explotation multimodaux pour routes urbaines*	2006
1159	VSS 2001/505		Geohydraulische Versuche in Fels *Essais géohydrauliques dans la roche*	2006
1160	OFROU 2003/005		Evaluation de la sécurité du trafic par microsimulation *Bewertung der Verkehrssicherheit mit Mikrosimulation*	2005
1162	ASTRA 1996/039		Tonminerale und Sulfate als Ursache für druckhaftes Verhalten von Gesteinen Ursachen und Wirkungen des Quellvorganges *Les minéraux argileux et les sulfates - origine de pressions développées par des roches Origine et effets du processus de gonflement*	2005
1163	VSS 2000/466		Lärmimmissionen von Parkierungsanlagen *Immissions de bruit d'installations de stationnement*	2006
1164	SVI 2000/388		Kernfahrbahnen auf Ausserortsstrecken *Chaussées à voie centrale banalisée hors des localités*	2006
1165	SVI 2002/001		Fussgängerstreifenlose Ortszentren *Centres de localité sans passages pour piétons*	2006
1166	ASTRA 2004/009		Überprüfung der VSS-Normen hinsichtlich Relevanz und Defiziten bezüglich Verkehrssicherheit *Analyse de la pertinence et des insuffisances des normes VSS relativement à la sécurité*	2006
1167	SVI 2001/523		Road Pricing Modelle auf Autobahnen und in Stadtregionen *Modèles de péages routiers sur les autoroutes et dans les régions urbaines*	2006
1168	SVI 2001/524		Entkopplung zwischen Verkehrs- und Wirtschaftswachstum *Découplage entre accroissement du trafic et croissance économique*	2006
1169	VSS 1999/265		Systeme für die automatische Verkehrsüberwachung (Monitoring) mit digitaler Bildverarbeitung *Systèmes de surveillance automatique du trafic (monitorage) par le traitement digital d'image*	2006
1170	VSS 2003/902		Schweizerische Bedürfnisse für den Austausch von Verkehrsinformatonen in Europa *Exigences suisses pour l'échange d'information*	2006

Bericht-Nr.	Projekt Nr.	Alte Nr.	Titel	Datum
			routière en Europe	
1171	VSS 1992/005		Kalibrieren, Vergleichen und Harmonisieren der Griffigkeitsmessungen und der Oberflächenrauhigkeits-messungen mit internationalen Institutionen (AIPCR-Ringversuch 1992) *Calibrage, comparaison et harmonisation des mesures d'adhérence et de la texture des couches de roulement avec les institutions internationales*	2006
1172	SVI 2004/013		Genderfragen in der Verkehrsplanung Vorstudie *Genre et mobilité, étude préliminaire*	2006
1173	VSS 1999/240		Vernetzung von Lebensräumen bei der Gestaltung von Verkehrsträgern *Les réseaux des habitats lors de l'aménagement des voies de trafic*	2006
1174	ASTRA 2006/012		Alpentransitbörse: Untersuchung der Praxistauglichkeit *La bourse du transit alpin: Etude de faisabilité pratique*	2007
1175	ASTRA 2004/012		Landschaftszerschneidung Schweiz Zerschneidungsanalyse 1885-2002 und Folgerungen für die Verkehrs- und Raumplanung *Morcellement du paysage en Suisse Analyse du morcellement 1885-2002 et implications pour la planification du trafic et l'aménagement du territoire*	2007
1176	SVI 2002/002		Verfahren zur Berücksichtigung der Zuverlässig-keit in Evaluationen *Procédure de prise en compte de la fiabilité dans les évaluations*	2007
1177	SVI 2001/504		Überlegungen zu einem Marketingansatz im Fuss- und Veloverkehr *Réflexions sur une approche marketing pour le trafic piétonnier et cycliste*	2007
1178	SVI 2001/542		Konfliktanalyse beim Mischverkehr *Analyse de conflits pour des situations de circulation mixte*	2007
1179	ASTRA 2002/012		Wirkung von Schallschirmen bei Inversionslagen und Wind *Efficacité des écrans sonores lors d'inversions de température et par temps de vent*	2007
1180	VSS 2001/501		Kombinierte Beläge Belagsüberzüge auf Betondecken, Kompositbeläge *Structures mixtes Resurfaçages sur chaussées en béton et structures composites*	2007
1181	VSS 1999/291		Zustandsbewertung von EM-Anlagen *Evaluation de l'état des installations électromécaniques*	2007
1182	ASTRA 2000/422		Unterhalt 2000, Forschungspaket 4: Dauerhafte Beläge *Unterhalt 2000, paquet de recherche 4: Revêtements durables*	2007

Bericht-Nr.	Projekt Nr.	Alte Nr.	Titel	Datum
1183	VSS 2000/453		Zusammenhang zwischen PAK-Gehalt in teerhaltigem Recycling-Granulat und in den emittierten Dämpfen beim Wiedereinbau *Relation entre la teneur en HAP des granulats recyclés renfermant du goudron et celle des vapeurs émises lors*	2007
1184	ASTRA 2004/010		Prise en compte du développement durable lors des prestations de recherche et de normalisation de la VSS *Einbindung der Nachhaltigkeit in die Normungs- und Forschungsvorhaben des VSS*	2007
1185	VSS 1999/280		Mechanical properties of porous asphalt, recommendations for standardization *Mechanische Eigenschaften von offenporigem Asphalt, Empfehlungen für die Normierung*	2006
1186	VSS 2005/911		Akzeptanz von Mobility Pricing *Acceptation du Mobility Pricing*	2007
1187	VSS 2005/912		Bedeutung von Mobility Pricing für die Verkehrsfinanzierung der Zukunft *Importance du Mobility Pricing pour le financement futur des transports*	2007
1188	VSS 2005/913		Importance de projets pilotes pour le Mobility Pricing *Bedeutung von Mobility Pricing Pilotversuchen*	2007
1189	VSS 2005/916		Verkehrstechnische Aspekte des Mobility Pricing *Aspects techniques de circulation du Mobility Pricing*	2007
1190	VSS 2005/917		Auswirkungen des europäischen elektronischen Mautdienstes auf die Schweiz *Effets du péage Electronique Européen sur la Suisse*	2007
1191	SVI 2005/004		Einbezug von Reisekosten bei der Modellierung des Mobilitätsverhaltens *Intégration des frais de déplacements dans la modélisation du comportement de mobilité*	2008
1192	VSS 2003/901		Datenverarbeitung für eine verkehrsträgerübergreifende Mobilitätssteuerung *Traitement de données pour une gestion de la mobilité basée sur l'interopérabilité des modes de déplacement*	2008
1193	ASTRA 2004/008		Swiss Contribution to Eureka Project Logchain Footprint E!2486 *Schweizer Beitrag zu Eureka Project Logchain Footpring E!2486*	2007
1194	VSS 2005/914		Systemtechnische und betriebswirtschaftliche Aspekte des Mobility Pricing *Aspects technologiques et d'exploitation du Mobility Pricing*	2007
1195	VSS 2005/503		Lanzeiterfassung des Schichtenverbunds - Relation zwischen Prüfwert nach Einbau und Langzeit-verhalten *Performance à long termes de la liaison entre les couches des revêtements bitumineux*	2007
1196	VSS 1999/277		Prüfung von Haftklebern *Preuves du résultat des émulsions pour couches d'accrochage*	2007
1197	SVI 2004/096		Ausgestaltung von multimodalen Umsteigepunkten *Equipement des points de transfert multimodaux*	2007
1198	SVI 2001/539		Überbreite Fahrstreifen und zweistreifige Schmalfahr-	2007

Bericht-Nr.	Projekt Nr.	Alte Nr.	Titel	Datum
			bahnen *Voies de circulation extra-larges et chaussées étroites à deux voies de circulation*	
1199	VSS 2005/204		Externe Kosten im Strassenverkehr: Grundlagen zur Durchführung einer Kosten-Nutzen-Analyse *Coûts externes du trafic routier: Principes pour la réalisation d'une analyse coûts/avantages*	2007
1200	VSS 2005/205		Ermittlung repräsentativer Betriebskostensätze für Kraftfahrzeuge zur Bewertung von Massnahmen im Strassenverkehr *Calcul des coûts unitaires représentatifs d'utilisation des automobiles en vue de l'évaluation des mesures en matière de circulation routière*	2007
1201	VSS 2003/601		Optimierung der Verkehrsicherheit und des Verkehrs-flusses im Winter durch den Einsatz moderner Kommunikationstechnologie im Strassenbetrieb *Optimiser la sécurité et le trafic routier en hiver par l'utilisation de moyens de communication modernes dans la gestion routière*	2007
1202	VSS 1999/298		Grundlagen zur Revision der Griffigkeitsnormen *Bases pour la révision des normes sur l'adhérence*	2007
1203	VSS 2005/304		Verkehrsregelungssysteme- Grundlagen für das Erhaltungsmanagement *Les systèmes de régulation du trafic - les bases pour la gestion de l'entretien*	2008
1204	SVI 2000/384		Fahrten- und Fahrleistungsmodelle: Erste Erfahrungen *Les systèmes de contingentement des trajets: Les premières expériences*	2007
1205	FGU 2004/001		*Die zerstörungsfreie Untersuchung von Leckstellen in zweischaligen Untertagbauwerken* *L'étude non destructive de points de fuite dans des ouvrages souterrains à deux parois*	2006
1206	ASTRA 2006/019		Short-term Forecasts for Transport Models *Prévision à court terme pour les modèles de transport*	2007
1207	VSS 2003/602		Sécurité routière: Importance du paysage dans la lisibilité de la route *Strassensicherheit: Bedeutung der Landschaft-gestaltung für die Lesbarkeit der Strasse*	2007
1208	SVI 2005/005		Quantitative Auswirkungen von Mobility Pricing Szenarien auf das Mobilitätsverhalten und auf die Raumplanung *Effets quantitifs des scénarios du Mobility Pricing sur la mobilité et le développement territorial*	2007
1209	VSS 2005/901		Einfluss von Fahrerassistenzsystemen auf die Leistungsfähigkeit von Strassennetzen *Influence des systèmes d'assistance à la conduite sur la capacité des réseaux routiers*	2008
1210	VSS 2005/915		Organisatorische und rechtliche Aspekte des Mobility Pricing *Aspects organisationnels et juridiques du Mobility Pricing*	2007
1211	VSS 1998/192		Minikreisel *Mini-giratoires*	2008

Bericht-Nr.	Projekt Nr.	Alte Nr.	Titel	Datum
1212	VSS 2007/501		D-A-CH - Forscungsprojekt Nutzungszeiten offenporiger Asphaltdeckschichten *D-A-CH - Projet de recherche Durabilité des revêtements en enrobé drainant*	2007
1213	VSS 2002/706		NAVAROU Potentiel d'utilisation des données routières de la navigation automobile pour l'entretien routier *Potenzial der Nutzung von Fahrzeugnavigationsdaten für das Strassenverkehrsmanagement*	2008
1214	VSS 2004/901		Darstellung und Verwendung von Verkehrssignalen in Strassendatenbanken *Implementation and use of traffic signs in road databases*	2007
1215	VSS 2000/456		Bewirtschaftungssysteme für Parkierungsanlagen *Concepts de gestion et d'exploitation d'installations de stationnement*	2008
1216	VSS 1998/195		Für Motorfahrzeuge und leichte Zweiräder befahrbare und für den Füssgängerverkehr ganz oder teilweise zugängliche Streifen in der Mitte der Fahrbahn (Mehrzweckstreifen) *Voies de circulation en milieu de chaussée destinées au trafic motorisé et au trafic des deux-roues légers, partiellement ou entièrement accessibles au trafic des piétons (voies à affectation variable)*	2008
1217	SVI 2006/001		Forschungspaket "Güterverkehr", Initialprojekt "Bestandesaufnahme und Konkretisierung des Forschungspakets" *Paquet de recherche "transport de marchandises", projet initial "inventaire et concrétisation du paquet de recherche"*	2008
1218	VSS 1999/271		Querungen für den Fuss- und leichten Zweiradverkehr *Traversées à l'usage des piétons et des deux-roues légers*	2008
1219	VSS 2003/603		Faunagerechte Sanierung von bestehende Gewässerdurchlässen *Adaptation des voûtages pour la petite faune terrestre et la faune piscicole*	2008
1220	VSS 2005/910		Mobility Pricing Synthesebericht *Mobility Pricing Rapport de Synthèse*	2007
1221	ASTRA 2004/019		Maladies et causes d'absences dans le service d'entretien des routes *Diseases and reasons for absences in the road maintenance services*	2008
1222	SVI 2004/074		Freizeitverkehr innerhalb von Agglomerationen *Trafic de loisirs dans les agglomérations*	2008
1223	VSS 2003/302		Auswirkungen und Massnahmen im HVS-Netz bei Rampenbewirtschaftung *Répercussions et mesures sur le réseau des routes principales en présence d'une gestion des rampes*	2008
1224	VSS 1999/276		Filler - Influence des phyllosilicates pour l'utilisation dans la construction routière *Füller - Einfluss von Schichtsilikaten für die*	2008

Bericht-Nr.	Projekt Nr.	Alte Nr.	Titel	Datum
			Verwendung im Strassenbau	
1225	SVI 1999/328		Gesetzmässigkeiten des Anlieferverkehrs *Caractéristiques du transport de livraison*	2008
1226	ASTRA 2003/007		Kommunale Strassennetze in der Schweiz: Formen neuer Public Private Partnership (PPP) - Kooperationen für den Unterhalt *Réseaux routiers communaux en Suisse:* *Formes de nouveaux partenariats publics-privés (PPP)-coopérations pour l'entretien*	2008
1227	VSS 2004/601		Umweltbauabnahme (UBA) *Réception environnementale des travaux (RET)*	2008
1228	SVI 2001/508		Mobilitätsmuster zukünftiger Rentnerinnen und Rentner: eine Herausforderung für das Verkehrssystem 2030? *Mobilité des futurs retraités - un défi pour le système des transport en 2030?*	2008
1229	SVI 2004/081		Modal Split Funktionen im Güterverkehr *Fonctions de répartition modale pour le trafic de marchandises*	2008
1230	SVI 2004/090		Monitoring und Controlling des Gesamtverkehrs in Agglomerationen *Monitoring et controlling de l'ensemble du trafic dans les agglomérations*	2008
1231	SVI 2004/045		Mobilitätsmanagement in Betrieben- Motive und Wirksamkeit *Gestion de la mobilité dans les entreprises-motifs et efficacité*	2008
1232	ASTRA 2005/008		Low Power Wireless Sensor Network for Monitoring Civil Infrastructure *Drahtloses Sensornetzwerk zur Infrastrukturüberwachung*	2009
1233	ASTRA 2000/420		Unterhalt 2000 Forschungsprojekt FP2 Dauerhafte Komponenten bitumenhaltiger Belagsschichten *Components durables des couches bitumineux*	2009
1234	VSS 2006/504		Expérimentation in situ du nouveau drainomètre européen *In Situ Validierung des neuen europäischen Drainometers*	2008
1235	VSS 2004/711		Forschungspaket Masssnahmenplanung im EM von Fahrbahnen Standardisierte Erhaltungsmassnahmen *Mesures d'entretiens standardisées*	2008
1236	ASTRA 2008/008_7		Analytische Gegenüberstellung der Strategie- und Tätigkeitsschwerpunkte ASTRA-AIPCR *Analyse Comparative des accents stratégiques et des champs d'action prioritaires de l'OFROU et de l'AIPCR*	2008
1237	VSS 2007/903		Grundlagen für eCall in der Schweiz *Bases pour eCall en Suisse*	2009

Bericht-Nr.	Projekt Nr.	Alte Nr.	Titel	Datum
1238	VSS 2005/303		Verkehrssicherheit an Tagesbaustellen und bei Anschlüssen im Baustellenbereich von Hochleistungs-strassen *Sécurité routière pour chantiers de courte durée et aux jonctions dans la zone d'un chantier de route à grand débit*	2008
1239	VSS 2000/450		Bemessungsgrundlagen für das Bewehren mit Geokunststoffen *Bases de dimensionnement pour le renforcement par géosyntétiques*	2009
1240	ASTRA 2002/010& 2005/009		L'acceptabilité du péage de congestion: Résultats et analyse de l'enquête réalisée en Suisse *Die Akzeptanz von Gebühren zur Vermeidung von Stau auf Strassen: Resultate und Analysen von Untersuchungen in der Schweiz*	2009
1241	ASTRA 2001/052		Erhöhung der Aussagekraft des LCPC Spurbildungstests *Amélioration des informations fournies par l'essai d'orniérage LCPC*	2009
1242	VSS 2005/451		Recycling von Ausbauasphalt in Heissmischgut: Initialprojekt *Recyclage des matériaux bitumeux de démolition dans les enrobés à chaud: projet initial*	2007
1243	VSS 2000/463		Kosten des betrieblichen Unterhalts von Strassen-anlagen *Les coûts de l'entretien courant des routes*	2008
1244	VSS 2004/714		Masssnahmenplanung im Erhaltungsmanagement von Fahrbahnen Gesamtnutzen und Nutzen-Kosten-Verhältnis von standardisierten Erhaltungsmassnahmen *Bénéfice total - rapport avantages / coûts des mesures d'entretien standardisées*	2008
1246	VSS 2004/713		Massnahmenplanung im Erhaltungsmanagement von Fahrbahnen Bedeutung Oberflächenzustand und Tragfähigkeit sowie gegenseitige Beziehung für Gebrauchs- und Substanzwert *Influences et interactions de l'état de surface et de la portance sur la valeur intrinsèque et la valeur d'usage*	2009